



Universitat Autònoma de Barcelona

ADVERTIMENT. L'accés als continguts d'aquesta tesi doctoral i la seva utilització ha de respectar els drets de la persona autora. Pot ser utilitzada per a consulta o estudi personal, així com en activitats o materials d'investigació i docència en els termes establerts a l'art. 32 del Text Refós de la Llei de Propietat Intel·lectual (RDL 1/1996). Per altres utilitzacions es requereix l'autorització prèvia i expressa de la persona autora. En qualsevol cas, en la utilització dels seus continguts caldrà indicar de forma clara el nom i cognoms de la persona autora i el títol de la tesi doctoral. No s'autoritza la seva reproducció o altres formes d'explotació efectuades amb finalitats de lucre ni la seva comunicació pública des d'un lloc aliè al servei TDX. Tampoc s'autoritza la presentació del seu contingut en una finestra o marc aliè a TDX (framing). Aquesta reserva de drets afecta tant als continguts de la tesi com als seus resums i índexs.

ADVERTENCIA. El acceso a los contenidos de esta tesis doctoral y su utilización debe respetar los derechos de la persona autora. Puede ser utilizada para consulta o estudio personal, así como en actividades o materiales de investigación y docencia en los términos establecidos en el art. 32 del Texto Refundido de la Ley de Propiedad Intelectual (RDL 1/1996). Para otros usos se requiere la autorización previa y expresa de la persona autora. En cualquier caso, en la utilización de sus contenidos se deberá indicar de forma clara el nombre y apellidos de la persona autora y el título de la tesis doctoral. No se autoriza su reproducción u otras formas de explotación efectuadas con fines lucrativos ni su comunicación pública desde un sitio ajeno al servicio TDR. Tampoco se autoriza la presentación de su contenido en una ventana o marco ajeno a TDR (framing). Esta reserva de derechos afecta tanto al contenido de la tesis como a sus resúmenes e índices.

WARNING. The access to the contents of this doctoral thesis and its use must respect the rights of the author. It can be used for reference or private study, as well as research and learning activities or materials in the terms established by the 32nd article of the Spanish Consolidated Copyright Act (RDL 1/1996). Express and previous authorization of the author is required for any other uses. In any case, when using its content, full name of the author and title of the thesis must be clearly indicated. Reproduction or other forms of for profit use or public communication from outside TDX service is not allowed. Presentation of its content in a window or frame external to TDX (framing) is not authorized either. These rights affect both the content of the thesis and its abstracts and indexes.



**Exploring an
artificial
chromoplast
system for
enrichment of
plant leaves in
isoprenoid
vitamins**

Luca Morelli

PhD thesis,
Barcelona, 2021



**Universitat Autònoma
de Barcelona**

UNIVERSITAT AUTÒNOMA DE BARCELONA

FACULTAT DE BIOCÈNCIES

Programa de Doctorat en Biologia i Biotecnologia Vegetal

**EXPLORING AN ARTIFICIAL CHROMOPLAST
SYSTEM FOR ENRICHMENT OF PLANT LEAVES IN
ISOPRENOID VITAMINS**

Luca Morelli

2021



UNIVERSITAT AUTÒNOMA DE BARCELONA

FACULTAT DE BIOCÈNCES

Programa de Doctorat en Biologia i Biotecnologia Vegetal

PhD thesis

EXPLORING AN ARTIFICIAL CHROMOPLAST
SYSTEM FOR ENRICHMENT OF PLANT LEAVES IN
ISOPRENOID VITAMINS

Dissertation presented by Luca Morelli for the degree of Doctor of Plant Biology and Biotechnology at Autonomous University of Barcelona. This work was developed in the Centre for Research in Agricultural Genomics.

Thesis Director

Thesis Tutor

Candidate

Prof. Manuel

Prof. Benet Gunsè Forcadell

Luca Morelli

Rodriguez Concepcion

Barcelona, 2021



The project that gave rise to these results received the support by "la Caixa" Foundation (ID 100010434) with the PhD INPhINIT fellowship LCF/BQ/IN18/11660004. This project has received funding from the European Union's Horizon 2020 research and innovation programme under the Marie Skłodowska-Curie grant agreement No. 713673.

Acknowledgements

I decided I wanted to do a PhD when I had already started one, and it was the scariest leap backward I ever had to face. But, on a closer inspection, it was a leap far forward. And, despite every fall and difficulty, all this work is part of me. Thanks to Manuel, for that video call that made me take the decisive step. For the trust, supervision, and support. It is said that every researcher's approach comes from his teachers and I am grateful you took part in shaping my scientific thinking. Thanks to Jaume for really contributing to my advances with ideas, suggestions, and support. Thanks to prof. Felix Kessler and to Balaji for hosting me in the laboratory in Neuchatel and helping me to realize a big piece of all this work. Thanks to Ricard Benito to have managed to illustrate in the cover what I really wanted to be a graphical representation of my work. Thanks to the CRAG technical support and facilities staff for greatly facilitating this research activity with your work, and thanks to the Obra Social La Caixa for the fellowship that allowed me to do this PhD. Thanks to the Caixa people because we were all together in this, and things made in group are easier. Thanks to Poonam for always knowing what to say and never trying to sweeten pills. Sometimes making people see the reality is the best gift someone could make. Thanks to all my colleagues from lab 2.01 because I would have never expected to be part of a team, more than of a research group. Thanks to Ari, because we are twin, we are connected, and everything it's easier when you have someone on your side that understand you by simply looking in your direction. Alba, Arantxa, Edu, Silvia, Esteban. I would have never endured all this without you. Lo que el bacallà pudent une, nada lo separa. Julian, thank you for what you made to support me when maybe was more difficult than ever.

Thanks to my family that always brace me in this choice, sometimes going against their own desires. You were, are, and always will be my strength and the origin of my dedication and I really want to dedicate this to you. Especially at the end of this crazy and painful year.

Thanks to everyone who was part of this travel with me, for the whole path, or just for a bit. You settled a stone, for sure.

“De cada fin, nace un principio necesario. Un trampolín, y volver a saltar con gente afin hasta el confín. A veces siento la herida de la partida. Pero hay recompensas que al llegar lo equilibran. Siempre viene un fuego nuevo que va y vuelve. Y los amigos te animan.”

Buen Viaje. LDS

Isoprenoids are one of the largest families of metabolites in nature, and they are especially diverse in the plant kingdom. Among them, carotenoids, tocopherols and phylloquinone are interesting for their role as vitamins. Plants synthesize these compounds in chloroplasts to contribute to photosynthesis and photoprotection. In the case of carotenoids, their highest levels are found in specialized plastids named chromoplasts, which are typically found in non-green pigmented organs such as flower petals and ripe fruits but only occasionally in leaves. The general goal of this thesis has been testing new strategies for the enrichment of leafy vegetables in isoprenoid vitamins through a system developed in our lab to induce the conversion of chloroplasts into chromoplasts in leaves. The tool is based on the capacity of the crtB enzyme from the bacterium *Pantoea ananatis* to boost the production of phytoene and the ability of leaves to convert this extra phytoene into downstream carotenoids with the concomitant changes in plastid ultrastructure. The availability of this system allowed to define two specific objectives: (1) to characterize the physiological context of the crtB-induced phenotype in *Nicotiana benthamiana* leaves and (2) to test different strategies exploiting this crtB-based system to improve leaf biofortification.

In the first part of the thesis, we demonstrate that the non-reversible chloroplast-to-chromoplast differentiation phenotype triggered by plastid-localized crtB is associated with a rapid loss of photosynthetic activity caused by the accumulation of phytoene. This phenomenon makes the chloroplast competent for chromoplastogenesis. The transition is then completed once phytoene is converted into downstream carotenoids by endogenous enzymes. We also demonstrate that treatments that cause altered redox balance of the photosystems and oxidative stress facilitate chromoplast differentiation. In the second part of the thesis, we characterize the structural changes associated with crtB-mediated chromoplast differentiation in leaves. During the process plastoglobules increase in number and size. Plastoglobules are used to store phytoene and other isoprenoids (including pro-vitamin A β -carotene, vitamin E tocopherols, and vitamin K phylloquinone). We also show that plastoglobules are the site of localization and action of the crtB protein and demonstrate that conditions that promote plastoglobule proliferation (such as high light) can be used to further promote the accumulation of isoprenoid vitamins. Our results show that the combination of crtB with genes involved in the biosynthesis of such vitamins can further increase their levels. Lastly, we show that β -carotene can be further accumulated by combining the crtB-mediated chromoplastogenesis with an engineered extraplastidial pathway. We also show that the optimizations of the crtB system can be applied to biofortify edible green leafy vegetables such as lettuce, hence contributing to the development of new functional foods.

Los isoprenoides son una de las familias más grande de metabolitos en la naturaleza y son especialmente diversos en el reino vegetal. Entre ellos, los carotenoides, los tocoferoles y la filoquinona tienen un interés especial por su papel como vitaminas. Las plantas sintetizan estos compuestos en cloroplastos para contribuir a la fotosíntesis y fotoprotección. En el caso de los carotenoides, sus niveles más altos se encuentran en plastos especializados llamados cromoplastos, que se encuentran típicamente en órganos pigmentados no verdes como pétalos de flores y frutos maduros, pero solo ocasionalmente en hojas. El objetivo general de esta tesis ha sido probar nuevas estrategias para el enriquecimiento de verduras en vitaminas isoprenoides a través de un sistema desarrollado en nuestro laboratorio para inducir la conversión de cloroplastos en cromoplastos en hojas. La herramienta se basa en la gran capacidad de la enzima *crtB* de la bacteria *Pantoea ananatis* para producir fitoeno y la capacidad de las hojas para convertir este fitoeno adicional en carotenoides posteriores con cambios concomitantes en la ultraestructura de los plástos. La disponibilidad de este sistema permitió definir dos objetivos específicos: (1) caracterizar el contexto fisiológico del fenotipo inducido por *crtB* en hojas de *Nicotiana benthamiana* y (2) probar diferentes estrategias aprovechando este sistema basado en *crtB* para mejorar la biofortificación de hojas. En la primera parte de la tesis, demostramos que el fenotipo no reversible de diferenciación de cloroplasto a cromoplasto desencadenado por *crtB* en plastos se asocia con una rápida pérdida de actividad fotosintética causada por la acumulación de fitoeno. Este fenómeno hace que el cloroplasto pase a ser competente para la cromoplastogénesis. Luego, la transición se completa una vez que el fitoeno se convierte en carotenoides posteriores mediante enzimas endógenas. También demostramos que los tratamientos que causan un equilibrio redox alterado de los fotosistemas y un estrés oxidativo facilitan la diferenciación de los cromoplastos. En la segunda parte de la tesis, caracterizamos los cambios estructurales asociados con la diferenciación de cromoplastos mediada por *crtB* en hojas. Durante el proceso, los plastoglobulos aumentan en número y tamaño y se utilizan para almacenar fitoeno y otros isoprenoides, incluidos β -caroteno (pro-vitamina A), tocoferoles (vitamina E) y filoquinona (de vitamina K). Los plastoglobulos son el sitio de localización y acción de la proteína *crtB* y demostramos que las condiciones que estimulan la proliferación de plastoglobulos (como la luz intensa) se pueden utilizar para promover aún más la acumulación de vitaminas isoprenoides. Nuestros resultados muestran que la combinación de *crtB* con genes involucrados en la biosíntesis de dichas vitaminas puede aumentar aún más sus niveles. Por último, mostramos que β -caroteno se puede acumular aún más combinando la cromoplastogénesis mediada por *crtB* con una vía extraplástica sintética. También demostramos que las optimizaciones del sistema *crtB* se pueden aplicar para biofortificar vegetales de verduras como la lechuga, contribuyendo así al desarrollo de nuevos alimentos.

Table of contents

<i>General introduction</i>	1
o.1. Isoprenoids in nature	1
o.2. Isoprenoids as health promoting compounds.	2
o.3. Isoprenoid biosynthetic pathways.....	4
o.3.1. Carotenoid pathway	5
o.3.2. Tocochromanol and prenylquinone pathways.....	6
o.4. Isoprenoid storage in plastids.....	8
o.5. Role of isoprenoids in photosynthesis and photoprotection	12
o.6. Isoprenoid biotechnology.	13
<i>Objectives</i>	19
<i>Chapter 1. Artificial generation of chromoplasts in green leaves: exploring the physiological context.</i> ..	23
o.7. Introduction	23
o.8. Results.....	25
1.2.1. Transient expression of the bacterial <i>crtB</i> gene strongly and irreversibly impacts photosynthesis	25
1.2.2. Artificial chromoplastogenesis is exacerbated by PAP-mediated retrograde signaling.....	29
1.2.3. Endogenous hormones do not control the leaf chromoplastogenesis process	31
1.2.4. Enhanced supply of phytoene in chloroplasts is necessary but not sufficient to trigger chromoplastogenesis in leaves.	35
1.3. Discussion	39
1.4. Materials and methods.....	44
1.4.1. Plant material and growth conditions	44
1.4.2. Gene constructs.....	44
1.4.3. Transient expression assays.....	45
1.4.4. Transcript analyses	46
1.4.5. Metabolite analyses.....	46
1.4.6. Photosynthetic measurements.....	47
1.4.7. Protein extraction and analysis	48
<i>Chapter 2. Use of light to promote the crtB-mediated transition from chloroplast to chromoplasts.</i>	53
2.1. Introduction.....	53
2.1.1. An enrichment in FR also impacts the efficiency of photosynthesis.....	56
2.2. Results.....	57

2.2.1. <i>N. benthamiana</i> plants exposed to FR show reduced photosynthetic pigment content and activity.....	57
2.2.2. Different Brassicaceae species present divergent photoacclimation responses	59
2.2.3. Genetic impairment of low R:FR perception impacts elongation and photosynthetic responses to shade but not photoacclimation capacity.	62
2.2.4. Exposure of shade-avoider plants to low R:FR improves their photoacclimation to low PAR. 65	
2.2.5. Simulated shade treatment facilitates the chromoplast differentiation process but results in a lower production of total carotenoids.	71
2.2.6. Exposure to high PAR can also promote crtB-induced chromoplastogenesis.....	75
2.3. Discussion.....	77
2.4. Material and methods.....	81
2.4.1. Plant material and growth conditions	81
2.4.2. Gene constructs.....	82
2.4.3. Transient expression assay.....	83
2.4.4. Photosynthetic measurements and pigment quantification.....	83
2.4.5. Microarray data analyses.....	83
2.4.6. Transmission electron microscopy.....	84
2.4.7. ROS histochemical staining.....	84
<i>Chapter 3. Exploiting the formation of new storage structures in artificially obtained chromoplasts to boost the accumulation of isoprenoid vitamins in leaves.</i>	<i>89</i>
3.1. Introduction.....	89
3.2. Results.....	91
3.2.1. The overexpression of <i>crtB</i> triggers disorganization of photosynthetic complexes followed by proliferation of PG as leaf chloroplasts turn into chromoplasts.	91
3.2.2. Artificial chromoplasts accumulate isoprenoids that distribute differentially in plastid substructures.....	99
3.2.3. High light acclimation and dark-induced senescence are effective for the enrichment of leaves in plastidial isoprenoids.....	104
3.2.4. <i>crtB</i> can be combined with isoprenoid biosynthetic genes for an additional enhancement effect	107
3.2.5. Physical treatments and metabolic engineering can be combined for additional enhancement.....	109
3.2.6. <i>crtB</i> overexpression can be used to biofortify edible leaves	112
3.3. Discussion.....	115
3.4. Material and methods.....	120
3.4.1. Plant material and growth conditions	120
3.4.2. Gene constructs.	121

3.4.3. Transient expression assays	121
3.4.4. Chloroplast isolation and fractionation	122
3.4.5. Protein extraction and western blot	122
3.4.6. Metabolite analyses.....	123
3.4.7. Microscopy.....	124
3.4.8. Antioxidant capacity	125
3.4.9. Photosynthetic measurements	125
<i>Chapter 4. Carotenoid biofortification beyond plastids.....</i>	<i>129</i>
4.1. Introduction.....	129
4.2. Results	131
4.2.1 Extraplasmidial phytoene and lycopene accumulate at levels so high that they eventually impact photosynthetic activity.....	131
4.2.2. The engineered cytosolic pathway can be extended to produce β -carotene in the cytosol	133
4.2.3. Cytosolic production of carotenoids can be combined with chromoplast development for further carotenoid enrichment of leaves	135
4.2.4. Providing more plastidial precursors does not improve carotenoid levels due to a bottleneck at the phytoene desaturation level.	136
4.3. Discussion.....	138
4.4. Material and methods.....	142
4.4.1. Plant material and growth conditions	142
4.4.2. Gene constructs.....	142
4.4.3. Transient expression assay.....	142
4.4.4. Photosynthetic measurements.....	142
4.4.5. Antioxidant capacity	143
4.4.6. Metabolite analysis	143
<i>General discussion</i>	<i>147</i>
5.1. Chromoplast differentiation in green leaves	147
5.1.1. A non-reversible chloroplast-to-chromoplast differentiation phenotype triggered by plastid-localized crtB	147
5.1.2. The crtB-mediated phytoene boost makes the chloroplasts competent to become chromoplasts.....	148
5.1.3. Chloroplast stress is signalled to the nucleus to support chromoplast differentiation	149
5.2. New ways to improve isoprenoid content in leaves.	150
5.2.1. Artificial chromoplasts develop structures that produce and store healthy isoprenoids ...	150
5.2.2. The crtB protein is localized in PG, the main storage structure for the newly formed plastidial isoprenoids.....	151

5.2.3. Artificial chromoplastogenesis can be combined with extraplastidial carotenoid biosynthesis to boost the production of healthy carotenoids.....	153
<i>Conclusions</i>	157
<i>References</i>	161
<i>Appendices</i>	182
<i>Appendix I</i>	184
<i>Appendix II</i>	185
<i>Annex I</i>	i
<i>Annex II</i>	ii
<i>Annex III</i>	iii
<i>Annex IV</i>	iv

List of figures

General introduction

Figure 0.1. Schematic representation of the main pathways that lead to the synthesis of isoprenoid precursors and their localization in the plant cell.....	5
Figure 0.2. Schematic representation of carotenoid biosynthetic pathway.....	6
Figure 0.3. Schematic representation of prenylquinones biosynthetic pathway.....	8
Figure 0.4. Schematic representation of the main typologies of plant plastids.....	9
Figure 0.5. Schematic representation of the main structural changes happening during chromoplast development (Adapted from (Egea et al., 2010)).....	10

Chapter 1

Figure 1.1. Overexpression of <i>crtB</i> in <i>N. benthamiana</i> leaves results in a yellow phenotype.....	25
Figure 1.2. Plastid-localized <i>crtB</i> triggers the loss of photosynthetic activity.....	26
Figure 1.3. The transformation of chloroplasts into chromoplasts is characterized by deep changes in photosynthetic apparatus connected to carotenoid accumulation in a time-dependent manner.	28
Figure 1.4. Lack of OR protein or carotenoid cleavage enzymes does not stop <i>crtB</i> protein to trigger chromoplastogenesis but <i>sal1</i> mutant plants show an accelerated phenotype.....	30-31
Figure 1.5. Exogenous application of hormones can impact chromoplast establishment by influencing phytoene content and <i>crtB</i> expression.....	34
Figure 1.6. Phytoene accumulation is a necessary step to impair plastid photosynthesis and allow chromoplastogenesis.....	36
Figure 1.7. Pharmacological inhibition of photosynthetic processes allows to recover <i>crtB</i> -like phenotype.....	37
Figure 1.8. Model of the chloroplast-to-chromoplast differentiation process.....	38

Chapter 2

Figure 2.1. Schematic representation of the various shade conditions to which a plant can be subjected.....	54
Figure 2.2. . Schematic representation of the main molecular factors controlling the response to low R:FR.....	55
Figure 2.3. <i>Nicotiana benthamiana</i> reacts to shade signal lowering its pigment content and photosynthetic competence.....	58
Figure 2.4. <i>Arabidopsis thaliana</i> and <i>Cardamine hirsuta</i> show antagonistic photoacclimation responses to high and low PAR.....	60
Figure 2.5. Brassicaceae plants can be grouped with either <i>Arabidopsis thaliana</i> or <i>Cardamine hirsuta</i> based on their photoacclimation responses.....	62
Figure 2.6. Mutations that alter sensitivity to low R:FR do not impact photoacclimation responses.....	63
Figure 2.7. Activation of low R:FR signaling reduces photosynthetic activity.....	65
Figure 2.8. Exposure to low R:FR triggers changes in photosynthetic gene expression that are attenuated in the hyposensitive <i>At-pifq</i> mutant.	66
Figure 2.9. Low R:FR triggers ultrastructural changes in <i>Arabidopsis</i> chloroplasts.....	67
Figure 2.10. Pre-exposure to low R:FR improves the photoacclimation to low PAR in shade-avoider plants.....	69-70
Figure 2.11. Exposure to low R:FR impacts crtB-induced chromoplast formation.....	72
Figure 2.12. Shade effect can make chloroplasts competent for conversion into chromoplasts.....	73
Figure 2.13. Shade affects the rate of conversion of phytoene into downstream carotenoids impacting chromoplast development.....	74
Figure 2.14. Acclimation to different light intensities impact carotenoids accumulation.....	76

Chapter 3

Figure 3.1. Plastids obtained through crtB overexpression have different structures compared to leaf chloroplasts.....	91
Figure 3.2. crtB-induced chromoplast development is associated with the loss of photosynthetic membranes.....	93
Figure 3.3. crtB-induced chromoplast development generates proliferation of electrodense globular structures.....	95-96
Figure 3.4. crtB chromoplasts induce only minor changes in most envelope proteins.....	100-101
Figure 3.5. crtB chromoplasts accumulate isoprenoids other than carotenoids.....	100
Figure 3.6. crtB-induced chloroplast to chromoplast transition is associated with changes in internal structures of the plastid.....	101-102
Figure 3.7. Isoprenoids are distributed differently in plastidial compartments, but PG are the only structure able to store all the isoprenoids in detectable amounts.....	103
Figure 3.8. High-PAR pre-acclimation can impact the accumulation of plastidial isoprenoids.....	105
Figure 3.9. Senescence can drastically increase the level of some plastidial isoprenoid.....	106
Figure 3.10. Levels of isoprenoid in crtB-chromoplasts can be improved by overexpressing genes involved in tocopherol biosynthesis.....	108-109
Figure 3.11. High-PAR acclimation provides additional improvement to metabolite content.....	110
Figure 3.12. Senescence provides additional improvement to metabolite content.....	111
Figure 3.13. crtB can improve isoprenoid content of green leafy vegetables.....	113
Figure 3.14. Exposure to high-PAR can improve metabolite content in lettuce.....	114

Chapter 4

Figure 4.1. Schematic representation of the two strategies (cytosolic and plastidic) used in this chapter for carotenoid biofortification.....	130
---	-----

Figure 4.2. Accumulation of extraplastidial phytoene and lycopene indirectly impacts photosynthesis 133

Figure 4.3. β -carotene can be produced in cytosol by adding the crtY gene to the combination 134

Figure 4.4. Extraplastidial synthesis of β -carotene can be combined with chromoplast generation for additional improvement 136

Figure 4.5 An increased amount of plastidial precursors does not improve the carotenoid content of the combined pathway 137

General discussion

Figure 5.1. Schematic model that defines the progression of chromoplast development in leaves..... 150

List of abbreviations

ACAT	Acetyl-CoA C-acetyltransferase
ATP	Adenosine triphosphate
CDP-ME	4-Diphosphocytidyl-2-C-methyl-D-erythritol
CDP-MEP	4-Diphosphocytidyl-2-C-methyl-D-erythritol 2-phosphate
CFP	Cyan fluorescent protein
CMK	4-Diphosphocytidyl-2-C-methyl-D-erythritol kinase
CMS	4-Diphosphocytidyl-2-C-methyl-D-erythritol synthase
CRTISO	Prolycopene isomerase
CS	Chorismate synthase
DAHHP	3-Deoxy-D-arabinoheptulosonate 7-phosphate
DAHPS	3-Deoxy-D-arabinoheptulosonate 7-phosphate synthase
DCMU	3-(3,4-dichlorophenyl)-1,1-dimethylurea
DES	De-epoxidation state
DGDG	Digalactosyldiacylglycerol
DHNA	1,4-dihydroxy-2-naphthoate
DHQ	3-Dehydroquininate
DHQ-D	3-Dehydroquininate dehydrogenase
DHQS	3-Dehydroquininate synthase
DHS	3-Dehydroshikimic acid
DMAPP	Dimethylallyl diphosphate
dMPBQ	2,3-dimethyl-6-phytyl-1,4-benzoquinone
<i>dpi</i>	<i>Days post inoculation</i>
DXP	Deoxyxylulose 5-phosphate
DXR	DXP reductoisomerase
DXS	DXP synthase
<i>e.g.</i>	<i>Exempli gratia</i> (“for example”)
E4P	D-erythrose 4-phosphate
EPSP	5-enolpyruvylshikimate-3-phosphate

EPSPS	5-enolpyruvylshikimate-3-phosphate synthase
ETR	Electron transport rate
FBN	Fibrillin
FPP	Farnesyl diphosphate
FR	Far-Red
G₃P	Glyceraldehyde-3-phosphate
GFP	Green fluorescent protein
GGPP	Geranylgeranyl diphosphate
GGPPS	GGPP synthases
GLI	Grana lateral irregularity
GPP	Geranyl diphosphate
HDR	(E)-4-hydroxy-3-methylbut-2-enyl diphosphate reductase
HDS	4-hydroxy-3-methylbut-2-enyl diphosphate synthase
HGA	Homogentisic acid
HMB-PP	(E)-4-Hydroxy-3-methylbut-2-enyl diphosphate
HMG-CoA	hydroxy-3-methyl glutaryl-CoA
HMGR	HMG-CoA reductase
HMGS	HMG-CoA synthase
<i>hpi</i>	Hours post-infiltration
HPLC	High Performance Liquid Chromatography
HPT	Homogentisate phytyltransferase
HST	Homogentisate solanesyltransferase
<i>i.e.</i>	Id est ('that is')
IDI	IPP/DMAPP isomerase
IPP	Isopentenyl diphosphate
kDa	Kilodalton
LB	Luria-Bertani
LC	Light curve
LCYB	Lycopene beta cyclase
LCYE	Lycopene epsilon cyclase
LD	Long day

LHC	Ligh harvesting complex
LMV	Lettuce mosaic virus
LUT₁	Carotene epsilon-monooxygenase
LUT₅	Carotene beta-monooxygenase
MCS	2-C-Methyl-D-erythritol synthase
MDD	Mevalonate diphosphate decarboxylase
MEcPP	2-C-Methyl-D-erythritol-2,4-cyclopyrophosphate
MEP	Methylerythritol 4-phosphate
MGDG	Monogalactosyldiacylglycerol
MPBQ	2-methyl-6-phytyl-1,4-benzoquinol
MSBQ	2-methyl-6-prenyl-1,4-benzoquinol
MVA	Mevalonic acid
MVA₅P	Mevalonate 5-phosphate
MVA-PP	Mevalonate diphosphate
MVK	Mevalonate kinase
NF	Norflurazon
NPQ	Non-photochemical quenching
NSY	Neoxanthin synthase
OD	Optical density
PAM	Pulse Amplitude Modulation
PAR	Photosynthetically active radiation
PC	Plastochromanol
PC-8	Platochromanol-8
PCR	Polymerase chain reaction
PDS	Phytoene desaturase
PEP	Phosphoenolpyruvate
PG	Plastoglobules
PIF	Phytochrome interacting factor
PMK	Phosphomevalonate kinase
PQ	Plastoquinone
PQ-9	Plastoquinone-9

PSI / PSII	Photosystem I / photosystem II
PSY	Phytoene synthase
QTOF	Quadrupole time-of-flight
RFP	Red fluorescent protein
ROS	Reactive oxygen species
rpm	Revolutions per minute
S₃P	Shikimate-3-phosphate
SD	Short day
SHK	Shikimic acid
SHK-D	Shikimic acid dehydrogenase
TC	Tocopherol cyclase
TEM	Transmission electron microscopy
TQ	Tocoquinone
TuMV	Turnip mosaic virus
tyrA	Prephenate dehydrogenase
UPLC-MS	Ultra Performance Liquid Chromatography mass spectrometry
UQ	Ubiquinone
VDE	Violaxanthin de-epoxidase
VTE₅	Phytol kinase
VTE₆	Phytyl-P kinase
WT	Wild type
ZIS	ζ-carotene isomerase
ZDS	ζ-carotene desaturase
ZEP	Zeaxanthin epoxidase
α-TC	α-tocopherol
α-TQ	α-tocoquinone
γ-TC	γ-tocopherol
γ-TMT	γ-tocopherol methyltransferase

General introduction

General introduction

Plants contain sophisticated biochemical machineries intended to produce a wide array of compounds that perform vital cellular functions. Being sessile organisms unable to flee from the threats of the environment, plants evolved over time to build their defence weapons through a wide secondary metabolism. Some of these compounds are so effective that have become important to human agriculture, industry, medicine, and nutrition.

o.1. Isoprenoids in nature

Isoprenoids (also known as terpenoids) are one of the largest families of plant metabolites, showing a wide variety of chemical structures (Vickers et al., 2014) Some plant isoprenoids are considered “primary” metabolites and are present in almost all plant species because they have an irreplaceable function in many vital metabolic processes. Among such essential isoprenoids, many are involved in plastid functions (including photosynthesis and photoprotection) or depend on the plastid for their synthesis (Rodríguez-Concepción and Boronat, 2015) In this category are included: chlorophylls (the main pigments involved in light harvesting and energy transfer), phylloquinones and plastoquinones (prenylquinones that are part of the electron transport chain system, especially associated with photosystem I, PSI), carotenoids (accessory pigments to harvest light for photosynthesis and photoprotectants against excessive light energy) and tocopherols (tocochromanols with an important role in the protection of membranes from oxidation). Other essential isoprenoids are ubiquinone (a prenylquinone that is fundamental in the respiratory electron transport chain in mitochondria), phytosterols (compounds involved in the maintenance of membrane fluidity and stability), and several groups of plant hormones (including brassinosteroids, cytokinins, gibberellins, and carotenoid-derived strigolactones and abscisic acid). Most plant isoprenoids, however, are considered “secondary” metabolites and participate in very specialized processes mostly related with plant-environment interaction. Usually, these specialized isoprenoids are confined to specific plant species or/and tissues and they are often produced in response to environmental challenges. In some cases, compounds with a “primary” role in some tissues play “secondary” roles in others. For example, carotenoids and derived cleavage products have a vital ecological role in non-photosynthetic tissues, contributing to the colours and aromas of many fruits and flowers to attract animals for pollination and seed dispersal. Isoprenoids with roles as pigments, volatiles and defence

molecules are also of use for human needs as colourants, flavours, chemicals, and drugs (Rodríguez-Concepción and Boronat, 2015; Vickers et al., 2014).

Among essential isoprenoids involved in photosynthesis and photoprotection, carotenoids, tocopherols and phyloquinones are particularly interesting because they have strong implication for human and animal health as vitamins (Tetali, 2019). In the case of carotenoids, animals take them through the diet and use them as pigments and as a source of retinoids, including vitamin A. Only a few animals have evolved to overcome this rule. The pea aphid *Acyrtosiphon pisum*, for example, produces its own carotenoids using biosynthetic genes of fungal origin that were integrated in its genome (Moran and Jarvik, 2010). Also, photosynthetic sea slugs like *Elysia timida* were reported to integrate plastids from their algal food and to maintain their full functionality. This process, called kleptoplasty, grants the animal the possibility to use the metabolic machinery of the chloroplasts to actively synthesize carotenoids and take advantage of their photoprotective functions (Cartaxana et al., 2019). Tocopherols (vitamin E) and phyloquinones (vitamin K₁) are only synthesized by photosynthetic organisms but most of our understanding of their chemical properties and functions come from studies in artificial membranes and animal systems.

o.2. Isoprenoids as health promoting compounds.

Isoprenoids show biological activities which have been exploited in prevention and treatment of human diseases (Britton, 1995). Hundreds of isoprenoid compounds and their derivatives have been tested for their pharmacological activities. The demonstrated biological effect of various classes of terpenoids from *in vitro* and *in vivo* studies include anti-inflammatory, anti-oxidative, anti-aggregatory, anti-coagulative, anti-tumour, sedative, and analgesic activities (Zhao et al., 2016). These compounds bring health benefits by interacting with key molecular players in animal and human physiology (Nuutinen, 2018). The main biological function of carotenoids in mammals is their role as precursors of retinoids (including vitamin A) that play fundamental roles for vision, growth, cell differentiation, and other physiological processes (Rodríguez-Concepción et al., 2018). Only carotenoids with at least one β -ring without any oxygen and with a polyenic chain with at least 11 carbon atoms can be converted into vitamin A. Thus, the most relevant provitamin A carotenoid is β -carotene (two β -rings), but other good sources are α -carotene (one β -ring) and some derived xanthophylls and apocarotenoids. Vitamin A is particularly important for the correct development of sight, but non-provitamin A carotenoids such as phytoene and lycopene are also important (Rodríguez-Concepción et al., 2018). The xanthophylls lutein and zeaxanthin are accumulated in the macula lutea within the eye (Ma and

Lin, 2010) where they act as a filter for blue light attenuating in about 40% the light that reaches photoreceptors reducing their damages and providing protection against photooxidation caused by the retina simultaneous exposition to light and oxygen (ROS).

Vitamin E is the general term for tocochromanols, of which α -tocopherol has the highest biological activity. Tocochromanols interact with polyunsaturated acyl groups and protect membrane lipids (especially polyunsaturated fatty acids) from oxidative damage by scavenging lipid peroxy radicals. Termination of polyunsaturated fatty acid free radical chain reactions by tocochromanols results in a "tocopherol radical." In mammals, the tocopherol radical is recycled back to the corresponding tocopherol allowing each tocopherol to participate in many lipid-peroxidation chain-breaking events before being degraded (DellaPenna and Pogson, 2006). Vitamin K occurs naturally in two forms. Phylloquinone (2-methyl-3-phytyl-1,4-naphthoquinone) or vitamin K₁ and menaquinones or vitamin K₂. The first one is present in high amounts in green leafy vegetables and is the form majoritarily uptaken in western diet. Physiologically, vitamin K is known for its role as a cofactor for a series of endoplasmic enzymes involved in blood coagulation and cell apoptosis. Some in vitro and animal studies point also to protective roles for vitamin K against oxidative stress and inflammatory processes, two phenomena associated with age-associated neurodegenerative diseases (DiNicolantonio et al., 2015).

A common valuable function of carotenoids together with tocochromanols and prenylquinones is related to their antioxidant properties. In biological systems, lipids constitute most of the cellular membranes and internal structures and lipid oxidation harms the functionality of the membranes and their integrity. Since carotenoids, tocochromanols and prenylquinones are stocked in these structures, they can delay the radical propagation generated by lipid oxidation and have a recognized role as membrane antioxidants. Epidemiological studies have shown that the consumption of carotenoid, tocopherol and phylloquinone-rich fruits and vegetables is associated with a lower risk of cardiovascular diseases. Carotenoids and tocopherols interact with polyunsaturated acyl groups and protect membrane lipids, especially polyunsaturated fatty acids, from oxidative damage by scavenging lipid peroxy radicals and chemically reacting with singlet oxygen and other ROS. Other studies suggested an inverse relationship between the high consumption of carotenoids, tocopherols and phylloquinones-enriched foods and a low incidence of cancer relating their protective role to the modulation of growth factor signalling, cell cycle progression, cell differentiation and apoptosis (Niranjana et al., 2015). It is widely acknowledged that the consumption of these isoprenoids within a vegetal matrix is more effective to cause health benefits than the intake of individual dietary supplements.

0.3. Isoprenoid biosynthetic pathways

Isoprenoids are built from the head-to-tail union of various units of the 5-carbon (C₅) compound isopentenyl diphosphate (IPP) and its allylic isomer dimethylallyl diphosphate (DMAPP). In plants, IPP and DMAPP can derive from two metabolic pathways acting in distinct cell compartments: the cytosolic mevalonic acid pathway (MVA) and the plastidial methylerythritol 4-phosphate (MEP) pathway (Rodríguez-Concepción and Boronat, 2002) (Figure 0.1). In the cytosolic pathway, IPP is formed from three molecules of acetyl-CoA. Two of them are combined to generate acetoacetyl-CoA and the third molecule is then incorporated through an aldolic addition that leads to the formation of hydroxy-3-methyl glutaryl-CoA (HMG-CoA). The reduction of the latter by HMG-CoA reductase (HMGR) leads to the formation of mevalonic acid (MVA) that is later transformed into compound IPP through two successive phosphorylations. MVA-derived IPP is then isomerized to DMAPP by the enzyme IPP/DMAPP isomerase (IDI). Two IPP molecules added to a DMAPP core form C₁₅ farnesyl diphosphate (FPP), the substrate for the formation of sesquiterpenes (C₁₅) and triterpenes (C₃₀) such as sterols (Hsieh and Goodman, 2005). Other prenyldiphosphate precursors formed using MVA-derived IPP and DMAPP include C₂₀ geranylgeranyl diphosphate (GGPP) to produce C₂₀ diterpenoids and prenylated proteins as well as polyterpenes.

The MEP pathway starts with the production of deoxyxylulose 5-phosphate (DXP) from glyceraldehyde-3-phosphate and pyruvate by DXP synthase (DXS). DXP is then rearranged and reduced by the enzyme DXP reductoisomerase (DXR) to MEP. The latter is then converted into a mixture of IPP and DMAPP in five enzymatic steps (Rodríguez-Concepción, 2010). Even if this pathway can produce both isoprenoid substrates at once, an isomerization activity interconverting IPP and DMAPP is still necessary to balance the relative ratios of these two compounds (Figure 0.1). IPP and DMAPP are then condensed to form the C₁₀ compound geranyl pyrophosphate (GPP), the precursor of monoterpenes (C₁₀). However, most plastidial isoprenoids derive from GGPP produced by plastidial GGPP synthases (GGPPS). MEP-derived GGPP is the common precursor of carotenoids and the prenyl moiety of chlorophylls, tocochromanols (including tocopherols and plastochromanol-8) and prenylquinones (such as phyloquinones, tocoquinones, and plastoquinone-9) in the plastid.

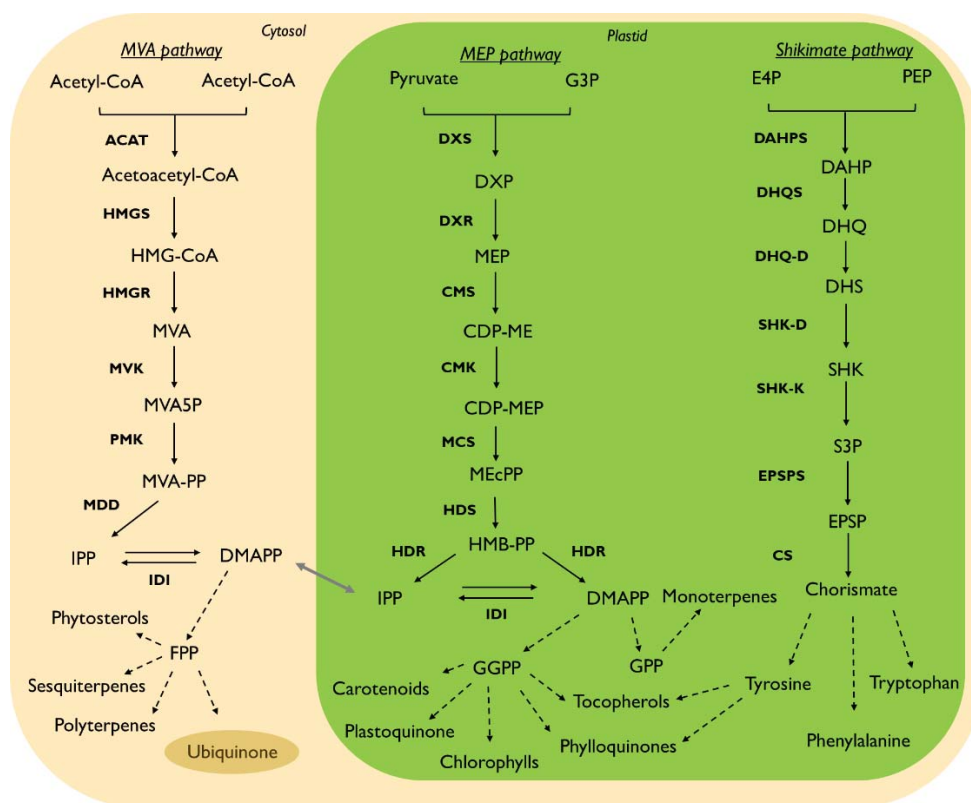


Figure 0.1. Schematic representation of the main pathways that lead to the synthesis of isoprenoid precursors and their localization in the plant cell. IPP and DMAPP, the universal C₅ isoprenoid units, are produced by the MVA pathway in the cytosol and the MEP pathway in plastids and can be transported between the two cellular compartments. The shikimate pathway provides moieties for the formation of tocopherols and prenylquinones in plastids. See List of abbreviations for acronyms.

0.3.1. Carotenoid pathway

GGPP can be channelled into the carotenoid biosynthetic pathway through the action of the enzyme phytoene synthase (PSY). This enzyme catalyses the tail-to-tail condensation of two molecules of GGPP into 15-*cis*-phytoene (Rodriguez-Concepcion et al., 2018). PSY is the main rate-limiting enzyme in the carotenoid biosynthetic flux (Fraser et al., 2002) and, for this reason, it has been repeatedly used as a preferential target for genetic manipulation. The core carotenoid pathway is conserved but some species can synthesize specific carotenoids via unique biosynthetic branches generating a huge diversity of carotenoid molecules (Maresca et al., 2008). In plants and cyanobacteria, phytoene undergoes dehydrogenation and isomerization in four enzymatic steps to produce all-*trans*-lycopene (Rodriguez-Concepcion et al., 2018). The desaturation reactions transform the colourless phytoene into the red-coloured lycopene because they introduce a series of carbon-carbon double bonds that form the chromophore in the carotenoid molecule. In higher plants, cyclization of the lycopene molecule ends produces two types of rings: β or ϵ . Introduction of β -rings transforms lycopene into γ -carotene (one β -ring)

and, subsequently, β -carotene (two β -rings). A second branch starts by introducing one ϵ -ring to produce δ -carotene and then one β -ring in the other end to generate α -carotene. Introduction of two ϵ -rings is rare and it only occurs in a few plant species such as lettuce (Ruiz-Sola and Rodríguez-Concepción, 2012). After this branching step, β -carotene and α -carotene are converted into xanthophylls (i.e., oxygenated carotenoids produced thank to ring-specific hydroxylation reactions). Hydroxylation of β -carotene first produces β -cryptoxanthin and then zeaxanthin while hydroxylation of α -carotene eventually leads to lutein. Other β , β -xanthophylls derived from β -carotene include violaxanthin (originated by the epoxidation of zeaxanthin) and neoxanthin. Both violaxanthin and neoxanthin can be used for the formation of the carotenoid-derived hormone ABA, while β -carotene is the precursor of strigolactones (Rodríguez-Concepción et al., 2018) (Figure 0.2).

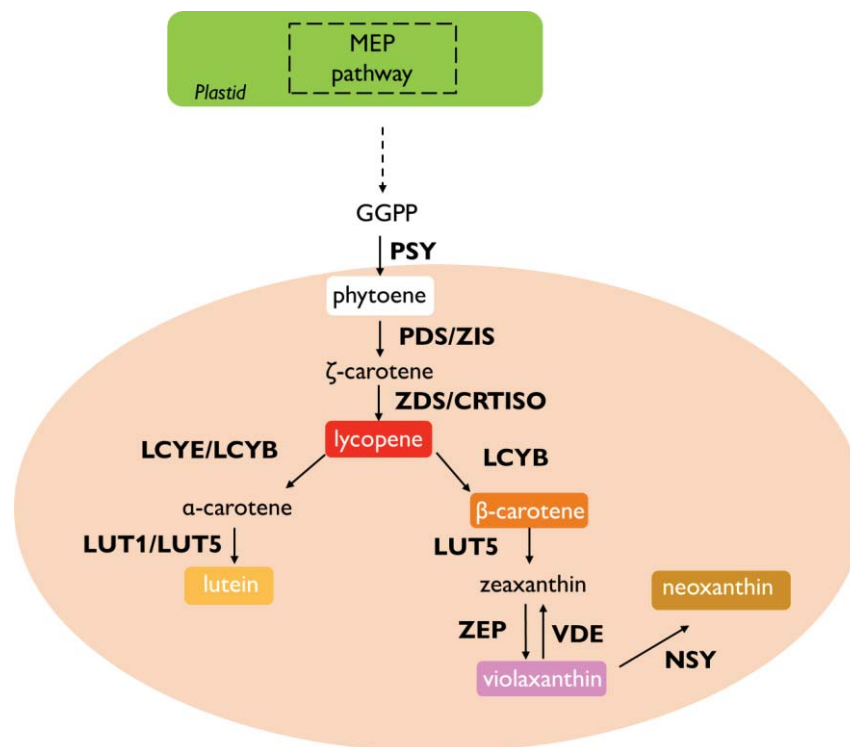


Figure 0.2. Schematic representation of carotenoid biosynthetic pathway. See List of abbreviations for acronyms.

0.3.2. Tocochromanol and prenylquinone pathways

Tocochromanols and prenylquinones have moieties derived from the MEP pathway and the shikimate pathway (Figure 0.3). The combination of the GGPP-derived prenyl moieties phytyl diphosphate (PPP) or solanesyl diphosphate (SPP) with chorismate-derived aromatic head groups homogentisic acid (HGA) or 1,4-dihydroxy-2-naphthoate (DHNA) eventually forms

tocopherols and tocoquinones (PPP and HGA), plastoquinone-9 and plastochromanol-8 (SPP and HGA) or phylloquinones (PPP and DHNA). The precursor of HGA is p-hydroxyphenyl pyruvate formed from chorismate via prephenate, arogenate and Tyr. However, arogenate can be also the precursor of Phe that is the base for a multitude of secondary metabolites such as lignin and flavonoids and, for this reason, only a small amount of photosynthetically obtained carbon is incorporated into Tyr. The saturated tail from tocopherols is derived from PPP that is either produced *de novo* from GGPP by GGPP reductase (GGR) or formed by recycling of the phytol released from chlorophyll degradation (Figure 0.3). The enzymes phytol kinase and phytyl-P kinase encoded by the genes *VTE5* and *VTE6*, respectively, convert phytol to PPP (DellaPenna and Pogson, 2006; Fritsche et al., 2017; Ischebeck et al., 2006). In the first committed step of tocopherol biosynthesis, PPP and HGA are fused by a membrane-bound homogentisate phytyltransferase encoded by the *HPT/VTE2* gene to form MPBQ (2-methyl-6-phytyl-1,4-benzoquinol). This metabolite can be converted into dMPBQ (2,3-dimethyl-6-phytyl-1,4-benzoquinone) by a methyltransferase encoded by *VTE3* or into δ -tocopherol by a tocopherol cyclase encoded by *VTE1*. The latter also synthesizes γ -tocopherol from dMPBQ (Collakova and DellaPenna, 2003; Lushchak and Semchuk, 2012). Finally, a tocopherol methyltransferase encoded by *VTE4* converts δ - and γ -tocopherol into β - and α -tocopherol, respectively. The antioxidant activity of α -tocopherol results in its conversion to α -tocoquinone.

The same benzene quinone ring precursor HGA can be used to synthesize plastoquinone-9 or plastochromanol-8. MEP-derived SPP is condensed with HGA by the plastidial enzyme homogentisate solanesyltransferase (HST) to produce 2-methyl-6-prenyl-1,4-benzoquinol (MSBQ). Steps catalyzed by enzymes that also participate in tocopherol biosynthesis transform MSBQ into plastoquinol 9 (*VTE3*), which is then cyclized into plastochromanol-8 (*VTE1*) or oxidized to form plastoquinone-9 (Liu and Lu, 2016; Szymańska and Kruk, 2010). Lastly, phylloquinone (vitamin K₁) is structurally like menaquinone (Vitamin K₂), a compound that can be synthesized by red algae, diatoms, and prokaryotes (Hu et al., 2012). In photosynthetic organisms like plants, phylloquinone is synthesized in nine consecutive reactions from the chorismate-derived DHNA produced by the shikimate pathway. The first four enzymes of phylloquinone biosynthesis, which convert chorismate to o-succinylbenzoate, are nuclear-encoded and localized in chloroplasts. The next three biosynthetic steps occur in the peroxisome and lead to the formation of DHNA that is then transported into plastids. There, DHNA phytyltransferase (MenA/ABC₄) attaches the PPP chain to the naphthoate ring of DHNA and then it is converted to phylloquinone after a methylation step catalysed by MenG (Shimada et al., 2005).

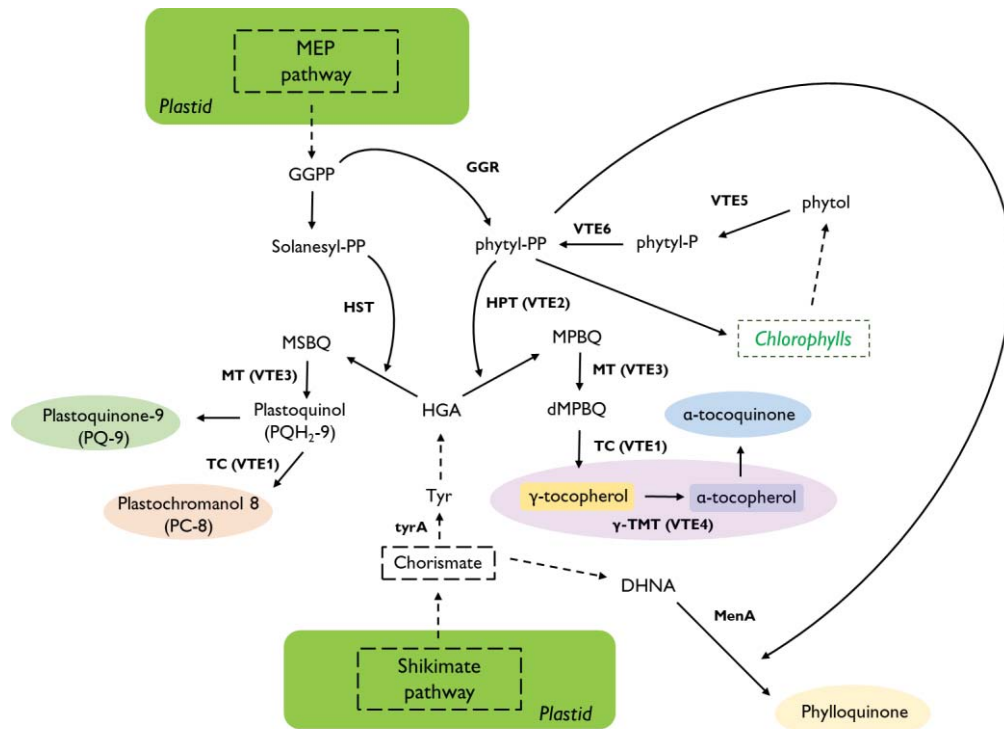


Figure 0.3. Schematic representation of prenylquinones biosynthetic pathway. See List of abbreviations for acronyms.

0.4. Isoprenoid storage in plastids

Plastids are essential and ubiquitously found in higher plants. They vary greatly in their morphology and function according to the ecophysiological state of the plant or its development. Based on their morphology and functions plastids are classified in distinct subtypes. 1) Proplastids are small, colourless, and undifferentiated that are usually present in meristematic tissues. 2) Etioplasts occur during the growth of plants in darkness and are characterized by the absence of chlorophylls and the presence of an internal membrane network called prolamellar body that constitutes the precursor of the thylakoids. 3) Chloroplasts are the photosynthetic plastids characteristic of light-grown plants; they contain the green pigment chlorophyll and an internal system of thylakoid discs where the light reactions of photosynthesis happen. 4) Leucoplasts are colourless plastids that can be differentiated in various subtypes depending on the compound stored: amyloplasts if they accumulate starch, elaioplasts if they accumulate lipids and proteoplasts if they store proteins. 5) Chromoplasts are pigmented plastids due to the accumulation of carotenoids and the absence of chlorophylls; they are typical of ripe fruits, flowers and some plant roots but only occasionally develop in leaves. 6) Gerontoplasts arise from the degeneration of chloroplasts during plant senescence and show disorganized thylakoidal

membranes and a proliferation of large plastoglobules (PG) that typically store tocopherols and other products of the degradation of chlorophylls (Jarvis and López-Juez, 2013; Sadali et al., 2019) (Figure 0.4).

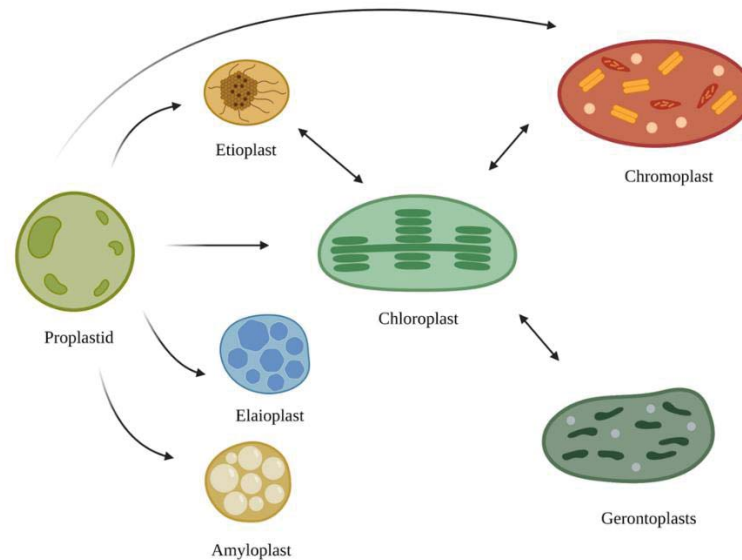


Figure 0.4. Schematic representation of the main typologies of plant plastids. Proplastid are the common ancestor for all the plastids except gerontoplasts and plastidial identity changes depending on the compound accumulated (elaioplasts accumulate proteins, amyloplast accumulate starch). Etioplasts are typically present in young non-photosynthetic tissues and differentiate in chloroplasts upon light exposition. Chloroplasts differentiate in chromoplasts in fruits and flowers. In old leaves chloroplasts degenerate into senescent gerontoplasts.

Plastids, particularly chloroplasts, chromoplasts and gerontoplasts, are a major site for isoprenoids biosynthesis and storage. Etioplasts synthesize a set of carotenoids like lutein and violaxanthin that are critical for optimizing the transition to photosynthetic development and, together with tocopherols, are fundamental to protect seedlings emerging from a dark environment (i.e., underground) from photodamage by avoiding the oxidation of chlorophyll precursors and the derived ROS production (Rodríguez-Villalón et al., 2009, Park et al., 2002). Violaxanthin and lutein in etioplasts are also essential for the correct assembly of prolamellar bodies. In chloroplasts, most carotenoids are often associated with proteins in different complexes of the photosynthetic apparatus localized in the thylakoidal membranes: light-harvesting complexes (LHCs) mostly contain xanthophylls, whereas β -carotene is usually located in both photosystems (PSI and PSII) and the cytochrome b6f complex. Lower carotenoid levels can also be found in the envelope (Lichtenthaler, 2007). The carotenoid composition in chloroplasts of most plant species is rather standard, and the most abundant carotenoids are

lutein (45% of the total), β -carotene (25-30%), violaxanthin (10-15%) and neoxanthin (10-15%) (Britton, 1995; Phillip and Young, 1995). In chloroplasts, tocopherols are stored mainly in the envelope and in thylakoid-derived vesicles named PG, where the enzymes necessary for their synthesis are located. Most of the α -tocopherol synthesized is partitioned between the chloroplast envelope and thylakoid membranes and it is stored in PG only in some cases. The proportion with other forms of tocopherols depends on the plant species. For example, α -, β -, and γ -forms of tocopherol occur in the thylakoids of spinach at molar ratios of 1:0.06:0.02, respectively (DellaPenna and Pogson, 2006). Plastoquinones are also present in thylakoids (where they are part of the photosynthetic electron transport chain) and in PG (where they are stored in their non-photoactive form) (Pralon et al., 2020). Pheophytinones, on the other hand are present mostly in PG (Van Wijk and Kessler, 2017).

Chloroplasts transform into chromoplasts by losing their chlorophyll and accumulating carotenoid pigments during the development of many flowers and the ripening of many fruits in a process, named chromoplastogenesis (Egea et al., 2010). Chromoplasts develop internal structures that can sequester and store carotenoids while the photosynthetic membranes are degraded (Figure 0.5).

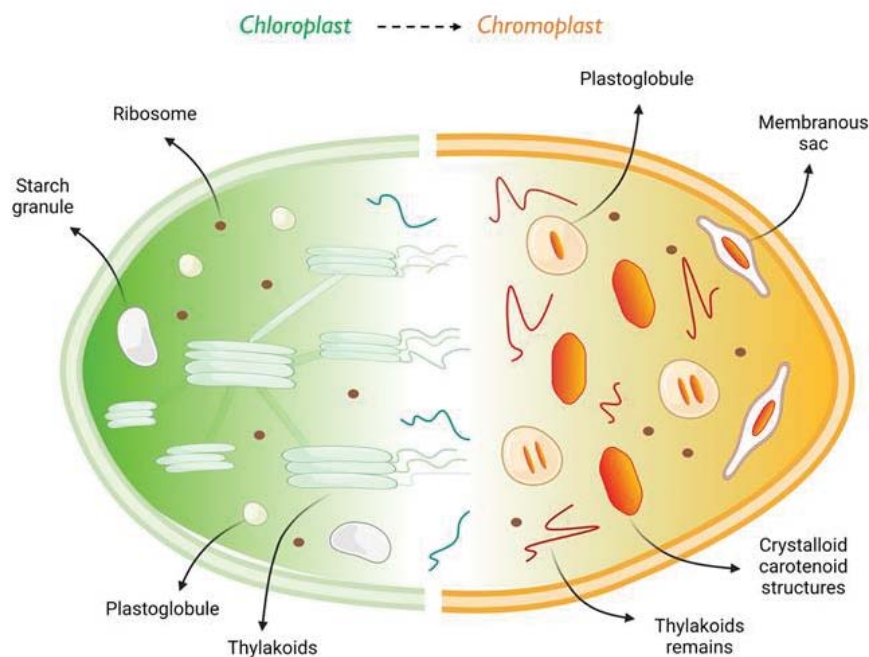


Figure 0.5. Schematic representation of the main structural changes happening during chloroplast to chromoplast transition (Adapted from (Egea et al., 2010)). During chromoplast development, starch grains are broken down together with thylakoid membranes. Plastoglobules increase in size and number and carotenoids are stored in membranous structures or in crystalloid formations.

The main examples of chromoplast structures are crystalline bodies observed in tomato and carrot chromoplasts, tubular structures present in some flower petals or abundant PG in chromoplasts of some fleshy fruit such as mango (Grilli Caiola and Canini, 2004). Some of these structures are permanent while others are transient and disappear in senescent chromoplasts. The most common carotenoid-containing structures present in chromoplasts are PG, usually distributed singly or in group in the chromoplast stroma. PG are plastid lipoprotein particles surrounded by a membrane lipid monolayer and contain small, specialized proteomes and metabolomes depending on the plastid type where they develop. While PG in chloroplasts are associated with thylakoids and have a role in multiple developmental processes (metabolism of prenyl lipids, redox and photosynthetic regulation; plastid biogenesis; and senescence), PG in chromoplasts are highly enriched in carotenoid esters and enzymes involved in carotenoid metabolism (Van Wijk and Kessler, 2017). During chromoplast maturation their number and size increase and accumulate carotenoids partially derived from the degradation of thylakoid membranes or synthesized anew through an internal biosynthetic machinery. Nonetheless, PG do not necessarily contain. In the late stage of chromoplast development carotenes can accumulate either as crystals or as long tubules because of the concentration increase (i.e., crystals of β -carotene in carrot roots or lycopene in tomato fruits). Tubules are thin undulated structures with an irregular shape in the cross section. They are usually in contact with PG and sometimes they pierce them establishing a connection between several globules. Many chromoplasts also develop special membranes called *chromoplast internal membranes (CIMs)* from invagination of plastidial envelope and from degradation of thylakoidal membranes. These formations contain carotenoids but never contain chlorophylls. The dependence of chromoplast structures upon the type of pigments was characterized by treating plants with bleaching herbicides: tulip tree flowers treated with SAN 9789 (a chemical that blocks β -carotene synthesis), for example, developed long thin tubules growing out of PG instead of β -carotene crystals (Ljubecic et al., 1991)

The membrane structures that form in chromoplasts also contribute to carotenoid biosynthesis through providing a proper environment to carotenoid biosynthetic enzymes, many of which are membrane-associated (Ruiz-Sola and Rodríguez-Concepción, 2012). Therefore, the development of chromoplasts results in enhanced carotenoid accumulation by combining a “pull” effect (by providing a suitable environment for the storage of carotenoids) with a “push” effect (by improving the activity of biosynthetic enzymes and hence the production of these compounds) (Ruiz-Sola and Rodríguez-Concepción, 2012). While carotenoid distribution inside chromoplasts greatly varies and impacts plastid morphology, tocochomanols and prenylquinones are mainly stored in PG where part of their biosynthetic machinery is also located. Depending on the degree

of thylakoid degradation part of tocopherols (mainly α -tocopherol) can also be found associated with the residues of the membranes. (Van Wijk and Kessler, 2017; Bréhélin et al., 2007).

During leaf senescence chloroplasts degenerate into gerontoplasts. During this conversion, chloroplasts lose progressively their internal organization and their photosynthetic competence. All photosynthetic pigments (chlorophylls and carotenoids) decline during senescence but chlorophylls are degraded at a faster rate compared to carotenoids causing the typical yellow, orange, and brown colour of autumn leaves. In many gerontoplasts the retained carotenoids are esterified. The formation of xanthophyll acyl esters results in more stable pigments. Leaf senescence is also associated with the formation of oxidation products of β -carotene. During the transition from chloroplasts to gerontoplasts the breakdown of the thylakoidal membranes provides material for the formation of a high number of small PG that, at the late stage of the process merge to generate a low number of large osmophilic PG that are the distinctive feature of the gerontoplasts. Tocopherols mainly formed using phytol recycled from chlorophyll degradation represent the main content of gerontoplast large PG but in some cases also traces of carotenoids are present (Lichtenthaler, 2007).

0.5. Role of isoprenoids in photosynthesis and photoprotection

Many secondary isoprenoids functions are linked to light and photosynthesis. Chlorophylls cannot absorb much light in the 450-550nm region, where carotenoids act as light-harvesting pigments. In oxygenic photosynthetic organisms, the reaction centres and the core complexes of the photosystems mainly contain β -carotene while the composition of the peripheral LHCs contains a mixture of lutein, neoxanthin, zeaxanthin and violaxanthin to efficiently transfer energy to chlorophylls (Liguori et al., 2017). The most important role of carotenoids, however, is their photoprotective action to prevent damages related to the formation of reactive oxygen species (ROS) by quenching excited chlorophyll triplets. When the excited state of carotenoids relaxes to the ground state, energy is harmlessly released as heat in a process known as non-photochemical quenching (NPQ) and based on xanthophyll cycles for optimal function (Nilkens et al., 2010; Murchie and Niyogi, 2011). Xanthophyll cycles consist in the transformation of epoxidized xanthophylls to de-epoxidized ones under excess light, which facilitates the dissipation of excitation energy through a conformational change able to rearrange LHC proteins (Latowski et al., 2011). Tocopherols, unlike carotenoids are not indispensable for photoprotection but they can contribute to provide general protection of thylakoidal membranes through their antioxidant action (Lichtenthaler, 2007). As for plastoquinones (PQ), they are involved in the

electron transport chain of oxygenic photosynthesis (Liu and Lu, 2016). In plastids PQ navigate quickly through the thylakoid lipid bilayer to shuttle electrons from PSII to PSI. The proportion of PQ that participates in electron transport in the thylakoid membrane is considered as the photoactive PQ pool; whereas the remaining proportion, which is approximately 60–70% of the total PQ, constitutes the non-photoactive pool (Pralon et al., 2020). Redox state of PQ also constitutes an important signal in the regulation of many physiological processes within the chloroplast such as gene expression, carotenoid biosynthesis, and antioxidant activity (Suzuki et al., 2012).

o.6. Isoprenoid biotechnology.

Currently, only a few commercially relevant carotenoids and tocopherols (including lycopene, β -carotene, lutein, capsanthin, astaxanthin, canthaxanthin and α -tocopherol) can be industrially produced. However, their increased importance for industry and human health led to explore multiple strategies to increase the amount of these components in plants. Different experimental strategies have been used to enhance isoprenoid content and composition in crops, including conventional breeding, or marker-assisted breeding, and genetic engineering. The first one allowed over time to select improved lines, but the process is slow and time-consuming. Vitamin A biofortification in maize, sweet potato, and cassava, however, are examples in which conventional breeding has been a success (Hotz et al., 2012; Ceballos et al., 2013). Genetic manipulation, on the other end, requires a short time and has been shown feasible and efficient in many plant species. Carotenoid and tocopherols engineering strategies involve direct intervention to boost the accumulation of target compounds by 1) increasing the metabolic flux through the pathway by overexpressing rate-limiting enzymes and eliminating metabolic bottlenecks ("push" strategy) 2) suppressing competing pathway downstream of branch points to avoid the diversion of intermediates to the synthesis of other compounds or the degradation of the compound of interest ("block" strategy) 3) creating sequestering structures to increase plastid sink capacity to store isoprenoid compounds ("pull" approach). The combination of more than one approach is also possible for refined control over the metabolic pathways (Botella-Pavía and Rodríguez-Concepción, 2006; DellaPenna and Pogson, 2006).

In the case of carotenoid content, there are several successful examples by using push strategies. The most famous one is maybe the "Golden Rice": a genetically engineered rice which has the genes necessary for β -carotene production introduced into its genome, as rice does not naturally express those genes in the endosperm. In the first version of Golden Rice a *PSY* gene from daffodil under an endosperm-specific glutelin promoter was introduced via *Agrobacterium*-

mediated transformation, as well as the *crtI* gene from *Pantoea ananatis* under the constitutive CaMV 35S promoter and a *LCYB* gene from daffodil under the glutelin promoter. This strategy produced at least one line with 1.6 µg/g of carotenoid content in the endosperm, most of that being β-carotene (Ye and Beyer, 2000). The second version of the product saw a major improvement in pro-vitamin A content after many plant *PSY* genes were tested and a maize *PSY* was used. This strategy was able to produce in one line 37 µg/g (Paine et al., 2005). In other studies, the constitutive overexpression of *A. thaliana* genes encoding for DXR and type I DXS in carrot plants (*Daucus carota*) allowed an increase in α-carotene and β-carotene (up to 3.6 and 2.7-fold, respectively) levels in roots (Simpson et al., 2016). The overexpression of *PSY*-encoding gene in carrot roots, also, led to an increase of total carotenoid content and the development of crystalloid structures in either carrot roots or *A. thaliana* seedlings (Maass et al., 2009). Then, in canola seeds (*Brassica napus*), the overexpression of the bacterial *crtB* (the bacterial phytoene synthase) using a seed-specific promoter increased resulted in a 50-fold increase of total carotenoid content (Shewmaker et al., 1999).

The best results for carotenoid biofortification, however, came from the combination of multiple bacterial genes (Majer et al., 2017; [Andersen et al., 2021](#)). For example, co-overexpression of *Chlamydomonas reinhardtii* β-carotene ketolase and *Hematococcus pluvialis* β-carotene hydroxylase in tomato succeeded into a massive accumulation of astaxanthin in leaves and esterified astaxanthin in fruits coupled with a 16-fold increase on total carotenoids levels (Huang et al., 2013). In potato, the co-expression of bacterial *crtB*, *crtI* and *crtY* (lycopene cyclase) resulted in a significant increase of carotenoid content (especially β-carotene) that maintained a relative stability during tubers propagation (Diretto et al., 2007). Other successful examples were the use of a combination of a “push” and a “block” strategy through the silencing of the endogenous *LCYE* gene expressing an antisense RNA construct that led to 14-fold more β-carotene avoiding the conversion of lycopene in α-carotene and the use of a block strategy to increase carotenoids amount by silencing potato β-carotene hydroxylase (*BCH*) gene. This resulted in the inhibition of the conversion of β-carotene in zeaxanthin forcing a 331-fold improvement of this carotenoid and a 2.5-fold improvement of lutein (Diretto et al., 2006). In another example, the silencing of the gene encoding *ZEP* led to tubers with a 133-fold increase in zeaxanthin content coupled with a 3.4-fold increase in β-carotene (Diretto et al., 2007; Römer and Fraser, 2005).

The pull strategies rely mainly on the formation of suitable structures for the storage of carotenoids (i.e., carotenoid sink) and on their stabilization to avoid their degradation. The most promising strategy is to trigger chromoplasts differentiation in the tissue of interest. The *Or* gene

encodes a protein containing DnaJ cysteine-rich zinc finger domain and was found to induce carotenoid accumulation by triggering the differentiation of non-coloured plastids into chromoplasts (Li et al., 2001). This discovery has made this approach feasible for some types of plants or specific tissues, the most relevant being callus, endosperm of cereals and tubers. *Or* effect seems to be context-specific, in some cases contributing to the increase of carotenoid content by stabilizing the PSY protein (Zhou et al., 2015) in some cases triggering the differentiation of chromoplasts. The overexpression of *A. thaliana Or* gene in the white endosperm of maize and in potato tubers generated an increased total carotenoid content likely by stabilizing the endogenous PSY protein and increasing its activity resulting in the formation of chromoplasts (Lopez et al., 2008). The fruit specific RNAi-mediated suppression of the morphogenesis regulatory gene *DET1* in tomato resulted also in an increased number of chloroplasts per area with a higher volume generating in this way an increase in the sink capacity of the organ (Enfissi et al., 2010).

Because of their central role in photosynthesis, the success with the carotenoid increase in green tissues, was limited. Nonetheless, recent reports have shown that *N. benthamiana* leaves overexpressing regulators of carotenoid gene expression and storage were able to double their carotenoid content in chloroplasts, and promising results were obtained by using transcription factors (TF) involved in plastid development and belonging to the MYB and bHLH families. For example, the overexpression of the TF *MYB7* from kiwifruit (*Actinidia deliciosa*) in *N. benthamiana* leaves resulted in an increase between 2 and 2.5-fold times in carotenoid content, likely because of an interaction of this factor with the promoter of the *LCY-B* gene. (Ampomah-Dwamena et al., 2019; D'Amelia et al., 2019; Llorente et al., 2020; Wang et al., 2018).

Green leafy vegetables have been tested mostly for the enrichment of vitamin E and folate (Dellapenna, 2007). There are two basic goals of vitamin E metabolic engineering in plants: 1) increasing the flux through the vitamin E biosynthetic pathway to enhance the levels of total tocochromanols and 2) altering the tocochromanols composition towards the α -tocopherol for its higher antioxidant potential (Chen et al., 2006). The overexpression in tobacco leaves of *Saccaromyces cerevisiae* prephenate dehydratase (*PDH* or *tyrA*) for the direct synthesis of HPP from prephenate together with the overexpression of *Arabidopsis HPPD* gene resulted in an 8-fold increase of tocochromanols in leaves with a massive accumulation of tocotrienols (Rippert et al., 2004). On the other hand, the combined overexpression of *VTE2* gene from *Arabidopsis* together with the gene encoding the γ -tocopherol methyltransferase enzyme (*VTE4*) resulted then in a 12-fold increase in vitamin E converting the whole pool of γ - and δ - tocopherol to α - and β -tocopherols. Then overexpression of *VTE1* gene in *Arabidopsis* leaves resulted in up to a 7-

fold increase in tocopherols and a dramatic shift of tocopherols composition from α -tocopherol to γ -tocopherol. Playing with the genes encoding the different steps of tocopherol biosynthetic pathway is also the way to impact tocopherol composition in plants favouring the accumulation of α -tocopherols. The co-expression of *Arabidopsis VTE₃* and *VTE₄* genes from in soybean, for example, resulted in a 5-fold increase of vitamin E activity with an accumulation of more than 95% of α -tocopherol in seeds changing the natural composition of soybean seeds that normally contain 20-30% of δ -tocopherols, 5% of β -tocopherol, 60-70% of γ -tocopherols and 10-20% of α -tocopherols (Van Eenennaam et al., 2003). Compared with seeds, leaves usually contain mostly α -tocopherol so the major goal relies on the improvement of total tocopherols levels without changing the tocopherol composition. The overexpression of tocopherol cyclase (*VTE₁*) and γ -TMT (*VTE₄*) was reported to have a major effect on tocopherol amount in tobacco and lettuce leaves (Yabuta et al., 2013). In some cases, the increased amount of vitamin E can be also a strategy to preserve the carotenoid content avoiding oxidative degradation (Che et al., 2016). Vitamin K content, however, compared to the other two isoprenoids previously discussed, is more difficult to improve. The reason is related to its complicated and poorly known biosynthetic pathway that includes steps located in plants peroxisomes. Most of the strategies that allowed to increase the amount of phylloquinones, in fact, were intended to increase the levels of other compounds like salicylic acid and resulted in the collateral increase of vitamin K because of alternative channelling of precursors (Babujee et al., 2010).

Objectives

Objectives

Carotenoids, tocopherols and phyloquinones are plant isoprenoid compounds with a high commercial value either from the industrial point of view or for their health-related properties being the principal precursors and components of vitamin A, E and K, respectively. Humans require a minimum daily intake of essential nutrients and vitamins to maintain an optimal body state. Malnutrition has been one of the central problems of the 20th century, especially in underdeveloped countries. In well-developed countries, the biofortification of processed foods with micronutrients and vitamins solved part of the problem but in developing countries, the low industrial level of the agriculture and a limited food-processing and distribution scheme led to the failure of this strategy. To solve the necessities of these populations the direct biofortification of the original crop is necessary (Dellapenna, 2007). Various trials were successful in enhancing the content of isoprenoids vitamins in different plant structures like fruits, seeds, or tubers. However, the biofortification of green leafy vegetables has been more challenging. Indeed, this type of products would be very good candidates for biofortification because of the faster, easier, and less expensive growth conditions of most green leaf edible products like spinaches, lettuce, or alfalfa.

The general objective of this thesis is to test new strategies for the biofortification of leafy vegetables. At the beginning of this work, a new tool able to induce the accumulation of high amounts of carotenoids in green leaves was being developed in the lab. The tool is based on the transient overexpression of the *crtB* gene from the bacterium *P. ananatis* under the control of a strong constitutive promoter. When the encoded protein, a bacterial phytoene synthase, entered the chloroplast, a yellow leaf phenotype was developed and the level of carotenoids was doubled concomitantly with the transformation of leaf chloroplasts into chromoplasts (Llorente et al., 2020). The availability of this system in the laboratory allowed to define 2 major objectives for this thesis.

Objective 1: To characterize the physiologic context of the crtB-induced phenotypes in leaves. The goal was to perform an in-depth analysis of the changes that *crtB* overexpression caused in leaf plastid physiology.

Objective 2: To Test different strategies exploiting the crtB-based system to improve leaf biofortification.

Environmental treatments known to influence plastid physiology and structure (such as dark-induced like senescence, high light intensity and altered light quality) as well as metabolic

engineering strategies will be separately explored and, if possible, combined to achieve optimal levels of pro-vitamin A carotenoids but also vitamin E tocopherols and vitamin K phyloquinone in leaves.

Chapter 1

Chapter 1. Artificial generation of chromoplasts in green leaves: exploring the physiological context.

Note: Part of the results shown in this chapter were published in Llorente et al., 2020. See Annex I.

0.7. Introduction

Plastids comprise a group of morphologically and functionally diverse plant organelles capable of differentiating from one plastid type to another in response to developmental and physiological stimuli (Jarvis and López-Juez, 2013; Sadali et al., 2019). These plastidial conversions are essential to sustain many fundamental biological processes and largely contribute to cell specialization in the different plant tissues and developmental phases. Among the different plastid types, chromoplasts are of great importance in nature and agriculture because of their capacity to accumulate high levels of carotenoids, plant pigments of isoprenoid nature that provide colour in the yellow to red range (Egea et al., 2010; Sun et al., 2018). Carotenoids such as β -carotene (pro-vitamin A) are health-promoting nutrients that animals cannot normally synthesize but take up in their diets. They are also added-value compounds widely used in cosmetics, pharma, food, and feed industries as natural pigments and phytonutrients (Rodriguez-Concepcion et al., 2018; Giuliano, 2017).

Chromoplasts differentiate from pre-existing plastids such as proplastids (i.e., undifferentiated plastids), leucoplasts (i.e., uncoloured plastids in non-photosynthetic tissues), and chloroplasts (i.e., photosynthetic plastids). Chromoplasts usually function in the synthesis and storage of carotenoid pigments in flowers and fruits. The Colouration of petals by chromoplasts is an evolutionary strategy adopted by some angiosperms to attract pollinators (Egea et al., 2010) whereas the differentiation of chromoplasts in fruit provides colour to inform animals on the ripening stages for them to disperse the incorporated seeds (Li and Yuan, 2013; Pesaresi et al., 2014; Llorente et al., 2016).

Only a few plant species differentiate chromoplasts in green leaves. For example, the box tree (*Buxus sempervirens* L.) leaves become red during autumn and winter due to the de novo synthesis of red carotenoids. This is a response to photoinhibitory conditions during winter acclimation and it is reversed on exposure to warmer temperatures (Hormaetxe et al., 2004). Structurally, the leaf chloroplasts differentiate into globular chromoplasts, which in turn de-

differentiate into chloroplasts again in warmer weather (Koiwa et al., 1986). This provides an interesting example of reversible chromoplast differentiation based on environmental cues (Sadali et al., 2019; Sun et al., 2018). It is important to note that the yellow to red colours that leaves from most plant species acquire as they senesce (e.g., in the autumn) are due to chloroplast carotenoids becoming visible when the chlorophylls degrade. This senescence process does not involve the transformation of chloroplasts into chromoplasts but into a completely different type of plastids named gerontoplasts (Sadali et al., 2019; Jarvis and López-Juez, 2013)

The most prominent changes during chloroplast-to-chromoplast differentiation are the reorganization of the internal plastid structures, together with a concurrent loss of photosynthetic competence and overaccumulation of carotenoid pigments (Sadali et al., 2019; Jarvis and López-Juez, 2013; Egea et al., 2010; Sun et al., 2018). The remodelling of the internal photosynthetic membrane system provides material such as lipids and proteins to build new storage structures and thus it generates an increased metabolic sink capacity while promoting carotenoid biosynthesis (Egea et al., 2010). The control of chromoplast differentiation hence appears as a very promising strategy for improving the nutritional and health benefits of crops (Sun et al., 2018). The overall process is known to involve changes in gene expression (e.g., via retrograde signalling from plastids to the nucleus), hormonal regulation, protein quality control, and plastid protein import (Sadali et al., 2019; Egea et al., 2010; Wurtzel, 2019; Sun et al., 2018). However, very few inducers of chromoplast development have been identified to date. Carotenoid-associated proteins and Orange (OR) chaperones are among the best characterized, but they only work in some tissues like callus or cauliflower curd, and the specific mechanism by which they promote chromoplast differentiation remains unclear (Welsch et al., 2018). The experimental manipulation of chromoplast differentiation for fundamental studies and biotechnological applications therefore requests a much better understanding of the mechanisms regulating this process.

The first committed step of the carotenoid biosynthetic pathway is the conversion of geranylgeranyl diphosphate (GGPP) to the colourless carotenoid phytoene, catalysed by phytoene synthase (referred to as PSY in plants and *crtB* in bacteria) (Figure 1.1A). Virus-mediated expression of a bacterial *crtB* gene in tobacco (*Nicotiana tabacum* and *Nicotiana benthamiana*), tomato (*Solanum lycopersicum*), *Arabidopsis thaliana* and several other plants, was found to cause leaf yellowing due to increased accumulation of coloured endogenous carotenoids downstream of phytoene (Majer et al., 2017). Further work demonstrated that untagged or chloroplast-targeted *crtB*, herein referred to as (p)*crtB*, but not a version retained in

the cytosol due to the presence of an N-terminal GFP fusion, referred to as (c)crtB, were able to trigger the conversion of chloroplasts into plastids with ultrastructural features resembling those found in chromoplasts ([Llorente et al., 2020](#)) (Figure 1.1B). Here we used the agroinfiltration system in *N. benthamiana* leaves to further investigate the dynamics of this process at the physiological and molecular levels.

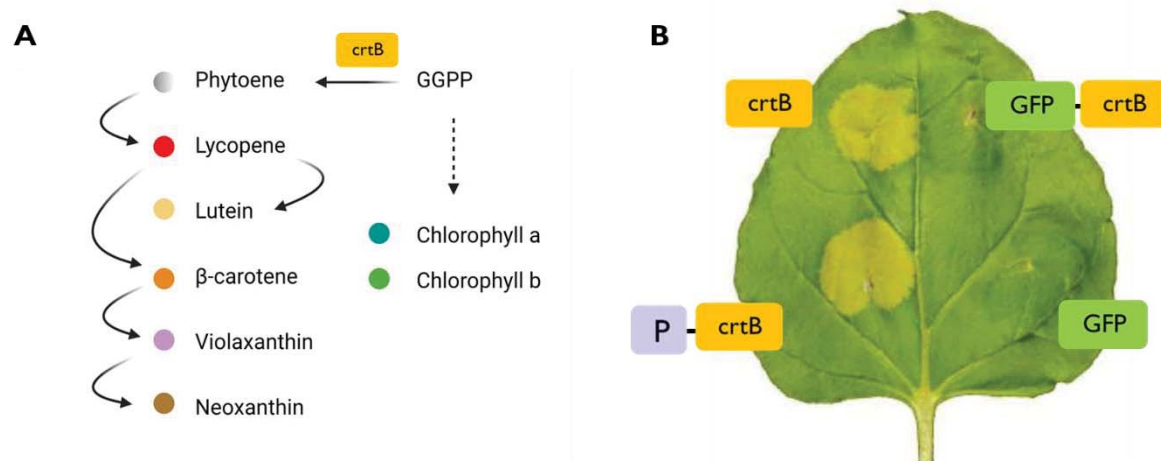


Figure 1.1. Overexpression of *crtB* in *N. benthamiana* leaves results in a yellow phenotype. (A) Schematic view of carotenoid biosynthetic pathway. *crtB* protein catalyses the conversion of GGPP into phytoene that can be converted into downstream carotenoids (B) Leaf tissue producing *crtB* proteins able to enter the plastid (either for their natural cryptic transit peptide or for the addition of a transit peptide) show a stable yellow phenotype while leaves producing *crtB* protein in the cytosol or a control GFP protein stay green

0.8. Results

1.2.1. Transient expression of the bacterial *crtB* gene strongly and irreversibly impacts photosynthesis

Agroinfiltration of *N. benthamiana* leaves with *crtB* or (p)*crtB* constructs did not initially reduce chlorophyll levels compared to leaf tissues agroinfiltrated with GFP or (c)*crtB* ([Llorente et al., 2020](#)). However, estimation of photosynthesis-related parameters such as effective quantum yield of PSII (ϕ PSII) and non-photochemical quenching (NPQ) showed that both *crtB* and (p)*crtB*, but not (c)*crtB* or GFP, had a dramatic impact on photosynthetic function. For instance, ϕ PSII was reduced to values near 0.1, typical of a non-photosynthetic tissue and coherent with the transition from functional chloroplasts to chromoplasts (Figure 1.2A). A plastid-targeted version of GFP did not cause any yellowing or ϕ PSII defect confirming that the disturbance of chloroplast photosynthesis observed in leaves agroinfiltrated with *crtB* or (p)*crtB* was not caused

by the targeting and accumulation of a foreign protein in chloroplasts but specifically by *crtB* activity (Figure 1.2B). Agroinfiltrated leaves did not experience re-greening and their low ϕ PSII was maintained for weeks. About a week after agroinfiltration with *crtB*, chlorophylls started to decrease. Carotenoids also decreased but not as much as chlorophylls, eventually resulting in a higher carotenoid-to-chlorophyll ratio and, therefore, a stronger yellow colour that was clear at 16 days post-inoculation (dpi) (Figure 1.2C, 1.2D).

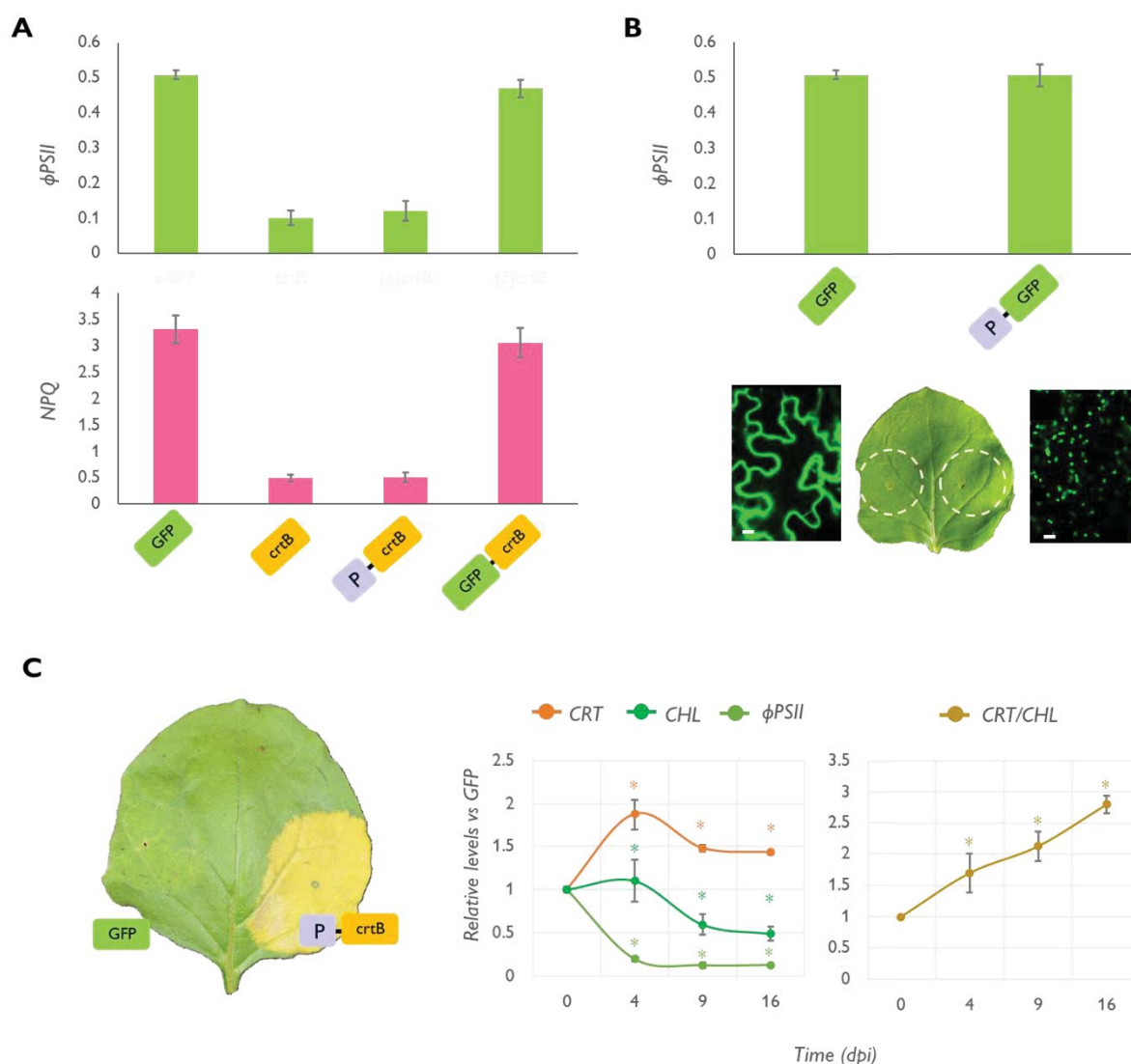
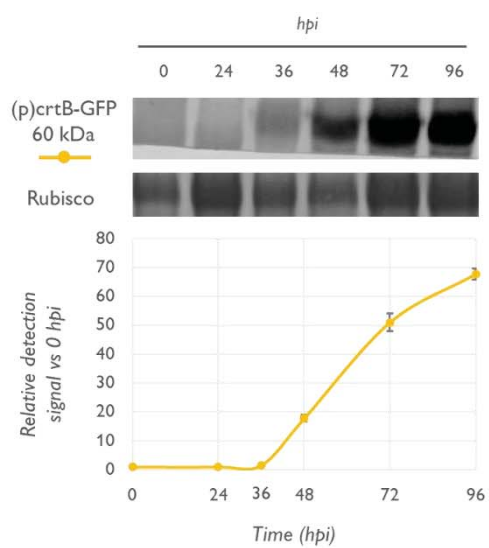


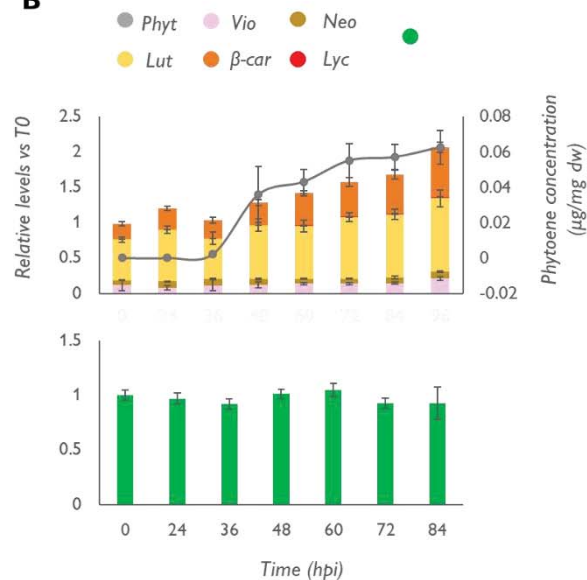
Figure 1.2. Plastid-localized *crtB* triggers loss of photosynthetic activity. (A) Effective quantum yield (ϕ PSII) and Non-photochemical quenching (NPQ) values of leaves overexpressing the indicated constructs. (B) ϕ PSII of leaves overexpressing two versions of GFP proteins. The lower panel shows the subcellular localization of the protein observed with the confocal microscope. (C) Visual phenotype, pigment content, and ϕ PSII of leaves overexpressing *crtB* for 16 days. Plots show the mean and SD of $n=3$ independent samples. Asterisks in (D) plots mark statistically significant changes relative to 0 dpi (t-test, $P < 0.05$).

To investigate the dynamics of the crtB-dependent chromoplast differentiation process, we next followed the time course of photosynthetic changes along with the accumulation of the (p)crtB-GFP protein estimated by immunoblot analysis using an α -GFP antibody. We also monitored phytoene production and downstream carotenoid accumulation in the same samples (Figure 1.3A, B). After agroinfiltration of *N. benthamiana* leaves with the (p)crtB-GFP construct, the (p)crtB-GFP protein became detectable between 36 hpi and 48 hpi and peaked 72 hpi. The product of this protein activity, phytoene, started to accumulate at 36 hpi and suddenly increased at 48 hpi coherently following the protein accumulation profile. Downstream carotenoids began to increase starting from 48 hpi, i.e., they expectedly showed a slight delay compared to phytoene accumulation. To follow the dynamics of photosynthesis as chloroplast membranes were remodelled during chromoplastogenesis, we monitored ϕ PSII, NPQ, maximum quantum yield of PSII (Fv/Fm), de-epoxidation state of the xanthophyll cycle (DES) (Cartaxana et al., 2019), and thylakoidal protein levels (Figure 1.3). While Fv/Fm remained unchanged until 48 hpi, ϕ PSII, and NPQ started to change at 36 hpi, paralleling the onset of phytoene accumulation. The 12-hour delay in the decrease of Fv/Fm is likely to be related to the lower sensitivity of the Fv/Fm value over small scale changes. In the case of NPQ, the total value of energy dissipation decreased starting from 36 hpi but the most variable component of NPQ to decrease was the fast-developing qE. This component is dependent on proton flux through thylakoid membrane and its decreasing could be related to the dismantling of these structures. DES decreased in (p)crtB samples at 48 hpi compared to GFP-agroinfiltrated control samples. In fact, in (p)crtB leaves the lack of proton motion force would result in the impossibility to dynamically convert violaxanthin into zeaxanthin upon light stress increasing thus the DES value (Figure 1.3D, E). Taken together, these results suggest that the crtB-mediated production of phytoene causes a fast disruption of the chloroplast photosynthetic functionality (estimated as changes in ϕ PSII and NPQ values) before downstream carotenoids start to over accumulate. Later, carotenoid overaccumulation parallels the decrease in DES and thylakoid protein levels, likely reflecting the loss of thylakoid membranes.

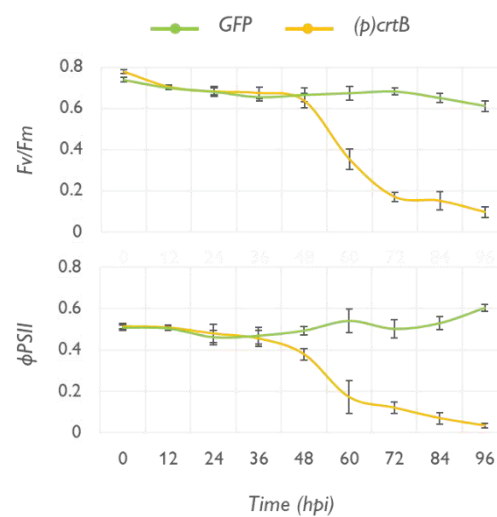
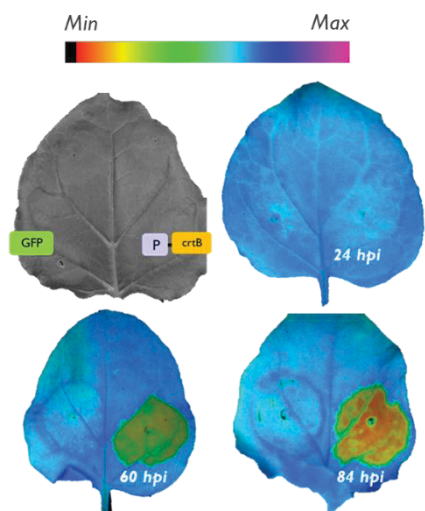
A



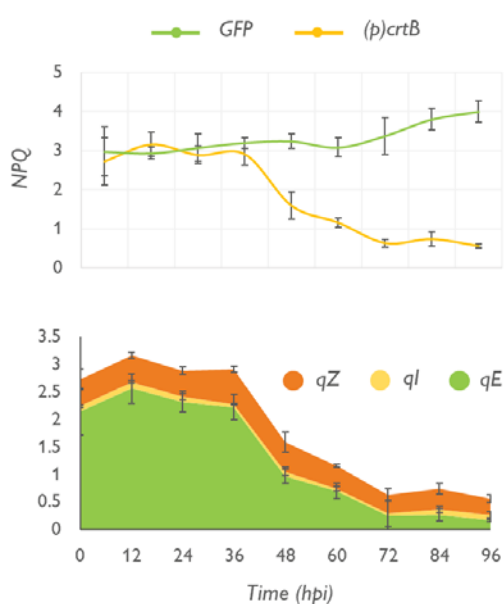
B



C



D



E

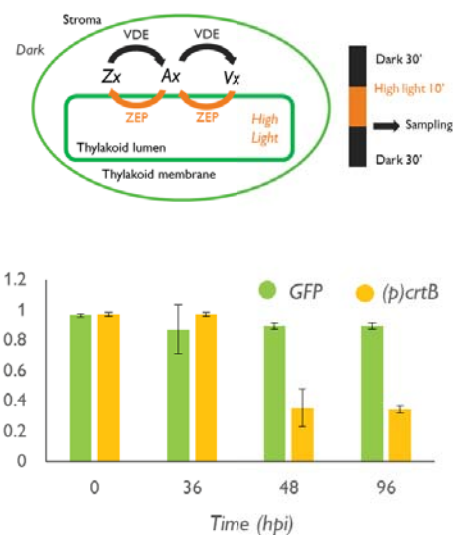
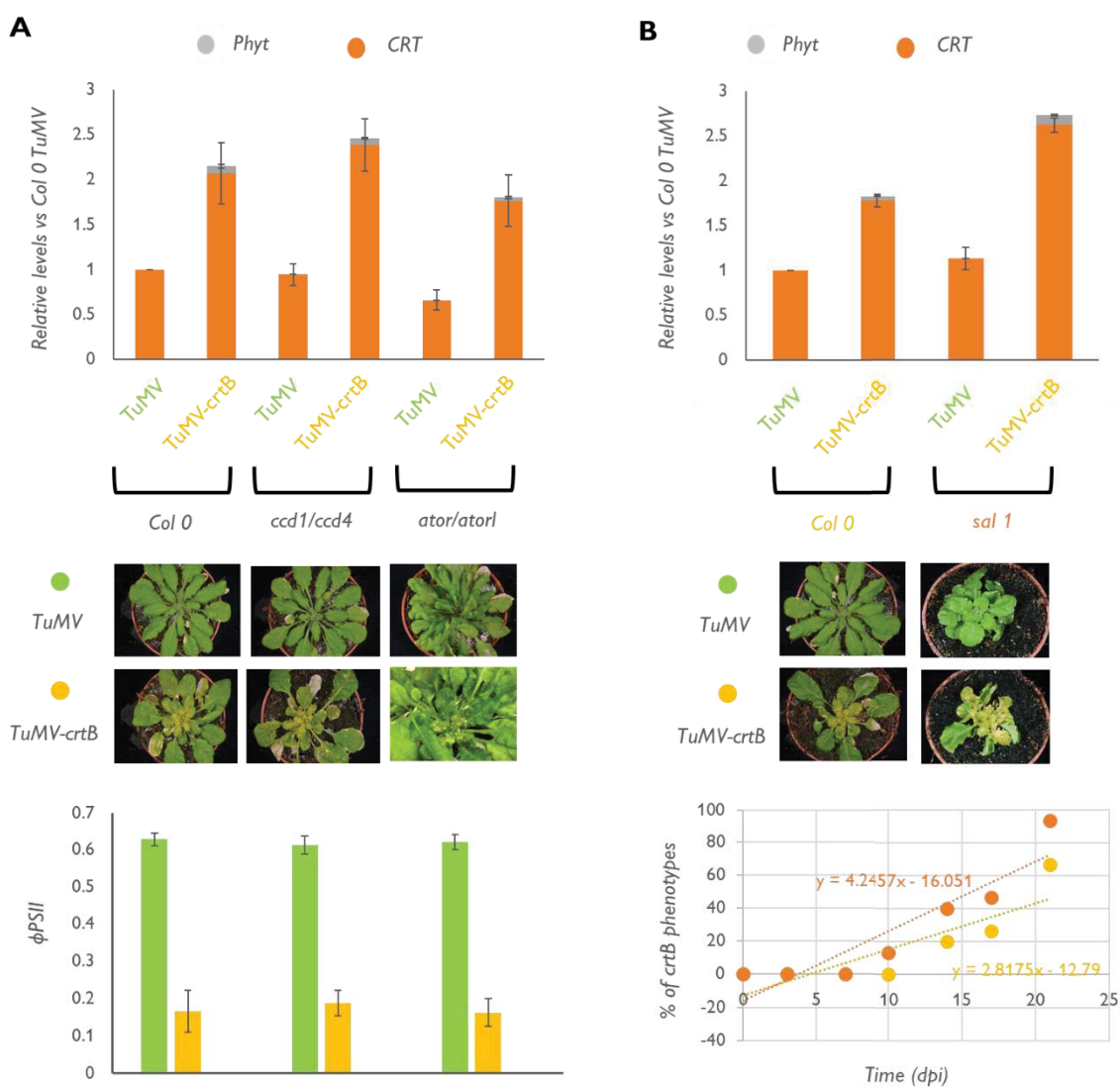


Figure 1.3: The transformation of chloroplasts into chromoplasts is characterized by deep changes in photosynthetic apparatus connected to carotenoid accumulation in a time-dependent manner. (A) Levels of (p)crtB-GFP protein in leaves. The protein was detected by probing the membrane with an anti-GFP antibody and quantified based on the intensity of Rubisco (B) Absolute phytoene levels and relative downstream carotenoids and chlorophylls levels in (p)crtB samples. Values were relativized to the one obtained in leaves sampled 0 hpi. The legend shows an abbreviated name for detected carotenoids (Phyt: phytoene, vio: violaxanthin, neo:neoxanthin, lut: lutein, β -car: β -carotene, lyc: lycopene, CHL: total chlorophylls. (C) Representative chlorophyll fluorescence Images, Fv/Fm and ϕ PSII values. (D) Total NPQ value in (p)crtB and GFP samples and evolutions of the different component of NPQ (qE, qI and qZ) in (p)crtB samples. (E), Leaves producing GFP or (p)crtB treated as shown in the panel and then collected to quantify their carotenoid levels. De-epoxidation state (DES) was calculated as $(Zx+0.5Ax)/(Zx+Ax+Vx)$, where Zx, Ax and Vx are the concentrations of zeaxanthin, antheraxanthin, and violaxanthin, respectively. All the values shown in this figure represent mean and SD of at least 3 replicates.

1.2.2. Artificial chromoplastogenesis is exacerbated by PAP-mediated retrograde signaling.

After having identified phytoene as one of the main factors regulating the progress of leaf chromoplast differentiation triggered by crtB we next used *Arabidopsis* double mutants defective in OR chaperones (AtOR and AtOR-LIKE) to test whether the differentiation process involved pathways depending on these well-characterized promoters of carotenoid metabolism and chromoplast development. OR has a stabilising effect on endogenous PSY activity allowing the enzyme to work at higher production rates but it also appears to prevent carotenoid degradation and to promote the differentiation of chromoplasts in different plant tissues but not in leaves (Welsch et al., 2018, Sun et al., 2018). We also tested double mutants lacking cytosolic and plastidial carotenoid cleavage dioxygenases (CCD₁ and CCD₄, respectively) to investigate the possible contribution of carotenoid degradation and/or signalling molecules derived from enzymatic cleavage of carotenoids (i.e., apocarotenoids) in the differentiation mechanism (Havaux, 2020). Because chloroplast transformation into chromoplasts is also expected to impact plastid redox balance, we also used *sal1* mutants that constitutively produce the redox-related retrograde signal 3-phosphoadenosine 5-phosphate (PAP) (Estavillo et al., 2011). We mechanically inoculated *A. thaliana* leaves from wild-type (Col 0) and mutant lines (*ator atrol*, *ccd1 ccd4* and *sal1*) with tissue from *N. benthamiana* leaves previously infected with a TuMV viral vector carrying the crtB gene (TuMV-crtB). Virus-mediated production of crtB protein in double *ator atrol* and *ccd1 ccd4* mutants resulted in leaves showing the characteristic yellow phenotype associated with carotenoid overaccumulation and loss of photosynthetic activity observed in the wild-type (Figure 1.4A), suggesting that signals derived from OR activity or from the enzymatic

cleavage of carotenoids are not required for the process. In *sal1* plants, however, this *crtB*-phenotype appeared to develop faster. To quantitative support this observation, the percentage of plants developing the characteristic yellow phenotype was counted every 5 days after inoculation with TuMV-*crtB* for a total of 25 days. The slope of the line obtained by plotting the percentage of *crtB*-induced phenotypes over time was found to be lower in the wild type (2.8) than in *sal1* plants (4.2), confirming a faster rate of chromoplastogenesis in the mutant (Figure 1.4B). Leaves from TuMV-*crtB*-inoculated mutant plants also showed significantly higher levels of phytoene and total carotenoids compared to wild type controls (Figure 1.4B). From these results we concluded that accumulation of the redox stress-related retrograde signal PAP promotes the *crtB*-mediated differentiation of chromoplasts. Besides leaves, yellowing was widespread in all other green tissues of *A. thaliana* wild type and mutant plants, including cauline leaves, stems, sepals, and siliques, where it remained stable until plants died hence confirming the inability of plants to revert over time to a chloroplast status (Figure 1.4C).



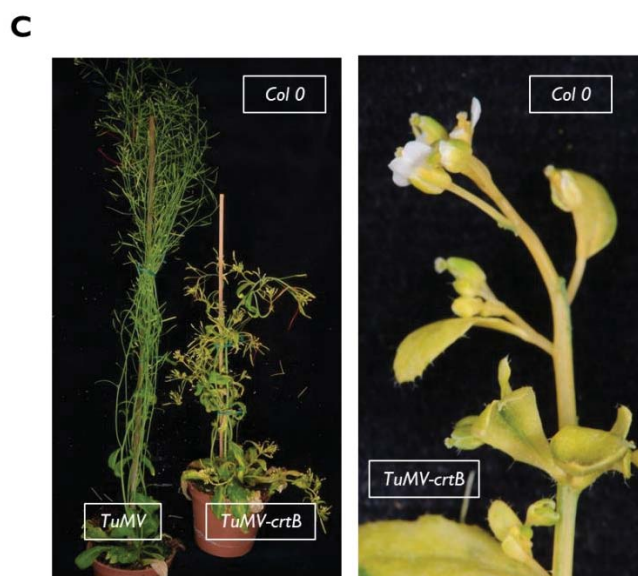


Figure 1.4. Lack of OR protein or carotenoid cleavage enzymes does not stop crtB protein to trigger chromoplastogenesis but *sal1* mutant plants show an accelerated phenotype. (A) Carotenoid relative level, effective quantum yield (ϕ PSII) and representative images at 14 dpi of *Arabidopsis* (Col) WT and double mutant plants grown under short day conditions (8 h of low light and 16 h of darkness) for 2 wk (WT and *ccd1/ccd4*) or 5 wk (*ator/ator1*) and then inoculated with the indicated viral vectors. (B) Carotenoid level, representative pictures of the phenotype and speed of crtB-phenotype establishment (expressed as % of crtB phenotype) in *sal 1* mutant plants inoculated with the same viral vectors. Plot shows the mean and SD of $n=3$ independent samples. Carotenoid levels are represented relative to those in WT samples inoculated with the empty vector control (TuMV). Bars represent total carotenoid amount except phytoene (CRT) and relative phytoene level (phyt). (C) Representative *Arabidopsis* WT plants at 38 dpi and particular of flower stem.

1.2.3. Endogenous hormones do not control the leaf chromoplastogenesis process

The *sal1* mutation has been found to impact expression of genes associated with ABA and methyl jasmonate as well as auxin homeostasis (Rodríguez-Concepción, 2010; Chan et al., 2016; Phua et al., 2018). Interestingly, hormones have also been described to impact chromoplast development in plants, especially in fruits. The hormonal regulation of fruit ripening can be classified as either ethylene-dependent (climacteric) or ethylene independent (non-climacteric). Common examples of climacteric fruits are tomato and most stone fruits, whereas non-climacteric fruits include citrus and pepper (Giovannoni, 2004). In climacteric fruit, the hormone ethylene induces chromoplast differentiation and the accumulation of metabolites responsible for colour and aroma. In non-climacteric fruit ethylene effects are usually limited to colour break, and it has no apparent effect on the internal ripening process or fruit quality (Giovannoni, 2004; Klee and

Giovannoni, 2011). To investigate the effect of hormones on chromoplastogenesis in leaves we tested exogenous hormones application. The decrease rate of Φ PSII was used as a reliable physiological marker to monitor the speed of chromoplast development considering that, in multiple experimental settings, the pattern of photosynthetic capacity loss in (p)crtB leaves was always comparable. We tested the effect of appropriate concentrations of various growth regulators (Table 1) by applying the compound with a fine brush on the surface of the leaf 2 hours after the agroinfiltration with either GFP or (p)crtB (i.e, once the agroinfiltration halo was dried). Φ PSII was calculated every 12 hours using a non-destructive Imaging PAM system to estimate the proceeding speed of the process.

Table 1. List of compounds applied to test hormonal regulation of chromoplast development in leaves. All the compounds were diluted to the enlisted concentration in water with the addition of 0.05% of Tween20 and then painted with a fine brush on leaf surface.

<i>Hormone class</i>	<i>Compound</i>	<i>Short name</i>	<i>Concentration</i>
Cytokinins	2-isopentenyladenine	2-iP	10 μ M
Cytokinins	Zeatin	ABA	10 μ M
Ethylenes	Etephon	ETH	1,5 mM
Jasmonates	Methyl Jasmonate	MJA	100 μ M
Salicylic acid	Salicylic acid	SA	300 μ M
Abscisic acid	Abscisic acid	ABA	10 μ M
Brassinosteroids	Epibrassinolide	EBR	10 μ M
Gibberellins	Gibberellic acid	GA ₃	100 μ M
Gibberellins biosynthesis inhibitors	Paclobutrazol	PAC	10 μ M
Auxins	Picloram	PIC	50 μ M
Auxins	Indole-3-acetic acid	IAA	50 μ M
Auxins	2,4-Dichlorophenoxyacetic acid	2,4-D	50 μ M
Auxins biosynthesis inhibitors	L-kynurenine	L-Kyn	500 μ M
Strigolactones	GR24	GR24	100 μ M
Strigolactones biosynthesis inhibitors	hydroxamic acid	D2	100 μ M

Most plant hormones listed in Table 1 showed no significant changes in Φ PSII or carotenoid content compared to the leaves overexpressing (p)crtB and treated with a mock solution (Figure 1.5A). However, gibberellins promoted the establishment of the crtB-induced phenotype whereas

auxins and strigolactones delayed it. In particular, the application gibberellic acid (GA_3) resulted in a significant decrease of ϕ PSII in (p)crtB samples already at 36 hpi compared to the control. On the other side, the application of the artificial strigolactone GR24 and of different auxins (including the synthetic picloram, PIC) resulted in a significantly higher ϕ PSII in all the time points evaluated. The modulation of the chromoplastogenesis speed also affected metabolite accumulation. At 96 hpi, GA_3 treatment led to a higher content of carotenoids compared to mock-treated control leaves while the PIC and GR24 treatments resulted in lower levels (Figure 1.5B). To test whether the internal amounts of these growth regulators could also regulate the chromoplastogenesis process we repeated the same experiment but using inhibitors of the endogenous biosynthesis pathways of the selected hormones. We used paclobutrazol to block gibberellin biosynthesis (Tsegaw et al., 2005). L-kynurenine to decrease the activity of key enzymes in the indole-3-pyruvic acid pathway of auxin biosynthesis (He et al., 2011) and the hydroxamic acid D2 to inhibit strigolactone biosynthesis through the antagonist action to the enzymes CCD7 and CCD8 (Harrison et al., 2015). The application of these inhibitors after agroinfiltration with (p)crtB did not show any effect on ϕ PSII or carotenoid contents compared to plants treated with the mock solution (Figure 1.5C).

We then analysed the expression of the (p)crtB gene over time in plants treated with GA_3 , GR24 or PIC to investigate whether hormone application impacted chromoplastogenesis through changes in the levels of the triggering factor. Transcripts encoding (p)crtB were reported to peak at 48 hpi (Llorente et al., 2020) so we concentrated the analysis at 0, 24, 36 and 48 hpi. The application of GR24 and PIC resulted in a lower expression of the (p)crtB transgene in all the evaluated time points while the application of GA_3 was associated with a higher expression compared to the control. We also found a correlation between this expression pattern and phytoene amount at 48 hpi: GA_3 treated plants showed a significantly higher content of phytoene compared to the control while GR24 and PIC treated plants accumulated a much lower amount (Figure 1.5D). These results strongly suggested that exogenous application of gibberellins, auxins and strigolactones can influence the expression of the transgene and thus affect the accumulation of phytoene, eventually resulting in an altered chromoplastogenesis rate.

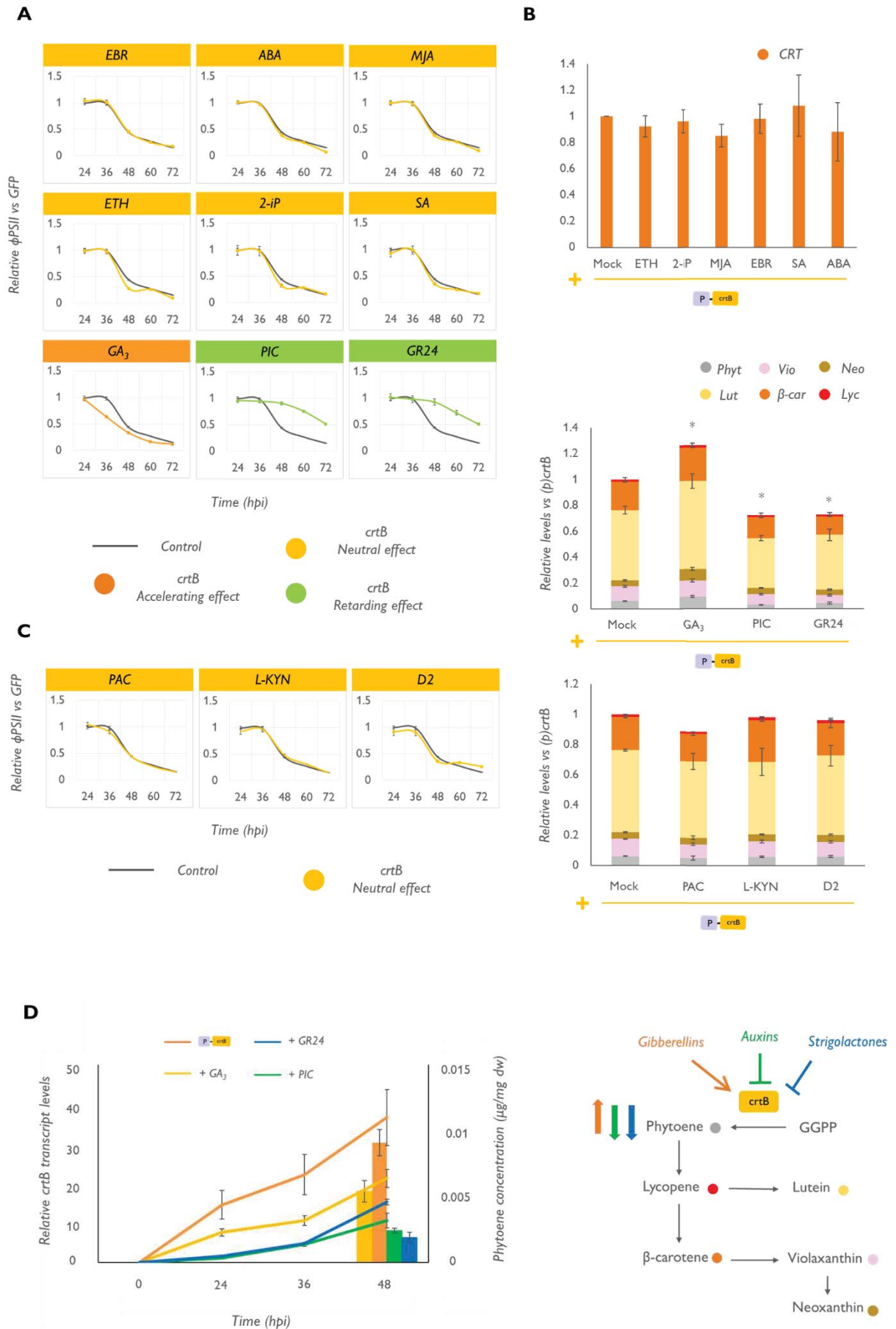


Figure 1.5. Exogenous application of hormones can impact chromoplast establishment by influencing phytoene content and *crtB* expression. (A) Relative effective quantum yield and carotenoid levels of samples treated with compounds enlisted in table 1. The rate of photosynthetic loss defines substances with neutral effect (yellow line), accelerating effect (orange line) or retarding effect (green line) on *crtB*-phenotype. (B) Carotenoid content of leaves overexpressing (*p*)*crtB* and treated with the enlisted compounds. Carotenoid levels were relative to the one found in leaves overexpressing (*p*)*crtB* and treated with a mock solution. (C) Application of inhibitors of endogenous hormone synthesis does not affect chromoplast development and has no effect on photosynthetic loss and carotenoids amount. (D) Levels of (*p*)*crtB*-encoding transcripts relative to the maximum in samples overexpressing (*p*)*crtB* 0, 24, 36 and 48h and phytoene content 48 hpi. The model in the right panel represents the possible effect of the different compounds on chromoplasts formation: fluctuations in the expression of *crtB* result in variation in phytoene level anticipating or delaying the beginning of the conversion process. Relative Φ PSII plots show the mean and SD obtained from 3 different measures for each plant and a minimum of 3 plants (n=9) while plots of carotenoid content show the mean and SD of 3 independent experiments (n=3). Asterisks in D plots mark statistically significant changes relative to 0 dpi (t-test, $P < 0.05$).

1.2.4. Enhanced supply of phytoene in chloroplasts is necessary but not sufficient to trigger chromoplastogenesis in leaves.

From all the previous results we developed the hypothesis that the increase in the levels of phytoene could be the main factor triggering chromoplast differentiation upon *crtB* overexpression. To next confirm whether impairment of chloroplast functionality was due to phytoene overaccumulation, we used norflurazon (NF), an inhibitor of the plant phytoene desaturase (PDS) enzyme that prevents phytoene conversion into downstream carotenoids (Ortiz-Alcaide et al., 2019). *N. benthamiana* leaves were agroinfiltrated with constructs to produce GFP, (*p*)*crtB* and *PAR1*, an *Arabidopsis* transcription cofactor that promotes total carotenoid biosynthesis but not phytoene accumulation in photosynthetic tissues (Roig-Villanova et al., 2007). At 24 hpi, some agroinfiltrated leaves were treated with NF. Untreated leaves transiently expressing the *Arabidopsis PAR1* gene accumulated higher levels of carotenoids downstream of phytoene but did not exhibit changes in Φ PSII compared to GFP controls. NF treatment resulted in phytoene accumulation, reduced levels of downstream carotenoids, and decreased Φ PSII in all the samples. The reduction in Φ PSII in these NF-treated samples correlated with the accumulation of phytoene (the higher the levels of phytoene the stronger the reduction of Φ PSII) (Figure 1.6). However, the reduction in Φ PSII was modest compared to that observed in (*p*)*crtB* samples lacking NF in which phytoene conversion into downstream carotenoids led to the differentiation of chromoplasts. We concluded that phytoene overaccumulation by itself disturbs photosynthesis but does not abolish chloroplast identity, resulting in a relatively modest

reduction in ϕ PSII. The much stronger decrease in ϕ PSII that takes place in (p)crtB samples would not be directly because of phytoene on photosynthetic activity but resulted from the dismantling of the photosynthetic apparatus as chloroplasts accumulate downstream carotenoids and differentiate into chromoplasts. Interestingly, PAR₁-mediated accumulation of carotenoids but not phytoene was unable to trigger the massive drop in ϕ PSII and the yellow leaf phenotype characteristic of chromoplast differentiation. We therefore conclude that the accumulation of phytoene causes a concentration-dependent disruption of the photosynthetic identity of chloroplasts, a condition that might be necessary for them to become chromoplasts upon the subsequent production and accumulation of downstream carotenoids in correlation with the physical disruption of the internal membranes system.

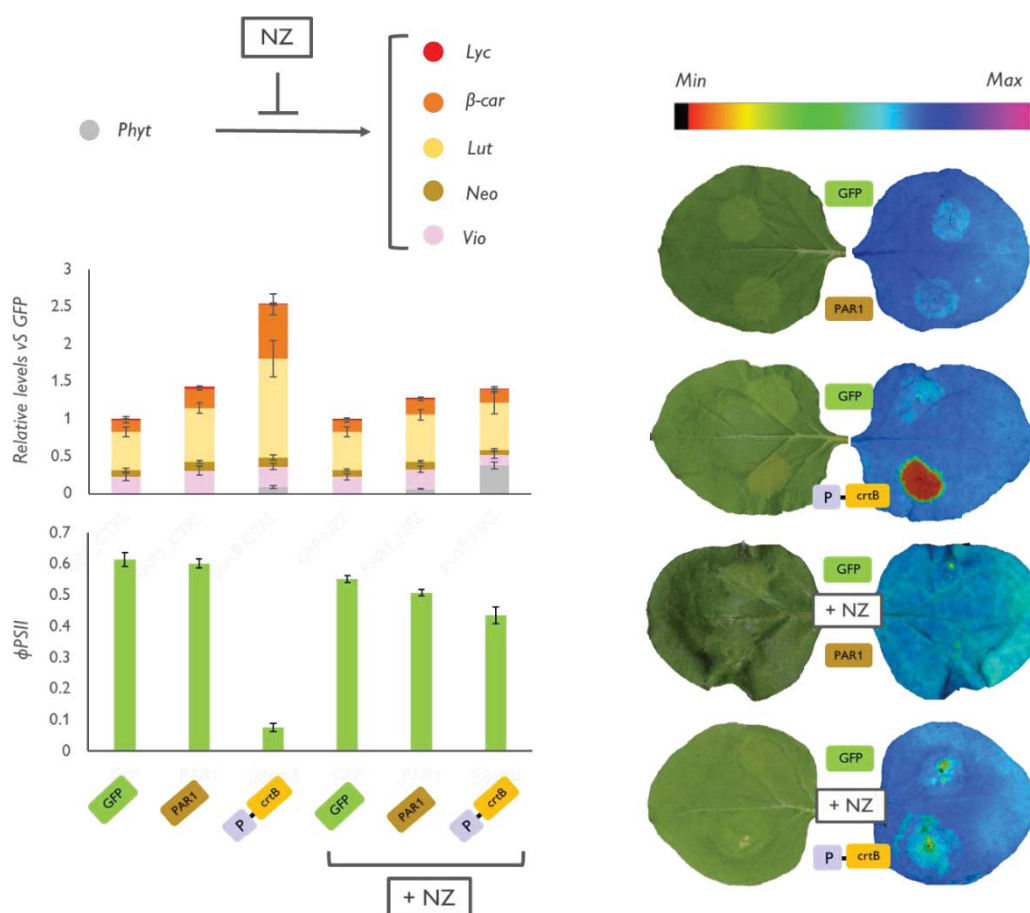


Figure 1.6. Phytoene accumulation is a necessary step to impair plastid photosynthesis and allow chromoplastogenesis. Values of ϕ PSII and relative carotenoid levels in plants overexpressing GFP, PAR₁ and (p)crtB and treated with NF. Plots represent the mean and SD of at least 3 samples for experiment. The right panel resume the experiment and show the different phenotype obtained.

In contrast with the results using crtB but similar to those with PAR₁, overexpression of PSY-encoding genes from *Arabidopsis* and tomato could not elicit the characteristic yellow leaf

phenotype associated with chromoplast differentiation (Llorente et al., 2020) and resulted only in a modest increase in total carotenoid content (Fraser et al., 2007; Lätari et al., 2015). Interestingly, the plant enzymes yielded significantly lower levels of phytoene compared to crtB and did not substantially impact photosynthesis to the same extent as deduced from ϕ PSII values (Llorente et al., 2020). We hence speculated that phytoene might act as a metabolic threshold switch that only alters the photosynthetic performance of chloroplasts when exceeding a certain level. To artificially overcome this putative threshold and to introduce a situation of photosynthetic impairment we treated *N. benthamiana* leaves with a sublethal dose of DCMU (3-(3,4-dichlorophenyl)-1,1-dimethylurea, diuron), a widely used inhibitor of photosynthesis that interrupts the photosynthetic electron transport chain at the level of PSII. The next day, treated and untreated control leaves were agroinfiltrated with constructs encoding either GFP or the *Arabidopsis* PSY enzyme. At 96 hpi, DCMU-treated GFP leaf sections showed a decrease in ϕ PSII compatible with the application of the inhibitor, but unchanged carotenoid levels compared to untreated samples. By contrast, DCMU-treated PSY sections showed a more dramatic drop in ϕ PSII and much higher levels of carotenoids than untreated PSY or GFP controls. Consequently, PSY leaf sections treated with DCMU turned yellow, like that observed when chloroplast-to-chromoplast differentiation was triggered by crtB in the absence of inhibitor (Figure 1.7).

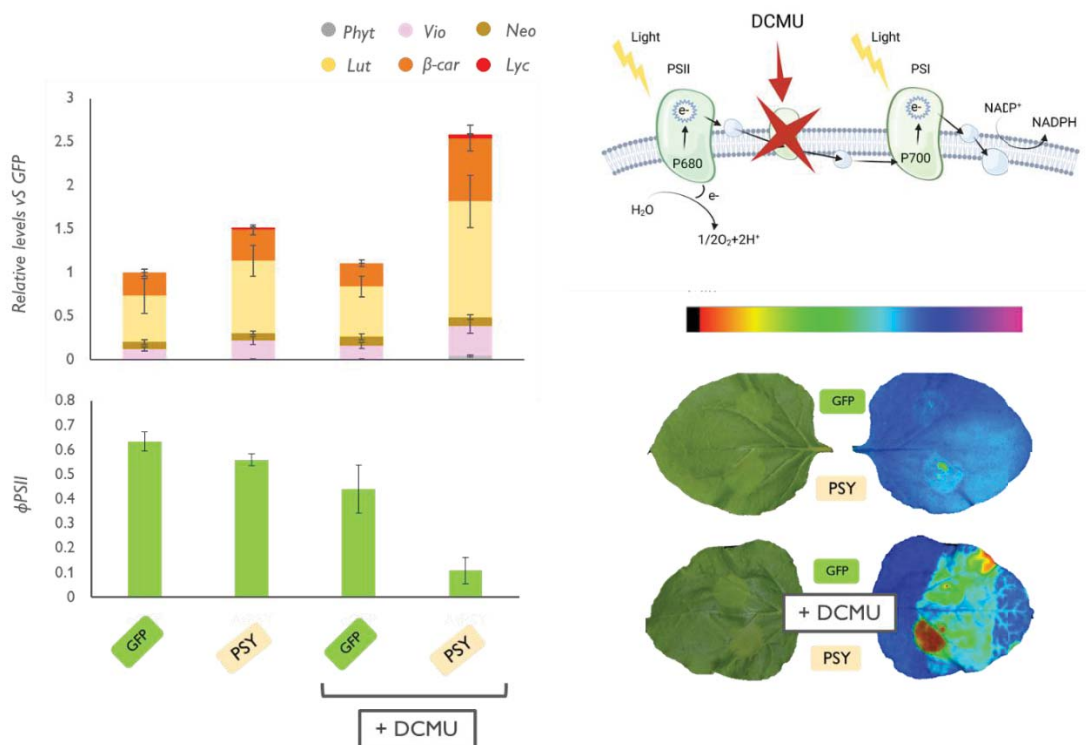


Figure 1.7. Pharmacological inhibition of photosynthetic processes allows to recover crtB-like phenotype. ϕ PSII and relative carotenoid levels of plants overexpressing GFP or PSY and treated with DCMU. Plots show the mean and SD of 3 independent samples for experiment. The right panel shows the obtained phenotypes

In summary, our results are consistent with the existence of a two-step process responsible for the *crtB*-mediated transformation of leaf chloroplasts into chromoplasts. Firstly, chloroplast identity is weakened by overaccumulation of phytoene and, secondly, increased production of carotenoids in pre-conditioned chloroplasts allows the differentiation of chromoplasts (Figure 1.8). Without pre-conditioning, carotenoid levels can increase but chromoplasts do not differentiate, as shown in untreated leaves producing *PAR1* or *PSY*. Moreover, if carotenoids downstream of phytoene are not produced, pre-conditioned chloroplasts remain unchanged, as shown in NF-treated (p)*crtB* leaves.

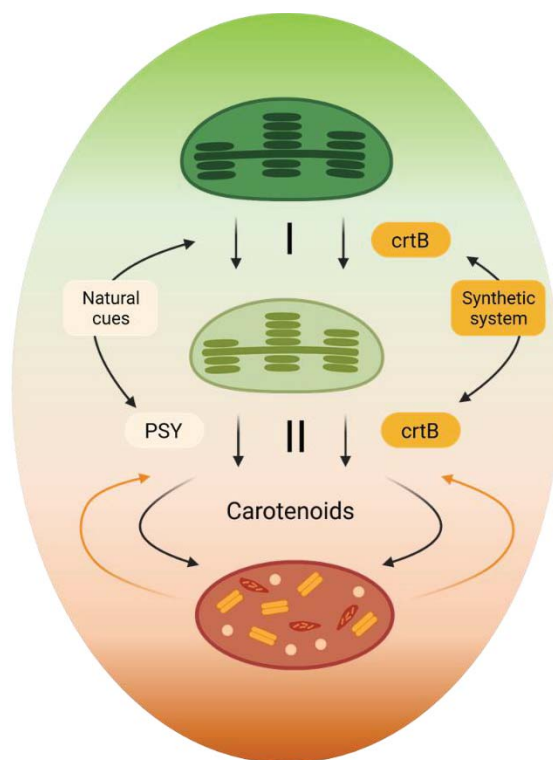


Figure 1.8. Model of the chloroplast-to-chromoplast differentiation process. Plant developmental programs create organs with different degrees of photosynthetic capacity and, hence, chloroplast identity, from strong (e.g., leaves) to weak (e.g., green fruits) or absent (e.g., roots). Weakening of chloroplast identity appears to be the first phase (I) in chromoplast differentiation. In a second phase (II), developmental cues promote the expression of genes encoding *PSY* and other carotenoid biosynthetic enzymes. Enhanced production of carotenoids then reprograms plastid-to-nucleus communication, changes plastid ultrastructure, and results in the differentiation of chromoplasts, which, in turn, promote biosynthesis and improve storage of carotenoids. The two phases can be synthetically engineered in leaves by overproducing phytoene using *crtB*. When phytoene exceeds a certain level, it interferes with the photosynthetic capacity of leaf chloroplasts. This acts as a metabolic switch that allows the formation of chromoplasts after phytoene is converted into downstream carotenoids by endogenous enzymes.

1.3. Discussion

The regulation of plastid identity is a core process in plants that remains poorly defined especially because of the intersection of this process with environmental and eco-physiological cues. Our results show that chromoplasts can be synthetically differentiated from leaf chloroplasts in all plants tested, even though only a few species can carry on the process in nature and only under some environmentally challenging situations (Hormaetxe et al., 2004). The dynamic characterization of our synthetic system has allowed us to propose a model for chromoplast differentiation that also applies to natural systems. In a first phase (I), chloroplasts must become competent (i.e., pre-conditioned) by lowering their photosynthetic capacity, whereas increased production of carotenoids completes the differentiation of chromoplasts in a second phase (II) (Figure 1.8).

In the described synthetic system, phase I was very fast (hours) and required enough phytoene to break chloroplast identity in leaves. In chloroplasts, carotenoids such as lutein, β -carotene, violaxanthin, and neoxanthin are required to maintain the properties of photosynthetic membranes and pigment-protein complexes responsible for harvesting sunlight and transferring excitation energy to the photosystems. Two species of carotenoids are present in the photosynthetic membranes: carotenes and their oxygenated derivatives, xanthophylls. The main carotene, β -carotene, is mainly associated with the core of PSI and PSII (Llorente et al., 2016; Lado et al., 2015) and it is present in all organisms performing oxygenic photosynthesis. The xanthophylls (in plants mainly lutein, neoxanthin, violaxanthin and zeaxanthin) are preferentially bound to the light-harvesting complexes (LHCs) that act as peripheral antennae increasing the absorption cross-section of both photosystems (Xu et al., 2020; Liguori et al., 2017). Phytoene is not normally detected in leaf chloroplasts as it is readily converted into downstream (photosynthesis-related) carotenoids (Figure 1.2A). Overaccumulation of phytoene (or a phytoene derivative) might somehow compete with endogenous carotenoids for their binding to photosynthetic protein complexes and membranes, interfere with their functions, and eventually cause the changes that we observed in photosynthetic competence (Figure 1.3C, Figure 1.6). Consistent with this hypothesis, engineered accumulation of non-chloroplast carotenoids such as astaxanthin in plants alters the properties of thylakoids and grana and interferes with the photosynthetic machinery at several other levels (Liguori et al., 2017; Rödning et al., 2015). Production of astaxanthin and other ketocarotenoids in tobacco resulted in leaf plastids that lost their chloroplast features and exhibited a proliferation of disordered membrane systems and plastoglobules and a loss of stability of PSII supercomplexes similar to our results (Xu et al., 2020). It was described that LHCs can accommodate different xanthophylls but are unable to

fold in presence of other carotenoids like β -carotene. Also, PSII assembly has been suggested to require the presence of carotenes while PSI is stable also in absence of carotenoids suggesting that, in a condition of carotenoid species disequilibrium the physical structure of at least one of the photosystems could be impaired. In our system, the sudden increase in phytoene levels (Figure 1.3B) could alter the protein stability of the PSII by steric hindrance competing with other carotenes for their binding site inside the complexes and triggering a series of signals that end up lowering the photosynthetic competence, not only at the level of energy transfer but also at the level of energy dissipation. A further confirmation of this is the major decrease in the fast-responding component of NPQ (qE) that requires the build-up of a proton gradient and relaxes within seconds to minutes. Usually, a decrease of pH in the thylakoid lumen is an immediate signal of excessive light that triggers the feedback regulation of light harvesting by qE. The development of qE is associated with the xanthophyll cycle, i.e., the reversible interconversion of zeaxanthin and violaxanthin. Under normal light, the enzyme zeaxanthin epoxidase converts zeaxanthin to violaxanthin. When light saturation is reached, however, the proton concentration within the thylakoid lumen increases and this induces the activation of the enzyme violaxanthin de-epoxidase that converts violaxanthin back to zeaxanthin via antheraxanthin. Zeaxanthin has a key role in qE because it directly quenches the singlet-excited chlorophyll and alters the sensitivity of qE to the pH changes. In conditions where no thylakoid membranes are present or where this proton build-up is impossible (e.g. when chloroplasts are converted into chromoplasts) the conversion of violaxanthin to zeaxanthin cannot happen and the fast-relaxing component qE decreases (Zhao et al., 2021)(Figure 1.3D, 1.3E).

In nature, chloroplasts might become competent for differentiation into chromoplasts without the need of a phytoene boost. In tomato and red pepper fruits, the chloroplasts of immature green fruit are much less photosynthetically active than those of leaves (Lado et al., 2015; Cocaliadis et al., 2014). Thus, tomato green fruit and other organs, tissues or/and developmental stages in which chloroplast identity is weak or non-existent (e.g., in dark-grown calli, tubers, or roots) might be considered as “naturally competent” to differentiate chromoplasts when carotenoid biosynthesis is upregulated. In agreement with this idea, overproduction of plant PSY enzymes resulted in chromoplast-like structures arising in green tomato fruit and non-photosynthetic *Arabidopsis* tissues but had no effect on leaves (Fraser et al., 2007; Lätari et al., 2015) unless previously conditioned by shutting down their photosynthetic capacity (Figure 1.7). Similarly, upregulation of OR triggers carotenoid overaccumulation and chromoplast differentiation in tomato fruit, potato tubers, cauliflower curds, or *Arabidopsis* calli, but not in the leaves of any of these plants (Lopez et al., 2008). OR has been shown to promote PSY activity and stability, and some OR mutants prevent carotenoid (particularly β -carotene) metabolism

(Welsch et al., 2018; Tzuri et al., 2015). Interestingly, OR does not appear to be required for *crtB*-mediated differentiation of leaf chloroplasts into chromoplasts (Figure 1.4A). We propose that the PSY-activating activity of OR is enough to trigger chromoplastogenesis in tissues with “naturally competent” plastids (i.e., those with minimal chloroplast identity) but not in those with strong photosynthetic activity, in which a much higher production of phytoene would be needed to interfere with photosynthetic functions. A corollary to this conclusion is that the level of phytoene reached through PSY or OR overexpression in leaves is not enough to trigger chromoplastogenesis. It is most likely that the tight regulation of plant PSY activity by OR and other factors could be bypassed by the bacterial *crtB* protein, hence allowing very high levels of phytoene to be produced in leaves (a tissue with an active MEP pathway providing metabolic precursors for carotenoids).

After the photosynthetic impairment provided by the phytoene boost in phase I of our system, enhanced expression of carotenoid-related genes likely contributes to activate the endogenous biosynthetic pathway in phase II. During this phase, carotenoid accumulation occurs concomitantly with the remodelling of the internal plastid structures, with both factors synergistically activating each other. Strikingly, in agroinfiltrated *N. benthamiana* leaves, this process takes place before chlorophylls start to degrade (Figure 1.3B). These results confirm that, especially in photosynthetically active leaves, chlorophyll breakdown and chromoplast differentiation are independent processes, as already shown in mutants such as tomato green flesh (*gf*), in which impairment of chlorophyll degradation during fruit ripening has no effect on the formation of chromoplast membranes and the accumulation of carotenoids (Cheung et al., 1993). They also show that and that the mere presence of chlorophyll does not necessarily involve photosynthetic competence. Also, it is known from the process of senescence (which involves the conversion from chloroplasts to gerontoplasts) that chlorophylls and carotenoids are degraded at different rates depending on the complexes where they are associated. The permanence of chlorophylls in *crtB*-overexpressing leaves might be due to a strong association of these pigments to some complexes like LHC proteins that would degrade over longer times. The new structures created following the disassembly of photosynthetic grana and thylakoids likely contribute to reaching high carotenoid levels by accommodating increasing amounts of carotenoids and by preventing their degradation (Sadali et al., 2019; Egea et al., 2010; Lado et al., 2015; Llorente et al., 2016). They might additionally enhance carotenoid production by stimulating the activity of endogenous carotenoid biosynthetic enzymes (including the same endogenous PSY), many of which are membrane-associated (Ruiz-Sola and Rodríguez-Concepción, 2012).

The build-up of carotenoids and the structural changes associated with the chloroplast-to-chromoplast transformation involve reorganization of the plastidial protein content but also a global reprogramming of nuclear gene expression and primary metabolism (Llorente et al., 2020). It is likely that implementing these changes (as well as others required to readapt plastid protein import and quality control mechanisms to chromoplast differentiation) relies on retrograde signals produced by differentiating plastids. Carotenoid degradation can generate signaling molecules that regulate many developmental processes in plants, including plastid development (Wang et al., 2019). The observation that *Arabidopsis ccd1/ccd4* mutants defective in carotenoid cleavage dioxygenase activity in the cytosol (via CCD1) and the plastids (via CCD4) were not affected in the *crtB*-dependent leaf phenotype suggests that signals independent of CCDs or carotenoids are responsible for eliciting the changes in nuclear gene expression and cell metabolism supporting chromoplast biogenesis (Figure 1.4A). It is possible that retrograde signals might derive from the changes occurring at the level of photosystems or the photosynthetic electron transport chain. Indeed, the exacerbation of the *crtB*-dependent yellow leaf phenotype and the enhanced accumulation of carotenoids in leaves of the *sal1* mutant support a role for the retrograde signal PAP, which accumulates after stress episodes causing impairment of plastid redox homeostasis (Figure 1.3B). This process, in fact, is important for natural chromoplast development in boxwood leaves, where the accumulation of red carotenoids (eschscholtzanthin, monoanhydroeschscholtzanthin, anhydroeschscholtzanthin) is a response to photoinhibitory conditions during winter acclimation and it is coupled with the operation of other photoprotective systems (Hormaetxe et al., 2004). Our experiments appear to exclude an eventual participation of endogenous hormone signals in the artificial, *crtB*-dependent chromoplastogenesis process. While transcriptomic analyses found similarities between our *crtB*-induced chromoplastogenesis in leaves and the naturally occurring chloroplast-to-chromoplast differentiation process during tomato fruit ripening (Llorente et al., 2020) hormones reported to control the process in tomato such as ethylene did not show any decisive impact on the *crtB*-mediated leaf chromoplast development. Our results showed that the three hormones impacting leaf chromoplast formation (gibberellins, auxins and strigolactones) were indirect regulators that altered the expression of the *crtB* transgene (Figure 1.5). However, other effects cannot be excluded. The exogenous application of GA₃ accelerated chromoplastogenesis in *N. benthamiana* leaves but it was reported to have a role in delaying fruit ripening of persimmon and colour change of citrus fruit peel (Goldschmidt, 1988) by contrasting chlorophyll degradation and carotenoids accumulation. But other works identified a carotenoid-associated protein in cucumber flowers named CHRC whose coding gene was early up-regulated by the exogenous application of GA₃ resulting in an increased level of carotenoids (Vishnevetsky

et al., 1997). CHRC belongs to the PAP/fibrillin family of proteins that are fundamental components of chromoplasts (Vishnevetsky et al., 1997; Bian et al., 2011). Also, gibberellins are reported to have a role in influencing chloroplasts division and number (Jiang et al., 2012) so the exogenous application of GA₃ could simply provide a bigger pool of chloroplasts to be converted into chromoplasts in *crtB*-overexpressing leaves. Opposite to gibberellins, treatment with auxins delay chromoplast development in leaves resulting in a decreased level of carotenoids. Auxins were identified as retardant agents in tomato fruit ripening, significantly reducing lycopene accumulation but leading to ABA-dependent regulation of ethylene synthesis (Su et al., 2015). The application of strigolactones also resulted in a delayed chromoplast development and a lower content of carotenoids in leaves. However, the observation that chromoplastogenesis was not impacted by inhibitors of endogenous hormone synthesis but correlated with exogenous hormone effects on *crtB* expression and phytoene accumulation led us to conclude that the observed effects of hormones are connected to the moment when phytoene reaches the necessary threshold to disrupt chloroplast identity.

In summary, we show that chromoplast differentiation only requires metabolic cues (i.e., enough phytoene and downstream carotenoid production). While our conclusions are based on a synthetic system (i.e., the expression of a bacterial gene in leaf cells), the similarity of the transcriptomic profiles between this process and fruit ripening (Llorente et al., 2020) strongly supports that this is a basic general mechanism for chloroplasts to become chromoplasts. In nature, however, developmental cues play a fundamental role by making chloroplasts competent (phase I) and by regulating the expression of carotenoid biosynthetic genes (phase II) (Figure 1.8). Signals produced by differentiating plastids are also hardwired to the process as they support the organellar transformation by reprogramming nuclear gene expression and whole-cell metabolism. Besides serving to successfully address a long-standing question in plant biology (i.e., plastid identity), the very simple and straightforward system that we describe here to induce chloroplast-to-chromoplast differentiation on demand is a powerful biotechnological tool that appears to work in every plant-tested so far (Majer et al., 2017). Thus, creating an organellar sink to improve both the production and the storage of carotenoids and maybe other plastidial phytonutrients in leaves and other chloroplast-containing tissues once their photosynthetic activity is dispensable (e.g., just before harvesting) should allow to boost the nutritional quality of green vegetables and forage crops. Our results with hormone application could also provide a way to modify the rate of this biofortification process. Increasing the speed of the system could be interesting to have high amounts of compounds of interest in a shorter time, hence saving production costs. On the other side, slowing down the process might allow to reach an

equilibrium between the photosynthetic requirements of the plant and the phytonutrient enrichment.

1.4. Materials and methods

1.4.1. Plant material and growth conditions

Nicotiana benthamiana plants used for the transient expression assays were grown in a greenhouse under standard long-day conditions (LD, 14 h light at $26 \pm 1^\circ\text{C}$ and 10 h dark at $21 \pm 1^\circ\text{C}$). *Arabidopsis thaliana* seeds (wild type and mutants) were surface sterilized by consecutively washing them in EtOH 70% + 0.5% Tween 20 for 5 minutes, EtOH 96% for 10 seconds and leaving them to dry under continuous sterile air flow. Sterile seeds were sown on solid 0.5 x Murashige and Skoog Medium (MS) without vitamins or sucrose. After stratification for 3 days at 4°C in the dark, plates were incubated in a climate-controlled growth chamber at 24°C and illuminated for 14 h with fluorescent white light at a photosynthetic photon flux density of $140 \mu\text{mol m}^{-2} \text{s}^{-1}$. 7–10-day seedlings were then transferred to soil and grown under standard short-day conditions (SD, 10 h light at $27 \pm 1^\circ\text{C}$ and 14 h dark at $22 \pm 1^\circ\text{C}$) to promote the development of a bigger leaf surface. Growth of double mutants *ccd1/ccd4* (Zhou et al., 2015) and *ator/ator1* (Schaub et al., 2018) both in the Col background, was facilitated by transferring them to low light ($40 \mu\text{mol photons m}^{-2} \text{s}^{-1}$) 7 days after germination while *sal1* mutant plants (also in Col background) were grown under standard short-day conditions. 4 weeks-old plants were used for the inoculation with the viral vector. Plant tissue of interest for further analysis was detached, frozen in liquid nitrogen, freeze-dried for 24 hours in a laboratory freeze drier (A 2-4 LD plus, CHRIST) and stored at -80°C until further analysis.

1.4.2. Gene constructs.

The different versions of crtB constructs (35S:crtB-pGWB405, 35S:(p)crtB-pGWB405, 35S:(p)crtB-GFP-pGWB405, 35S:GFP-crtB-pGWB506) and 35S:AtPSY-pGWB405 were already available in the lab and were generated as described by [Llorente et al., 2020](#). The pGTuMV-UK1 and TuMV-crtB vectors were kindly provided by prof. José Antonio-Daròs (IBMCP-Valencia, Spain) and generated as described by [Llorente et al., 2020](#).

1.4.3. Transient expression assays.

For transient expression studies using viral vectors, leaves of 4- to 6-week-old *Arabidopsis* plants were mechanically inoculated with crude extracts from frozen-stored infected plant tissue and collected upon the appearance of the yellowing phenotype as described previously (Majer et al., 2017). For agroinfiltration assays, the second or the third youngest leaves of 4-5-week-old *N. benthamiana* plants were infiltrated in the abaxial part of leaves. *A. tumefaciens* GV3101 strains were transformed with constructs of interest and grown on Luria-Bertani (LB) agar plates with the corresponding antibiotics at 28°C for 3 days. A single PCR-confirmed colony per construct was inoculated in 5 mL antibiotic-complemented LB media and incubated overnight at 28 °C in 300 rpm continuous agitation. 200 µL of the grown culture were then inoculated in 15 mL of LB media and incubated overnight at 28 °C in 300 rpm continuous agitation the day before performing agroinfiltration. OD₆₀₀ of each liquid culture was spectrophotometrically measured and then cultures were centrifuged at 4400 rpm for 10 min. Bacterial pellets were resuspended in infiltration buffer (10 mM MES pH 5.5-6, 10 mM MgCl₂, 150 µM acetosyringone) to reach a final OD₆₀₀ of 0.5. Cultures were mixed in identical proportions for the various combinations. Gene silencing was prevented by co-agroinfiltration with an agrobacterium strain EHA101 carrying the helper component protease (HcPro) of the watermelon mosaic virus (WMV) in plasmid HcProWMV-pGWB702 (a kind gift of Juan José López-Moya and Maria Luisa Domingo-Calap (CRAG-Barcelona, Spain)). For the inoculation of plants with the TuMV viral vector, *N. benthamiana* plants were infiltrated with suspensions cultures of agrobacterium carrying the assembled TuMV viral vector, following the procedure described before. 7 days after the infiltration tissue showing clear symptoms of infection was collected and frozen in liquid nitrogen. The same tissue was then ground and mixed with an inoculation buffer (TI: 50 mM K₃PO₄, 1% PVP-10, 1% PEG-6000, 10 mM β-mercapto-ethanol, pH 8). The resulting solution was mechanically inoculated on plant leaves with the support of silicon carbide as an abrasive agent. For growth regulators treatments, Gibberellic Acid (GA₃), Picloram (PIC) and GR24 were diluted in water and 0.05 % Tween 20 (to lower superficial tension and delay the evaporation of the solution) at the respective concentrations of 100 µM, 50 µM and 100 µM. The endogenous synthesis inhibitors Paclobutrazol (PAC), L-kynurenine (L-Kyn) and D2 were diluted at the same way at the respective concentrations of 10 µM, 500 µM and 100 µM. All the other compounds were diluted in the same way at the concentrations enlisted in *table 1*. All the substances were applied on the leaf surface with a fine paintbrush 24 h before agroinfiltration. For pharmacological treatments, norflurazon (NF) or diuron (DCMU) were diluted in water and 0.05 % Tween 20. The treatments with NF (2 µM) were performed by infiltration with a syringe

of leaf areas that had been agroinfiltrated with different constructs 24 h earlier. DCMU (10 μ M) was applied on the leaf surface with a fine paintbrush 24 h before agroinfiltration.

1.4.4. Transcript analyses

Total RNA was extracted from leaves with the Maxwell 16 LEV Plant RNA Kit (Promega) and quantified with a NanoDrop (Thermo Scientific) as described (Majer et al., 2017). For reverse transcription-quantitative PCR (RT-qPCR) analyses, the First Strand cDNA Synthesis Kit (Roche) was used to generate cDNA according to the manufacturer's instructions, with anchored oligo(dT)₁₈ primers and 500 ng of total RNA. Relative mRNA abundance was evaluated via quantitative PCR using LightCycler 480 SYBR Green I Master Mix (Roche) on a LightCycler 480 real-time PCR system (Roche). Primers used for the experiment are enlisted in *Appendix 1*.

1.4.5. Metabolite analyses

Leaf carotenoids and chlorophylls were extracted in 2 mL Eppendorf tubes from 4 mg of freeze-dried leaf tissue, using 375 μ L of methanol as extraction solvent and 25 μ L of 10% (w/v) solution of canthaxanthin in chlorophorm (Sigma) as internal standard. After vortexing for 10 s and lysing the tissue with 4 mm glass beads for 1 min at 30 Hz in a TissueLyser II (QIAGEN), 400 μ L of Tris-NaCl pH 7.5 were added followed by 1 min of TissueLyser. After this, samples were added with 800 μ L of chlorophorm and processed again with the TissueLyser for 1 min. Samples were then centrifuged for 5 min at 13,000 rpm and 4 °C. Organic phase (lower) was transferred in a new tube and evaporated for 1 h using a SpeedVac system (Eppendorf Concentrator plus). Extracted metabolites were then completely re-dissolved in 200 μ L of acetone by sonicating them for 15 seconds and filtered with 0.2 μ m filters into amber-coloured 2 mL glass vials. A 10- μ L aliquot of each sample was then injected onto an Agilent Technologies 1200 series HPLC system. A C₃₀ reverse-phase column (YMC Carotenoid, 250 \times 4.6 mm \times 3 μ m) was used, with three mobile phases consisting of methanol (A), water/methanol (20/80 v/v) containing 0.2% ammonium acetate (w/v) (B), and tert-methyl butyl ether (C). Metabolites were separated with the following gradient: 95% A, 5% B isocratically for 12 min, a step-up to 80% A, 5% B, 15% C at 12 min, followed by a linear gradient up to 30% A, 5% B, 65% C by 30 min. The flow rate was maintained at 1 ml/min. The HPLC equipment was coupled to a Photometric Diode Array (PDA) detector (Santa Clara, CA) allowing the detection of the full UV-visible absorption spectra of the different metabolites. Peak areas of chlorophylls at 650 nm, carotenoids at 472 nm (lycopene, lutein, β -carotene, violaxanthin, neoxanthin, canthaxanthin) or 290 nm (phytoene) were

determined using the *Agilent ChemStation* software. A fluorescence detector at 330 nm was used for tocopherols identification. The quantification of the compounds of interest was done by using a concentration curve built with a commercial standard (Sigma).

1.4.6. Photosynthetic measurements

Photosynthetic efficiencies were assessed by measuring chlorophyll a fluorescence with a MAXI-PAM fluorometer (Heinz Walz GmbH). Leaves were placed under the camera and effective quantum yield ($\Delta F/F_m'$) was measured as $(F_m' - F_s)/F_m'$, where F_m' and F_s are, respectively, the maximum and the minimum fluorescence of light exposed plants. The light intensity chosen was 21 PAR for all the leaf areas analysed (actinic light, $AL=2$) as the last value able to generate a response in the (p)crtB-infiltrated areas before having a null photosynthetic activity. Each value is the average result of three biological replicates and three different AOI for each replicate. NPQ was also measured using the MAXI-PAM unit. All recordings were performed every day at the same time slot, but the order of the samples was randomized to reduce the bias related to the length of the light stress recovery protocol. Plants were dark-adapted for 30 min before measurement and then submitted to a continuous 801 PAR light ($AL=17$) for 10 min. After this period plants were left recovering in darkness for 40 min. During the whole protocol, F_t was monitored and F_m' values were estimated with a saturating pulse (SAT) every 60 seconds. NPQ and its relative components qE , qZ and qI were calculated as described (Coate et al., 2013) with some modifications. Briefly: NPQ was calculated as $(F_m - F_{m_0})/F_m$, where F_m and F_{m_0} are the maximum fluorescence after the dark acclimation and after the light stress, respectively. The relative contributions of qE , qZ and qI to NPQ were estimated by monitoring NPQ relaxation kinetics in the dark: following the 10 min exposure to saturating light used to measure NPQ, leaves were left in darkness, and F_{m_0} was measured again after 10 and 40 min. The qE component of NPQ relaxes within 10 min of a leaf being placed in darkness such that NPQ persisting after 10 min in the dark consists of $qZ + qI$. The qZ component of NPQ relaxes within tens of minutes so that NPQ persisting after 40 min in the dark (when the F_t value is linear) consists of qI , which is either irreversible in the dark or requires several hours to relax. Consequently, $(qI + qZ)$ was calculated as $(F_m - F_{m_1})/F_{m_1}$, where F_{m_1} is the value of F_m measured after 10 min in the dark following NPQ measurement. qZ was calculated as $(F_m - F_{m_2})/F_{m_2}$, where F_{m_2} is the value of F_m measured after 40 min in the dark following measurement of NPQ_{max}. qE was calculated as $NPQ - (qI + qZ)$ and qI was calculated as $(qI + qZ) - qZ$. For the calculation of the de-epoxidation state (DES), agroinfiltrated leaf areas were exposed for 10 min to a continuous 801 PAR light ($AL=17$) in the MAXI-PAM unit, sampled under the same light and immediately frozen

before pigment extraction and quantification. The operation of the xanthophyll cycle, comprising the sequential de-epoxidation of the pigments violaxanthin (Vx) to antheraxanthin (Ax) and zeaxanthin (Zx) was followed by calculating DES as $(Zx+0.5 \times Ax)/(Zx+Ax+Vx)$, where Zx, Ax and Vx are the concentrations of the corresponding xanthophylls.

1.4.7. Protein extraction and analysis

For the quantification of (p)crtB-GFP protein a total protein extract was used. The detailed protocol is enlisted in the *chapter 3*.

Chapter 2

Chapter 2. Use of light to promote the crtB-mediated transition from chloroplast to chromoplasts.

Note: Part of the results shown in this chapter were published in Molina-Contreras et al., 2019 and Morelli et al., 2021. See Annex II and Annex III.

2.1. Introduction

Our previous results highlighted a fundamental role of photosynthesis in the crtB-mediated chloroplast-to-chromoplast transition in green leaves. Weakening photosynthesis was found to be necessary for *Nicotiana benthamiana* leaf chloroplasts to become competent for chromoplastogenesis. Treatment with chemicals but also exposure to certain environmental stimuli can be effective to downregulate photosynthesis in leaves and hence facilitate the differentiation of chromoplasts upon crtB production. Light is the most important environmental regulator of photosynthesis. Besides acting as the source of energy, it provides key environmental information. When growing in search for light, plants can experience continuous or occasional shading by other plants. Shading by nearby individuals can reduce photon supply and hence compromise photosynthetic activity and growth, a situation that can be considered particularly problematic in intensive cropping systems. To deal with the outcomes of mutual shading, plants have developed response mechanisms based on the perception of light quality, i.e., spectral information (Casal, 2013; Martínez-García et al., 2010). The preferential absorbance of red light (R) and reflection of far-red light (FR) by photosynthetic tissues results in a decreased ratio of R to FR (R:FR) when light is reflected from or filtered through green stems and leaves. Plants growing one next to the other will experience a moderate reduction of the R:FR even in the absence of actual shading. We refer to this condition as proximity shade: the amount of photons is not reduced but the plant interprets the low R:FR signal as the presence of nearby vegetation that might become competitors for light. When the plant is actually shaded (i.e., covered by another plant), the light intensity decreases and R is more drastically reduced compared to FR, resulting in a much lower R:FR. This situation is referred to as canopy shade, and it involves a more intense plant acclimation reaction (Roig-Villanova and Martínez-García, 2016) (Figure 2.1). The low R:FR signal is perceived by phytochromes, a family of photoreceptors that function in the R and FR range (660nm and 730nm, respectively). Phytochromes exist in a dynamic photoequilibrium between the ground state (Pr, a cytosolic inactive form) and the

signalling state (Pfr, the biologically active form mainly found in the nucleus). The Pr form preferentially absorbs R to form the Pfr state, which migrates to the nucleus to regulate gene expression by interacting with specific transcription factors. Pfr preferentially absorb FR to be converted back to Pr and migrate to the cytosol. Under sunlight (high R:FR), the active Pfr is the most abundant, whereas exposure to low R:FR results in its inactivation by conversion to the inactive Pr form the nucleus (Leivar and Monte, 2014).

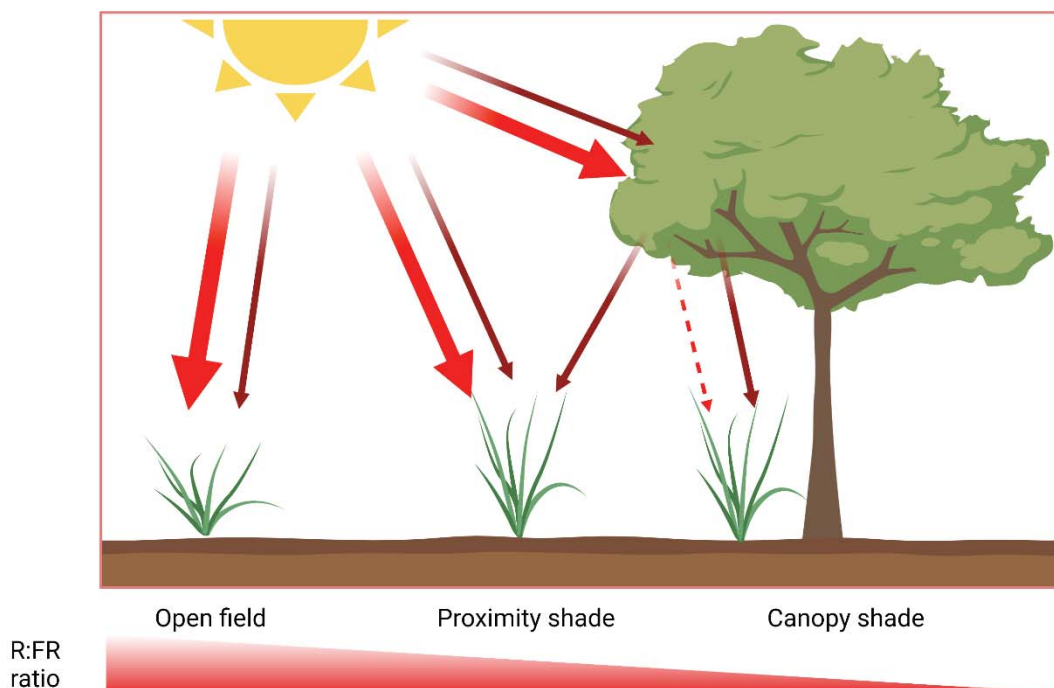


Figure 2.1. Schematic representation of the various shade conditions to which a plant can be subjected. In open field plants are exposed to light with more red (R) than far-red (FR), i.e., of high R:FR. When plants grow near each other the R:FR decreases because of a supplement of FR radiation that is reflected by neighbour plants (proximity shade). When plants are covered by a taller plant the R:FR utterly decreases because, R, but not FR, is absorbed by the competitor plant (canopy shade).

Plants growing in ecosystems where access to light is restricted (e.g., in forest understories) show a shade-tolerant habit by adapting their light capture and utilization systems to low light intensity conditions. By contrast, plants growing in open habitats are shade-avoiders (also referred to as shade-intolerant or sun-loving). In shade-avoider plant species, such as *Arabidopsis thaliana* and most sun-loving crops, perception of the low R:FR signal by the phytochromes activates a signalling pathway that eventually triggers a set of responses known as the shade avoidance syndrome (SAS). The most prominent phenotype following exposure to low R:FR is elongation (e.g., of seedling hypocotyl, leaf petiole and stem internode tissues), intended to

overgrow neighbouring competitors and outcompete them in the access to light. If the neighbouring individuals overgrow and eventually shade the plant, the consequent reduction in light quantity (i.e., in the amount of radiation available for photosynthesis) results in additional and stronger SAS responses such as reduced leaf size, attenuated defence mechanisms and early flowering (Roig-Villanova and Martínez-García, 2016). The most extensively studied SAS response by far is hypocotyl elongation in *Arabidopsis*. In this species, low R:FR inactivates phytochrome B (phyB), releasing basic helix-loop-helix (bHLH) transcription factors of the PHYTOCHROME INTERACTING FACTORS (PIFs) subfamily that can then regulate gene expression and promote elongation growth. This elongation response is also repressed by negative SAS regulators such as the basic leucine zipper (bZIP) transcription factor ELONGATED HYPOCOTYL 5 (HY5), amongst many others (Cifuentes-Esquivel et al., 2013; Ciolfi et al., 2013). Biological activity of these transcription factors can be modulated by additional components of the SAS regulatory network such as LONG HYPOCOTYL IN FAR-RED 1 (HFR1, which binds PIFs to prevent their binding to target genes) and PHYTOCHROME A (phyA, which gets stabilized in shade and then promotes HY5 accumulation) (Ciolfi et al., 2013; Martínez-García et al., 2014; Yang et al., 2018) (Figure 2.2). Both HFR1 and phyA hence act as additional SAS repressors that were recently found to be instrumental for the adaptation to shade (Molina-Contreras et al., 2019; Paulišić et al., 2021). (Figure 2.2).

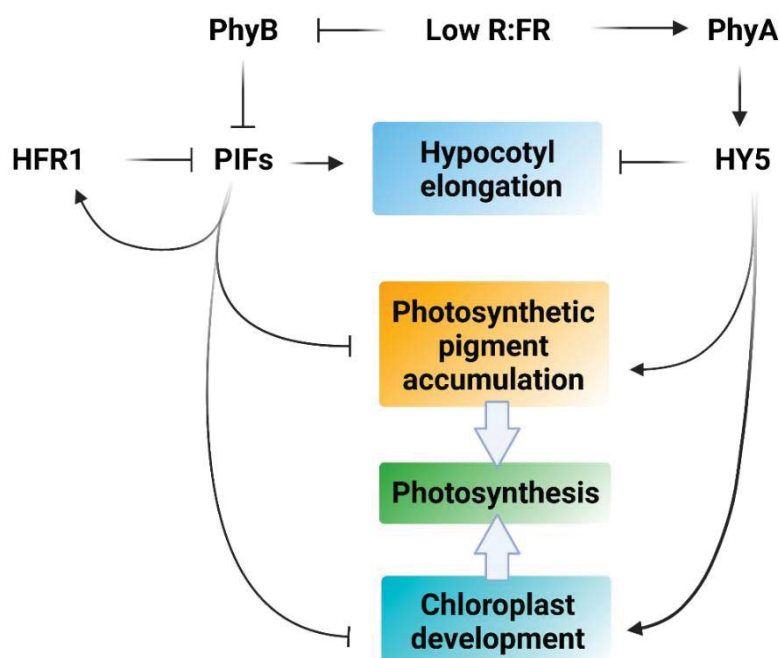


Figure 2.2. Schematic representation of the main molecular factors controlling the response to low R:FR. The decrease in the ratio of R:FR has effect on transcription factors such as PIFs and HY5 that regulate photosynthetic pigment accumulation and chloroplast development which likely ends up impacting photosynthesis.

Besides elongation, another typical SAS response involves the decrease in photosynthetic pigments levels (Roig-Villanova et al. 2007; Molina-Contreras et al., 2019; Cagnola et al., 2012; Bou-Torrent et al., 2015). The light-induced up-regulation of transcripts for carotenoid and chlorophyll biosynthetic enzymes during photomorphogenesis is mainly mediated by phytochromes, PIFs of the so-called PIF quartet (PIFq, encompassing PIF1, PIF3, PIF4 and PIF5) and HY5 (Toledo-Ortiz et al., 2010; Bou-Torrent et al., 2015; Ortiz-Alcaide et al., 2019). These factors also regulate chloroplast development (Leivar et al. 2012, Leivar and Monte 2014, Toledo-Ortiz et al. 2010) (Figure 2.2)

The shade-tolerant *Cardamine hirsuta*, a close relative of *Arabidopsis*, does not elongate when exposed to low R:FR unless the function of phyA or HFR₁ is genetically lost in mutant plants (Molina-Contreras et al., 2019, Paulišić et al., 2021). Differences between shade-avoider and shade-tolerant species are not restricted to changes in elongation after exposure to low R:FR. *Arabidopsis* and *Cardamine* also show a differential response to low R:FR in terms of photosynthetic pigment accumulation. Chlorophyll and carotenoid levels drop about 20 % in *Arabidopsis* plants grown under low R:FR conditions, whereas the decrease is attenuated in *Cardamine* plants (Molina-Contreras et al., 2019). Photoacclimation also varies in these two plant categories: Photoacclimation is defined as the ability of green organisms to respond with specific phenotypic adjustments to changes in the incident light. The shade-avoider *Arabidopsis* showed a lower capacity to acclimate to reduced photosynthetically active radiation (low PAR) but a higher capacity to acclimate to intense light (high PAR) compared to the shade-tolerant *Cardamine* (Molina-Contreras et al., 2019). This physiological behaviour is like the one described for shade-avoider and shade-tolerant ecotypes of *Tradescantia spp.* (Benkov et al., 2019). Whether photosynthetic capacity and/or chloroplast ultrastructure is differentially impacted by low R:FR in shade-avoider and shade-tolerant plants remains unknown.

2.1.1. An enrichment in FR also impacts the efficiency of photosynthesis.

The photosynthetic apparatus of higher plants is optimized to harvest sunlight and exploits its energy to generate an electron flow from water to NADPH, which is then used to produce organic molecules from CO₂. This electron transport involves the coordinated activity of several membrane embedded complexes (PSII, the cytochrome b6f and PSI) that are functionally connected by diffusible electron carriers, such as plastoquinone (PQ), which ensures the electron transport between PSII and cytochrome b6f). While PSII and PSI work electrochemically in series, the reaction centers differ in their absorption properties and use light quanta of different wavelengths. Excitation imbalances between the two photosystems can disturb both the redox chemistry in the transport chain and its coordination with CO₂ fixation. FR (700-770 nm)

preferentially energizes PSI and it thereby oxidizes the intersystem electron carriers, including PQ (Zhen and van Iersel, 2017). Therefore, an excess of FR can also impair photosynthesis by disrupting the energetic equilibrium between the two photosystems. Interference with the redox state of the PQ pool is expected to impact the phytoene desaturation steps that require oxidized PQ as an electron carrier (Ruiz-Sola and Rodriguez-Concepcion, 2012). With all this information available we explored how different light regimes impacted photosynthesis and hence crtB-mediated chromoplastogenesis in the leaves of different plants with the final goal of finding optimal conditions to improve the leaf carotenoid biofortification process with minimal negative effects on plant fitness and to better characterize the role of light in chromoplast development.

2.2. Results.

2.2.1. *N. benthamiana* plants exposed to FR show reduced photosynthetic pigment content and activity.

Exposure to reduced R:FR leads to reduced photosynthetic pigment content, particularly in shade avoider species such as *Arabidopsis* (Roig-Villanova et al. 2007, Cagnola et al., 2012, Bou-Torrent et al., 2015, Molina-Contreras et al., 2019). We hypothesized that this effect might eventually result in a photosynthetic impairment and hence could be used as an optimal alternative to the pharmacological inhibition of photosynthesis to improve crtB-mediated chromoplast development. To test this hypothesis, 3-4 weeks old *N. benthamiana* plants growing in the greenhouse were transferred for 4 days to chambers equipped with either white light (W, high R:FR) or W supplemented with FR (W+FR, low R:FR). Plants exposed to W+FR (herein referred to as simulated shade) displayed reduced accumulation of total chlorophylls and carotenoids compared to controls grown under W. These results were also evident at the naked eye as W+FR plants showed paler leaves compared to W plants (Figure 2.3A, C). Stem length was also significantly higher in *N. benthamiana* plants grown under W+FR light (Figure 2.3D). These results are consistent with the conclusion that *N. benthamiana* is a shade avoider plant that responds to low R:FR by elongating and reducing the accumulation of photosynthetic pigments, like *Arabidopsis*. Most interestingly, the decreased accumulation of chlorophylls and carotenoids in *N. benthamiana* plants irradiated with simulated shade correlated with a significantly lower maximum quantum yield (F_v/F_m) and effective quantum yield (ϕ_{PSII}), suggesting that exposure to low R:FR can be used to lower photosynthetic efficiency in plants (Figure 2.3C). The next set of experiments were designed to better understand how shade impacts photosynthesis by

exploiting genetic diversity in the response to shade generated by nature (i.e., different species and ecotypes) and in the lab (i.e., *Arabidopsis* and *Cardamine* mutants).

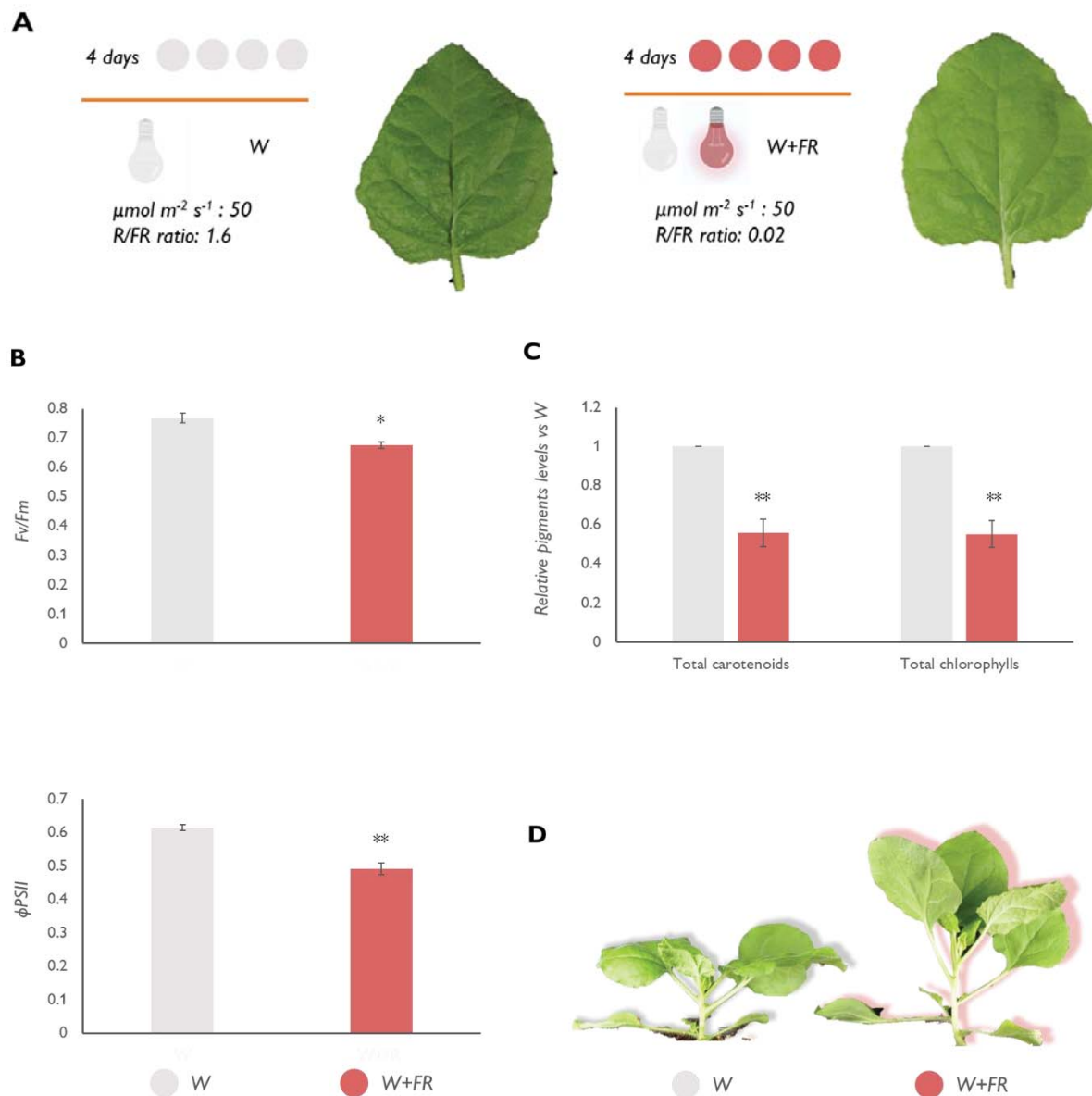


Figure 2.3. *Nicotiana benthamiana* reacts to shade signal lowering its pigment content and photosynthetic competence. (A) schematic representation of the experimental setting. Plants were exposed for 4 days to either white light or white light supplemented with FR. (B) Maximum quantum yield and effective quantum yield calculated after the 4 days of treatment. Plots show the mean and SD of 6 measures for each treatment (n=6). (C) Relative levels of carotenoids and chlorophylls in plants grown under W or W+FR. Plots shows means and SD of 3 plants for experiment. Values are relativised to the amount in plant grown under W. (D) Picture showing the different phenotypes developed by plants grown under W or FR. Asterisks mark statistically significant changes (t-test * $P < 0.05$, ** $P < 0.01$) in plant exposed to FR relative to W.

2.2.2. Different Brassicaceae species present divergent photoacclimation responses

To explore the effect of shade on photosynthesis we initially screen plants of the Brassicaceae family with the aim to classify them as shade avoider or shade tolerant based on their photoacclimation response to different intensities of light. It was previously shown that, compared to sun-loving *Arabidopsis* (At), shade-tolerant *Cardamine* (Ch) exhibits a better ability to maintain photosynthesis after transfer to low PAR but a stronger chlorophyll loss when light intensity increases (Molina-Contreras et al, 2019). To better characterize the photoacclimation responses of these two Brassicaceae species, both At and Ch were germinated and grown for 7 days under control PAR conditions (W_{20} , 20-24 $\mu\text{mol m}^{-2} \text{s}^{-1}$) and then transferred to either lower PAR (W_4 , 4 $\mu\text{mol m}^{-2} \text{s}^{-1}$) or higher PAR (W_{200} , 200 $\mu\text{mol m}^{-2} \text{s}^{-1}$) for up to 7 more days. Light curve analysis at day 3 after the transfer already showed clearly opposite responses of At and Ch (i.e., a better photosynthetic activity of Ch compared to At when transferred to W_4 and a better activity of At compared to Ch when transferred to W_{200}). Derived parameters such as maximum electron transport rate (ETR_m) and photosynthetic rate in light-limited region of the light curve (α) also illustrated that At performed better than Ch after transfer to higher light (W_{200}) but worst after transfer to lower light (W_4). In favourable light conditions, plants tend to maintain stable values of electron transport rate, without reaching the saturation point (i.e., the plateau typically reached immediately before of photoinhibitory processes) (Figure 2.4A, 2.4B). Other photosynthetic parameters such as maximum and effective quantum efficiency of PSII (F_v/F_m and ϕPSII , respectively) also showed differences between At and Ch at day 3 after transfer, but these differences became clearer at longer times of exposure to either W_{200} or W_4 . Specifically, F_v/F_m values were lower in Ch than in At after transfer to higher light, while the opposite was observed when transferred to lower light. A similar trend was observed in the case of ϕPSII (Figure 2.4C). These results together indicate that Ch tolerates better the transfer to lower PAR (consistent with Ch being more tolerant to shade), while an increase in light irradiance compromises photosynthetic efficiency in Ch more than in shade-avoider At. Based on these results, we used light curve analysis at day 3 or earlier to estimate photoacclimation to lower PAR and F_v/F_m measurements at day 7 to estimate photoacclimation to higher PAR.

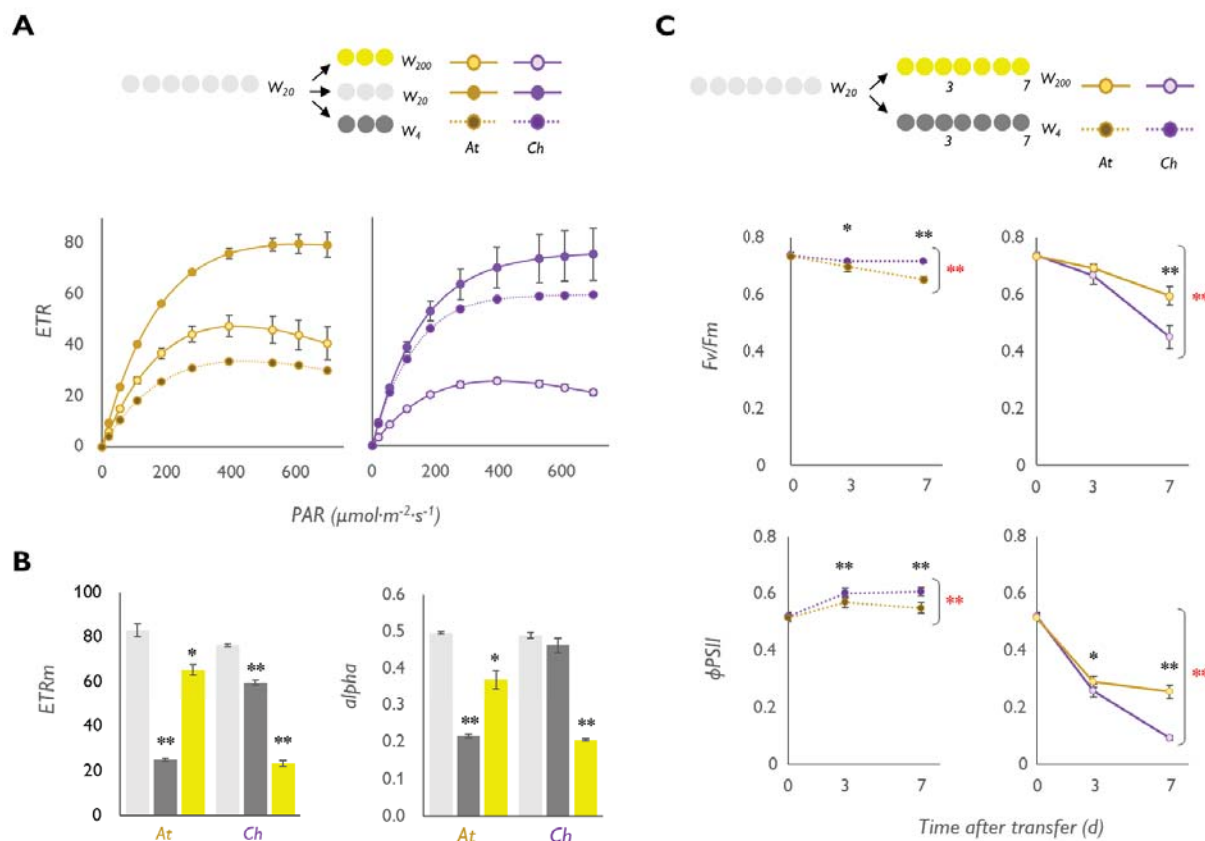


Figure 2.4. *Arabidopsis thaliana* and *Cardamine hirsuta* show antagonistic photoacclimation responses to high and low PAR. (A) Light curves of *Arabidopsis* (At) and *Cardamine* (Ch) seedlings germinated and grown under 20 $\mu\text{mol}\cdot\text{m}^{-2}\cdot\text{s}^{-1}$ PAR (W_{20}) for 7 days and then either kept under W_{20} or transferred to either 200 (W_{200}) or 4 (W_4) $\mu\text{mol}\cdot\text{m}^{-2}\cdot\text{s}^{-1}$ PAR for 3 more days. Values represent the mean and standard error of $n=3$ plants for treatment. (B) Maximum relative electron transport rate (ETRm) and photosynthetic rate in the light-limited region of the light curve (alpha) calculated from the curves shown in (A). Asterisks mark statistically significant changes (t-test * $P < 0.05$, ** $P < 0.01$) in seedlings exposed to W_4 or W_{200} relative to W_{20} . (C) Maximum photochemical efficiency of PSII in the dark-adapted state (Fv/Fm) and effective quantum yield calculated at growth light (ϕPSII) of seedlings germinated and grown for 7 days under W_{20} and then transferred to either W_{200} or W_4 for more 7 days. Data were taken at 0, 3 and 7 days after the transfer. Values are mean and standard error of $n=7$ seedlings per treatment. Two-way ANOVA showed that photosynthetic performance under W_4 is significantly increased (** $P < 0.01$) in *Cardamine* than *Arabidopsis* over time while, in seedlings grown under W_{200} , Fv/Fm and ϕPSII are significantly higher in *Arabidopsis* than *Cardamine*.

Besides At and Ch, the Brassicaceae family (mustards) includes many food crops (e.g., cauliflower, broccoli, radish, cabbage, kale, and similar green leafy vegetables) and a diversity of wild species from forested and open habitats. As a first step to explore the possible connection between low PAR and low R:FR responses, we analysed photoacclimation and hypocotyl elongation in six different Brassicaceae species or accessions, including At and Ch as controls. The selected wild mustards were *Arabis alpina* (Aa), two accessions of *Capsella bursa-pastoris*, Freiburg-1 (Cb-F) and Strasbourg-1 (Cb-S), *Capsella rubella* (Cr), *Nasturtium officinale* (No), and *Sisymbrium irio* (Si). Initially, we aimed to classify them as shade-avoider or shade-tolerant based on photoacclimation responses. After germination and growth for 7 days under W, seedlings were either kept under control W_{20} or transferred to lower light (W_4). Light curve analyses at day 1 after the transfer already showed differential responses that served to classify the accessions in two groups. Like the shade-avoider At, seedlings of Cb-F, Cb-S and Cr showed a lowering of the curve under W_4 conditions, whereas those of Aa, No and Si behaved as the shade-tolerant Ch and showed virtually identical light curves under W_{20} and W_4 (Figure 2.5A). ETR_m and α values also illustrated that the W_4 treatment led to decreased photosynthetic performance in At, Cb-F, Cb-S and Cr but not in Ch, Aa, No and Si (Figure 2.5B). We next studied photoacclimation to increased irradiation quantifying F_v/F_m before or after transferring 7-day-old W_{20} -grown seedlings to W_{200} for 7 additional days. Again, At grouped together with the two accessions of Cb and with Cr as they acclimated much better to high PAR compared to the group formed by Ch, Aa, No and Si. Together, these photoacclimation results led to classify the former group as shade-avoiders, and the latter as shade-tolerant species (Figure 2.5C). This classification, however, only partially correlated with the hypocotyl elongation response typically used to classify plants as shade tolerant or shade avoiders ([Morelli et al., 2021](#)). Nonetheless, accessions classified as shade-avoider exhibit a range of clear elongation responses to low R:FR whereas plant species with a shade-tolerant photoacclimation responses display either null or mild hypocotyl elongation when exposed to low R:FR.

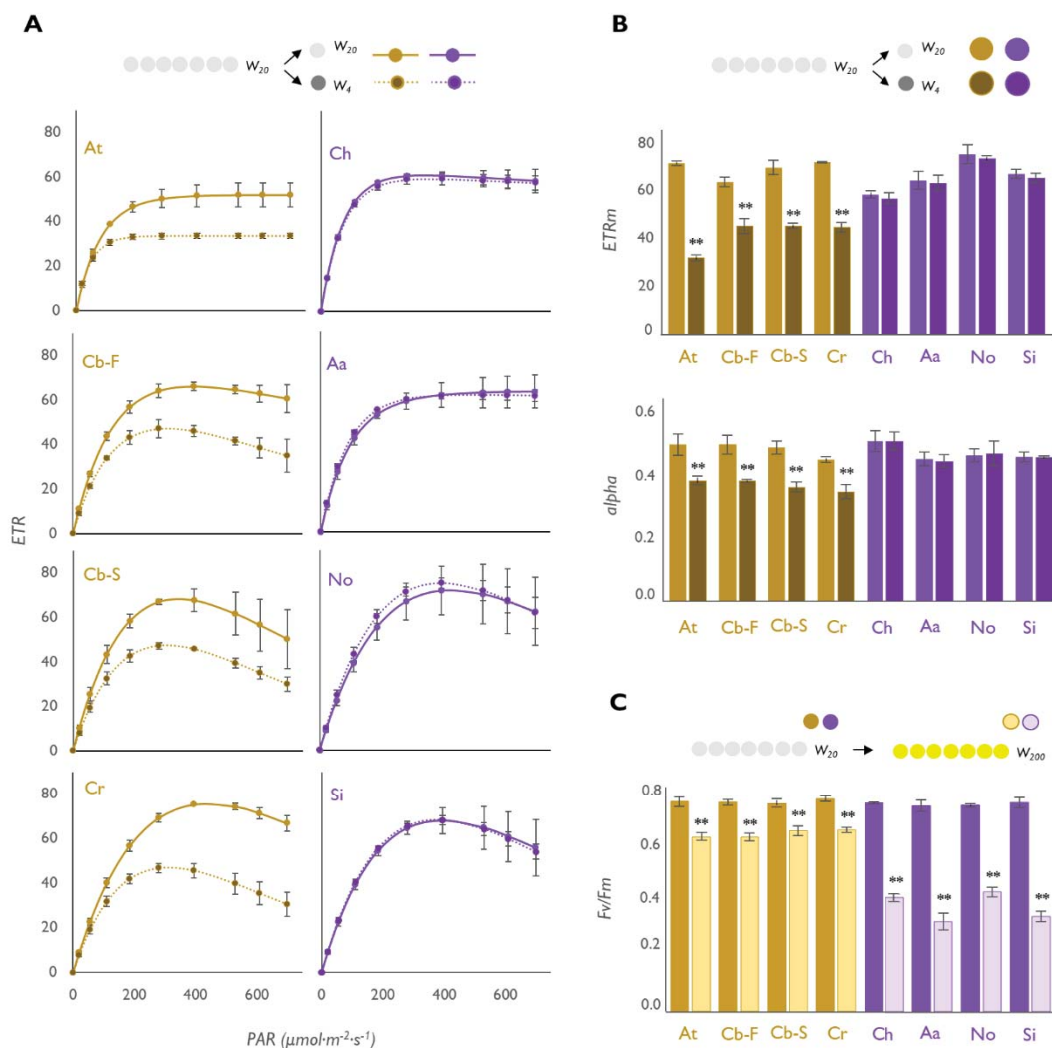


Figure 2.5. Brassicaceae plants can be grouped with either *Arabidopsis thaliana* or *Cardamine hirsuta* based on their photoacclimation responses. (A) Light curves of *Arabidopsis thaliana* (At), *Capsella bursa-pastoris* (Cb-F and Cb-S), *Capsella rubella* (Cr), *Cardamine hirsuta* (Ch), *Arabis alpina* (Aa), *Nasturtium officinale* (No), and *Sisymbrium imbrioides* (Si) seedlings germinated and grown under $20 \mu\text{mol}\cdot\text{m}^{-2}\cdot\text{s}^{-1}$ PAR (W_{20}) for 7 days and then either kept under W_{20} or transferred to $4 \mu\text{mol}\cdot\text{m}^{-2}\cdot\text{s}^{-1}$ PAR (W_4) for 1 more day. Values represent the mean and standard error of $n=3$ plants for treatment. (B) ETRm and alpha values calculated from the curves shown in (A). (C) Fv/Fm values of seedlings grown for 7 days under W_{20} and then transferred to $200 \mu\text{mol}\cdot\text{m}^{-2}\cdot\text{s}^{-1}$ PAR (W_{200}) for 7 more days. Mean and standard error of $n=9$ seedlings per treatment are represented. Asterisks mark statistically significant changes (t -test $** P<0.01$) in seedlings exposed to W_4 or W_{200} relative to W_{20}

2.2.3. Genetic impairment of low R:FR perception impacts elongation and photosynthetic responses to shade but not photoacclimation capacity.

The shade-avoider or shade-tolerant elongation phenotype in response to low R:FR can be reversed by manipulating the levels of specific SAS regulators. Previous results have shown that At lines overexpressing HY5 (*At-HY5ox*) display an attenuated hypocotyl response to low R:FR

(Ortiz-Alcaide et al., 2019), whereas a similar but weaker response was observed in a quadruple mutant defective in all members of the photolabile PIF quartet (*At-pifq*) (Bou-Torrent et al., 2015). Despite the different degrees of elongation response to low R:FR, we found that these two lines showed photoacclimation responses to lower PAR very similar to those of wild-type (*At-WT*) controls. In fact, both light curves and ETRm values were almost identical in *At-WT* plants and mutants hyposensitive to low R:FR (*At-HY5ox* and *At-pifq*). In the case of *C. hirsuta*, lines deficient in phyA (*Ch-sis1*) or HFR1 (*Ch-hfr1*) gain the ability to elongate when exposed to low R:FR (Molina-Contreras et al., 2019; Paulišić et al., 2021). In contrast to the shade-hyposensitive *At* mutants, the hypersensitive *Ch* mutant lines appeared to gain a partial shade-avoider phenotype in terms of photoacclimation to low PAR, as lower values of light curves and ETRm were observed under W_4 compared to W_{20} . However, photoacclimation to increased PAR (W_{200}) estimated from Fv/Fm values and from chlorophyll levels (Molina-Contreras et al., 2019) was similar for *Ch-WT*, *Ch-sis1* and *Ch-hfr1* plants (Figure 2.6A, B, C). We therefore concluded that manipulation of the plant ability to elongate in response to proximity shade hardly impacts their photoacclimation capacity, at least when plants are growing in the absence of the low R:FR signal.

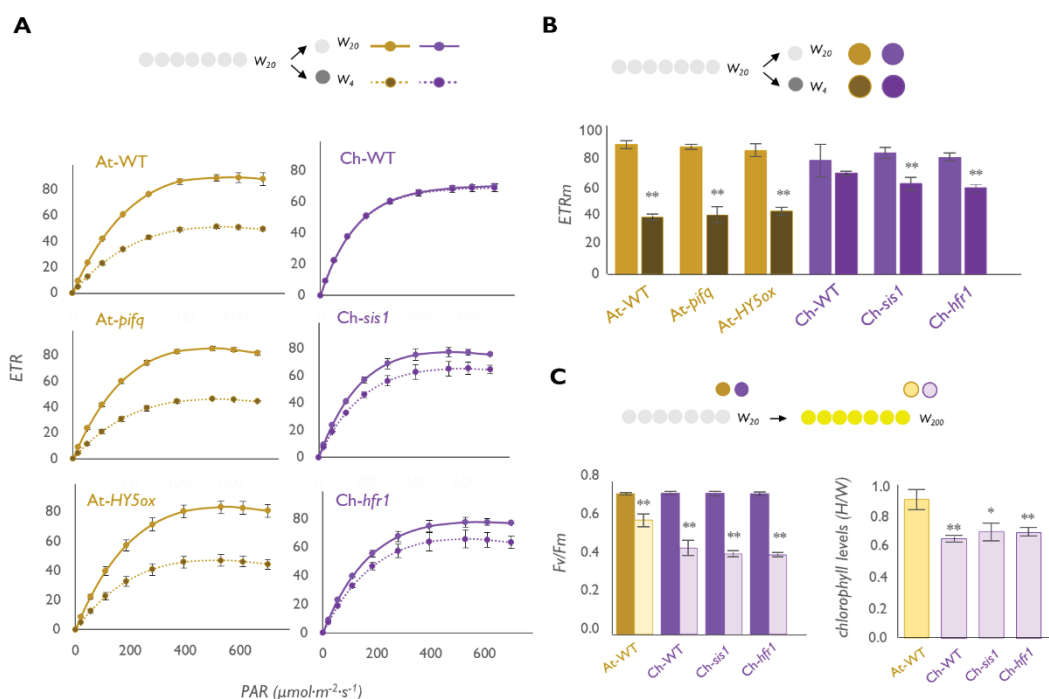
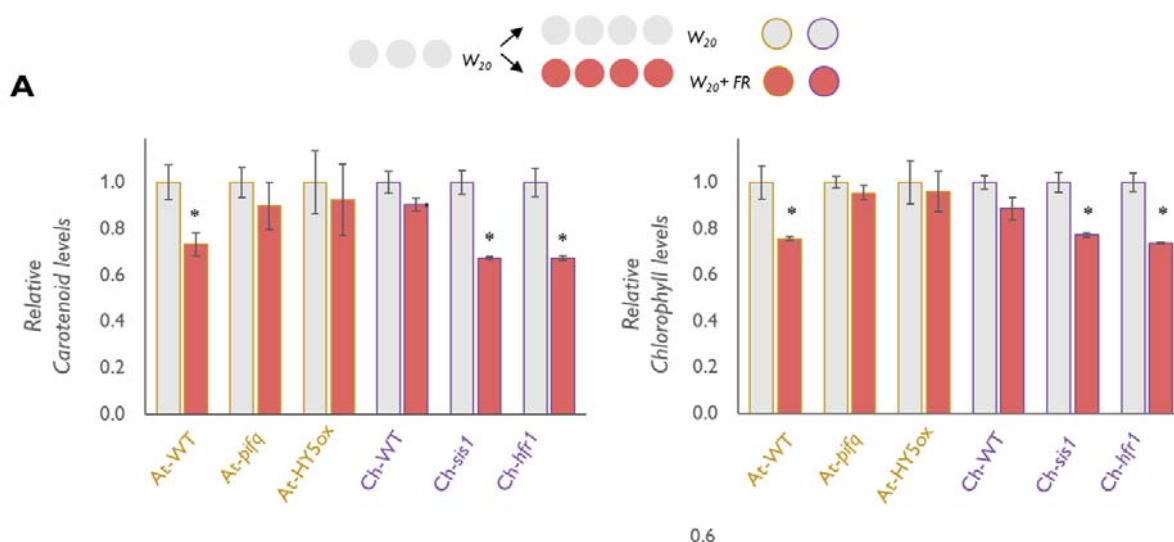


Figure 2.6. Mutations that alter sensitivity to low R:FR do not impact photoacclimation responses. (A) Light curves of *Arabidopsis* and *Cardamine* wild-type and mutant seedlings germinated and grown under $20 \mu\text{mol}\cdot\text{m}^{-2}\cdot\text{s}^{-1}$ PAR (W_{20}) for 7 days and then either kept under W_{20} or transferred to $4 \mu\text{mol}\cdot\text{m}^{-2}\cdot\text{s}^{-1}$ PAR (W_4) for 1 more day. Values represent the mean and standard error of $n=3$ plants for treatment. (B) ETRm values calculated from the curves shown in (A). (C) Fv/Fm values and HPLC-determined chlorophyll levels of seedlings grown for 7 days under W_{20} and then transferred to $200 \mu\text{mol}\cdot\text{m}^{-2}\cdot\text{s}^{-1}$ PAR (W_{200}) for 7 more days. Mean and standard error of $n=9$ seedlings (Fv/Fm) or $n=3$

independent pools (HPLC) per treatment are represented. Asterisks mark statistically significant changes (t -test, * $P < 0.05$, ** $P < 0.01$) in seedlings exposed to W_4 or W_{200} relative to W_{20}

When grown under $W+FR$, however, *Cardamine* hypersensitive mutants *Ch-sis1* and *Ch-hfr1* displayed a stronger reduction in photosynthetic pigment contents compared to *Ch-WT* while *Arabidopsis* hyposensitive mutants *At-pifq* and *At-HY5ox* showed an attenuated reduction of pigment contents compared to *At-WT* (Figure 2.7A). To test whether the observed decreases in photosynthetic pigment levels driven by simulated shade exposure might affect photosynthetic activity in *At* and *Ch* lines like that shown in *N. benthamiana* (Figure 2.3), we next measured F_v/F_m and $\phi PSII$ in seedlings grown either under W_{20} or under $W_{20}+FR$. Indeed, low R:FR was found to result in decreased photosynthetic activity in the lines with strong pigment loss responses independently on the species (*At-WT*, *Ch-sis1* and *Ch-hfr1*) (Figure 2.7A, B, C). ETRm and α parameters also tended to be lower in $W+FR$ -exposed *At-WT*, *Ch-sis1* and *Ch-hfr1* seedlings compared to W controls (Figure 2.7C). The effect of low R:FR on photosynthesis was much less dramatic in the rest of the lines (*At-pifq*, *At-HY5ox* and *Ch-WT*), which consistently displayed a reduced impact of $W_{20}+FR$ exposure on their photosynthetic pigment levels.



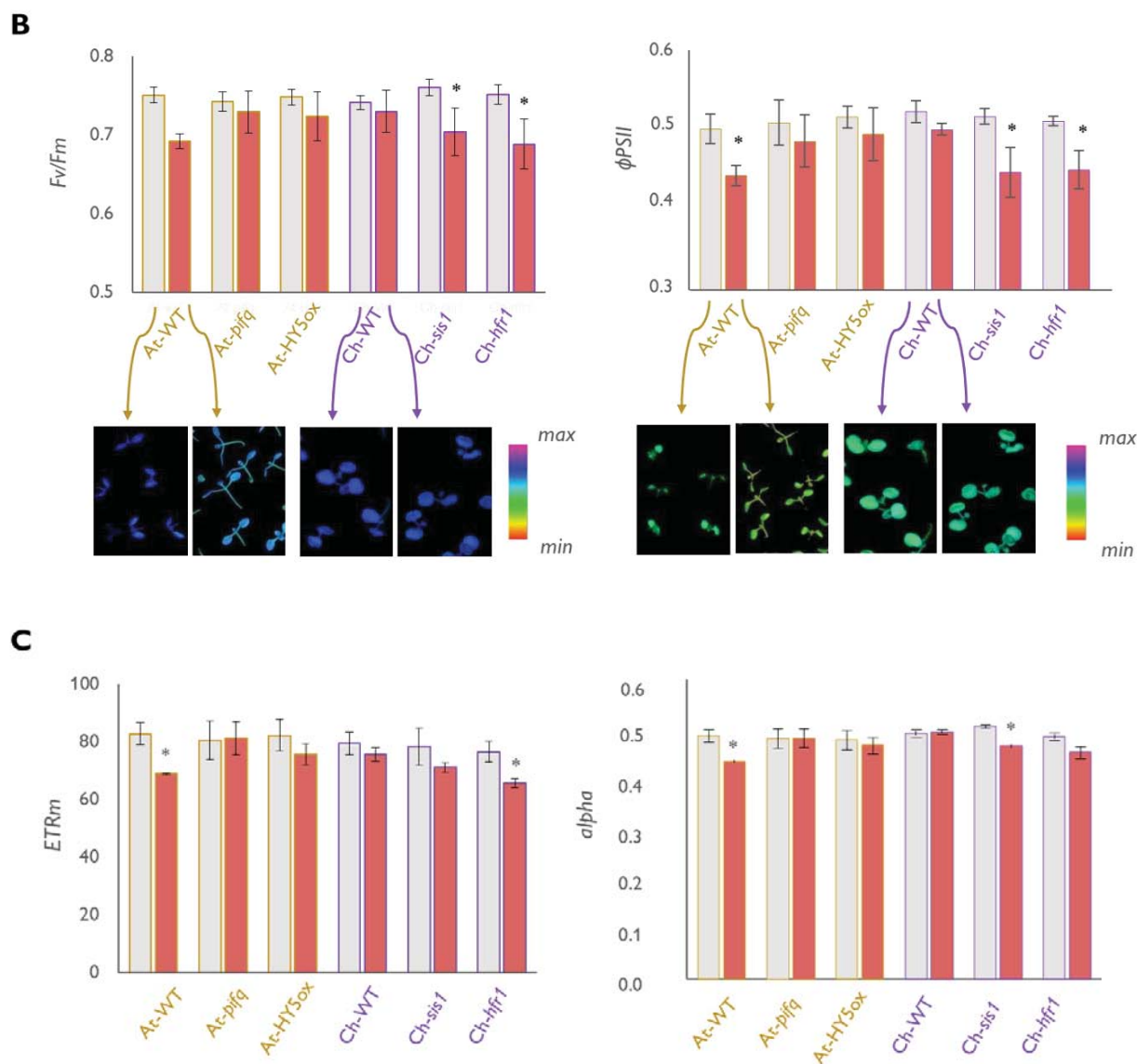


Figure 2.7: Activation of low R:FR signaling reduces photosynthetic activity. (A) Relative carotenoid and chlorophyll level, (B) Fv/Fm and ϕ PSII values and (C) ETRm and alpha of seedlings germinated and grown as indicated at the top of the section. Pictures in panel B show false-Colour images of the corresponding parameter in wild-type seedlings. Mean and standard error of $n=9$ seedlings per treatment are represented. Asterisks mark statistically significant changes in $W_{20}+FR$ relative to W_{20} (t-test, * $P<0.05$).

2.2.4. Exposure of shade-avoider plants to low R:FR improves their photoacclimation to low PAR.

The observation that exposure of low R:FR caused a decreased in photosynthetic activity of At-WT seedlings and shade-hypersensitive Ch mutants prompted us to analyse whether this light signal may also cause changes in gene expression and/or chloroplast ultrastructure. Proximity shade signals have also found to impact photosynthesis at the level of gene expression. Analyses of low R:FR-triggered transcriptomic changes showed reduced levels of transcripts encoding

photosynthesis-related proteins (e.g., enzymes involved in chlorophyll and carotenoid biosynthesis, components of the photosynthetic apparatus, and/or members of the carbon fixation process) in several species, including alfalfa, maize, tomato, and *Arabidopsis* (Lorenzo et al., 2019; Cagnola et al., 2012; Leivar et al., 2012). Interestingly, we observed that the changes in the expression of photosynthesis-related genes triggered by low R:FR are attenuated in the *At-pifq* mutant compared to *At-WT* seedlings (**Figure 2.8**). This is particularly evident in the case of low R:FR-repressed photosynthetic genes, suggesting that the PIF-mediated regulation of gene expression in response to low R:FR contributes for the observed changes in photosynthesis.

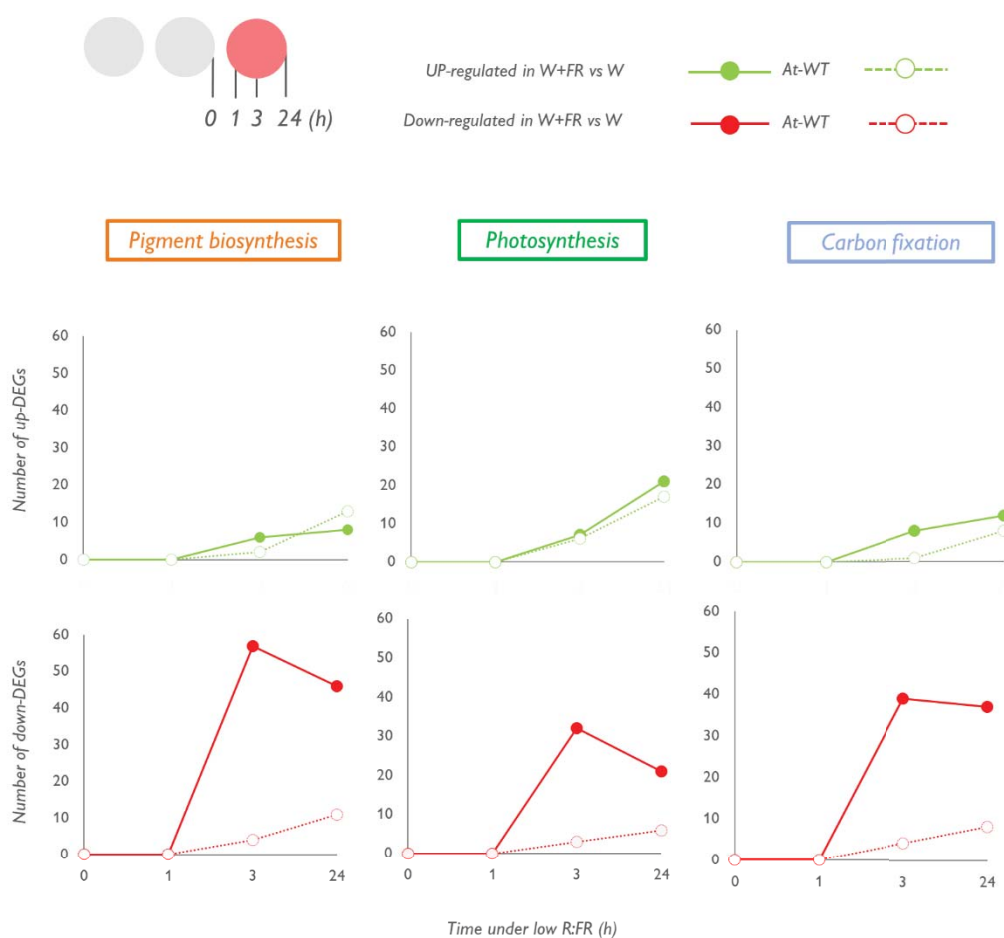


Figure 2.8. Exposure to low R:FR triggers changes in photosynthetic gene expression that are attenuated in the hypersensitive *At-pifq* mutant. Data were extracted from a publicly available experiment (Leivar et al., 2012). The data sets used were originally filtered for statistical significance ($P < 0.05$). *At-WT* and *At-pifq* lines were germinated and grown under $20 \mu\text{mol}\cdot\text{m}^{-2}\cdot\text{s}^{-1}$ PAR white light (W_{20}) for 2 days and exposed to low R:FR ($W_{20}+\text{FR}$) for 0, 1, 3 or 24 h. Plots represent the number of differentially expressed genes (DEGs) either up-regulated or down-regulated in $W_{20}+\text{FR}$ vs. W_{20} that are involved in photosynthetic pigment biosynthesis (KEGG pathways *atho0906* and *atho0860*), photosynthesis (*atho0195* and *atho0196*), and carbon fixation (*atho0710*).

Next, we investigated whether low R:FR exposure also resulted in changes in chloroplast ultrastructure. Cotyledons from At-WT seedlings germinated and grown for 2 days under W_{20} and then either kept in W_{20} or transferred to W_{20} +FR for 5 additional days were collected and used for transmission electron microscopy (TEM). Chloroplasts from W +FR samples were found to exhibit larger grana stacks and contain less and smaller plastoglobules (PG) compared to W -grown controls (Figure 2.9). Interestingly, similar changes are associated to low PAR photoacclimation, when plants need to increase their light harvesting complexes to maximise their photon catching ability (Lichtenthaler, 2007; Rozak et al., 2002; Wood et al., 2018). We therefore reasoned that exposure to low R:FR in the absence of any light intensity change might trigger responses that anticipate a foreseeable shading involving a decrease in PAR.

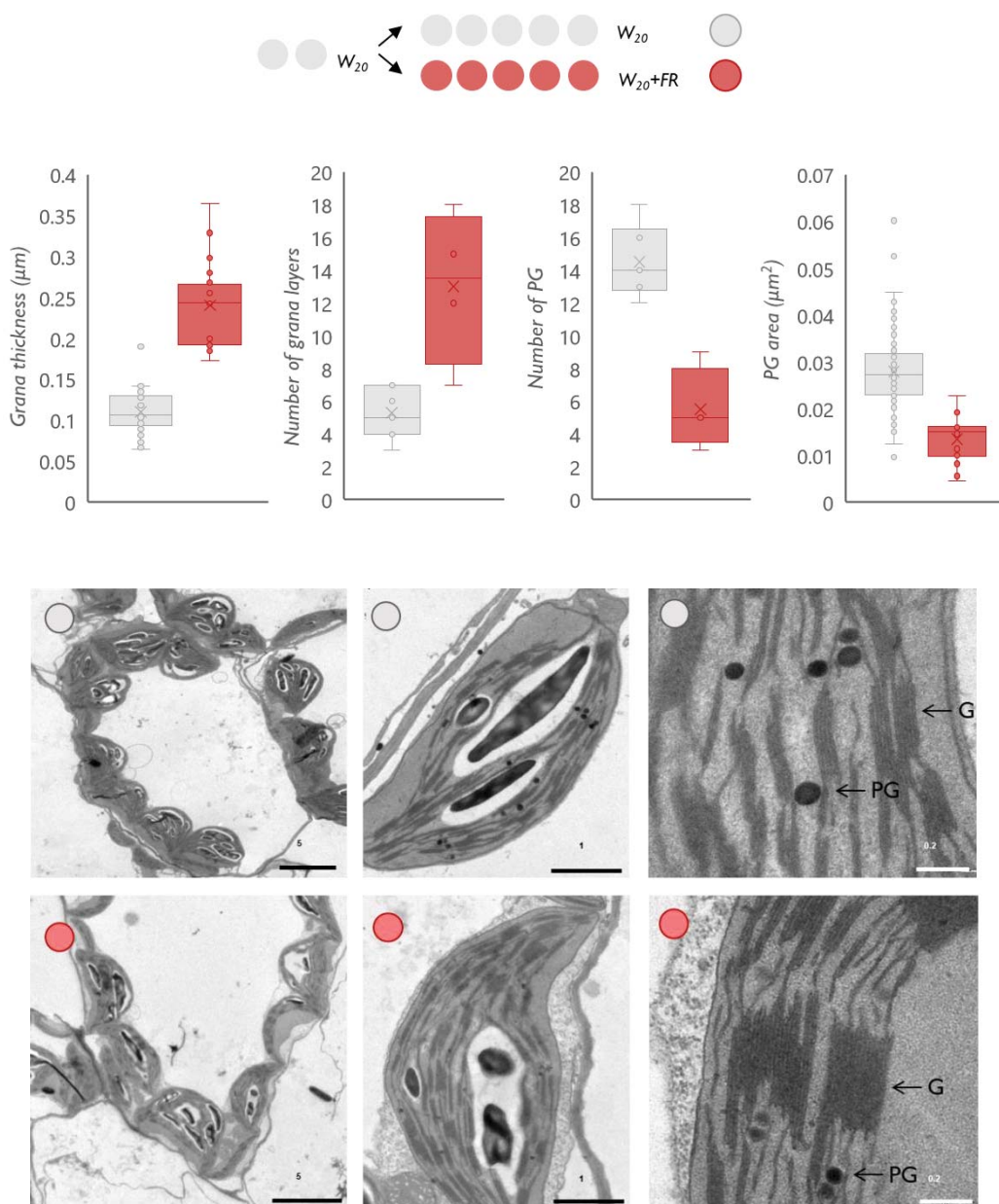
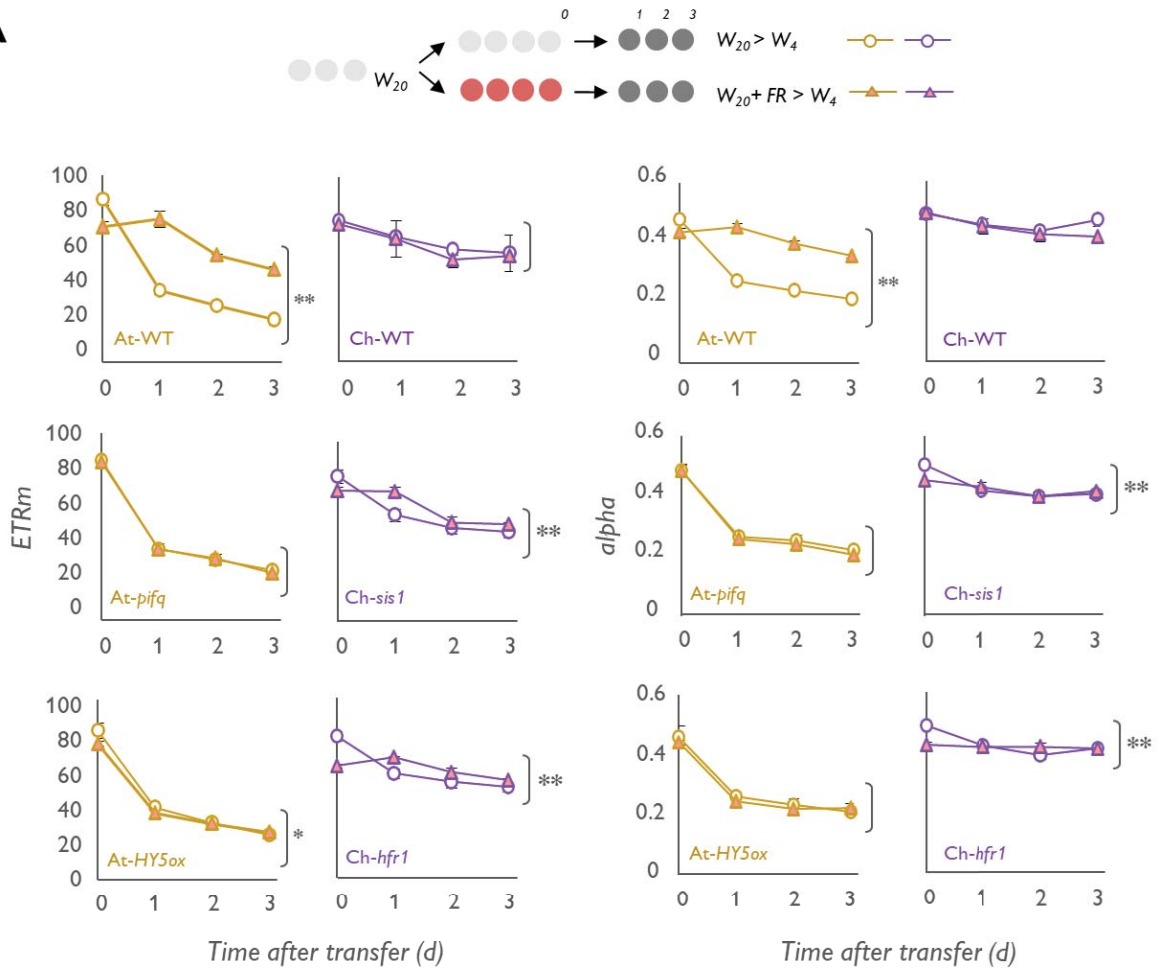


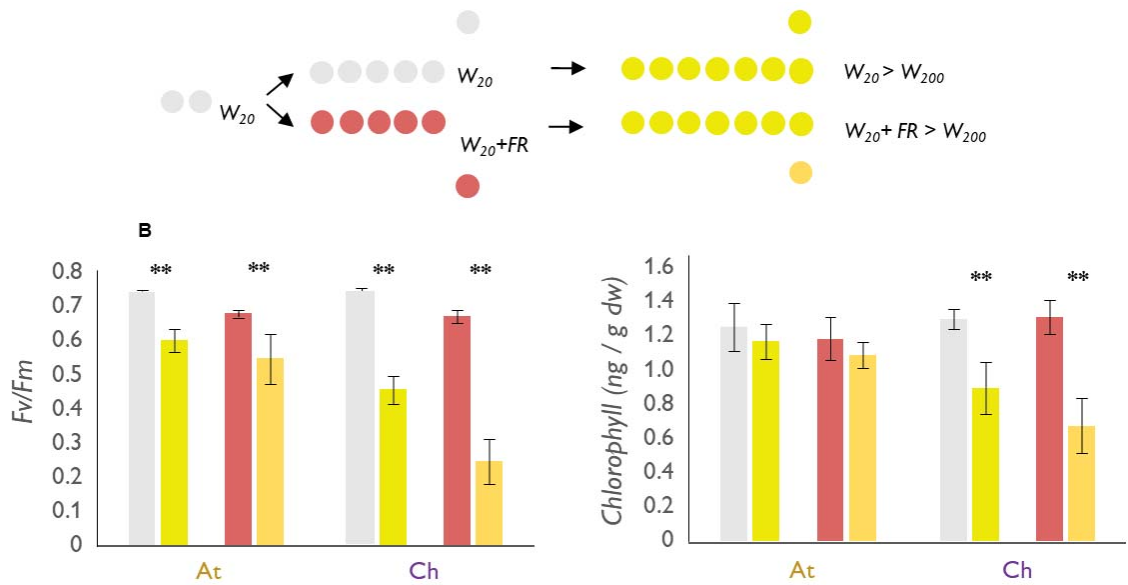
Figure 2.9. Low R:FR triggers ultrastructural changes in *Arabidopsis* chloroplasts. At-WT seeds were germinated and grown under under $20 \mu\text{mol}\cdot\text{m}^{-2}\cdot\text{s}^{-1}$ PAR (W_{20}) for 2 days and then either kept under W_{20} or transferred to low R:FR ($W_{20}+\text{FR}$) for 5 more days. Cotyledons were then used for TEM analysis of chloroplast ultrastructure. Representative pictures at different scales (numbers indicate μm) are shown. Boxplots show quantification of the indicated parameters from the images. Boxes show the values between the upper and the lower quartile, the cross represents the mean, the horizontal line the median, the whiskers the upper and lower extremes. The circles represent the single data with the ones located outside of the whiskers limit being the outliers. The area was measured for all the PG (W_{20} n=87, $W_{20}+\text{FR}$ n=22). For the number of grana layers, 4 major grana complexes were measured (only those from higher magnifications were employed). For the grana thickness all the distinguishable structures were used (W_{20} n=30, $W_{20}+\text{FR}$ n=20). For the measurements at least 6 individual chloroplasts for each treatment were used.

To test this hypothesis, we analysed light curves of WT and mutant seedlings grown in either W_{20} or $W_{20}+\text{FR}$ and then transferred to lower PAR (W_4) for 3 days (Figure 2.10). Pre-exposure of At-WT seedlings to low R:FR ($W_{20}+\text{FR}$) resulted in a strongly attenuated reduction in ETRm after their transfer to lower PAR. By contrast, hyposensitive At mutants lost this photoacclimation response to lower PAR (W_4). Pre-treatment with $W_{20}+\text{FR}$ had virtually no effect on the photoacclimation of Ch-WT seedlings to lower PAR (W_4) but caused a slight but significant improvement of ETRm in shade-hypersensitive Ch mutants at day 1 after transfer to W_4 . When analysing photoacclimation to higher PAR, pre-exposure of At-WT or Ch-WT seedlings to $W_{20}+\text{FR}$ resulted in no improvement compared to W_{20} -grown controls (Figure 2.10A). If anything, Ch-WT seedlings grown under $W_{20}+\text{FR}$ photoacclimated worse than W_{20} -grown seedlings when exposed to higher light intensity (Figure 2.10B). The battery of mustards that grouped together with At in terms of photoacclimation responses (Cb-F, Cb-S and Cr) also showed improved photoacclimation to reduced PAR when pre-exposed to low R:FR, whereas the simulated shade signal did not have an effect on those clustered with Ch (Aa, No and Si) (Figure 2.10C).

A



B



C

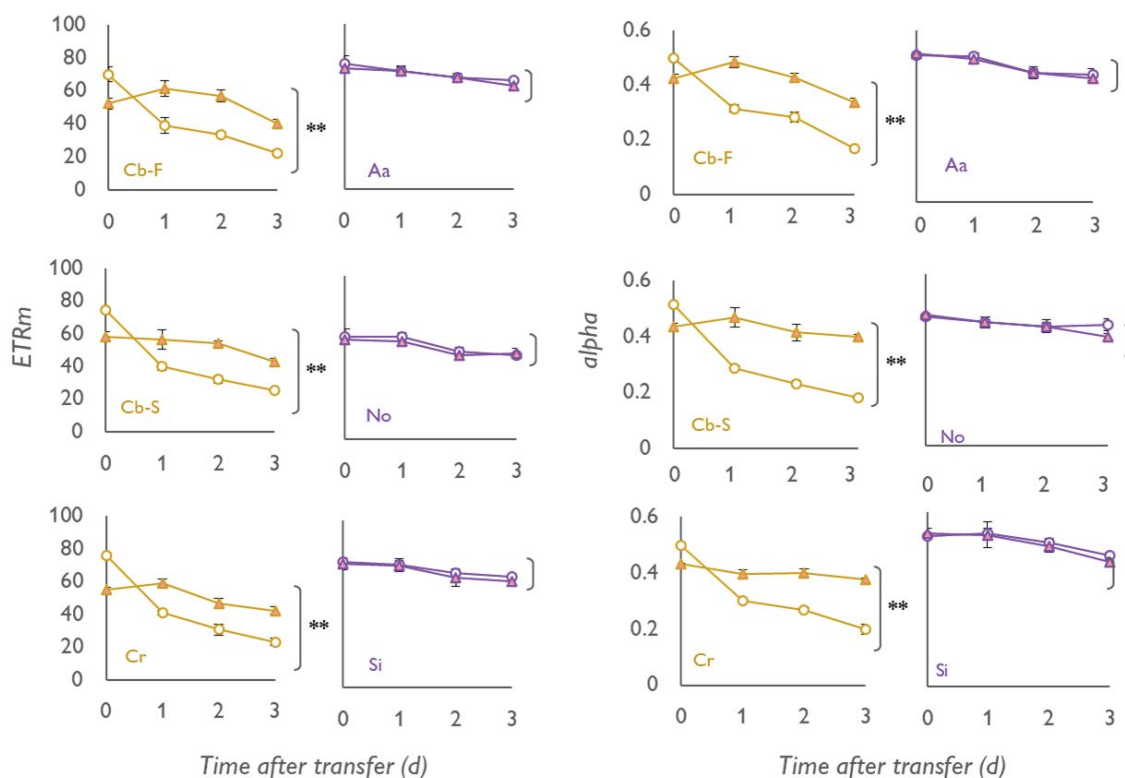


Figure 2.10. Pre-exposure to low R:FR improves the photoacclimation to low PAR in shade-avoider plants. (A, C) The indicated genotypes were germinated and grown under $20 \mu\text{mol}\cdot\text{m}^{-2}\cdot\text{s}^{-1}$ PAR (W_{20}) for 3 days, transferred to either W_{20} or $W_{20}+\text{FR}$ for 4 days, and then exposed to $4 \mu\text{mol}\cdot\text{m}^{-2}\cdot\text{s}^{-1}$ PAR (W_4) for 3 more days. Mean and standard error of ETRm values at 0, 1, 2 and 3 days after transfer to W_4 are shown ($n=3$ seedlings per treatment). (B) Wild-type *Arabidopsis* and *Cardamine* lines were germinated and grown under W_{20} for 2 days, transferred to either W_{20} or $W_{20}+\text{FR}$ for 5 days, and then exposed to $200 \mu\text{mol}\cdot\text{m}^{-2}\cdot\text{s}^{-1}$ PAR (W_{200}) for 7 more days. Fv/Fm values and chlorophyll levels were determined. Mean and standard error of $n=7$ seedlings (Fv/Fm) or $n=3$ independent pools (HPLC) per treatment are represented. In (A) and (C) Two-way ANOVA showed that photosynthetic performance under W_4 is significantly increased ($* P < 0.05$, $** P < 0.01$) by $W_{20}+\text{FR}$ exposure in genotypes classified as shade avoiders while, in genotypes classified as shade tolerant the changes are not statistically significant. In (B) asterisks mark statistically significant changes between values before and after exposing to W_{200} for the indicated time (t-test, $* P < 0.05$, $** P < 0.01$).

Based on these data we concluded that, detection and transduction of low R:FR signals not only allows shade-avoider plants to overgrow their neighbours but also to pre-adapt their photosynthetic machinery to foreseeable conditions of actual shading involving reduced PAR. By contrast, shade-tolerant plants have a better adapted capacity to grow under reduced PAR and do not seem to use the low R:FR signal. Also, we noticed that the exposure to a low R:FR influences plastid ultrastructure, and this could be the reason at the base of a lower photosynthetic competence either for a physical reason (a low-PAR-type plastid living in a

condition of light not suitable for its acclimation state) or because of a signal derived from the same photosystems stimulated by differential light wavelengths.

2.2.5. Simulated shade treatment facilitates the chromoplast differentiation process but results in a lower production of total carotenoids.

After having established the relationship between a low R:FR and photosynthesis and knowing that *N. benthamiana* behaves as a shade-avoider, we decided to test whether exposure to simulated shade impacted the crtB-mediated carotenoid-overaccumulation and chromoplast differentiation phenotype. We grew *N. benthamiana* plants in the greenhouse and then transferred them to chambers under W or W+FR for 4 days. At the end of the 4-day exposure, we agroinfiltrated half of the leaf with the (p)crtB construct and the other half with the GFP control and then moved the plants back to the greenhouse. As expected, W+FR-exposed plants were paler and displayed a lower photosynthetic activity compared to plants grown in W at 0 hpi (Figure 2.11B). At later timepoints, Φ PSII was always lower in W+FR plants (despite the normalization of growth light condition) and the yellow colour indicative of chromoplast differentiation also developed faster, being clearly visible in (p)crtB leaves at 48 hpi (Figure 2.11A, B). Despite the more evident phenotype, the final total carotenoid amount in crtB leaves pre-exposed to W+FR was lower compared to the amount detected in control W leaves. Considering that W+FR plants started with a reduced content of pigments, however, crtB overexpression granted a higher percentual increase of carotenoids compared to what happened in W plants (Figure 2.11D). These results support our model described in the previous chapter that reducing photosynthetic activity in leaf chloroplasts could speed up the crtB-dependent chromoplastogenesis process. Intriguingly, a higher amount of phytoene was found at 48 and 96 hpi in W+FR plants compared to W controls (Figure 2.11C, D).

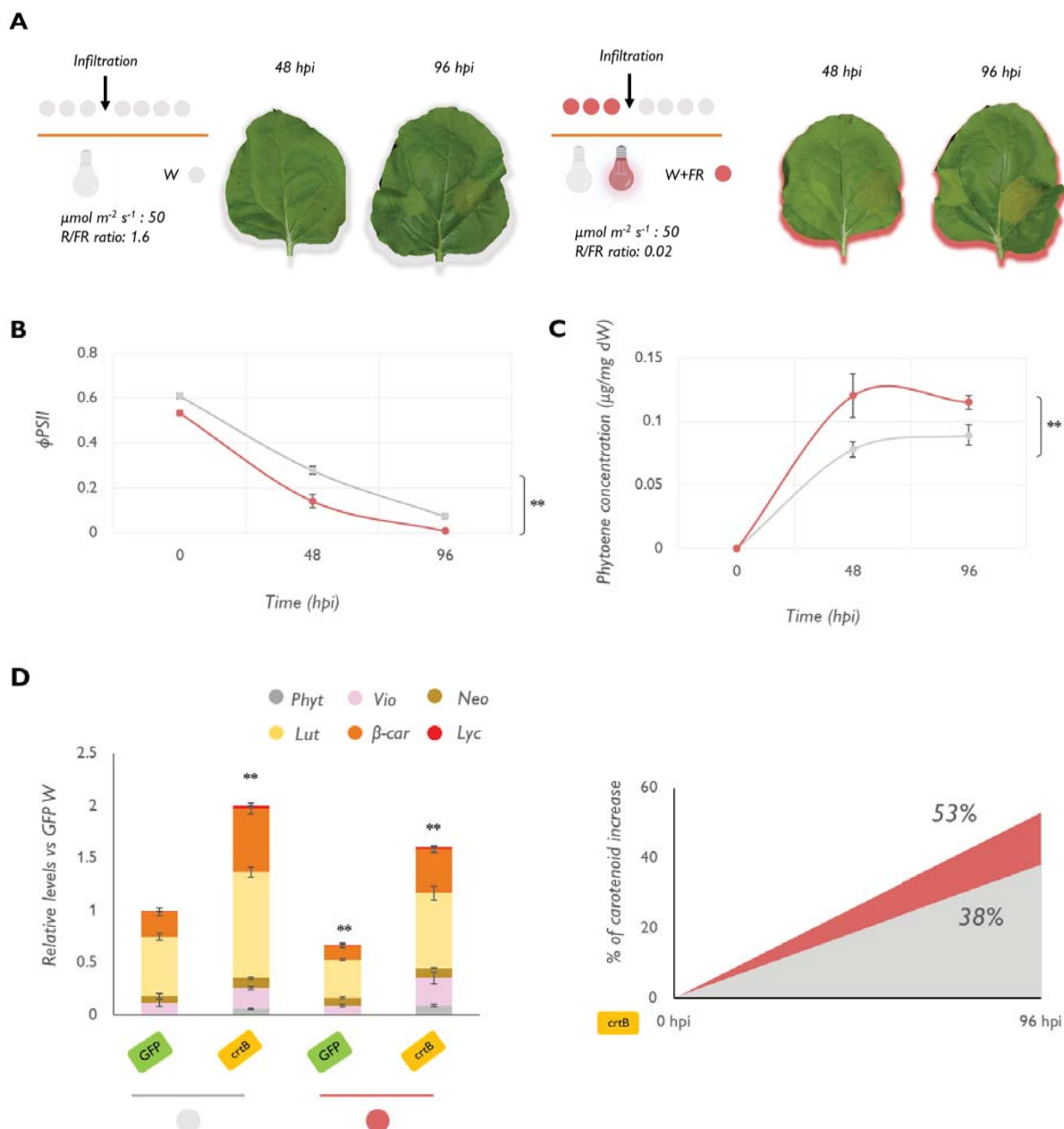


Figure 2.11. Exposure to low R:FR impacts *crtB*-induced chromoplast formation. (A) schematic representation of the experimental setting. Plants pre-exposed to FR light develop the phenotype faster than plants grown in W. (B) effective quantum yield of plants pre-acclimated to W or W+FR and overexpressing *crtB* for 96h. Plots show the mean and SD of 3 different plants for each experiment. (C) Phytoene amount determined 0, 48 and 96 hpi in plant acclimated to W or to W+FR and overexpressing *crtB*. Plots show the value of 3 plants for each treatment. Values are relativised to plants acclimated to W. (D) Relative carotenoid level in plants acclimated to W or W+FR. The values are relative to the amount detected in plants overexpressing *GFP* and acclimated to W. The right panel shows the relative percentual increase of carotenoids in *crtB* plants acclimated to different light conditions. The legend shows a shortened name for the carotenoids detected (Phyt: phytoene, vio: violaxanthin, neo:neoxanthin, lut: lutein, β -car: β -carotene, lyc: lycopene). Plots show means and SD of 3 plants for each treatment. In (B) and (C) Two-way ANOVA showed that photosynthetic performance under and phytoene amount is significantly impacted (* $P < 0.05$, ** $P < 0.01$) by W_{20} +FR exposure. In (D) asterisks mark statistically significant changes compared to the respective control for the indicated treatment (t-test, * $P < 0.05$, ** $P < 0.01$).

We hypothesized that the W+FR treatment should also allow plant PSY enzymes to trigger the chloroplast-to-chromoplast differentiation process in *N. benthamiana* leaves, in a similar fashion to that observed with the application of the photosynthesis inhibitor DCMU (Chapter 1, Figure 1.7). Indeed, PSY-overexpressing leaf areas showed the yellow colour, photosynthetic drop, and carotenoid overaccumulation characteristic of chromoplast differentiation only when pre-exposed to W+FR (Figure 2.12). PSY also caused a higher amount of phytoene in leaves pre-exposed to W+FR compared with W controls (Figure 2.12). These results again strengthened the conclusion that interfering with chloroplast physiology can be useful to improve the strategies for the accumulation of secondary metabolites.

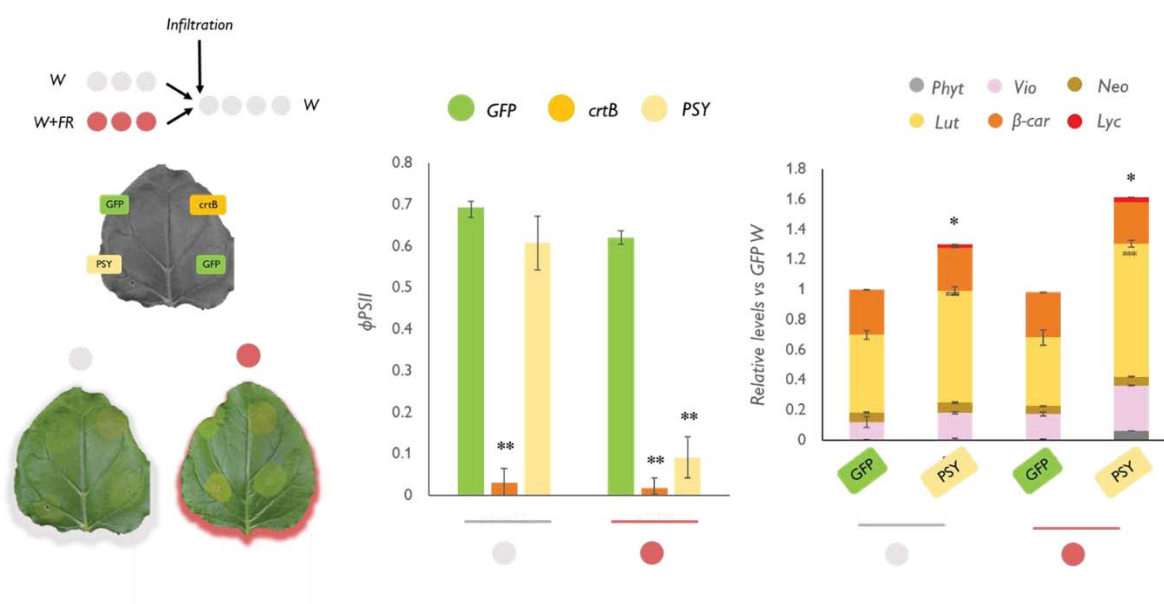


Figure 2.12. Shade effect can make chloroplasts competent for conversion into chromoplasts. Plants were grown in W light or in W+FR for three days before infiltrating the leaves with the enlisted constructions. Plant exposed to a low R:FR recover a crtB-like phenotype when overexpressing PSY and the infiltrated zones show a low photosynthetic activity and an increased amount of phytoene and total carotenoids. Carotenoid levels are relative to the one in leaves overexpressing GFP and growing in W. Asterisks mark statistically significant changes compared to GFP (t-test, * $P < 0.05$, ** $P < 0.01$).

Previous studies reported that exposure to FR light can preferentially channel the electrons to the PSI and thus can be used to fully oxidise the PQ pool (Pralon et al., 2020). When white light is supplemented with FR, however, the prevalence of electrons at the level of PSI, could interfere with the normal electron transport chain ratio and generates an increase of the excitation pressure on the PSII (i.e., the amount of energy reaching closed PSII reaction centres (Sonoike, 2011; Zivcak et al., 2014; Landi et al., 2020; Fan et al., 2007) increasing the level of reduced PQ and thus reducing the amount of oxidised PQ required for the regeneration of desaturase enzymes

responsible for the conversion of phytoene into downstream carotenoids (Figure 2.13A) (Ruiz-Sola and Rodriguez-Concepcion, 2012). We therefore reasoned that the increased levels of phytoene, but reduced levels of downstream carotenoids observed in *crtB*-expressing W+FR plants compared to W controls might be due, at least in part, to a defective conversion of phytoene. To test whether the W+FR treatment resulted in changes in the redox state of the PQ pool, we used a parameter called $1-qP$, i.e., the proportion of reaction centres that are closed generating excitation pressure on PSII with 1 corresponds to the full closure of the centres (Kornyeyev et al., 2010). The $1-qP$ value, which denotes the relative PQ reduction level, increased during *crtB*-triggered chromoplast differentiation, coherently with the loss of the chloroplast ability to handle the redox equilibrium of the PQ pool (already observed in the previous chapter with the OJIP test). This value, however, was significantly higher in W+FR leaves, suggesting a higher excitation pressure, more reduced PQ, and so a lower availability of oxidized PQ for phytoene desaturation (Figure 2.13B). To indirectly test whether the activity of desaturase enzymes that convert phytoene into lycopene was indeed altered by W+FR, we used 2-(4-chlorophenylthio) triethylamine hydrochloride (CPTA) to prevent the conversion of lycopene into downstream carotenoids (Figure 2.13A). Leaves from plants exposed to either W or W+FR were infiltrated with *crtB* and CPTA and carotenoid levels were measured at 96 hpi. Phytoene levels increased under W+FR compared to W whereas lycopene levels decreased, supporting the conclusion that the simulated shade treatment inhibits the desaturation steps converting phytoene into lycopene (Figure 2.13C).

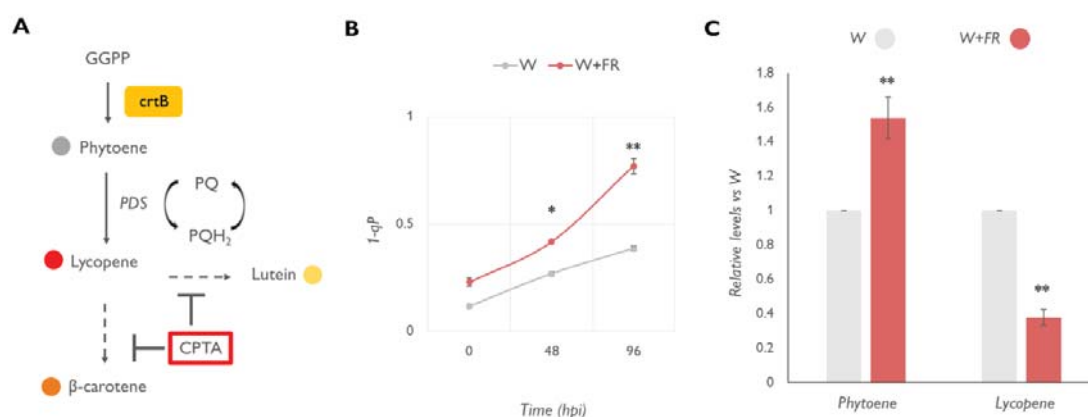


Figure 2.13. Shade affects the rate of conversion of phytoene into downstream carotenoids impacting chromoplast development. (A) Schematic view of carotenoid biosynthetic pathway evidencing the effect of CPTA. (B) $1-qP$ value calculated in plants overexpressing *crtB* and pre-acclimated with W or W+FR before the infiltration. Plot shows the mean and SD of 3 plants for each treatment. (C) Relative levels of phytoene and lycopene in plants pre-acclimated with W or W+FR and overexpressing *crtB* for 96 hours after treatment with CPTA. Levels are relative to the amount of the two metabolites in W. Asterisks mark statistically significant changes compared to W (t-test, * $P < 0.05$, ** $P < 0.01$).

2.2.6. Exposure to high PAR can also promote crtB-induced chromoplastogenesis.

Photoacclimation to altered light quantity (i.e., changing PAR) also involves changes in the photosynthetic apparatus that might weaken photosynthesis to a level that it could facilitate the crtB-mediated chromoplastogenesis process. To test this hypothesis, we grew *N. benthamiana* plants in the greenhouse and transferred them for 3 days to chambers with different light intensities, namely control PAR (W_{50} , $50 \mu\text{mol m}^{-2} \text{s}^{-1}$), lower PAR (W_{10} , $10 \mu\text{mol m}^{-2} \text{s}^{-1}$) and higher PAR (W_{500} , $500 \mu\text{mol m}^{-2} \text{s}^{-1}$). Then, they were agroinfiltrated with (p)crtB or GFP constructs and returned to the greenhouse for the 4 days necessary for the yellow phenotype to develop (Figure 2.14A). The analysis of light curves at 0 hpi confirmed the photoacclimation, with a higher ETR_m value in W_{500} plants a lower one in W_{10} plants compared to the W_{50} controls (Ralph and Gademann, 2005) (Figure 2.14B). At 96 hpi, the overexpression of crtB in W_{10} plants resulted in a lower accumulation of total carotenoids but a higher amount of violaxanthin compared to W_{50} plants, causing an increased ratio xanthophylls/ β -carotene. By contrast, W_{500} plants showed significantly higher levels of total carotenoids and, particularly, β -carotene compared to W_{10} controls. Interestingly all the GFP sections maintained the same carotenoid pattern at 96 hpi regardless of PAR treatment, suggesting that a photosynthetically functional chloroplasts can fully restore the pigment composition after photoacclimation (Figure 2.14C). We also found out that high PAR-treated plants were faster in establishing the yellow phenotype and displayed a faster decaying of ϕPSII (Figure 2.14D). Interestingly, staining of reactive oxygen species (ROS) with 3,3'-diaminobenzidine (DAB, which produces a brown precipitate when oxidized by H_2O_2) and nitrotetrazolium blue chloride (NBT, which reacts with O_2^- to form a dark blue insoluble compound) showed increased levels in W_{500} plants compared to W_{50} controls at 0 hpi (Figure 2.14E). A burst of ROS was also observed during chromoplast formation in crtB-inoculated areas of both W_{50} and W_{500} plants (Figure 2.14E).

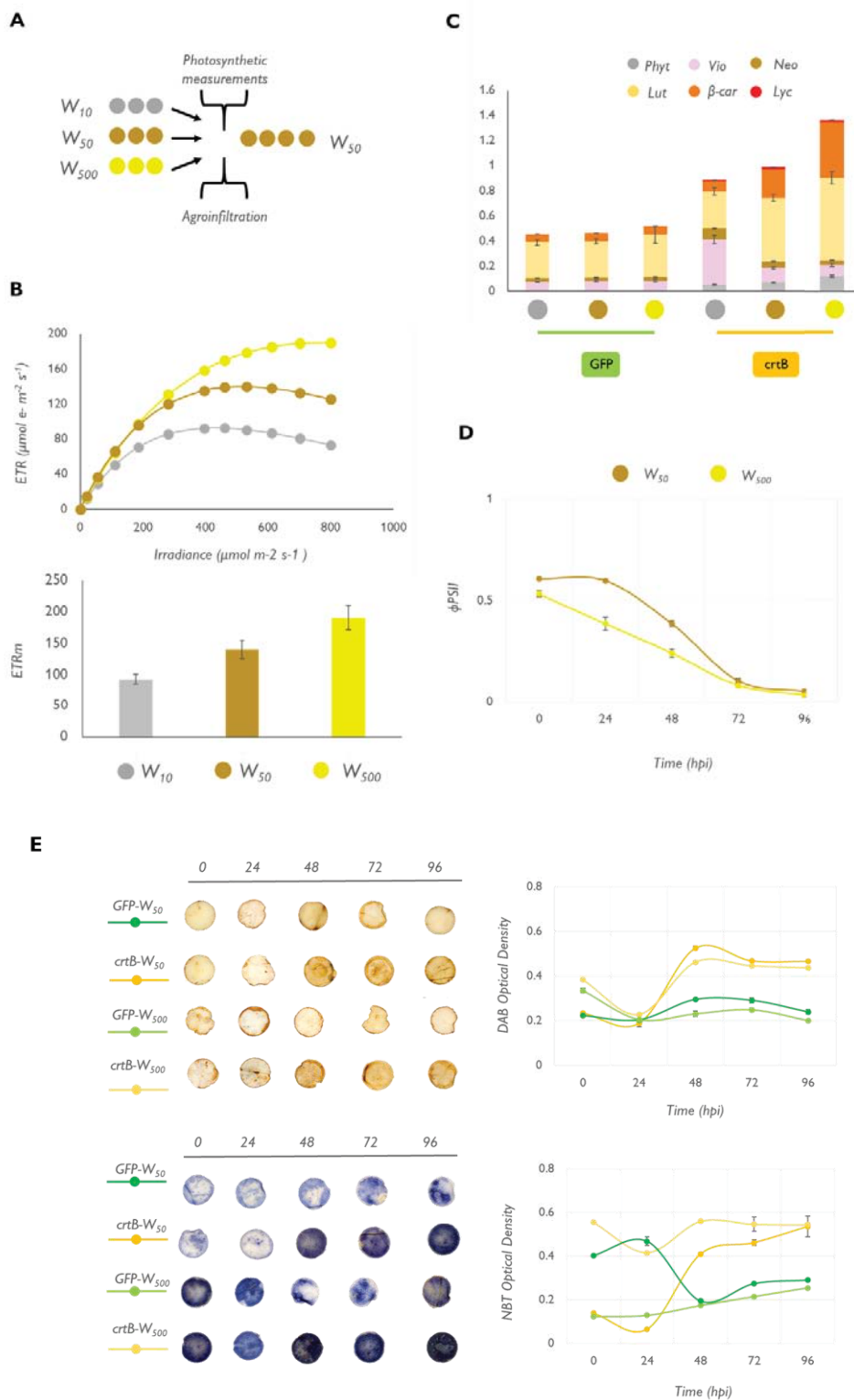


Figure 2.14. acclimation to different light intensities impact carotenoids accumulation (A) schematic view of the experimental setting and different light conditions. ETR vs irradiance curves of plants maintained for 3 days under W_{10} , W_{50} and W_{500} . **(B)** ETRm value obtained by plotting ETR vs Irradiance curves with the mathematical plot of Platt. Confirming the reached photoacclimation state **(C)** Relative levels of carotenoids in plants acclimated to different light intensities. Values are relative to the amount detected in crtB leaf sections acclimated to W_{50} . Plots show the mean and SD of 3 plants for experiment. **(D)** Effective quantum yield loss in W_{500} vs W_{50} acclimated plants **(E)** ROS content in

leaves determined by DAB and NBT histochemical staining and quantification by ImageJ software. Leaf discs acclimated to W_{500} have a higher content of ROS and develop the phenotype faster. Plots show the mean and SD of 5 different disks for every treatment.

2.3. Discussion

Changes in light quantity and quality can have a negative impact on photosynthesis. In this Chapter, we show that this impact could be productively used to improve our crtB-based system for chromoplast differentiation and carotenoid biofortification of leaves. According to our model of two steps in the chloroplast-to-chromoplast conversion pathway, factors challenging leaf photosynthetic performance (i.e., chloroplast identity) would make chloroplasts more competent to differentiate into chromoplasts upon induction of carotenoid production (i.e., by crtB). In Chapter 1 we showed that this increased competence could be achieved by mimicking plastidial stress in PAP-overaccumulating *sal1* mutants and by specifically interfering with photosynthesis using DCMU (which interrupts the electron flow from PSII to PQ). Here we explored the effect of light treatments and found that high light intensity, irradiation with R, and exposure to simulated shade (W+FR) can all result in a faster rate of chloroplast-to-chromoplast differentiation. Along the way, we learned that *N. benthamiana* is a shade avoider and that photoacclimation responses to changes in light quality (low R:FR) and quantity (lower and higher PAR) are characteristic of shade avoider and shade tolerant plants.

Plants have been traditionally classified as shade avoider and tolerant based mostly on their natural habitat. Although virtually all plants are exposed to at least some degree of shade during their lifetime some of them can develop a preference for a particular light environment. As an ecological concept, shade tolerance refers to the capacity of a given plant to tolerate low light levels, but it is also associated with a wide range of traits, including phenotypic plasticity to optimize light capture. (Valladares and Niinemets, 2008). By analysing a range of caulescent herbs, it was suggested that the elongation response upon exposure to low R:FR was dependent on the shade habit, the shade-avoiders elongating the most and the shade-tolerants showing a mild or no elongation response (Paulišić et al., 2021). Indeed, elongation might not be the best solution for plants that spend all their lives under a canopy or permanently shaded by other plants because it supposes a great energetic waste and in small herbaceous plants could not provide an actual solution to the shading from another plant. Nonetheless, another important parameter to ascertain the degree of shade tolerance of a plant is photoacclimation capacity, which is essential for plant fitness in environments with changing light input conditions like

those where nearby plants can suddenly compromise the access to an optimal amount of light (Landi et al., 2020). By considering both parameters (the hypocotyl elongation response and the capacity to acclimate to low or high PAR), we analysed the responses to shade of several Brassicaceae species, including the closely related mustard model systems *Arabidopsis* and *Cardamine* (Figure 2.4). As a rule of thumb, we observed that *Cardamine* and other species showing a good photoacclimation response to lower PAR (and badly performing after transfer to higher PAR) showed a poor or null elongation response to low R:FR, whereas shade-avoider species like *Arabidopsis* showed a weak photosynthetic performance under low PAR but they strongly elongated when exposed to low R:FR (Figure 2.5). The coordination between the elongation and the photoacclimation responses is maintained in a wide range of mustards with a certain degree of variability but always coherently with the hypothesis. Furthermore, mutation of genes encoding SAS regulators can dramatically change the elongation response to low R:FR without improving the photoacclimation phenotype. Together, these results confirm that the capacity for photosynthetic acclimation to changing irradiance is a species-specific trend (Bailey et al., 2001) and a reliable indicator of shade tolerance, especially in an eco-physiological context.

Our results also unveiled that an activation of low R:FR signalling in shade-avoider species such as *Arabidopsis* (At-WT) and shade-tolerant *Cardamine* plants with mutations causing low R:FR hypersensitivity (Ch-*sis1* and Ch-*hfr1*) regulated photosynthesis at multiple levels (Figure 2.6, 2.7). We confirmed that exposure to W+FR caused a substantial decrease in the levels of photosynthetic pigments (chlorophylls and carotenoids) in these lines (Bou-Torrent et al, 2015; [Molina-Contreras et al, 2019](#); Paulišić et al, 2021; Roig-Villanova et al, 2007) and proved that the changes had a direct impact on decreasing photosynthetic activity. Low R:FR treatments are known to trigger changes in gene expression within minutes (Kohnen et al., 2016). These changes, which are often instrumental for altering rapid growth responses, such as hypocotyl or petiole elongation, are usually mediated by PIFs (Cifuentes-Esquivel et al., 2013; de Wit et al., 2015; Galstyan et al., 2011). PIFs were also found to regulate longer-term changes in gene expression such as those affecting photosynthetic genes. Because loss of PIFQ function in the At-*pifq* mutant resulted in a much-attenuated response to W+FR compared to At-WT in terms of photosynthetic gene expression, but it also prevented photosynthetic pigment and activity loss, we propose that stabilization of PIFQ proteins following low R:FR exposure triggers a reprogramming of photosynthesis-related gene expression that eventually results in lower pigment levels and reduced photosynthetic activity (Figure 2.8). Based on the results obtained with other mutants, we speculate that this signalling network is further influenced by factors such as HFR₁ and HY5, which prevent PIF binding to target genes by heterodimerization (Hornitschek et al., 2009) or competition for promoter binding sites (Toledo-Ortiz et al, 2014).

Concomitant with the described molecular and physiological changes, we discovered that low R:FR treatment of At-WT seedlings triggered ultrastructural changes in the chloroplast endomembrane systems resembling those occurring after transfer to low PAR. Grana with more thylakoid layers and increased thickness were observed in the chloroplasts of At seedlings exposed to simulated shade together with a low number of small PG, characteristics that are common to leaves that develop under low PAR. In fact, low light acclimated leaves have chloroplasts with less PG (which are derived from thylakoid membranes) and more thylakoids per granum because these changes in chloroplast ultrastructure contribute to optimize photosynthesis when relatively less photons are available. (Rozak et al., 2002; Lichtenthaler, 2007; Wood et al., 2018). Based on these results, we suggest that the chloroplast ultrastructural changes observed in At-WT plants grown under low R:FR are most likely aimed to acclimate their photosynthetic machinery to perform better under low PAR by, for instance, allowing a more efficient energy transfer or by avoiding the necessity of massive internal remodelling when the light condition effectively changes (Figure 2.9). In agreement, pre-treatment with low R:FR improved photoacclimation to low PAR of At-WT seedlings but had no effect in At mutants defective in low R:FR signalling. Further experiments showed that the observed positive effect of low R:FR exposure for acclimation to low PAR can be observed in At-WT plants growing under different light conditions and in other shade-avoider Brassicaceae (Cb-F, Cb-S and Cr), but not in shade-tolerant species such as Ch, Aa, No and Si most likely because in the latter the chloroplast is already provided of characteristics either from the metabolic or the structural point of view that allow it to lead with low photon flux (Figure 2.10).

Regardless of the signalling pathway connecting low R:FR perception to reduced photosynthesis and respiration, this is likely part of an anticipation mechanism for shade-avoider plants to prepare for the foreseeable reduction in PAR associated with shading. Indeed, low R:FR signals are perceived before actual shading takes place and light becomes limiting, and hence they are considered to act as a warning signal that shading might occur (Casal, 2013; Martinez-Garcia et al, 2010). When shade-avoider plants such as *Arabidopsis* and most crops (including tomato, cereals, or legumes) grow among taller plants or in a forest understory, they will use the low R:FR signals coming from a closing canopy to elongate (to overgrow its neighbours) but also to readapt its photosynthetic machinery to low PAR before actual shading takes place. By contrast, shade-tolerant plants are adapted to grow under dim light and hence photoacclimation to low PAR is hardly improved even when hypersensitive mutants that show shade-avoider responses in terms of elongation and photosynthesis are pre-exposed to low R:FR.

The photosynthetic responses to low R:FR irradiation have clear consequences for crtB-dependent chromoplast development in shade avoider plants such as *N. benthamiana*. We showed that the crtB-induced phenotype in shade-primed plants develops faster than in plants grown in normal conditions of light (i.e., high R:FR) even if this phenomenon is not associated to an eventually higher content of carotenoids downstream of phytoene (Figure 2.11). While the faster chromoplastogenesis rate might be the consequence of chloroplasts becoming more competent due to shade-triggered photosynthetic decline, the lower production of carotenoids is likely an indirect effect. By applying CPTA we were able to confirm that the W+FR treatment caused a lower rate of desaturation activities that transform crtB-produced phytoene into lycopene (Figure 2.13). Plants irradiated with a low R:FR are naturally showing a higher flux of electrons in the PSI (preferentially excited by this wavelength of light) and a higher rate of reduced PQ. Because the electrons involved in the oxidation reactions catalysed by the desaturase enzymes are subsequently transferred to reduce PQ (Sonoike, 2011) the lower pool of oxidized PQ is certainly expected to slow down the desaturation of phytoene and hence the production of downstream carotenoids (Figure 2.13). The higher pool of phytoene that accumulates in shade-treated plants could also contribute to more rapidly reaching the threshold necessary for the de-differentiation of chloroplasts. It is also expected that the accumulation of PIFs in plants exposed to W+FR could also contribute to reduced chloroplast identity and carotenoid accumulation, as these transcription factors are well-established repressors of chloroplast development and photosynthetic pigment biosynthesis (Toledo-Ortiz et al., 2010, Bou-Torrent et al., 2015).

Moving from light quality to light quantity, acclimation to high light leads to the accumulation of β -carotene either for its antioxidant power (Müller et al., 2011) or for its association with photosystems. On the other side low light acclimated plants accumulate a higher amount of violaxanthin, necessary for its light harvesting properties and for being a key compound in xanthophyll cycle (Lichtenthaler et al. 2007). Coherently with this, plants exposed to W_{500} and then agro-inoculated with crtB showed a higher level of total carotenoids with an increase of β -carotene content compared to W_{50} controls (40% of the total carotenoid content in W_{500} plants compared to 25% in W_{50} plants), while those exposed to W_{10} showed an increased content of violaxanthin (40% of the total) at the expenses of β -carotene (10% of the total) despite not increasing the total amount of carotenoids (Figure 2.14). These results together with the increased production of ROS in W_{500} leaves and the results reported in Chapter 1 with the *A. thaliana sal1* mutant identified the redox status of the plastid as one of the major factors controlling chromoplast development. Multiple observations suggest that oxidative stress regulates carotenoid biosynthesis during the chloroplast to chromoplast transition in plants. For

example, in *Reseda odorata* leaves, rodoxanthin, a chromoplast-specific carotenoid, shows a *de novo* accumulation following stem bark removal and thus a generation of oxidative stress caused by changes in turgor pressure (Bouvier et al., 1998). Second, in *Aloe vera* and *Cryptomeria*, stress from drought and high irradiance or low temperatures induces the *de novo* accumulation of rodoxanthin in chloroplasts, which subsequently undergo a transformation into photosynthetically active chlorochromoplasts (Bouvier et al. 1998). In red pepper fruits also was demonstrated that the induction of ROS formation through the application of chemicals such as t-tert-butyl hydroperoxide caused the pronounced induction of different carotenogenic gene expression whereas the downregulation of the catalase system through the application of amitrole (3-amino-1,2,4-triazole) resulted in a massive increase in expression of different carotenogenic gene transcripts and the parallel *de novo* synthesis of the chromoplast-specific carotenoid, capsanthin associated with a faster chromoplast formation in fruit pericarp (Bouvier et al. 1998). We conclude that the oxidative stress by itself can contribute to determine the speed of chromoplast formation in leaves and that this specific biochemical regulation is conserved among different typologies of chromoplast differentiation (including our artificial system) (Figure 2.14). Also, considering that the formation of chromoplasts in leaves is associated with the loss of photosynthetic and photoprotective competence, the process itself contributes to ROS production self-sustaining its own rhythm. Our results therefore contribute to better understand the controversial role of photosynthesis in chromoplast development in leaves: something that is necessary for the process but, at the end, must be lost.

2.4. Material and methods

2.4.1. Plant material and growth conditions

Arabis alpina (*pepi-1* mutant) (Wang et al., 2009) *Arabidopsis thaliana* (Col-o accession), *Cardamine hirsuta* (Oxford, Ox accession) (Molina-Contreras et al, 2019), *Capsella bursa-pastoris* (accessions Strasbourg-1, Str-1 and Freiburg-1, Fre-1), *Capsella rubella* and *Sisymbrium irio* plants were grown in the greenhouse under long-day photoperiods (LD, 16 h light and 8 h dark) to produce seeds, as described (Gallemí et al., 2017). Seeds of *C. bursa-pastoris* were collected by Ruben Alcazar (University of Barcelona, Spain) from wild populations in Strasbourg (France, coordinates: 48.612436, 7.767881; Str-1) and Freiburg (Germany, coordinates: 47.994945, 7.861979; Fre-1). Seeds of *Capsella rubella*, collected from wild populations in Crete (Greece, coordinates 35.29, 24.42; accession 879) were previously described (Koenig et al, 2019). Seeds of *Sisymbrium irio* were collected from wild populations in Bellaterra (Barcelona, Spain, coordinates: 41.497731,

2.109558). Seeds of *Nasturtium officinale* were provided by a seed company (www.semillasfito.es). *A. thaliana* and *C. hirsuta* mutant and transgenic lines were previously available in our collaborator's laboratories ([Molina-Contreras et al, 2019](#); [Ortiz-Alcaide et al, 2019](#); [Paulišić et al, 2021](#)).

For the light acclimation experiments seedlings were germinated and grown in Petri dishes containing solid medium without sucrose (0.5x MS-): 2.2 g/L MS basal salt mixture (Duchefa), 1% (w/v) agar, 0.25 g/L MES (Sigma Aldrich), pH 5.7. Normal light conditions refer to white light (W) produced by cool-white vertical fluorescent tubes (PAR of 20-24 $\mu\text{mol photons m}^{-2} \text{s}^{-1}$, W_{20}) with a R:FR of 1.5-3.3. Low light and high light conditions corresponded to W of PAR values of 4 (W_4) and 200 (W_{200}) $\mu\text{mol m}^{-2} \text{s}^{-1}$, respectively, produced by horizontal fluorescent tubes. Low R:FR treatment was produced by supplementing W_{20} with FR ($W_{20}+\text{FR}$). FR was emitted from a GreenPower LED module HF far-red (Philips), providing a R:FR of 0.02 ([Martinez-Garcia et al, 2014](#)). Light fluence rates were measured with a Spectrosense2 meter (Skye Instruments Ltd), which measures PAR (400–700 nm), and 10 nm windows of R (664–674 nm) and FR (725–735 nm) regions to calculate the R:FR ([Martinez-Garcia et al, 2014](#)). Full spectra photon distribution of W and W+FR treatments have been described elsewhere ([Molina-Contreras et al, 2019](#)). *Nicotiana benthamiana* plants were grown under standard conditions as described in the previous chapter. For the light acclimation experiments, tobacco plants were grown in a visitable cabin and then moved to an ARALAB 600 fitoclima plant growth chamber where they were maintained for three days in three different light conditions: Low PAR (W_{10}): 10 $\mu\text{mol photons m}^{-2} \text{s}^{-1}$, normal PAR (W_{50}): 50 $\mu\text{mol photons m}^{-2} \text{s}^{-1}$ and high PAR (W_{500}): 500 $\mu\text{mol m}^{-2} \text{s}^{-1}$ photons under a LD light regime. After the agroinfiltration plants were all maintained in the W_{50} condition. For the simulated shade experiment plants were grown for three days in a visitable chamber in LD light conditions supplemented with the same FR lamp described above synchronized with the photoperiod. After the agroinfiltration plants were moved to the same light conditions eliminating the FR. Agroinfiltration with constructs of interest was realised as described in the previous chapter. For the CPTA treatment, the chemical was diluted in water at the final concentration of 50 μM and infiltrated in the leaves 24 hours after the agroinfiltration.

2.4.2. Gene constructs

The crtB versions used for this study (35S:(p)crtB-GFP-pGWB405 and 35S:(p)crtB-pGWB405) and were available in the laboratory and were obtained as described by [Llorente et al. 2020](#).

2.4.3. Transient expression assay

Agroinfiltration experiments were performed as described in the previous chapter. Gene silencing was prevented by co-agroinfiltration with an agrobacterium strain EHA101 carrying the helper component protease (HcPro) of the watermelon mosaic virus (WMV) in plasmid HcProWMV-pGWB702 (a kind gift of Juan José López-Moya and Maria Luisa Domingo-Calap (CRAG-Barcelona, Spain)).

2.4.4. Photosynthetic measurements and pigment quantification

Whole seedlings were harvested, ground in liquid nitrogen, and the resulting powder was used for quantification of chlorophylls and carotenoids spectrophotometrically (Bou-Torrent et al, 2015). or by HPLC as described in the previous chapter. Chlorophyll fluorescence measurements were carried out on seedlings using a MAXI-PAM fluorometer (Heinz Walz GmbH) Briefly, for every measurement the whole cotyledons of 7 seedlings were considered. Effective quantum yield of photosystem II (PSII) under growth light, ϕ_{PSII} , was measured as $\Delta F/F_m'$, where ΔF corresponds to $F_m' - F$ (the maximum minus the minimum fluorescence of light-exposed plants). Maximum quantum yield of PSII, F_v/F_m , was calculated as $(F_m - F_o)/F_m$, where F_m and F_o are respectively the maximum and the minimum fluorescence of dark-adapted samples. For dark acclimation, plates were incubated for at least 30 minutes in darkness to allow the full relaxation of photosystems. Light curves were constructed with 10 incremental steps of actinic irradiance (E ; 0, 20, 55, 110, 185, 280, 395, 530, 610, 700 $\mu\text{mol photons m}^{-2} \text{s}^{-1}$ PAR). For each step, ϕ_{PSII} was monitored every minute and electron transport rate (ETR, $\mu\text{mol e}^{-} \text{m}^{-2} \text{s}^{-1}$) was calculated as $E \times \phi_{PSII} \times 0.84 \times 0.5$ (where 0.84 is light absorptance by an average green leaf and 0.5 is the fraction of absorbed quanta available for PSII). The light response and associated parameters ETR_m (maximum electron transport rate, $\mu\text{mol electrons m}^{-2} \text{s}^{-1}$) and alpha (α , photosynthetic rate in light-limited region of the light curve, $\mu\text{mol electrons m}^{-2} \text{s}^{-1} [\mu\text{mol photons m}^{-2} \text{s}^{-1}]^{-1}$) were characterized by fitting iteratively the model of the ETR versus E curves using MS Excel Solver (Platt et al., 1980). The fit was very good in all the cases ($r > 0.98$). Excitation pressure as $1 - qP$ where $qP = (F_m' - F)/(F_m' - F_o')$ where F_m' and F_o' are respectively maximal and minimal fluorescence yield of illuminated sample.

2.4.5. Microarray data analyses

Microarray data corresponding to *Arabidopsis* Col-o (At-WT) and *At-pifq* seedlings exposed to low-R:FR for 0, 1, 3 and 24 h (Leivar et al, 2012) were analysed to select for differentially expressed

genes (DEGs) specifically related to photosynthesis. The reported list of DEGs was further filtered using cut-offs of FDR <0.05 and log₂-transformed fold change (log₂FC) higher than 0.585 for upregulated genes and lower than -0.599 for downregulated genes. Then, photosynthesis-related genes were identified by using the KEGG (Kyoto Encyclopedia of Genes and Genomes) Mapper tool (Kanehisa and Sato, 2020).

2.4.6. Transmission electron microscopy

Transmission electron microscopy (TEM) was carried out as described (Flores-Pérez et al., 2008). Chloroplast features in the pictures were quantified by using the FIJI-ImageJ software (Schindelin et al., 2012).

2.4.7. ROS histochemical staining

H₂O₂ stained in plant tissue by using diaminobenzidine (DAB). Briefly, *N. benthamiana* leaf disks were infiltrated with a solution of 1 mg/ml of DAB-HCl, pH=3.8 by using a capped syringe moving the plunger up and down 10-15 times. Infiltrated leaf disks were then incubated at room temperature for 16 hours. O₂⁻ was stained by using nitroblue tetrazolium (NBT). Leaf disks were infiltrated with a solution of 0.1% NBT in 50 mM of potassium phosphate, pH=7.8 for 2 hours. In both cases the material was distained by incubating in a solution made of ethanol:lactic acid:glycerol, 3:1:1 for 8 hours. Once fully distained, disks were mounted on transparent paper in 60% glycerol and scanned for further analysis.

Chapter 3

Chapter 3. Exploiting the formation of new storage structures in artificially obtained chromoplasts to boost the accumulation of isoprenoid vitamins in leaves.

3.1. Introduction

The demand for plant-derived isoprenoids with vitamin activity such as carotenoids (pro-vitamin A), phyloquinones (vitamin K₁) and tocochromanols (vitamin E) dramatically increased in the last years after the discovery of their anticarcinogenic and antioxidant effects. The improvement of isoprenoid levels in plants can be obtained through three main different strategies: 1) increasing the metabolic flux (push strategy), 2) suppressing competing and degradation pathway to enhance substrate availability and avoid product degradation (block strategy) and 3) promoting the formation of new storage structures (pull strategy). Biotechnological approaches have shown that achieving high yields of carotenoids and tocopherols in crops following one or several of these strategies is feasible (Botella-Pavia and Rodriguez-Concepcion, 2006). Nonetheless, our major challenge still resides in the limited knowledge of the mechanisms and signals controlling plant metabolism (including the interaction among metabolic pathways) and metabolite sequestration (Dellapenna and Pogson, 2006; Rodriguez-Concepcion et al., 2018). The “pull” strategy, based on the development of new storage structures, appears to be the most compromised by our scarce knowledge of the underlying mechanisms despite it is particularly promising considering the central role of plastids in both the synthesis and the storage of secondary isoprenoids. Chloroplasts, for example, possess a complex membrane system where carotenoids, tocopherols and prenylquinones are produced and accumulated, including the outer and inner envelope and the thylakoid membranes (Sadali et al., 2019). The envelope membranes are debited to protein import and have a series of channels and translocation complexes composed by translocons at the outer and inner envelope membrane (Toc and Tic complexes, respectively) that mediate the recognition of preproteins and their translocation across the membrane (Breuers et al., 2012). The thylakoid membrane system is the place for the light-dependent reactions of photosynthesis that adopts different structural states to cope with different light conditions (Oikawa et al., 2008). Attached to the thylakoids and enclosed by a lipid monolayer that is a continuation of the outer thylakoid membrane are also found the plastoglobules (PG), that are basically vesicles filled with lipophilic metabolites such as chromanols and quinones and enzymes involved in their metabolism. PG serve as dynamic lipid reservoirs whose abundance increases under unfavourable environmental conditions and under certain developmental stages (Van Wijk and Kessler, 2017). Despite their potential, however,

chloroplasts cannot be fully exploited as metabolite reservoirs because of their fundamental role as photosynthetic machinery and the delicate metabolite equilibrium that is necessary for their functioning.

Chromoplasts, on the other hand, are more suitable for a “pull” strategy because they are naturally differentiated for the massive accumulation of isoprenoids (especially carotenoids) (Mellor et al., 2018). The substructures for the sequestration and storage of carotenoids serve to classify chromoplasts as crystalline, globular, tubular, or membranous. Every structure can be characteristic of a particular carotenoid, but more than one pigment-bearing substructures or different types of chromoplasts can co-exist in the same plant species. Crystalline bodies are observed, for example, in chromoplasts of tomato and carrot where the major pigments are, respectively, lycopene and β -carotene (Harris and Spurr, 1969). Crystal structures are accumulated inside the lumina of thylakoid-like structures that may be formed from the degeneration of the original chloroplast thylakoids (Egea et al. 2010). As other examples, mango fruits contain chromoplasts with a high concentration of PG where the major carotenoid detected was β -cryptoxanthin while watermelon and butternut fruits show prominence of membranous chromoplasts (Jeffery et al., 2012). Chromoplasts of red pepper are characterized by many globules with fibrillar extensions of carotenoids (Laborde and Spurr, 1973). In these chromoplasts, carotenoids, together with tocopherols and prenylquinones, are sequestered in a central core and surrounded by a layer of polar lipids which then are surrounded by an outer layer of fibrillins (Deruere et al., 1994). PG in red ripe pepper chromoplasts were reported to contain several enzymes involved in carotenoid biosynthesis (Br  h  lin et al., 2007). However, a general contribution of PG to the biosynthesis of carotenoids in plastids is still unclear.

Surprisingly little is known on the factors involved in natural differentiation of chloroplasts into chromoplasts (Sadali et al, 2019; Sun et al, 2018). Among the few molecular tools available that allow the formation of chromoplasts, the most known is the ORANGE (OR) protein (Giuliano and Diretto, 2007, Sun et al., 2019). The OR protein is, however, unable to trigger chromoplast differentiation in photosynthetic tissues other than tomato green fruit. The only described tool for the transformation of photosynthetically strong chloroplasts (such as those of leaves) into chromoplasts is the overexpression of the bacterial *crtB* gene (Llorente et al., 2020). Chromoplasts obtained through this tool showed the presence of several electron-dense globules that seemingly increased in number during the chromoplastogenesis process (Llorente et al., 2020). These structures are likely to be PG that might provide increased sink strength but also enhanced biosynthetic capacity to produce plastidial isoprenoids other than carotenoids. In this chapter we confirm that these structures were indeed PG and characterize their formation and

their role in the production and accumulation of different plastidial isoprenoids in *crtB*-chromoplasts. We further explore multiple connected strategies to maximise the accumulation of such nutritionally valuable isoprenoids.

3.2. Results

3.2.1. The overexpression of *crtB* triggers disorganization of photosynthetic complexes followed by proliferation of PG as leaf chloroplasts turn into chromoplasts.

Chloroplasts present in green leaves and unripe fruits are characterized by a regular network of thylakoidal membranes and a moderate number of PG. In chromoplasts developing in tomato and red pepper, the number and size of PG increase (Egea et al. 2010). Transmission electron microscopy (TEM) images of leaf areas infiltrated with *Agrobacterium tumefaciens* carrying a vector overexpressing the bacterial (*p*)*crtB* gene also showed what appeared to be a proliferation of PG among other structural features found in naturally occurring chromoplasts (Figure 3.1).

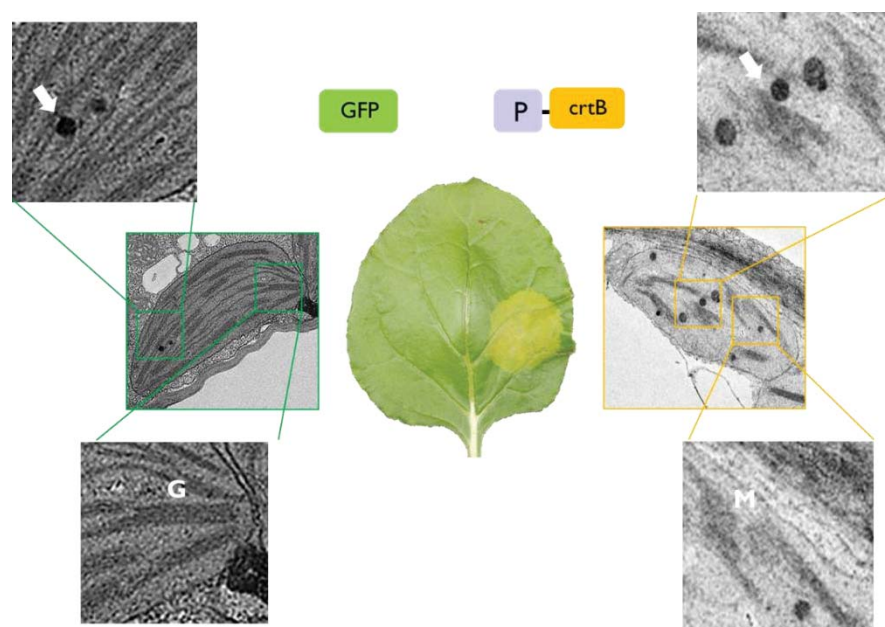


Figure 3.1. Plastids obtained through *crtB* have different structures compared to leaf chloroplasts. TEM pictures evidencing the main structural differences in plastids obtained through the overexpression of (*p*)*crtB* in leaves. Magnifications show the thylakoid grana (G), membranous formations (M) and electron dense globules identified as PG (white arrow).

The thylakoidal membrane system in the area overexpressing (*p*)*crtB* disappeared as chloroplasts were transformed. To quantify the thylakoid degradation, we calculated the grana lateral irregularity (GLI) value. In a chloroplast, the grana have a highly regular structure that fits into a cylindrical shape with very few deviations. The GLI is an estimation of the lateral irregularity of the membranes system and is calculated as the ratio between the mean and the standard deviation of the length of the different thylakoidal disks that compose a granum. In an ideal situation of a highly cylindrical shape, this value is around 0 while in a situation of complete irregularity the value is near 1 (Kowalewska et al., 2016). In our analysis, the GLI value for GFP samples was around 0.1 (indicating a diffused regularity in grana around the chloroplasts) but in (*p*)*crtB* sections it increased to around 0.6, highlighting the disgregation of the thylakoidal membranes (Figure 3.2A). Coherently with the disruption of thylakoidal membranes we found a lower amount of galactolipids in (*p*)*crtB* samples compared to GFP controls (Figure 3.2A). In particular, the galactolipids with a prokaryotic origin that are associated with the thylakoidal membranes (MGDG 18:3/16:3 and DGDG 18:3/16:3) showed a reduction between 40% and 60% compared to GFP samples (Figure 3.2A). We further analysed the differences in abundance of marker proteins that compose the photosynthetic apparatus in leaf material overexpressing (*p*)*crtB* and GFP for 96 hours (Figure 3.2B). We analysed PsbA as a constituent of the D1 protein of PS₂, PsaD as part of the ferredoxin complex in PS₁, PsbO as part of the oxygen splitting complex, PetC as one of the subunits of the cytochrome b₆-f complex, and Lhcb₂ as a component of the light-harvesting complex (Peltier et al., 2000). All the studied proteins showed a reduction in the (*p*)*crtB* samples compared to GFP; the only exception was Lhcb₂, that remained unchanged between the two samples (Figure 3.2B). We further explored the evolution of some of these marker proteins (PsbA, PetC, PsaD, and Lhcb₂) in leaf material sampled 0, 24, 36, 48, 72 and 96 hours after the infiltration (hpi) with (*p*)*crtB* (Figure 3.2C). Unlike Lhcb₂, that maintains its stability over the course of the conversion from chloroplast to chromoplast-like plastids, the other three studied proteins decreased between 36 and 48 hpi, consistent with the photosynthetic impairment previously detected at these time points (Figure 1.3). The absence of changes in the amount of Lhcb₂ could explain the stability in chlorophyll content of (*p*)*crtB* overexpressing leaves (Figure 1.2) as this protein is usually part of complexes that bind the pigment (Pietrzykowska et al., 2014).

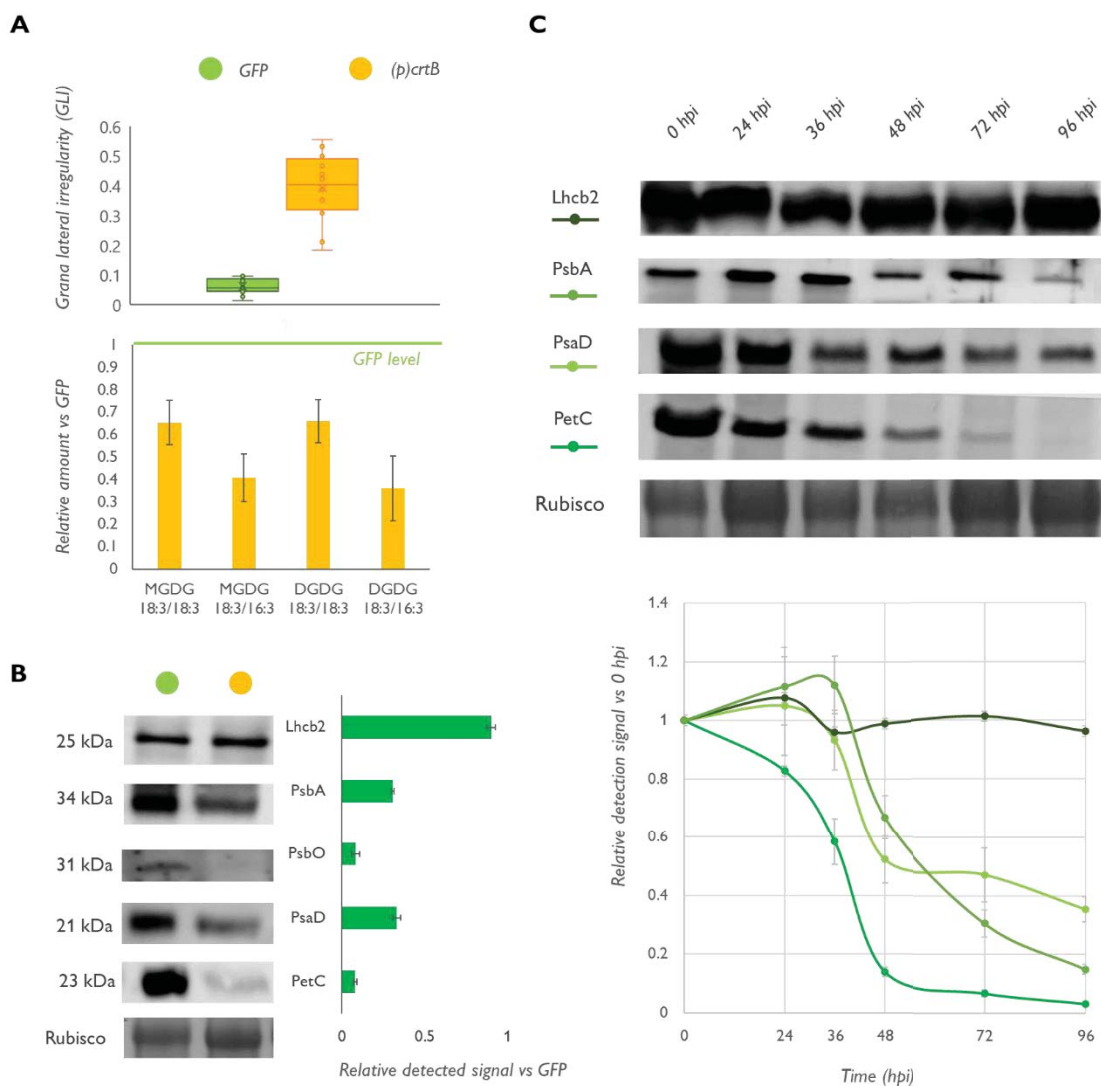


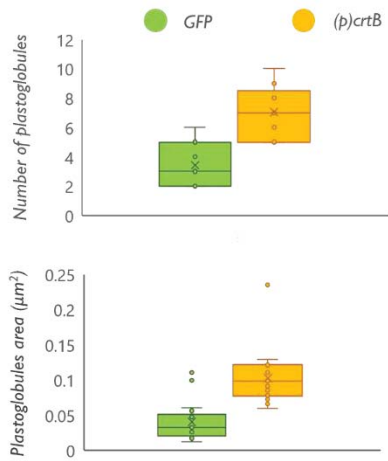
Figure 3.2. *crtB*-induced chromoplast development is associated with the loss of photosynthetic membranes.

(A) Grana lateral irregularity (GLI) value calculated in plastid overexpressing (*p*)*crtB* and GFP and evidencing the degree of degradation of thylakoidal membranes and associated to relative levels of galactolipids in (*p*)*crtB* samples. The amount is relative to the amount detected in GFP controls (indicated by the green line) (B) Relative protein amount in plants overexpressing *crtB* or *GFP* and sampled 96 hpi. (C) Protein amount 0, 24, 36, 48, 72 and 96 hpi in samples overexpressing *crtB*. Values are and calculated based on the intensity of Rubisco protein stained with amidoblack staining and relative to the intensity at 0 hpi. Plots in (A) show mean and SD of 3 different replicates for experiment ($n=3$) while plots in (B) and (C) show mean and SD of 5 replicates for each experiment ($n=5$).

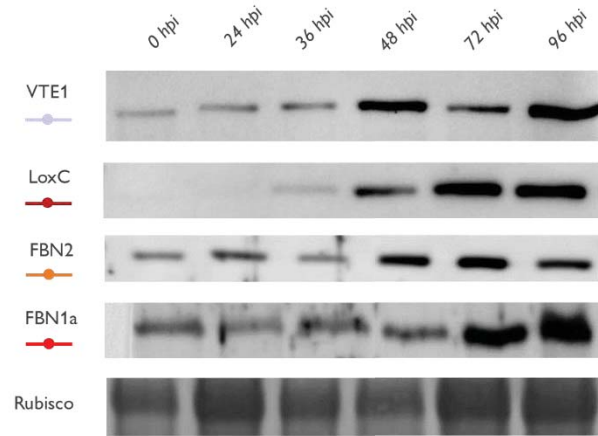
The chromoplasts present in leaves overexpressing (*p*)*crtB* contained a higher number of electrodense globular structures compared to chloroplasts observed in the control GFP leaves. These globules, tentatively identified as PG, were found to be about 50% bigger and more abundant in the chromoplasts of *crtB* samples compared to equivalent structures in chloroplasts

from GFP controls (Figure 3.3A). Similarly, tomato fruit chromoplasts increase in number and size during chloroplast-to-chromoplast transformation, consequent to the liberation of lipids from the thylakoidal membranes (Egea et al. 2010). To further confirm their PG identity, a set of marker proteins related to PG structure and metabolism were analysed in *crtB* and GFP leaves (Figure 3.3A). They included FBN1a, FBN2, and FBN4 as part of the PG core and envelope, and VTE1 and LoxC as PG-associated enzymes involved in the metabolism of tocopherols and membrane lipids (Van Wijk and Kessler, 2017). In the first comparison between leaf areas overexpressing (p)*crtB* and GFP sampled at 96 hpi, we observed a general increase in all the analysed proteins. FBN1a, FBN2, FBN4 and VTE1 doubled their content in (p)*crtB*-overexpressing samples while LoxC experienced a massive 6-fold increase (Figure 3.3B). When analysing a subset of proteins in a time-course manner we observed that FBN1a, FBN2 and VTE1 increased between 48 and 72 hpi while LoxC up-regulation started earlier (Figure 3.3C). These results were confirmed using the PG marker proteins fibrillin FBN7a (PGL34) and VTE1 (Vidi et al., 2006, 2007). Both proteins were equipped with an RFP tag to allow their localization and they were expressed under the control of glucocorticoid-induced promoters. The rationale of using induced promoters was to prevent putative interferences with the differentiation process arising from the constitutive presence of high levels of PG-associated proteins. Tobacco leaves were agroinfiltrated with the RFP-fused PG marker protein constructs together with either GFP or (p)*crtB*, and localization of the fluorescent marker proteins was analysed by confocal laser scanning microscopy (CLSM) at 0, 48 and 96 hpi, after their expression was induced by applying 17 β -Estradiol 24 h earlier (Figure 3.3D). The marker proteins were localized as several dots inside the chloroplasts in a pattern compatible with the described PG localization (Vidi et al. 2006). When the marker proteins were co-expressed with the (p)*crtB* protein the number of globular formations progressively increased from an average of 2 per plastid at 0 hpi to an average of 5 at 96 hpi (Figure 3.3D, E). By contrast, these PG-associated signals remained unchanged in GFP samples. Interestingly, a GFP-tagged version of (p)*crtB* was perfectly co-localized with the RFP-tagged PG markers (Figure 3.3F). Co-immunoprecipitation experiments carried out in *N. benthamiana* (p)*crtB*-GFP leaves demonstrated that *crtB* did not directly interact with PG or thylakoidal proteins (Figure 3.3G), suggesting that the PG localization of *crtB* is an intrinsic feature of the protein and not a consequence of its interaction with other proteins. These results confirmed that the overexpression of *crtB* and the subsequent conversion from chloroplasts to chromoplasts is associated with a proliferation of PG, globular storage structures that could also contain the *crtB* protein itself.

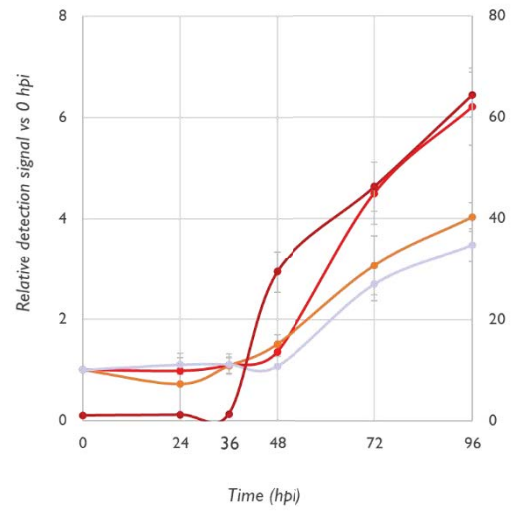
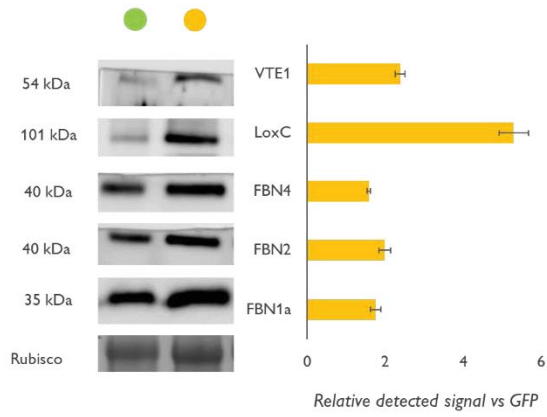
A



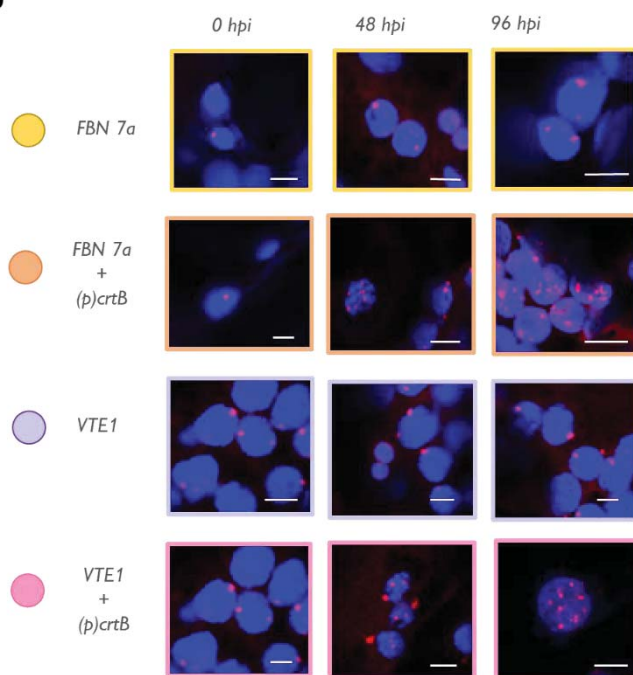
C



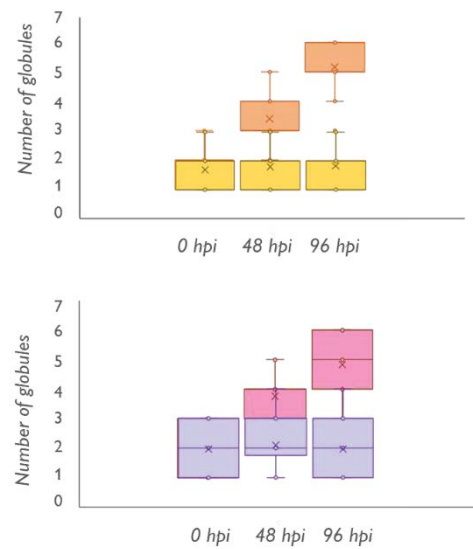
B



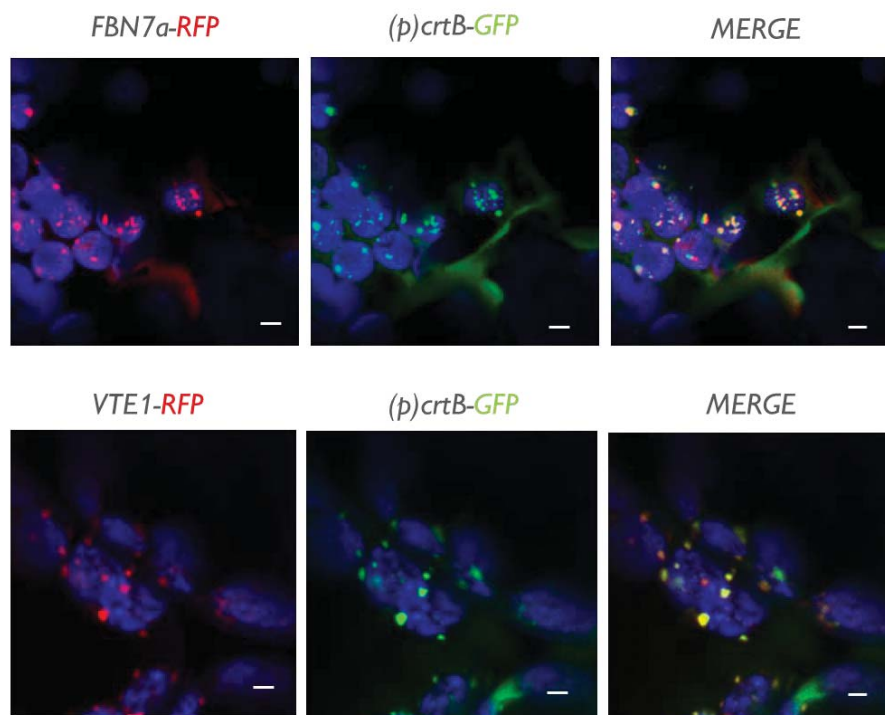
D



E



F



G

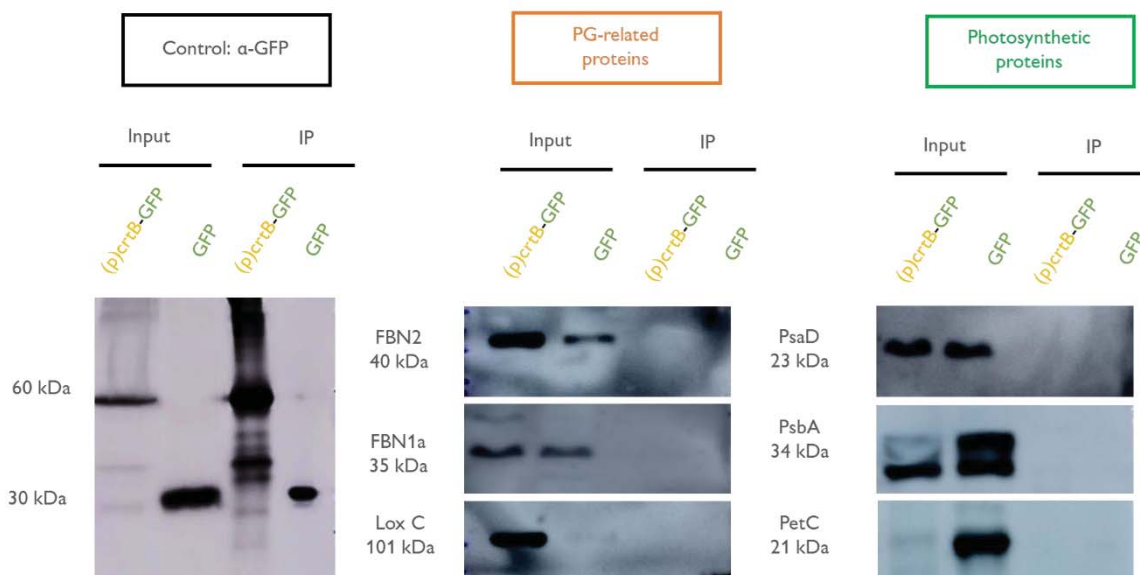
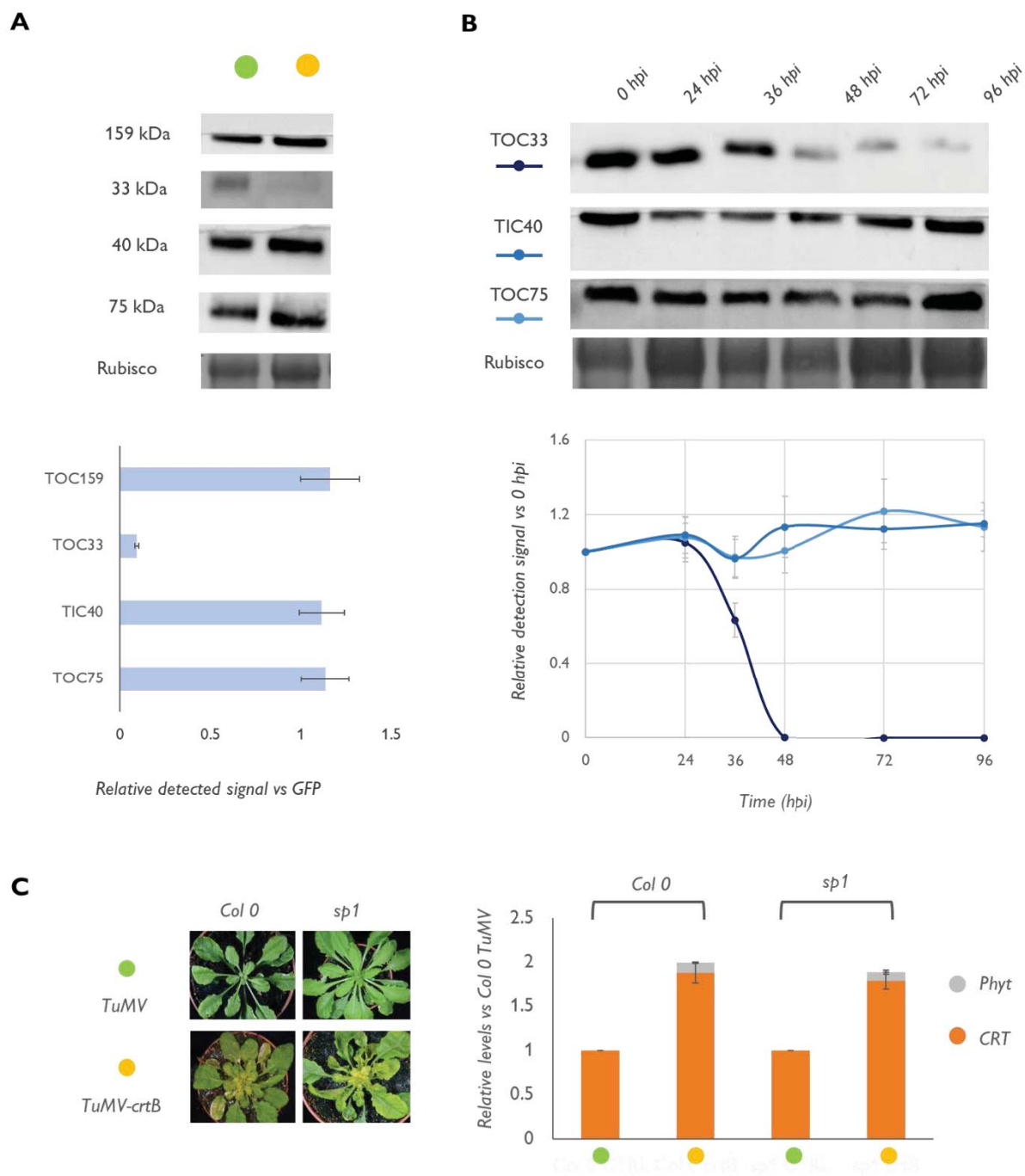


Figure 3.3. crtB-induced chromoplast development generates the proliferation of electrodense globular structures. (A) Number and area of globular formations detected in TEM pictures of plastid overexpressing (p)crtB and GFP (B) Relative PG-related protein amount in plants overexpressing (p)crtB or GFP and sampled 96 hpi. (C) Protein evolution 0, 24, 36, 48, 72 and 96 hpi in samples overexpressing crtB. Values are calculated based on the intensity of Rubisco protein stained with amidoblack staining and relative to the intensity at 0 hpi (D) Confocal microscopy pictures showing the localization of PG markers and the progressive increase of globular formation when

overexpressing (*p*)*crtB*, blue colour corresponds to the autofluorescence of chlorophylls while red colour corresponds to the protein tagged with RFP (E) Boxplots show the evolution of globules number 0, 48 and 96 hpi in plants overexpressing the marker only or the marker together with (*p*)*crtB*. (F) Co-localization picture of PG marker and (*p*)*crtB*-GFP protein showing the plastoglobular localization of the latter. White bar corresponds to 5 μ m. Plots in (B) and (C) show mean and SD of 5 replicates for each experiment (n=5). (G) *crtB* protein does not specifically interact with PG or photosynthetic proteins. The (*p*)*crtB*-GFP protein was produced in *N. benthamiana* leaves and complexes containing it were isolated by immunoprecipitation using anti-GFP magnetic beads. Protein extracts before (Input) and after immunoprecipitation (IP) were used for immunoblotting analysis with antibodies against GFP or the indicated endogenous proteins.

We also studied the changes in the amount of TOC159, TOC75, TOC33, and TIC40, a set of marker proteins of import-export complexes situated in the chloroplast envelope, a structure supposed to be stable during chromoplastogenesis (Sadali et al., 2019). The amount of TOC159, TOC75 and TIC40 did not change in *crtB* samples compared to GFP (Figure 3.4A). TOC33, however, showed a strong decrease. When analysing a subset in a time-course manner, TOC75 and TIC40 confirm their stability with only a slight fluctuation over time while we confirmed that TOC33 amount strongly decreases starting from 36 hpi (Figure 3.4B). TOC33 together with TOC159 and TOC75 are major TOC components mainly involved in the import of photosynthesis-related proteins, and all three of them are targeted for ubiquitination and degradation by the RING-type ubiquitin E3 ligase SP1 in *Arabidopsis* (Ling and Jarvis, 2015; Ling et al., 2021) SP1 activity hence modifies the balance between different substrate-specific translocons and the operation of substrate-specific protein import pathways to facilitate the plastid differentiation (e.g., etioplasts to chloroplasts or chloroplasts to gerontoplasts). Recent evidence also indicates that the tomato SP1 homologues regulate the transition of chloroplasts into chromoplasts during fruit ripening (Ling et al., 2021). Upregulated levels of SP1 proteins in tomato led to reduced levels of TOC75 but not TIC40, as expected. However, *crtB*-dependent chromoplast differentiation in tobacco leaves did not involve changes in the levels of SP1 targets such as TOC75 or TOC159 (Figure 3.4A, B). Furthermore, virus-mediated expression of *crtB* in *Arabidopsis* mutant plants defective in SP1 resulted in leaves showing the characteristic yellow phenotype and carotenoid overaccumulation observed in the wild-type (Figure 3.4C), suggesting that SP1 activity is not required *crtB*-mediated chromoplastogenesis. We reasoned that the decrease in TOC33 observed when *crtB* is expressed in tobacco leaves might be a SP1-independent process that selectively targets this TOC component to prevent the import of photosynthetic proteins. By using CFP-fused marker proteins of the envelope outer and inner membranes (TOC64 and TIC40, respectively) (Breuers et al., 2012), we further confirmed a similar localization of the markers in GFP and *crtB* samples at all stages (Figure 3.4D), which

together with the absence of vesicles forming from inner envelope membranes in TEM images (Figure 3.1) argues against the envelope membranes as major contributors to the newly-formed internal membrane systems that develop in *crtB*-triggered chromoplasts. Instead, it is most likely that the disintegration of thylakoid membranes is responsible for the formation of the dense membrane stacks and proliferating PG observed in these plastids.



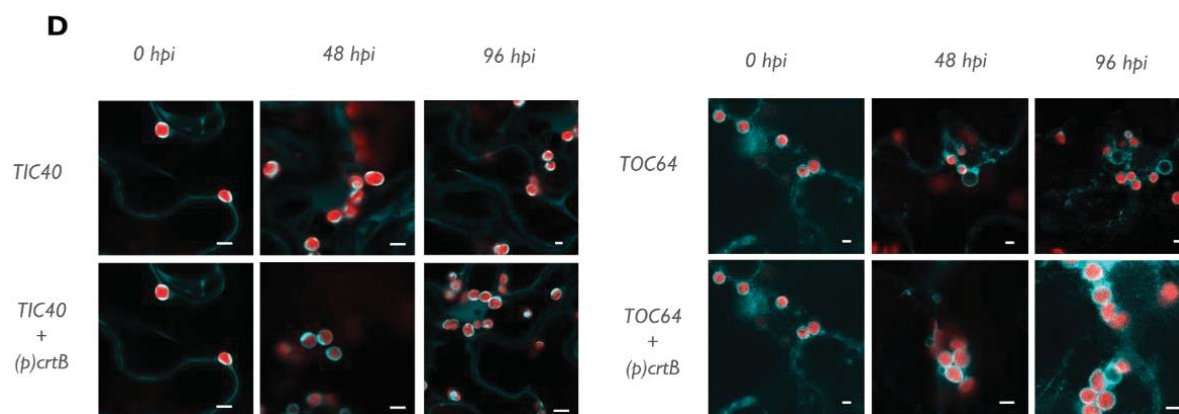


Figure 3.4. crtB chromoplasts induce only minor changes in most envelope proteins (A) Relative protein amount in plants overexpressing (p)crtB or GFP and sampled 96 hpi. (B) Protein evolution 0, 24, 36, 48, 72 and 96 hpi in samples overexpressing (p)crtB. Values are and calculated based on the intensity of Rubisco protein stained with amido black staining and relative to the intensity at 0 hpi. (C) Pictures showing the phenotype of *Arabidopsis* Colo and sp1 mutants inoculated with TuMV as a control or with TuMV-crtB and relative amount of phytoene (phyt) and total carotenoids excluding phytoene (CRT). (D) Confocal microscopy pictures showing the localization of inner and outer envelope markers and the absence of changes during (p)crtB overexpression. Red colour indicates the autofluorescence of chlorophyll while the light blue colour corresponds to the CFP-tagged envelope proteins. Plots in (A) and (B) show mean and SD of 5 replicates for each experiment (n=5). Plots in (C) show mean and SD of 3 different replicates (n=3) and are relative to the ones obtained in Col 0 inoculated with TuMV.

3.2.2. Artificial chromoplasts accumulate isoprenoids that distribute differentially in plastid substructures.

After having demonstrated the generation of new structures that could potentially store different types of plastidial isoprenoids besides carotenoids, we investigated if the levels of these metabolites were altered in artificially obtained chromoplasts (Figure 3.5B). We were able to observe a 1.5 to 2-fold increase in the levels of total tocopherols and phylloquinone in (p)crtB-triggered artificial chromoplasts compared to the amount observed in the green chloroplasts of GFP control leaves. Additionally, (p)crtB-overexpressing leaves contained similar increases in the amount of α -tocoquinone (α -TQ) and plastochromanol 8 (PC-8), a vitamin E tocochromanol derived from plastoquinone 9 (PQ-9). Only PQ-9 was decreased in (p)crtB samples, likely as an effect of the disgregation of thylakoidal membranes coherently with what detected in tomato fruits in previous studies (Van Wijk and Kessler, 2017). The amount of ubiquinone (UQ), a mitochondrial isoprenoid, did not change between the two samples and for this reason constituted an optimal control that the observed changes in plastidial isoprenoids were likely the result of altering the ultrastructure of plastids (Figure 3.5B).

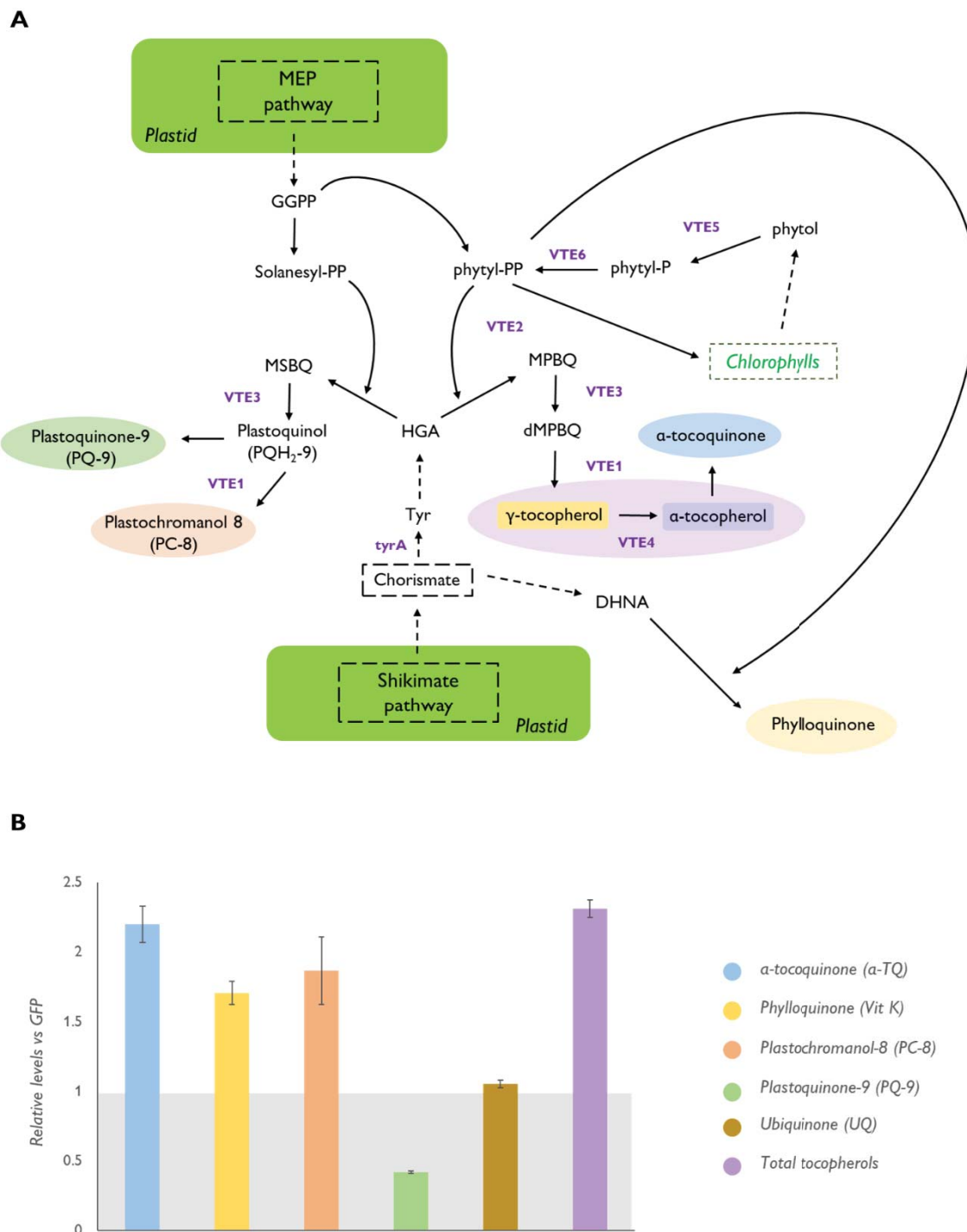
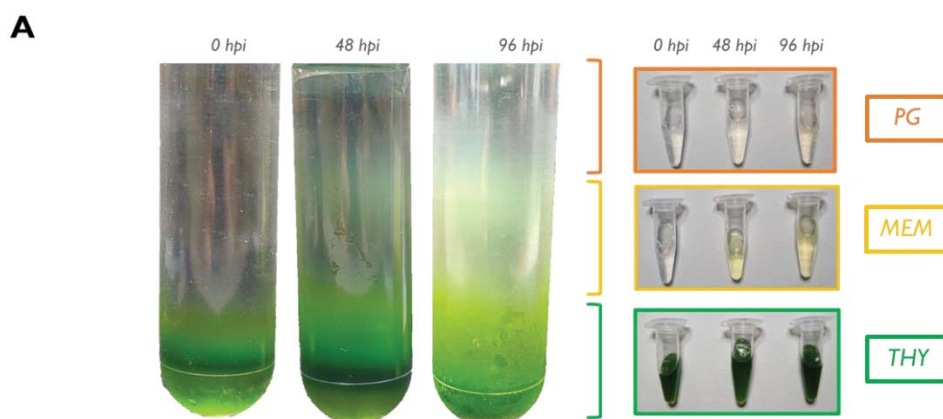


Figure 3.5. Artificial chromoplasts accumulate isoprenoids other than carotenoids. (A) Schematic representation of the prenylquinones biosynthetic pathway indicating the corresponding genes for every step. (B) UPLC-MS data showing the array of prenylquinones detected in (*p*)*crtB*-overexpressing leaves. Values are relative to the amount present in GFP control samples (shaded in gray). Plots show the mean and SD of 3 replicates ($n=3$).

Once demonstrated that chromoplast generation triggered by *crtB* was associated with accumulation of a wide array of isoprenoid, we hypothesized that the different metabolites could be distributed differently in the plastid as already described for chloroplasts and tomato fruit chromoplasts. Van Wijk and Kessler, 2017). We performed, thus, a chloroplast fractionation by ultracentrifuging chloroplast membranes on a sucrose gradient (Vidi et al., 2006) using material coming from plants overexpressing (p)*crtB*-GFP for 0, 48, and 96 hpi (Figure 3.6). The lower part of the gradient was expected to contain the thylakoid membranes or its remnants. The intermediate layers (15% and 20% sucrose) did not show any Colouration at 0 hpi while at 48 hpi the same section of the gradient contained traces of green material and at 96 hpi acquired a yellowish colour. The upper part of the gradient (5% sucrose) was mainly transparent but took an oily consistency and a brownish colour as the chromoplastogenesis process advanced (Figure 3.6A). These observations suggested a possible variation of the metabolites contained in different sections of gradient.

By probing the different fractions with antibodies against FBN1a, TOC75 and Lhcb2 (to localize PG, envelope and thylakoidal membranes, respectively), we divided the gradient into three differential zones: PG zone (fractions 1-10 in the 5% sucrose part of the column with FBN1a), membranous zone (fractions 11-20 in the 15% and 20% sucrose part where TOC75 but not Lhcb2 was localized), and thylakoidal zone (fractions 21-30 in the 38% and 45% sucrose gradient zones, where only Lhcb2 was found) (Figure 3.6B). The localization of the *crtB*-GFP protein was restricted to the PG fraction at 48 hpi and 96 hpi (Figure 3.6C). In the same PG fractions, we were able to detect the PG markers FBN1a and FBN2, whereas Lhcb2 and PsaD proteins were only found in the thylakoidal fraction and Rubisco was only present in the stroma (Figure 3.6C). These results not only validate the subplastidial fractionation method but additionally confirm our previous conclusion that *crtB* specifically localizes in PG.



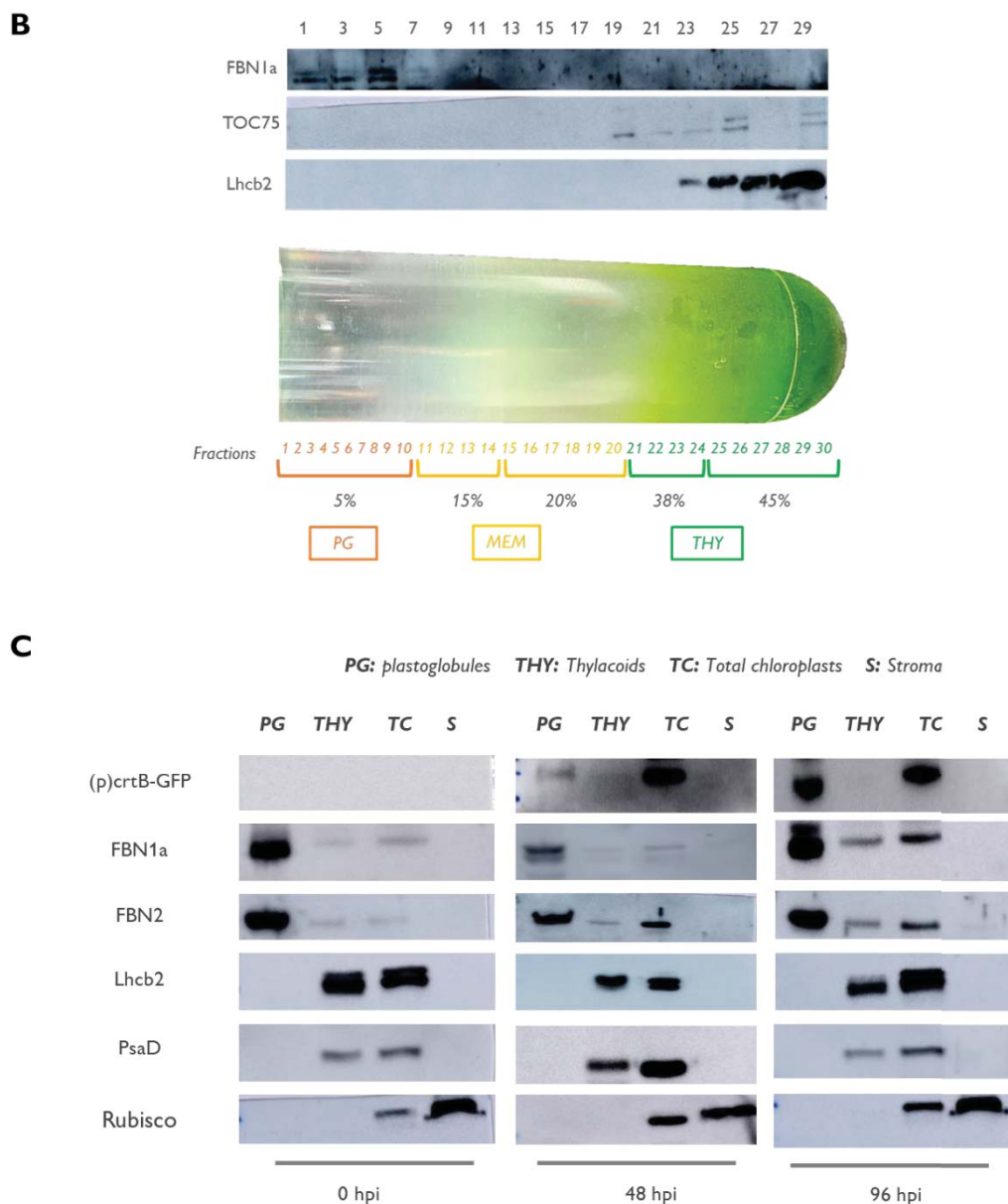


Figure 3.6. crtB-induced chloroplast to chromoplast transition is associated with changes in internal structures of the plastid (A) Pictures of the sucrose gradient ultracentrifugation result. Tubes containing fractionated membranes of leaves expressing (p)crtB for 0, 48 and 96 hours show different colour gradients. (B) Western blot probing the localization of FBN1a, TOC75 and Lhcb2 proteins in the gradient. (C) Western blot showing (p)crtB-GFP protein localization in pooled fractions of the plastids. Anti-GFP binds in the pool of PG fractions co-localising with two PG markers: FBN1a and FBN2.

We next analysed the metabolite composition of these zones by using the fractions for UPLC-MS analysis (Figure 3.7). We observed that in the PG zone the total amount of isoprenoid metabolites highly increased over time. The major compounds at 0 hpi were tocopherols while carotenoids became the most abundant isoprenoids from 48 hpi. Large increases in the rest of the plastidial isoprenoids were also detected at 48 hpi. At 96 hpi the levels of all the compounds

further increased except for PQ-9. Observing the carotenoid composition in detail, we found a significant enrichment in the amount of β -carotene at 48 hpi and 96 hpi. The presence of phytoene was almost exclusively associated to this PG zone at the same time points (Figure 3.7), suggesting that the crtB protein is enzymatically active in the PG. The membranous zone showed a general decrease of tocopherols and PQ-9 and an increase of carotenoids, with the prevalent presence of lutein (likely responsible for yellow colour of the fractions). The thylakoidal zone hardly showed an increase in the total amount of metabolites compared with the other two zones, suggesting that the accumulation of compounds is mainly carried on by other plastid substructures. In this zone, only xanthophylls and tocopherols increased as chromoplasts developed whereas PG-9 decreased (Figure 3.7).

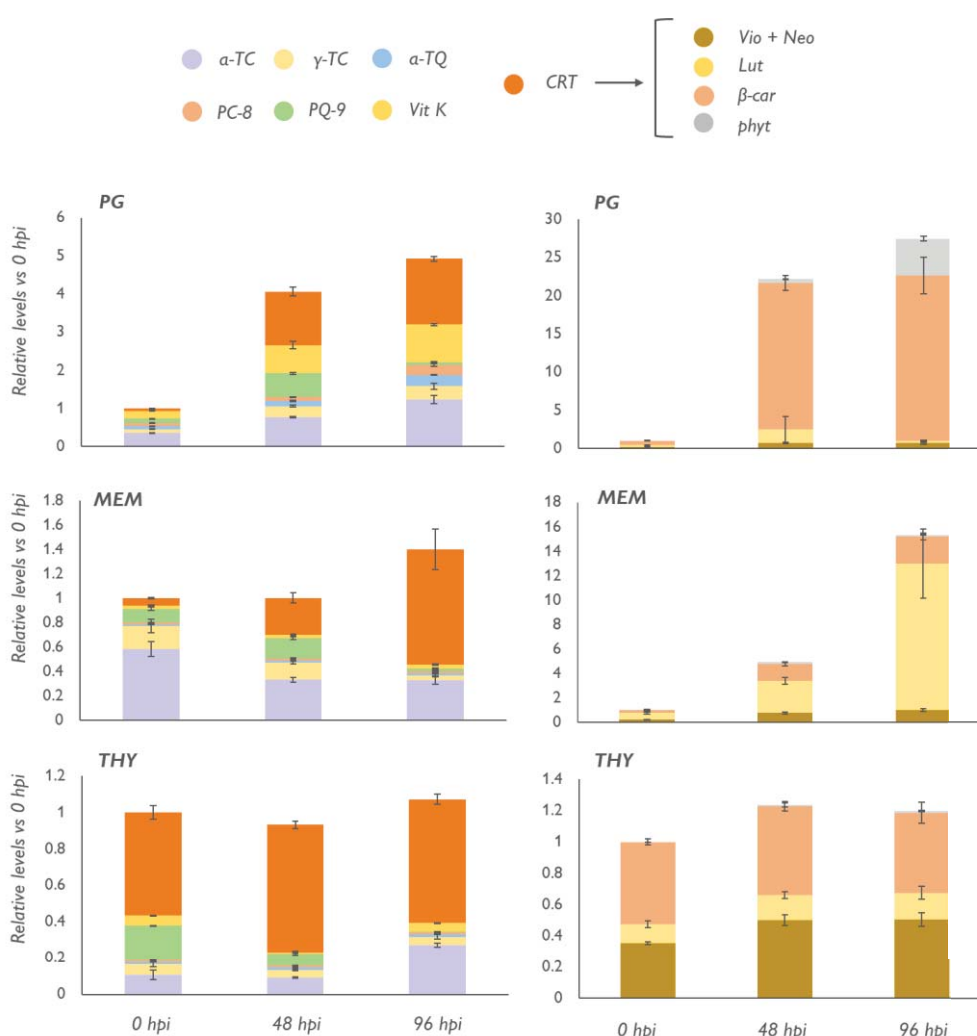


Figure 3.7. Isoprenoids are distributed differently in plastidial compartments, but PG are the only structure able to store all the isoprenoids in detectable amounts. Relative levels of plastidial isoprenoids (left) and proportion of carotenoids (right) detected in leaves overexpressing (p)crtB for 0, 48 and 96 hpi. Values are relative to 0 hpi. Plots show the mean and SD of values calculated from samples obtained from 3 independent fractionations. The first row corresponds to the metabolites found in the plastoglobular fractions (PG), the second to the ones found in the membranous fraction (MEM), and the third row corresponds to the content of the thylakoidal fractions (THY).

These results, together, showed that *crtB*-triggered chromoplasts develop different internal storage structures able to produce and store isoprenoids and confirmed that the *crtB* protein is localised in PG, which are the main storage structures for these newly synthesized plastidial isoprenoids (including phytoene and β -carotene).

3.2.3. High light acclimation and dark-induced senescence are effective for the enrichment of leaves in plastidial isoprenoids.

After having described the major relevance of PG for plastidial isoprenoid synthesis and storage in *crtB*-induced chromoplasts, we next explored strategies to improve PG accumulation with the eventual goal of enriching leaves in these health-promoting metabolites. We started by analysing the effect of environmental conditions able to promote the formation of PG, e.g., high-PAR exposure and dark induced senescence (Lichtenthaler et al., 2007). Other than the increase in carotenoid content previously reported in chapter 2, the overexpression of (*p*)*crtB* in high-PAR (W_{500}) acclimated plants resulted in an increase in total tocopherols level with a prevalent increment of α -tocopherol, likely connected to the high antioxidant activity of this compound. The acclimation to higher intensity of light did not show any significant effect on the content of α -TQ or PC-8 but produced a significant increase in the amount of phylloquinone (Vit-K) and PQ-9 compared to the one present in plants grown under W_{50} (normal PAR) generating thus a higher improvement compared to the content in green leaves overexpressing GFP and growing under W_{50} (Figure 3.8). This variation can be related to the photosynthetic remodelling of the thylakoidal apparatus. Despite the increase, PQ-9 level was still lower than the one in GFP overexpressing plants.

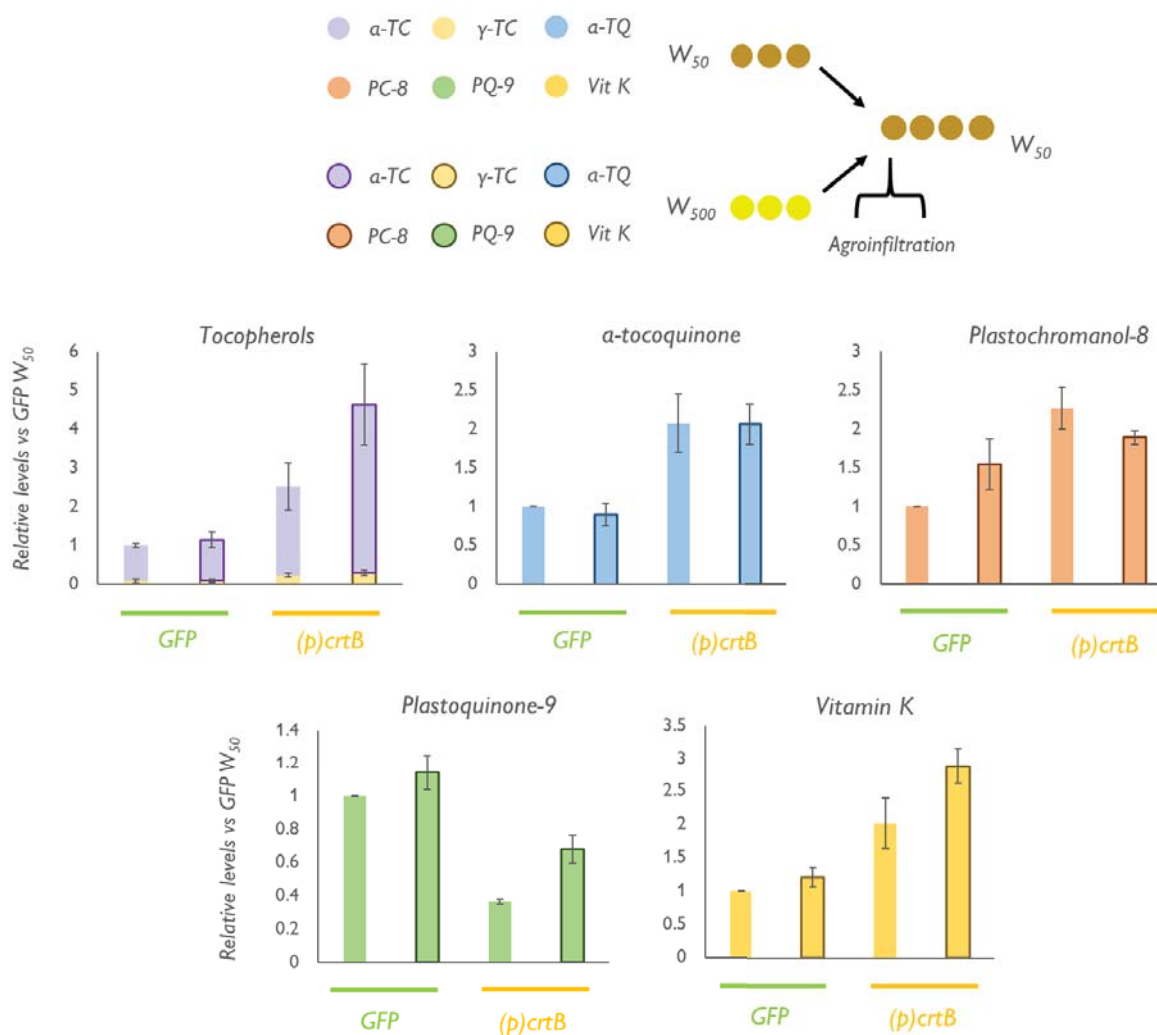


Figure 3.8. High-PAR pre-acclimation can impact the accumulation of plastidial isoprenoids. *N. benthamiana* plants were grown for 3 days either under normal or high-PAR (W_{50} and W_{500} respectively) and after the infiltration were all moved to W_{50} for 4 days. The graphs show the relative amount of plastidial isoprenoids in leaves from plants pre-acclimated to W_{50} or to W_{500} that were later agroinfiltrated with GFP (green) or (p)crtB (orange) constructs and collected at 96 hpi. Values are relative to the amount detected in GFP control samples from plants acclimated to W_{50} . Plots show mean and SD of 3 different plants ($n=3$). Asterisks mark significant differences between the amount of metabolite detected in leaf sectors overexpressing (p)crtB in W_{500} -acclimated plants compared to plants acclimated to W_{50} and expressing the same construction. (t-test, * $P<0.05$).

We tested then the impact on metabolite composition of dark-induced senescence as the biological process where the PG amount and size is maximum to allow chlorophyll degradation products mobilization (Besagni and Kessler, 2013). GFP- and (p)crtB-overexpressing leaves were collected from the plant at 96 hpi and kept in the dark for 10 days, which resulted in a pale green-yellow colour (Figure 3.9A). Senescent GFP-overexpressing leaves accumulated 3-fold times more α -TQ, 2.6-fold times more PC-8, 1.8-fold times more PQ-9, and 4.8-fold times more

tocopherols compared to non-senescent GFP controls (Figure 3.9B). Interestingly the senescence treatment had no effects on Vit-K content but decreased total carotenoid contents. Senescent (p)crtB-overexpressing leaves, on the other hand, showed a higher increase in metabolite contents compared to non-senescent GFP controls: α -TQ increased by 11-fold times, PC-8 by 7.5-fold times, and total tocopherols by 11-fold times (With α -TC increasing 10-fold times). Differently to what has been observed in GFP sectors Vit-K content also increased 2.5-fold times in senescent (p)crtB while PQ-9 showed no changes probably because an increase was then compensated by the natural lowering occurring during the generation of chromoplasts. (Figure 3.9B). Dark-induced senescence however also resulted in a slight loss of carotenoids in (p)crtB sectors. The loss of carotenoid pigments is a hindrance for the applicability of this strategy.

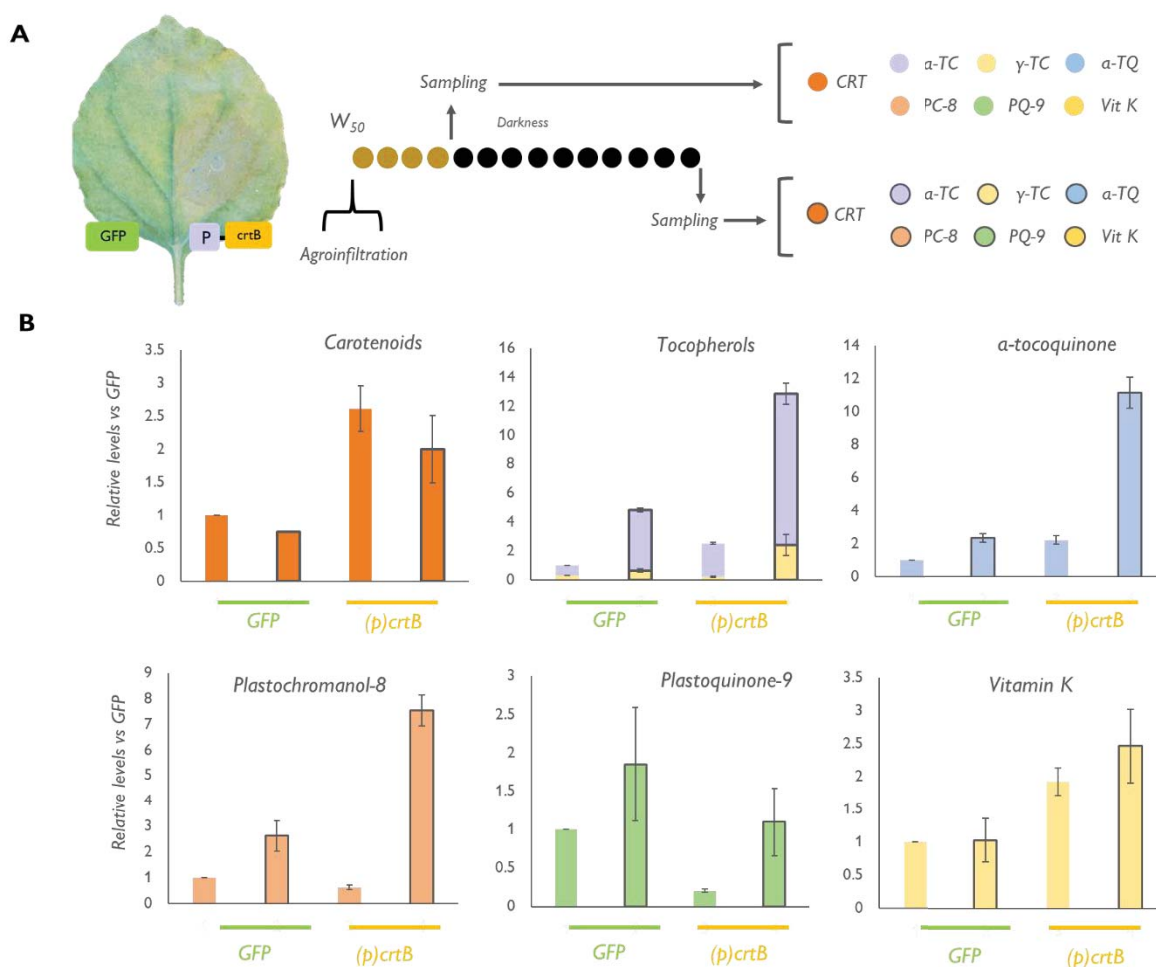
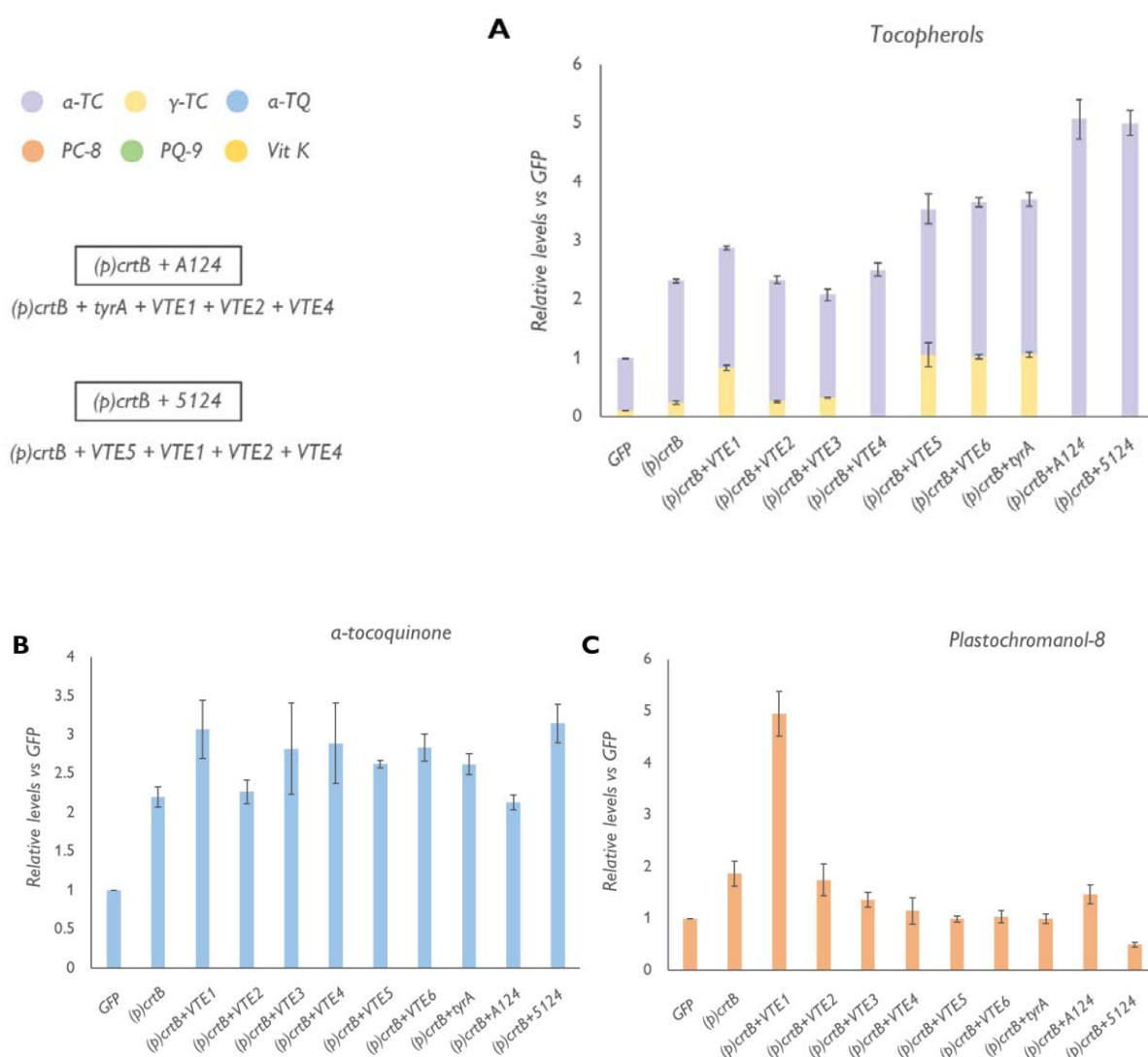


Figure 3.9. Senescence can drastically increase the level of some plastidial isoprenoid (A) schematic representation of the experimental setting and phenotype of dark-induced senescent leaves. Plants were infiltrated with (p)crtB or GFP constructs and after 4 days leaves were detached and left in darkness for 10 additional days before sampling them for further analysis (B) Relative amount of plastidial isoprenoid identified in senescent GFP leaves (upper panel) or in senescent (p)crtB-sectors. Values are relative to the ones found in not-senescent GFP samples (represented by the grey square). Plots show the means and SD of 3 replicates (n=3).

3.2.4. crtB can be combined with isoprenoid biosynthetic genes for an additional enhancement effect

Given that the *crtB*-dependent increase in carotenoid level is accompanied with an increase of other healthy isoprenoids such as tocopherols likely due to an improved storage, we speculated that the co-overexpression of tocopherol biosynthetic genes might boost the vitamin E contents of agroinfiltrated leaves as appropriate structures for their sequestration were in place. We tested single genes of the tocopherol biosynthetic pathway (Figure 3.3, 3.5) in combination with the (*p*)*crtB* gene: *VTE1*, *VTE2*, *VTE3*, *VTE4*, *VTE5*, *VTE6* and *tyrA* (a bacterial gene able to catalyse the formation of tyrosine starting from prephenate avoiding the feedback inhibition problem related to this compound). We also tested several gene combinations to produce exclusively α -tocopherol: *tyrA+VTE1+VTE2+VTE4+(p)crtB* and *VTE5+VTE1+VTE2+VTE4+(p)crtB* (Figure 3.10). The overexpression of *VTE2* or *VTE3* in combination with (*p*)*crtB* did not produce any relevant increase in tocopherol content compared to the overexpression of only the (*p*)*crtB* gene. The overexpression of the *VTE1* gene together with (*p*)*crtB* increased the levels of total tocopherols by means of increasing 3 times the amount of γ -tocopherol compared to (*p*)*crtB* alone. The overexpression of *VTE4* and (*p*)*crtB* resulted in total tocopherols level comparable to the one obtained by overexpressing (*p*)*crtB* alone but with α -tocopherol as the only tocopherol, as expected from the known role of *VTE4*. The overexpression of enzymes required for the synthesis of precursors like *VTE5*, *VTE6* and *tyrA* together with (*p*)*crtB* resulted all in a similar increase in the level of total tocopherols (1.3-fold) compared to the overexpression of the single (*p*)*crtB* gene suggesting that the availability of substrates either from the phytol side or from the tyrosine side is a major limiting factor to control the outcome of the tocopherol biosynthetic pathway. The two multigene combinations *tyrA+VTE1+VTE2+VTE4+(p)crtB* and *VTE5+VTE1+VTE2+VTE4+(p)crtB* resulted in increased levels of total tocopherols (likely because of the higher availability of precursors) with the sole presence of α -TC due to the presence of the *VTE4* gene in the combinations (Figure 3.10A). None of the combinations analysed provided a significant increase in the amount of α -TQ compared to the overexpression of the single (*p*)*crtB* gene (Figure 3.10B). Vit K amount was also very stable in all the combinations except in *VTE5+(p)crtB* and *VTE6+(p)crtB*, that resulted in an increased accumulation of this isoprenoid vitamin likely because of the activated supply of the phytol-PP moiety required in the phylloquinone metabolic pathway (Figure 3.10C). PC-8 was increased by the combination of (*p*)*crtB* and *VTE1*, as expected (Figure 3.10D) while PQ-9 was decreased in all the combinations following the same trend observed when overexpressing (*p*)*crtB* alone (Figure 3.10E).

Interestingly the co-overexpression of $(p)crtB$ and VTE_3 resulted in levels of PQ-9 comparable to the ones observed in green leaves overexpressing GFP . According to the presence of a high amount of α -tocopherol, the samples overexpressing $tyrA+VTE_1+VTE_2+VTE_4+(p)crtB$ and $VTE_5+VTE_1+VTE_2+VTE_4+(p)crtB$ showed the highest antioxidant activity. This information is very relevant because the overexpression of these genes did not impact the levels of carotenoids accumulated through $(p)crtB$ (Figure 3.10F, G) suggesting that the increase in the levels of tocopherols could have a protective effect against carotenoid oxidation and that the difference in antioxidant activity of the extract would be dependent mostly on variations in vitamin E content.



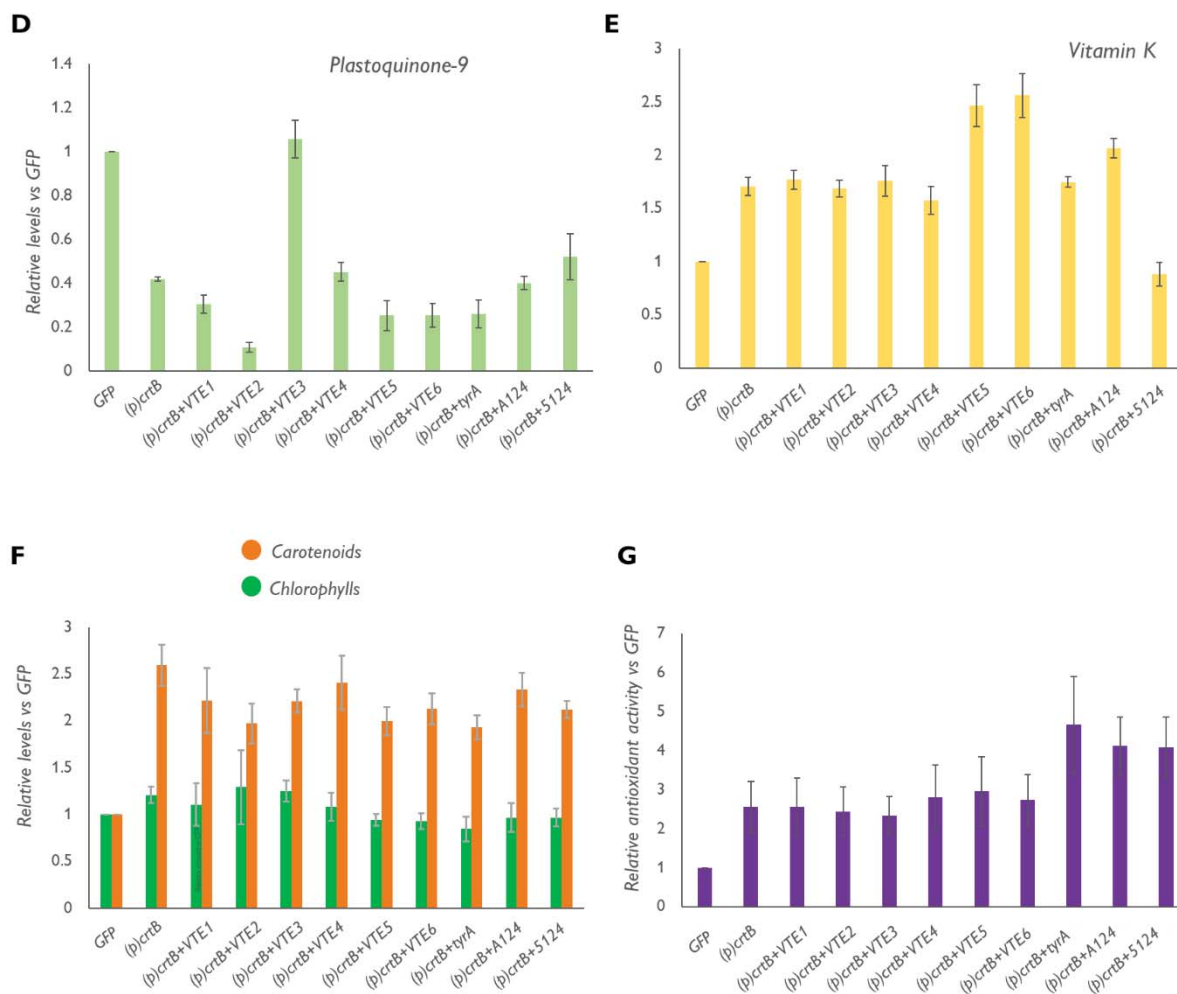


Figure 3.10. Levels of isoprenoid in *crtB*-chromoplasts can be improved by overexpressing genes involved in tocopherol biosynthesis. (A,B,C,D,E) Relative amount of isoprenoids in plants overexpressing (*p*)*crtB* together with different genes involved in tocopherol biosynthesis. Leaves were co-infiltrated with agrobacterium solutions carrying out the plasmids of interest and leaf material was collected 96 hpi. Values are relative to GFP overexpressing sectors. (F) Relative levels of chlorophylls and carotenoids in the same combinations (G) Relative antioxidant activity calculated as μM of Trolox equivalent of extracts coming from plants overexpressing different combinations of genes for 96 hours. Plots show mean and SD of 3 different replicates ($n=3$).

3.2.5. Physical treatments and metabolic engineering can be combined for additional enhancement

The “pull” strategy based on treatments able to increase storage capacity (i.e., PG proliferation), and the “push” strategy based on the overexpression of biosynthetic genes were able to improve isoprenoid content of leaves separately. We hypothesized that the two approaches could be combined to sum their positive outcomes. First, we tested the effect of W_{500} pre-acclimation and the combinations *VTE1+(p)crtB*, *VTE4+(p)crtB*, *VTE5+(p)crtB* and *VTE5+VTE1+VTE2+VTE4+(p)crtB* (i.e., the best performing gene combinations among the ones

previously presented). All the combinations showed an increased level of total carotenoids (particularly β -carotene) compared to $(p)crtB$ -overexpressing plants grown in normal light (Figure 3.11). This increase was coherent with the one observed in the previous trial (Figure 3.8) and highlighted the reproducibility of the treatment. Tocopherols were also increased by the high-PAR treatment in a similar way while the combination of $VTE_5+VTE_1+VTE_2+VTE_4+(p)crtB$ resulted in an increased pool of α -tocopherol (Figure 3.11). The co-overexpression of $(p)crtB$ and VTE_5 maintained the improved accumulation of vitamin K amount already observed in plants that were not exposed to high-PAR (Figure 3.11). These results confirmed that the improvements obtained with the pre-acclimation to high light were maintained when overexpressing tocopherol biosynthetic genes.

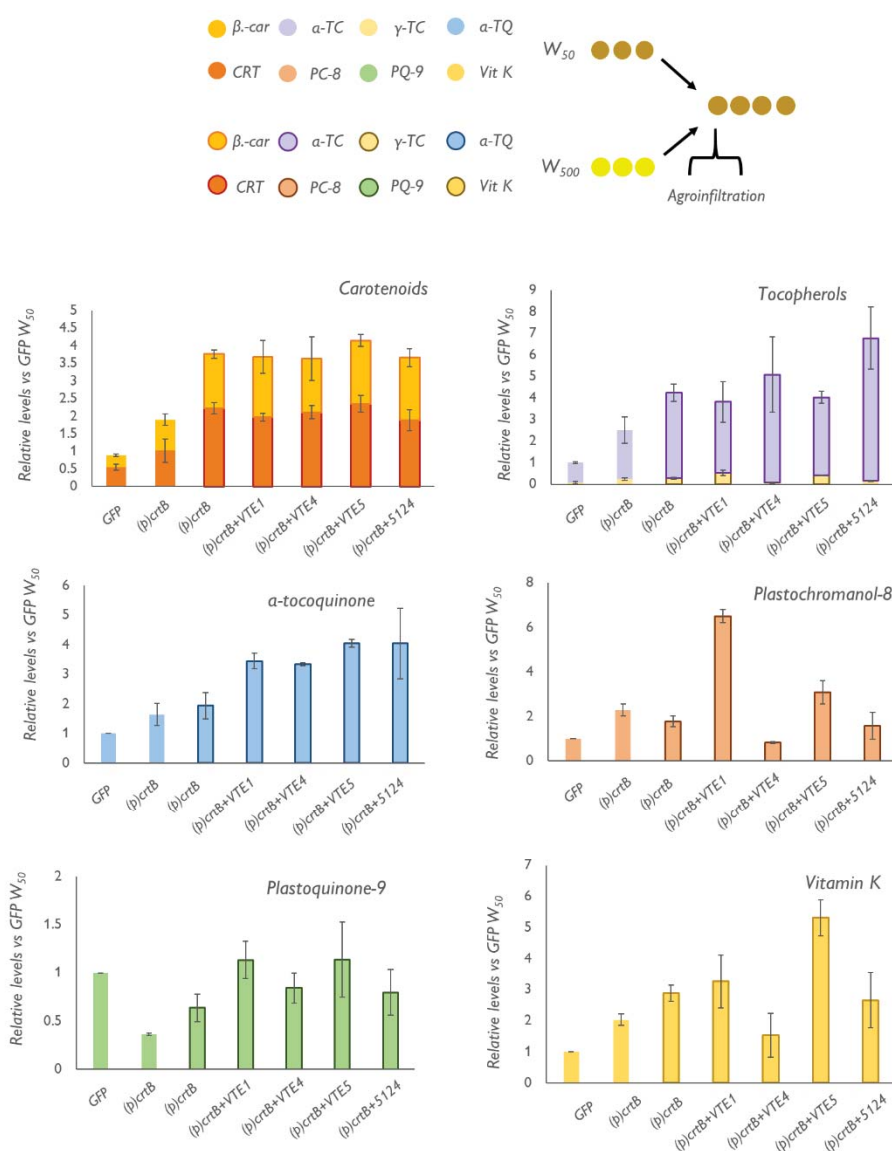
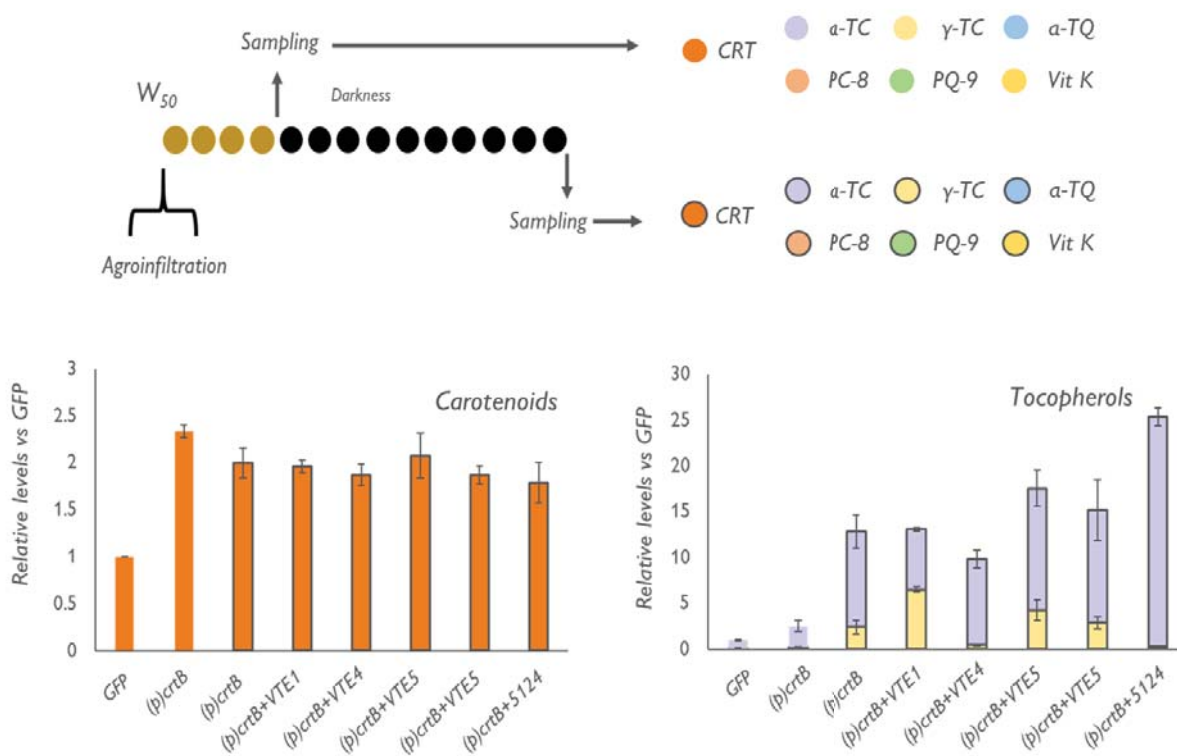


Figure 3.11. High-PAR acclimation provides additional improvement to metabolite content. Relative metabolite levels of isoprenoids in plants acclimated to high-PAR (W_{500}) for 3 days and then moved to normal-PAR (W_{50}) for 96 hours to express the combination of constructs enlisted. Values are relative to the ones obtained from plants acclimated to W_{50} and overexpressing the control GFP. Plots show means and SD of 3 different replicates ($n=3$).

We then tested the effect of dark-induced senescence on the combinations of $VTE_{1+(p)crtB}$, $VTE_{4+(p)crtB}$, $VTE_{5+(p)crtB}$, $VTE_{6+(p)crtB}$, $VTE_{5+VTE_{1+VTE_{2+VTE_{4+(p)crtB}}$. We included VTE_6 in the combinations because of its role in the senescence process where, together with VTE_5 , has a key role in the recycling of the phytol group from chlorophyll. We again observed a slight reduction in the content of total carotenoids compared with non-senescent leaves overexpressing $(p)crtB$ (Figure 3.12). The increase of tocopherols, on the other hand, was drastic, especially in the multiple combinations $VTE_{5+VTE_{1+VTE_{2+VTE_{4+(p)crtB}}$ where the levels increased 25-fold. Again, the overexpression of VTE_5 and VTE_6 resulted into an increased amount of Vit K (6- and 7- fold times, respectively) (Figure 3.12). These results confirmed that, like what deduced for high PAR treatments, the metabolic effects observed in senescent chromoplasts can be combined with the metabolic engineering approach and that the obtained improvements are drastic for some specific compounds.



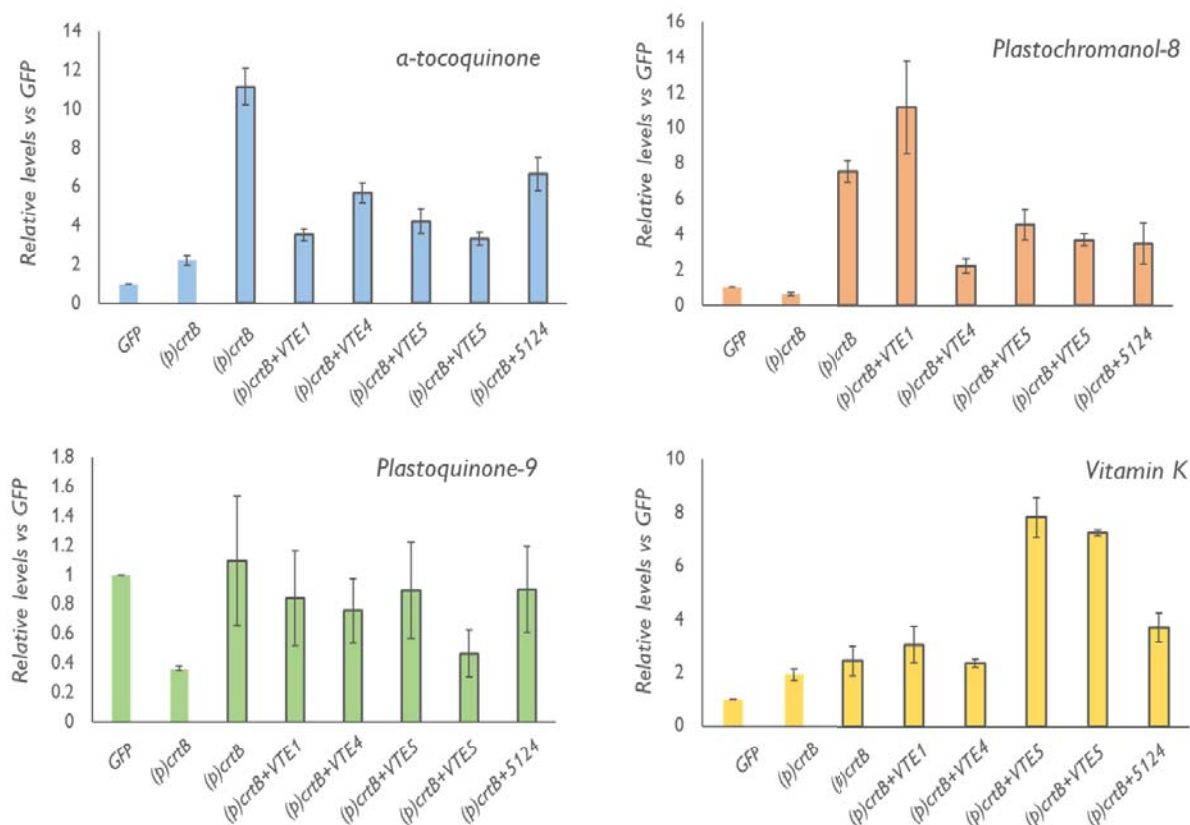


Figure 3.12. Senescence provides additional improvement to metabolite content. Relative metabolite levels in plants overexpressing (p)crtB for 96 hours and subjected to dark-induced senescence (10 days in darkness). Control leaves overexpressing GFP or (p)crtB were collected 96 hpi and not subjected to the treatment. Values are relative to the ones obtained from GFP control leaves. Plots show means and SD of 3 different replicates (n=3).

3.2.6. crtB overexpression can be used to biofortify edible leaves

We have previously shown that *crtB* overexpression was able to trigger chromoplast differentiation and a bright yellow-orange colour in plants other than tobacco like zucchini and lettuce (Llorente et al., 2020). We hypothesized that besides the expected carotenoid accumulation, this strategy might also enrich the leaves in tocopherols and other isoprenoid vitamins, making it a suitable method for multivitamin biofortification of edible leaves. The *crtB* gene was expressed in two lettuce varieties (*Trocadero* and *Romana*) by infiltrating them with an agrobacterium suspension carrying the LMV-*crtB* virus construct (Llorente et al., 2020). 2 weeks after the infiltration lettuce leaves developed a yellow colour due to a 2.5-fold increase in carotenoid content in both varieties (Figure 3.13A). Lettuce leaves also accumulated a species-specific carotenoid named lactucaxanthin that also increased in *crtB* samples. We also found increased levels of tocopherols even if, compared to *N. benthamiana*, the major form present was γ -tocopherol. Like that observed for *N. benthamiana*, *crtB*-induced chromoplast development in

lettuce correlated with an increased amount of PG markers FBN1a and FBN2 (Figure 3.13B). By contrast, a decreased amount of Lhcb2 protein was observed in lettuce leaves infected with LMV-crtB compared to control leaves (Figure 3.13B). This result correlated with a loss of chlorophyll content, a factor usually related with virus-induced necrosis (Majer et al., 2017) (Figure 3.13C). This result strengthened our hypothesis of an association of chlorophyll pigments and LHC protein complexes in *N. benthamiana* plants.

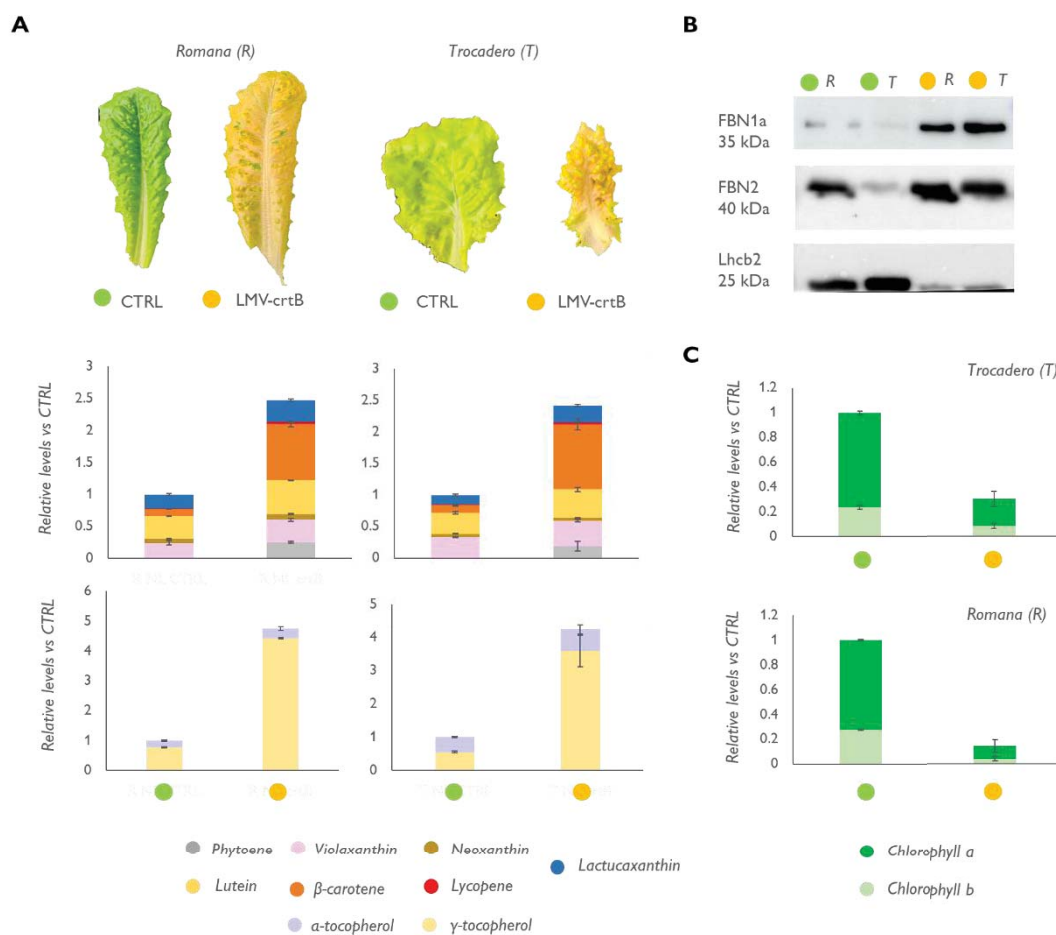


Figure 3.13. crtB can improve isoprenoid content of green leafy vegetables. (A) pictures showing the yellow colour of lettuce leaves overexpressing *crtB* and their relative levels of carotenoids (upper row) and tocopherols (lower row) compared to a control (i.e., not inoculated) leaf (B) Relative content of chlorophylls in lettuce leaves overexpressing *crtB*. (C) Western blot showing the same increase of fibrillins detected in *N. benthamiana* and a lower amount of Lhcb2. Plots show means and SD of 3 different replicates ($n=3$).

We next-tested the effect of high light acclimation on metabolite accumulation in lettuce (Figure 3.14A). We started by testing the number of days necessary for the two varieties of lettuce to reach a stable photoacclimation state. We noticed a constant increase in the value of ETRm

during the exposure to W_{500} but we detected no changes between 5 and 7 days of exposure (Figure 3.14B) concluding, thus, that 5 days was the necessary time to reach a photoacclimation state in this plant. We then exposed plants for 5 days to W_{500} starting from 6 days after the infiltration with the LMV-crtB viral vector (i.e., when the first yellow spots on the leaves were noticed) and we left them for 2 additional days under W_{50} for a recovery. We observed a colour change of colour in W_{500} -acclimated lettuce leaves from yellow to reddish-orange (Figure 3.14A). This was likely due to an increase in carotenoid content, especially orange-colour β -carotene, coherently with what was observed in *N. benthamiana* leaves. Tocopherol level was also increased through the W_{500} treatment with a small increase in the α -tocopherol fraction of tocopherols, likely related to its high antioxidant potential necessary to cope with oxidative stress induced by high irradiance (Figure 3.14A). In the case of the *Trocadero* variety the intense reddish colour was also due to an enhanced accumulation of purple-colour anthocyanins accumulation likely to protect the normally pale leaf (Figure 3.14C), likely to protect the normally pale leaf of this lettuce variety. We demonstrated, thus, that crtB-mediated chromoplast development is an effective tool for metabolites enrichment in non-experimental species and that the isoprenoid accumulation response is conserved among different species.

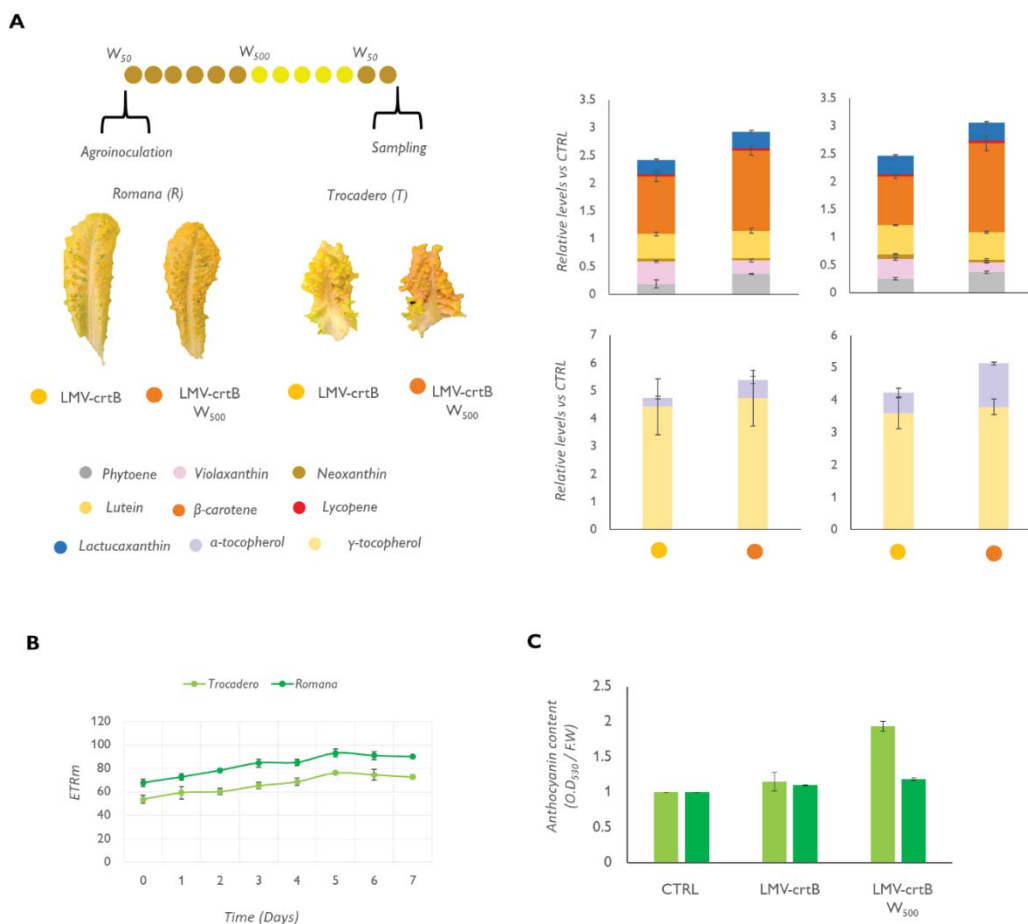


Figure 3.14. Exposure to high-PAR can improve metabolite content in lettuce. (A) Schematic representation of the experimental setting. After agroinoculation plants were left 6 days under W_{50} to allow the virus particle to multiply. 6 dpi plants are moved for 5 days to W_{500} for the high PAR treatment and then moved again to W_{50} for 2 days before the sampling. The pane shows the colour of leaves overexpressing *crtB* after W_{50} or W_{500} acclimation and respective relative carotenoid and tocopherols content. Values are relative to control, not inoculated, leaf. (B) ETRm follow up defining the amount of time needed for photoacclimation in lettuce. (C) Relative amount of anthocyanin in lettuce leaves exposed to different intensities of light. Plots show means and SD of 3 different replicates (n=3).

3.3. Discussion

The generation of chromoplasts is one of the most promising strategies for the biofortification of green leaves despite the few number of tools available to date to control the process. Chromoplasts most distinctive feature resides is their set of substructures that constitute a suitable environment for the storage and metabolism of a wide array of metabolites, including isoprenoids (Sadali et al., 2019). The transition from chloroplasts to chromoplasts has been extensively characterized from the biochemical and molecular point of view mainly in fruits like tomato, red pepper and papaya (Barsan et al., 2010, 2012; Egea et al., 2010) this process can be different depending on the plant structures where these organelles develop (for example, flower petal chromoplasts develop differently compared to fruit chromoplasts). Different structures can coexist in the same chromoplast and hybrid chromoplasts with characteristics coming from different typologies exist (Schweiggert et al., 2011). In nature, chromoplasts derived from chloroplasts of green leaves (like the case of boxwood) are implied as a temporary measure to respond to environmental stimuli and they tend to conserve a high number of photosynthetic structures to revert to chloroplasts in optimal ecological situation (Hormaetxe et al., 2004). In our *crtB* system, however, no re-greening process was observed meaning that the differentiation is not subjected to a retroactive regulation like the few cases identified in nature. However, the high number of photosynthetic structures present at the beginning of the process could interfere with their complete degradation. The massive production of phytoene likely causes photosynthetic apparatus proteins in the (*p*)*crtB*-overexpressing samples to decay starting at 36 hpi (Figure 3.2B, C). The loss of photosynthesis-related proteins is a commonly reported event in several processes of chromoplastogenesis in fruits like tomato and pepper (Rödiger et al., 2021). Interestingly, Lhcb2, one of the proteins of the light-harvesting complex, does not decrease during the transition likely because, starting from a highly competent chloroplast, the transition is not completely efficient and there is the permanence of proteins bound to the chlorophyll molecule. Lhcb proteins in fact are part of the proximal antenna system and bind most of the photosynthetic pigments (Pietrzykowska et al., 2014). The prevalence of this protein would also

explain why the *crtB*-overexpressing leaves do not show a lower amount of chlorophyll compared to normal green leaves until at least 16 days post infiltration when the leaves start to enter a senescence process and the remaining photosynthetic complexes are dismantled ([Llorente et al. 2020](#)).

Considering the decreased amount of thylakoid specific galactolipids in *crtB*-overexpressing samples (Figure 3.2A), it is logic to think that the disassembly of thylakoids can provide lipids for the formation or the increase in size of structures like with PG. The increased number of globular formations can be clearly observed in TEM images and in confocal microscope localization experiments and it is coherent with PG-related proteins increase: FBN1a, FBN2 and FBN4 almost double their amount coherently with what was detected in pepper fruits in the last stage of ripening ([Rodiger et al. 2021](#)). Fibrillins control the formation as well as structure and shape of the PG that have been proposed to “bud” from the thylakoid membrane. The increased presence of these proteins in *crtB*-induced chromoplasts is likely to be connected either to the formation of PG anew or to their derivation from the rests of thylakoidal membranes ([Shanmugabalaji et al., 2013](#)). The increased levels of LoxC, a lipoxygenase debited to the liberation of lipids from the membranes definitively highlights the massive membrane remodelling happening during the conversion. The slight delay in the accumulation of PG-associated fibrillins and VTE1 compared to LoxC could be identified as a “remodelling delay” or, in other words, a period necessary to break down the previous membranes and re-use the obtained bricks to build the new storage system (e.g., PG). Contrary to the previously enlisted proteins, envelope proteins do not normally change during the *crtB*-induced chromoplastogenesis with the only exception of TOC33, which showed a complete decay synchronized with the loss of photosynthetic processes. TOC33 is a protein whose role is to import precursors for the establishment of the photosynthetic apparatus. Its loss is likely to be part of a signal imposing the stop of the chloroplastic functions. Interestingly, TOC159 did not show variations in *crtB* samples compared to green leaves despite having a clear implication in de-etiolation and chloroplast biogenesis ([Shanmugabalaji et al., 2018](#)). Other proteins of the envelope and export complex like TOC75 and TIC40 remain stable during the conversion process indicating that a massive reorganization of the TOC complex is not connected to changes in these two structures (Figure 3.4A, B). Our data suggest that the drop in TOC33 is not dependent on the E3 ligase SP1 as its absence does not affect leaf chromoplast development in *Arabidopsis* (Figure 3.4C). We propose the presence of multiple layers of control operating during chromoplastogenesis, so that failure of the SP1 pathway may eventually be compensated for by other regulatory systems, such as transcriptional control or different proteolytic pathways ([Ling et al., 2021](#)). In the specific case of *crtB*-induced chromoplasts, thus, a complete reorganization of the complexes could not be necessary once the main importer of

photosynthetic proteins precursors (i.e., TOC₃₃) is degraded. The lack of interactions between *crtB* and the various structural proteins suggests, also, that the detected changes in protein levels are the result of the chromoplastogenesis process and that these proteins are not recruited to trigger the process itself.

Chromoplasts obtained through *crtB* also show divergences with classical chromoplasts concerning the secondary metabolites they accumulate. The high capacity of accumulation of carotenoids of *crtB*-plastids was already discussed ([Llorente et al., 2020](#)) but we additionally observe an increased number of total vitamin E tocopherols and vitamin K phyloquinone (Figure 3.5). This metabolite enrichment can have two different explanations. First, the overexpression of *crtB* could trigger an increase in the transcript levels of key biosynthetic enzymes, including those of MEP pathway that may provide a higher availability of isoprenoid precursors that would explain the increase in tocopherols and phyloquinones. A second reason could be due to the proliferation of internal structures induced by *crtB* overexpression that could provide an improved environment for the activity of the biosynthetic enzymes and the channelling and storage of their intermediates and products. This is supported by the increased amount of PC-8 and α -TQ. Chromoplasts in red fruits and flowers are reported to have low amount of these two compounds, even though, the main enzymes necessary for their biosynthesis and redox recycling and repair, VTE₁ and NDC₁, are localized in PG ([Van Wijk and Kessler, 2017](#)). Also, the scavenging of lipid peroxy radicals by α -TC results in the formation of the tocopherol oxidation product α -TQ. Therefore, the enrichment in these metabolites in chromoplasts derived from leaf chloroplasts can be related to a double process: from one side an increased amount of storage and synthesis sites linked to the proliferation of PG that contains the enzymes for their biosynthetic pathways, and on the other hand the increased oxidative stress can give rise to amount of these products as a degradation of other metabolites like tocopherols ([Vidi et al., 2006](#); [Spicher and Kessler, 2015](#); [Piller et al., 2014](#)).

crtB protein was reported to be associated with inflated invaginations of the internal membrane of the plastid envelope and with intergranal lamellae in tomato fruits. Here the protein would work with lycopene cyclase to convert the excess of phytoene stored in PG into lycopene. ([Nogueira et al., 2013](#)). When overexpressed in leaves, however, *crtB* protein localised exclusively in the PG fraction together with typical PG marker proteins such as FBN_{1a} and FBN₂. The analysis of the isoprenoids contained in the different subplastidial fractions clearly shows that the PG zone is the only one where all the different isoprenoids detected in *crtB*-chromoplasts are accumulated as chromoplasts differentiate. PG predominantly store β -carotene and phytoene (Figure 3.7). The latter was detected in PG fractions at the same time as the detection of *crtB*

protein (i.e., starting at 48 hpi) and we concluded that crtB protein is actively acting in PG to convert GGPP into phytoene. The presence of β -carotene in these structures, on the other hand, could be explained because the concentration reached in crtB-chromoplasts is not high enough for this compound to crystallize (like it happens in carrot root chromoplasts) and thus the compound is moved to a highly lipophilic environment (i.e., PG) as in the cases of citrus, pumpkin fruits and microalgae like *Euglena gracilis* or *Dunaliella salina* cells (Kato et al., 2017; Polle et al., 2020). The identification of PG as central compartments for isoprenoid accumulation in crtB chromoplasts granted useful insights about how to improve the system. We tested a pull strategy and a push strategy. In the first case, we exploited the capacity of the plant to produce more PG in response to higher light exposure as this condition is also widely reported to impact PG proliferation (Rey et al., 2000; Van Wijk and Kessler, 2017). The effect of light acclimation on carotenoid profile was already discussed in chapter 2 but here we showed that plants acclimated to high PAR also showed a higher level of tocopherols and vitamin K. The synthesis of tocopherols and phylloquinone and their accumulation in thylakoid membranes and plastoglobules is a well-known phenomenon which has been demonstrated to occur in response to oxidative stress coherently with the necessity of an antioxidant buffer (Vidi et al., 2007). A certain degree of lipid peroxidation caused by higher light exposure in non-photoprotective plastids could provide a bigger pool of precursors for phylloquinone biosynthesis. PQ-9 also increased upon exposure to high PAR, especially in the form of plastoquinol (Figure 3.8). Plastoquinol, which is a component of the electron transport chain in photosynthesis, was shown to have antioxidant activity like or even higher than that of tocopherols in vitro (Kruk and Szymańska, 2012; Szymańska and Kruk, 2010) mainly because, in contrast to tocopherols, both the head group and the isoprenoid side chain of plastoquinol can scavenge singlet oxygen which makes this compound an excellent membrane-localized antioxidant. Under higher light most of the plastoquinol is photochemically non-active and it is localized outside thylakoids in PG, which are the storage site for the plastoquinol acting as an antioxidant in the thylakoids (Szymanska and Kruk, 2010). High PAR-acclimated chloroplasts could be able to produce more of this compound before having a reduction in total PQ amount debited to the transformation to chromoplasts. Dark-induced senescence, on the other hand, was also effective in increasing the amount of some compounds because of its drastic effect on PG proliferation (Lushchak and Semchuk, 2012). The push strategy consisted of the overexpression of genes involved in the synthesis of tocopherols (Figure 3.10). As previously stated, the overexpression of the (*p*)crtB gene already provides enrichment in the content of total tocopherols. No significant improvements were obtained when this gene was combined with *VTE2* and *VTE3*. These results agree with other studies that reported a similar fold when overexpressing *VTE2* in *A. thaliana* or

in tomato under a constitutive promoter (Collakova and DellaPenna, 2003). The overexpression of *VTE3*, however, was able to recover the amount of PQ-9 bringing it to a similar level to the ones of a normal green leaf being one of the genes involved in its biosynthesis. Since tocopherol composition was not altered but there was an increase in MPBQ levels, it is logical to locate the main focal point of tocopherol biosynthesis in the *VTE1* and *VTE4* genes. The overexpression of *VTE1* along with *(p)crtB* yielded the highest improvement in tocopherol content between all the combinations, probably due to its localization in PG and the proliferation of these structures when expressing *(p)crtB* (Vidi et al., 2006; Llorente et al., 2020). Moreover, this combination resulted in a higher increase in γ -TC than the other combinations, which corresponds with the product of this enzyme.

The improvement of total tocopherol content obtained in this study is similar or larger than the results obtained in other research, where *VTE1* was overexpressed in lettuce and tobacco (Kanwischer et al., 2005; Yabuta et al., 2013). Additionally, the overexpression of *VTE1* gene provided an increase in the amount of PC-8, one of the direct products in another branch of the pathway. The overexpression of *VTE4* in combination with *(p)crtB* resulted in the conversion of the entire pool of tocopherols in the α form suggesting then that, in a situation of increased metabolic flux, provided by *(p)crtB*, the overexpression of *VTE4* can change tocopherol composition. The overexpression of the precursors generating genes *VTE5*, *VTE6* and *tyrA* increases in the level of total tocopherols (γ - and α - in a similar fashion). This is likely because the availability of phytol is the most limiting factor in vitamin E biosynthesis as determined by studies in cell cultures. At the same time, the major availability of phytol allows increasing the amount of vitamin K because of it being a common precursor in both pathways. The overexpression of *VTE5* and *VTE6* allows, thus, to improve a pathway usually very difficult to engineer. Also, the overexpression of the bacterial *tyrA* enzyme provides tyrosine without the normal feedback inhibition removing the bottleneck in that side of the pathway an effect already recorded by Lushchak and Semchuk (2012). The combination of all the genes previously enlisted allowed to convert the whole content of tocopherols into α -tocopherol maximizing then the amount of this compound. The prevalence of the highly antioxidant isoform is reflected by the increased antioxidant potential of the extracts that increase with the amount of α -TC. The combination of the physical treatments previously presented, and the metabolic engineering strategies allowed us to combine the positive results of both strategies. The high light acclimation results a balanced strategy able to moderately increase carotenoids, tocopherols, and vitamin K levels while the senescence treatment was again drastic but at the expenses of the carotenoids level that was lower compared to not-treated *crtB*-overexpressing sectors. Considering that the presented senescence experiment was lasting only 10 days we can't exclude

that over longer periods of time the loss of carotenoid could be more drastic because of the natural degradation occurring during the conversion to gerontoplasts (Figure 3.12).

We demonstrated also that the (p)crtB system shows a high versatility and can be applied to edible species like lettuce. The progress of the phenotype in this species follows the same pattern as in *N. benthamiana* with an increase in the level of carotenoids and an increase in the amount of PG related proteins. Lhcb2 proteins decrease could be associated with a direct effect of the virus similarly to what described in other virus-plant interaction (Kushwaha et al., 2019) (Figure 3.13) where the infection by chilli leaf curl virus resulted in a downregulation of photosynthesis related genes and a degradation of photosynthetic proteins. Also, the virus-induced chlorosis could cause a faster degradation of the chlorophyll binding protein coordinated with the loss of chlorophyll compared to what observed in agroinfiltrated leaves. In the case of lettuce, *crtB* overexpression provided an increased amount of lactucaxanthin in both varieties. This unique carotenoid derived from ϵ - ϵ -carotene is reported to have a potential anti-diabetic role in humans and a higher antioxidant activity than lycopene (Gopal et al., 2017). The overexpression of *crtB*, thus, is not only able to increase the typical downstream carotenoids but in different plants can be used to improve the levels of endogenous compounds that are specific of particular plant species. Also, high-PAR acclimation reproduced in lettuce the same effect described for *N. benthamiana* (i.e., an increase content of carotenoid, in particular β -carotene, but also of tocopherols) confirming to be a reliable method for metabolite enrichment (Figure 3.14). In summary, in this chapter, we were successful in determining the singular characteristics of the artificial chromoplasts obtained through the action of *crtB* and to test several strategies that can be used to further improve leaf nutritional value in a greenhouse or vertical farming context.

3.4. Material and methods

3.4.1. Plant material and growth conditions

Nicotiana benthamiana and lettuce plants (var. *Trocadero* and *Romana*) used for the transient expression assays and for the virus inoculation were grown in a greenhouse under standard long-day conditions (LD, 14 h light at $26 \pm 1^\circ\text{C}$ and 10 h dark at $21 \pm 1^\circ\text{C}$). *A. thaliana* Col 0 and *spi-1* mutants plants used for the virus inoculation were grown under standard short-day conditions (SD, 10 h light at $27 \pm 1^\circ\text{C}$ and 14 h dark at $22 \pm 1^\circ\text{C}$) to promote the development of a bigger leaf surface. *Sp1-1* seeds were kindly provided by dr. Venkatasalam Shanmugabalaji (University of

Neuchâtel, Neuchâtel, Switzerland). High PAR acclimation was performed in an ARALAB 600 fitoclima providing $500 \mu\text{mol m}^{-2} \text{s}^{-1}$ photons under a LD light regime.

3.4.2. Gene constructs.

The crtB versions used for this study (35S:(p)crtB-GFP-pGWB405 and 35S:(p)crtB-pGWB405) were available in the laboratory and were obtained as described by [Llorente et al. 2020](#). cDNA sequences encoding for the FBN7a (PGL34), TIC40 and TOC64 proteins were amplified from *A. thaliana* leaves. Transcript encoding for VTE1 protein was obtained from *A. thaliana* seeds ([Breuers et al., 2012](#), [Vidi et al., 2006](#), [Vidi et al., 2007](#)) and VTE2, VTE3, VTE4, VTE5, VTE6 proteins from *A. thaliana* leaves. For the sequence encoding for the tyrA protein, a culture of *E. coli* was used as a template. Primers used for this amplification are enlisted in the *Appendix 1*. PCR products were cloned using the Gateway system first into plasmid pDONR-207 and then into plasmid pGWB454 provided with an RFP fluorescent tag ([Nakagawa et al., 2007](#)) to generate 35S:VTE1-pGWB454, 35S:VTE2-pGWB454, 35S:VTE3-pGWB454, 35S:VTE4-pGWB454, 35S:VTE5-pGWB454, 35S:VTE6-pGWB454, 35S:tyrA-pGWB454. For the co-localization experiment cDNA sequence encoding for the FBN7a and VTE1 proteins were amplified and cloned into a pDONR-207 plasmid and later into plasmid pGWB454. The 35S:PGL34-pGWB454 generated and 35S:VTE1-pGWB454 were then used as a template to obtain the proteins fused with the fluorescent tag by using a universal gateway primer annealing with sequence encoding RFP. These two amplicons were then cloned into pDONR207 plasmid and then into the β estradiol-inducible vector pER8 to obtain PGL34:RFP-pER8 and VTE1:RFP-pER8. cDNA sequence encoding for TIC40 and TOC64 proteins were amplified and cloned into a pDONR-207 plasmid and later into β estradiol-inducible vector pMDC7 (provided with a CFP fluorescent tag) to obtain TIC40-pMDC7 and TOC64-pMDC7. LMV-crtB construction was kindly provided by prof. Josè Antonio Daròs (IBMCP, Valencia, Spain) and was obtained as described ([Llorente et al., 2020](#)).

3.4.3. Transient expression assays.

Agroinfiltration experiments were performed as described in the previous chapters. Gene silencing was prevented by co-agroinfiltration with an agrobacterium strain EHA101 carrying the helper component protease (HcPro) of the watermelon mosaic virus (WMV) in plasmid HcProWMV-pGWB702 (a kind gift of Juan José López-Moya and Maria Luisa Domingo-Calap (CRAG-Barcelona, Spain)). For the inoculation of lettuce, 3 leaves of 3-4 weeks old plant were infiltrated in, at least, 6 different spot each with the same agro-infiltration solution used for *N.*

benthamiana and described in the previous chapters. TuMV-crtB virus inoculation of *A. thaliana* plants was performed as described in the previous chapters.

3.4.4. Chloroplast isolation and fractionation

For the isolation of total chloroplasts, leaves were blended into a Waring mixer with 200 ml of HB buffer (Sorbitol 450 mM, Tricine/KOH pH 8.4 20 mM, EDTA pH 8.5 10mM, NaHCO₃ 10 mM, MgCl₂ 1mM, Na-ascorbate 5mM, PMSF 1mM). The mixture was then filtered through 2 layers of cheesecloth and one layer of miracloth at 4°C and then centrifuged for 10 minutes at 2.200 rpm. The pellet was resuspended in 2 mL of HB buffer and used to measure the chlorophyll concentration. Then the volume was increased to 50 mL with HB buffer and the samples were centrifuged again at 4°C at 3.600 rpm for 2 minutes. The upper phase was removed, and the pellet resuspended into 0.6M sucrose solution (in TED buffer: Tricine pH 7.5 500mM, EDTA 20mM, DTT 20mM) to obtain a final chlorophyll concentration of 2 mg/ml. Chloroplast suspension was then diluted with 3 volumes of TED buffer 1X, manually homogenized, and then centrifuged for 1 hour at 27.000 rpm. The upper phase (stroma) was removed and frozen for further analysis, the pellet was resuspended into 45% sucrose in TED buffer at a concentration of 3 mg of chlorophyll and the suspension was homogenized again in a glass potter. The obtained resuspended membranes were then pipetted into a polycarbonate UltraClear SW28 tube. A gradient of 5%-38% sucrose in TED buffer 1X was then layered on top of the membranes (6 ml 38% sucrose, 6 ml 20% sucrose, 4 ml 15% sucrose, 6 ml 5% sucrose). The obtained gradient was then centrifuged at 27.000 rpm for 16 hours, single fractions, separated by density gradient flotation, were then collected, and stored for further analysis (Vidi et al., 2006, Shanmugabalaji et al., 2013).

3.4.5. Protein extraction and western blot

For total protein extraction approximately 5 mg of freeze-dried leaf, material was ground with 300 ul of lysis buffer (100 mM Tris-HCl pH 7.7, 2% SDS, 0.1% protease inhibitor (SIGMA), vigorously shaken for 1 minute, and then incubated at 37°C for 30 minutes with constant shaking. After that samples were centrifuged for 15 minutes at 10.000 g, the supernatant was collected, and the protein amount was calculated by mixing the sample with the Bradford reagent and measuring the optical absorbance at 595 nm. Proteins were precipitated by adding 4 volumes of acetone and by incubating the samples at -20°C for 30 minutes. After centrifuging the samples for 15 minutes at max speed at 4°C the upper phase was removed and the pellet washed with 500

ul of 80% acetone, then centrifuged for 10 minutes at max speed. The pellet was then dried and resuspended in protein loading buffer (10% SDS, 500mM DTT, 50% Glycerol, 500mM Tris-HCL, and 0.05% bromophenol blue dye) to obtain a final concentration of 2 μ g/ μ l. Before loading the gel, samples were boiled for 10 minutes at 95°C. For the isolation of proteins of the chloroplast fractions, 200 μ l of sucrose gradient fractions were collected and precipitated by adding acetone as before. After the addition of loading buffer, single samples were pooled together by washing a single sample in the successive to maximize protein amount for western blot. SDS-PAGE and immunoblotting were performed as described (Shanmugabalaji et al. 2018). After protein transfer, the nitrocellulose membranes were stained with amido black. To probe the blots, primary antibodies recognizing TOC159, TOC75, TOC33, TIC40, FBN1A, FBN2, FBN4, VTE1, LoxC, were used. To detect photosynthesis-associated proteins, antibodies recognizing RBCS, PetC, PsaD, PSBA, PSBO, and LHCB2 were purchased from Agrisera, Sweden. Additional antibodies recognizing anti-GFP (Sigma) were used. Secondary antibodies were anti-rabbit IgG conjugated with horseradish peroxidase (Millipore) or anti-mouse IgG conjugated with horseradish peroxidase (Sigma). For the Immunoprecipitation total proteins were extracted in lysis buffer containing 50 mM Tris-HCl pH 8, 150 mM NaCl, 1% Triton X-100, 0.2% v/v protease inhibitors (Sigma P9599), 20mM MG132, and 10% glycerol. Anti-GFP antibodies conjugated to microbeads (mMACS GFP-tagged beads; Miltenyi Biotec) were used to isolate the immunoprotein complexes. The eluates were resolved by SDS-PAGE, crtB-GFP and GFP were detected using anti-GFP antibody. The interaction with other proteins was checked by probing the membranes with primary antibodies recognizing FBN1a, FBN2, PsaD, PetC, VTE1, and LoxC and the same secondary antibodies listed before. Chemiluminescence was detected using ECL Plus Western Blotting Detection Reagents (Pierce) and developed using a GE Amersham Imager600. Band intensities were quantified using ImageJ software.

3.4.6. Metabolite analyses.

Leaf areas of interest were harvested, snap-frozen in liquid nitrogen, and lyophilized until they were completely dry. For the prenylquinone analysis approximately 7 mg of freeze-dried tissue was mixed with 500 μ l of THF:MeOH (Analytical grade, Normapur) 1:1 buffered with a 10% of water (v/v), mixed for 1 minute at 30 MHz, centrifuged and then transferred to an amber vial for appropriate UPLC-QTOF-MS analysis. For the metabolite analysis of the chloroplast fractions 100 μ l of 5 different fractions from the PG zone, the membranous zone and the thylakoid zone were pooled together. The sucrose was removed by adding the same volume of ethyl acetate, mixing roughly and then centrifuging for 10 minutes at 14,000 rpm. The upper phase was collected and dried to be later resuspended into 500 μ l of THF:MeOH 1:1. All samples were injected into a Waters Acquity UPLC™ (Milford, MA) coupled to a Waters Synapt G2 MS QTOF equipped with

an atmospheric pressure chemical ionization (APCI) source. Prenylipids were separated on an Acquity BEH C18 column (50 × 2.1 mm, 1.7 μm) under the following conditions: Solvent A = water; Solvent B = MeOH; 90-100% B in 1.5 min, 100% B for 2.5 min, re-equilibration at 90% B for 0.5 min. The flow rate was 800 μL/min, and the injection volume was 2.5 μL. The temperature of the column was set to 60°C and the autosampler chamber was kept at 15°C. Standards of HPLC grade (≥ 99.5%) were purchased from Sigma-Aldrich (Steinheim, Germany). PQ-9 and PC-8 standards were provided by Jerzy Kruk (Jagiellonian University, Kraków, Poland). (Martinis et al., 2011). For phytoene quantification in the fractions, the temperature of the column was settled at 70°C and the mobile phases were H₂O+NH₄OH 0.1% (phase A) and MeOH+NH₄OH 0.1% (phase B). The flow rate was set at 0.4 mL/min and a gradient of 80-100% B in 6 min was applied, followed by a hold at 100% for 3 min and re-equilibration at 80% B for 4 min. The injection volume was 2.5 μL. Phytoene was monitored at 285 nm in UV (RT 8.26 min) and at m/z 545.509 in MS (RT 8.30 min) using electrospray positive ionization. The MS source parameters were set as follows: capillary voltage +2.8 kV, cone voltage +40V, source temperature 120°C, desolvation temperature 450°C, cone gas flow 50 L/h, desolvation gas flow 900 L/h. The instrument was used in resolution mode (RFWHM = 20'000 at m/z 556). To increase sensitivity, the enhanced duty cycle (EDC) mode centred on m/z 545 was activated. To ensure accurate mass measurements, the mass spectrometer was internally calibrated with a solution of leucine-enkephaline infused at 15 μL/min via the Lockspray probe. Quantification was performed by external calibration using five calibration solutions of a phytoene reference standard ranging from 0.1-20 μg/mL.

Anthocyanins were extracted as described by (Nakata et al., 2013). Briefly, freeze-dried leaves were grinded to a fine powder and were homogenized with 5 volumes of extraction buffer (45% MeOH, 5% Acetic acid). Samples were then centrifuged at 12.000 g for 5 minutes at room temperature, supernatant was moved to another tube and the centrifugation was repeated. The supernatant was then used to measure absorbance at 530 nm and 657 nm. Anthocyanin content (Abs₅₃₀ /g F.W.) was calculated by $[Abs_{530} - (0.25 \times Abs_{657})] \times 5$.

3.4.7. Microscopy

Subcellular localization of GFP, CFP and RFP-tagged proteins was observed by direct examination of agroinfiltrated leaf tissue at 4 dpi with a Leica TCS SP8-MP Confocal Laser Scanning Microscope. GFP fluorescence was detected using a BP515-525 filter after excitation at 488 nm while CFP was detected after excitation at 440 nm. Chlorophyll autofluorescence was detected using a 610-700 nm filter after excitation at 568 nm. The RFP signal was detected after excitation at 532 nm laser line and detected at 588 nm. Transmission electron microscopy was

realized as described (Llorente et al. 2020). Subcellular structures were quantified by using the ImageJ software (Schindelin et al, 2012).

3.4.8. Antioxidant capacity

Metabolite extracts prepared as described above were diluted in 400 μL of diethyl-ether and saponified by adding 100 μL of 10%(w/v) KOH in methanol to avoid interference from chlorophylls. Samples were left shaking for 30 min at 4 $^{\circ}\text{C}$ and then diluted with 400 μL of milliQ water before centrifugation for 5 min at 13 000 rpm and 4 $^{\circ}\text{C}$. The upper phase was collected, dried in a SpeedVac, and resuspended in 200 μL of acetone. ABTS assay to calculate the total antioxidant capacity of the mixture was carried out as described (Re et al., 1999). Briefly ABTS^{o+} was prepared by adding to a 7mM solution of ABTS (SIGMA), APS to a final concentration of 2.45 mM. The solution was then diluted with water to reach an absorbance of 0.700 ± 0.020 at 30 $^{\circ}\text{C}$. 100 μl of diluted sample were added to 1 ml of ABTS^{o+} and absorbance at 734 nm was measured after 4 minutes. The obtained values were plotted against a standard curve made by substituting the sample with increasing 6-hydroxy-2,5,7,8-tetramethylchroman-2-carboxylic acid (Trolox) concentrations: 11 μM , 22 μM , 44 μM , 88 μM to calculate the antioxidant activity as μM of Trolox equivalents.

3.4.9. Photosynthetic measurements

Photosynthetic efficiencies for lettuce plants were assessed by measuring chlorophyll fluorescence with a Handy-GFP fluorcam (Photon system instruments (PSI)) fluorometer. Light curves were constructed with 11 incremental steps of actinic irradiance (E; 0, 21, 56, 111, 186, 281, 396, 461, 531, 611, 701, 801). For each step, the effective quantum yield of PSII ($\Delta F/F_m'$) was monitored every min and electron transport rate (ETR, $\mu\text{mol electrons m}^{-2} \text{s}^{-1}$) was calculated as $E \times \Delta F/F_m'$. The maximum electron transport rate (ETR_m) was calculated by fitting iteratively, using MS Excel Solver, the model of Platt (1980) the ETR versus E curves. The fit was very good in all the cases ($r > 0.98$).

Chapter 4

Chapter 4. Carotenoid biofortification beyond plastids.

Note: Part of the results shown in this chapter were published in Andersen et al., 2021. See Annex IV.

4.1. Introduction

Biofortification of carotenoid content in plants is an open challenge with multiple possible ways, of which only a handful has been experimentally explored (Zheng et al., 2020). While several successful strategies have been described for non-photosynthetic tissues, including Golden Rice, manipulation of carotenoid levels in photosynthetic tissues has been much more challenging because chloroplast carotenoid levels are finely balanced with those of chlorophylls for the efficient assembly and functionality of photosynthetic complexes (Domonkos et al., 2013; Esteban et al., 2015; Hashimoto et al., 2018). While plant carotenoids are only produced and stored in plastids, their metabolic C₅ precursors (IPP and DMAPP) are also present in the cytosol due to the activity of the mevalonate (MVA) pathway (Rodriguez-Concepcion and Boronat, 2015) (Figure 4.1). In the first step of the MVA pathway, two molecules of acetyl-CoA generate acetoacetyl-CoA and then a third molecule is incorporated to produce hydroxy-3-methyl glutaryl-CoA (HMG-CoA). The reduction of HMG-CoA catalysed by HMG-CoA reductase (HMGR) enzymes leads to the formation of MVA, which is later transformed into IPP in three enzymatic steps. MVA-derived IPP is interconverted into DMAPP by cytosolic IPP/DMAPP isomerase enzymes. An attempt of using cytosolic IPP and DMAPP to produce carotenoids outside plastids was carried out using virus-mediated expression of bacterial genes encoding GGPP synthase (*crtE*), phytoene synthase (*crtB*) and a desaturase/isomerase transforming phytoene into lycopene (*crtI*) in tobacco (*Nicotiana tabacum*) leaves (Majer et al., 2017) (Figure 4.1). Virus infected tissues accumulated lycopene to levels up to 10% of the total leaf carotenoid content, but only for 1–2 days, as carotenoid-producing leaves soon became necrotized either (1) as a side effect of the viral infection, (2) as a negative steric interference of lipophilic lycopene with cell membrane function, or (3) because of the diversion of the metabolic substrates away from the cytosolic isoprenoid pathways. MVA-derived IPP and DMAPP are mostly used to produce C₁₅ farnesyl diphosphate (FPP), the precursor of sesquiterpenes, triterpenes, and sterols (the major product of the pathway), while minor levels of GGPP are synthesized for diterpenes and protein prenylation. Although the subcellular compartmentation of the MEP

pathway in plastids and the MVA pathway in the cytosol allows both pathways to operate independently in plants, there is evidence that they cooperate in the biosynthesis of certain metabolites in some plants, tissues, or/and developmental stages (Rodríguez-Concepcion and Boronat, 2015). An uptake of IPP from the cytosol into isolated plastids was reported in several plants (Kleinig, 1989; Soler et al., 1993) whereas the transport of IPP in the plastid-to-cytosol direction appears to be mediated by a plastidial proton symport system (Milborrow, 2001). Other prenyl-diphosphates of increasing size might be also exchanged between the cytosol and the plastids, with efficiency decreasing as the molecule size increases (Hemmerlin et al., 2003). In the case of carotenoids, the MEP pathway is the main supplier of metabolic precursors under normal growth conditions but a minor contribution of the MVA pathway under some specific conditions cannot be excluded (Rodríguez-Concepción, 2010; Ruiz-Sola et al., 2016). (Figure 4.1)

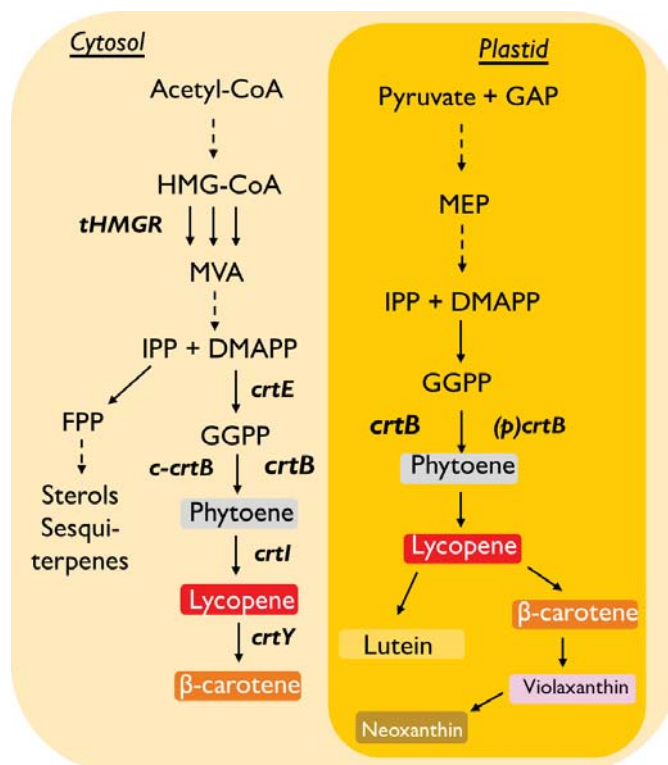


Figure 4.1. Schematic representation of the two strategies (cytosolic and plastidic) used in this chapter for carotenoid biofortification.

In this chapter we retook the idea of using the MVA pathway for the extraplastidial production of carotenoids. Instead of viral vectors, we used our optimized transient expression system via agroinfiltration in *Nicotiana benthamiana* leaves. As initial target carotenoid products, we selected phytoene and lycopene. The choice of these carotenoid intermediates was based on three main reasons. First, they are virtually absent in non-engineered leaves as they are readily converted into downstream chloroplast carotenoids (Marano et al., 1993; Rodríguez-Concepcion et al., 2018). Second, they are health-promoting phytonutrients that are only found in a few food

sources (Rodriguez-Concepcion et al., 2018; Mapelli-Brahm et al., 2018; Müller et al., 2011). And third, their supply is essential for the eventual production of any downstream carotenoid of interest such as β -carotene, the main precursor of vitamin A. As a proof of concept, the second part of the work was directed to produce β -carotene by introducing an extra step in the engineered cytosolic pathway (the lycopene β -cyclase encoded by the bacterial *crtY* gene) and to combine this strategy with the *crtB*-mediated differentiation of leaf chromoplasts

4.2. Results

4.2.1 Extraplastidial phytoene and lycopene accumulate at levels so high that they eventually impact photosynthetic activity.

To produce phytoene and lycopene in the cytosol without the deleterious effects previously observed using viral vectors (Majer et al., 2017), we used a combination of strategies using agroinfiltration of *N. benthamiana* as a less aggressive transient expression system (Schwach et al., 2005). To convert MVA-derived IPP and DMAPP into carotenoids, the bacterial *Pantoea ananatis* genes encoding *crtE* (to produce GGPP), *crtB* (to transform GGPP into phytoene) and *crtI* (to synthesize lycopene from phytoene) were used. Unmodified versions of these three bacterial enzymes are active and synthesize lycopene in the cytosol of tobacco leaf cells (Majer et al., 2017). Only the unmodified *crtB* protein can be found in the cytosol and the plastid when fused to GFP and expressed in plant cells (Llorente et al. 2020). To prevent the chromoplastogenesis associated to *crtB* activity in plastids, a version of the *crtB* enzyme with GFP fused to its N-terminus (referred to as GFP-*crtB*) was used to construct the cytosolic pathway. This version was reported to be retained in the cytosol of agroinfiltrated *N. benthamiana* leaf cells in an enzymatically active form (Llorente et al., 2020; Andersen et al., 2021). To avoid competition for IPP and DMAPP with endogenous cytosolic isoprenoid pathways, an extra amount of these metabolic intermediates was supplied by using a truncated version of HMGR, the main rate-limiting enzyme of the MVA pathway. This truncated version, referred to as tHMGR (van Herpen et al., 2010) is not feedback-regulated and localizes to the cytosol as a soluble protein as it lacks the N-terminal transmembrane domain that anchors the enzyme to the endoplasmic reticulum (ER) (Figure 4.2). Constructs encoding tHMGR were co-infiltrated with those encoding the enzymes *crtE* (to convert IPP and DMAPP into GGPP), GFP-*crtB* (to transform GGPP into phytoene) or/and *crtI* (to transform phytoene into lycopene) in *N.*

benthamiana leaves and their carotenoid profile was analysed at different time points (Figure 4.2C). Co-agroinfiltration of constructs for tHMGR, crtE and GFP-crtB (HEcB combination) led to a steady increase in the production of phytoene up to 7 dpi. Further addition of crtI (HEcBI combination) resulted in the incomplete conversion of this cytosolic phytoene into lycopene, probably reflecting differential enzymatic working rates or complications in accessing the substrate. In these HEcBI leaves, lycopene showed a steady increase to 5 dpi and then remained high for at least two more days before gradually fainting as the leaves started to show signals of necrosis (Figure 4.2B). The level of cytosolic carotenoids accumulated in HEcB and HEcBI leaves was comparable to the content of endogenous chloroplast carotenoids ([Andersen et al. 2021](#)). Interestingly, the levels of chloroplast carotenoids in HEcB and HEcBI leaves remained unchanged with time (Figure 4.2C), suggesting a lack of exchange of carotenoid precursors between cytosol (where they were produced in excess) and plastids.

The massive levels of lycopene that accumulated in HEcBI *N* leaves resulted in a characteristic red colour in the sectors that produced the pigment (Figure 4.2A). By contrast, HEcB areas producing only phytoene were visually indistinguishable from agroinfiltrated control HE areas, as expected due to the colourless nature of phytoene. Chlorophyll levels in HEcBI leaves started to decrease at 5 dpi and by 7 dpi they had dropped about 20% (Figure 4.2C). In HEcB leaves, however, the reduction in chlorophyll contents occurred later (at 7 dpi) and to a lower degree (10%) compared to lycopene-producing HEcBI leaf tissues. No changes in carotenoid or chlorophyll levels were observed in control HE leaves, suggesting that the decrease in chlorophyll levels observed in leaves producing phytoene and lycopene is not due to the agroinfiltration procedure but to the accumulation of those carotenoids outside chloroplasts. We deduced that the accumulation of these compounds, despite being circumscribed to the cytosol, might eventually impact in some way the activity of chloroplasts. To test this possibility, we next quantified effective quantum yield of photosystem II (ϕ PSII) at different time points after agroinfiltration with HE, HEcB or HEcBI combinations (Figure 4.2B). Phytoene-producing HEcB leaves only showed a statistically significant decrease in ϕ PSII value at 7 dpi, whereas HEcBI tissues producing lycopene showed a stronger reduction even at earlier time points (Figure 4.2B). These results demonstrated that leaf cells were remaining photosynthetically active despite accumulating phytoene and lycopene at levels like those of photosynthesis-related chloroplast carotenoids with only a limited drop of photosynthetic functionality.

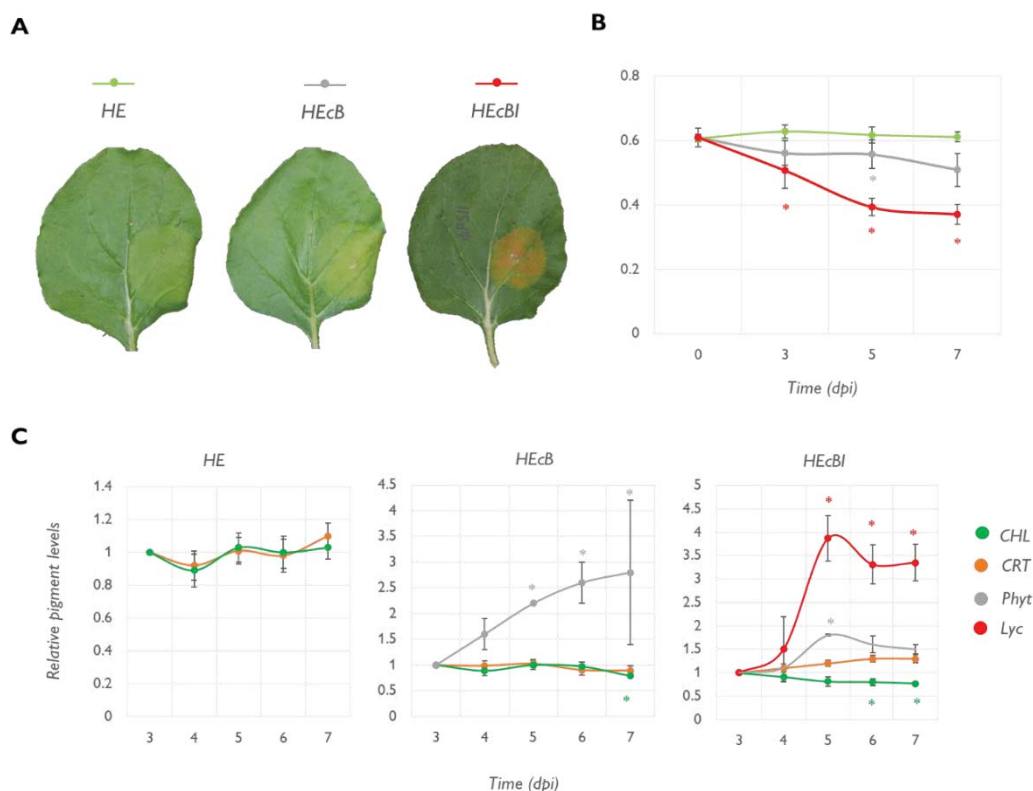


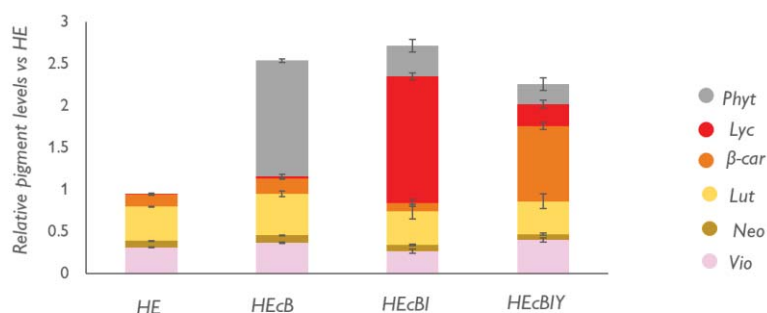
Figure 4.2. Accumulation of extraplastidial phytoene and lycopene indirectly impacts photosynthesis. (A) Representative pictures of *N. benthamiana* leaves agroinfiltrated in their lower left-hand side with constructs to express HE, HEcB and HEcBI combinations (B) effective quantum yield (ϕ PSII) of the infiltrated area (C) Photosynthetic pigment levels in HE, HEcB and HEcBI leaf areas at the indicated times after agroinfiltration. Carotenoid contents (CRT) refer to endogenous (i.e., chloroplastic) species, excluding phytoene and lycopene. Abbreviations correspond to total chlorophylls (CHL), phytoene (phyt) and lycopene (lyc). Values are the mean and standard error of $n \geq 3$ independent samples relative to levels at 3 dpi. Asterisks mark statistically significant changes (t-test, $P < 0.05$) relative to 3 dpi.

4.2.2. The engineered cytosolic pathway can be extended to produce β -carotene in the cytosol

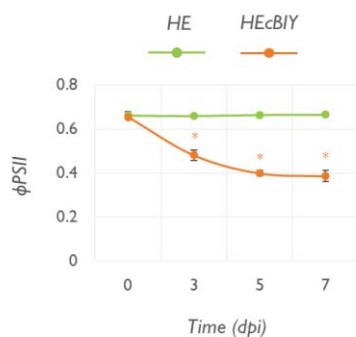
As previously discussed, β -carotene is one of the most interesting carotenoids from the nutritional point of view because of its prime pro-vitamin A activity (Rodriguez-Concepcion et al. 2018). Despite the relatively high amount of this carotenoid in leaf tissues, its physical and functional association with photosynthetic membranes can prevent its overaccumulation and negatively impact its bioavailability. We hence decided to explore the possibility to extend the engineered cytosolic pathway tested above by adding the *P. ananatis* gene encoding the lycopene β cyclase crtY, which catalyses the conversion of lycopene into β -carotene (Figure 4.3A). After agroinfiltrating leaves with a combination of tHMGR, crtE, GFP-crtB, crtI and crtY (combination named HEcBIY), samples were collected for analysis at 6 dpi. The accumulation of β -carotene in

HEcBIY leaves (resulting from the sum of chloroplast levels plus engineered cytosolic contents) was 6-fold higher than the levels measured in HE leaves (corresponding to only chloroplast levels). The production of β -carotene in the cytosol, however, was limited by the activity of the bacterial enzymes as deduced from the high levels of lycopene and phytoene still present in HEcBIY leaves (Figure 4.3A). The remaining amount of lycopene could also be the reason behind the reddish colour of the HEcBIY leaves. The loss of photosynthetic activity (ϕ PSII) was also comparable to that obtained in HEcBI samples (Figure 4.3B), suggesting that the production of a new carotenoid in the cytosol did not have additional negative effects on plastid functionality. Having demonstrated the possibility to accumulate β -carotene in the cytosol we then checked whether the cytosolic carotenoids were conserving an antioxidant effect. Extracts coming from leaves accumulating phytoene, lycopene and β -carotene showed a higher antioxidant activity compared to extracts coming from the control HE leaf, suggesting that cytosolic carotenoids keep their bioactive properties, in particular lycopene that showed the highest antioxidant activity (in accordance to its relative antioxidant contribution described by Muller et al. 2011) (Figure 4.3C).

A



B



C

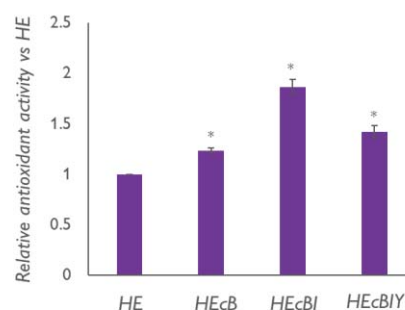


Figure 4.3. β -carotene can be produced in cytosol by adding the crtY gene to the combination. (A Pigment levels in HE, HEcB, HEcBI and HEcBI leaf areas. The legend shows a shortened name for the carotenoids detected

(Phyt: phytoene, vio: violaxanthin, neo:neoxanthin, lut: lutein, β -car: β -carotene, lyc: lycopene. (B) ϕ PSII value of leaves overexpressing the HE and HEcBIY combinations of genes (C) Relative antioxidant activity in extracts from leaves overexpressing different combinations of constructs calculated as μ M of Trolox equivalents. Values are the mean and standard error of $n \geq 3$ independent samples and relative to levels in HE. Asterisks mark statistically significant changes (t-test, $P < 0.05$) relative to 3 dpi

4.2.3. Cytosolic production of carotenoids can be combined with chromoplast development for further carotenoid enrichment of leaves

With the previous experiment we successfully demonstrated that it is possible to accumulate a large amount of β -carotene outside a plastid context. This very promising strategy allows to pass from a 20% to a 40% of this compound relative to the total amount of carotenoids in a green leaf (Figure 4.2). We have also shown in previous Chapters that, when chromoplasts are differentiated from chloroplasts in crtB-producing green leaves, β -carotene is one of the most enriched carotenoids because of its association with globular and membranous structures. We hypothesized that the two strategies could be combined, i.e., the plastidial crtB-mediated conversion of chloroplasts into chromoplasts (*strategy P*) with the engineered cytosolic pathway leading to β -carotene (*strategy C*). To explore this idea, we first tested whether using the unmodified version of crtB known to localize in both the cytosol and the plastids and to efficiently work in strategy P (Llorente et al. 2020) could also be used for strategy C. We transiently overexpressed in *N. benthamiana* leaves a combination of tHMGR, crtE and one of three crtB versions: unmodified crtB (HEB), cytosolic GFP-crtB (HEcB) or plastidial (p)crtB (HEpB) (Figure 4.4A). As expected, only HEB and HEpB combinations, but not HEcB, led to a clear visual yellow phenotype of agroinfiltrated areas, indicative of successful chromoplast differentiation (Figure 4.4A). HPLC analysis of carotenoid contents showed that the amount of phytoene in HEB samples was roughly the sum of the levels detected in HEcB (i.e., exclusively cytosolic) plus those in HEpB (i.e., exclusively plastidial) (Figure 4.4B). When crtI and crtY were added to each of the combinations, the resulting profile was also consistent with the conclusion that unmodified crtB was working for strategies C and P with no apparent loss of efficiency compared to GFP-crtB or (p)crtB, respectively (Figure 4.4C). The results also demonstrated an additive phenotype, confirming the feasibility of combining the two strategies. The levels of total carotenoids in HEBYI samples increased almost 3-fold compared to HE controls, but the increase in β -carotene was much higher, changing the Colour of the leaf agroinfiltration area to orange. As expected, a drastic decrease of photosynthetic capacity was present only when the combination contained the crtB versions able to enter the plastid to trigger chromoplastogenesis (Figure 4.4C).

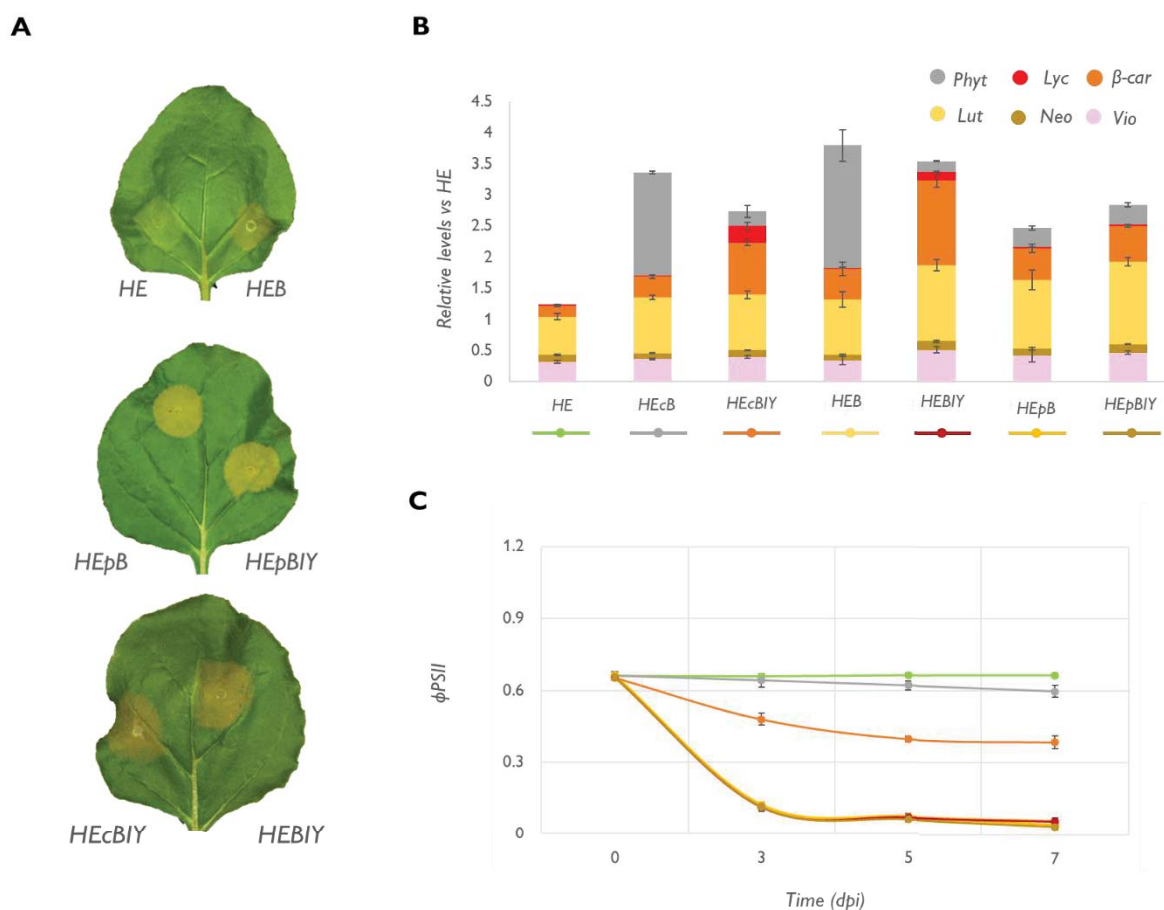


Figure 4.4. Extraplantid synthesis of β -carotene can be combined with chromoplast generation for additional improvement (A) Leaves showing the phenotype obtained through the overexpression of different combinations (B) Carotenoid levels during the overexpression of different versions of the pathway. Values are the mean and standard error of $n \geq 3$ independent samples relative to levels in HE. (C) Effective quantum yield in leaf sectors overexpressing the enlisted combinations of genes.

4.2.4. Providing more plastidial precursors does not improve carotenoid levels due to a bottleneck at the phytoene desaturation level.

The incorporation of tHMGR to increase the MVA pathway flux in the extraplantid strategy (C) was found to boost the production of cytosolic carotenoids (Andersen et al. 2021). We therefore reasoned that increasing the metabolic flux through the MEP pathway might also contribute to improve the production of plastidial carotenoids with the crtB strategy (P). The enzyme deoxyxylulose 5-phosphate synthase (DXS) catalyzes the first and main rate-determining step of the MEP pathway (Rodríguez-Concepción and Boronat, 2015). We tried three different sources of DXS activity from plants: tomato DXS₁ and DXS₂ and *A. thaliana* DXS (also referred to as CLA₁) (Lois et al., 2000; Paetzold et al., 2010). The three isoforms were transiently expressed in *N. benthamiana* leaves in combination with *crtB-GFP* to assess their effect on the final pigment

amount. Of the three isoforms, only DXS₁ led to a small but statistically significant increase in carotenoid levels downstream of phytoene compared to using only *crtB*. Interestingly, DXS₁ in combination with *crtB* resulted in a massive accumulation of phytoene that correlated with a faster decrease in ϕ PSII compared to the single *crtB* overexpression (Figure 4.5A, B). The very high accumulation of phytoene suggested the existence of a limiting step for its conversion into lycopene and downstream carotenoids. Indeed, no improvement in the contents of β -carotene or any other carotenoid besides phytoene was observed when DXS₁ was incorporated to the HEBIY combination (named HEBIYD) (Figure 4.5C).

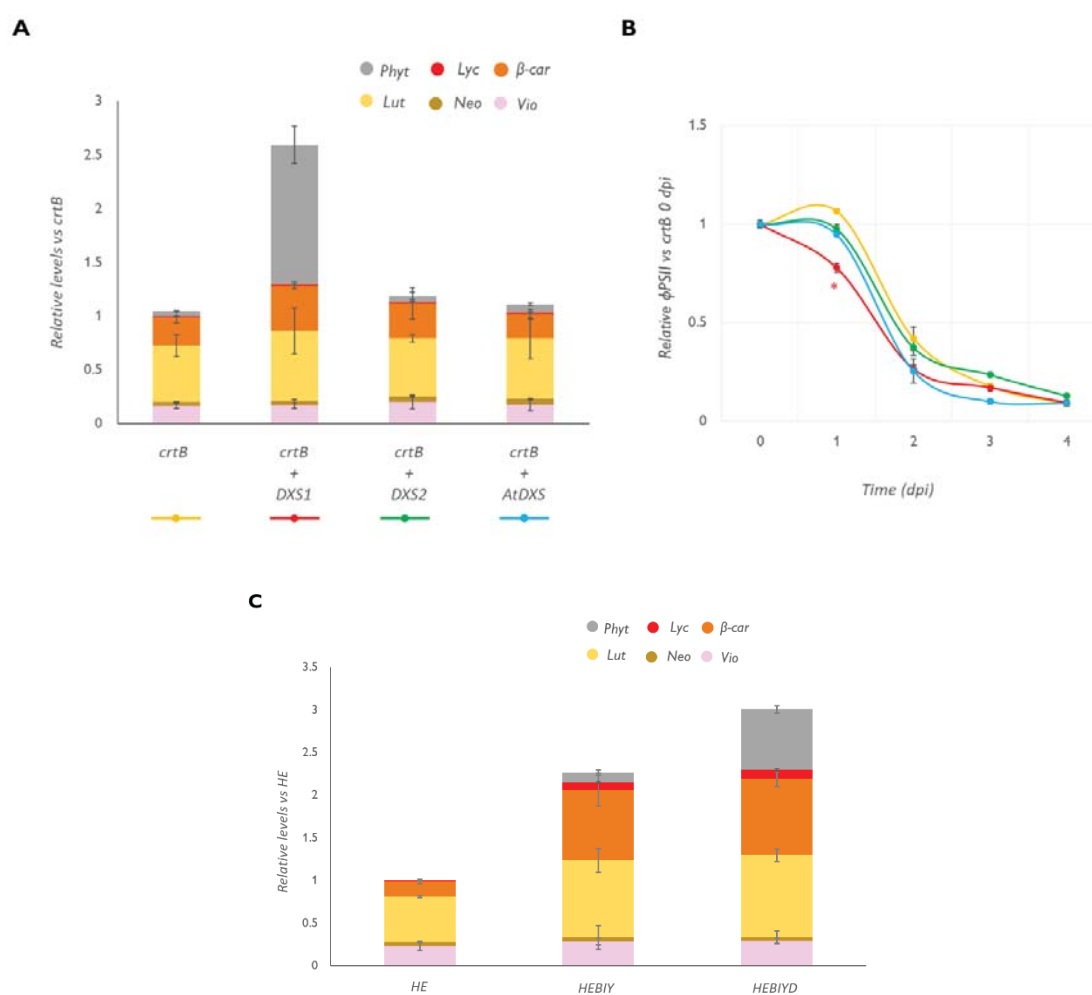


Figure 4.5. An increased amount of plastidial precursors does not improve the carotenoid content of the combined pathway. (A) Relative carotenoid levels in plants overexpressing *crtB* alone or in combination with different isoforms of DXS. Values are relative to the amount detected in *crtB*. (B) Relative effective quantum yield in the same samples. Only the overexpression of *crtB* and DXS₁ can effectively accelerate the loss of photosynthetic capacity. (C) Relative levels of carotenoids obtained by adding DXS to the HEBIY combination. Plots show means and SD of 3 different replicates ($n=3$) and relative to *crtB* (A) or HE (C). Asterisks mark statistically significant changes (t -test, $P < 0.05$) relative to 0 dpi.

4.3. Discussion

In this Chapter, we show that carotenoids can be produced and accumulated in very high amounts for over a week in the cytosol and that this strategy can be combined with the crtB-mediated chromoplastogenesis process that also results in an enhanced production and accumulation of carotenoids in plastids. The possibility to produce carotenoids in compartments other than plastids open the door for multiple possibilities for the biofortification of agricultural products. Very little attention has been paid to carotenoid biofortification of green vegetables to date, in part because of the challenges associated with changing the balance between carotenoids and chlorophylls (Domonkos et al., 2013; Esteban et al., 2015; Hashimoto et al., 2016; Zheng et al., 2020). Nonetheless, recent reports have shown that *N. benthamiana* leaves overexpressing regulators of carotenoid gene expression and storage were able to double their carotenoid content in chloroplasts (Ampomah-Dwamena et al., 2019; D'Amelia et al., 2019; Llorente et al., 2020). Our strategy C leads to a similar twofold increase in total carotenoid levels in *N. benthamiana* leaves, whereas the combination of strategies C and P leads to an even higher increase (Figure 4.4C).

The production of carotenoids in the cytosol (strategy C) offers multiple advantages over those modifying the plastidial carotenoid content. Firstly, the composition of chloroplast carotenoids remains unchanged and therefore their photosynthetic and photoprotective functions are not directly impacted. Although a likely secondary effect does cause photosynthesis to slow down (Figures 4.2, 4.3, 4.4), it is not blocked and can therefore continue to support plant growth while the extraplastidial carotenoids are produced and stored. Secondly, strategy C separates the carotenoid intermediates from those plastidial enzymes that convert them into downstream products or degrade them into cleavage products, including apocarotenoid signals (Rodriguez-Concepcion et al., 2018). While non-enzymatic degradation could still occur, it does not appear to be a problem to achieve high titres of extraplastidial carotenoids in our system. Together with the unexpected capacity of leaf cells to accumulate carotenoids outside chloroplasts, this resulted in levels of cytosolic carotenoids (phytoene, lycopene and β -carotene) up to 1 mg/g DW (Figure 4.4) (Andersen et al., 2021), which are in the range of those found in chromoplasts from natural sources such as ripe tomato fruit (D'Andrea et al., 2018; Diretto et al., 2020; Flores et al., 2016; Massaretto et al., 2018; Nogueira et al., 2013; Pankratov et al., 2016; Suzuki et al., 2015). Thirdly, the system is very flexible, and the incorporation of additional enzymes catalysing downstream steps is feasible so that a much broader variety of carotenoids could be produced (Nogueira et al., 2019). Fourthly, once the pigments were synthesized in the cytosol, they maintained their high antioxidant potential, in particular lycopene (Figure 4.2C). And finally, we demonstrate that this

strategy can be combined with strategy P to further improve carotenoid levels of green tissues such as leaves.

In this chapter, we have shown that leaves can be enriched with considerable amounts of phytoene and lycopene, two carotenoids that are normally present only in trace amounts in chloroplasts. Furthermore, this strategy C also works for β -carotene, whose levels can be further increased by combination with strategy C. Lycopene has been found to generate crystals that break plastid membranes when present in high amounts, like in tomato fruits (Ben-Shaul and Naftali, 1969). When produced in the leaf cytosol, lycopene also forms crystals that are very similar to those naturally formed in the chromoplasts of tomato ripe fruit ([Andersen et al. 2021](#)). It is likely that cytosolic lycopene is initially stored in association with cell membranes before reaching a concentration high enough to crystallize. In the case of phytoene and β -carotene, fruits that produce high amounts of these carotenoids store it in PG and other lipophilic vesicles inside chromoplasts that are sometimes released into the cytosol, probably to remove excess amounts accumulated in plastidial membranes (Lado et al., 2015; Nogueira et al., 2013). The site where the massive amounts of cytosolic phytoene and β -carotene produced in *N. benthamiana* leaves are sequestered remains unknown. The amount of phytoene stored in the cytosol through the extraplastidial pathway is far higher than the one described generated by the plastidial crtB protein, but the impossibility to penetrate and cross the plastid envelope membranes does not allow the trigger the chromoplastogenesis process (Figure 4.2). These data also support the conclusion that carotenoid compounds produced with a cytosolic pathway are unable to be translocated into the plastid and thus to greatly affect its physiology. Nevertheless, the formation of cytosolic lycopene crystals and the accumulation of similarly high levels of phytoene and β -carotene in extraplastidial locations had a negative effect on chlorophyll levels and photosynthesis (Figures 4.2, 4.3, 4.4). We speculate that this is a secondary effect and that the primary impact of extraplastidial carotenoid accumulation is in overall cell fitness. Indeed, several signs of cell damage and senescence, including chlorosis and eventual necrosis, developed about a week after agroinfiltration with strategy C constructs. Consistently, the earliest changes associated with leaf senescence occur in the chloroplast and cause chlorosis before necrotic symptoms are observed (Majer et al., 2017). It seems likely that these deleterious, senescence-like effects might be related to cell damage caused by the disruption of normal cell compartments, functions and/or metabolism upon accumulation of extraplastidial carotenoids. Alternatively, signals derived from the cleavage of cytosolic phytoene, lycopene, β -carotene, or intermediate carotenoid species might be transduced to regulate chloroplast function, including photosynthetic activity (Avendaño-Vázquez et al., 2014; Cazzonelli et al., 2020)

In our experiments we showed that the addition of the bacterial lycopene cyclase *crtY* to the cytosolic pathway allowed to produce β -carotene in the cytosol but with a high level of lycopene and phytoene left (Figure 4.4). The mechanism of cyclization of lycopene is quite mysterious and at the present it is believed to be initiated by electrophilic protons. Lycopene β -cyclase is a flavoprotein that generally has an NAD(P)/FAD-binding motif. There are aromatic and carboxyl amino acid residues in the FAD-binding motif and catalytic domain of cyclase, and these residues may represent negative point charges related to the coordination of the incipient carotenoid carbocations. FAD(H₂) and NAD(P)(H), which were identified as the cofactors, might involve redox reactions. FAD needs to be noncovalently bound to the enzyme, and NADPH functions as the FAD reductant. As the reaction progresses, hydrogen is not transferred from the dinucleotide cofactors to β -carotene (Mialoundama et al., 2010). It is possible that the high concentration of enzymes in the cytosol could lack precursors to maintain their maximum activity so, higher the number of enzymes, lower the conversion rate to downstream products. Alternatively, the crystallization of lycopene might prevent easy access of *crtY* to its substrate.

The amount of β -carotene was increased when the cytosolic version of *crtB* (GFP-*crtB*) was substituted for the unmodified version that can enter the chloroplast through a cryptic transit peptide and trigger the development of chromoplasts (strategy P) (Llorente et al. 2020). This led to the accumulation of β -carotene in the cytosol and in the newly formed chromoplasts resulting in an increased amount of this compound (Figure 4.4). The results indicate that the plastidial MEP pathway and the cytosolic MVA pathway are compatible and can work together at the same time without downregulating each other. The lack of improvement in β -carotene levels when using the plastid targeted version of (p)*crtB* or when enhancing the flux of the MEP pathway with *DXS_I* further confirmed the lack of metabolite exchange between these two pathways in our system. By combining *crtB* and *DXS_I* overexpression (Figure 4.5), however, we obtained a considerably high increase in the level of phytoene. This result suggested that (1) the *DXS_I* enzyme was working to stimulate the MEP pathway flux, (2) that the endogenous GGPP synthase enzymes could efficiently convert the extra supply of MEP-derived IPP and DMAPP into GGPP, (3) that the plastid-localized *crtB* enzyme was able to convert enhanced levels of GGPP into phytoene, and (4) that the conversion of phytoene into downstream carotenoids was limiting in *N. benthamiana* leaves. Several explanations for the poor phytoene conversion are possible. It has been shown that when the activity of the main rate-determining step of the carotenoid pathway (i.e., phytoene synthase) is increased (e.g., when *crtB* is present), the control of the pathway flux is shifted to downstream enzymes, many of which are under redox control (Busch et al., 2002; Fraser et al., 2002). While it is possible that biosynthetic and storage mechanisms could already be saturated in *crtB*-containing samples, thus limiting further

increases upon enhancing the supply of phytoene with DXS₁, it is also possible that this additional phytoene cannot be easily accessed by endogenous desaturase enzymes due to differential compartmentation. Indeed, in Chapter 3 we showed that most crtB-derived phytoene is produced and stored in PG whereas desaturases have been mainly localized in envelope membranes and the stroma (Ruiz-Sola and Rodriguez-Concepcion 2012; Nogueira et al., 2013). Nonetheless, the DXS₁-mediated increase in the synthesis of precursors combined with the activity of crtB results in the accumulation of a considerable amount of phytoene that allows the crtB-induced phenotype to proceed faster at least in the first phases of its establishment (i.e., when the overaccumulation of carotenoids is not the main factor controlling chromoplast establishment but the photosynthetic impairment is connected to phytoene amount), in a similar fashion to what observed when blocking phytoene desaturation with norflurazon (Llorente et al. 2020) (Figure 5).

N. benthamiana is particularly well suited to produce high titres of valuable enzymes and metabolites for molecular pharming due to a fast growth rate and a natural ability to express heterologous gene sequences, among other traits (Lomonosoff and D'Aoust, 2016). While agroinfiltration assays can be scaled up for industrial production of carotenoids and other metabolites in *N. benthamiana*, adaptation to crops such as lettuce for human or animal consumption should require further efforts in the development and optimization of safe and reliable transient expression methods with no health risks. Stable expression of transgenes appears as a valid alternative from the technical point of view. However, the poor consumer acceptance of transgenesis has turned the attention to genome editing. New varieties of leafy food (e.g., lettuce, spinach, cabbage, kale, chard) and forage crops (e.g., alfalfa, grasses) could be generated by editing endogenous genes to overaccumulate carotenoids in both plastidial and extraplastidial locations. Flux-controlling enzymes involved in isoprenoid biosynthesis (including HMGR, GGPP synthase and phytoene synthase) are encoded by small gene families in most plants. In the case of GGPP synthase, cytosolic isoforms are naturally present (Ruiz-Sola et al., 2016). For the rest, CRISPR-Cas9 technology could be used to remove the N-terminal region from non-essential and/or tissue-specific isoforms of HMGR (to create truncated forms similar to the tHMGR version used here) and carotenoid biosynthetic enzymes such as phytoene synthase (to remove the plastid transit peptide and create a cytosolic version for strategy C or to make it more stable and active to be used in strategy C upon weakening chloroplast identity using a light treatment like those described in Chapter 2). Furthermore, our results open the door to the biofortification of leafy vegetables with other health-promoting isoprenoids such as tocopherols (vitamin E) and phyloquinones (vitamin K₁) by combining extraplastidial biosynthetic pathways

using MVA-derived precursors with the crtB-mediated chromoplastogenesis system complemented as described in Chapter 3.

4.4. Material and methods.

4.4.1. Plant material and growth conditions

Nicotiana benthamiana used for the transient expression assays were grown in a greenhouse under standard long-day conditions (LD, 14 h light at $26 \pm 1^\circ\text{C}$ and 10 h dark at $21 \pm 1^\circ\text{C}$).

4.4.2. Gene constructs

Constructions used in this study for the assembling of the extraplastidial pathway were available in the lab and were generated as described by [Andersen et al. 2020](#). Constructions overexpressing the different isoforms of tomato DXS (35S:SIDXS₁-pGWB₂₁ and 35S:SIDXS₂-pGWB₄₅₄) were a kindly provided by Xueni Di (IBMCP, Valencia, Spain) while 35S:AtDXS-pGWB₄₀₅ was available in the lab.

4.4.3. Transient expression assay

Agroinfiltration experiments were performed as described in the previous chapters. Gene silencing was prevented by co-agroinfiltration with an agrobacterium strain EHA₁₀₁ carrying the helper component protease (HcPro) of the watermelon mosaic virus (WMV) in plasmid HcProWMV-pGWB₇₀₂ (a kind gift of Juan José López-Moya and Maria Luisa Domingo-Calap (CRAG-Barcelona, Spain)).

4.4.4. Photosynthetic measurements

Photosynthetic efficiencies were assessed by measuring chlorophyll a fluorescence with a MAXI-PAM fluorimeter (Heinz Walz GmbH). Photosynthetic parameters were evaluated at 0, 3, 5 and 7 dpi in plants that were previously kept in darkness for at least 30 min to fully open and relax PSII reaction centres. Effective quantum yield of PSII (ϕPSII) was measured as $(F_m' - F_s)/F_m'$, where F_m' and F_s are the maximum and minimum fluorescence of light-exposed plants, respectively. The chosen light intensity was 21 PAR (AL=2). Average values were calculated from three biological replicates with three different leaf areas for each replicate. To assess the effective

quantum yield of PSII (Φ PSII) of plants overexpressing the different DXS isoforms, fluorescence was measured with a Handy GFP Cam (PSI (Photon Systems Instruments) spol. s r.o.) with the same light intensity.

4.4.5. Antioxidant capacity

Total antioxidant capacity was calculated as described in the previous chapter.

4.4.6. Metabolite analysis

Metabolite content of the leaf areas overexpressing the combinations of interest was evaluated as described in the previous chapters.

General discussion

General discussion

5.1. Chromoplast differentiation in green leaves.

5.1.1. A non-reversible chloroplast-to-chromoplast differentiation phenotype triggered by plastid-localized crtB

Chromoplasts are a very studied and yet little-known typology of plastids. They are involved in the synthesis and storage of carotenoid pigments in flowers, roots and fruits but only occasionally develop in leaves. The differentiation of chromoplasts is fundamental in fruit ripening, for example in tomato or bell pepper, because it is associated with the accumulation of several important compounds such as carotenoids and other isoprenoids (Egea et al., 2010; Li and Yuan, 2013). As some isoprenoids have important nutritional value, chromoplast generation is seen as an interesting strategy of biofortification.

Leaves are an interesting target for secondary metabolites enrichment because green leafy vegetables are easy and fast to grow. Unfortunately, they are the most recalcitrant organ to develop chromoplasts and in nature are reported few cases. *Buxus sempervirens* leaves, for example, show a conversion of their chloroplasts into chromoplasts that accumulate carotenoids to face photoinhibitory stress during winter. The photosynthetic efficiency of these leaves progressively decreases during chromoplastogenesis accumulating high levels of carotenoids with photoprotective activity (Hormaetxe et al., 2004). However, conversely to fruit or petal chromoplasts, the plastids of red leaves of this species can revert to chloroplasts once the winter is over. The synthetic system studied in this thesis work is based on the overexpression of the bacterial gene *crtB*, a homologue of the plant gene *PSY* that codifies for the enzyme phytoene synthase. In its natural conformation, crtB protein likely has a cryptic transit peptide that allows it to be partially translocated inside the chloroplast (Majer et al., 2017, [Llorente et al., 2020](#)). When this happens, the level of phytoene and subsequently of downstream carotenoids highly increases and the chloroplast irreversibly converts to a chromoplast, a phenotype that is visually detectable because the leaf colour changes from green to yellow. The differentiation process is associated with a progressive loss of photosynthetic activity as reported in fruits like tomato or bell pepper, where this transition naturally occurs during the ripening process (Egea et al., 2010). The loss of chloroplast functionality however is not directly caused by the accumulation of downstream carotenoids, but it starts with the burst in the amount of phytoene. Most

importantly, this thesis work demonstrates that the reduction of the photosynthetic capacity of leaf chloroplasts is not just a consequence of chromoplast differentiation but a requirement that makes chloroplasts competent to embark in the differentiation process.

5.1.2. The crtB-mediated phytoene boost makes the chloroplasts competent to become chromoplasts

Phytoene is a Colourless carotenoid synthesized in the first committed step of pathway. In chloroplasts, it does not naturally accumulate as it is transformed into downstream carotenoids of the photosynthetic apparatus, where the efficient energy transfer is guaranteed by the presence in light harvesting complexes of β -carotene and xanthophylls (i.e., lutein, violaxanthin and zeaxanthin). With crtB overexpression the levels of phytoene sudden increase and the excessive presence of this intermediate could result in a disruption of the photosystem equilibrium (Liechtenthaler et al., 2007). The functioning of a highly efficient photosynthetic antenna, in fact, depends entirely on the specific structures of the apo-proteins of the light-harvesting complexes that must bind sufficient pigments to maximize absorption and energy dissipation. In plants where the carotenoid biosynthetic flux is perturbed and only one compound is accumulated (e.g., phytoene), for example by silencing the gene codifying for phytoene desaturase (i.e., *PDS*) enzyme, the thylakoidal membrane system is highly impacted with changes in the protein composition that results in a lower photosynthetic efficiency (Wang et al., 2010). Our results show that the higher the levels of phytoene, the higher the photosynthetic efficiency loss. Chloroplasts, in fact, can compensate to a certain extent for the disequilibrium in the photosynthetic apparatus composition when they retain functionality and can redistribute the internal levels of carotenoids to avoid major fractures of the photosynthetic apparatus (Liechtentaler et al., 2007, Xu et al., 2020).

Once photosynthesis is impaired (e.g., by high enough phytoene levels), phytoene must be converted into downstream carotenoids for chromoplast differentiation to proceed. Therefore, crtB-mediated chromoplastogenesis can be divided into two phases. In the first phase, photosynthetic efficiency must be lowered, likely constituting a signal that mark the chloroplast as “non-active”. The high availability of phytoene as a precursor, then, allows the endogenous biosynthetic machinery to proceed and the level of downstream carotenoids increases. This event triggers the formation of internal storage structures that in turn activate the carotenoid biosynthetic process and the storage capacity as the chromoplasts differentiate. In a natural context, such as during fruit ripening, the chloroplasts of green fruit exhibit fewer thylakoid membranes and a marginal electron transport activity (i.e., photosynthetic function) (Carrara et

al., 2001). In such naturally competent chloroplasts, the developmentally regulated overexpression of an endogenous gene (i.e., *PSY*), associated with the ripening process, allows to synthesize enough carotenoids to proceed with chromoplast differentiation (Sadali et al., 2019, [Llorente et al., 2020](#)). The need of a low or null photosynthetic activity to proceed with chromoplast development is also supported by the observation that the ORANGE (OR) protein only promotes chromoplastogenesis in green fruits or non-photosynthetic tissues like tubers or calli (Osorio, 2019).

5.1.3. Chloroplast stress is signalled to the nucleus to support chromoplast differentiation

We propose that a *crtB*-dependent signal must travel from the plastid to the nucleus (i.e., retrograde) to unleash the observed changes in plastid ultrastructure and metabolism that take place as chloroplasts differentiate into chromoplasts. Chemical or physical treatments able to weaken photosynthetic activity of leaf chloroplasts facilitate transition to chromoplasts when carotenoid biosynthesis is stimulated (e.g., by *PSY* overexpression) and increase the speed of the *crtB*-driven process. This suggests that alterations in the redox poise and excitation balance between photosystem II (PSII) and photosystem I (PSI) (Bellaflore et al., 2005) that promote the formation of plastid reactive oxygen species (ROS) (Chan et al., 2016) might be part of the signalling pathway. ROS are part of a complex net of retrograde signalling from chloroplast to the nucleus that allows the plant to respond to perturbations in plastid function due to environmental and developmental cues. Events such as exposure to low R:FR (Ortiz-Alcaide et al., 2019), high light (Estavillo et al., 2011) or phytoene overproduction by *crtB* lead to the formation of ROS molecules like H_2O_2 and $O^{\cdot-}$ at PSI and singlet oxygen ($^1O^2$) at PSII, which alter stromal redox state and plastid metabolism (Strand et al., 2015) impacting chromoplast formation. A parallelism can be seen with natural chromoplastogenesis considering that, during fruit ripening or flower petal development, several peaks of ROS production can be observed that correspond to the starting point of chromoplast development (Muñoz and Munné-Bosch, 2018). It is possible that rather than (or in addition to) losing photosynthetic identity, leaf chloroplasts must experience a malfunctioning situation at the level of their photosynthetic chain that produces signals of distress to the nucleus. Chloroplast stress is known to result in the accumulation of metabolites able to regulate nuclear gene expression, including methylerythritol 2,4-cyclodiphosphate (MEcPP, a MEP pathway intermediate) (Xiao et al. 2012), β -cyclocitral (produced by the non-enzymatic oxidative cleavage of β -carotene) (Ramel et al. 2012), and 3'-phosphoadenosine 5'-phosphate (PAP) (Estavillo et al. 2011). The accelerated

chromoplastogenesis observed in the PAP-overaccumulating *A.thaliana salı* mutant suggests that PAP might be one of the signals sensing the chloroplast stress and transducing it to regulate nuclear gene expression for chromoplast differentiation to occur. However, the participation of MEcPP, β -cyclocitral, and maybe other retrograde signals cannot be excluded. Regardless of their identity, such signals might tag the plastid as a “dead man walking” losing its identity of source organ and starting the transition towards a sink structure (i.e., chromoplast). How fast the chloro-chromoplast conversion can occur might therefore depend on how intense the production of these signalling molecules is. For this reason, conditions that result in a higher level of phytoene or conditions directly associated with ROS production at the level of the photosystems impact the speed of chromoplast development, even if, in some cases, do not directly affect the final carotenoid content (Figure 5.1).

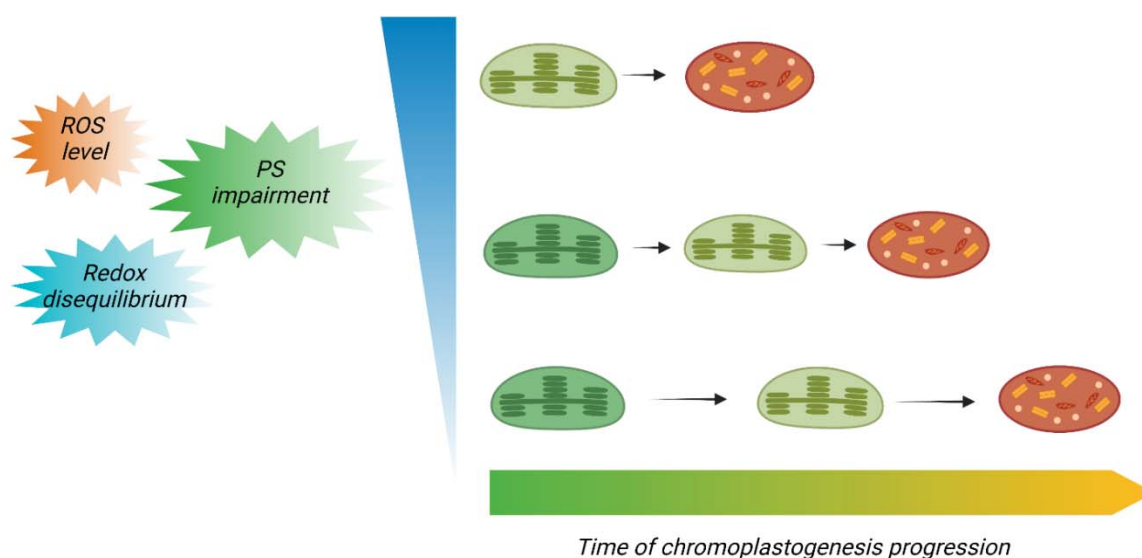


Figure 5.1: Representation of the schematic model that define the progression of chromoplast development in leaves. The accumulation of ROS, changes in redox equilibrium or the impairment of photosystems trigger the generation of plastidial signals that speed up the chromoplastogenesis process.

5.2. New ways to improve isoprenoid content in leaves.

5.2.1. Artificial chromoplasts develop structures that produce and store healthy isoprenoids

During the natural chloroplast-to-chromoplast transition, the most conspicuous changes happen in biochemical composition (e.g., the elevation of carotenoid contents) and structural organization (e.g., degradation of thylakoids and development of carotenoid-sequestering

structures) (Sadali et al., 2019). Chromoplasts internal structures allow to classify them as crystalline, membranous, tubular, or globular. These structures accumulate different carotenoids, depending on the chemical nature of the pigment and its concentration (Sadali et al., 2019, Egea et al., 2010). Our crtB chromoplasts do not show crystalline formations (typically associated with lycopene) but contain a high number of dispersed membranes and show more and larger PG compared to green leaf chloroplasts mirrored by increased levels of PAG-associated proteins (Van Wijk and Kessler, 2017). Additionally, most proteins markers associated with the photosynthetic apparatus disappear during chromoplast formation, coherently with what described for tomato or red pepper fruit (Rödiger et al., 2021). An exception is Lhcb2, which does not change during the process likely because of an association protein-pigment that results in the conservation of chlorophylls. On the other hand, while other studies had described a central role for the envelope-located translocon complexes in the import-export of proteins involved into chromoplast development (Ling et al., 2021; Rödiger et al., 2021), chromoplastogenesis triggered by crtB does not cause changes in the levels of translocon-associated proteins with the only exception of a downregulation of TOC33 by a SP1-independent pathway.

The tightly packed membranes in that develop in our artificial leaf chromoplasts resemble the ones observed in flower petals from daffodil or *Thunbergia alata* (Sadali et al., 2019; Ljubešić et al., 1996). The membranous and tubular chromoplasts found in these flowers, however, usually display a low number of PG. By contrast, crtB-induced chromoplasts show more and larger PG similar to ripe fruit chromoplasts. In other plant tissues, such as the pulp of *Citrus* fruits, the type of chromoplast substructures was related to the presence of specific carotenoids. Chromoplasts from fruit with an elevated content of colourless carotenes (e.g., phytoene) showed abundant PG-like vesicles while other varieties with a prevalence of lycopene showed thin crystalline formations (Lado et al., 2015). Differences in carotenoid composition or accumulation, thus, are mirrored by the development of diverse chromoplast types, revealing the plasticity of these organelles to rearrange carotenoids inside different structures to allow massive accumulation and chemical stability of these lipophilic metabolites.

5.2.2. The crtB protein is localized in PG, the main storage structure for the newly formed plastidial isoprenoids

Besides carotenoids, the globular-membranous chromoplasts that develop in crtB-producing leaves accumulate increased levels of α -tocoquinone, plastochromanol 8, tocopherols and phylloquinone but a lower level of plastoquinones-9. These isoprenoids are typically stored in PG

(Van Wijk and Kessler, 2017) that, in *crtB*-chromoplasts are the only structures to show increased levels of all the isoprenoids while others (e.g., the membranous formations) show almost no detectable levels of compounds such as phylloquinone or tocoquinone. Among the carotenoid stored, the PG fraction of synthetic chromoplasts show a prevalence of phytoene and β -carotene. Phytoene is normally undetectable in plant leaves because it is readily converted to downstream product but is reported to be accumulated in PG when excessively produced in tomato fruit (Ruiz-Sola and Rodríguez-Concepción, 2012; Nogueira et al., 2013). Interestingly, the *crtB* protein was found associated with PG and internal membranes in tomato fruit chromoplasts where it would work with endogenous enzymes to produce lycopene. In synthetic chromoplasts, most of the *crtB* protein localizes in PG, and only part of its phytoene product is converted into downstream carotenoids. PG were also described to contain enzymes involved in carotenoid biosynthesis and degradation in some fruit chromoplasts (Brehelin et al., 2007, Rottet et al., 2016). In leaf chromoplasts, PG-localized enzymes might also convert part of the pool of phytoene into β -carotene. In this case these structures would increase the sink strength of the plastid and at the same time the source strength participating actively in the synthesis and sequestration of compounds (Vishnevetsky et al., 1997). The main proteins involved in the finalization of the tocopherol biosynthesis pathway (i.e., VTE₄ and VTE₁) are localised and act in the PG (Brehelin et al., 2007, Vidi et al., 2006). The overexpression of these genes allowed to increase the levels of isoprenoids also in *crtB*-overexpressing leaves likely because of the higher availability of enzyme-localization sites (i.e., PG). The combination with genes involved in the synthesis of prenylquinones precursors (i.e., VTE₅ and VTE₆) also allowed to increase at the same time the amount of phylloquinones and tocopherols indicating that the enrichment of leaves in multiple vitamins is possible by using this strategy. Interestingly, none of these gene combinations resulted in a lower amount of carotenoids compared to the overexpression of *crtB* alone, suggesting that the availability of common MEP-derived precursors is not limiting. This conclusion was supported by the experiments using DXS₁, in which carotenoids levels hardly increased despite the supply of precursors was boosted.

It's logic to think that conditions that promote PG proliferation and enlargement such as abiotic stress or senescence might have an impact on the content of the molecules enlisted above. Under oxidative conditions caused by stress. PG would deliver isoprenoids to thylakoid membranes to scavenge reactive oxygen species via the structural connection with thylakoids (Brehelin et al., 2007). When chloroplasts harbouring increased PG levels (e.g., after high-light acclimation) are transformed into chromoplasts, the metabolic profile adjust to the greater sink strength and results in increased levels of carotenoids and other isoprenoids such as tocopherols or phylloquinone. The same principle applies when leaves developing chromoplasts undergo dark

induced senescence causing the formation of massive PG and, additionally, the mobilization of high amount of phytol coming from chlorophyll degradation that increase the availability of precursors for several prenylquinones (Van Wijk and Kessler, 2017). In senescent leaves, however, carotenoids are also degraded constituting a limitations for the use of this treatment with biofortification purposes (Rottet et al., 2016). More importantly, the use of *crtB* in combination with PG-promoting treatments allowed to double the levels of carotenoids and tocopherols also in edible species such as lettuce that mirrored the protein and metabolic profile of *N. benthamiana*. Especially this plant showed higher levels of the carotenoid lactucaxanthin indicating that the overexpression of *crtB* provide enough precursors to boost the synthesis of species-specific compounds.

5.2.3. Artificial chromoplastogenesis can be combined with extraplastidial carotenoid biosynthesis to boost the production of healthy carotenoids.

One interesting feature of the *crtB* system is its possibility to be combined with other strategies to synthesize health-promoting isoprenoids. The use of a synthetic pathway engineered with bacterial enzymes and a deregulated version of the main rate-determining enzyme of the MVA pathway allowed the production of very high levels of phytoene and lycopene in the cytosol (Andersen et al., 2021). Using a similar approach on the plastidial MEP pathway, however, did not work that well because the combination of DXS and *crtB* results in a limited increase of downstream carotenoids and an overaccumulation of phytoene. This bottleneck effect is likely due to a limit in the amount of *crtB*-synthesized phytoene that can be converted by the downstream enzymes that could not have access or could not handle the whole pool stored in PG (Nogueira et al., 2013). In this thesis, the synthetic cytosolic pathway was extended by adding an extra gene allowing the conversion of lycopene into β -carotene, the main pro-vitamin A carotenoid. Furthermore, the use of the original *crtB* protein (which localizes to both the cytosol and plastids) allowed the production of high β -carotene levels in the cytosol and, at the same time, triggering chromoplast development and providing additional compartments for the storage of healthy plastidial isoprenoids, including β -carotene.

With this work, thus, we have characterized a new biotechnological tool that exhibits great flexibility to biofortify green leaves in health-promoting isoprenoids such as pro-vitamin A carotenoids, vitamin E tocopherols or vitamin K, and we demonstrated the possibility to use it on edible plants. The system could be used to enrich the vitamin content in leaves once the photosynthesis become dispensable (e.g., immediately before harvest). The possibility to modulate the speed of the process through physical or chemical treatments would help to adapt the yield to different species of plant or to different growth strategies (i.e., open field or

greenhouse). For example, the exogenous application of phytohormones or the supplement with a low R:FR, able to accelerate chromoplast development, would be handy to reach high vitamin levels faster and reducing the cost of maintenance of plants. Also, being a system of transient expression, the tool would avoid the generation of transgenic plants saving time and money.

Conclusions

Conclusions

1. A non-reversible chloroplast-to-chromoplast differentiation phenotype is triggered in leaves by the bacterial *crtB* protein acting in plastids.
2. The activity of *crtB* produces a boost in phytoene content that causes a loss of photosynthetic activity. This makes the chloroplasts competent to become chromoplasts when phytoene is converted into downstream carotenoids.
3. Altered redox balance in chloroplasts might be signalled by PAP to facilitate chromoplast differentiation.
4. Application of exogenous hormones can modulate *crtB* expression levels, eventually impacting phytoene amount and subsequent chromoplastogenesis speed.
5. Weakening of photosynthetic activity of leaf chloroplasts by chemical or physical treatments also facilitates transition to chromoplasts.
6. Exposure to simulated shade (low R:FR) facilitates acclimation to low light in shade avoider plants. It also decreases the levels of photosynthetic pigments and activity that increases the speed of chromoplastogenesis upon activation of phytoene production.
7. Higher levels of reduced plastoquinone in plants exposed to low R:FR slow down phytoene desaturation and result in increased levels of phytoene in *crtB* overexpressing leaves, hence explaining the faster development of chromoplasts.
8. Plants exposed to high light conditions and experiencing more oxidative stress at the plastid level are also faster in developing chromoplasts.
9. Chromoplasts differentiated after the overexpression of *crtB* show the proliferation of structures used to sequestrate and store carotenoids. Thylakoidal membranes are degraded, and new membrane formations develop, while plastoglobules increase. Envelope stays stable during the conversion.
10. These artificial chromoplasts accumulate plastidial isoprenoids other than carotenoids. While α -tocoquinone, tocopherols, plastochromanol 8, and phylloquinone double their levels, plastoquinone-9 decreases.

11. The crtB protein is localized in plastoglobules, which are the main storage structure for the newly formed plastidial isoprenoids, including phytoene and β -carotene.
12. Conditions that promote plastoglobules proliferation such high-light and dark-induced senescence, can be used to further improve isoprenoid content in crtB leaves. Senescence, however, results in a loss of carotenoids.
13. Overexpression of isoprenoid biosynthetic genes can further improve the content of these metabolites in crtB-triggered chromoplasts.
14. Lettuce leaves overexpressing crtB and exposed to high light show an isoprenoid accumulation response like *N. benthamiana* leaves.
15. Increasing supply of MEP-derived isoprenoid precursors in plastids with crtB results in much higher levels of phytoene but not downstream carotenoids in chromoplasts, suggesting a bottleneck in the endogenous carotenoid pathway that prevents further carotenoid enrichment of leaves.
16. Carotenoids such as phytoene, lycopene and β -carotene can be accumulated in the cytosol by building an extraplastidial synthetic pathway and enhancing the supply of isoprenoid precursors through the cytosolic MVA pathway.
17. The amount of β -carotene can be further increased by using a version of the crtB protein able to function in the cytosol with the synthetic pathway but also enter the plastid and trigger chromoplast differentiation.
18. The new biotechnological tools developed here allow biofortification of leaves and green tissues in health-promoting carotenoids (such as phytoene) and vitamins (such as β -carotene, tocopherols and phylloquinones) once photosynthesis is dispensable (e.g., just before harvest).

References

References

- Ampomah-Dwamena, C., Thrimawithana, A.H., Dejnopratt, S., Lewis, D., Espley, R. V., and Allan, A.C.** (2019). A kiwifruit (*Actinidia deliciosa*) R2R3-MYB transcription factor modulates chlorophyll and carotenoid accumulation. *New Phytol.* **221**: 309–325.
- Andersen, T.B., Llorente, B., Morelli, L., Torres-Montilla, S., Bordanaba-Florit, G., Espinosa, F.A., Rodriguez-Goberna, M.R., Campos, N., Olmedilla-Alonso, B., Llansola-Portoles, M.J., Pascal, A.A., and Rodriguez-Concepcion, M.** (2021). An engineered extraplastidial pathway for carotenoid biofortification of leaves. *Plant Biotechnol. J.* **19**: 1008–1021.
- Avendaño-Vázquez, A.O., Cordoba, E., Llamas, E., San Román, C., Nisar, N., De la Torre, S., Ramos-Vega, M., de la Luz Gutiérrez-Nava, M., Cazzonelli, C.I., Pogson, B.J., and León, P.** (2014). An uncharacterized apocarotenoid-derived signal generated in ζ -carotene desaturase mutants regulates leaf development and the expression of chloroplast and nuclear genes in *Arabidopsis*. *Plant Cell* **26**: 2524–2537.
- Babujee, L., Wurtz, V., Ma, C., Lueder, F., Soni, P., Van Dorselaer, A., and Reumann, S.** (2010). The proteome map of spinach leaf peroxisomes indicates partial compartmentalization of phylloquinone (vitamin K₁) biosynthesis in plant peroxisomes. *J. Exp. Bot.* **61**: 1441–1453.
- Bailey, S., Walters, R.G., Jansson, S., and Horton, P.** (2001). Acclimation of *Arabidopsis thaliana* to the light environment: The existence of separate low light and high light responses. *Planta* **213**: 794–801.
- Barsan, C., Sanchez-Bel, P., Rombaldi, C., Egea, I., Rossignol, M., Kuntz, M., Zouine, M., Latché, A., Bouzayen, M., and Pech, J.C.** (2010). Characteristics of the tomato chromoplast revealed by proteomic analysis. *J. Exp. Bot.* **61**: 2413–2431.
- Barsan, C., Zouine, M., Maza, E., Bian, W., Egea, I., Rossignol, M., Bouyssié, D., Pichereaux, C., Purgatto, E., Bouzayen, M., Latché, A., and Pech, J.C.** (2012). Proteomic analysis of chloroplast-to-chromoplast transition in tomato reveals metabolic shifts coupled with disrupted thylakoid biogenesis machinery and elevated energy-production components. *Plant Physiol.* **160**: 708–725.
- Bellaflora, S., Barneche, F., Peltler, G., and Rochalx, J.D.** (2005). State transitions and light

adaptation require chloroplast thylakoid protein kinase STN7. *Nature* **433**: 892–895.

- Ben-Shaul, Y. and Naftali, Y.** (1969). The development and ultrastructure of lycopene bodies in chromoplasts of *Lycopersicum esculentum*. *Protoplasma* **67**: 333–344.
- Benkov, M.A., Yatsenko, A.M., and Tikhonov, A.N.** (2019). Light acclimation of shade-tolerant and sun-resistant *Tradescantia* species: photochemical activity of PSII and its sensitivity to heat treatment. *Photosynth. Res.* **139**: 203–214.
- Besagni, C. and Kessler, F.** (2013). A mechanism implicating plastoglobules in thylakoid disassembly during senescence and nitrogen starvation. *Planta* **237**: 463–470.
- Bian, W., Barsan, C., Egea, I., Purgatto, E., Chervin, C., Zouine, M., Latché, A., Bouzayen, M., and Pech, J.-C.** (2011). Metabolic and Molecular Events Occurring during Chromoplast Biogenesis. *J. Bot.* **2011**: 1–13.
- Botella-Pavía, P. and Rodríguez-Concepción, M.** (2006). Carotenoid biotechnology in plants for nutritionally improved foods. *Physiol. Plant.* **126**: 369–381.
- Bou-Torrent, J., Toledo-Ortiz, G., Ortiz-Alcaide, M., Cifuentes-Esquivel, N., Halliday, K.J., Martínez-García, J.F., and Rodríguez-Concepción, M.** (2015). Regulation of carotenoid biosynthesis by shade relies on specific subsets of antagonistic transcription factors and cofactors. *Plant Physiol.* **169**: 1584–1594.
- Bouvier, F., Backhaus, R.A., and Camara, B.** (1998). Induction and control of chromoplast-specific carotenoid genes by oxidative stress. *J. Biol. Chem.* **273**: 30651–30659.
- Bréhélin, C., Kessler, F., and van Wijk, K.J.** (2007). Plastoglobules: versatile lipoprotein particles in plastids. *Trends Plant Sci.* **12**: 260–266.
- Breuers, F.K.H., Bräutigam, A., Geimer, S., Welzel, U.Y., Stefano, G., Renna, L., Brandizzi, F., and Weber, A.P.M.** (2012). Dynamic remodeling of the plastid envelope membranes - A tool for chloroplast envelope *in vivo* localizations. *Front. Plant Sci.* **3**: 1–10.
- Britton, G.** (1995). Structure and properties of carotenoids in relation to function. *FASEB J.* **9**: 1551–1558.
- Busch, M., Seuter, A., and Hain, R.** (2002). Functional analysis of the early steps of carotenoid biosynthesis in tobacco. *Plant Physiol.* **128**: 439–453.
- Cagnola, J.I., Ploschuk, E., Benech-Arnold, T., Finlayson, S.A., and Casal, J.J.** (2012). Stem

- transcriptome reveals mechanisms to reduce the energetic cost of shade-avoidance responses in tomato. *Plant Physiol.* **160**: 1110–1119.
- Carrara, S., Pardossi, A., Soldatini, G.F., Tognoni, F., and Guidi, L.** (2001). Photosynthetic activity of ripening tomato fruit. *Photosynthetica* **39**: 75–78.
- Cartaxana, P., Morelli, L., Jesus, B., Calado, G., Calado, R., and Cruz, S.** (2019). The photon menace: Kleptoplast protection in the photosynthetic sea slug *Elysia timida*. *J. Exp. Biol.* **222**.
- Casal, J.J.** (2013). Photoreceptor signaling networks in plant responses to shade. *Annu. Rev. Plant Biol.* **64**: 403–427.
- Cazzonelli, C.I., Hou, X., Alagoz, Y., Rivers, J., Dhami, N., Lee, J., Marri, S., and Pogson, B.J.** (2020). A cis-carotene derived apocarotenoid regulates etioplast and chloroplast development. *Elife* **9**: 1–32.
- Ceballos, H., Morante, N., Sánchez, T., Ortiz, D., Aragón, I., Chávez, A.L., Pizarro, M., Calle, F., and Dufour, D.** (2013). Rapid cycling recurrent selection for increased carotenoids content in cassava roots. *Crop Sci.* **53**: 2342–2351.
- Chan, K.X., Mabbitt, P.D., Phua, S.Y., Mueller, J.W., Nisar, N., Gigolashvili, T., Stroehrer, E., Grassl, J., Arlt, W., Estavillo, G.M., Jackson, C.J., and Pogson, B.J.** (2016). Sensing and signaling of oxidative stress in chloroplasts by inactivation of the SAL1 phosphoadenosine phosphatase. *Proc. Natl. Acad. Sci. U. S. A.* **113**: E4567–E4576.
- Che, P., Zhao, Z.Y., Glassman, K., Dolde, D., Hu, T.X., Jones, T.J., Gruis, D.F., Obukosia, S., Wambugu, F., and Albertsen, M.C.** (2016). Erratum: Elevated vitamin E content improves all-trans β -carotene accumulation and stability in biofortified sorghum (*Proc Natl Acad Sci USA* (2016) **113**:39 (11040–11045) DOI: 10.1073/pnas.1605689113). *Proc. Natl. Acad. Sci. U. S. A.* **113**: E8209.
- Chen, S., Li, H., and Liu, G.** (2006). Progress of vitamin E metabolic engineering in plants. *Transgenic Res.* **15**: 655–665.
- Cheung, A.Y., McNellis, T., and Piekos, B.** (1993). Maintenance of chloroplast components during chromoplast differentiation in the tomato mutant green flesh. *Plant Physiol.* **101**: 1223–1229.
- Cifuentes-Esquivel, N., Bou-Torrent, J., Galstyan, A., Gallemí, M., Sessa, G., Salla Martret, M., Roig-Villanova, I., Ruberti, I., and Martínez-García, J.F.** (2013). The bHLH proteins BEE and BIM positively modulate the shade avoidance syndrome in *Arabidopsis* seedlings. *Plant J.* **75**:

989–1002.

- Ciolfi, A., Sessa, G., Sassi, M., Possenti, M., Salvucci, S., Carabelli, M., Morelli, G., and Ruberti, I.** (2013). Dynamics of the shade-avoidance response in *Arabidopsis*. *Plant Physiol.* **163**: 331–353.
- Coate, J.E., Powell, A.F., Owens, T.G., and Doyle, J.J.** (2013). Transgressive physiological and transcriptomic responses to light stress in allopolyploid *Glycine dolichocarpa* (Leguminosae). *Heredity* (Edinb). **110**: 160–170.
- Cocaliadis, M.F., Fernández-Muñoz, R., Pons, C., Orzaez, D., and Granell, A.** (2014). Increasing tomato fruit quality by enhancing fruit chloroplast function. A double-edged sword? *J. Exp. Bot.* **65**: 4589–4598.
- Collakova, E. and DellaPenna, D.** (2003). Homogentisate phytyltransferase activity is limiting for tocopherol biosynthesis in *Arabidopsis*. *Plant Physiol.* **131**: 632–642.
- D'Amelia, V., Raiola, A., Carputo, D., Filippone, E., Barone, A., and Rigano, M.M.** (2019). A basic Helix-Loop-Helix (SIARANCIO), identified from a *Solanum pennellii* introgression line, affects carotenoid accumulation in tomato fruits. *Sci. Rep.* **9**: 1–10.
- D'Andrea, L., Simon-Moya, M., Llorente, B., Llamas, E., Marro, M., Loza-Alvarez, P., Li, L., and Rodriguez-Concepcion, M.** (2018). Interference with Clp protease impairs carotenoid accumulation during tomato fruit ripening. *J. Exp. Bot.* **69**: 1557–1568.
- Dellapenna, D.** (2007). Levels By Metabolic Engineering. **104**: 3675–3676.
- DellaPenna, D. and Pogson, B.J.** (2006). Vitamin synthesis in plants: Tocopherols and carotenoids. *Annu. Rev. Plant Biol.* **57**: 711–738.
- Deruere, J., Romer, S., d'Harlingue, A., Backhaus, R.A., Kuntz, M., and Camara, B.** (1994). Fibril assembly and carotenoid overaccumulation in chromoplasts: A model for supramolecular lipoprotein structures. *Plant Cell* **6**: 119–133.
- DiNicolantonio, J.J., Bhutani, J., and O'Keefe, J.H.** (2015). The health benefits of Vitamin K. *Open Hear.* **2**: 1–7.
- Diretto, G. et al.** (2020). Manipulation of β -carotene levels in tomato fruits results in increased ABA content and extended shelf life. *Plant Biotechnol. J.* **18**: 1185–1199.
- Diretto, G., Tavazza, R., Welsch, R., Pizzichini, D., Mourgues, F., Papacchioli, V., Beyer, P.,**

- and Giuliano, G.** (2006). Metabolic engineering of potato tuber carotenoids through tuber-specific silencing of lycopene epsilon cyclase. *BMC Plant Biol.* **6**.
- Diretto, G., Welsch, R., Tavazza, R., Mourgues, F., Pizzichini, D., Beyer, P., and Giuliano, G.** (2007). Silencing of beta-carotene hydroxylase increases total carotenoid and beta-carotene levels in potato tubers. *BMC Plant Biol.* **7**.
- Domonkos, I., Kis, M., Gombos, Z., and Ughy, B.** (2013). Carotenoids, versatile components of oxygenic photosynthesis. *Prog. Lipid Res.* **52**: 539–561.
- Van Eenennaam, A.L. et al.** (2003). Engineering Vitamin E Content: From Arabidopsis Mutant to Soy Oil. *Plant Cell* **15**: 3007–3019.
- Egea, I., Barsan, C., Bian, W., Purgatto, E., Latché, A., Chervin, C., Bouzayen, M., and Pech, J.C.** (2010). Chromoplast differentiation: Current status and perspectives. *Plant Cell Physiol.* **51**: 1601–1611.
- Enfissi, E.M.A., Barneche, F., Ahmed, I., Lichtlé, C., Gerrish, C., McQuinn, R.P., Giovannoni, J.J., Lopez-Juez, E., Bowler, C., Bramley, P.M., and Fraser, P.D.** (2010). Integrative transcript and metabolite analysis of nutritionally enhanced DE-ETIOLATED₁ downregulated tomato fruit. *Plant Cell* **22**: 1190–1215.
- Enfissi, E.M.A., Fraser, P.D., Lois, L.M., Boronat, A., Schuch, W., and Bramley, P.M.** (2005). Metabolic engineering of the mevalonate and non-mevalonate isopentenyl diphosphate-forming pathways for the production of health-promoting isoprenoids in tomato. *Plant Biotechnol. J.* **3**: 17–27.
- Estavillo, G.M. et al.** (2011). Evidence for a SAL1-PAP chloroplast retrograde pathway that functions in drought and high light signaling in Arabidopsis. *Plant Cell* **23**: 3992–4012.
- Esteban, R., Moran, J.F., Becerril, J.M., and García-Plazaola, J.I.** (2015). Versatility of carotenoids: An integrated view on diversity, evolution, functional roles and environmental interactions. *Environ. Exp. Bot.* **119**: 63–75.
- Fan, D.Y., Nie, Q., Hope, A.B., Hillier, W., Pogson, B.J., and Chow, W.S.** (2007). Quantification of cyclic electron flow around Photosystem I in spinach leaves during photosynthetic induction. *Photosynth. Res.* **94**: 347–357.
- Flores-Pérez, Ú., Sauret-Güeto, S., Gas, E., Jarvis, P., and Rodríguez-Concepción, M.** (2008). A mutant impaired in the production of plastome-encoded proteins uncovers a mechanism for

the homeostasis of isoprenoid biosynthetic enzymes in Arabidopsis plastids. *Plant Cell* **20**: 1303–1315.

Flores, P., Hernández, V., Hellín, P., Fenoll, J., Cava, J., Mestre, T., and Martínez, V. (2016). Metabolite profile of the tomato dwarf cultivar Micro-Tom and comparative response to saline and nutritional stresses with regard to a commercial cultivar. *J. Sci. Food Agric.* **96**: 1562–1570.

Fraser, P.D., Enfissi, E.M.A., Halket, J.M., Truesdale, M.R., Yu, D., Gerrish, C., and Bramley, P.M. (2007). Manipulation of phytoene levels in tomato fruit: Effects on isoprenoids, plastids, and intermediary metabolism. *Plant Cell* **19**: 3194–3211.

Fraser, P.D., Romer, S., Shipton, C.A., Mills, P.B., Kiano, J.W., Misawa, N., Drake, R.G., Schuch, W., and Bramley, P.M. (2002). Evaluation of transgenic tomato plants expressing an additional phytoene synthase in a fruit-specific manner. *Proc. Natl. Acad. Sci. U. S. A.* **99**: 1092–1097.

Fritsche, S., Wang, X., and Jung, C. (2017). Recent advances in our understanding of tocopherol biosynthesis in plants: An overview of key genes, functions, and breeding of vitamin E improved crops. *Antioxidants* **6**.

Gallemí, M., Molina-Contreras, M.J., Paulišić, S., Salla-Martret, M., Sorin, Ç., Godoy, M., Franco-Zorrilla, J.M., Solano, R., and Martínez-García, J.F. (2017). A non-DNA-binding activity for the ATHB4 transcription factor in the control of vegetation proximity. *New Phytol.* **216**: 798–813.

Galstyan, A., Cifuentes-Esquivel, N., Bou-Torrent, J., and Martinez-Garcia, J.F. (2011). The shade avoidance syndrome in Arabidopsis: A fundamental role for atypical basic helix-loop-helix proteins as transcriptional cofactors. *Plant J.* **66**: 258–267.

Giovannoni, J.J. (2004). Genetic regulation of fruit development and ripening. *Plant Cell* **16**: 170–181.

Giuliano, G. (2017). Provitamin A biofortification of crop plants: a gold rush with many miners. *Curr. Opin. Biotechnol.* **44**: 169–180.

Goldschmidt, E.E. (1988). Minireview regulatory aspects of chloro-chromoplast interconversions in senescing citrus fruit peel. *Isr. J. Bot.* **37**: 123–130.

Gopal, S.S., Lakshmi, M.J., Sharavana, G., Sathaiah, G., Sreerama, Y.N., and Baskaran, V. (2017). Lactucaxanthin-a potential anti-diabetic carotenoid from lettuce (*Lactuca sativa*) inhibits α -amylase and α -glucosidase activity in vitro and in diabetic rats. *Food Funct.* **8**: 1124–

1131.

- Grilli Caiola, M. and Canini, A.** (2004). Ultrastructure of chromoplasts and other plastids in *Crocus sativus* L. (Iridaceae). *Plant Biosyst.* **138**: 43–52.
- Harris, W.M. and Spurr, A.R.** (1969). Chromoplasts of Tomato Fruits. II. the Red Tomato. *Am. J. Bot.* **56**: 380–389.
- Harrison, P.J., Newgas, S.A., Descombes, F., Shepherd, S.A., Thompson, A.J., and Bugg, T.D.H.** (2015). Biochemical characterization and selective inhibition of β -carotene cis-trans isomerase D27 and carotenoid cleavage dioxygenase CCD8 on the strigolactone biosynthetic pathway. *FEBS J.* **282**: 3986–4000.
- Hashimoto, H., Uragami, C., Yukihiro, N., Gardiner, A.T., and Cogdell, R.J.** (2018). Understanding/unravelling carotenoid excited singlet states. *J. R. Soc. Interface* **15**.
- Havaux, M.** (2020). β -Cyclocitral and derivatives: Emerging molecular signals serving multiple biological functions. *Plant Physiol. Biochem.* **155**: 35–41.
- He, W. et al.** (2011). A small-molecule screen identifies L-Kynurenine as a competitive inhibitor of TAA1/TAR activity in Ethylene-Directed Auxin Biosynthesis and root growth in *Arabidopsis*. *Plant Cell* **23**: 3944–3960.
- Hemmerlin, A., Hoeffler, J.F., Meyer, O., Tritsch, D., Kagan, I.A., Grosdemange-Billiard, C., Rohmer, M., and Bach, T.J.** (2003). Cross-talk between the cytosolic mevalonate and the plastidial methylerythritol phosphate pathways in tobacco bright yellow-2 cells. *J. Biol. Chem.* **278**: 26666–26676.
- van Herpen, T.W.J.M., Cankar, K., Nogueira, M., Bosch, D., Bouwmeester, H.J., and Beekwilder, J.** (2010). *Nicotiana benthamiana* as a production platform for artemisinin precursors. *PLoS One* **5**.
- Hormaetxe, K., Hernández, A., Becerril, J.M., and García-Plazaola, J.I.** (2004). Role of red carotenoids in photoprotection during winter acclimation in *Buxus sempervirens* leaves. *Plant Biol.* **6**: 325–332.
- Hornitschek, P., Lorrain, S., Zoete, V., Michielin, O., and Fankhauser, C.** (2009). Inhibition of the shade avoidance response by formation of non-DNA binding bHLH heterodimers. *EMBO J.* **28**: 3893–3902.
- Hotz, C., Loechl, C., Lubowa, A., Tumwine, J.K., Masawi, G.N., Baingana, R., Carriquiry, A., de**

- Brauw Meenakshi, A., and Gilligan, D.O.** (2012). Introduction of β -Carotene-Rich orange sweet potato in rural Uganda resulted in increased vitamin A intakes among children and women and improved vitamin A status among children. *J. Nutr.* **142**: 1871–1880.
- Hsieh, M.H. and Goodman, H.M.** (2005). The Arabidopsis IspH homolog is involved in the plastid nonmevalonate pathway of isoprenoid biosynthesis. *Plant Physiol.* **138**: 641–653.
- Hu, J., Baker, A., Bartel, B., Linka, N., Mullen, R.T., Reumann, S., and Zolman, B.K.** (2012). Plant peroxisomes: Biogenesis and function. *Plant Cell* **24**: 2279–2303.
- Huang, J.C., Zhong, Y.J., Liu, J., Sandmann, G., and Chen, F.** (2013). Metabolic engineering of tomato for high-yield production of astaxanthin. *Metab. Eng.* **17**: 59–67.
- Ischebeck, T., Zbierzak, A.M., Kanwischer, M., and Dörmann, P.** (2006). A salvage pathway for phytol metabolism in Arabidopsis. *J. Biol. Chem.* **281**: 2470–2477.
- Jarvis, P. and López-Juez, E.** (2013). Biogenesis and homeostasis of chloroplasts and other plastids. *Nat. Rev. Mol. Cell Biol.* **14**: 787–802.
- Jeffery, J., Holzenburg, A., and King, S.** (2012). Physical barriers to carotenoid bioaccessibility. Ultrastructure survey of chromoplast and cell wall morphology in nine carotenoid-containing fruits and vegetables. *J. Sci. Food Agric.* **92**: 2594–2602.
- Jiang, X., Li, H., Wang, T., Peng, C., Wang, H., Wu, H., and Wang, X.** (2012). Gibberellin indirectly promotes chloroplast biogenesis as a means to maintain the chloroplast population of expanded cells. *Plant J.* **72**: 768–780.
- Kanehisa, M. and Sato, Y.** (2020). KEGG Mapper for inferring cellular functions from protein sequences. *Protein Sci.* **29**: 28–35.
- Kanwischer, M., Porfirova, S., Bergmüller, E., and Dörmann, P.** (2005). Alterations in tocopherol cyclase activity in transgenic and mutant plants of Arabidopsis affect tocopherol content, tocopherol composition, and oxidative stress. *Plant Physiol.* **137**: 713–723.
- Kato, S., Soshino, M., Takaichi, S., Ishikawa, T., Nagata, N., Asahina, M., and Shinomura, T.** (2017). Suppression of the phytoene synthase gene (*Egcr1B*) alters carotenoid content and intracellular structure of *Euglena gracilis*. *BMC Plant Biol.* **17**: 1–10.
- Klee, H.J. and Giovannoni, J.J.** (2011). Genetics and control of tomato fruit ripening and quality attributes. *Annu. Rev. Genet.* **45**: 41–59.

- Kleinig, H.** (1989). The Role of Plastids in Isoprenoid Biosynthesis. *Annu. Rev. Plant Physiol. Plant Mol. Biol.* **40**: 39–59.
- Kohnen, M. V., Schmid-Siegert, E., Trevisan, M., Petrolati, L.A., Sénéchal, F., Müller-Moulé, P., Maloof, J., Xenarios, I., and Fankhauser, C.** (2016). Neighbor detection induces organ-specific transcriptomes, revealing patterns underlying hypocotyl-specific growth. *Plant Cell* **28**: 2889–2904.
- Koiwa, H., Ikeda, T., and Yoshida, Y.** (1986). Reversal of chromoplasts to chloroplasts in *Buxus* leaves. *Bot. Mag. Tokyo* **99**: 233–240.
- Kornyeyev, D., Logan, B.A., and Holaday, A.S.** (2010). Excitation pressure as a measure of the sensitivity of photosystem II to photoinactivation. *Funct. Plant Biol.* **37**: 943–951.
- Kowalewska, Ł., Mazur, R., Suski, S., Garstka, M., and Mostowska, A.** (2016). Three-dimensional visualization of the tubular-lamellar transformation of the internal plastid membrane network during runner bean chloroplast biogenesis. *Plant Cell* **28**: 875–891.
- Kruk, J. and Szymańska, R.** (2012). Singlet oxygen and non-photochemical quenching contribute to oxidation of the plastoquinone-pool under high light stress in *Arabidopsis*. *Biochim. Biophys. Acta - Bioenerg.* **1817**: 705–710.
- Küpper, H., Benedikty, Z., Morina, F., Andresen, E., Mishra, A., and Trtílek, M.** (2019). Analysis of OJIP chlorophyll fluorescence kinetics and Q A reoxidation kinetics by direct fast imaging 1[OPEN]. *Plant Physiol.* **179**: 369–381.
- Kushwaha, N.K., Mansi, Sahu, P.P., Prasad, M., and Chakrabroty, S.** (2019). Chilli leaf curl virus infection downregulates the expression of the genes encoding chloroplast proteins and stress-related proteins. *Physiol. Mol. Biol. Plants* **25**: 1185–1196.
- Laborde, J.A. and Spurr, A.R.** (1973). Chromoplast Ultrastructure As Affected By Genes Controlling Grana Retention and Carotenoids in Fruits of *Capsicum Annuum*. *Am. J. Bot.* **60**: 736–744.
- Lado, J., Zacarías, L., Gurrea, A., Page, A., Stead, A., and Rodrigo, M.J.** (2015). Exploring the diversity in Citrus fruit colouration to decipher the relationship between plastid ultrastructure and carotenoid composition. *Planta* **242**: 645–661.
- Landi, M., Zivcak, M., Sytar, O., Brestic, M., and Allakhverdiev, S.I.** (2020). Plasticity of photosynthetic processes and the accumulation of secondary metabolites in plants in response to monochromatic light environments: A review. *Biochim. Biophys. Acta - Bioenerg.* **1861**:

148131.

- Lätari, K., Wüst, F., Hübner, M., Schaub, P., Beisel, K.G., Matsubara, S., Beyer, P., and Welsch, R.** (2015). Tissue-specific apocarotenoid glycosylation contributes to carotenoid homeostasis in arabidopsis leaves. *Plant Physiol.* **168**: 1550–1562.
- Latowski, D., Kuczyńska, P., and Strzałka, K.** (2011). Xanthophyll cycle - a mechanism protecting plants against oxidative stress. *Redox Rep.* **16**: 78–90.
- Leivar, P. and Monte, E.** (2014). PIFs: Systems integrators in plant development. *Plant Cell* **26**: 56–78.
- Leivar, P., Tepperman, J.M., Cohn, M.M., Monte, E., Al-Sady, B., Erickson, E., and Quail, P.H.** (2012). Dynamic antagonism between phytochromes and PIF family basic helix-loop-helix factors induces selective reciprocal responses to light and shade in a rapidly responsive transcriptional network in Arabidopsis. *Plant Cell* **24**: 1398–1419.
- Li, L., Paolillo, D.J., Parthasarathy, M. V., DiMuzio, E.M., and Garvin, D.F.** (2001). A novel gene mutation that confers abnormal patterns of β -carotene accumulation in cauliflower (*Brassica oleracea* var. botrytis). *Plant J.* **26**: 59–67.
- Li, L. and Yuan, H.** (2013). Chromoplast biogenesis and carotenoid accumulation. *Arch. Biochem. Biophys.* **539**: 102–109.
- Lichtenthaler, H.K.** (2007). Biosynthesis, accumulation and emission of carotenoids, α -tocopherol, plastoquinone, and isoprene in leaves under high photosynthetic irradiance. *Photosynth. Res.* **92**: 163–179.
- Liguori, N., Xu, P., Van Stokkum, I.H.M., Van Oort, B., Lu, Y., Karcher, D., Bock, R., and Croce, R.** (2017). Different carotenoid conformations have distinct functions in light-harvesting regulation in plants. *Nat. Commun.* **8**: 1–9.
- Ling, Q. and Jarvis, P.** (2015). Regulation of chloroplast protein import by the ubiquitin E3 ligase SP1 is important for stress tolerance in plants. *Curr. Biol.* **25**: 2527–2534.
- Ling, Q., Sadali, N.M., Soufi, Z., Zhou, Y., Huang, B., Zeng, Y., Rodriguez-Concepcion, M., and Jarvis, R.P.** (2021). The chloroplast-associated protein degradation pathway controls chromoplast development and fruit ripening in tomato. *Nat. Plants* **7**: 655–666.
- Liu, M. and Lu, S.** (2016). Plastoquinone and ubiquinone in plants: Biosynthesis, physiological function and metabolic engineering. *Front. Plant Sci.* **7**: 1–18.

- Ljubescic, N., Wrischer, M., and Devide, Z.** (1991). Chromoplasts - the last stages in plastid development. *Int. J. Dev. Biol.* **35**: 251–258.
- Ljubešić, N., Wrischer, M., and Devidé, Z.** (1996). Chromoplast structures in *Thunbergia* flowers. *Protoplasma* **193**: 174–180.
- Llorente, B. et al.** (2020). Synthetic conversion of leaf chloroplasts into carotenoid-rich plastids reveals mechanistic basis of natural chromoplast development. *Proc. Natl. Acad. Sci. U. S. A.* **117**: 21796–21803.
- Llorente, B., D'Andrea, L., and Rodríguez-Concepción, M.** (2016). Evolutionary recycling of light signaling components in fleshy fruits: New insights on the role of pigments to monitor ripening. *Front. Plant Sci.* **7**: 1–7.
- Lois, L.M., Rodríguez-Concepción, M., Gallego, F., Campos, N., and Boronat, A.** (2000). Carotenoid biosynthesis during tomato fruit development: Regulatory role of 1-deoxy-D-xylulose 5-phosphate synthase. *Plant J.* **22**: 503–513.
- Lomonosoff, G.P. and D'Aoust, M.A.** (2016). Plant-produced biopharmaceuticals: A case of technical developments driving clinical deployment. *Science (80-.)*. **353**: 1237–1240.
- Lopez, A.B., Van Eck, J., Conlin, B.J., Paolillo, D.J., O'Neill, J., and Li, L.** (2008). Effect of the cauliflower or transgene on carotenoid accumulation and chromoplast formation in transgenic potato tubers. *J. Exp. Bot.* **59**: 213–223.
- Lorenzo, C.D., Alonso Iserte, J., Sanchez Lamas, M., Antonietti, M.S., Garcia Gagliardi, P., Hernando, C.E., Dezar, C.A.A., Vazquez, M., Casal, J.J., Yanovsky, M.J., and Cerdán, P.D.** (2019). Shade delays flowering in *Medicago sativa*. *Plant J.* **99**: 7–22.
- Lushchak, V.I. and Semchuk, N.M.** (2012). Tocopherol biosynthesis: Chemistry, regulation and effects of environmental factors. *Acta Physiol. Plant.* **34**: 1607–1628.
- Ma, L. and Lin, X.M.** (2010). Effects of lutein and zeaxanthin on aspects of eye health. *J. Sci. Food Agric.* **90**: 2–12.
- Maass, D., Arango, J., Wüst, F., Beyer, P., and Welsch, R.** (2009). Carotenoid crystal formation in *Arabidopsis* and carrot roots caused by increased phytoene synthase protein levels. *PLoS One* **4**.
- Majer, E., Llorente, B., Rodríguez-Concepción, M., and Daròs, J.A.** (2017). Rewiring carotenoid biosynthesis in plants using a viral vector. *Sci. Rep.* **7**: 1–10.

- Mapelli-Brahm, P., Desmarchelier, C., Margier, M., Reboul, E., Meléndez Martínez, A.J., and Borel, P.** (2018). Phytoene and Phytofluene Isolated from a Tomato Extract are Readily Incorporated in Mixed Micelles and Absorbed by Caco-2 Cells, as Compared to Lycopene, and SR-BI is Involved in their Cellular Uptake. *Mol. Nutr. Food Res.* **62**: 1–9.
- Marano, M.R., Serra, E.C., Orellano, E.G., and Carrillo, N.** (1993). The path of chromoplast development in fruits and flowers. *Plant Sci.* **94**: 1–17.
- Maresca, J.A., Graham, J.E., and Bryant, D.A.** (2008). The biochemical basis for structural diversity in the carotenoids of chlorophototrophic bacteria. *Photosynth. Res.* **97**: 121–140.
- Martínez-García, J.F., Gallemí, M., Molina-Contreras, M.J., Llorente, B., Bevilaqua, M.R.R., and Quail, P.H.** (2014). The shade avoidance syndrome in Arabidopsis: The antagonistic role of phytochrome A and B differentiates vegetation proximity and canopy shade. *PLoS One* **9**.
- Martínez-García, J.F., Galstyan, A., Salla-Martret, M., Cifuentes-Esquivel, N., Gallemí, M., and Bou-Torrent, J.** (2010). Regulatory Components of Shade Avoidance Syndrome. *Adv. Bot. Res.* **53**: 65–116.
- Martinis, J., Kessler, F., and Glauser, G.** (2011). A novel method for prenylquinone profiling in plant tissues by ultra-high pressure liquid chromatography-mass spectrometry.
- Massaretto, I.L., Albaladejo, I., Purgatto, E., Flores, F.B., Plasencia, F., Egea-Fernández, J.M., Bolarin, M.C., and Egea, I.** (2018). Recovering tomato landraces to simultaneously improve fruit yield and nutritional quality against salt stress. *Front. Plant Sci.* **8**: 71.
- Mellor, S.B., Behrendorff, J.B.Y.H., Nielsen, A.Z., Jensen, P.E., and Pribil, M.** (2018). Non-photosynthetic plastids as hosts for metabolic engineering. *Essays Biochem.* **62**: 41–50.
- Mialoundama, A.S., Heintz, D., Jadid, N., Nkeng, P., Rahier, A., Deli, J., Camara, B., and Bouvier, F.** (2010). Characterization of plant carotenoid cyclases as members of the flavoprotein family functioning with no net redox change. *Plant Physiol.* **153**: 970–979.
- Milborrow, B. V.** (2001). The pathway of biosynthesis of abscisic acid in vascular plants: A review of the present state of knowledge of ABA biosynthesis. *J. Exp. Bot.* **52**: 1145–1164.
- Molina-Contreras, M.J. et al.** (2019). Photoreceptor Activity Contributes to Contrasting Responses to Shade in Cardamine and Arabidopsis Seedlings. *Plant Cell* **31**.
- Moran, N.A. and Jarvik, T.** (2010). Lateral transfer of genes from fungi underlies carotenoid production in aphids. *Science (80-.)*. **328**: 624–627.

- Morelli, L., Paulišić, S., Qin, W., Iglesias-Sanchez, A., Roig-Villanova, I., Florez-Sarasa, I., Rodriguez-Concepcion, M., and Martinez-Garcia, J.F.** (2021). Light signals generated by vegetation shade facilitate acclimation to low light in shade-avoider plants. *Plant Physiol.*: 1–15.
- Morris, W.L., Ducreux, L.J.M., Hedden, P., Millam, S., and Taylor, M.A.** (2006). Overexpression of a bacterial 1-deoxy-D-xylulose 5-phosphate synthase gene in potato tubers perturbs the isoprenoid metabolic network: Implications for the control of the tuber life cycle. *J. Exp. Bot.* **57**: 3007–3018.
- Mujer, C. V., Andrews, D.L., Manhart, J.R., Pierce, S.K., and Rumpho, M.E.** (1996). Chloroplast genes are expressed during intracellular symbiotic association of *Vaucheria litorea* plastids with the sea slug *Elysia chlorotica*. *Proc. Natl. Acad. Sci. U. S. A.* **93**: 12333–12338.
- Müller, L., Fröhlich, K., and Böhm, V.** (2011). Comparative antioxidant activities of carotenoids measured by ferric reducing antioxidant power (FRAP), ABTS bleaching assay (α TEAC), DPPH assay and peroxy radical scavenging assay. *Food Chem.* **129**: 139–148.
- Muñoz, P. and Munné-Bosch, S.** (2018). Photo-oxidative stress during leaf, flower and fruit development. *Plant Physiol.* **176**: 1004–1014.
- Murchie, E.H. and Niyogi, K.K.** (2011). Manipulation of photoprotection to improve plant photosynthesis. *Plant Physiol.* **155**: 86–92.
- Nakagawa, T. et al.** (2007). Improved gateway binary vectors: High-performance vectors for creation of fusion constructs in transgenic analysis of plants. *Biosci. Biotechnol. Biochem.* **71**: 2095–2100.
- Nakata, M., Mitsuda, N., Herde, M., Koo, A.J.K., Moreno, J.E., Suzuki, K., Howe, G.A., and Ohme-Takagi, M.** (2013). A bHLH-type transcription factor, ABA-INDUCIBLE BHLH-TYPE TRANSCRIPTION FACTOR/JA-ASSOCIATED MYC2-LIKE1, acts as a repressor to negatively regulate jasmonate signaling in *Arabidopsis*. *Plant Cell* **25**: 1641–1656.
- Nilkens, M., Kress, E., Lambrev, P., Miloslavina, Y., Müller, M., Holzwarth, A.R., and Jahns, P.** (2010). Identification of a slowly inducible zeaxanthin-dependent component of non-photochemical quenching of chlorophyll fluorescence generated under steady-state conditions in *Arabidopsis*. *Biochim. Biophys. Acta - Bioenerg.* **1797**: 466–475.
- Niranjana, R., Gayathri, R., Nimish Mol, S., Sugawara, T., Hirata, T., Miyashita, K., and Ganesan, P.** (2015). Carotenoids modulate the hallmarks of cancer cells. *J. Funct. Foods* **18**: 968–985.

- Nogueira, M., Enfissi, E.M.A., Welsch, R., Beyer, P., Zurbriggen, M.D., and Fraser, P.D.** (2019). Construction of a fusion enzyme for astaxanthin formation and its characterisation in microbial and plant hosts: A new tool for engineering ketocarotenoids. *Metab. Eng.* **52**: 243–252.
- Nogueira, M., Mora, L., Enfissi, E.M.A., Bramley, P.M., and Fraser, P.D.** (2013). Subchromoplast sequestration of carotenoids affects regulatory mechanisms in tomato lines expressing different carotenoid gene combinations. *Plant Cell* **25**: 4560–4579.
- Nuutinen, T.** (2018). Medicinal properties of terpenes found in *Cannabis sativa* and *Humulus lupulus*. *Eur. J. Med. Chem.* **157**: 198–228.
- Oikawa, K., Yamasato, A., Kong, S.G., Kasahara, M., Nakai, M., Takahashi, F., Ogura, Y., Kagawa, T., and Wada, M.** (2008). Chloroplast outer envelope protein Chup1 is essential for chloroplast anchorage to the plasma membrane and chloroplast movement. *Plant Physiol.* **148**: 829–842.
- Ortiz-Alcaide, M., Llamas, E., Gomez-Cadenas, A., Nagatani, A., Martínez-García, J.F., and Rodríguez-Concepción, M.** (2019). Chloroplasts modulate elongation responses to canopy shade by retrograde pathways involving *hy5* and abscisic acid. *Plant Cell* **31**: 384–398.
- Osorio, C.E.** (2019). The Role of Orange Gene in Carotenoid Accumulation: Manipulating Chromoplasts Toward a Coloured Future. *Front. Plant Sci.* **10**.
- Paetzold, H., Garms, S., Bartram, S., Wieczorek, J., Urós-Gracia, E.M., Rodríguez-Concepción, M., Boland, W., Strack, D., Hause, B., and Walter, M.H.** (2010). The isogene 1-deoxy-D-xylulose 5-phosphate synthase 2 controls isoprenoid profiles, precursor pathway allocation, and density of tomato trichomes. *Mol. Plant* **3**: 904–916.
- Pankratov, I., McQuinn, R., Schwartz, J., Bar, E., Fei, Z., Lewinsohn, E., Zamir, D., Giovannoni, J.J., and Hirschberg, J.** (2016). Fruit carotenoid-deficient mutants in tomato reveal a function of the plastidial isopentenyl diphosphate isomerase (*IDI1*) in carotenoid biosynthesis. *Plant J.* **88**: 82–94.
- Park, H., Kreunen, S.S., Cuttriss, A.J., DellaPenna, D., and Pogson, B.J.** (2002). Identification of the carotenoid isomerase provides insight into carotenoid biosynthesis, prolamellar body formation, and photomorphogenesis. *Plant Cell* **14**: 321–332.
- Paulišić, S., Qin, W., Arora Verasztó, H., Then, C., Alary, B., Nogue, F., Tsiantis, M., Hothorn, M., and Martínez-García, J.F.** (2021). Adjustment of the PIF7-HFR1 transcriptional module activity controls plant shade adaptation. *EMBO J.* **40**: 1–16.

- Peltier, J.B., Friso, G., Kalume, D.E., Roepstorff, P., Nilsson, F., Adamska, I., and Van Wijk, K.J.** (2000). Proteomics of the chloroplast: Systematic identification and targeting analysis of lumenal and peripheral thylakoid proteins. *Plant Cell* **12**: 319–341.
- Pesaresi, P., Mizzotti, C., Colombo, M., and Masiero, S.** (2014). Genetic regulation and structural changes during tomato fruit development and ripening. *Front. Plant Sci.* **5**: 1–14.
- Phillip, D. and Young, A.J.** (1995). Occurrence of the carotenoid lactucaxanthin in higher plant LHC II. *Photosynth. Res.* **43**: 273–282.
- Phua, S.Y., Yan, D., Chan, K.X., Estavillo, G.M., Nambara, E., and Pogson, B.J.** (2018). The arabidopsis SAL1-PAP pathway: A case study for integrating chloroplast retrograde, light and hormonal signaling in modulating plant growth and development? *Front. Plant Sci.* **9**: 1–8.
- Pietrzykowska, M., Suorsa, M., Semchonok, D.A., Tikkanen, M., Boekema, E.J., Aro, E.M., and Jansson, S.** (2014). The light-harvesting chlorophyll a/b binding proteins Lhcb1 and Lhcb2 play complementary roles during state transitions in Arabidopsis. *Plant Cell* **26**: 3646–3660.
- Piller, L.E., Glauser, G., Kessler, F., and Besagni, C.** (2014). Role of plastoglobules in metabolite repair in the tocopherol redox cycle. *Front. Plant Sci.* **5**: 1–10.
- Platt, T., Gallegos, C.L., and Harrison, W.G.** (1980). Photoinhibition of Photosynthesis in Natural Assemblages of Marine Phytoplankton. *J. Mar. Res.* **38**: 687–701.
- Polle, J.E.W., Roth, R., Ben-Amotz, A., and Goodenough, U.** (2020). Ultrastructure of the green alga *Dunaliella salina* strain CCAP19/18 (Chlorophyta) as investigated by quick-freeze deep-etch electron microscopy. *Algal Res.* **49**: 101953.
- Pralon, T., Collombat, J., Pipitone, R., Ksas, B., Shanmugabalaji, V., Havaux, M., Finazzi, G., Longoni, P., and Kessler, F.** (2020). Mutation of the Atypical Kinase ABC1K3 Partially Rescues the PROTON GRADIENT REGULATION 6 Phenotype in Arabidopsis thaliana. *Front. Plant Sci.* **11**: 1–18.
- Ralph, P.J. and Gademann, R.** (2005). Rapid light curves: A powerful tool to assess photosynthetic activity. *Aquat. Bot.* **82**: 222–237.
- Rey, P., Gillet, B., Römer, S., Eymery, F., Massimino, J., Peltier, G., and Kuntz, M.** (2000). Over-expression of a pepper plastid lipid-associated protein in tobacco leads to changes in plastid ultrastructure and plant development upon stress. *Plant J.* **21**: 483–494.
- Rippert, P., Scimemi, C., Dubald, M., and Matringe, M.** (2004). Engineering Plant Shikimate

- Pathway for Production of Tocotrienol and Improving Herbicide Resistance. *Plant Physiol.* **134**: 92–100.
- Rödiger, A., Agne, B., Dobritsch, D., Helm, S., Müller, F., Pötzsch, N., and Baginsky, S.** (2021). Chromoplast differentiation in bell pepper (*Capsicum annuum*) fruits. *Plant J.* **105**: 1431–1442.
- Röding, A., Dietzel, L., Schlicke, H., Grimm, B., Sandmann, G., and Büchel, C.** (2015). Production of ketocarotenoids in tobacco alters the photosynthetic efficiency by reducing photosystem II supercomplex and LHCII trimer stability. *Photosynth. Res.* **123**: 157–165.
- Rodríguez-Concepcion, M. et al.** (2018). A global perspective on carotenoids: Metabolism, biotechnology, and benefits for nutrition and health. *Prog. Lipid Res.* **70**: 62–93.
- Rodríguez-Concepción, M.** (2010). Supply of precursors for carotenoid biosynthesis in plants. *Arch. Biochem. Biophys.* **504**: 118–122.
- Rodríguez-Concepción, M. and Boronat, A.** (2015). Breaking new ground in the regulation of the early steps of plant isoprenoid biosynthesis. *Curr. Opin. Plant Biol.* **25**: 17–22.
- Rodríguez-Concepción, M. and Boronat, A.** (2002). Elucidation of the methylerythritol phosphate pathway for isoprenoid biosynthesis in bacteria and plastids. A metabolic milestone achieved through genomics. *Plant Physiol.* **130**: 1079–1089.
- Rodríguez-Villalón, A., Gas, E., and Rodríguez-Concepción, M.** (2009). Phytoene synthase activity controls the biosynthesis of carotenoids and the supply of their metabolic precursors in dark-grown *Arabidopsis* seedlings. *Plant J.* **60**: 424–435.
- Roig-Villanova, I., Bou-Torrent, J., Galstyan, A., Carretero-Paulet, L., Portolés, S., Rodríguez-Concepción, M., and Martínez-García, J.F.** (2007). Interaction of shade avoidance and auxin responses: A role for two novel atypical bHLH proteins. *EMBO J.* **26**: 4756–4767.
- Roig-Villanova, I. and Martínez-García, J.F.** (2016). Plant responses to vegetation proximity: A whole life avoiding shade. *Front. Plant Sci.* **7**: 1–10.
- Römer, S. and Fraser, P.D.** (2005). Recent advances in carotenoid biosynthesis, regulation and manipulation. *Planta* **221**: 305–308.
- Rottet, S., Devillers, J., Glauser, G., Douet, V., Besagni, C., and Kessler, F.** (2016). Identification of plastoglobules as a site of carotenoid cleavage. *Front. Plant Sci.* **7**: 1–11.
- Rozak, P.R., Seiser, R.M., Wacholtz, W.F., and Wise, R.R.** (2002). Rapid, reversible alterations in

spinach thylakoid appression upon changes in light intensity. *Plant, Cell Environ.* **25**: 421–429.

Ruiz-Sola, M.Á., Barja, M.V., Manzano, D., Llorente, B., Schipper, B., Beekwilder, J., and Rodríguez-Concepción, M. (2016). A single arabidopsis gene encodes two differentially targeted geranylgeranyl diphosphate synthase isoforms. *Plant Physiol.* **172**: 1393–1402.

Ruiz-Sola, M.Á. and Rodríguez-Concepción, M. (2012). Carotenoid Biosynthesis in Arabidopsis: A Colourful Pathway. *Arab. B.* **10**: e0158.

Russell, A.W., Critchley, C., Robinson, S.A., Franklin, L.A., Seaton, G.G., Chow Wah Soon, Anderson, J.M., and Osmond, C.B. (1995). Photosystem II regulation and dynamics of the chloroplast D₁ protein in Arabidopsis leaves during photosynthesis and photoinhibition. *Plant Physiol.* **107**: 943–952.

Sadali, N.M., Sowden, R.G., Ling, Q., and Jarvis, R.P. (2019). Differentiation of chromoplasts and other plastids in plants. *Plant Cell Rep.* **38**: 803–818.

Schaub, P., Rodríguez-Franco, M., Cazzonelli, C.I., Alvarez, D., Wüst, F., and Welsch, R. (2018). Establishment of an Arabidopsis callus system to study the interrelations of biosynthesis, degradation and accumulation of carotenoids. *PLoS One* **13**: 1–28.

Schindelin, J. et al. (2012). Fiji: An open-source platform for biological-image analysis. *Nat. Methods* **9**: 676–682.

Schwach, F., Vaistij, F.E., Jones, L., and Baulcombe, D.C. (2005). An RNA-dependent RNA polymerase prevents meristem invasion by potato virus X and is required for the activity but not the production of a systemic silencing signal. *Plant Physiol.* **138**: 1842–1852.

Schweiggert, R.M., Steingass, C.B., Heller, A., Esquivel, P., and Carle, R. (2011). Characterization of chromoplasts and carotenoids of red- and yellow-fleshed papaya (*Carica papaya* L.). *Planta* **234**: 1031–1044.

Shanmugabalaji, V., Besagni, C., Piller, L.E., Douet, V., Ruf, S., Bock, R., and Kessler, F. (2013). Dual targeting of a mature plastoglobulin/fibrillin fusion protein to chloroplast plastoglobules and thylakoids in transplastomic tobacco plants. *Plant Mol. Biol.* **81**: 13–25.

Shanmugabalaji, V., Chahtane, H., Accossato, S., Rahire, M., Gouzerh, G., Lopez-Molina, L., and Kessler, F. (2018). Chloroplast Biogenesis Controlled by DELLA-TOC159 Interaction in Early Plant Development. *Curr. Biol.* **28**: 2616–2623.e5.

Shewmaker, C.K., Sheehy, J.A., Daley, M., Colburn, S., and Ke, D.Y. (1999). Seed-specific

- overexpression of phytoene synthase: Increase in carotenoids and other metabolic effects. *Plant J.* **20**: 401–412.
- Shimada, H., Ohno, R., Shibata, M., Ikegami, I., Onai, K., Ohto, M.A., and Takamiya, K.I.** (2005). Inactivation and deficiency of core proteins of photosystems I and II caused by genetical phyloquinone and plastoquinone deficiency but retained lamellar structure in a T-DNA mutant of *Arabidopsis*. *Plant J.* **41**: 627–637.
- Simpson, K., Quiroz, L.F., Rodriguez-Concepción, M., and Stange, C.R.** (2016). Differential contribution of the first two enzymes of the MEP pathway to the supply of metabolic precursors for carotenoid and chlorophyll biosynthesis in carrot (*Daucus carota*). *Front. Plant Sci.* **7**: 1–10.
- Soler, E., Clastre, M., Bantignies, B., Marigo, G., and Ambid, C.** (1993). Uptake of isopentenyl diphosphate by plastids isolated from *Vitis vinifera* L. cell suspensions. *Planta* **191**: 324–329.
- Sonoike, K.** (2011). Photoinhibition of photosystem I. *Physiol. Plant.* **142**: 56–64.
- Spicher, L. and Kessler, F.** (2015). ScienceDirect Unexpected roles of plastoglobules (plastid lipid droplets) in vitamin K₁ and E metabolism. *Curr. Opin. Plant Biol.* **25**: 123–129.
- Strand, D.D., Livingston, A.K., Satoh-Cruz, M., Froehlich, J.E., Maurino, V.G., and Kramer, D.M.** (2015). Activation of cyclic electron flow by hydrogen peroxide in vivo. *Proc. Natl. Acad. Sci. U. S. A.* **112**: 5539–5544.
- Su, L., Diretto, G., Purgatto, E., Danoun, S., Zouine, M., Li, Z., Roustan, J.P., Bouzayen, M., Giuliano, G., and Chervin, C.** (2015). Carotenoid accumulation during tomato fruit ripening is modulated by the auxin-ethylene balance. *BMC Plant Biol.* **15**: 1–12.
- Sun, T., Yuan, H., Cao, H., Yazdani, M., Tadmor, Y., and Li, L.** (2018). Carotenoid Metabolism in Plants: The Role of Plastids. *Mol. Plant* **11**: 58–74.
- Suzuki, M. et al.** (2015). Plastid proteomic analysis in tomato fruit development. *PLoS One* **10**: 1–25.
- Suzuki, N., Koussevitzky, S., Mittler, R., and Miller, G.** (2012). ROS and redox signalling in the response of plants to abiotic stress. *Plant, Cell Environ.* **35**: 259–270.
- Szymańska, R. and Kruk, J.** (2010). Plastoquinol is the main prenyllipid synthesized during acclimation to high light conditions in *Arabidopsis* and is converted to plastochromanol by tocopherol cyclase. *Plant Cell Physiol.* **51**: 537–545.
- Tetali, S.D.** (2019). Terpenes and isoprenoids: a wealth of compounds for global use. *Planta* **249**: 1–8.

- Toledo-Ortiz, G., Huq, E., and Rodríguez-Concepción, M.** (2010). Direct regulation of phytoene synthase gene expression and carotenoid biosynthesis by phytochrome-interacting factors. *Proc. Natl. Acad. Sci. U. S. A.* **107**: 11626–11631.
- Tsegaw, T., Hammes, S., and Robbertse, J.** (2005). Paclobutrazol-induced leaf, stem, and root anatomical modifications in potato. *HortScience* **40**: 1343–1346.
- Tzuri, G. et al.** (2015). A “golden” SNP in CmOr governs the fruit flesh Colour of melon (*Cucumis melo*). *Plant J.* **82**: 267–279.
- Valladares, F. and Niinemets, Ü.** (2008). Shade tolerance, a key plant feature of complex nature and consequences. *Annu. Rev. Ecol. Evol. Syst.* **39**: 237–257.
- Vickers, C.E., Bongers, M., Liu, Q., Delatte, T., and Bouwmeester, H.** (2014). Metabolic engineering of volatile isoprenoids in plants and microbes. *Plant, Cell Environ.* **37**: 1753–1775.
- Vidi, P.A., Kanwischer, M., Baginsky, S., Austin, J.R., Csucs, G., Dörmann, P., Kessler, F., and Bréhélin, C.** (2006). Tocopherol cyclase (VTE₁) localization and vitamin E accumulation in chloroplast plastoglobule lipoprotein particles. *J. Biol. Chem.* **281**: 11225–11234.
- Vidi, P.A., Kessler, F., and Bréhélin, C.** (2007). Plastoglobules: A new address for targeting recombinant proteins in the chloroplast. *BMC Biotechnol.* **7**: 1–12.
- Vishnevetsky, M., Ovadis, M., Itzhaki, H., and Vainstein, A.** (1997). CHRC, encoding a chromoplast-specific carotenoid-associated protein, is an early gibberellic acid-responsive gene. *J. Biol. Chem.* **272**: 24747–24750.
- Wang, J.Y. et al.** (2019). The apocarotenoid metabolite zaxinone regulates growth and strigolactone biosynthesis in rice. *Nat. Commun.* **10**: 1–9.
- Wang, M., Wang, G., and Ji, J.** (2010). Suppression of the phytoene desaturase gene influence on the organization and function of photosystem II (PSII) and antioxidant enzyme activities in tobacco. *Environ. Exp. Bot.* **67**: 460–466.
- Wang, R., Farrona, S., Vincent, C., Joecker, A., Schoof, H., Turck, F., Alonso-Blanco, C., Coupland, G., and Albani, M.C.** (2009). PEP₁ regulates perennial flowering in *Arabidopsis thaliana*. *Nature* **459**: 423–427.
- Welsch, R., Zhou, X., Yuan, H., Álvarez, D., Sun, T., Schlossarek, D., Yang, Y., Shen, G., Zhang, H., Rodríguez-Concepción, M., Thannhauser, T.W., and Li, L.** (2018). Clp Protease and OR Directly Control the Proteostasis of Phytoene Synthase, the Crucial Enzyme for Carotenoid

- Biosynthesis in Arabidopsis. *Mol. Plant* **11**: 149–162.
- Van Wijk, K.J. and Kessler, F.** (2017). Plastoglobuli: Plastid Microcompartments with Integrated Functions in Metabolism, Plastid Developmental Transitions, and Environmental Adaptation.
- de Wit, M., Ljung, K., and Fankhauser, C.** (2015). Contrasting growth responses in lamina and petiole during neighbor detection depend on differential auxin responsiveness rather than different auxin levels. *New Phytol.* **208**: 198–209.
- Wood, W.H.J., MacGregor-Chatwin, C., Barnett, S.F.H., Mayneord, G.E., Huang, X., Hobbs, J.K., Hunter, C.N., and Johnson, M.P.** (2018). Dynamic thylakoid stacking regulates the balance between linear and cyclic photosynthetic electron transfer. *Nat. Plants* **4**: 116–127.
- Wurtzel, E.T.** (2019). Changing form and function through carotenoids and synthetic biology. *Plant Physiol.* **179**: 830–843.
- Xu, P., Chukhutsina, V.U., Nawrocki, W.J., Schansker, G., Bielszynski, L.W., Lu, Y., Karcher, D., Bock, R., and Croce, R.** (2020). Photosynthesis without β -carotene. *Elife* **9**: 1–16.
- Yabuta, Y., Tanaka, H., Yoshimura, S., Suzuki, A., Tamoi, M., Maruta, T., and Shigeoka, S.** (2013). Improvement of vitamin E quality and quantity in tobacco and lettuce by chloroplast genetic engineering. *Transgenic Res.* **22**: 391–402.
- Yang, C., Xie, F., Jiang, Y., Li, Z., Huang, X., and Li, L.** (2018). Phytochrome A Negatively Regulates the Shade Avoidance Response by Increasing Auxin/Indole Acetic Acid Protein Stability. *Dev. Cell* **44**: 29–41.e4.
- Zhao, D.D., Jiang, L.L., Li, H.Y., Yan, P.F., and Zhang, Y.L.** (2016). Chemical components and pharmacological activities of terpene natural products from the genus paeonia. *Molecules* **21**.
- Zhao, W., Zhang, Q.S., Tan, Y., Liu, Z., Ma, M.Y., Wang, M.X., and Luo, C.Y.** (2021). An underlying mechanism of qE deficiency in marine angiosperm *Zostera marina*. *Photosynth. Res.*
- Zhen, S. and van Iersel, M.W.** (2017). Far-red light is needed for efficient photochemistry and photosynthesis. *J. Plant Physiol.* **209**: 115–122.
- Zheng, X., Giuliano, G., and Al-Babili, S.** (2020). Carotenoid biofortification in crop plants: citius, altius, fortius. *Biochim. Biophys. Acta - Mol. Cell Biol. Lipids* **1865**: 158664.
- Zhou, X., Welsch, R., Yang, Y., Álvarez, D., Riediger, M., Yuan, H., Fish, T., Liu, J., Thannhauser, T.W., and Li, L.** (2015). Arabidopsis OR proteins are the major

posttranscriptional regulators of phytoene synthase in controlling carotenoid biosynthesis. *Proc. Natl. Acad. Sci. U. S. A.* **112**: 3558–3563.

Zivcak, M., Brestic, M., Kalaji, H.M., and Govindjee (2014). Photosynthetic responses of sun- and shade-grown barley leaves to high light: Is the lower PSII connectivity in shade leaves associated with protection against excess of light? *Photosynth. Res.* **119**: 339–354.

Appendices

Appendix I

List of primers used in this work

Use	No.	Name	Sequence (5'-3')
Cloning	1	PGL34-B1	GGGGACAAGTTTGTACAAAAAAGCAGGCTTTATGGCATTGATCCAACAT
Cloning	2	PGL34-B2	GGGGACCACTTTGTACAAGAAAGCTGGGTTACTGTTGTATTCAAGATT
Cloning	3	TIC40-B1	GGGGACAAGTTTGTACAAAAAAGCAGGCTTTATGGAGAACCTTACCCTAGT
Cloning	4	TIC40-B2	GGGGACCACTTTGTACAAGAAAGCTGGGTTACCCGTCATTCTCTGGGAAGA
Cloning	5	TOC64-B1	GGGGACAAGTTTGTACAAAAAAGCAGGCTTTATGATGGCGTCTCAAGCTGCGAA
Cloning	6	TOC64-B2	GGGGACCACTTTGTACAAGAAAGCTGGGTTCTGGAATTTTCTCAGTCTCTC
Cloning	7	VTE1-B1	GGGGACAAGTTTGTACAAAAAAGCAGGCTTTATGGAGATACGGAGCTTGAT
Cloning	8	VTE1-B2	GGGGACCACTTTGTACAAGAAAGCTGGGTTCTCAGACCCGGTGGCTTGAAGAA
Cloning	9	VTE2-B1	GGGGACAAGTTTGTACAAAAAAGCAGGCTTTATGGAGTCTCTGCTCTCTAG
Cloning	10	VTE2-B2	GGGGACCACTTTGTACAAGAAAGCTGGGTTCTTCAAAAAGGTAACAGCA
Cloning	11	VTE3-B1	GGGGACAAGTTTGTACAAAAAAGCAGGCTTTATGGCCTCTTTGATGCTCAA
Cloning	12	VTE3-B2	GGGGACCACTTTGTACAAGAAAGCTGGGTTGATGGGTTGGTCTTTGGGAA
Cloning	13	VTE4-B1	GGGGACAAGTTTGTACAAAAAAGCAGGCTTTATGAAAGCAACTCTAGCAGC
Cloning	14	VTE4-B2	GGGGACCACTTTGTACAAGAAAGCTGGGTTGAGTGGCTTCTGGCAAGTGATGAT
Cloning	15	VTE5-B1	GGGGACAAGTTTGTACAAAAAAGCAGGCTTTATGGCAGCAACCTTACCTCT
Cloning	16	VTE5-B2	GGGGACCACTTTGTACAAGAAAGCTGGGTTATATCCGAAACTTAAATAAG
Cloning	17	VTE6-B1	GGGGACAAGTTTGTACAAAAAAGCAGGCTTTATGCTTTCGTCGGGAAGTAG
Cloning	18	VTE6-B2	GGGGACCACTTTGTACAAGAAAGCTGGGTTCTTGACCCAGTTCTGGAGTAT
Cloning	19	tyrA-B1	GGGGACAAGTTTGTACAAAAAAGCAGGCTTTATGGTTGCTGAATTGACCGC
Cloning	20	tyrA-B2	GGGGACCACTTTGTACAAGAAAGCTGGGTTCTGGCGATTGTCATTGCCT
Cloning	21	mRFP-B2	GGGGACCACTTTGTACAAGAAAGCTGGGTTGGCGCCGGTGGAGTGGCGGC
RT-qPCR	22	crtB-F	TATTGCTCGCGATATTGTGG
RT-qPCR	23	crtB-R	TTTCAGGTGCCGCATAATTC
RT-qPCR	24	ACT-F	TAAGGTTGTTGCACCACCAG
RT-qPCR	25	ACT-R	ACATCTGCTGGAATGTGCTG

Appendix II

List of constructs used in this work

Name	Plasmid	Template	TAG	Primers	Source
35S:crtB-pGWB405	pGWB405	<i>P. ananatis</i> genomic DNA	GFP	-	Llorente et al., 2020
35S:(p)crtB-pGWB405	pGWB405	<i>P. ananatis</i> genomic DNA	GFP	-	Llorente et al., 2020
35S:(p)crtB-pGWB405-STOP	pGWB405	<i>P. ananatis</i> genomic DNA	-	-	Llorente et al., 2020
35S:GFP-crtB-pGWB506	pGWB506	<i>P. ananatis</i> genomic DNA	GFP	-	Llorente et al., 2020
35S:VTE1-pGWB454	pGWB454	<i>A.thaliana</i> seeds cDNA	RFP	7+8	This thesis
35S:VTE2-pGWB454	pGWB454	<i>A.thaliana</i> rosetta leaves cDNA	RFP	9+10	This thesis
35S:VTE3-pGWB454	pGWB454	<i>A.thaliana</i> rosetta leaves cDNA	RFP	11+12	This thesis
35S:VTE4-pGWB454	pGWB454	<i>A.thaliana</i> rosetta leaves cDNA	RFP	13+14	This thesis
35S:VTE5-pGWB454	pGWB454	<i>A.thaliana</i> rosetta leaves cDNA	RFP	15+16	This thesis
35S:VTE6-pGWB454	pGWB454	<i>A.thaliana</i> rosetta leaves cDNA	RFP	17+18	This thesis
35S:tyrA-pGWB454	pGWB454	<i>E. coli</i> genomic DNA	RFP	19+20	This thesis
X:VTE1-RFP-pER8	pER8	35S:VTE1:pGWB454	RFP	7+21	This thesis
35S:PGL34-pGWB454	pGWB454	<i>A.thaliana</i> rosetta leaves cDNA	RFP	1+2	This thesis
X:PGL34-RFP-pER8	pER8	35S:PGL34:pGWB454	RFP	1+21	This thesis
X:TIC40-pMDC7	pMDC7	<i>A.thaliana</i> rosetta leaves cDNA	CFP	3+4	This thesis
X:TOC64-pMDC7	pMDC7	<i>A.thaliana</i> rosetta leaves cDNA	CFP	5+6	This thesis
35S:AtPSY-pGWB405	pGWB405	<i>A.thaliana</i> rosetta leaves cDNA	GFP	-	Llorente et al., 2020
35S:SIDXS1-pGWB21	pGWB21	<i>Solanum lycopersicum</i> fruit cDNA	10 x Myc	-	This thesis
35S:SIDXS2-pGWB454	pGWB454	<i>Solanum lycopersicum</i> fruit cDNA	RFP	-	This thesis
35S:AtDXS-pGWB405	pGWB405	<i>A.thaliana</i> rosetta leaves cDNA	GFP	-	Andersen et al., 2021
35S:(t)HMGR-pEAQ USER	pEAQ USER	<i>A.thaliana</i> rosetta leaves cDNA	-	-	Andersen et al., 2021
35S:crtE-pGWB405	pGWB405	<i>P. ananatis</i> genomic DNA	GFP	-	Andersen et al., 2021
35S:crtI-pGWB405	pGWB405	<i>P. ananatis</i> genomic DNA	GFP	-	Andersen et al., 2021
35S:crtY-pGWB405	pGWB405	<i>P. ananatis</i> genomic DNA	-	-	Andersen et al., 2021
HcPROWMV-pGWB702	pGWB702	Watermelon mosaic virus cDNA	-	-	Domingo-Calap et al. 2021
TuMV-UK1-pG35Z	pG35Z	Turnip mosaic virus cDNA	-	-	Llorente et al., 2020
TuMV-UK1-crtB-pG35Z	pG35Z	<i>P. ananatis</i> genomic DNA	-	-	Llorente et al., 2020
LMV-crtB-pG35Z	pG35Z	<i>P. ananatis</i> genomic DNA	-	-	Llorente et al., 2020

Annex I

Synthetic conversion of leaf chloroplasts into carotenoid-rich plastids reveals mechanistic basis of natural chromoplast development.

Llorente, B., Torres-Montilla, S., **Morelli, L.**, Florez-Sarasa, I., Matus, J.T., Ezquerro, M., D'Andreas, L., Houhou, F., Majer, E., Picò, B., Cebolla, J., Troncoso, A., Fernie, A.R., Daròs, J.A., Rodriguez-Concepcion, M.

The PhD candidate contributed with his work to the following datasets:

Figure 1C, 1D

Figure 3D

Figure 4C,4D

Figure 5A, 5B

Figure S5A, S5B



Synthetic conversion of leaf chloroplasts into carotenoid-rich plastids reveals mechanistic basis of natural chromoplast development

Briardo Llorente^{a,b,c,1}, Salvador Torres-Montilla^a, Luca Morelli^a, Igor Florez-Sarasa^a, José Tomás Matus^{a,d}, Miguel Ezquerro^a, Lucio D'Andrea^{a,e}, Fakhreddine Houhou^f, Eszter Majer^f, Belén Picó^g, Jaime Cebolla^g, Adrian Troncoso^h, Alisdair R. Fernie^e, José-Antonio Daròs^f, and Manuel Rodríguez-Concepción^{a,f,1}

^aCentre for Research in Agricultural Genomics (CRAG) CSIC-IRTA-UAB-UB, Campus UAB Bellaterra, 08193 Barcelona, Spain; ^bARC Center of Excellence in Synthetic Biology, Department of Molecular Sciences, Macquarie University, Sydney NSW 2109, Australia; ^cCSIRO Synthetic Biology Future Science Platform, Sydney NSW 2109, Australia; ^dInstitute for Integrative Systems Biology (I2SysBio), Universitat de València-CSIC, 46908 Paterna, Valencia, Spain; ^eMax-Planck-Institut für Molekulare Pflanzenphysiologie, 14476 Potsdam-Golm, Germany; ^fInstituto de Biología Molecular y Celular de Plantas, CSIC-Universitat Politècnica de València, 46022 Valencia, Spain; ^gInstituto de Conservación y Mejora de la Agrodiversidad, Universitat Politècnica de València, 46022 Valencia, Spain; and ^hSorbonne Universités, Université de Technologie de Compiègne, Génie Enzymatique et Cellulaire, UMR-CNRS 7025, CS 60319, 60203 Compiègne Cedex, France

Edited by Krishna K. Niyogi, University of California, Berkeley, CA, and approved July 29, 2020 (received for review March 9, 2020)

Plastids, the defining organelles of plant cells, undergo physiological and morphological changes to fulfill distinct biological functions. In particular, the differentiation of chloroplasts into chromoplasts results in an enhanced storage capacity for carotenoids with industrial and nutritional value such as beta-carotene (provitamin A). Here, we show that synthetically inducing a burst in the production of phytoene, the first committed intermediate of the carotenoid pathway, elicits an artificial chloroplast-to-chromoplast differentiation in leaves. Phytoene overproduction initially interferes with photosynthesis, acting as a metabolic threshold switch mechanism that weakens chloroplast identity. In a second stage, phytoene conversion into downstream carotenoids is required for the differentiation of chromoplasts, a process that involves a concurrent reprogramming of nuclear gene expression and plastid morphology for improved carotenoid storage. We hence demonstrate that loss of photosynthetic competence and enhanced production of carotenoids are not just consequences but requirements for chloroplasts to differentiate into chromoplasts.

carotenoid | chromoplast | differentiation | phytoene | synthetic

Plastids comprise a group of morphologically and functionally diverse plant organelles capable of differentiating from one plastid type to another in response to developmental and environmental stimuli (1, 2). Such plastidial conversions are essential to sustain many fundamental biological processes and largely contribute to cell specialization in the different plant tissues. Among the different plastid types, chromoplasts are of great importance in nature and agriculture because of their capacity to accumulate high levels of carotenoids, plant pigments of isoprenoid nature that provide color in the yellow to red range (3–5). Carotenoids such as beta-carotene (provitamin A) are health-promoting nutrients that animals cannot synthesize but take up in their diets. They are also added-value compounds widely used in cosmetics, pharma, food, and feed industries as natural pigments and phytonutrients (4, 6).

Chromoplasts differentiate from preexisting plastids such as proplastids (i.e., undifferentiated plastids), leucoplasts (i.e., uncolored plastids in nonphotosynthetic tissues), and chloroplasts (i.e., photosynthetic plastids). Chloroplasts transform into chromoplasts during the development of many flowers and fruits, but only a few plant species differentiate chromoplasts in leaves (1, 5). The yellow to red colors that some leaves acquire as they senesce (e.g., in the autumn or when they are exposed to continuous darkness) are due to chloroplast carotenoids becoming visible when the chlorophylls degrade. This senescence process, however, does not involve the transformation of chloroplasts into

chromoplasts but into a completely different type of plastids named gerontoplasts (1, 2).

The most prominent changes during chloroplast-to-chromoplast differentiation are the reorganization of the internal plastid structures, together with a concurrent loss of photosynthetic competence and overaccumulation of carotenoid pigments (1–3, 5, 7, 8). The remodeling of the internal plastid structures generates an increased metabolic sink capacity but it also promotes carotenoid biosynthesis. The control of chromoplast differentiation appears as a very promising strategy for improving the nutritional and health benefits of crops (5–9). The overall process is known to involve changes in gene expression (e.g., via retrograde signaling from plastids to the nucleus), hormonal regulation, protein quality control, and plastid protein import (1, 3, 5). However, very few inducers of chromoplast development have been identified to date. Orange (OR) chaperones are among the best characterized,

Significance

Carotenoids are natural pigments whose properties as provitamin A and health-promoting phytonutrients make them ideal targets for biofortification. Here, we show that plastids specialized in carotenoid overaccumulation named chromoplasts can be synthetically produced in plant tissues that do not naturally develop them. We further demonstrate that differentiation of chromoplasts from leaf chloroplasts not just causes but requires both a reduction in photosynthetic activity and a stimulation of carotenoid biosynthesis in a process hardwired to a major reprogramming of global gene expression and cell metabolism. The synthetic system that we report here should allow to boost the nutritional quality of green vegetables and forage crops once their photosynthetic activity is dispensable (e.g., just before harvesting).

Author contributions: B.L., S.T.-M., L.M., I.F.-S., E.M., J.-A.D., and M.R.-C. designed research; B.L., S.T.-M., L.M., I.F.-S., J.T.M., M.E., L.D., F.H., E.M., B.P., J.C., and A.T. performed research; B.L., S.T.-M., L.M., I.F.-S., J.T.M., M.E., B.P., J.C., A.T., A.R.F., J.-A.D., and M.R.-C. contributed new reagents/analytic tools; B.L., S.T.-M., L.M., I.F.-S., J.T.M., M.E., L.D., F.H., E.M., B.P., J.C., A.T., A.R.F., J.-A.D., and M.R.-C. analyzed data; and B.L. and M.R.-C. wrote the paper.

The authors declare no competing interest.

This article is a PNAS Direct Submission.

Published under the PNAS license.

¹To whom correspondence may be addressed. Email: briardo.llorente@mq.edu.au or manuelrc@ibmcp.upv.es.

This article contains supporting information online at <https://www.pnas.org/lookup/suppl/doi:10.1073/pnas.2004405117/-DCSupplemental>.

First published August 19, 2020.

but they only work in some tissues, and the specific mechanism by which they promote chloroplast differentiation remains unclear (5). The experimental manipulation of chloroplast differentiation for fundamental studies and biotechnological applications therefore requests a much better understanding of the mechanisms regulating this process.

Results

The Bacterial *crbB* Enzyme Induces the Transformation of Leaf Chloroplasts into Plastids of Chromoplast Features. The first committed step of the carotenoid pathway is the conversion of geranylgeranyl diphosphate (GGPP) to phytoene, catalyzed by phytoene synthase (referred to as PSY in plants and *crbB* in bacteria). We previously found that the virus-mediated expression of a bacterial *crbB* gene in tobacco (*Nicotiana tabacum* and *Nicotiana benthamiana*), tomato (*Solanum lycopersicum*), *Arabidopsis thaliana*, and several other plants caused leaf yellowing due to increased accumulation of colored endogenous carotenoids downstream of phytoene (10). When the production of *crbB* was optimized using appropriate viral vectors for specific target hosts, an intense and widespread yellow phenotype was achieved in edible leaves such as those of lettuce (*Lactuca sativa*) (Fig. 1A) and green vegetables such as zucchini (*Cucurbita pepo*) (Fig. 1B). These results illustrate the potential of this approach to boost the nutritional value of green (i.e., chloroplast-containing) plant tissues, which are particularly recalcitrant to carotenoid enrichment. To further investigate the mechanism underlying the characteristic yellow phenotype of *crbB*-expressing tissues, we used transmission electron microscopy (TEM) to analyze plastid ultrastructure in leaves from *N. tabacum* and *Arabidopsis* plants treated with *crbB*-harboring viral vectors. Yellow sectors in infected leaves contained plastids with a distinctive ultrastructure that were absent in empty vector controls (Fig. 2A and B). Very similar plastids were observed when the *crbB* gene was transiently expressed from *Agrobacterium tumefaciens*-delivered vectors in agroinfiltrated *N. benthamiana* leaves (Fig. 2C). These plastids were devoid of the organized photosynthetic thylakoids and grana found in typical chloroplasts but contained electron-dense (i.e., lipid-containing) membrane stacks much more tightly appressed than grana (Fig. 2D). The stacks were connected by what appeared to be remnants of thylakoid membranes. Plastids of *crbB* sectors also showed a proliferation of small electron-dense round vesicles identified as plastoglobules (Fig. 2). Loss of thylakoid and grana integrity as well as proliferation of plastoglobules and new membrane systems are features typically observed when chloroplasts differentiate into chromoplasts (3, 8, 11). TEM examination of dark-incubated senescent *N. benthamiana* leaves showed that the plastids found in *crbB*-producing cells were completely different from gerontoplasts (Fig. 2E).

To further substantiate the identity of the chromoplast-like plastids that developed in *crbB*-producing leaves, we analyzed chloroplast and chromoplast marker proteins by immunoblot analysis (Fig. 2F). Virus- or *A. tumefaciens*-mediated expression of *crbB* in *N. tabacum* or *N. benthamiana* leaves, respectively, resulted in increased levels of fibrillin, a protein associated with chromoplast development (12, 13). In contrast, the levels of D1 (also known as PsbA), a core component of photosystem II (PSII) that is highly down-regulated during chloroplast-to-chromoplast differentiation (14, 15), decreased in *crbB*-producing leaves (Fig. 2F). These results together suggest that expressing the bacterial *crbB* gene in leaf cells is sufficient to differentiate chloroplasts into chromoplast-like plastids.

We next used *Arabidopsis* double mutants defective in OR chaperones (AtOR and AtOR-LIKE) to test whether the differentiation process triggered by *crbB* involved pathways depending on these well-characterized promoters of chromoplast development (5, 16). Similarly, double mutants lacking cytosolic and plastidial carotenoid cleavage dioxygenases (CCD1 and CCD4, respectively) were used to investigate the possible contribution of

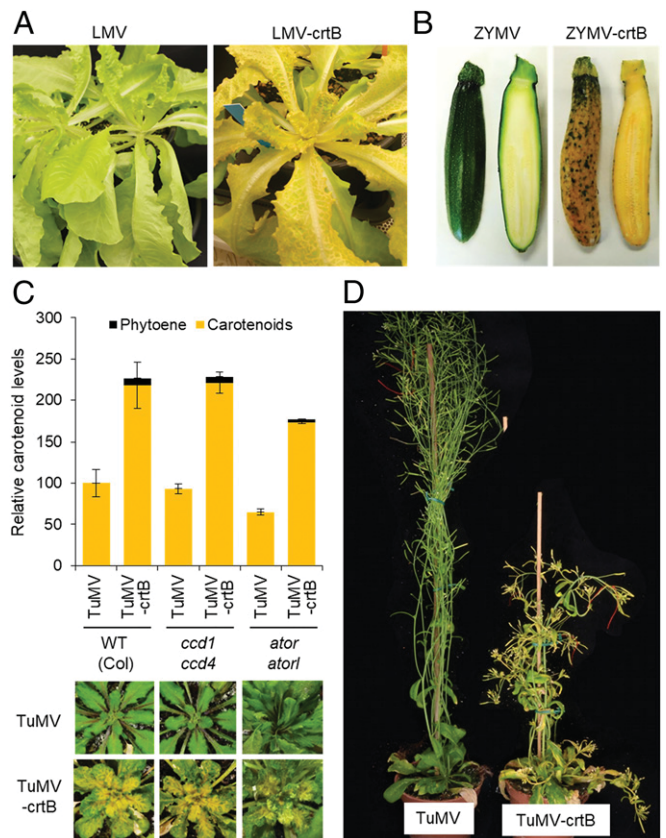


Fig. 1. Virus-mediated production of *crbB* causes leaf yellowing due to carotenoid overaccumulation. (A) Lettuce at 12 d postinoculation (dpi) with a *crbB*-expressing Lettuce mosaic virus (LMV)-derived vector or an empty control. (B) Zucchini from plants at 14 dpi with a *crbB*-expressing Zucchini yellow mosaic virus (ZYMV)-derived vector or an empty control. (C) Carotenoid analysis and representative images at 14 dpi of *Arabidopsis* (Col) WT and double mutant plants grown under short day conditions (8 h of low light and 16 h of darkness) for 2 wk (WT and *ccd1 ccd4*) or 5 wk (*ator ator*) and then inoculated with the indicated viral vectors. Plot shows the mean and SD of $n = 3$ independent samples. Carotenoid levels are represented relative to those in WT samples inoculated with the empty vector control (TuMV). (D) Representative *Arabidopsis* WT plants at 38 dpi.

signaling molecules derived from enzymatic degradation of carotenoids in the differentiation mechanism (17–19). Virus-mediated expression of *crbB* in these mutants resulted in leaves showing the characteristic yellow phenotype and carotenoid overaccumulation observed in the WT (Fig. 1C), suggesting that OR activity or enzymatic cleavage of carotenoids are not required for the process. Besides leaves, yellowing was widespread in all other green tissues, including cauline leaves, stems, sepals, and siliques, where it remained stable until plants died (Fig. 1D).

The *crbB* Enzyme Only Triggers Chloroplast-to-Chromoplast Differentiation When Localized in Plastids. Low scores for plastidial targeting were obtained for *crbB* with TargetP and ChloroP servers, indicating a nonreliable prediction. However, the 12-aa-long noncatalytic N-terminal region of this protein contains some features found in plastid-targeting peptides, including five hydrophobic and two hydroxylated residues. A C-terminal fusion of the full-length *crbB* enzyme to the green fluorescent protein (*crbB*-GFP) mainly localized to the cytosol in *N. benthamiana* leaf cells, but some fluorescence was also detected in chloroplasts (10). By optimizing the transient expression conditions (using only young leaves and adding the helper component protease of the

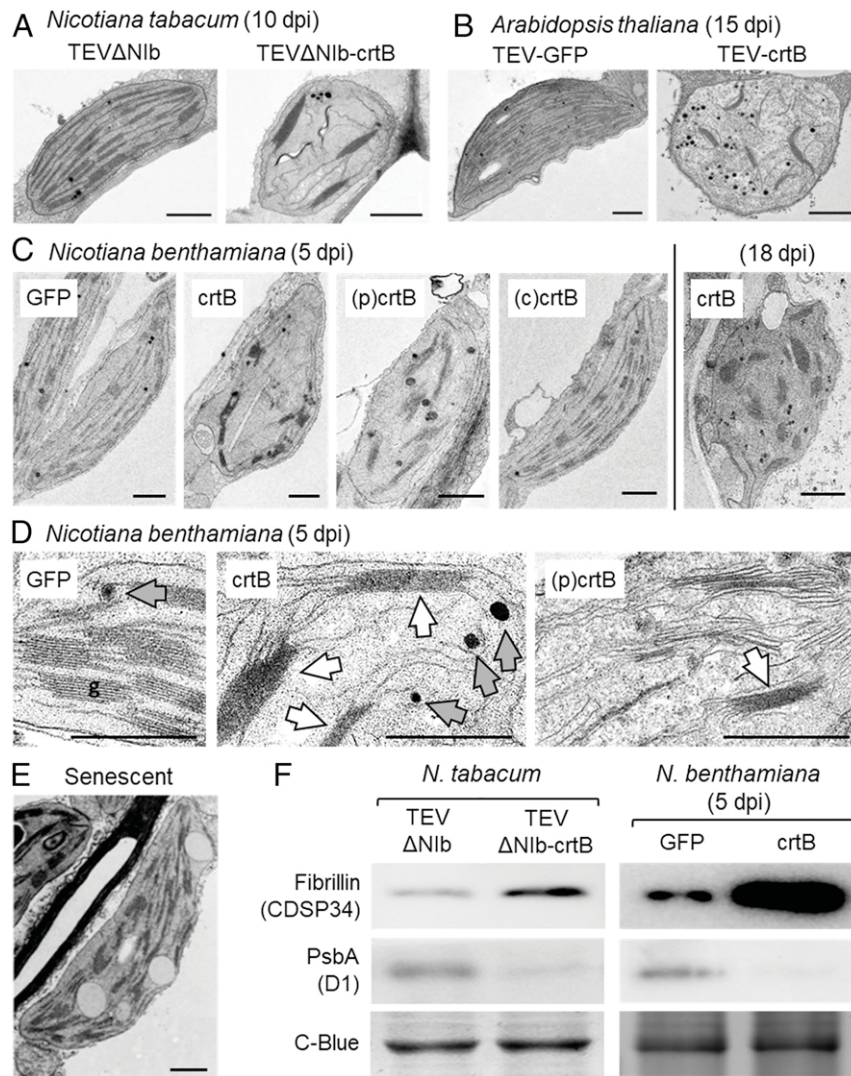


Fig. 2. Chromoplast-like plastids develop from chloroplasts in leaves producing crtB or a plastid-targeted version of the enzyme. TEM images of representative plastids from the indicated species and treatments are shown. (A) Plastids from *N. tabacum* leaves collected 10 dpi with TEV Δ Nlb (empty vector) or TEV Δ Nlb-crtB. (B) Plastids from *A. thaliana* (Ler) leaves inoculated with TEV (empty vector) or TEV-crtB at 15 dpi. (C) Plastids from *N. benthamiana* leaves agroinfiltrated with the indicated constructs and collected at 5 dpi (first four images) or 18 dpi (Right). (D) Magnification of plastids from *N. benthamiana* leaves agroinfiltrated with the indicated constructs and collected at 5 dpi. Grana are marked as "g," membrane stacks with white arrows, and plastoglobules with gray arrows. (E) Gerontoplast from a *N. benthamiana* leaf harvested from the plant and kept in the dark for 10 d (senescent). (F) Immunoblot analysis of plastidial proteins in leaves treated as described in A and C. Coomassie blue (C-Blue) staining is shown as a loading control. (Scale bars, 1 μ m.)

Watermelon mosaic virus to prevent gene silencing), crtB-GFP fluorescence was detected at a much higher intensity. This allowed to confirm that the crtB-GFP protein was present in both cytosol and chloroplasts of agroinfiltrated cells (SI Appendix, Fig. S1A). When GFP was fused to the N terminus of crtB, the resulting protein (GFP-crtB) was completely excluded from chloroplasts (SI Appendix, Fig. S1A). It is therefore likely that the bacterial crtB enzyme harbors a cryptic plastid-targeting signal in its N terminus that becomes blocked and, hence, inactivated in the GFP-crtB protein. To unambiguously target crtB to the chloroplast, we next added the plastid-targeting sequence of the *Arabidopsis* enzyme HDS (20) to the crtB-GFP reporter. As expected, the resulting (p)crtB-GFP protein was only found in chloroplasts (SI Appendix, Fig. S1A). Agroinfiltrated leaf tissues expressing either crtB or (p)crtB developed the characteristic yellow phenotype at 4–5 d postinoculation (dpi), whereas tissues expressing the cytosolic GFP-crtB version—renamed as (c)crtB—remained green as the controls expressing GFP (Fig. 3A). Analysis of carotenoid contents showed identical profiles for leaf sections

agroinfiltrated with GFP and (c)crtB and confirmed that, similarly to crtB, (p)crtB triggered carotenoid overaccumulation (Fig. 3B). Agroinfiltration of *N. benthamiana* leaves with crtB or (p)crtB constructs did not initially reduce chlorophyll levels compared to leaf tissues agroinfiltrated with GFP or (c)crtB (Fig. 3B). However, estimation of photosynthesis-related parameters such as effective quantum yield of PSII (Φ PSII) and nonphotochemical quenching (NPQ) showed that both crtB and (p)crtB, but not (c)crtB or GFP, had a dramatic impact on chloroplast function (Fig. 3C). A plastid-targeted version of GFP did not cause any yellowing or Φ PSII defect (SI Appendix, Fig. S1B), confirming that disturbance of chloroplast photosynthesis is not caused by the accumulation of a foreign protein in chloroplasts but specifically by crtB. TEM analyses confirmed that (p)crtB induced the differentiation of chromoplast-like plastids very similar to those found in leaf tissues expressing the untargeted crtB enzyme, whereas only chloroplasts were present in leaves producing either (c)crtB or GFP (Fig. 2 C and D). These results confirm that crtB elicits a synthetic

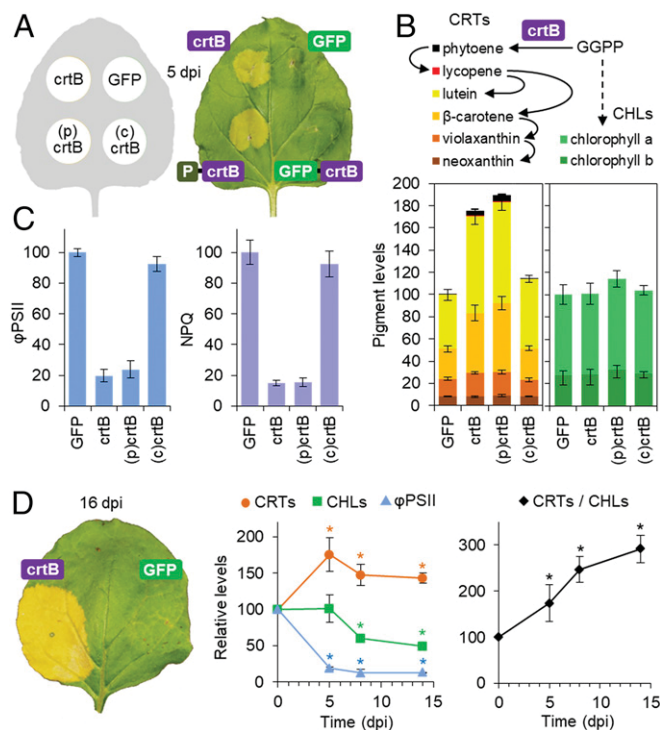


Fig. 3. Leaf tissues producing *crtB* show a stable phenotype of high carotenoid levels and impaired photosynthesis. (A) *N. benthamiana* leaf 5 d after agroinfiltration (dpi) with the indicated constructs in different sections. (B) Levels of carotenoids (CRTs) and chlorophylls (CHLs) in leaf sections like those shown in A. (C) ϕ PSII and NPQ in leaf sections like those shown in A. (D) Changes in CRTs, CHLs, ϕ PSII, and carotenoid-to-chlorophyll ratio (CRTs/CHLs) in leaf sections at different time points after agroinfiltration with *crtB*. A representative leaf at 16 dpi is shown at *Left*. Plots show the mean and SD of $n = 3$ independent samples. Values are represented relative to those in GFP controls. Asterisks in D plots mark statistically significant changes relative to 0 dpi (t test, $P < 0.05$).

(i.e., nonnatural) differentiation of chromoplasts only when localized in plastids, where carotenoids are made.

Differentiated leaf chromoplasts (Fig. 2C) and associated features such as high carotenoid levels and low ϕ PSII (Fig. 3D) were maintained for weeks after agroinfiltration, and no reversions to chloroplasts or green color were ever observed. About a week after agroinfiltration with *crtB*, chlorophylls started to decrease. Carotenoids also decreased but not as much as chlorophylls, eventually resulting in a higher carotenoid-to-chlorophyll ratio and, as a consequence, a stronger yellow color as leaves became older (Fig. 3D). The strong yellow phenotype associated with chromoplast differentiation and carotenoid enrichment was also stably maintained when the *crtB* gene was expressed from a viral vector in *Arabidopsis*, lettuce, and zucchini (Fig. 1), strongly suggesting that the mechanism by which *crtB* overexpression eventually results in chromoplastogenesis is conserved in plants.

Synthetic Chromoplast Biogenesis Induces Profound Changes in Nuclear Gene Expression and Primary Cell Metabolism. The vast majority of plastidial proteins are encoded by nuclear genes (2). We therefore reasoned that the drastic remodeling of plastidial ultrastructure associated with *crtB*-triggered chromoplast differentiation would require changes in nuclear gene expression. RNA-sequencing (seq) analyses of *N. benthamiana* leaf samples at 96 h postinfiltration (hpi) showed that about 5,000 genes were differentially expressed in yellow (p)*crtB* sections compared to green GFP controls (Dataset S1). Such a massive reprogramming of gene expression included the up-regulation of 3,183

genes and the down-regulation of 1,803 genes in chromoplast-containing samples. Gene Ontology (GO) term enrichment analyses (Dataset S2) showed overrepresentation of genes involved in protein folding and binding to RNA and ribosomes among those induced by (p)*crtB* (SI Appendix, Fig. S2). Enrichment of genes with roles in transmembrane transport, cell signaling (protein phosphorylation, calcium binding), and nuclear gene expression (transcription factors) was observed among those repressed when chromoplast biogenesis was induced (SI Appendix, Fig. S2). This profile was strikingly similar to that of ripening tomato fruits (where chromoplasts naturally differentiate from chloroplasts) but very different from that of senescent *Arabidopsis* leaves (SI Appendix, Fig. S2). Many of the genes potentially involved in carotenoid biosynthesis were up-regulated during *crtB*-triggered transformation of leaf chloroplasts into chromoplasts (SI Appendix, Fig. S3). However, the changes in carotenoid-related gene expression detected during chromoplastogenesis in *N. benthamiana* leaves were modest compared to those taking place in tomato ripening fruit (SI Appendix, Fig. S3 and Dataset S3).

Energy and carbon required for carotenoid biosynthesis rely on photosynthesis (i.e., the Calvin–Benson cycle) in chloroplasts. Given that leaf chromoplast differentiation was associated with impairment of photosynthesis (Fig. 3), we asked whether primary cell metabolism might also be reprogrammed. Of 52 metabolites detected by gas chromatography/time-of-flight/mass spectrometry analysis in *N. benthamiana* leaves (Dataset S4), 13 displayed statistically significant changes in (p)*crtB* sections compared to GFP controls (SI Appendix, Fig. S4 and Table S1). We observed reductions in the levels of ascorbate and hexoses (glucose and fructose, the main soluble carbohydrate stores and respiration substrates). This, together with increments in tricarboxylic acid (TCA) cycle intermediates (citrate, 2-oxoglutarate, and malate) and amino acids (valine, isoleucine, aspartate, and glutamate), suggested that sugars were used to produce ATP through the TCA cycle to sustain amino acid and carotenoid biosynthesis (and likely other cellular functions). Indeed, respiration rate—determined as total oxygen consumption in the dark—was higher in chromoplast-containing leaf tissues (SI Appendix, Fig. S4). While an increased respiration is also associated with the onset of carotenoid overproduction in tomato and other climacteric fruits, the metabolic changes that we observed in (p)*crtB*-producing *N. benthamiana* leaves are often opposite to those occurring during chromoplast differentiation in tomato (11, 21). In particular, hexoses and ascorbate do not decrease but increase. We speculate that this might be because leaf metabolism is devoted to produce and export photoassimilates, whereas tomatoes are sink organs that have been selected to accumulate sugars and acids as positive taste attributes. In any case, our data together show that the activity of *crtB* in leaf chloroplasts is sufficient to trigger a deep reprogramming of nuclear gene expression and whole-cell metabolism associated with the differentiation of chromoplasts, a plastid type that is not naturally found in tobacco or *Arabidopsis* leaves.

Enhanced Supply of Phytoene in Chloroplasts Can Interfere with Photosynthesis. To investigate the dynamics of the *crtB*-dependent chromoplast differentiation process, we next followed the time course of *crtB* expression, phytoene production, and downstream carotenoid accumulation after agroinfiltration of *N. benthamiana* leaves with the (p)*crtB* construct. Transcripts encoding (p)*crtB* were reliably detected at 24 hpi and peaked at 48 hpi (Fig. 4A), whereas phytoene started to accumulate between 24 and 36 hpi and suddenly increased at 48 hpi (Fig. 4B). Downstream carotenoids began to increase at 48 hpi (Fig. 4B). To follow chloroplast membrane remodeling dynamics, we also monitored ϕ PSII, NPQ, and D1 protein levels as estimators of photosynthesis, photoprotection, and photodamage, respectively. Both ϕ PSII (Fig. 4C)

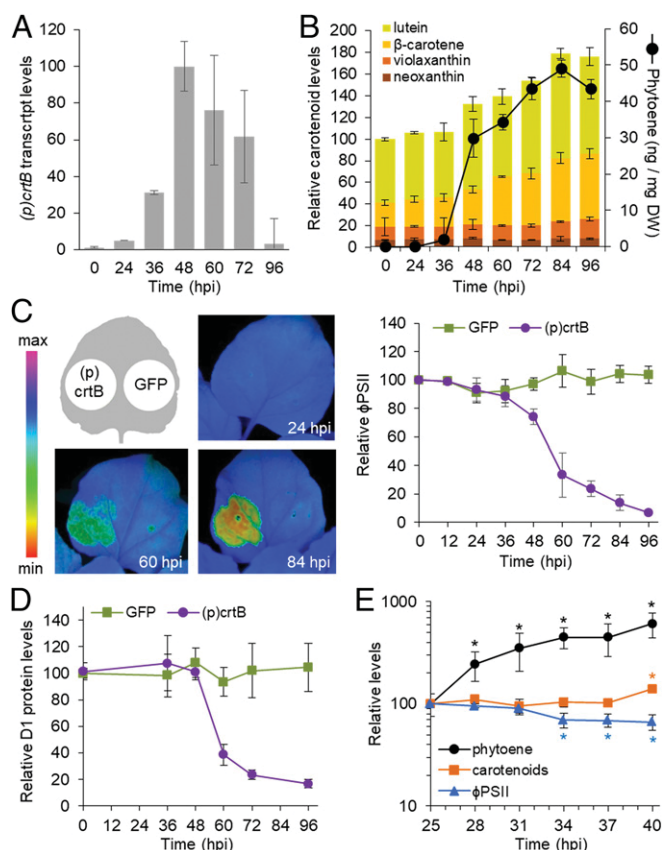


Fig. 4. Time-course of chloroplast-to-chromoplast differentiation in leaves. *N. benthamiana* leaves were agroinfiltrated with the indicated constructs, and samples were collected at the indicated time points (hours after agroinfiltration). (A) Levels of (p)crtB-encoding transcripts relative to the maximum in (p)crtB samples. (B) Absolute phytoene levels and relative downstream carotenoid contents in (p)crtB samples. (C) Representative chlorophyll fluorescence images and ϕ PSII values. (D) D1 (PsbA) protein contents. (E) Levels of phytoene, downstream carotenoids, and ϕ PSII in (p)crtB samples relative to those at 25 hpi. Asterisks mark significant changes relative to the 25 hpi values (t test, $P < 0.05$). Note the logarithmic scale. In all of the plots, values correspond to mean and SD values of $n = 3$ independent samples.

and NPQ (*SI Appendix, Fig. S5*) remained unchanged up to 36 hpi, and then decreased as the levels of both phytoene and downstream carotenoids increased (Fig. 4). The levels of D1 started to decrease later, between 48 and 60 hpi (Fig. 4D), likely as a result of photodamage. A higher temporal resolution analysis of both ϕ PSII and carotenoid levels between 25 and 40 hpi showed that phytoene levels increased before ϕ PSII decreased, whereas downstream carotenoids took a bit longer to accumulate (Fig. 4E). Taken together, these results suggest that the crtB-mediated production of phytoene causes a disruption of the chloroplast photosynthetic functionality before carotenoids start to overaccumulate.

To next confirm whether impairment of chloroplast functionality was due to phytoene overaccumulation, we used norflurazon (NF) to prevent phytoene conversion into downstream carotenoids (22). *N. benthamiana* leaves were agroinfiltrated with constructs to produce GFP, (p)crtB, and PAR1, an *Arabidopsis* transcription cofactor that promotes total carotenoid biosynthesis but not phytoene accumulation in photosynthetic tissues (23). At 24 hpi, some agroinfiltrated leaves were treated with NF (Fig. 5). Untreated leaves transiently expressing the *Arabidopsis* PAR1 gene accumulated higher levels of carotenoids downstream of phytoene but did not exhibit changes in ϕ PSII compared to GFP controls. NF treatment resulted in phytoene

accumulation, reduced levels of downstream carotenoids, and decreased ϕ PSII in all of the samples (Fig. 5). The reduction in ϕ PSII in these NF-treated samples correlated with the accumulation of phytoene (the higher the levels of phytoene, the stronger the reduction of ϕ PSII). However, the reduction in ϕ PSII was modest compared to that observed in (p)crtB samples lacking NF (Fig. 5A), in which phytoene conversion into downstream carotenoids led to the differentiation of chromoplasts. We concluded that phytoene overaccumulation by itself disrupts photosynthesis but does not abolish chloroplast identity, resulting in a relatively modest reduction in ϕ PSII. The much stronger decrease in ϕ PSII that takes place in (p)crtB samples would not be directly due to the effect of phytoene on photosynthetic activity but resulted from the dismantling of the photosynthetic apparatus as chloroplasts accumulate downstream carotenoids and differentiate into chromoplasts. Interestingly, PAR1-mediated accumulation of carotenoids but not phytoene (Fig. 5A) was unable to trigger the massive drop in ϕ PSII and the yellow leaf phenotype characteristic of chromoplast differentiation (Fig. 5B). We therefore conclude that the accumulation of phytoene causes a concentration-dependent disruption of the photosynthetic identity of chloroplasts, a condition that might be necessary for them to become chromoplasts upon the subsequent production and accumulation of downstream carotenoids.

Pharmacological Inhibition of Photosynthetic Activity Reduces the Phytoene Threshold to Initiate Chloroplast-to-Chromoplast Transition in Leaves. In contrast with the results using crtB but similar to those with PAR1, overexpression of PSY-encoding genes from *Arabidopsis* and tomato could not elicit the characteristic yellow leaf phenotype associated with chromoplast differentiation (Fig. 5 and *SI Appendix, Fig. S6*) (11, 24, 25). Interestingly, the plant enzymes

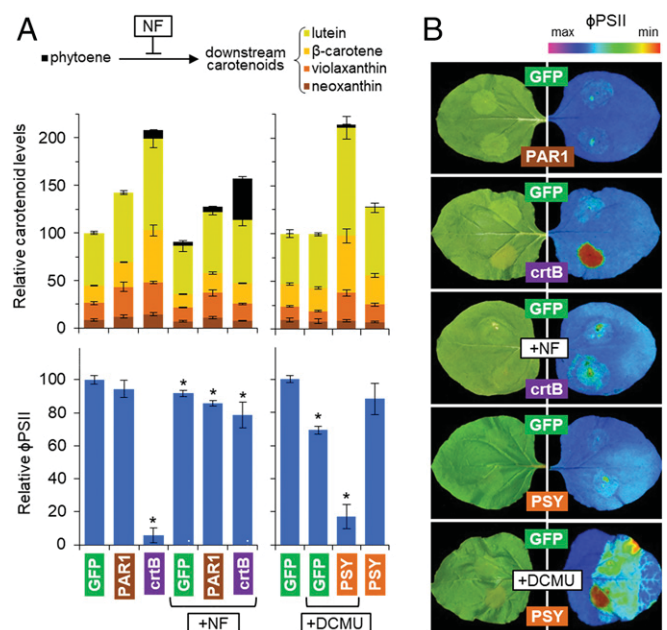


Fig. 5. Transformation of leaf chloroplasts into chromoplasts requires a reduction of photosynthetic capacity and production of carotenoids downstream of phytoene. (A) Carotenoid levels and ϕ PSII in leaves 96 h after agroinfiltration with the indicated constructs. In all cases, plot values correspond to mean and SD values of $n = 3$ independent samples. Asterisks in ϕ PSII plots mark statistically significant changes relative to untreated GFP controls (t test, $P < 0.05$). Samples infiltrated with NF at 24 hpi or treated with DCMU 24 h before agroinfiltration are indicated. (B) Representative images of agroinfiltrated leaves at 96 hpi and their corresponding chlorophyll fluorescence for ϕ PSII.

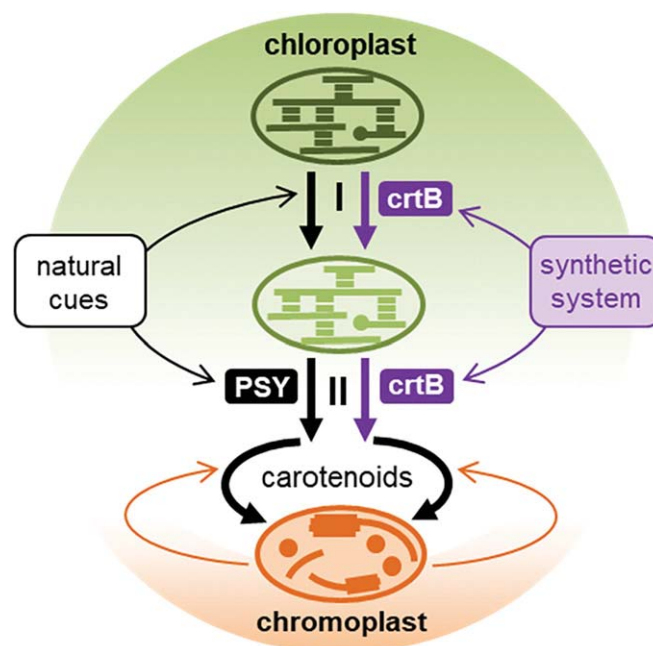


Fig. 6. Model of the chloroplast-to-chromoplast differentiation process. Plant developmental programs create organs with different degrees of photosynthetic capacity and, hence, chloroplast identity, from strong (e.g., leaves) to weak (e.g., green fruits) or absent (e.g., roots). Weakening of chloroplast identity appears to be the first phase (I) in chromoplast differentiation. In a second phase (II), developmental cues promote the expression of genes encoding PSY and other carotenoid biosynthetic enzymes. Enhanced production of carotenoids then reprograms plastid-to-nucleus communication, changes plastidial ultrastructure, and results in the differentiation of chromoplasts, which, in turn, promote biosynthesis and improve storage of carotenoids. The two phases can be synthetically engineered in leaves by overproducing phytoene using crtB. When phytoene exceeds a certain level, it interferes with the photosynthetic capacity of leaf chloroplasts. This acts as a metabolic switch that allows the formation of chromoplasts after phytoene is converted into downstream carotenoids by endogenous enzymes.

photosynthetically active than those of leaves (8, 30). Thus, tomato green fruit and other organs, tissues, or/and developmental stages in which chloroplast identity is weak or nonexistent (e.g., dark-grown calli, tubers, or roots) might be considered as “naturally competent” to differentiate chromoplasts when carotenoid biosynthesis is up-regulated. In agreement, overproduction of plant PSY enzymes resulted in chromoplast-like structures arising in green tomato fruit and nonphotosynthetic *Arabidopsis* tissues but had no effect on leaves (11, 24, 25) unless previously conditioned by shutting down their photosynthetic capacity (Fig. 5). Similarly, up-regulation of OR triggers carotenoid overaccumulation and chromoplast differentiation in tomato fruit, potato tubers, cauliflower curds, or *Arabidopsis* calli, but not in the leaves of any of these plants (31–34). Interestingly, OR does not appear to be required for crtB-mediated differentiation of leaf chloroplasts into chromoplasts (Fig. 1C). OR has been shown to promote PSY activity and stability, and some OR mutants prevent carotenoid (particularly beta-carotene) metabolism (5, 16, 35, 36). Our results suggest that no extra function would be required for OR up-regulation to cause chromoplast development from plastids with weak or no chloroplast identity. Interestingly, a role for OR in repressing chloroplast development in etiolated seedlings has been recently proposed (37).

In phase II, which likely overlaps with phase I, enhanced expression of carotenoid-related genes (*SI Appendix, Fig. S3*) likely contributes to activate the endogenous biosynthetic pathway. During this phase, carotenoid accumulation occurs concomitantly

yielded significantly lower levels of phytoene compared to crtB and did not substantially impact photosynthesis as deduced from ϕ PSII values (Fig. 5 and *SI Appendix, Fig. S6*). We hence speculated that phytoene might act as a metabolic threshold switch that only alters the photosynthetic performance of chloroplasts when exceeding a certain level. To overcome this putative threshold, we treated *N. benthamiana* leaves with DCMU (3-(3,4-dichlorophenyl)-1,1-dimethylurea, diuron), a widely used inhibitor of photosynthesis that interrupts the photosynthetic electron transport chain. The next day, treated and untreated control leaves were agroinfiltrated with constructs encoding either GFP or the *Arabidopsis* PSY enzyme. At 96 hpi, DCMU-treated GFP leaf sections showed a decrease in ϕ PSII but unchanged carotenoid levels compared to untreated samples (Fig. 5). By contrast, DCMU-treated PSY sections showed a more dramatic drop in ϕ PSII and much higher levels of carotenoids than untreated PSY or GFP controls (Fig. 5A). As a consequence, PSY leaf sections treated with DCMU turned yellow (Fig. 5B), similar to that observed when chloroplast-to-chromoplast differentiation was triggered by crtB in the absence of inhibitor. In summary, our results are consistent with the existence of a two-step process responsible for the crtB-mediated transformation of leaf chloroplasts into chromoplasts (Fig. 6). First, chloroplast identity is weakened by overaccumulation of phytoene and, second, increased production of carotenoids in preconditioned chloroplasts allows the differentiation of chromoplasts. Without preconditioning, carotenoid levels can increase but chromoplasts do not differentiate, as shown in untreated leaves producing PAR1 or PSY. Moreover, if carotenoids downstream of phytoene are not produced, preconditioned chloroplasts remain unchanged, as shown in NF-treated (p) crtB leaves (Fig. 5).

Discussion

The regulation of plastid identity is a core process in plants that remains poorly defined. Our work shows that chromoplasts can be synthetically differentiated from leaf chloroplasts in all plants tested, despite this is something that only a few species can do in nature. This synthetic system has allowed us to propose a model for chromoplast differentiation that also applies to natural systems (Fig. 6). In a first phase (I), chloroplasts must become competent (i.e., preconditioned) by lowering their photosynthetic capacity, whereas increased production of carotenoids completes the differentiation of chromoplasts in a second phase (II).

In our synthetic system, phase I was very fast (hours) and required a sufficient amount of phytoene to weaken chloroplast identity in leaves. In chloroplasts, carotenoids such as lutein, beta-carotene, violaxanthin, and neoxanthin are required to maintain the properties of photosynthetic membranes and pigment-protein complexes responsible for harvesting sunlight and transferring excitation energy to the photosystems (4, 26, 27). Phytoene is not normally detected in leaf chloroplasts as it is readily converted into downstream (photosynthesis-related) carotenoids. Overaccumulation of phytoene (or a phytoene derivative) might somehow compete with endogenous carotenoids for their binding to photosynthetic protein complexes and membranes, interfere with their functions, and eventually cause the changes that we observed in photosynthetic competence. Consistent with this hypothesis, engineered accumulation of non-chloroplast carotenoids such as astaxanthin in plants alters the properties of thylakoids and grana and interferes with the photosynthetic machinery at several other levels (27, 28). Production of astaxanthin and other ketocarotenoids in tobacco actually resulted in leaf plastids that lost their chloroplast features and exhibited a proliferation of disordered membrane systems and plastoglobules (28, 29), similar to our results (Fig. 2).

In nature, chloroplasts might become competent for differentiation into chromoplasts without the need of a phytoene boost. In tomato, the chloroplasts of green fruit are much less

with the remodeling of the internal plastid structures, with both factors synergistically activating each other (Fig. 6). Strikingly, in agroinfiltrated *N. benthamiana* leaves, this process takes place before chlorophylls start to degrade (Fig. 3). These results confirm that chlorophyll breakdown and chromoplast differentiation are independent processes, as already shown in mutants such as tomato *green flesh* (*gf*), in which impairment of chlorophyll degradation during fruit ripening has no effect on the formation of chromoplast membranes and the accumulation of carotenoids (38). The new structures created following the disassembly of photosynthetic grana and thylakoids (Fig. 2) likely contribute to reaching high carotenoid levels by accommodating increasing amounts of carotenoids and by preventing their degradation (1–3, 5, 7, 8). They might additionally enhance carotenoid production by stimulating the activity of endogenous carotenoid biosynthetic enzymes (including PSY), many of which are membrane-associated (39).

The buildup of carotenoids and the structural changes associated with the chloroplast-to-chromoplast transformation involve reorganization of the plastidial protein content (Fig. 2F) but also a global reprogramming of nuclear gene expression (SI Appendix, Fig. S2) and primary metabolism (SI Appendix, Fig. S4). It is likely that implementing these changes (as well as others required to readapt plastid protein import and quality control mechanisms to chromoplast differentiation) relies on retrograde signals produced by differentiating plastids. Carotenoid degradation can generate signaling molecules that regulate many developmental processes in plants, including plastid development (18, 19). The observation that *Arabidopsis ccd1 ccd4* mutants defective in carotenoid cleavage dioxygenase activity in the cytosol (via CCD1) and the plastids (via CCD4) were not affected in the crtB-dependent leaf phenotype (Fig. 1C) suggests that signals independent of CCDs or carotenoids are responsible for eliciting the changes in nuclear gene expression and cell metabolism supporting chromoplast biogenesis. The specific nature of such signals remains to be discovered.

In summary, we show that chromoplast differentiation only requires metabolic cues (i.e., enough phytoene and downstream carotenoid production). While our conclusions are based on a synthetic system (i.e., the expression of a bacterial gene in leaf cells), the similarity of the transcriptomic profiles between this process and fruit ripening (SI Appendix, Fig. S2) strongly supports that this is a basic general mechanism for chloroplasts to become chromoplasts. In nature, however, developmental cues play a fundamental role by making chloroplasts competent (phase I) and by regulating the expression of carotenoid biosynthetic genes (phase II). Signals produced by differentiating plastids are also hardwired to the process as they support the organellar transformation by reprogramming nuclear gene expression and whole-cell metabolism. Besides serving to successfully address a long-standing question in plant biology (i.e., plastid identity), the very simple and straightforward system that we describe here to induce chloroplast-to-chromoplast differentiation on demand is a powerful biotechnological tool that appears to work in every plant tested so far (Fig. 1) (10). Thus, creating an organellar sink to improve both the production and the storage of carotenoids and other plastidial phytonutrients in chloroplast-containing tissues once their photosynthetic activity is dispensable (e.g., just before harvesting) should allow to boost the nutritional quality of green vegetables and forage crops.

Materials and Methods

Plant Material and Growth Conditions. *N. tabacum* Xanthi nc, *N. benthamiana* RDR6i, and *A. thaliana* Columbia-0 (Col) and Landsberg *erecta* (Ler) plants were grown under standard conditions as described previously (10, 40). Growth of double mutants *ccd1 ccd4* (16) and *ator ator1* (17), both in the Col background, was facilitated by transferring them to low light (40 $\mu\text{mol photons}\cdot\text{m}^{-2}\cdot\text{s}^{-1}$) days after germination. For generating dark-induced leaf

senescence, detached leaves were maintained inside dark, humid chambers until visible yellowing occurred. Collected plant material was frozen in liquid nitrogen, lyophilized, and then homogenized to a fine powder using a Tissuelyser system (Qiagen) for further analyses.

Transmission Electron Microscopy. Transmission electron microscopy of plant leaves was performed as previously described (41).

Gene Constructs. See SI Appendix, Materials and Methods for details.

Transient Expression Assays. For transient expression studies using viral vectors, leaves of 4- to 6-wk-old *N. tabacum* and *Arabidopsis* plants were mechanically inoculated with crude extracts from frozen-stored infected plant tissue and collected upon the appearance of the yellowing phenotype as described previously (10). For agroinfiltration experiments, the second or third youngest leaves of 4- to 6-wk-old *N. benthamiana* plants were infiltrated with *A. tumefaciens* strain GV3101 carrying vectors of interest following the procedure described previously (42). Gene silencing was prevented by co-agroinfiltration with a strain carrying the helper component protease (HC-Pro) of the *Watermelon mosaic virus* (WMV) in vector HcProWMV-pGWB702 (kindly provided by Juan José López-Moya and Maria Luisa Domingo-Calap, CRAG, Barcelona, Spain). Infiltration cultures were grown on Luria-Bertani medium at 28 °C and used at optical density at 600 nm (OD_{600}) of 0.5. For pharmacological treatments, NF or diuron (DCMU) were diluted in water and 0.05% Tween 20. The treatments with NF (2 μM) were performed by infiltration with a syringe of leaf areas that had been agroinfiltrated with different constructs 24 h earlier. DCMU (10 μM) was applied on the leaf surface with a fine paintbrush 24 h before agroinfiltration.

Transcript Analyses. See SI Appendix, Materials and Methods for details.

Protein Extraction and Immunoblot Analyses. Protein extraction, quantification, and immunoblot analyses were performed as described (43) using anti-brilliant (44) or anti-PsbA serum (Agriseria).

Metabolite Analyses. Carotenoids were analyzed as previously described (40). Phytoene was quantified using a concentration curve with a commercial standard (Sigma). Primary metabolites were extracted and analyzed as described in SI Appendix, Materials and Methods.

Photosynthetic and Respiration Measurements. See SI Appendix, Materials and Methods for details.

Statistical Analyses. Differentially expressed genes (DEGs) were identified by comparing crtB and GFP RNA-seq datasets with the DESeq2 statistical method in the AIR platform. The resulting crtB/GFP list was filtered using cut-offs of false discovery rate <0.05 and \log_2 -transformed fold change ($\log_2\text{FC}$) >0.585 for up-regulated genes and <-0.599 for down-regulated genes. GO enrichments were identified by the Parametric Analysis of Gene Set Enrichment (PAGE) function of the AgriGO v2.0 web-based tool (bioinfo.cau.edu.cn/agriGO/) after transforming the gene IDs to the Niben v04.4 annotation. For the comparison of different biological systems, we selected the significantly enriched gene ontologies from our *N. benthamiana* RNA-seq experiment (P and q values <0.05) and compared their Z-score values with those obtained from the analysis of published RNA-seq data of tomato fruit ripening and *Arabidopsis* leaf senescence. In particular, we used the reads per million mapped reads values of the total pericarp at mature green (MG), light ripe (LR), and red ripe (RR) stages (45) and the fragments per kilobase million mapped reads values of the 16D and 30D senescence stages (46). DEGs resulting from LR/MG, RR/MG, and 30D/16D comparisons were filtered as described above for *N. benthamiana* crtB/GFP. Student's t tests were used for the rest of statistical analyses using GraphPad Prism 5.0a (GraphPad Software). Carotenoid-related genes in *N. benthamiana* were identified by BLASTp using tomato sequences. Heatmaps were made using the pheatmap package in R (<https://cran.r-project.org/web/packages/pheatmap/index.html>).

Data Availability. RNA-seq data were deposited in the Sequence Read Archive (SRA) database of the National Center for Biotechnology Information (NCBI) under the accession SRP238752 (BioProject ID PRJNA597608). The rest of the data presented in the paper are available in the main text and SI Appendix. Biological materials are available from the corresponding authors upon request.

All study data are included in the article and SI Appendix.

ACKNOWLEDGMENTS. We greatly thank Jaume F. Martínez-García and Ralf Welsch for fruitful discussions on the manuscript; Ralf Welsch and Li Li for providing seeds of the *Arabidopsis ccd1 ccd4* and *ator atorl* mutants, respectively; Juan José López-Moya and María Luisa Domingo-Calap for the gift of the HProWMV-pGW702 vector; and M. Rosa Rodríguez-Goberna for excellent technical support. The help of Martí Bernardo, Fidel Lozano, Lidia Jiménez, and members of the CRAG core facilities is also appreciated. This work was funded by the European Regional Development Fund and Spanish Agencia Estatal de Investigación Grants BIO2017-84041-P, BIO2017-83184-R, BIO2017-90877-REDT, BES-2017-080652, and AGL2017-85563-C2-1-R; Ministry of Education, Culture and Sports Grants AP2012-3751 and FPU16/04054;

and Generalitat de Catalunya Grant 2017SGR-710. We also thank the financial support of the European Union's Horizon 2020 (EU-H2020) COST Action CA15136 (EuroCaroten) and Marie S. Curie Action (MSCA) 753301 (Arcatom), the Severo Ochoa Programme for Centres of Excellence in R&D 2016-2019 Grant SEV-2015-0533 and the Generalitat de Catalunya CERCA Programme (to CRAG). B.L. is supported by grants from the CSIRO Synthetic Biology Future Science Platform and Macquarie University. L.M. is supported by La Caixa Foundation PhD INPhINIT Fellowship LCF/BQ/IN18/11660004, which received funding from the EU-H2020 through MSCA Grant 713673. A.R.F. is supported by Deutsche Forschungsgemeinschaft Grant DFG TRR 175.

- N. M. Sadali, R. G. Sowden, Q. Ling, R. P. Jarvis, Differentiation of chromoplasts and other plastids in plants. *Plant Cell Rep.* **38**, 803–818 (2019).
- P. Jarvis, E. López-Juez, Biogenesis and homeostasis of chloroplasts and other plastids. *Nat. Rev. Mol. Cell Biol.* **14**, 787–802 (2013).
- I. Egea *et al.*, Chromoplast differentiation: Current status and perspectives. *Plant Cell Physiol.* **51**, 1601–1611 (2010).
- M. Rodríguez-Concepción *et al.*, A global perspective on carotenoids: Metabolism, biotechnology, and benefits for nutrition and health. *Prog. Lipid Res.* **70**, 62–93 (2018).
- T. Sun *et al.*, Carotenoid metabolism in plants: The role of plastids. *Mol. Plant* **11**, 58–74 (2018).
- G. Giuliano, Provitamin A biofortification of crop plants: A gold rush with many miners. *Curr. Opin. Biotechnol.* **44**, 169–180 (2017).
- B. Llorente, J. F. Martínez-García, C. Stange, M. Rodríguez-Concepción, Illuminating colors: Regulation of carotenoid biosynthesis and accumulation by light. *Curr. Opin. Plant Biol.* **37**, 49–55 (2017).
- J. Lado, L. Zacarias, M. J. Rodrigo, Regulation of carotenoid biosynthesis during fruit development. *Subcell. Biochem.* **79**, 161–198 (2016).
- E. T. Wurtzel, Changing form and function through carotenoids and synthetic biology. *Plant Physiol.* **179**, 830–843 (2019).
- E. Majer, B. Llorente, M. Rodríguez-Concepción, J. A. Daròs, Rewiring carotenoid biosynthesis in plants using a viral vector. *Sci. Rep.* **7**, 41645 (2017).
- P. D. Fraser *et al.*, Manipulation of phytoene levels in tomato fruit: Effects on isoprenoids, plastids, and intermediary metabolism. *Plant Cell* **19**, 3194–3211 (2007).
- J. Deruère *et al.*, Fibril assembly and carotenoid overaccumulation in chromoplasts: A model for supramolecular lipoprotein structures. *Plant Cell* **6**, 119–133 (1994).
- D. K. Singh, T. W. McNellis, Fibrillin protein function: The tip of the iceberg? *Trends Plant Sci.* **16**, 432–441 (2011).
- C. Barsan *et al.*, Proteomic analysis of chloroplast-to-chromoplast transition in tomato reveals metabolic shifts coupled with disrupted thylakoid biogenesis machinery and elevated energy-production components. *Plant Physiol.* **160**, 708–725 (2012).
- S. Kahlau, R. Bock, Plastid transcriptomics and translationalomics of tomato fruit development and chloroplast-to-chromoplast differentiation: Chromoplast gene expression largely serves the production of a single protein. *Plant Cell* **20**, 856–874 (2008).
- X. Zhou *et al.*, Arabidopsis OR proteins are the major posttranscriptional regulators of phytoene synthase in controlling carotenoid biosynthesis. *Proc. Natl. Acad. Sci. U.S.A.* **112**, 3558–3563 (2015).
- P. Schaub *et al.*, Establishment of an Arabidopsis callus system to study the interrelations of biosynthesis, degradation and accumulation of carotenoids. *PLoS One* **13**, e0192158 (2018).
- X. Hou, J. Rivers, P. León, R. P. McQuinn, B. J. Pogson, Synthesis and function of apocarotenoid signals in plants. *Trends Plant Sci.* **21**, 792–803 (2016).
- J. Y. Wang *et al.*, The apocarotenoid metabolite zaxinone regulates growth and strigolactone biosynthesis in rice. *Nat. Commun.* **10**, 810 (2019).
- E. Gas, U. Flores-Pérez, S. Sauret-Güeto, M. Rodríguez-Concepción, Hunting for plant nitric oxide synthase provides new evidence of a central role for plastids in nitric oxide metabolism. *Plant Cell* **21**, 18–23 (2009).
- F. Carrari, A. R. Fernie, Metabolic regulation underlying tomato fruit development. *J. Exp. Bot.* **57**, 1883–1897 (2006).
- M. Ortiz-Alcaide *et al.*, Chloroplasts modulate elongation responses to canopy shade by retrograde pathways involving HYS and abscisic acid. *Plant Cell* **31**, 384–398 (2019).
- I. Roig-Villanova *et al.*, Interaction of shade avoidance and auxin responses: A role for two novel atypical bHLH proteins. *EMBO J.* **26**, 4756–4767 (2007).
- D. Maass, J. Arango, F. Wüst, P. Beyer, R. Welsch, Carotenoid crystal formation in Arabidopsis and carrot roots caused by increased phytoene synthase protein levels. *PLoS One* **4**, e6373 (2009).
- K. Lätari *et al.*, Tissue-specific apocarotenoid glycosylation contributes to carotenoid homeostasis in Arabidopsis leaves. *Plant Physiol.* **168**, 1550–1562 (2015).
- I. Domonkos, M. Kis, Z. Gombos, B. Ughy, Carotenoids, versatile components of oxygenic photosynthesis. *Prog. Lipid Res.* **52**, 539–561 (2013).
- N. Liguori *et al.*, Different carotenoid conformations have distinct functions in light-harvesting regulation in plants. *Nat. Commun.* **8**, 1994 (2017).
- A. Röding *et al.*, Production of ketocarotenoids in tobacco alters the photosynthetic efficiency by reducing photosystem II supercomplex and LHCII trimer stability. *Photosynth. Res.* **123**, 157–165 (2015).
- Y. Lu *et al.*, Horizontal transfer of a synthetic metabolic pathway between plant species. *Curr. Biol.* **27**, 3034–3041.e3 (2017).
- M. F. Cocaliadis, R. Fernández-Muñoz, C. Pons, D. Orzaez, A. Granell, Increasing tomato fruit quality by enhancing fruit chloroplast function. A double-edged sword? *J. Exp. Bot.* **65**, 4589–4598 (2014).
- L. Li, D. J. Paolillo, M. V. Parthasarathy, E. M. Dimuzio, D. F. Garvin, A novel gene mutation that confers abnormal patterns of beta-carotene accumulation in cauliflower (*Brassica oleracea* var. botrytis). *Plant J.* **26**, 59–67 (2001).
- A. B. Lopez *et al.*, Effect of the cauliflower or transgene on carotenoid accumulation and chromoplast formation in transgenic potato tubers. *J. Exp. Bot.* **59**, 213–223 (2008).
- H. Yuan *et al.*, A single amino acid substitution in an ORANGE protein promotes carotenoid overaccumulation in Arabidopsis. *Plant Physiol.* **169**, 421–431 (2015).
- M. Yazdani *et al.*, Ectopic expression of ORANGE promotes carotenoid accumulation and fruit development in tomato. *Plant Biotechnol. J.* **17**, 33–49 (2019).
- G. Tzuri *et al.*, A “golden” SNP in CmOr governs the fruit flesh color of melon (*Cucumis melo*). *Plant J.* **82**, 267–279 (2015).
- R. Welsch *et al.*, Clp protease and OR directly control the proteostasis of phytoene synthase, the crucial enzyme for carotenoid biosynthesis in Arabidopsis. *Mol. Plant* **11**, 149–162 (2018).
- T. Sun *et al.*, ORANGE represses chloroplast biogenesis in etiolated Arabidopsis cotyledons via interaction with TCP14. *Plant Cell* **31**, 2996–3014 (2019).
- A. Y. Cheung, T. McNellis, B. Piekos, Maintenance of chloroplast components during chromoplast differentiation in the tomato mutant green flesh. *Plant Physiol.* **101**, 1223–1229 (1993).
- M. A. Ruiz-Sola, M. Rodríguez-Concepción, Carotenoid biosynthesis in Arabidopsis: A colorful pathway. *Arabidopsis Book* **10**, e0158 (2012).
- B. Llorente *et al.*, Tomato fruit carotenoid biosynthesis is adjusted to actual ripening progression by a light-dependent mechanism. *Plant J.* **85**, 107–119 (2016).
- L. D'Andrea *et al.*, Interference with Clp protease impairs carotenoid accumulation during tomato fruit ripening. *J. Exp. Bot.* **69**, 1557–1568 (2018).
- I. A. Sparkes, J. Runions, A. Kearns, C. Hawes, Rapid, transient expression of fluorescent fusion proteins in tobacco plants and generation of stably transformed plants. *Nat. Protoc.* **1**, 2019–2025 (2006).
- P. Pulido *et al.*, Specific Hsp100 chaperones determine the fate of the first enzyme of the plastidial isoprenoid pathway for either refolding or degradation by the stromal clp protease in Arabidopsis. *PLoS Genet.* **12**, e1005824 (2016).
- A. J. Simkin *et al.*, Fibrillin influence on plastid ultrastructure and pigment content in tomato fruit. *Phytochemistry* **68**, 1545–1556 (2007).
- Y. Shinozaki *et al.*, High-resolution spatiotemporal transcriptome mapping of tomato fruit development and ripening. *Nat. Commun.* **9**, 364 (2018).
- H. R. Woo *et al.*, Programming of plant leaf senescence with temporal and inter-organellar coordination of transcriptome in Arabidopsis. *Plant Physiol.* **171**, 452–467 (2016).

Supplementary Information for

Synthetic conversion of leaf chloroplasts into carotenoid-rich plastids reveals mechanistic basis of natural chromoplast development.

Briardo LLORENTE*, Salvador TORRES-MONTILLA, Luca MORELLI, Igor FLOREZ-SARASA, José Tomás MATUS, Miguel EZQUERRO, Lucio D'ANDREA, Fakhreddine HOUHOU, Eszter MAJER, Belén PICÓ, Jaime CEBOLLA, Adrian TRONCOSO, Alisdair R. FERNIE, José-Antonio DARÒS, Manuel RODRIGUEZ-CONCEPCION*

(*) Corresponding authors: BL, **Email:** briardo.llorente@mq.edu.au
MRC, **Email:** manuel.r.c@csic.es

This PDF file includes:

SI Materials and Methods

Figures S1 to S6

Tables S1 to S2

SI References

Other supplementary materials for this manuscript include the following:

Datasets S1 to S4

SI Materials and Methods

Gene constructs. Viral vectors used in this study have been described (1) with the following exceptions. A plasmid with recombinant clone TEV-GFP was constructed from plasmid pGTEVa (2) and used for *Arabidopsis* Ler plants. The binary plasmid pGTuMV-UK1 was used for *Arabidopsis* Col plants. Briefly, a cDNA of the UK1 isolate of *Turnip mosaic virus* (TuMV-UK1; GenBank accession number NC_002509.2) was cloned in vector pG35Z (3) flanked by the *Cauliflower mosaic virus* 35S promoter and terminator. To generate the different crtB versions, we amplified by PCR the *Pantoea ananatis* crtB gene (1). We also amplified cDNA sequences encoding the plastid-targeting peptide of *Arabidopsis* hydroxymethylbutenyl 4-diphosphate synthase (4), *Arabidopsis* PSY and tomato PSY2. Primers used for cloning procedures are listed in *SI Appendix*, Table S2. PCR products were cloned using the Gateway system first into plasmid pDONR-207 and then into plasmid pGWB405 (5) to generate 35S:crtB-pGWB405, 35S:(p)crtB-pGWB405, 35S:(p)crtB-GFP-pGWB405, 35S:AtPSY-pGWB405, and 35S:SIPSY2-pGWB405, or plasmid pGWB506 (5) to generate 35S:GFP-crtB-pGWB506. To generate TuMV-crtB and LMV-crtB, the crtB sequence was cloned by Gibson assembly between positions 8758 and 8759 of TuMV-UK1 and 9034 and 9035 of LMV after amplification with flanking sequences complementing the TuMV-UK1 and LMV nuclear inclusion a protease (NlaPro) cleavage sites, respectively (*SI Appendix*, Table S2) to mediate the release of the crtB protein from the viral polyproteins. ZYMV-crtB was generated as described (1).

Transcript analyses. Total RNA was extracted from leaves with the Maxwell 16 LEV Plant RNA Kit (Promega) and quantified with a NanoDrop (Thermo Scientific) as described (1). For reverse transcription-quantitative PCR (RT-qPCR) analyses, the First Strand cDNA Synthesis Kit (Roche) was used to generate cDNA according to the manufacturer's instructions, with anchored oligo(dT)₁₈ primers and 1 µg of total RNA. Relative mRNA abundance was evaluated via quantitative PCR using LightCycler 480 SYBR Green I Master Mix (Roche) on a LightCycler 480 real-time PCR system (Roche). Quantification of crtB-encoding transcripts was conducted by RT-qPCR using the *ACT* gene Niben101Scf03410g03002 for normalization and the primers listed in *SI Appendix*, Table S2. RNAseq service was performed by Sequentia Biotech SL (Barcelona, Spain). RNA concentration in each sample was assayed with a ND-1000 spectrophotometer (NanoDrop) and its quality assessed with the TapeStation 4200 (Agilent Technologies). Indexed libraries were prepared from 1 µg/ea purified RNA with TruSeq Stranded mRNA Sample Prep Kit (Illumina) according to the manufacturer's instructions. Libraries were quantified using the TapeStation 4200 and pooled such that each index-tagged sample was present in equimolar amounts, with final concentration of the pooled samples of 2 nM. The pooled samples were subject to cluster generation and sequencing using a NextSeq 500 System (Illumina) in a 2x75 paired end format at a final concentration of 1.8 pmol. The raw sequence files generated (.fastq files) underwent quality control analysis using FastQC (<http://www.bioinformatics.babraham.ac.uk/projects/fastqc/>). Data analysis was performed with the online platform AIR (www.transcriptomics.cloud) using the SolGenomics Network (<https://solgenomics.net/>) *N. benthamiana* 1.01 (Niben v101) reference genome (6).

Metabolite analyses. Primary metabolites were extracted as described previously (7) using approximately 20 mg of lyophilized leaf tissue. Derivatization and gas chromatography-time of flight-mass spectrometry (GC-TOF-MS) analyses were carried out as described previously (7). Metabolites were identified manually using the TagFinder software in combination with the reference library mass spectra and retention indices from the Golm Metabolome Database, <http://gmd.mpimp-golm.mpg.de>. The parameters used for the peak annotation of the 52

metabolites can be found in *SI Appendix*, Dataset S4, which follows recommended standards on the report of metabolite data (8). Data were normalized to the mean value of the GFP control samples (i.e., the value of all metabolites for GFP control samples was set to 1). The means and standard errors of five to six replicates at 96 hpi are presented in *SI Appendix*, Dataset S5.

Photosynthetic measurements. Photosynthetic efficiencies were assessed by measuring chlorophyll *a* fluorescence with a MAXI-PAM fluorometer (Heinz Walz GmbH). Leaves were placed under the camera and effective quantum yield ($\Delta F/F_m'$) was measured as $(F_m' - F_s)/F_m'$, where F_m' and F_s are, respectively, the maximum and the minimum fluorescence of light-exposed plants. The light intensity chosen was 21 PAR (actinic light, AL=2) as the last value able to generate a response in the (p)crtB-infiltrated areas before having a null photosynthetic activity. Each value is the average result of three biological replicates and three different AOI for each replicate. NPQ was also measured using the MAXI-PAM unit. All recordings were performed every day at the same time slot, but the order of the samples was randomized to reduce the bias related to the length of the light stress recovery protocol. Plants were dark-adapted for 30 min before measurement and then submitted to a continuous 801 PAR light (AL=17) for 10 min. After this period plants were left recovering in darkness for 40 min. During the whole protocol, F_t was monitored and F_m' values were estimated with a saturating pulse (SAT) every 60 seconds. NPQ and its relative components qE , qZ and qI were calculated as described (9) with some modifications. Briefly: NPQ was calculated as $(F_m - F_{m_0})/F_m$, where F_m and F_{m_0} are the maximum fluorescence after the dark acclimation and after the light stress, respectively. The relative contributions of qE , qZ and qI to NPQ were estimated by monitoring NPQ relaxation kinetics in the dark: following the 10 min exposure to saturating light used to measure NPQ, leaves were left in darkness, and F_{m_0} was measured again after 10 and 40 min. The qE component of NPQ relaxes within 10 min of a leaf being placed in darkness such that NPQ persisting after 10 min in the dark consists of $qZ + qI$. The qZ component of NPQ relaxes within tens of minutes so that NPQ persisting after 40 min in the dark (when the F_t value is linear) consists of qI , which is either irreversible in the dark or requires several hours to relax. Consequently, $(qI + qZ)$ was calculated as $(F_m - F_{m_1})/F_{m_1}$, where F_{m_1} is the value of F_m measured after 10 min in the dark following NPQ measurement. qZ was calculated as $(F_m - F_{m_2})/F_{m_2}$, where F_{m_2} is the value of F_m measured after 40 min in the dark following measurement of NPQmax. qE was calculated as $NPQ - (qI + qZ)$ and qI was calculated as $(qI + qZ) - qZ$. For the calculation of the de-epoxidation state (DES), agroinfiltrated leaf areas were exposed for 10 min to a continuous 801 PAR light (AL=17) in the MAXI-PAM unit, sampled under the same light and immediately frozen before pigment extraction and quantification. The operation of the xanthophyll cycle, comprising the sequential de-epoxidation of the pigments violaxanthin (Vx) to antheraxanthin (Ax) and zeaxanthin (Zx) was followed by calculating DES as $(Zx + 0.5 \times Ax)/(Zx + Ax + Vx)$, where Zx, Ax and Vx are the concentrations of the corresponding xanthophylls.

Respiration measurements. Before respiration measurements, *N. benthamiana* plants were placed in the dark for about 30 min to avoid light-enhanced dark respiration. Four leaf discs of 3.8 cm² each were harvested from leaf sections of two different plants infiltrated with the (p)crtB construct, weighted and placed into the respiration cuvette containing the respiration buffer (30 mM MES pH 6.2, 0.2 mM CaCl₂). Oxygen uptake rates were measured in darkness using a liquid-phase Clark-type oxygen electrode (Rank Brothers) at a constant temperature of 25°C. Dry weights from leaf discs were determined after drying for 2 days at 60°C.

SI Figures

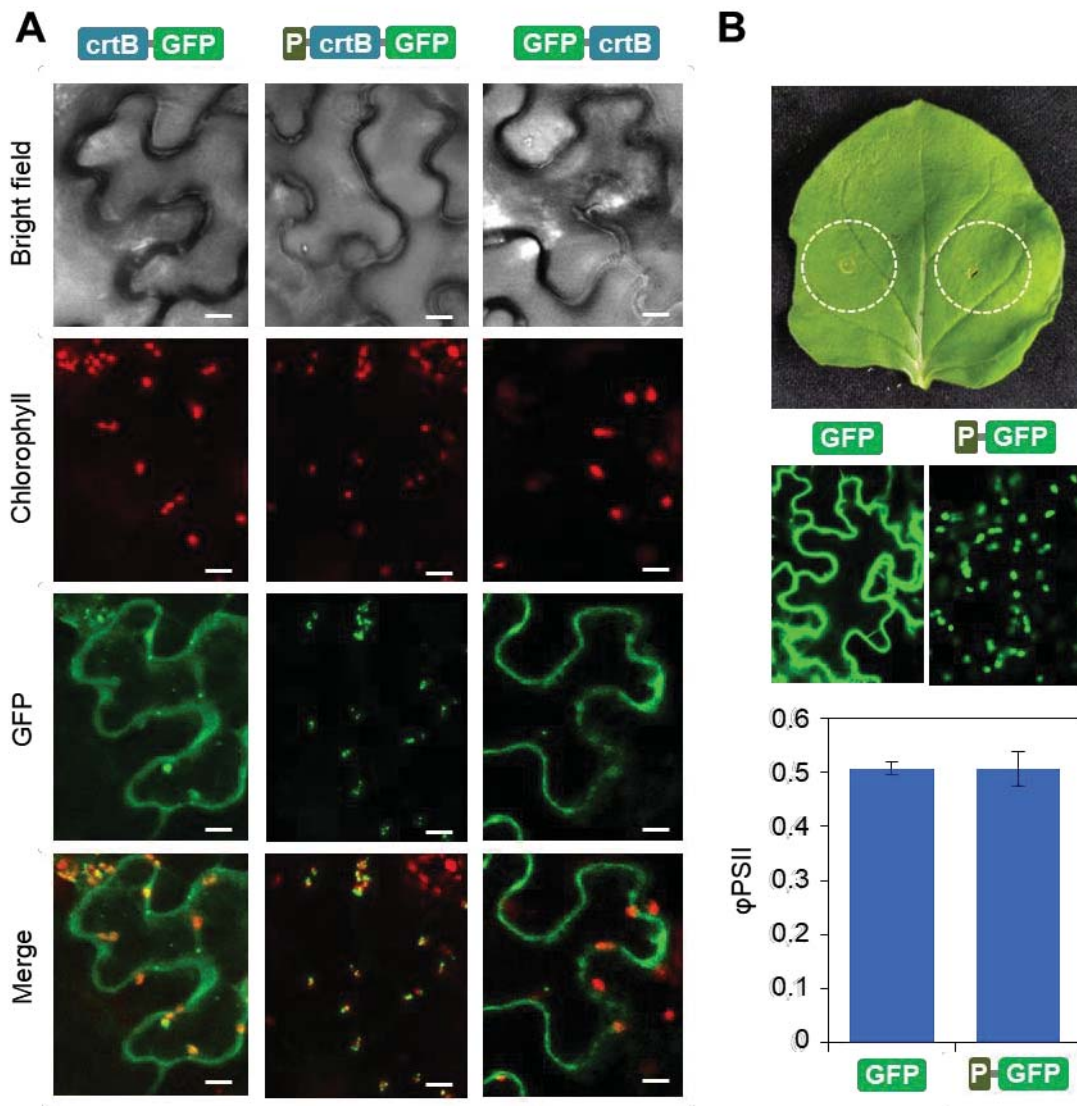


Figure S1. Localization of GFP-tagged proteins. A, Subcellular localization of the indicated constructs in agroinfiltrated *N. benthamiana* leaf cells by confocal laser scanning microscopy. Pictures were taken 3 days after agroinfiltration (72 hpi). Bars, 20 μ m. B, *N. benthamiana* leaf agroinfiltrated with constructs to express a plastid-targeted version of GFP (P-GFP) or the untargeted GFP protein (upper picture). At 72 hpi, GFP fluorescence was examined in agroinfiltrated tissue to confirm the localization of P-GFP in chloroplasts and GFP in the cytosol (middle pictures). Effective quantum yield of PSII was quantified at 96 hpi (lower plot).



Figure S2. Chromoplast differentiation triggered by crtB in *N. benthamiana* leaves resembles that associated to ripening in tomato fruit. Heatmap represents GO term enrichment values (Z-scores) calculated from log2FC values in *N. benthamiana* leaves 4 days after agroinfiltration with (p)crtB compared to GFP (lane NbB). Data publicly available from tomato fruit (light ripe vs. mature green, SIO, and red ripe vs. mature green, SIR) and *Arabidopsis* leaves (senescent -30D- vs. controls -16D-, AtS) are also shown. Only GO terms with a significant enrichment in the *N. benthamiana* experiment are shown.

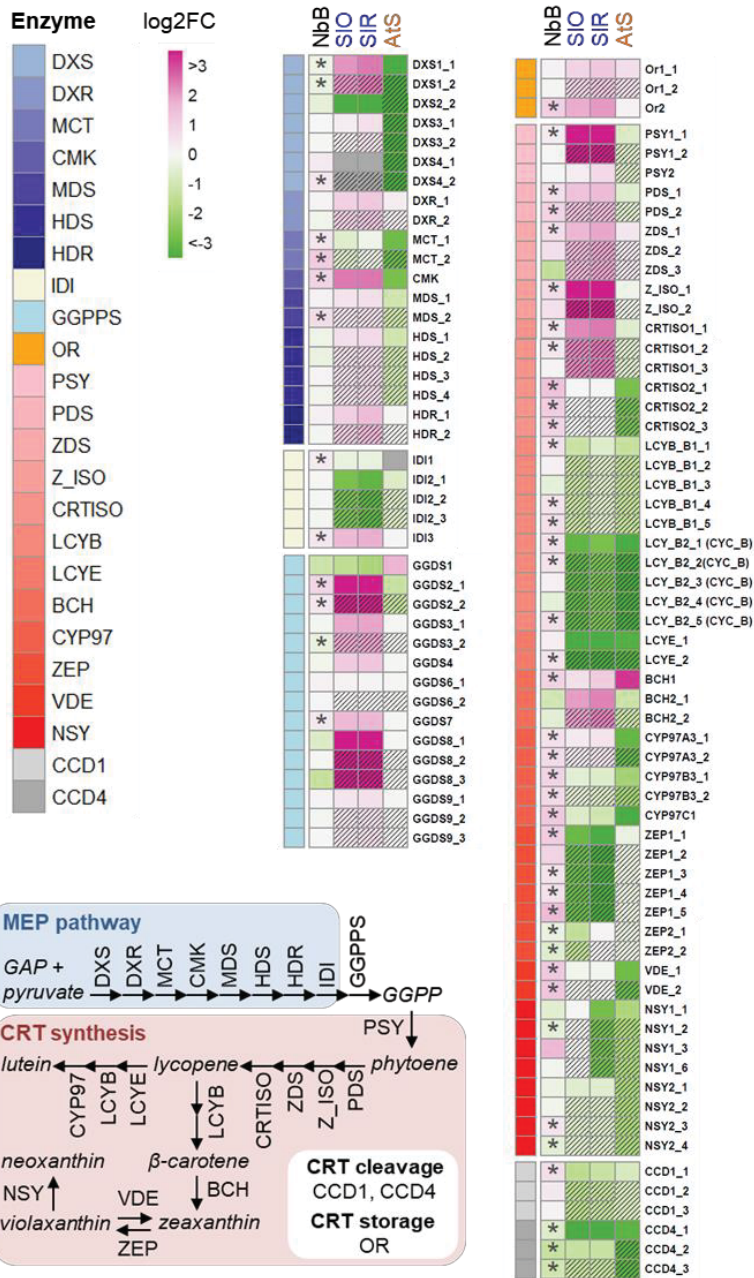


Figure S3. Level of transcripts for carotenoid-related proteins. Heatmap represents log₂FC values in *N. benthamiana* leaves 4 days after agroinfiltration with (p)crbB compared to GFP (lane NbB). Data publicly available from tomato fruit (light ripe vs. mature green, SIO, and red ripe vs. mature green, SIR) and Arabidopsis leaves (senescent -30D- vs. controls -16D-, AtS) are also shown. The position of enzymes in pathways and/or the biological function of the proteins selected are indicated in the cartoon and represented by colors. Stripped cells mark missing isogenes and their colors correspond to the closest homolog in the genome. Asterisks mark differentially expressed genes in the NbB lane (DESeq2, FDR ≤ 0.05).

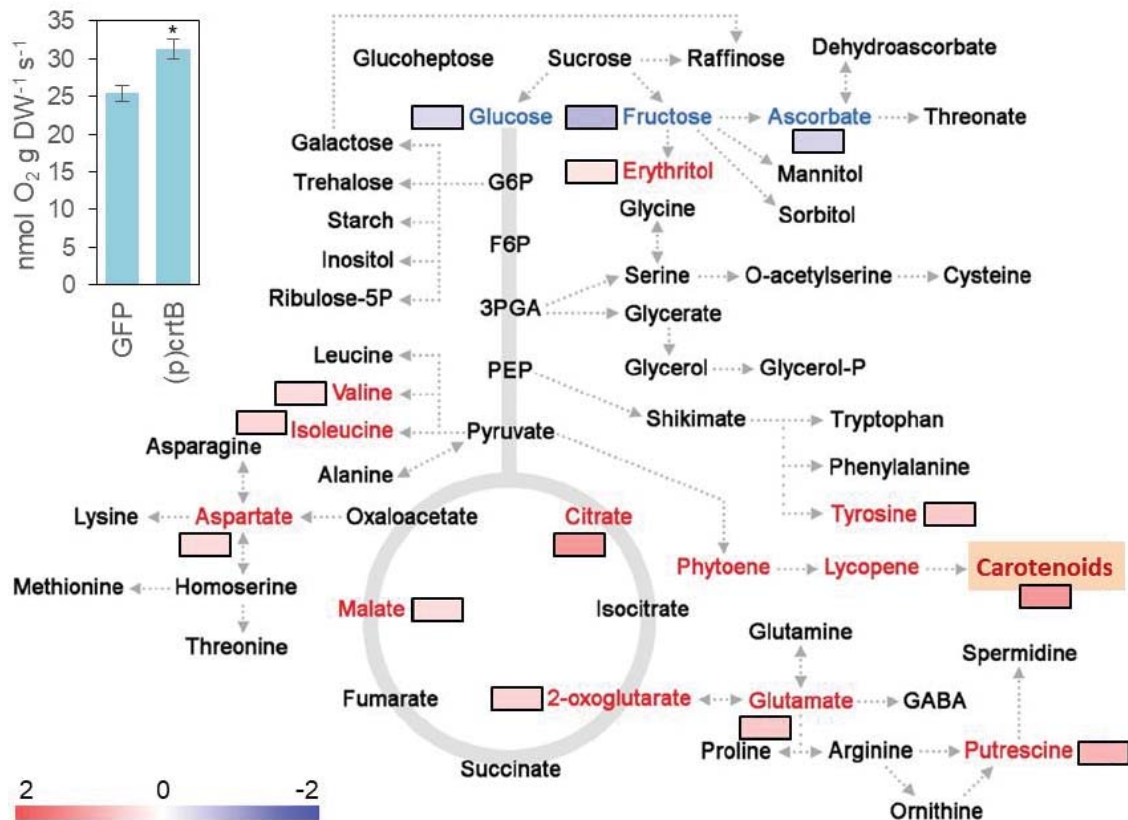


Figure S4. Chromoplast differentiation induces glycolytic and oxidative energy metabolism. Heatmap represents statistically significant FC (fold-change) values of metabolite levels in *N. benthamiana* leaves 4 days after agroinfiltration with (p)crtB relative to those in GFP controls. Inset represents respiration rates. Mean and standard deviation values of $n = 3$ independent samples are shown. Asterisk represents statistical significance (t test, $P < 0.05$).

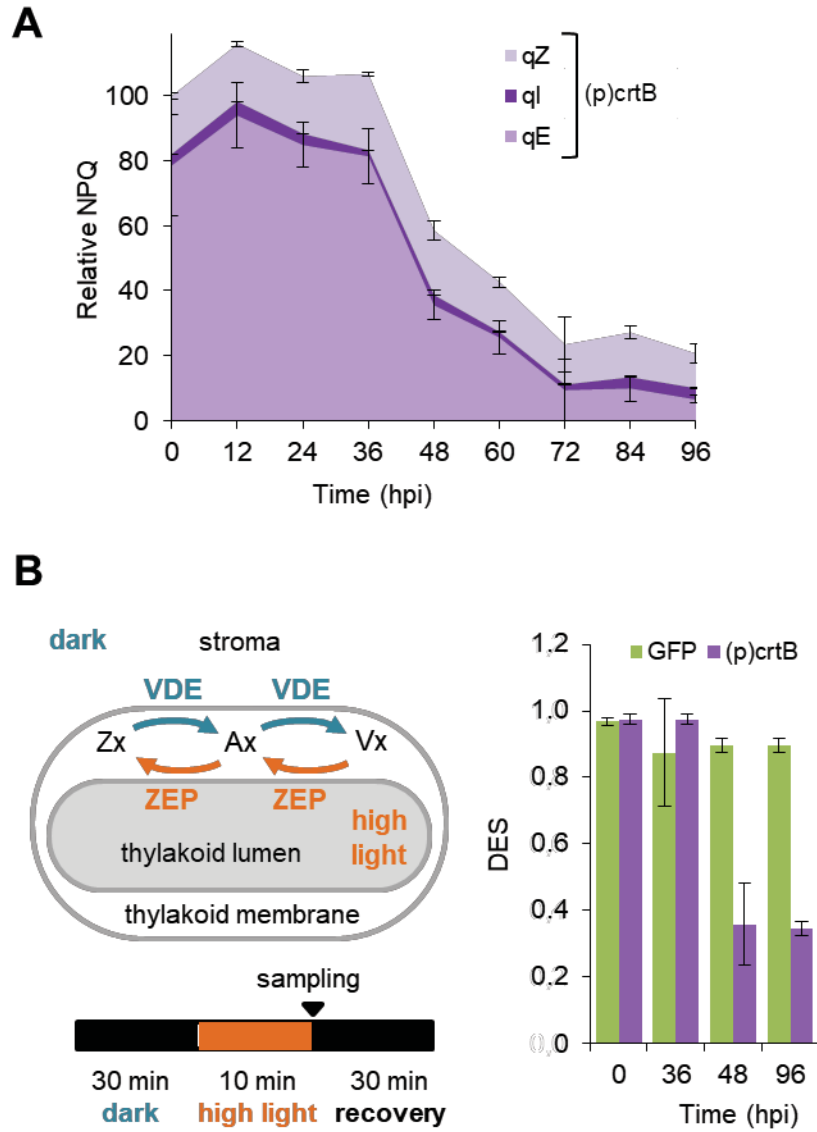


Figure S5. Chromoplast differentiation in leaves reduces NPQ and impairs the xanthophyll cycle. A, Non-photochemical quenching (NPQ) components in *N. benthamiana* leaf sections agroinfiltrated with (p)crtB. B, Leaves producing GFP or (p)crtB were treated as shown in the left panel and then collected to quantify their carotenoid levels. De-epoxidation state (DES) was calculated as $(Zx+0.5 \times Ax)/(Zx+Ax+Vx)$, where Zx, Ax and Vx are the concentrations of zeaxanthin, antheraxanthin, and violaxanthin, respectively.

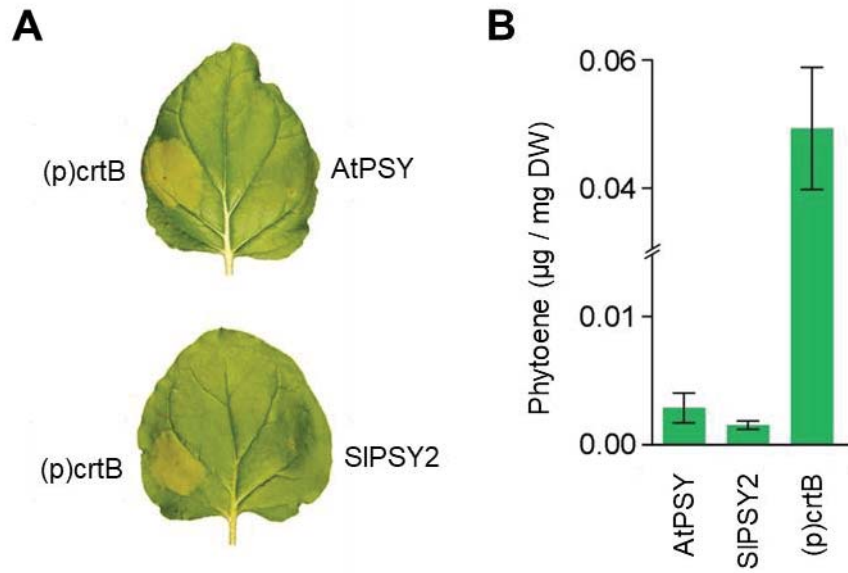


Figure S6. Plant PSY enzymes do not induce chromoplast differentiation in leaves. A, Phenotypes of *N. benthamiana* leaf sections producing the indicated proteins at 96 hpi. B, Phytoene content in the leaf sections shown in A.

SI Tables

Table S1. Relative metabolite levels in *N. benthamiana* leaf sections infiltrated with GFP and (p)crtB constructs. Data is presented as means \pm SE of five to six biological replicates normalized to the mean level of the control GFP samples.

Metabolite	GFP	crtB	Metabolite	GFP	crtB
Pyruvate	1 \pm 0.09	1.05 \pm 0.04	2-oxo-Glutarate	1 \pm 0.13	1.42 \pm 0.11
Valine	1 \pm 0.08	1.33 \pm 0.03	Fucose	1 \pm 0.08	1.19 \pm 0.06
Glycerol	1 \pm 0.10	0.8 \pm 0.12	Phenylalanine	1 \pm 0.10	1.03 \pm 0.08
Isoleucine	1 \pm 0.11	1.38 \pm 0.1	Asparagine	1 \pm 0.16	1.43 \pm 0.18
Glycine	1 \pm 0.34	0.88 \pm 0.2	3-deoxy-Glucosone	1 \pm 0.08	0.87 \pm 0.04
Phosphoric acid	1 \pm 0.08	1.2 \pm 0.08	Glycerol-3-P	1 \pm 0.10	0.89 \pm 0.08
Proline	1 \pm 0.18	1.04 \pm 0.26	Lysine	1 \pm 0.15	0.99 \pm 0.05
GABA	1 \pm 0.16	0.68 \pm 0.1	Dehydroascorbate	1 \pm 0.11	0.7 \pm 0.08
Alanine	1 \pm 0.15	1.41 \pm 0.49	Tyramine	1 \pm 0.08	1.02 \pm 0.05
Serine	1 \pm 0.14	1.01 \pm 0.11	Ascorbate	1 \pm 0.02	0.77 \pm 0.07
Succinate	1 \pm 0.10	1.1 \pm 0.11	myo-Inositol	1 \pm 0.07	0.83 \pm 0.1
Threonine	1 \pm 0.06	1.24 \pm 0.11	Tyrosine	1 \pm 0.13	1.53 \pm 0.15
Fumarate	1 \pm 0.11	0.85 \pm 0.07	trans-Caffeate	1 \pm 0.32	1.44 \pm 0.06
Maleate	1 \pm 0.12	1.28 \pm 0.12	Glucose-6-P	1 \pm 0.06	1.1 \pm 0.04
Nicotinate	1 \pm 0.07	1.08 \pm 0.1	Tryptophan	1 \pm 0.28	2.1 \pm 0.51
beta-alanine	1 \pm 0.07	1.22 \pm 0.08	Maltose	1 \pm 0.10	0.92 \pm 0.09
Erythritol	1 \pm 0.02	1.24 \pm 0.03	Trehalose	1 \pm 0.09	0.95 \pm 0.07
2-methyl-Malate	1 \pm 0.04	1.09 \pm 0.04	Glycerate	1 \pm 0.16	0.72 \pm 0.11
Aspartate	1 \pm 0.03	1.35 \pm 0.02	Malate	1 \pm 0.09	1.33 \pm 0.1
Methionine	1 \pm 0.14	1.03 \pm 0.12	Threonate	1 \pm 0.11	1.24 \pm 0.09
Ornithine	1 \pm 0.18	0.91 \pm 0.06	Sucrose	1 \pm 0.11	1.14 \pm 0.06
Glutamine	1 \pm 0.21	1.66 \pm 0.7	Quinic acid, 3-caffeoyl-, cis-	1 \pm 0.07	1.07 \pm 0.07
Xylose	1 \pm 0.09	1.13 \pm 0.04	Quinic acid, 3-caffeoyl-, trans-	1 \pm 0.08	1.02 \pm 0.06
Glutamate	1 \pm 0.15	1.55 \pm 0.17	Fructose	1 \pm 0.10	0.56 \pm 0.04
Rhamnose	1 \pm 0.07	1.17 \pm 0.05	Glucose	1 \pm 0.06	0.74 \pm 0.07
Putrescine	1 \pm 0.11	1.81 \pm 0.12	Citrate	1 \pm 0.09	2.28 \pm 0.31

Table S2. Primers used in this work.

Name	Sequence
PacrtB_N-tag_attB1-F	5'-GGGGACAAGTTTGTACAAAAAAGCAGGCTGGATGAATAATCCGTCGTTACTCAATC-3'
PacrtB_C-tag_attB2-R	5'-GGGGACCACTTTGTACAAGAAAGCTGGGTCTAGAGCGGGCGCTGCCAGAGATG-3'
PacrtB_STOP_attB2-R	5'-GGGGACCACTTTGTACAAGAAAGCTGGGTCTAGAGCGGGCGCTGCCAGAGATG-3'
AtHDS_N-tag_attB1-F	5'-GGGGACAAGTTTGTACAAAAAAGCAGGCTTCATGGCGACTGGAGTATTGCCAGCTC-3'
crtB-5'-AtHDS-3'-R	5'-GATTGAGTAACGACGGATTATTCATATCCGGATAACCGAAACTCTTCTC-3'
AtPSY_N-tag_attB1-F	5'-GGGGACAAGTTTGTACAAAAAAGCAGGCTTCATGTCAAGCTTAGTAGCAAGTCCTTC-3'
AtPSY_STOP_attB2-R	5'-GGGGACCACTTTGTACAAGAAAGCTGGGTTCATATCGATAGTCTTGAAGTTGAAG-3'
SIPSY2_N-tag_attB1-F	5'-GGGGACAAGTTTGTACAAAAAAGCAGGCTATGTCTGTTGCTTTGTTGTGGGTTG-3'
SIPSY2_STOP_attB2-R	5'-GGGGACCACTTTGTACAAGAAAGCTGGGTTCATGTCTTTGCTAGTGGGGAAGAAG-3'
PacrtE_N-tag_attB1-F	5'-GGGGACAAGTTTGTACAAAAAAGCAGGCTGGATGACGGTCTGCGCAAAAAACAC-3'
PacrtE_STOP_attB2-R	5'-GGGGACCACTTTGTACAAGAAAGCTGGGTTTATACTGACGGCAGCGAGTTTTTGTGTC-3'
TuMV-crtB-flank-5'	5'-GCAGGAGAA-3'
TuMV-crtB-flank-3'	5'-GCTGAAGCTTGCGTTTACCACCAA-3'
LMV-crtB-flank-5'	5'-GTGGACACA-3'
LMV-crtB-flank-3'	5'-GACATGGACGAAGTTTATCACCAA-3'
crtB_qPCR-F	5'-TATTGCTCGCGATATTGTGG-3'
crtB_qPCR-R	5'-TTTCAGGTGCCGCATAATTC-3'
ACT_qPCR-F	5'-TAAGGTTGTTGCACCACCAG-3'
ACT_qPCR-R	5'-ACATCTGCTGGAATGTGCTG-3'

SI References

1. E. Majer, B. Llorente, M. Rodriguez-Concepcion, J. A. Daros, Rewiring carotenoid biosynthesis in plants using a viral vector. *Scientific reports* **7**, 41645 (2017).
2. T. Berges, Guyonnet, D., Karst, F., The *Saccharomyces cerevisiae* mevalonate diphosphate decarboxylase is essential for viability, and a single Leu-to-Pro mutation in a conserved sequence leads to thermosensitivity. *J Bacteriol* **179(15)**, 4664-4670 (1997).
3. T. Cordero *et al.*, Dicer-Like 4 Is Involved in Restricting the Systemic Movement of Zucchini yellow mosaic virus in *Nicotiana benthamiana*. *Molecular plant-microbe interactions : MPMI* **30**, 63-71 (2017).
4. E. Gas, U. Flores-Perez, S. Sauret-Gueto, M. Rodriguez-Concepcion, Hunting for plant nitric oxide synthase provides new evidence of a central role for plastids in nitric oxide metabolism. *The Plant cell* **21**, 18-23 (2009).
5. T. Nakagawa *et al.*, Improved Gateway binary vectors: high-performance vectors for creation of fusion constructs in transgenic analysis of plants. *Bioscience, biotechnology, and biochemistry* **71**, 2095-2100 (2007).
6. A. Bombarely *et al.*, A draft genome sequence of *Nicotiana benthamiana* to enhance molecular plant-microbe biology research. *Mol. Plant Microbe Interact.* **25**, 1523-1530 (2012).
7. J. Lisec, N. Schauer, J. Kopka, L. Willmitzer, A. R. Fernie, Gas chromatography mass spectrometry-based metabolite profiling in plants. *Nature protocols* **1**, 387-396 (2006).
8. A. R. Fernie *et al.*, Recommendations for reporting metabolite data. *The Plant cell* **23**, 2477-2482 (2011).
9. J. E. Coate, A. F. Powell, T. G. Owens, J. J. Doyle, Transgressive physiological and transcriptomic responses to light stress in allopolyploid *Glycine dolichocarpa* (Leguminosae). *Heredity* **110**, 160-170 (2013).

SI Datasets

Dataset S1 (separate file). Genes UP-REGULATED and DOWN-REGULATED in (p)crtB vs GFP agroinfiltrated leaves of *N. benthamiana* collected at 96 hpi (DESeq2, $\log_2FC \geq 0.585$, FDR ≤ 0.05).

Dataset S2 (separate file). Parametric Analysis of Gene Set Enrichment (PAGE) by AgriGO. p value ≤ 0.05 ; q value ≤ 0.05

Dataset S3 (separate file). Expression values (\log_2FC) of carotenoid-related genes.

Dataset S4 (separate file). Metabolite Reporting (Checklist and Overview)

Annex II

Photoreceptor activity contributes to contrasting responses to shade in *Cardamine* and *Arabidopsis* seedlings.

Molina-Contreras, M.J., Paulisic, S., Then, C., Moreno-Romero, J., Pastor-Andreu, P., **Morelli, L.**,
Roig Villanova, I., Jenkins, H., Hallab, A., Gan, X., Gomez-Cadenas, A., Tsiantis, M., Rodríguez-
Concepción, M., Martínez-García, J.F.

The PhD candidate contributed with his work to the following datasets:

Figure S1B



Synthetic conversion of leaf chloroplasts into carotenoid-rich plastids reveals mechanistic basis of natural chromoplast development

Briardo Llorente^{a,b,c,1}, Salvador Torres-Montilla^a, Luca Morelli^a, Igor Florez-Sarasa^a, José Tomás Matus^{a,d}, Miguel Ezquerro^a, Lucio D'Andrea^{a,e}, Fakhreddine Houhou^f, Eszter Majer^f, Belén Picó^g, Jaime Cebolla^g, Adrian Troncoso^h, Alisdair R. Fernie^e, José-Antonio Daròs^f, and Manuel Rodríguez-Concepción^{a,f,1}

^aCentre for Research in Agricultural Genomics (CRAG) CSIC-IRTA-UAB-UB, Campus UAB Bellaterra, 08193 Barcelona, Spain; ^bARC Center of Excellence in Synthetic Biology, Department of Molecular Sciences, Macquarie University, Sydney NSW 2109, Australia; ^cCSIRO Synthetic Biology Future Science Platform, Sydney NSW 2109, Australia; ^dInstitute for Integrative Systems Biology (I2SysBio), Universitat de València-CSIC, 46908 Paterna, Valencia, Spain; ^eMax-Planck-Institut für Molekulare Pflanzenphysiologie, 14476 Potsdam-Golm, Germany; ^fInstituto de Biología Molecular y Celular de Plantas, CSIC-Universitat Politècnica de València, 46022 Valencia, Spain; ^gInstituto de Conservación y Mejora de la Agrodiversidad, Universitat Politècnica de València, 46022 Valencia, Spain; and ^hSorbonne Universités, Université de Technologie de Compiègne, Génie Enzymatique et Cellulaire, UMR-CNRS 7025, CS 60319, 60203 Compiègne Cedex, France

Edited by Krishna K. Niyogi, University of California, Berkeley, CA, and approved July 29, 2020 (received for review March 9, 2020)

Plastids, the defining organelles of plant cells, undergo physiological and morphological changes to fulfill distinct biological functions. In particular, the differentiation of chloroplasts into chromoplasts results in an enhanced storage capacity for carotenoids with industrial and nutritional value such as beta-carotene (provitamin A). Here, we show that synthetically inducing a burst in the production of phytoene, the first committed intermediate of the carotenoid pathway, elicits an artificial chloroplast-to-chromoplast differentiation in leaves. Phytoene overproduction initially interferes with photosynthesis, acting as a metabolic threshold switch mechanism that weakens chloroplast identity. In a second stage, phytoene conversion into downstream carotenoids is required for the differentiation of chromoplasts, a process that involves a concurrent reprogramming of nuclear gene expression and plastid morphology for improved carotenoid storage. We hence demonstrate that loss of photosynthetic competence and enhanced production of carotenoids are not just consequences but requirements for chloroplasts to differentiate into chromoplasts.

carotenoid | chromoplast | differentiation | phytoene | synthetic

Plastids comprise a group of morphologically and functionally diverse plant organelles capable of differentiating from one plastid type to another in response to developmental and environmental stimuli (1, 2). Such plastidial conversions are essential to sustain many fundamental biological processes and largely contribute to cell specialization in the different plant tissues. Among the different plastid types, chromoplasts are of great importance in nature and agriculture because of their capacity to accumulate high levels of carotenoids, plant pigments of isoprenoid nature that provide color in the yellow to red range (3–5). Carotenoids such as beta-carotene (provitamin A) are health-promoting nutrients that animals cannot synthesize but take up in their diets. They are also added-value compounds widely used in cosmetics, pharma, food, and feed industries as natural pigments and phytonutrients (4, 6).

Chromoplasts differentiate from preexisting plastids such as proplastids (i.e., undifferentiated plastids), leucoplasts (i.e., uncolored plastids in nonphotosynthetic tissues), and chloroplasts (i.e., photosynthetic plastids). Chloroplasts transform into chromoplasts during the development of many flowers and fruits, but only a few plant species differentiate chromoplasts in leaves (1, 5). The yellow to red colors that some leaves acquire as they senesce (e.g., in the autumn or when they are exposed to continuous darkness) are due to chloroplast carotenoids becoming visible when the chlorophylls degrade. This senescence process, however, does not involve the transformation of chloroplasts into

chromoplasts but into a completely different type of plastids named gerontoplasts (1, 2).

The most prominent changes during chloroplast-to-chromoplast differentiation are the reorganization of the internal plastid structures, together with a concurrent loss of photosynthetic competence and overaccumulation of carotenoid pigments (1–3, 5, 7, 8). The remodeling of the internal plastid structures generates an increased metabolic sink capacity but it also promotes carotenoid biosynthesis. The control of chromoplast differentiation appears as a very promising strategy for improving the nutritional and health benefits of crops (5–9). The overall process is known to involve changes in gene expression (e.g., via retrograde signaling from plastids to the nucleus), hormonal regulation, protein quality control, and plastid protein import (1, 3, 5). However, very few inducers of chromoplast development have been identified to date. Orange (OR) chaperones are among the best characterized,

Significance

Carotenoids are natural pigments whose properties as provitamin A and health-promoting phytonutrients make them ideal targets for biofortification. Here, we show that plastids specialized in carotenoid overaccumulation named chromoplasts can be synthetically produced in plant tissues that do not naturally develop them. We further demonstrate that differentiation of chromoplasts from leaf chloroplasts not just causes but requires both a reduction in photosynthetic activity and a stimulation of carotenoid biosynthesis in a process hardwired to a major reprogramming of global gene expression and cell metabolism. The synthetic system that we report here should allow to boost the nutritional quality of green vegetables and forage crops once their photosynthetic activity is dispensable (e.g., just before harvesting).

Author contributions: B.L., S.T.-M., L.M., I.F.-S., E.M., J.-A.D., and M.R.-C. designed research; B.L., S.T.-M., L.M., I.F.-S., J.T.M., M.E., L.D., F.H., E.M., B.P., J.C., and A.T. performed research; B.L., S.T.-M., L.M., I.F.-S., J.T.M., M.E., B.P., J.C., A.T., A.R.F., J.-A.D., and M.R.-C. contributed new reagents/analytic tools; B.L., S.T.-M., L.M., I.F.-S., J.T.M., M.E., L.D., F.H., E.M., B.P., J.C., A.T., A.R.F., J.-A.D., and M.R.-C. analyzed data; and B.L. and M.R.-C. wrote the paper.

The authors declare no competing interest.

This article is a PNAS Direct Submission.

Published under the PNAS license.

¹To whom correspondence may be addressed. Email: briardo.llorente@mq.edu.au or manuelrc@ibmcp.upv.es.

This article contains supporting information online at <https://www.pnas.org/lookup/suppl/doi:10.1073/pnas.2004405117/-DCSupplemental>.

First published August 19, 2020.



Photoreceptor Activity Contributes to Contrasting Responses to Shade in Cardamine and Arabidopsis Seedlings

Maria Jose Molina-Contreras,^{a,1} Sandi Paulišić,^{a,1} Christiane Then,^{a,1,2} Jordi Moreno-Romero,^a Pedro Pastor-Andreu,^a Luca Morelli,^a Irma Roig-Villanova,^{a,3} Huw Jenkins,^b Asis Hallab,^{c,4} Xiangchao Gan,^c Aurelio Gomez-Cadenas,^d Miltos Tsiantis,^c Manuel Rodríguez-Concepción,^a and Jaime F. Martínez-García^{a,e,5}

^aCentre for Research in Agricultural Genomics, Consejo Superior de Investigaciones Científicas -Institut de Recerca i Tecnologies Agroalimentaries - Universitat Autònoma de Barcelona - Universitat de Barcelona, 08193 Barcelona, Spain

^bDepartment of Plant Sciences, University of Oxford, Oxford OX1 3BR, United Kingdom

^cDepartment of Comparative Development and Genetics, Max Planck Institute for Plant Breeding Research, 50829 Cologne, Germany

^dDepartament de Ciències Agràries i del Medi Natural, Universitat Jaume I, 12071 Castello de la Plana, Spain

^eInstitució Catalana de Recerca i Estudis Avançats, 08010 Barcelona, Spain

ORCID IDs: 0000-0002-1474-4436 (M.J.M.-C.); 0000-0003-4696-5134 (S.P.); 0000-0001-8867-7080 (C.T.); 0000-0002-7352-1507 (J.M.-R.); 0000-0001-6320-0569 (P.P.-A.); 0000-0002-9968-0012 (L.M.); 0000-0001-9124-0429 (I.R.-V.); 0000-0003-2189-515X (H.J.); 0000-0002-2421-5431 (A.H.); 0000-0001-6398-5191 (X.G.); 0000-0002-4598-2664 (A.G.-C.); 0000-0001-7150-1855 (M.T.); 0000-0002-1280-2305 (M.R.-C.); 0000-0003-1516-0341 (J.F.M.-G.).

Plants have evolved two major ways to deal with nearby vegetation or shade: avoidance and tolerance. Moreover, some plants respond to shade in different ways; for example, Arabidopsis (*Arabidopsis thaliana*) undergoes an avoidance response to shade produced by vegetation, but its close relative *Cardamine hirsuta* tolerates shade. How plants adopt opposite strategies to respond to the same environmental challenge is unknown. Here, using a genetic strategy, we identified the *C. hirsuta slender in shade1* mutants, which produce strongly elongated hypocotyls in response to shade. These mutants lack the phytochrome A (*phyA*) photoreceptor. Our findings suggest that *C. hirsuta* has evolved a highly efficient *phyA*-dependent pathway that suppresses hypocotyl elongation when challenged by shade from nearby vegetation. This suppression relies, at least in part, on stronger *phyA* activity in *C. hirsuta*; this is achieved by increased *ChPHYA* expression and protein accumulation combined with a stronger specific intrinsic repressor activity. We suggest that modulation of photoreceptor activity is a powerful mechanism in nature to achieve physiological variation (shade tolerance versus avoidance) for species to colonize different habitats.

INTRODUCTION

Understanding how plants colonize different habitats requires identifying the genetic differences underlying physiological variation between species. In this work, we focus on angiosperm responses to changes in light produced by nearby vegetation, perception of which alerts the plant to potential resource competition by other plants. Nearby vegetation is perceived as changes in light parameters: whereas sunlight has a high red light (R) to far-red light (FR) ratio (R:FR > 1.1), proximity to vegetation

lowers this ratio (Smith, 1982). Because vegetation specifically reflects FR, proximity to other plants initially results in a mild reduction in R:FR (<0.7) due to the FR enrichment. Eventually, when the vegetation canopy closes, sunlight is filtered by photosynthetic tissues, strongly reducing the intensity of the PAR (400–700 nm, which includes blue and R) while marginally affecting FR. As a result, R:FR resulting from natural canopy shade typically drops to lower values (<0.05; Smith, 1982; Casal, 2012; Martínez-García et al., 2014; de Wit et al., 2016). In the laboratory, both vegetation proximity and canopy shade can be simulated by providing plants grown under white light (W; high R:FR) varying amounts of supplemental FR (W+FR; low or very low R:FR) while maintaining total PAR, a treatment known as simulated shade (Casal, 2012; Roig-Villanova and Martínez-García, 2016).

Plants have two main strategies to acclimate to vegetation proximity and shade: avoidance or tolerance. In the early stages of development, shade-avoider species invest energy into promoting elongation to overgrow their neighbors as part of the so-called shade avoidance syndrome (SAS). By contrast, shade-tolerant plants adopt other physiological and metabolic responses to adapt to a highly conservative utilization of resources, commonly accompanied by very low growth rates (i.e., do not involve promotion of elongation growth; Smith, 1982; Valladares and Niinemets, 2008).

¹ These authors contributed equally to this work.

² Current address: Institute for Epidemiology and Pathogen Diagnostics, Julius Kühn-Institut, Federal Research Institute for Cultivated Plants, 38104 Braunschweig, Germany.

³ Current address: Escola Superior d'Agricultura de Barcelona, Universitat Politècnica de Catalunya, Campus Baix Llobregat, Castelldefels, 08860 Barcelona, Spain.

⁴ Current address: IBG-2 Plant Sciences, Forschungszentrum Jülich, 52428 Jülich, Germany.

⁵ Address correspondence to jaume.martinez@cragenomica.es.

The author responsible for distribution of materials integral to the findings presented in this article in accordance with the policy described in the Instructions for Authors (www.plantcell.org) is: Jaime F. Martínez-García (jaume.martinez@cragenomica.es).

www.plantcell.org/cgi/doi/10.1105/tpc.19.00275

IN A NUTSHELL

Background: Plant development is strongly influenced by the proximity of other plants, as neighboring vegetation might shade and reduce light availability. Not enough light may compromise photosynthesis and hence plant growth. The so-called shade-avoiding species respond to vegetation proximity by trying to escape it. These responses include increased elongation (to overgrow neighboring competitors for light), reduced levels of photosynthetic pigments (to adjust photosynthesis to the available light) or flowering induction (to ensure a next generation). This is the case in *Arabidopsis thaliana*, in which exposure to plant shade leads to shade-avoidance responses. Those plants growing in forest understories or next to other plants tolerate and do not elongate in response to neighboring vegetation. One of these species is *Cardamine hirsuta*, whose hypocotyls are unresponsive to plant shade.

Question: We wondered how the elongation response is oppositely regulated in these plants. As these two species are closely related, we aimed to know if *C. hirsuta* uses the same or different components to regulate its hypocotyl elongation response to plant shade as *A. thaliana*.

Findings: Using a genetic approach, we identified *C. hirsuta* mutants with a restored ability to elongate hypocotyls in response to plant shade. We named these mutants *slender in shade 1 (sis1)*, which were deficient in the photoreceptor phytochrome A (*phyA*). Because *phyA* was already known to inhibit the shade-induced elongation of *Arabidopsis* seedlings, our results indicate that shade avoidance and tolerance in these plants have shared components to regulate this divergent response. In addition, *phyA* is more active in *Cardamine* than *Arabidopsis*, which results from a higher expression and a stronger intrinsic activity of this photoreceptor in *Cardamine* compared to *Arabidopsis*.

Next steps: Our knowledge can help attenuate plant responses to shade. As most crops are shade-avoiding species, this knowledge can result in shade-tolerant crop varieties that grow well at high planting density, maximizing land use. It can also lead to engineering shade-avoiding beneficial weeds (that provide refuge to beneficial animals or enhance soil quality) to thrive in shaded or semi-shaded areas to be used in conservation agriculture approaches.

Analyses of the shade-avoider *Arabidopsis* (*Arabidopsis thaliana*) laid the basis for our knowledge of the genetic components and mechanisms involved in the regulation of the SAS (Martínez-García et al., 2010; Casal, 2012; Roig-Villanova and Martínez-García, 2016). The shade signal is perceived by the phytochrome photoreceptors: phytochrome B (*phyB*) and *phyA* have major and antagonistic roles (respectively) in hypocotyl elongation, the most conspicuous *Arabidopsis* response to low R:FR (Mathews, 2010; Casal, 2012). Lowering the R:FR to resemble either vegetation proximity or canopy shading deactivates *phyB* in wild-type seedlings, resulting in the hypocotyl elongation promotion. By contrast, *phyA* accumulates and is strongly activated under very low R:FR to prevent excessive seedling elongation (Martínez-García et al., 2014; Yang et al., 2018). Consistent with this, *Arabidopsis* *phyB*-deficient mutants display constitutive shade responses under high R:FR, whereas *phyA* mutant seedlings show enhanced hypocotyl elongation only under very low R:FR conditions, which indicates that *phyA* antagonizes *phyB* activity under these specific canopy shade conditions (Yanovsky et al., 1995; Casal et al., 2014; Martínez-García et al., 2014; Yang et al., 2018).

SAS responses are mainly initiated because of the interaction of active phytochromes with PHYTOCHROME INTERACTING FACTORS (PIFs), eventually triggering rapid changes in the expression of dozens of genes that implement the SAS responses. Genetic analyses in *Arabidopsis* indicate that PIFs, which are basic helix-loop-helix transcription factors, have a role in positively regulating the shade-triggered hypocotyl elongation. The active form of *phyB* interacts with PIFs and inhibits their transcriptional activity (Martínez-García et al., 2010; Casal, 2012). After exposure to shade, the proportion of active *phyB* decreases and PIF activity increases. Enhanced PIF binding to G-boxes of auxin biosynthetic genes (e.g., *YUCCA* genes) then promotes their expression, which results in a rapid (1–4 h) increase in free

indole-3-acetic acid (IAA) that is required for the promotion of shade-induced hypocotyl elongation (Tao et al., 2008; Hornitschek et al., 2012; Li et al., 2012; Bou-Torrent et al., 2014). In addition, nuclear-pore complex components and chloroplast-derived signals also prevent an excessive response to shade, providing additional regulatory levels of this response (Gallemí et al., 2016; Ortiz-Alcaide et al., 2019).

There are, however, still major gaps in understanding the genetic and molecular regulation of SAS and, by extension, shade-tolerance traits. Comparative analyses using shade-avoiding and shade-tolerant species is expected to identify regulators of traits associated with shade tolerance habits (Gommers et al., 2013). Indeed, a comparative transcriptomic approach using two *Geranium* species with divergent petiole responses to shade unveiled components that might suppress growth in the shade-tolerant species (Gommers et al., 2017, 2018). The use of related species that are amenable for genetic analyses is expected to push this effort further to find regulatory components used in nature to modulate these divergent responses. This is what we are addressing in this work.

Comparing *Arabidopsis* and its close relative *Cardamine hirsuta* to understand the genetic basis for trait diversification between species is a powerful strategy to understand the evolution of morphological traits. Key to this approach is the wide morphological and physiological diversity between these species, such as differences in leaf morphology and seed dispersal mechanism among others (Barkoulas et al., 2008; Hay et al., 2014; Vlad et al., 2014; Hofhuis et al., 2016; Vuolo et al., 2016). Like *Arabidopsis*, *C. hirsuta* has a short generation time, small size, inbreeding habit, abundant progeny, and ease of large-scale cultivation (Hay et al., 2014; Hay and Tsiantis, 2016). It is a diploid species with a small genome and eight chromosomes that has been completely sequenced (Gan et al., 2016). Genetic transformation by floral

dipping, a dense genetic map, and chemically mutagenized populations provide the tools to identify the genetic components and molecular mechanisms underlying diversification or morphology and response to environment (Hay and Tsiantis, 2016). *C. hirsuta* is an invasive herbaceous plant that can grow in open sun but is often found in shaded or semishaded areas. Indeed, *C. hirsuta* does not need much light to grow, and their stems become purplish (likely to prevent oxidative damage) in strong sun (<http://edis.ifas.ufl.edu/pdffiles/EP/EP51100.pdf>; http://practicalplants.org/wiki/Cardamine_hirsuta; <http://www.asturnatura.com/especie/cardamine-hirsuta.html>; http://dnr.wi.gov/topic/Invasives/documents/classification/LR_Cardamine_hirsuta.pdf; <https://www.wildfooduk.com/edible-wild-plants/hairy-bittercress/>). These observations are consistent with *C. hirsuta* being shade-tolerant (Bealey and Robertson, 1992). In agreement, whereas seedlings of *Arabidopsis* elongate in response to shade, those of *C. hirsuta* are unresponsive to the same stimulus (Hay et al., 2014).

The divergent hypocotyl response to shade of *Arabidopsis* and *C. hirsuta* species led us to take a comparative approach to understand the genetic basis of the evolution of this physiological trait. We found that *C. hirsuta* has acquired a highly efficient phyA-dependent pathway that represses hypocotyl elongation and other SAS-associated responses when exposed to simulated shade. After complementing *Arabidopsis phyA* mutant plants with endogenous or *C. hirsuta phyA* molecules, we concluded that these two photoreceptors are not exchangeable. Differences in phyA intrinsic activity hence contribute to a different response of *C. hirsuta* and *Arabidopsis* to shade exposure.

RESULTS

C. hirsuta Seedlings Perceive Low R:FR but Do Not Elongate

A recent study revealed that different species of the *Tradescantia* genus with divergent tolerance to shade showed clear differences in maximum quantum efficiency of photosystem II (F_v/F_m) upon variations of the growth light (Benkov et al., 2019). In particular, the sun-resistant *T. sillamontana* (a succulent growing in semidesert regions of Mexico and Peru, hence adapted to high light intensities) was more tolerant to changes in irradiation intensity (i.e., showed a more constant F_v/F_m) than the shade-tolerant *T. fluminensis* (habitant of tropical rainforests and other shaded areas in southeastern Brazil and hence adapted to grow under low light intensities).

Using a similar experimental system, we aimed to confirm whether *C. hirsuta* is a shade-tolerant plant compared with *Arabidopsis* (a broadly accepted shade-avoider). Indeed, when wild-type seedlings of these two species (Ch^{WT} and At^{WT}) were transferred from normal W to conditions in which PAR was first increased 10-fold (high light [HL]) and then reduced fivefold relative to W (low light [LL]) or vice versa, F_v/F_m changes were much more pronounced in Ch^{WT} (Supplemental Figure 1A). The lower capacity of Ch^{WT} to adapt to intense irradiation was confirmed by the bleaching symptoms (e.g., lower chlorophyll contents) observed in Ch^{WT} (but not in At^{WT}) upon transferring to HL (Supplemental Figure 1B). Ch^{WT} seedlings only showed a better performance than At^{WT} when transferred from W to LL. Rapid light

curve analysis confirmed that Ch^{WT} was better able to maintain its level of photosynthetic activity under LL conditions than At^{WT} (Supplemental Figure 1C), as expected for a shade-tolerant plant (Han et al., 2015).

Besides differentially responding to decreased light quantity, plant species from open habitats show a stronger elongation response to reduced R:FR (i.e., light quality) compared with those from woodland shade habitats (Smith, 1982; Gommers et al., 2017). Further supporting the conclusion that *C. hirsuta* tolerates shade, Ch^{WT} failed to elongate their hypocotyls when exposed to a range of low R:FR treatments (i.e., W+FR) that mimic vegetation proximity (intermediate or low R:FR; 0.09–0.07) and canopy shade (very low R:FR; 0.02; Figure 1; Supplemental Figure 2). W-grown Ch^{WT} hypocotyls, as well as cotyledons, are substantially longer than those of At^{WT} growing under the same conditions. Ch^{WT} hypocotyls were also longer than those of At^{WT} when growing in the dark (Figure 1C), indicating that *C. hirsuta* is overall bigger than *Arabidopsis*. More importantly, when treated with growth stimulants, such as gibberellic acid (Hay et al., 2014) or picloram (a synthetic auxin), hypocotyls of both species elongate (Figure 1D). We therefore concluded that the elongation of *C. hirsuta* hypocotyls is not generally compromised, arguing against the possibility that this species displays a constitutive SAS phenotype.

In *Arabidopsis*, exposure to simulated shade also triggers the elongation of leaf petioles. We quantified the elongation response of the petiole and rachis in 2-week-old Ch^{WT} and At^{WT} plants subjected to 7 d of high (W) or low (W+FR) R:FR. In agreement with previous studies (Kozuka et al., 2010; Sasidharan et al., 2010; de Wit et al., 2015), shade-treated At^{WT} leaves showed substantially longer petioles than those of plants grown under W. Petiole and rachis length in Ch^{WT} , however, was similar in leaves from plants grown under W or W+FR (Figure 1E; Supplemental Figure 3). These results together suggest that elongation responses to low R:FR are dramatically arrested in *C. hirsuta* plants.

C. hirsuta Shows Other Attenuated Responses to Shade

Beyond elongation responses, low R:FR triggers a reduction in the levels of photosynthetic pigments (i.e., carotenoids and chlorophylls; Roig-Villanova et al., 2007; Cagnola et al., 2012; Bou-Torrent et al., 2015). While these pigments were also significantly reduced in shade-treated Ch^{WT} seedlings (Figure 1F), the decrease was less prominent than in At^{WT} . These results indicated that not all SAS responses are equally compromised in *C. hirsuta*.

We next used RNA sequencing (RNA-seq) to compare the genome-wide expression patterns of 7-d-old At^{WT} and Ch^{WT} whole seedlings in W versus 1 h of simulated shade (W+FR; Figure 2). Incorporating knowledge about gene orthology, 432 differentially expressed genes (DEGs) were categorized as rapidly regulated by shade in one species or in both. Plotting the W+FR versus W fold change in *C. hirsuta* against the same ratio in *Arabidopsis* resulted in a linear regression equation with a slope of 0.54 (Figure 2B), which supported that shade-modulated changes in gene expression are also attenuated in *C. hirsuta* compared with *Arabidopsis*. In *Arabidopsis*, shade treatment induced 246 genes (fold change > 1.5, $P < 0.05$) and repressed 58 genes (fold change ≤ 1.5 , $P < 0.05$). In *C. hirsuta*, this same treatment induced 181 genes and repressed 54 genes (Supplemental Figure 4A;

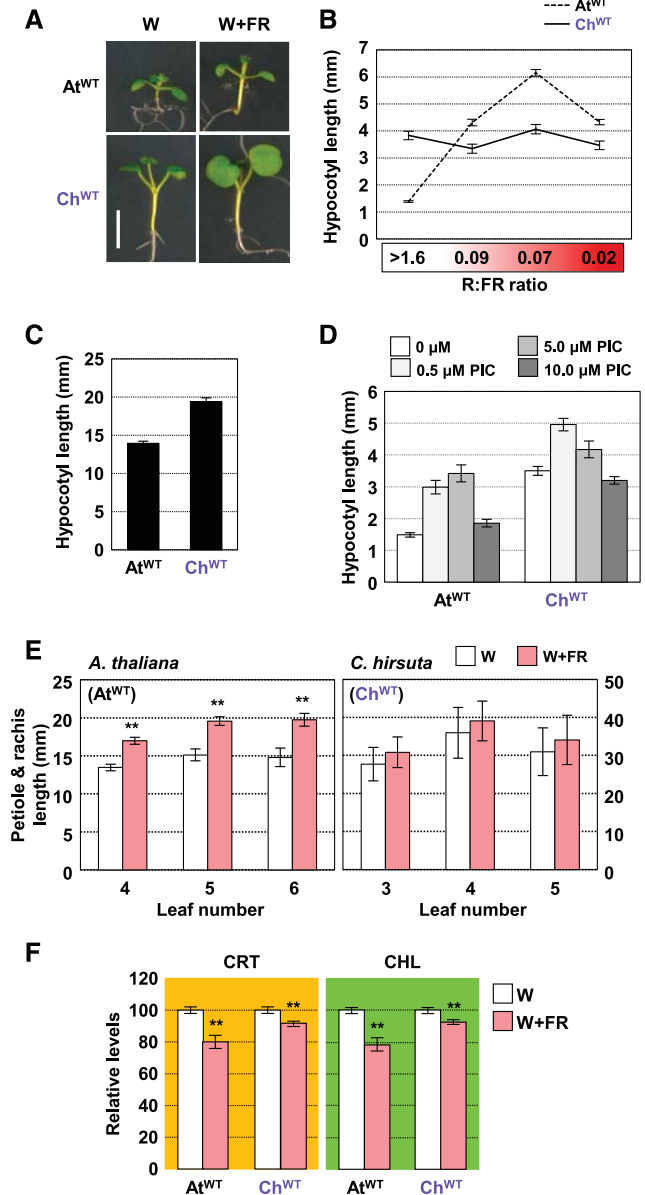


Figure 1. Arabidopsis and *C. hirsuta* Differ in the Hypocotyl Elongation Response to Neighboring Vegetation.

(A) Phenotype of representative seedlings of *At*^{WT} and *Ch*^{WT} after 3 d grown in W and retained in W (left panels) or transferred to W+FR (R:FR of 0.02; right panels) until day 7. Bar = 5 mm.
 (B) Hypocotyl length of day-7 *At*^{WT} and *Ch*^{WT} seedlings grown for the last 4 d under the indicated R:FR.
 (C) Hypocotyl length of day-4 *At*^{WT} and *Ch*^{WT} seedlings grown in darkness.
 (D) Hypocotyl length of day-7 *At*^{WT} and *Ch*^{WT} seedlings grown under W in medium supplemented with increasing concentrations of picloram (PIC).
 (E) Petiole and rachis length of 3-week-old leaves of *At*^{WT} and *Ch*^{WT} plants grown for the last 7 d under the indicated R:FR.
 (F) Carotenoid (CRT) and chlorophyll (CHL) levels of *At*^{WT} and *Ch*^{WT} seedlings grown in W and W+FR (as detailed in [A]). Values are means and SE of three to five independent samples. Asterisks indicate significant differences (**, *P* < 0.01) relative to W-grown plants.

Supplemental Data Sets 1 to 4). From the set of induced DEGs, 102 responded in both species. They included several of the well-known shade-marker genes in Arabidopsis and other species, such as *ARABIDOPSIS THALIANA HOMEBOX PROTEIN2 (ATHB2)*, *BRASSINOSTEROID-ENHANCED EXPRESSION1*, *BES1-INTERACTING MYC-LIKE1*, *LONG HYPOCOTYL IN FR1*, and *XYLOGLUCAN ENDOTRANSGLYCOSYLASE7* (Ueoka-Nakanishi et al., 2011; Karve et al., 2012; Cifuentes-Esquivel et al., 2013; Procko et al., 2014).

Gene Ontology (GO) and MapMan-Bin (MMB) functional prediction of these upregulated gene groups indicated that terms related to auxin were significantly overrepresented (Supplemental Data Sets 5 and 6), suggesting an early role for auxins in both

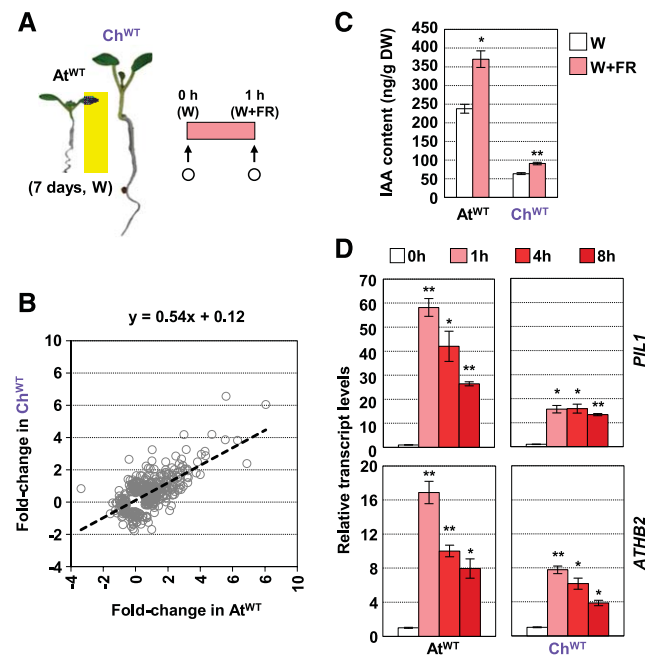


Figure 2. Arabidopsis and *C. hirsuta* Seedlings Respond to Neighboring Vegetation by Altering Gene Expression.

(A) RNA-seq was performed with RNA extracted from *At*^{WT} and *Ch*^{WT} seedlings that were grown in W for 7 d and then treated for 1 h with W+FR (R:FR = 0.02). White circles indicate the moment of harvesting for RNA extraction. Three independent biological replicates were used for each genotype and treatment.
 (B) Correlation between log-transformed fold change of 432 DEGs in *At*^{WT} and *Ch*^{WT}. The estimated regression equation is shown at the top of the graph.
 (C) IAA content in *At*^{WT} and *Ch*^{WT} seedlings grown and harvested as indicated in (A). Whole seedlings were collected and lyophilized to measure IAA levels. Data are presented as means and SE of three (*At*^{WT}) or four (*Ch*^{WT}) biological replicates. DW, dry weight.
 (D) Effects of W+FR treatment on *PIL1* and *ATHB2* expression in *At*^{WT} and *Ch*^{WT} seedlings (R:FR = 0.02). W-grown day-7 seedlings of Col-0 and Oxford were treated for 0, 1, 4, and 8 h with W+FR. Transcript abundance, normalized to EF1 α , is shown. Values are means and SE of three independent RT-qPCR biological replicates relative to values at 0 h for each species.
 In (C) and (D), asterisks indicate significant differences (**, *P* < 0.01 and *, *P* < 0.05) relative to 0-h samples.

Arabidopsis and *C. hirsuta*. Indeed, W+FR treatment for 1 h increased auxin (IAA) levels not only in *At*^{WT}, as published (Tao et al., 2008; Hornitschek et al., 2012; Bou-Torrent et al., 2014; Hersch et al., 2014), but also in whole *Ch*^{WT} seedlings (Figure 2C).

Using public transcriptomic data, we identified a group of 13 genes whose expression was induced in Arabidopsis wild-type seedlings but not in mutants that do not accumulate auxins (*shade avoidance3-2* and *pif7-1*) after 1 h of shade treatment (Tao et al., 2008; Li et al., 2012; Bou-Torrent et al., 2014). Based on our RNA-seq data, the expression of these genes was significantly upregulated in *At*^{WT} and, to a lower extent, *Ch*^{WT} seedlings (Supplemental Figure 5), consistent with the observed increase in IAA content in both species. Since only Arabidopsis elongates in response to shade exposure, either the observed early changes in gene expression and auxin levels are not reflecting the differences in hypocotyl growth between these species or the elongation is a consequence of differential later events.

In our RNA-seq analyses, 55 and 49 DEGs were specifically repressed in either *At*^{WT} or *Ch*^{WT} seedlings, respectively, and just 3 genes were repressed in both species. Regarding upregulated genes, 142 and 79 DEGs were specifically induced either in *At*^{WT} or *Ch*^{WT}, respectively (Supplemental Figure 4A). GO and MMB functional prediction of the 142 DEGs specific for *At*^{WT} showed genes related to several aspects of plant development, whereas the 79 DEGs specifically induced in *Ch*^{WT} showed enrichment for genes related to the photosynthetic machinery. Particularly, *C. hirsuta* rapidly responds by inducing the expression of genes encoding components of both PSI and PSII, the NADH dehydrogenase-like complex (involved in chlororespiration), and both small and large subunits of plastidial ribosomes (Supplemental Figure 5B; Supplemental Data Sets 5 and 6). Whether these rapid changes are maintained after prolonged exposure to shade or have any functional relevance is unknown. Nonetheless, these transcriptome differences support that the two mustard species employ alternative strategies to adapt to plant proximity and shade that go further from the modulation of elongation growth.

Comparative approaches have been used before to investigate the differential responses to shade of related species. Transcriptomic analyses using two *Geranium* species that display divergent shade-induced petiole elongation (*G. pyrenaicum* as a shade avoider or responsive and *G. robertianum* as a shade tolerant) identified a series of 31 upregulated genes that included a number of candidate regulators of differential shade avoidance (Gommers et al., 2017). In these two species, putatively orthologous transcript groups (OMCL) were defined, and the best BLAST hit with the Arabidopsis transcriptome was used to name *Geranium* OMCL groups (Gommers et al., 2017). When we compared our lists of shade-regulated genes with the *Geranium* OMCLs differentially regulated after 2 h of low R:FR in the petioles, we found that the number of genes upregulated in both shade-tolerant and shade-avoider species was higher for the *At*^{WT}/*Ch*^{WT} pair than between the *Geranium* species (Supplemental Figure 4C; Supplemental Data Sets 7 and 8). GO analyses did not identify any function from the lists of genes specifically induced in either *G. pyrenaicum* or *G. robertianum*. Overlap was very limited between the sets of repressed genes. Together, the contrasting rapid shade-induced gene expression changes might either support

differences in the early molecular mechanisms between the *Geranium* and mustard groups or just reflect the differences in tissues (whole seedlings versus leaf petioles) and/or shade and growth conditions (continuous light versus photoperiod) between experiments.

We also analyzed the changes in gene expression of *PIF3-LIKE1* (*PIL1*) and *ATHB2*, two typical shade-marker genes, in response to longer (up to 8 h) exposure to low R:FR. Expression of *PIL1* and *ATHB2* was rapidly induced in both mustard seedlings after simulated shade exposure. However, the relative induction of the expression of these genes was attenuated in *Ch*^{WT} compared with *At*^{WT} (Figure 2D). Together, our results indicate that *C. hirsuta* seedlings sense plant proximity and respond molecularly and metabolically to it; however, this signal does not promote hypocotyl elongation in *C. hirsuta* as it does in the shade-avoider Arabidopsis.

Shade-Induced Elongation in *C. hirsuta* Is Repressed

To explain the hypocotyl elongation differences between Arabidopsis and *C. hirsuta*, we hypothesized two mutually exclusive mechanisms: (1) uncoupling: shade perception is specifically unplugged from the endogenous mechanisms of control of hypocotyl elongation; and (2) suppression: there are mechanisms that strongly suppress the shade-induced elongation of hypocotyls. To distinguish between these possibilities, a genetic screening looking for *C. hirsuta* seedlings with long hypocotyls under simulated shade (>6 mm long) was performed, using an ethyl methane sulfonate-mutagenized population (Vlad et al., 2014). If suppression mechanisms exist, then loss-of-function mutants that unleash shade-induced hypocotyl elongation might be recovered. Indeed, from the various long-hypocotyl seedlings identified, we focused on two *slender in shade* (*sis*) mutants, shown to be recessive and allelic. After backcrossing these mutants twice with the *Ch*^{WT} plants, homozygous mutants had slightly longer hypocotyls in W than the wild type and had very long hypocotyls under W+FR. We named the mutants as *sis1-1* and *sis1-2* (Figure 3). These results indicated that (1) loss-of-function (recessive) mutations support the “suppression” mechanisms in *C. hirsuta* to establish shade tolerance and (2) a single gene, *SIS1*, is able to repress the elongation response to shade in *C. hirsuta*.

As a first step to explore *SIS1* identity, we determined whether light perception was altered in *sis1* mutants by analyzing hypocotyl length after deetiolation under monochromatic lights. We noticed that *Ch*^{WT} seedlings were quite hyposensitive to R compared with *At*^{WT} (Figure 3B), suggesting that an attenuated phyB signaling might result in a constitutive SAS hypocotyl response, causing the observed suppression of the shade-induced hypocotyl elongation. Considering the relationship between the attenuated responsiveness to R and the strength of the shade-induced hypocotyl elongation of the weak *phyB-4* and strong *phyB-1* Arabidopsis mutant seedlings (Figures 3C and 3D), the hyposensitivity to R observed in *Ch*^{WT} might contribute but is not enough to fully suppress the shade-induced hypocotyl elongation in this species. Therefore, additional components are required to establish the shade-tolerant hypocotyl habit in *C. hirsuta*. Indeed, mutant *sis1* seedlings, although slightly hyposensitive to R and

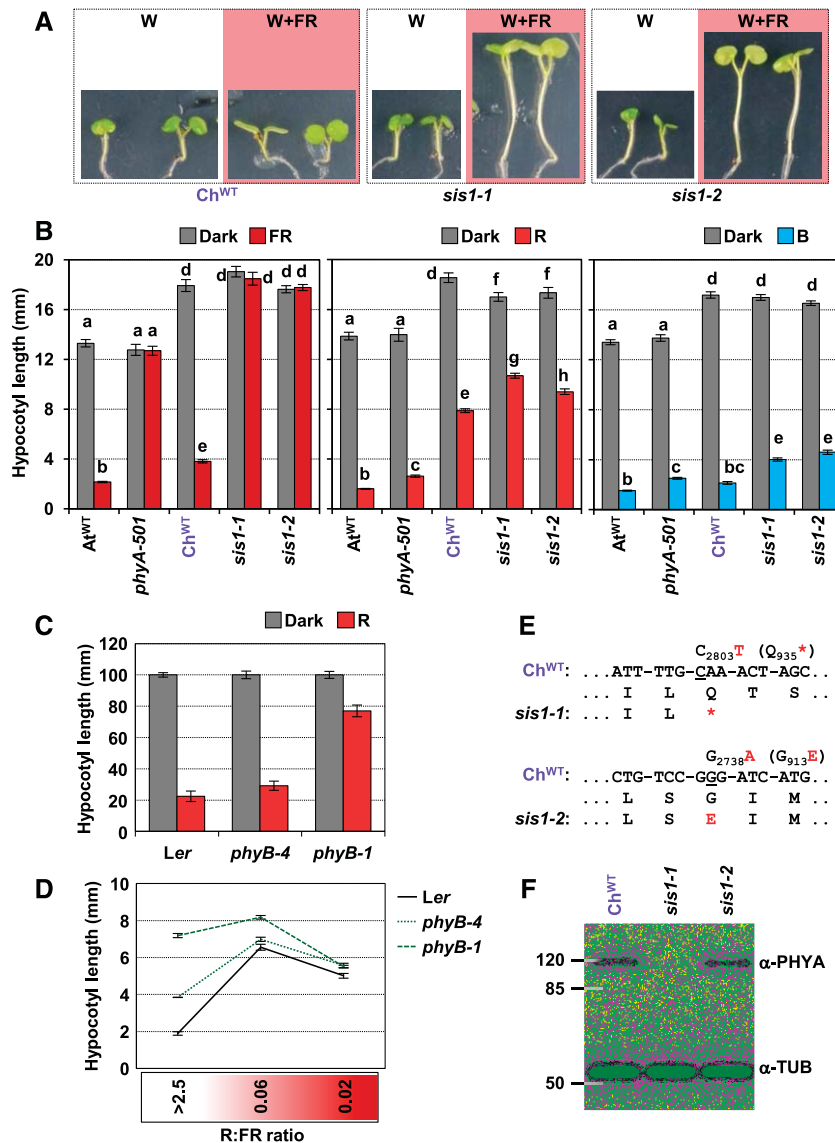


Figure 3. Mutant *sis1* Seedlings of *C. hirsuta* Are Deficient in *phyA* Activity.

(A) Phenotypes of representative seedlings of *Ch*^{WT}, *sis1-1*, and *sis1-2* after 3 d grown in W and retained in W (white panels) or transferred to W + FR (R:FR of 0.02; pink panels) until day 7. All panels are to the same scale.

(B) Hypocotyl length of *At*^{WT}, *phyA-501* (Arabidopsis), *Ch*^{WT}, *sis1-1*, and *sis1-2* (*C. hirsuta*) lines grown for 4 d in darkness (Dark) or under monochromatic FR (2.6 $\mu\text{mol m}^{-2} \text{s}^{-1}$), R (38.9 $\mu\text{mol m}^{-2} \text{s}^{-1}$), and blue light (B; 1.9 $\mu\text{mol m}^{-2} \text{s}^{-1}$).

(C) Hypocotyl length of Arabidopsis Landsberg *erecta* (*Ler*), *phyB-4*, and *phyB-1* seedlings grown for 4 d in darkness or under monochromatic R (40.6 $\mu\text{mol m}^{-2} \text{s}^{-1}$).

(D) Hypocotyl length of Arabidopsis *Ler*, *phyB-4*, and *phyB-1* seedlings under the indicated R:FR. Seedlings were grown for 2 d in W (R:FR > 2.5) and then kept in W (R:FR > 2.5) or transferred to W + FR (R:FR of 0.06 or 0.02) until day 7.

(E) Schematic diagram of the lesions found in the *ChPHYA* gene in the *sis1-1* and *sis1-2* alleles compared with the wild-type sequence (*Ch*^{WT}) and the predicted changes in the amino acid sequence.

(F) Immunoblot detection of *phyA* and tubulin with mouse monoclonal anti-*phyA* (073D) and anti-TUB antibodies in extracts of etiolated seedlings of *Ch*^{WT}, *sis1-1*, and *sis1-2* lines.

blue light, were fully blind to FR compared with *Ch*^{WT} seedlings (Figure 3B).

A very similar pattern of response was also shown by Arabidopsis *phyA*-deficient *phyA-501* seedlings (Figure 3B; Li et al., 2011), which suggested that *sis1* seedlings might be deficient in

phyA activity or signaling. Sequencing of the *C. hirsuta* *PHYA* (*ChPHYA*) gene from *sis1-1* and *sis1-2* plants showed point mutations (transitions) that introduced either a nonsense mutation in Gln-935 (in *sis1-1*) or a missense mutation in the conserved Gly-913 (in *sis1-2*; Figure 3E; Supplemental Figure 6A). Immunoblot

analyses using a specific monoclonal antibody against phyA (073D) indicated that only *sis1-1* was lacking phyA (Figure 3D). Consistent with this, *C. hirsuta* lines with reduced activity of phyA by overexpressing an RNA interference construct directed toward the *ChPHYA* gene (line 35S:RNAi-*ChPHYA*) also resulted in a *sis1* phenotype (Supplemental Figures 6B to 6D). Together, these results indicated that *sis1* are *C. hirsuta phyA*-deficient mutants (for clarity, we will keep the *sis1* mutant name in this article to distinguish it from the *phyA* mutants from Arabidopsis). They also suggested that shade tolerance in *C. hirsuta* might be caused by the existence of a phyA-dependent suppression mechanism that represses the hypocotyl elongation response to shade.

Molecular analyses showed that the relative induction of *PIL1* and *ATHB2* expression was enhanced in both *sis1* mutants compared with *Ch*^{WT} seedlings after more than 4 h of simulated shade exposure (Figure 4). This relatively late effect of *ChPHYA* absence (*sis1*) on gene expression is consistent with what was observed in Arabidopsis *phyA* mutants (Ciolfi et al., 2013). We also measured the levels of photosynthetic pigments (carotenoids and chlorophylls) after long-term exposure to low R:FR in wild-type and *phyA*-deficient Arabidopsis and *C. hirsuta* seedlings. Simulated shade triggered a stronger decrease in the accumulation of these pigments in *phyA-501*, *sis1-1*, and *sis1-2* seedlings compared with wild-type controls (Figure 4B), hence indicating that phyA represses this trait in both species, likely to avoid exaggerated losses of photosynthetic pigments in response to vegetation proximity and shade.

PhyA represses the shade-induced hypocotyl elongation in Arabidopsis caused by the deactivation of phyB only under conditions that mimic closed canopies (i.e., under very low R:FR; Yanovsky et al., 1995; Casal et al., 2014; Martínez-García et al., 2014). Indeed, Arabidopsis *phyA*-deficient mutants behaved almost like *At*^{WT} seedlings under various shade-mimicking conditions except for the lowest R:FR tested (Figure 4C). By contrast, *C. hirsuta sis1* mutants behaved differently than *Ch*^{WT} under all the low R:FR applied (Figure 4D), indicating that phyA has a broader role in suppressing the shade-induced hypocotyl elongation in *C. hirsuta* than in Arabidopsis.

C. *hirsuta* Has Higher phyA Activity Than Arabidopsis

Our results suggested the possibility that phyA activity is higher in the shade-tolerant *C. hirsuta* than in the shade-avoider Arabidopsis. Higher phyA activity can be achieved by at least two alternative and nonexclusive ways: higher phyA levels and/or higher specific (intrinsic) activity of the photoreceptor. To analyze these possibilities, we first aimed to compare *PHYA* expression levels in *At*^{WT} and *Ch*^{WT} seedlings. Data extracted from our RNA-seq experiment indicated that the expression of several commonly used reference genes, such as *EF1 α* or *YLS8* (Hornitschek et al., 2009; Kohnen et al., 2016; Gallemí et al., 2017), was within the same range (Supplemental Table 1). Then, we quantified *PHYA* expression levels in *At*^{WT} and *Ch*^{WT} seedlings growing under W or W+FR (Figure 5) using primers that recognize the sequences of the target gene (*PHYA*) and three normalizer genes (*EF1 α* , *SPC25*, and *YLS8*) in both species (Supplemental Figure 7). Expression of *PHYA* was significantly higher in *C. hirsuta* than in Arabidopsis seedlings (two-way ANOVA tests, $P < 0.05$) in

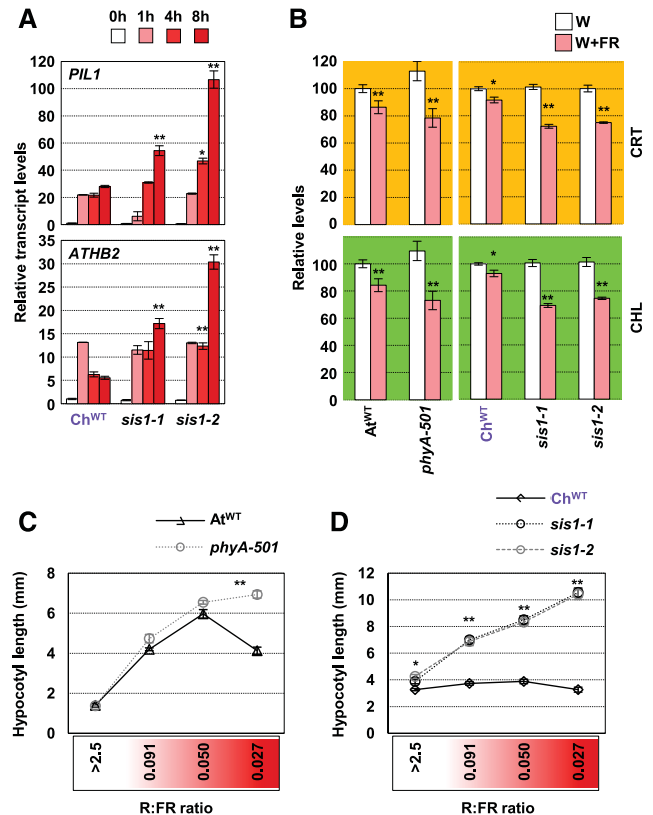


Figure 4. *C. hirsuta sis1* Seedlings Are Impaired in Their Tolerance to Plant Proximity.

(A) Effects of W+FR treatment on *PIL1* and *ATHB2* expression in *Ch*^{WT} *sis1-1* and *sis1-2* seedlings. Seedlings were grown as in Figure 2D. Transcript abundance, normalized to *EF1 α* , is shown. Values are means and SE of three independent RT-qPCR biological replicates relative to values at 0 h for each genotype. Asterisks indicate significant differences (**, $P < 0.01$) relative to 0-h samples.

(B) Carotenoid (CRT) and chlorophyll (CHL) levels of *At*^{WT} and *phyA-501* Arabidopsis and *Ch*^{WT}, *sis1-1*, and *sis1-2* *C. hirsuta* seedlings grown in W and W+FR (as detailed in Figure 1A). Values are means and SE of five independent samples. Asterisks indicate significant differences (*, $P < 0.05$ and **, $P < 0.01$) relative to W-grown plants.

(C) and **(D)** Hypocotyl length of day-7 *At*^{WT}, *phyA-501* (Arabidopsis; **C**) and *Ch*^{WT}, *sis1-1*, and *sis1-2* (*C. hirsuta*; **D**) seedlings grown for the last 4 d under the indicated R:FR. Asterisks indicate significant differences (*, $P < 0.05$ and **, $P < 0.01$) relative to the corresponding wild-type plant grown under the same R:FR. In **(D)**, asterisks apply for both *sis1* mutants.

seedlings of different ages grown under W or W+FR conditions (Figure 5B).

Higher expression of *PHYA* in *C. hirsuta* might result in higher phyA protein levels, contributing to an increased phyA activity in this species. Our immunoblot analyses showed that *PHYA* protein levels were significantly higher in *C. hirsuta* than in Arabidopsis etiolated seedlings (Figure 5D). More importantly, whereas *PHYA* levels almost disappear after 6 h of W exposure in both species, *C. hirsuta* seedlings maintained higher *PHYA* levels than Arabidopsis when exposed to W+FR for 6 to 10 h (Figures 5C and 5D). Together, these results support that *PHYA* levels in *C. hirsuta* are

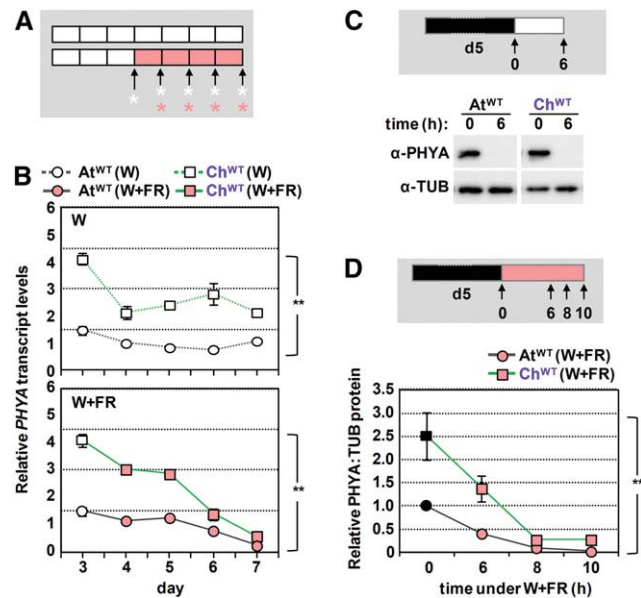


Figure 5. *C. hirsuta* Seedlings Have Higher *phyA* Levels Than Those of Arabidopsis.

(A) Cartoon showing the design of the experiment. *At*^{WT} and *Ch*^{WT}, grown as in Figure 1A, were harvested at the indicated times of W or W+FR treatments (asterisks) for RNA extraction.

(B) Evolution of *PHYA* transcript levels in *At*^{WT} and *Ch*^{WT} seedlings grown as detailed in (A). Primers used (Supplemental Figure 8A) allow quantifying and comparing expression levels by RT-qPCR between both species. *PHYA* transcript abundance was normalized to three reference genes (*EF1α*, *SPC25*, and *YLS8*). Values are means and *SE* of three independent RT-qPCR biological replicates relative to *PHYA* transcript levels of day-3 Arabidopsis seedlings. Two-way ANOVA showed that *PHYA* levels are significantly different (**, *P* < 0.01) between species under either W or W+FR.

(C) Immunoblot detection of *phyA* and tubulin with the antibodies indicated in Figure 3C in extracts of *At*^{WT} and *Ch*^{WT} seedlings grown as detailed at the top of the panel: 5-d-old etiolated seedlings were exposed to W light, and material was harvested before and after 6 h of W exposure (arrows).

(D) Evolution of relative *phyA* protein levels (*PHYA:TUB*) in *At*^{WT} and *Ch*^{WT} seedlings exposed to simulated shade, as detailed at the top of the panel: 5-d-old etiolated seedlings were exposed to W+FR light, and material was harvested before and after 6, 8, and 10 h of simulated shade exposure (arrows). Values are means and *SE* of four independent biological replicates relative to *PHYA:TUB* levels of etiolated *At*^{WT} seedlings. Two-way ANOVA showed that relative *PHYA* levels under W+FR are significantly increased (**, *P* < 0.01) in *C. hirsuta* over Arabidopsis.

generally higher than in Arabidopsis seedlings, even under shade conditions. This observation is consistent with the strongest difference in hypocotyl length under W of wild-type and *phyA*-deficient seedlings from *C. hirsuta* compared with Arabidopsis (Figures 4C and 4D; Supplemental Figure 6D; Martínez-García et al., 2014). Furthermore, transgenic overexpression of *PHYA* has been shown to attenuate shade-triggered hypocotyl elongation in Arabidopsis seedlings and stem elongation in other species (Heyer et al., 1995; Robson et al., 1996; Roig-Villanova et al., 2006).

To compare *AtphyA* and *ChphyA* specific (intrinsic) activities, complementation analyses of the Arabidopsis *phyA-501* mutant

were performed with the *AtPHYA* or *ChPHYA* gene under the control of the endogenous promoter of *AtPHYA* (*pAtPHYA:AtPHYA* or *pAtPHYA:ChPHYA*, respectively). The resulting lines were named as *phyA>AtPHYA* and *phyA>ChPHYA* (Figure 6). We obtained a total of five independent *phyA>AtPHYA* lines and

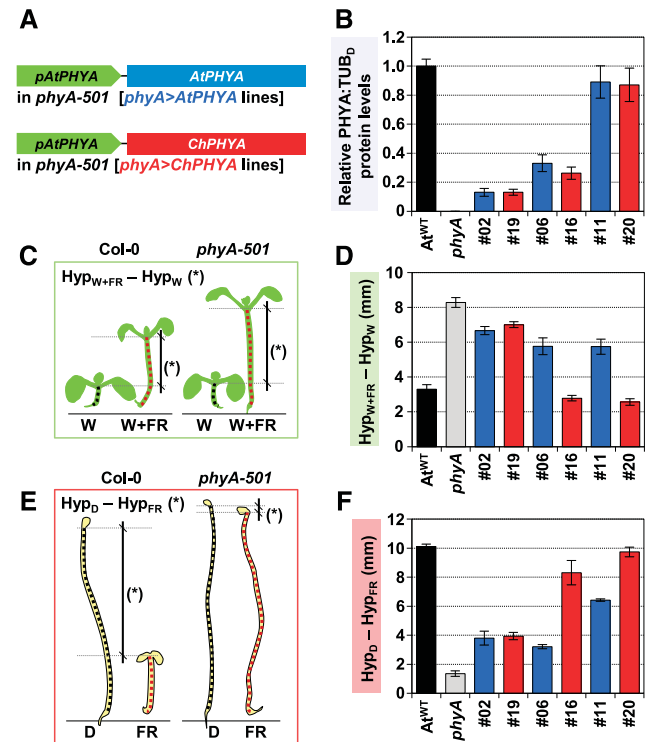


Figure 6. *ChphyA* Has a Stronger Activity Than *AtphyA* in Repressing Shade-Induced Hypocotyl Elongation.

(A) Cartoon detailing the constructs used to complement Arabidopsis *phyA-501* mutant plants.

(B) Relative *PHYA:TUB* in etiolated seedlings of *At*^{WT}, *phyA-501*, and selected *phyA>AtPHYA* (blue bars) and *phyA>ChPHYA* (red bars) complementation lines. Seedlings were grown as indicated in Supplemental Figure 8. Values are means and *SE* of four independent biological replicates relative to *PHYA:TUB* levels of etiolated *At*^{WT} seedlings.

(C) Cartoon illustrating how *phyA* activity in simulated shade was established as differences in hypocotyl length between simulated shade- and W-grown seedlings (*Hyp*_{W+FR} - *Hyp*_W). Seedlings were grown for 2 d under W and then for another 5 d under W or W+FR (R:FR = 0.02), when hypocotyls were measured.

(D) *Hyp*_{W+FR} - *Hyp*_W in seedlings of *At*^{WT}, *phyA-501*, and selected *phyA>AtPHYA* (blue bars) and *phyA>ChPHYA* (red bars) complementation lines. Values are the difference of means of hypocotyl length between seedlings grown under W+FR (*Hyp*_{W+FR}) and under W (*Hyp*_W). *SE* were propagated accordingly.

(E) Cartoon illustrating how *phyA* activity in deetiolation was established as differences in hypocotyl length between dark- and FR-grown seedlings (*Hyp*_D - *Hyp*_{FR}). Seedlings were grown as indicated in Figure 3B.

(F) *Hyp*_D - *Hyp*_{FR} in seedlings of *At*^{WT}, *phyA-501*, and selected *phyA>AtPHYA* (blue bars) and *phyA>ChPHYA* (red bars) complementation lines. Values are the difference of means of hypocotyl length between seedlings grown in the dark (*Hyp*_D) and under FR (*Hyp*_{FR}). *SE* were propagated accordingly.

In (C) and (E), mutant *phyA-501* seedlings have no *phyA* activity.

seven independent *phyA>ChPHYA* lines with different transcript and protein levels (Supplemental Figure 8). To estimate PHYA protein levels, we used etiolated seedlings, as *phyA* is photolabile. Because *PHYA* expression is repressed by light via *phyA* and *phyB* (Cantón and Quail, 1999), RNA was extracted from seedlings either grown in the dark or under W+FR (Supplemental Figure 8A). *PHYA* expression in seedlings grown in these two conditions correlated positively in both *phyA>AtPHYA* ($R^2 = 0.79$) and *phyA>ChPHYA* ($R^2 = 0.79$) lines (Supplemental Figure 8B). The slope of these equations, however, was significantly higher ($P < 0.05$) for *phyA>AtPHYA* (7.49) than for *phyA>ChPHYA* (2.81). Specifically, *phyA>AtPHYA* and *phyA>ChPHYA* lines with comparable *PHYA* expression levels in the dark showed lower *PHYA* expression under simulated shade when complemented by *ChPHYA* (*phyA>ChPHYA*) compared with *AtPHYA* (*phyA>AtPHYA*). These results pointed to a stronger activity for the ChphyA protein in repressing its own (*PHYA*) expression.

For the comparison of AtphyA and ChphyA activities, we initially studied their effects on the promotion of the shade-induced hypocotyl elongation in transgenic lines. *At*^{WT} and *phyA-501* seedlings were incorporated as controls. In these experiments, the difference in hypocotyl length between seedlings grown under W+FR versus W ($\text{Hyp}_{\text{W+FR}} - \text{Hyp}_{\text{W}}$) provided values indicative of the complementation level (or *phyA* biological activity) for the response analyzed. Consequently, in these analyses, the lower the $\text{Hyp}_{\text{W+FR}} - \text{Hyp}_{\text{W}}$ value, the higher the *phyA* activity. Opposite to that observed with transcript levels (Supplemental Figure 8C), $\text{Hyp}_{\text{W+FR}} - \text{Hyp}_{\text{W}}$ correlated well with ChPHYA but not with AtPHYA protein levels (Supplemental Figure 8D). These results together indicate that the two photoreceptors are not fully exchangeable and suggest different intrinsic qualities (i.e., biological activity) between the *phyA* receptors of *Arabidopsis* and *C. hirsuta*.

When lines with comparable PHYA protein levels were selected (Figure 6B), the response to shade ($\text{Hyp}_{\text{W+FR}} - \text{Hyp}_{\text{W}}$) was more strongly attenuated by ChPHYA (Figures 6C and 6D). As an additional way to test for *phyA* activity, we estimated hypocotyl elongation in seedlings etiolated (Hyp_{D}) and deetiolated under monochromatic FR (Hyp_{FR}). In this case, the higher the difference between these two values ($\text{Hyp}_{\text{D}} - \text{Hyp}_{\text{FR}}$), the stronger the activity of *phyA*. Similar to the shade-response analyses, ChphyA showed a stronger activity than AtphyA in deetiolating seedlings under FR (Figures 6E and 6F). A good correlation between these two *phyA*-mediated responses was also found when all the lines were considered together (Supplemental Figure 8E), reinforcing our interpretation that ChphyA is intrinsically more active than AtphyA.

The expression of dozens of auxin-responsive genes is repressed by *phyA* after just 1 h of very low R:FR treatment (Yang et al., 2018). As an additional and complementary test of *phyA* biological activity different from hypocotyl elongation, we evaluated the repressive effect of AtphyA and ChphyA on the expression of these genes. First, we selected *1-AMINO-CYCLOPROPANE-1-CARBOXYLATE SYNTHASE8* (*ACS8*), *GRETCHEN HAGEN3.3* (*GH3.3*), *INDOLE-3-ACETIC ACID INDUCIBLE19* (*IAA19*), and *IAA29*, four auxin-responsive genes described as repressed *phyA* targets (Yang et al., 2018). As expected, the shade-induced expression of these genes was attenuated in *At*^{WT} compared with *phyA-501* seedlings, but under

our shade conditions, the differences were most obvious after long exposure to W+FR (Figure 7).

The expression of the same genes was next quantified in seedlings from the various *phyA>AtPHYA* and *phyA>ChPHYA* lines grown for 24 h under W+FR. When plotting transcript levels of *phyA* target genes as a function of *PHYA* expression in these lines, the clouds of data corresponding to *phyA>ChPHYA* lines (red) were separated from those of *phyA>AtPHYA* lines (blue; Figure 7B). Importantly, the expression of all *phyA* target genes tested was overall lower in *phyA>ChPHYA* than in *phyA>AtPHYA*, indicating that ChphyA repressed more efficiently gene expression than AtphyA (Figure 7B). Consistent with this conclusion, the expression of these and other *phyA* target genes (Yang et al., 2018) was attenuated in shade-induced seedlings of *Ch*^{WT} compared with *At*^{WT} (Supplemental Figure 9). Together, these data further support that ChphyA is intrinsically more active than AtphyA.

DISCUSSION

Currently, the genetic basis of shade tolerance is poorly understood. To address this open question, we have focused on comparative analyses of the hypocotyl response to shade in young seedlings of two related mustards, *Arabidopsis* and *C. hirsuta*. Shade avoidance and tolerance are ecological concepts originated from the natural habitats of plant species (Callahan et al., 1997). Hence, defining the shade habit of a species is difficult because shade tolerance is not an absolute value but a relative concept; indeed, plants may exhibit different strategies during the juvenile and adult phases of their lives (Valladares and Niinemets, 2008). Despite the uncertainty, *Arabidopsis* is generally considered as a shade avoider and it is a model broadly used to study the SAS hypocotyl response, but there is little information referring to its physiological shade-responsiveness habit. *C. hirsuta*, by contrast, has been previously described as a shade-tolerant species whose hypocotyls are unresponsive to shade (Bealey and Robertson, 1992; Hay et al., 2014), but little is known about other shade-response mechanisms. Here, we confirm that, as expected for a shade-tolerant species, *C. hirsuta* showed a much better capacity to acclimate to LL than to HL compared with *Arabidopsis* (Supplemental Figure 1). Most strikingly, *C. hirsuta* seedlings failed to elongate in response to simulated proximity or canopy shade (Figure 1). Such a dramatic hypocotyl elongation response compared with *Arabidopsis* makes these two related species good candidates for comparative analyses of divergent responses to shade.

Our comparative and genetic analyses suggest that the absence of a shade-induced hypocotyl elongation in *C. hirsuta* is not caused by defects in the rapid biosynthesis of auxin in seedlings (Figure 2). Although we cannot exclude local defects in auxin biosynthesis (e.g., in hypocotyls) that might be masked by collecting whole seedlings, our conclusion is consistent with the lack of effect of *phyA* on the rapid shade-induced biosynthesis of auxin (Yang et al., 2018). On the contrary, we favor that the differences in hypocotyl elongation between these species is the result of a suppression mechanism sustained by the stronger activity of the ChphyA photoreceptor, likely enhanced by the attenuated ChphyB activity (Figure 3B). A stronger intrinsic (specific) repressor activity of ChphyA would result in a strong suppression of

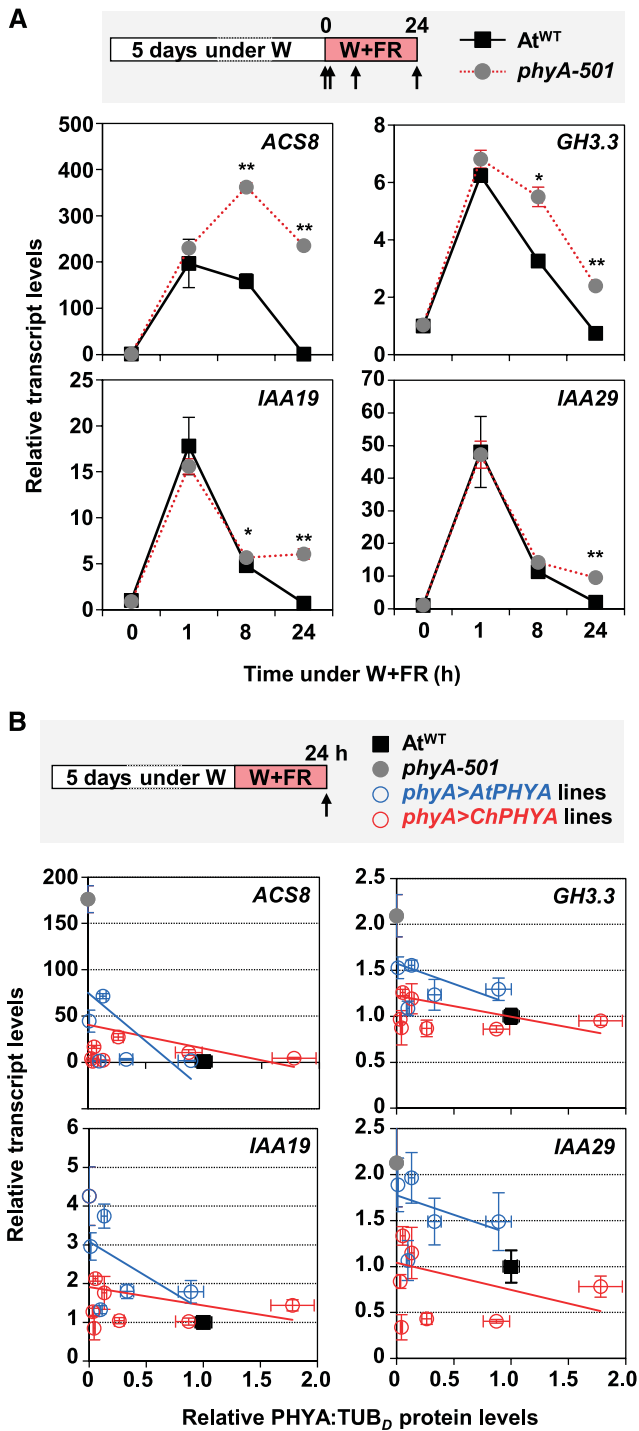


Figure 7. ChphyA Has a Stronger Activity Than AtphyA in Repressing Shade-Induced Expression of *ACS8*, *GH3.3*, *IAA19*, and *IAA29* Genes.

(A) Effects of phyA in the shade-induced expression of *ACS8*, *GH3.3*, *IAA19*, and *IAA29*. W-grown day-5 seedlings of *At*^{WT} and *phyA-501* were treated for 0, 1, 8, and 24 h with W+FR (R:FR = 0.02), when material was harvested for RNA extraction, as indicated at the top of the panel. Transcript abundance, normalized to EF1 α , is shown. Values are means and se of three independent RT-qPCR biological replicates relative to values at 0 h

the elongation of *C. hirsuta* seedlings when exposed to shade (Figure 8). The underlying mechanism likely relies, at least partly, upon suppression of auxin signaling via phyA directly binding and stabilizing AUX/IAA proteins, as has been shown in Arabidopsis (Yang et al., 2018). In this scenario, ChphyA seems to suppress not auxin biosynthesis but signaling more strongly than AtphyA, as deduced from the results with transgenic lines (Figure 7B) but also from the stronger repression in shade of auxin-responsive genes with a putative role in auxin signaling (e.g., several *IAA* and *SAUR* genes) detected in Ch^{WT} compared with At^{WT} (Supplemental Figure 9).

AtphyA and ChphyA might achieve different activities by changes in particular residues that could alter susceptibility to posttranslational modifications. For instance, phyA stability, Pfr-to-Pr reversion rate upon shade treatment, and/or interaction with protein partners (e.g., PIF1/PIF3, FHY1/FHL, and AUX/IAA) affect phyA activity in Arabidopsis (Kim et al., 2004; Seo et al., 2004; Dieterle et al., 2005; Genoud et al., 2008; Oka et al., 2012; Sheerin et al., 2015). These intrinsic differences might be also enhanced by changes in protein abundance of phyA and/or other components in its signaling pathway specifically acting in light-grown seedlings (see below). Comparison of the amino acid sequences of AtphyA and ChphyA, however, did not point to any obvious specific residue or region that could be responsible for the observed intrinsic differences in activity (Supplemental Figure 10). This is an issue that would need future research.

The genetic mechanisms underlying physiological evolution remain largely unknown, but changes in the timing, location, and levels of gene expression (i.e., *cis*-regulatory evolution of key genes) have caused much of morphological evolution changes (Carroll, 2008). Our data on *PHYA* expression and *PHYA* protein levels (Figure 5) agree with this view, but they go a step beyond by showing that differences in protein (ChphyA and AtphyA) intrinsic activities also contribute to differential responses to shade (Figures 6 and 7). As both components (levels versus intrinsic activity) are intimately connected (e.g., phyA represses its own expression in a light-dependent manner), at this stage it is difficult to quantify the specific contribution of each one. Moreover, additional components might contribute: while we show that phyA is a central component of a range of regulators that can be modulated in nature to implement shade tolerance, the observation

for *At*^{WT}. Asterisks indicate significant differences (**, $P < 0.01$ and *, $P < 0.05$) between *phyA-501* and *At*^{WT} seedlings exposed for the same time to W+FR.

(B) Correlation between *ACS8*, *GH3.3*, *IAA19*, and *IAA29* expression and relative levels of *PHYA* protein in the seedlings of *At*^{WT}, *phyA-501*, and *phyA>AtPHYA* (blue lines and dots) and *phyA>ChPHYA* (red lines and dots) complementation lines. Gene expression was quantified in W-grown day-5 seedlings exposed to W+FR (R:FR = 0.02) during 24 h, as indicated at the top of the panel. Transcript abundance was normalized to EF1 α . Relative *PHYA* protein levels (PHYA:TUB; data already shown in Supplemental Figure 8) were estimated in etiolated seedlings. Values are means and se of three independent RT-qPCR biological replicates relative to values of *At*^{WT}. The estimated regression lines for the *phyA>AtPHYA* (blue line) and *phyA>ChPHYA* (red line) complementation lines are shown for each correlation.

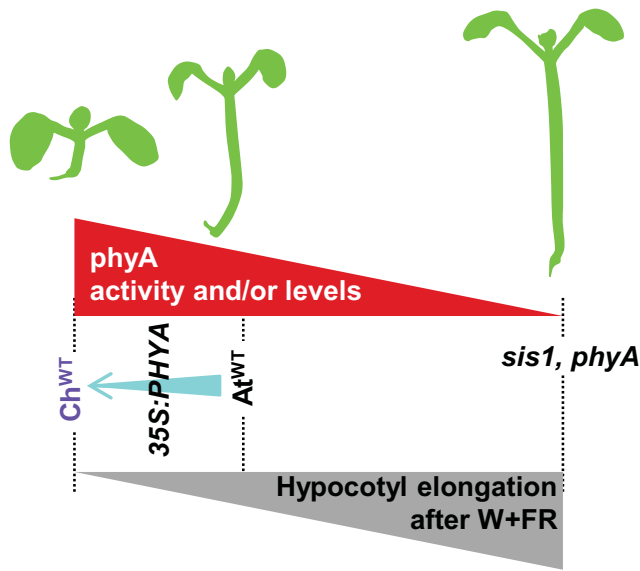


Figure 8. Model of How Increased *phyA* Activity in *C. hirsuta* Might Implement the Shade Tolerance of Hypocotyl Elongation.

Increases in *phyA* activity caused by the constitutive overexpression of *PHYA* also attenuate the shade-induced hypocotyl elongation in transgenic plants, and it results in partially tolerant Arabidopsis seedlings.

that none of the *phyA>ChPHYA* lines display a shade-tolerant habit (Supplemental Figure 8D) strongly suggests that additional downstream components of the shade-regulatory network are also participating in suppressing this response in *C. hirsuta* (e.g., differences in *phyB* activity). Indeed, it cannot be excluded that the mutant screen, despite identifying an important regulator, did not establish the causal difference between the two species in terms of shade-induced hypocotyl elongation. Nonetheless, our results unveil the importance of modulating photoreceptor activity as a powerful evolutionary mechanism in nature to achieve physiological variation between species, hence enabling the colonization of new, different habitats. In addition, searching for variability in *phyA* function could provide a suitable tool to modify the impact of neighbors' cues in crops to minimize yield losses.

METHODS

Plant Material and Plant Growth Conditions

Plants of Arabidopsis (*Arabidopsis thaliana*) Col-0 (*At*^{WT}) *phyA-501* (in the Col-0 background), *phyB-1*, *phyB-4* (both *phyB*-deficient lines are in the Landsberg *erecta* background), and *Cardamine hirsuta*, of the reference Oxford accession (*Ch*^{WT}), have been described (Reed et al., 1993; Hay et al., 2014; Martínez-García et al., 2014). Plant growth conditions have been described elsewhere (Martínez-García et al., 2014; Gallemí et al., 2016). Normal light conditions refer to W produced by cool-white vertical fluorescent tubes (PAR of 20–24 $\mu\text{mol m}^{-2} \text{s}^{-1}$). LL and HL conditions corresponded to PAR values of 4 and 200 $\mu\text{mol m}^{-2} \text{s}^{-1}$, respectively. Shade treatments in seedlings were provided by enriching W (R:FR of 2.5) with different intensities of FR LEDs (730-nm peak; Philips Greenpower Research modules) to produce the indicated R:FR (0.091–0.021) without altering PAR. Light spectra are presented in Supplemental Figure 2. For

estimating petiole and rachis length, rosette plants were grown under a long-day (16 h of light, 8 h of dark) photoperiod, in which W was generated by cool-white horizontal fluorescent tubes (PAR of $\sim 100 \mu\text{mol m}^{-2} \text{s}^{-1}$, R:FR of 3.0); for shade treatments, W was supplemented with FR (W+FR, PAR of $\sim 100 \mu\text{mol m}^{-2} \text{s}^{-1}$, R:FR of 0.05). Fluence rates were measured with a Spectrosense2 meter associated with a four-channel sensor (Skye Instruments), which measures PAR (400–700 nm) and 10-nm windows in the blue (464–473 nm), R (664–673 nm), and FR (725–734 nm) regions (Gallemí et al., 2017). Light spectra were generated using a Flame Model Spectrometer with Sony Detector (FLAME-S; Ocean Optics).

Hypocotyl, Petiole, and Rachis Measurements

For hypocotyl measurement, ~ 30 seeds of each genotype were germinated on the plates for observing the seedling phenotype and at least 20 seedlings were measured for quantification of hypocotyl length. All experiments were repeated at least three times with consistent results. Hypocotyl measurements from all the different experiments were averaged (Supplemental Data Set 9). For petiole measurement, ~ 30 seeds of each genotype were germinated under continuous W. One week later, 20 seedlings in a similar stage of development were transferred to individual pots and moved to a long-day growth chamber (R:FR of 3.0). After 1 week, half of the rosette plants stayed under W and the other half were moved to a W+FR shelf (R:FR of 0.05). After 1 week of differential R:FR treatment, leaves were harvested and petiole was measured; in the case of complex leaves from *C. hirsuta*, rachises were measured, covering the distance from the base of the leaf to the base of the main leaflet (Supplemental Figure 3). At least eight leaves were measured for quantification of petiole and rachis length for each leaf number. Experiments were repeated four times with consistent results. Petiole and rachis measurements from all four experiments were averaged (Supplemental Data Set 9).

Photosynthetic Pigment Quantification and Chlorophyll Fluorescence

Whole 7-d-old seedlings of the indicated genotypes grown under W or W+FR (Figures 1 and 4) or transferred to HL conditions (Supplemental Figure 1B) were harvested, ground in liquid nitrogen, and the resulting powder was used for quantification of chlorophylls and carotenoids spectrophotometrically or by HPLC, as described (Bou-Torrent et al., 2015).

Fluorescence measurements were performed on seedlings grown under different light regimes using a MAXI-PAM fluorometer (Heinz Walz). For every measurement, the whole cotyledons of seven seedlings were considered. F_v/F_m was calculated as $(F_m - F_0)/F_m$, where F_m and F_0 are the maximum and minimum fluorescence of dark-adapted samples, respectively. For dark acclimation, plates were incubated for at least 30 min in darkness to allow the full relaxation of photosystems. Rapid light curves were constructed with 10 incremental steps of actinic irradiance (E ; 0, 1, 21, 56, 111, 186, 281, 396, 531, and 701 $\mu\text{mol photons m}^{-2} \text{s}^{-1}$). For each step, the effective quantum yield of PSII ($\Delta F/F_m'$) was monitored every 1 min, and relative electron transport rate was calculated as $E \times \Delta F/F_m'$. The light response was characterized by fitting iteratively, using MS Excel Solver, the model of Platt et al., (1980) to relative electron transport rate versus E curves. The fit was very good in all the cases ($r > 0.98$).

Expression Analyses by RT-qPCR and RNA-Seq

RNA was extracted from whole seedlings of Arabidopsis and *C. hirsuta* (grown as detailed in each experiment, three biological replicates per time point, each biological replicate composed of 30–40 seedlings) using commercial kits (RNAeasy Plant Mini kit, Qiagen; or the semiautomatic Maxwell SimplyRNA kit, Promega). For real-time qPCR analysis, 2 μg of

RNA was reverse-transcribed using the M-MLV Reverse Transcriptase (Invitrogen) or Transcriptor First Strand cDNA synthesis (Roche). Reference genes used were *UBQ10*, *EF1 α* , *SPC25*, and/or *YLS8* (Supplemental Table 2).

For RNA-seq analyses, quantification of gene expression was performed as indicated elsewhere (Gan et al., 2016) and detailed in the Supplemental Data. From the lists of genes, we selected as differentially expressed those whose fold change was significantly (adjusted $P < 0.05$) higher than 1.5 (Supplemental Data Sets 1 and 3) or lower than 0.67 (Supplemental Data Sets 2 and 4) in seedlings treated for 1 h with W+FR compared with those grown under W in either *C. hirsuta* (Supplemental Data Sets 1 and 2) or *Arabidopsis* (Supplemental Data Sets 3 and 4).

GO and MapMan Analysis

A strict synteny-based approach was used to identify conserved orthologs between the two species. The *Arabidopsis* orthologs of the *C. hirsuta* genes were used for getting the GO term annotations and MMBs. The GO term annotations for *Arabidopsis* genes, used as a reference, were obtained from the Gene Ontology Consortium (<http://www.geneontology.org/>; Ashburner et al., 2000). The results are presented as Supplemental Data Set 5. For the MMB analyses, each list of genes was submitted to the Mercator gene function prediction pipeline (Lohse et al., 2014), which annotates the query genes with the hierarchical ontology MMBs (Thimm et al., 2004; Klie and Nikoloski, 2012). Based on these MMB annotations, exact Fisher's tests for function enrichment within the six groups of DEGs were performed and interpreted (Supplemental Data Set 6).

Protein Extraction and Immunoblot Analysis

Methods for extracting and detecting phyA protein levels in *Arabidopsis* or *C. hirsuta* seedlings (Martínez-García et al., 1999; Gallemí et al., 2017) are as follows. Protein extracts from *C. hirsuta* seedlings analyzed in Figure 3 and Supplemental Figure 6 were prepared following the direct extract protocol (Martínez-García et al., 1999) with the modifications described below. Extracts were prepared from Ch^{WT}, *sis1*, and RNAi-ChPHYA seedlings germinated and grown in the dark for 4 d. Ten seedlings per genotype were harvested in the dark and extracted in 1.5-mL microfuge tubes containing 300 μ L of Laemmli buffer supplemented with protease inhibitors (10 μ g/mL aprotinin, 1 μ g/mL E-64, 10 μ g/mL leupeptin, 1 μ g/mL pepstatin A, and 100 μ M PMSF). These extracts were prepared in duplicate and similar results were observed. Plant material was ground using disposable grinders in the Eppendorf tube at room temperature until the mixture was homogeneous (usually less than 15 s). Once all the samples were prepared, tubes were placed in boiling water for 3 min. Tubes were centrifuged in a microfuge at maximum speed (13,000g, 10 min) immediately before loading. Fifteen microliters of each extract, equivalent to ~ 0.5 seedlings, was loaded per lane in an SDS-8% PAGE device.

Protein extracts analyzed in Figure 5 were prepared from At^{WT} and Ch^{WT} seedlings grown as indicated in the figure legend. Extracts were obtained from four biological replicates. Protein extracts analyzed in Figure 6 were prepared from At^{WT}, *phyA-501*, *phyA>AtPHYA*, and *phyA>ChPHYA* seedlings germinated and grown in the dark for 4 d, as described (Gallemí et al., 2017). Extracts were obtained from three biological replicates. Each biological replicate was obtained from ~ 100 seedlings. Protein concentration in these extracts was determined using the Pierce BCA Protein Assay kit (catalog number 23225). Five or 7.5 μ g of each extract was loaded per lane in an SDS-8% PAGE device.

Immunoblot analyses of PHYA and TUB were performed at the same time with the antibodies (073D, commercial anti-TUB) and dilutions indicated elsewhere (Martínez-García et al., 2014). Anti-mouse horseradish

peroxidase-conjugated antibody (Promega) was used as a secondary antibody. ECL or ECL-plus chemiluminescence kits (GE Healthcare) were used for detection. Signal was visualized and quantified using the ChemiDoc Touch Imaging System (Bio-Rad).

Hormone Analyses

Hormone extraction and analysis were performed as described (Durgbanshi et al., 2005) with a few modifications. Briefly, 0.02 g of dry tissue (~ 150 At^{WT} seedlings and 100 Ch^{WT} seedlings) was extracted in 1 mL of ultrapure water after spiking with 50 ng of [²H₂]IAA in a ball mill (MillMix20, Dome). After centrifugation at 4000g at 4°C for 10 min, supernatants were recovered and pH adjusted to 3 with 30% (v/v) acetic acid. The water extract was partitioned twice against 2 mL of diethyl ether, and the organic layer was recovered and evaporated under vacuum in a centrifuge concentrator (Speed Vac, Jouan). Once dried, the residue was resuspended in a 10:90 methanol:water solution by gentle sonication. The resulting solution was filtered through 0.22- μ m polytetrafluoroethylene membrane syringe filters (Albet) and directly injected into an ultraperformance LC system (Acquity SDS, Waters). Chromatographic separations were performed on a reverse-phase C18 column (gravity, 50 \times 2.1 mm, 1.8- μ m particle size, Macherey-Nagel) using a methanol:water (both supplemented with 0.1% acetic acid) gradient at a flow rate of 300 μ L/min. IAA was quantified with a triple quadrupole mass spectrometer (Micromass) connected online to the output of the column through an orthogonal Z-spray electrospray ion source.

Data Availability

The Illumina RNA-seq reads are available from the website <http://chi.mpiz.mpg.de/assembly>. Source code of BAMLINK is available at <http://chi.mpiz.mpg.de/software>. The data that support the findings of this study are also available from the corresponding author on request.

Accession Numbers

Sequence data from this article can be found in the *Arabidopsis* Genome Initiative or the *C. hirsuta* (<http://chi.mpiz.mpg.de/assembly>) databases under the following accession numbers: *AtATHB2* (At4g16780), *ChATHB2* (CARHR223400), *AtPIL1* (At2g46970), *ChPIL1* (CARHR142340), *AtUBQ10* (At4g05320), *AtPHYA* (At1g09570), *ChPHYA* (CARHR009540), *ACS8* (At4g37770), *GH3.3* (At2g23170), *IAA19* (At3g15540), *IAA29* (At3g15540), *AtEF1 α* (At5g60390), *ChEF1 α* (CARHR274060 and CARHR274080), *SPC25* (At2g39960), *ChSPC25* (CARHR134880 and CARHR134890), *YLS8* (At5g08290), and *ChYLS8* (CARHR204840).

Supplemental Data

Supplemental Figure 1. Photosynthetic-related responses of *A. thaliana* and *C. hirsuta* seedlings to changing light conditions.

Supplemental Figure 2. Light spectra of the treatments used in this study.

Supplemental Figure 3. Longitudinal length of *A. thaliana* and *C. hirsuta* leaves respond differently to simulated shade.

Supplemental Figure 4. *A. thaliana* and *C. hirsuta* seedlings change gene expression differently in response to simulated shade.

Supplemental Figure 5. The expression of a set of shade-induced but auxin-dependent genes, identified in *A. thaliana*, is also shade-induced in *C. hirsuta*.

Supplemental Figure 6. Reduction of phyA activity in *C. hirsuta* seedlings results in a *sis* phenotype.

Supplemental Figure 7. Partial alignment of *ChPHYA/AtPHYA*, *ChEF1 α /AtEF1 α* , *ChSPC25/AtSPC25* and *ChYLS8/AtYLS8* sequences.

Supplemental Figure 8. Strategies to compare biological activity between *AtphyA* and *ChphyA* in transgenic lines.

Supplemental Figure 9. The expression of a set of shade-induced *phyA*-repressed genes, identified in *A. thaliana*, is attenuated in *C. hirsuta*.

Supplemental Figure 10. Alignment of *C. hirsuta* and *A. thaliana* *phyA* amino acid sequences.

Supplemental Table 1. RPKM of eight genes commonly used for normalizing in RT-qPCR analyses.

Supplemental Table 2. Primers used in this work.

Supplemental Data Set 1. Bioset of up-regulated genes in *C. hirsuta* seedlings in response to simulated shade.

Supplemental Data Set 2. Bioset of down-regulated genes in *C. hirsuta* seedlings in response to simulated shade.

Supplemental Data Set 3. Bioset of up-regulated genes in *A. thaliana* seedlings in response to simulated shade.

Supplemental Data Set 4. Bioset of down-regulated genes in *A. thaliana* seedlings in response to simulated shade.

Supplemental Data Set 5. Results of Venn diagrams of the GO categorization.

Supplemental Data Set 6. Functional enrichment groups based on the MapMan-Bin analyses.

Supplemental Data Set 7. Bioset of shade-regulated OMCL groups in *Geranium pyrenaicum* petioles in response to simulated shade.

Supplemental Data Set 8. Bioset of shade-regulated OMCL groups in *Geranium robertianum* petioles in response to simulated shade.

Supplemental Data Set 9. Summary of statistical tests.

ACKNOWLEDGMENTS

We thank Ester Botterweg and M. Rosa Rodríguez (Centre for Research in Agricultural Genomics [CRAG]) for their technical support; Victor González and Martí Bernardo (Bioinformatics Core unit, CRAG) for help in statistical analyses; Peter Quail (Plant Gene Expression Center) for providing the anti-*phyA* antibody; Fernando Valladares (National Museum of Natural History, Madrid, Spain) for discussions about the shade habit of *Arabidopsis* and *C. hirsuta*; and Charlotte Gommers (CRAG) for comments on the article. Support for this work was provided by the Spanish Ministerio de Economía y Competitividad (MINECO; FPI program predoctoral fellowship to M.J.M.-C.), the Agència d'Ajuts Universitaris i de Recerca (AGAUR-Generalitat de Catalunya; FI program predoctoral fellowship to S.P.), and La Caixa Foundation (INPhINIT fellowship LCF/BQ/IN18/11660004 to L.C.). Support was also provided by an International CRAG "Severo Ochoa" postdoctoral program fellowship and a postdoctoral contract funded by the European Commission (H2020-MSCA-IF-2017, Proposal 797473 to J.M.-R.), and by a Marie Curie postdoctoral contract funded by the European Commission and a CRAG short-term fellowship (FP7-PEOPLE-IEF-2008, Proposal 237492 to C.T.). Our research is supported by the Biotechnology and Biological Science Research Council (grant BB/H006974/1), by the Max Planck Society (core grant to M.T.), by MINECO-FEDER (grants BIO2017-85316-R and BIO2017-84041-P), and AGAUR (grants 2017-SGR1211, 2017-SGR710, and Xarba to J.F.M.-G. and M.R.C.). We also acknowledge the support of MINECO for the "Centro de Excelencia Severo Ochoa 2016-2019"

(award SEV-2015-0533) and by the CERCA Programme/Generalitat de Catalunya.

AUTHOR CONTRIBUTIONS

J.F.M.-G. conceived the original research plan and directed and coordinated the study; A.H., H.J., X.G., and M.T. performed RNA-seq and analyzed the data; A.G.-C. analyzed auxin levels; L.M. and M.R.-C. measured and analyzed photosynthetic parameters and pigment levels; M.J.M.-C., S.P., C.T., J.M.-R., P.P.-A., and I.R.-V. performed all the other experiments; all authors analyzed their data and discussed the results; J.F.M.-G. wrote the article with revisions of M.R.-C. and contributions and/or comments of all other authors.

Received April 17, 2019; revised July 22, 2019; accepted September 13, 2019; published September 17, 2019.

REFERENCES

- Ashburner, M., et al. (2000). Gene Ontology: Tool for the unification of biology. *Nat. Genet.* **25**: 25–29.
- Barkoulas, M., Hay, A., Kougioumoutzi, E., and Tsiantis, M. (2008). A developmental framework for dissected leaf formation in the *Arabidopsis* relative *Cardamine hirsuta*. *Nat. Genet.* **40**: 1136–1141.
- Bealey, C.E., and Robertson, P.A. (1992). Coppice management for pheasants. In *Ecology and Management of Coppice Woodlands*, G.P. Buckley, ed (Dordrecht: Springer), pp. 193–210.
- Benkov, M.A., Yatsenko, A.M., and Tikhonov, A.N. (2019). Light acclimation of shade-tolerant and sun-resistant *Tradescantia* species: Photochemical activity of PSII and its sensitivity to heat treatment. *Photosynth. Res.* **139**: 203–214.
- Bou-Torrent, J., Galstyan, A., Gallemí, M., Cifuentes-Esquivel, N., Molina-Contreras, M.J., Salla-Martret, M., Jikumaru, Y., Yamaguchi, S., Kamiya, Y., and Martínez-García, J.F. (2014). Plant proximity perception dynamically modulates hormone levels and sensitivity in *Arabidopsis*. *J. Exp. Bot.* **65**: 2937–2947.
- Bou-Torrent, J., Toledo-Ortiz, G., Ortiz-Alcaide, M., Cifuentes-Esquivel, N., Halliday, K.J., Martínez-García, J.F., and Rodríguez-Concepcion, M. (2015). Regulation of carotenoid biosynthesis by shade relies on specific subsets of antagonistic transcription factors and cofactors. *Plant Physiol.* **169**: 1584–1594.
- Cagnola, J.I., Ploschuk, E., Benech-Arnold, T., Finlayson, S.A., and Casal, J.J. (2012). Stem transcriptome reveals mechanisms to reduce the energetic cost of shade-avoidance responses in tomato. *Plant Physiol.* **160**: 1110–1119.
- Callahan, H.S., Pigliucci, M., and Schlichting, C.D. (1997). Developmental phenotypic plasticity: Where ecology and evolution meet molecular biology. *BioEssays* **19**: 519–525.
- Cantón, F.R., and Quail, P.H. (1999). Both *phyA* and *phyB* mediate light-imposed repression of *PHYA* gene expression in *Arabidopsis*. *Plant Physiol.* **121**: 1207–1216.
- Carroll, S.B. (2008). Evo-devo and an expanding evolutionary synthesis: A genetic theory of morphological evolution. *Cell* **134**: 25–36.
- Casal, J.J. (2012). Shade avoidance. *The Arabidopsis Book* **10**: e0157.
- Casal, J.J., Candia, A.N., and Sellaro, R. (2014). Light perception and signalling by phytochrome A. *J. Exp. Bot.* **65**: 2835–2845.
- Cifuentes-Esquivel, N., Bou-Torrent, J., Galstyan, A., Gallemí, M., Sessa, G., Salla Martret, M., Roig-Villanova, I., Ruberti, I., and Martínez-García, J.F. (2013). The bHLH proteins BEE and BIM

- positively modulate the shade avoidance syndrome in *Arabidopsis* seedlings. *Plant J.* **75**: 989–1002.
- Cioffi, A., Sessa, G., Sassi, M., Possenti, M., Salvucci, S., Carabelli, M., Morelli, G., and Ruberti, I.** (2013). Dynamics of the shade-avoidance response in *Arabidopsis*. *Plant Physiol.* **163**: 331–353.
- de Wit, M., Keuskamp, D.H., Bongers, F.J., Hornitschek, P., Gommers, C.M.M., Reinen, E., Martínez-Cerón, C., Fankhauser, C., and Pierik, R.** (2016). Integration of phytochrome and cryptochrome signals determines plant growth during competition for light. *Curr. Biol.* **26**: 3320–3326.
- de Wit, M., Ljung, K., and Fankhauser, C.** (2015). Contrasting growth responses in lamina and petiole during neighbor detection depend on differential auxin responsiveness rather than different auxin levels. *New Phytol.* **208**: 198–209.
- Dieterle, M., Bauer, D., Büche, C., Krenz, M., Schäfer, E., and Kretsch, T.** (2005). A new type of mutation in phytochrome A causes enhanced light sensitivity and alters the degradation and subcellular partitioning of the photoreceptor. *Plant J.* **41**: 146–161.
- Durgbanshi, A., Arbona, V., Pozo, O., Miersch, O., Sancho, J.V., and Gómez-Cadenas, A.** (2005). Simultaneous determination of multiple phytohormones in plant extracts by liquid chromatography-electrospray tandem mass spectrometry. *J. Agric. Food Chem.* **53**: 8437–8442.
- Galleli, M., Galstyan, A., Paulišić, S., Then, C., Ferrández-Ayela, A., Lorenzo-Orts, L., Roig-Villanova, I., Wang, X., Micol, J.L., Ponce, M.R., Devlin, P.F., and Martínez-García, J.F.** (2016). DRACULA2 is a dynamic nucleoporin with a role in regulating the shade avoidance syndrome in *Arabidopsis*. *Development* **143**: 1623–1631.
- Galleli, M., Molina-Contreras, M.J., Paulišić, S., Salla-Martret, M., Sorin, C., Godoy, M., Franco-Zorrilla, J.M., Solano, R., and Martínez-García, J.F.** (2017). A non-DNA-binding activity for the ATHB4 transcription factor in the control of vegetation proximity. *New Phytol.* **216**: 798–813.
- Gan, X., et al.** (2016). The *Cardamine hirsuta* genome offers insight into the evolution of morphological diversity. *Nat. Plants* **2**: 16167.
- Genoud, T., Schweizer, F., Tscheuschler, A., Debrieux, D., Casal, J.J., Schäfer, E., Hiltbrunner, A., and Fankhauser, C.** (2008). FHY1 mediates nuclear import of the light-activated phytochrome A photoreceptor. *PLoS Genet.* **4**: e1000143.
- Gommers, C.M., Keuskamp, D.H., Buti, S., van Veen, H., Koevoets, I.T., Reinen, E., Voeselek, L.A., and Pierik, R.** (2017). Molecular profiles of contrasting shade response strategies in wild plants: Differential control of immunity and shoot elongation. *Plant Cell* **29**: 331–344.
- Gommers, C.M., Visser, E.J., St. Onge, K.R., Voeselek, L.A., and Pierik, R.** (2013). Shade tolerance: When growing tall is not an option. *Trends Plant Sci.* **18**: 65–71.
- Gommers, C.M.M., Buti, S., Tarkowská, D., Pěnčík, A., Banda, J.P., Arricastes, V., and Pierik, R.** (2018). Organ-specific phytohormone synthesis in two *Geranium* species with antithetical responses to far-red light enrichment. *Plant Direct* **2**: e00066.
- Han, S., Jiang, J., Li, H., Song, A., Chen, S., and Chen, F.** (2015). The differential response of two *Chrysanthemum* cultivars to shading: Photosynthesis, chloroplast, and sieve element-companion cell ultrastructure. *HortScience* **50**: 1192–1195.
- Hay, A., and Tsiantis, M.** (2016). *Cardamine hirsuta*: A comparative view. *Curr. Opin. Genet. Dev.* **39**: 1–7.
- Hay, A.S., et al.** (2014). *Cardamine hirsuta*: A versatile genetic system for comparative studies. *Plant J.* **78**: 1–15.
- Hersch, M., Lorrain, S., de Wit, M., Trevisan, M., Ljung, K., Bergmann, S., and Fankhauser, C.** (2014). Light intensity modulates the regulatory network of the shade avoidance response in *Arabidopsis*. *Proc. Natl. Acad. Sci. USA* **111**: 6515–6520.
- Heyer, A.G., Mozley, D., Landschütze, V., Thomas, B., and Gatz, C.** (1995). Function of phytochrome A in potato plants as revealed through the study of transgenic plants. *Plant Physiol.* **109**: 53–61.
- Hofhuis, H., et al.** (2016). Morphomechanical innovation drives explosive seed dispersal. *Cell* **166**: 222–233.
- Hornitschek, P., Kohnen, M.V., Lorrain, S., Rougemont, J., Ljung, K., López-Vidriero, I., Franco-Zorrilla, J.M., Solano, R., Trevisan, M., Pradervand, S., Xenarios, I., and Fankhauser, C.** (2012). Phytochrome interacting factors 4 and 5 control seedling growth in changing light conditions by directly controlling auxin signaling. *Plant J.* **71**: 699–711.
- Hornitschek, P., Lorrain, S., Zoete, V., Michielin, O., and Fankhauser, C.** (2009). Inhibition of the shade avoidance response by formation of non-DNA binding bHLH heterodimers. *EMBO J.* **28**: 3893–3902.
- Karve, A.A., Jawdy, S.S., Gunter, L.E., Allen, S.M., Yang, X., Tuskan, G.A., Wulschleger, S.D., and Weston, D.J.** (2012). Initial characterization of shade avoidance response suggests functional diversity between *Populus* phytochrome B genes. *New Phytol.* **196**: 726–737.
- Kim, J.I., Shen, Y., Han, Y.J., Park, J.E., Kirchenbauer, D., Soh, M.S., Nagy, F., Schäfer, E., and Song, P.S.** (2004). Phytochrome phosphorylation modulates light signaling by influencing the protein-protein interaction. *Plant Cell* **16**: 2629–2640.
- Klie, S., and Nikoloski, Z.** (2012). The choice between MapMan and Gene Ontology for automated gene function prediction in plant science. *Front. Genet.* **3**: 115.
- Kohnen, M.V., Schmid-Siegert, E., Trevisan, M., Petrolati, L.A., Sénéchal, F., Müller-Moulé, P., Maloof, J., Xenarios, I., and Fankhauser, C.** (2016). Neighbor detection induces organ-specific transcriptomes, revealing patterns underlying hypocotyl-specific growth. *Plant Cell* **28**: 2889–2904.
- Kozuka, T., Kobayashi, J., Horiguchi, G., Demura, T., Sakakibara, H., Tsukaya, H., and Nagatani, A.** (2010). Involvement of auxin and brassinosteroid in the regulation of petiole elongation under the shade. *Plant Physiol.* **153**: 1608–1618.
- Li, J., Li, G., Wang, H., and Wang Deng, X.** (2011). Phytochrome signaling mechanisms. *The Arabidopsis Book* **9**: e0148, doi/10.1199/tab.0148.
- Li, L., et al.** (2012). Linking photoreceptor excitation to changes in plant architecture. *Genes Dev.* **26**: 785–790.
- Lohse, M., Nagel, A., Herter, T., May, P., Schroda, M., Zrenner, R., Tohge, T., Fernie, A.R., Stitt, M., and Usadel, B.** (2014). Mercator: A fast and simple web server for genome scale functional annotation of plant sequence data. *Plant Cell Environ.* **37**: 1250–1258.
- Martínez-García, J.F., Galleli, M., Molina-Contreras, M.J., Llorente, B., Bevilacqua, M.R., and Quail, P.H.** (2014). The shade avoidance syndrome in *Arabidopsis*: The antagonistic role of phytochrome A and B differentiates vegetation proximity and canopy shade. *PLoS One* **9**: e109275.
- Martínez-García, J.F., Galstyan, A., Salla-Martret, M., Cifuentes-Esquível, N., Galleli, M., and Bou-Torrent, J.** (2010). Regulatory components of shade avoidance syndrome. *Adv. Bot. Res.* **53**: 65–116.
- Martínez-García, J.F., Monte, E., and Quail, P.H.** (1999). A simple, rapid and quantitative method for preparing *Arabidopsis* protein extracts for immunoblot analysis. *Plant J.* **20**: 251–257.
- Mathews, S.** (2010). Evolutionary studies illuminate the structural-functional model of plant phytochromes. *Plant Cell* **22**: 4–16.
- Oka, Y., Ono, Y., Toledo-Ortiz, G., Kokaji, K., Matsui, M., Mochizuki, N., and Nagatani, A.** (2012). *Arabidopsis* phytochrome A is

- modularly structured to integrate the multiple features that are required for a highly sensitized phytochrome. *Plant Cell* **24**: 2949–2962.
- Ortiz-Alcaide, M., Llamas, E., Gomez-Cadenas, A., Nagatani, A., Martínez-García, J.F., and Rodríguez-Concepción, M.** (2019). Chloroplasts modulate elongation responses to canopy shade by retrograde pathways involving HY5 and abscisic acid. *Plant Cell* **31**: 384–398.
- Platt, T., Gallegos, C.L., and Harrison, W.G.** (1980). Photoinhibition of photosynthesis in natural assemblages of marine phytoplankton. *Journal of Marine Research* **38**: 687–701.
- Procko, C., Crenshaw, C.M., Ljung, K., Noel, J.P., and Chory, J.** (2014). Cotyledon-generated auxin is required for shade-induced hypocotyl growth in *Brassica rapa*. *Plant Physiol.* **165**: 1285–1301.
- Reed, J.W., Nagpal, P., Poole, D.S., Furuya, M., and Chory, J.** (1993). Mutations in the gene for the red/far-red light receptor phytochrome B alter cell elongation and physiological responses throughout Arabidopsis development. *Plant Cell* **5**: 147–157.
- Robson, P.R., McCormac, A.C., Irvine, A.S., and Smith, H.** (1996). Genetic engineering of harvest index in tobacco through overexpression of a phytochrome gene. *Nat. Biotechnol.* **14**: 995–998.
- Roig-Villanova, I., Bou, J., Sorin, C., Devlin, P.F., and Martínez-García, J.F.** (2006). Identification of primary target genes of phytochrome signaling: Early transcriptional control during shade avoidance responses in Arabidopsis. *Plant Physiol.* **141**: 85–96.
- Roig-Villanova, I., Bou-Torrent, J., Galstyan, A., Carretero-Paulet, L., Portolés, S., Rodríguez-Concepción, M., and Martínez-García, J.F.** (2007). Interaction of shade avoidance and auxin responses: A role for two novel atypical bHLH proteins. *EMBO J.* **26**: 4756–4767.
- Roig-Villanova, I., and Martínez-García, J.F.** (2016). Plant responses to vegetation proximity: A whole life avoiding shade. *Front. Plant Sci.* **7**: 236.
- Sasidharan, R., Chinnappa, C.C., Staal, M., Elzenga, J.T., Yokoyama, R., Nishitani, K., Voesenek, L.A., and Pierik, R.** (2010). Light quality-mediated petiole elongation in Arabidopsis during shade avoidance involves cell wall modification by xyloglucan endotransglucosylase/hydrolases. *Plant Physiol.* **154**: 978–990.
- Seo, H.S., Watanabe, E., Tokutomi, S., Nagatani, A., and Chua, N.H.** (2004). Photoreceptor ubiquitination by COP1 E3 ligase desensitizes phytochrome A signaling. *Genes Dev.* **18**: 617–622.
- Sheerin, D.J., Menon, C., zur Oven-Krockhaus, S., Enderle, B., Zhu, L., Johnen, P., Schleifenbaum, F., Stierhof, Y.D., Huq, E., and Hiltbrunner, A.** (2015). Light-activated phytochrome A and B interact with members of the SPA family to promote photomorphogenesis in Arabidopsis by reorganizing the COP1/SPA complex. *Plant Cell* **27**: 189–201.
- Smith, H.** (1982). Light quality, photoperception, and plant strategy. *Annu. Rev. Plant Physiol.* **33**: 481–518.
- Tao, Y., et al.** (2008). Rapid synthesis of auxin via a new tryptophan-dependent pathway is required for shade avoidance in plants. *Cell* **133**: 164–176.
- Thimm, O., Bläsing, O., Gibon, Y., Nagel, A., Meyer, S., Krüger, P., Selbig, J., Müller, L.A., Rhee, S.Y., and Stitt, M.** (2004). MAPMAN: A user-driven tool to display genomics data sets onto diagrams of metabolic pathways and other biological processes. *Plant J.* **37**: 914–939.
- Ueoka-Nakanishi, H., Hori, N., Ishida, K., Ono, N., Yamashino, T., Nakamichi, N., and Mizuno, T.** (2011). Characterization of shade avoidance responses in *Lotus japonicus*. *Biosci. Biotechnol. Biochem.* **75**: 2148–2154.
- Valladares, F., and Niinemets, U.** (2008). Shade tolerance, a key plant feature of complex nature and consequences. *Annu. Rev. Ecol. Evol. Syst.* **39**: 237–257.
- Vlad, D., et al.** (2014). Leaf shape evolution through duplication, regulatory diversification, and loss of a homeobox gene. *Science* **343**: 780–783.
- Vuolo, F., Mentink, R.A., Hajheidari, M., Bailey, C.D., Filatov, D.A., and Tsiantis, M.** (2016). Coupled enhancer and coding sequence evolution of a homeobox gene shaped leaf diversity. *Genes Dev.* **30**: 2370–2375.
- Yang, C., Xie, F., Jiang, Y., Li, Z., Huang, X., and Li, L.** (2018). Phytochrome A negatively regulates the shade avoidance response by increasing auxin/indole acetic acid protein stability. *Dev. Cell* **44**: 29–41.e24.
- Yanovsky, M.J., Casal, J.J., and Whitelam, G.C.** (1995). Phytochrome A, phytochrome B and HY4 are involved in hypocotyl growth responses to natural radiation in Arabidopsis: Weak de-etiolation of the phyA mutant under dense canopies. *Plant Cell Environ.* **18**: 788–794.

1 Photoreceptor Activity Contributes to Contrasting Responses 2 to Shade in Cardamine and Arabidopsis Seedlings

3
4 Maria Jose Molina-Contreras, Sandi Paulišić, Christiane Then, Jordi Moreno-
5 Romero, Pedro Pastor-Andreu, Luca Morelli, Irma Roig-Villanova, Huw Jenkins,
6 Asis Hallab, Xiangchao Gan, Aurelio Gómez-Cadenas, Miltos Tsiantis, Manuel
7 Rodríguez-Concepción, Jaime F. Martínez-García

9 SUPPLEMENTAL METHODS

11 Generation of *C. hirsuta* RNAi-ChPHYA plants

12 To generate an RNAi construct to silence the endogenous *ChPHYA*, a
13 fragment of 256 bp was PCR-amplified using the primers CTO31 and CTO32
14 (Supplemental Table 2) and cDNA from *C. hirsuta* seedlings treated with 1 h of
15 W+FR as a template. This ChPHYA region, corresponding to the first 256 bp of
16 the cDNA, was selected because it showed less similarity with other
17 phytochrome genes. PCR product was directionally subcloned into pCRII-TOPO
18 to generate pCT16. The pCT16 fragment was sequenced to confirm its identity.
19 An *EcoRI* fragment of pCT16 was subcloned into the same sites of pENTR3C
20 vector (Invitrogen), flanked by the attL1 and attL2 sites, to give pCT18. Using
21 the Gateway LR Clonase II (Invitrogen), *in vitro* recombination with the RNAi
22 destination vector pB7GWIWG2(I), containing attR1 and attR2 sites, generated
23 pCT31 (35S:attB1<RNAi-ChPHYA<attB2), which confers phosphinothricin
24 (PPT) resistance in plants. This binary vector was introduced in *Agrobacterium*
25 *tumefaciens* C₅₈C₁ (pGV2260) by electroporation, and transformed colonies
26 were selected in YEB media supplemented with Rifampicin (100 µg/mL),
27 Kanamycin (25 µg/mL) and Spectinomycin (100 µg/mL). *C. hirsuta* wild-type
28 plants (Ch^{WT}) were transformed by floral dipping and transgenic seedlings were
29 selected in media containing PPT (50 µg/mL). Transgene presence in T1 plants
30 was verified by PCR analysis using specific primers on plant genomic DNA
31 isolated from young leaves. Only lines with a single T-DNA insertion (as
32 estimated from the segregation of the marker gene in T2 populations) were
33 eventually selected, as described (Roig-Villanova *et al.*, 2006).

1 **Generation of *A. thaliana phyA-501* lines transformed with**
2 ***pAtPHYA:AtPHYA* and *pAtPHYA:ChPHYA***

3 As a source of the *A. thaliana PHYA* gene promoter (*pAtPHYA*), we
4 employed the plasmid APAG (pAPAG, kindly provided by A. Nagatani, Kyoto
5 University, Japan), which contains 2.9 kb of the promoter region (Toledo-Ortiz
6 *et al.*, 2010). A *XhoI-BamHI* fragment of pAPAG was subcloned in pBS-SK+
7 (Stratagene) digested with the same enzymes, generating pMJ70, which allows
8 to get an *XbaI* fragment covering ~2.0 Kbp of the *pAtPHYA* (from ATG to
9 -2,029; see below).

10 As a source of *AtPHYA*, we employed vector pET-PHYA (kindly provided
11 by P. Quail, UC-Berkeley, CA, USA), which contains the whole ORF of *AtPHYA*
12 in pET3c to be expressed in *E. coli* (Somers *et al.*, 1991). pET-PHYA was
13 digested first with *NheI* (and blunt-ended with Klenow, *NheI*^{be}) and next with
14 *BamHI*. The *NheI*^{be}-*BamHI* fragment, which contains the whole ORF of
15 *AtPHYA*, was then cloned in pBS-SK+ (Stratagene) digested with *EcoRV* and
16 *BamHI*, generating pMJ77. A *SaII-NotI* fragment of pMJ77 was subcloned into
17 the same sites of pENTR3C (attL1<*ccdB*<attL2; Invitrogen), generating pMJ78,
18 which contains *AtPHYA* flanked by recombination sites (attL1<*AtPHYA*<attL2).

19 The whole *ChPHYA* coding sequence was amplified using specific primer
20 CTO31 and MBO9 (Supplemental Table 2), and cDNA isolated from etiolated
21 seedlings as DNA template. The resulting fragment was cloned into pCRII-
22 TOPO to give pMJ65. After sequencing several independent colonies, we
23 focused in pMJ65.2 (it contained no or silent mistakes between the ATG and a
24 unique *AvrII* site within the *ChPHYA*) and pMJ65.6 (it contained no or silent
25 mistakes between the unique *AvrII* site and the stop codon). An *XbaI-AvrII*
26 fragment of pMJ65.2 was subcloned into the same sites of pMJ65.6 vector,
27 generating pMJ67, which contains the whole ORF of *ChPHYA* with no or silent
28 mistakes. An *EcoRI* fragment of pMJ67 was directionally subcloned into the
29 same sites of pENTR3C, generating pMJ72, which contains *ChPHYA* flanked
30 by recombination sites (attL1<*ChPHYA*^{*XbaI*}<attL2). pMJ72 was digested with
31 *XbaI*, refilled with Klenow and religated, to generate pMJ74
32 (attL1<*ChPHYA*<attL2), which removes an *XbaI* site located after the stop
33 codon but before the attL2 site.

1 The gateway binary vector NOB936 (Galbiati *et al.*, 2013), was digested
2 with *Aat*II (to release the *SEEDSTICK* promoter) and re-ligated to generate
3 pIR101. Using the Gateway LR Clonase II (Invitrogen), *in vitro* recombination
4 between pIR101 (attR1<*ccdB*<attR2) and pMJ74 (attL1<*ChPHYA*<attL2),
5 generated pMJ83 (attB1<*ChPHYA*<attB2). An *Xba*I fragment of pMJ70,
6 containing *pAtPHYA*, was directionally cloned in pMJ83 digested with the same
7 restriction enzyme, producing pMJ84 (pAtPHYA:attB1<*ChPHYA*<attB2).

8 Using the Gateway BP Clonase II (Invitrogen), pMJ84
9 (pAtPHYA:attB1<*ChPHYA*<attB2) was recombined with pDONR207
10 (attP1<*ccdB*-Cm^R<attP2) to generate pMJ85 (pAtPHYA:attR1<*ccdB*-
11 Cm^R<attB2), which was recombined (LR clonase) with pMJ78
12 (attL1<*AtPHYA*<attL2) to generate pMJ86 (pAtPHYA:attB1<*AtPHYA*<attB2).

13 These binary vectors (pMJ84 and pMJ86) were introduced in
14 *Agrobacterium tumefaciens* C₅₈C₁ (pGV2260) by electroporation, and
15 transformed colonies (selected in YEB media supplemented with 100 µg/mL
16 Rifampicin, 25 µg/mL Kanamycin and 100 µg/mL Spectinomycin), were used to
17 transform *A. thaliana phyA-501* plants by floral dipping (Figure 6A). Transgenic
18 seedlings were selected in media containing PPT (50 µg/mL); and characterized
19 as indicated before for *C. hirsuta*. Only lines with a single T-DNA insertion were
20 eventually selected, as described (Roig-Villanova *et al.*, 2006).

22 RNA sequencing analyses

23 We collected Illumina short-read transcription sequences for each
24 sample with 3 biological replicates. Paired-end reads were aligned to the
25 reference genome (tair10 for *A. thaliana* and CHIV1 for *C. hirsuta*) using
26 TopHat2 (Kim *et al.*, 2013) with parameters "--max-multihits 10 --coverage-
27 search --microexon-search --mate-std-dev 40 --max-intron-length 30000". Raw
28 read counts per gene were quantified with HTSeq v0.5.4p1 ([http://www-
29 huber.embl.de/users/anders/HTSeq](http://www-huber.embl.de/users/anders/HTSeq)) using the "--stranded=no -t CDS" option.
30 To facilitate cross-species comparisons, the reads within UTR regions were not
31 taken into account since UTR regions are generally more divergent than CDS
32 regions.

33 Differential expression between samples from the same species was
34 determined using DESeq (Anders and Huber, 2010). We found the most

1 sensitive parameter settings for the function estimateDispersions were
2 method="blind", and sharingMode="fit-only" (Mott *et al.*, 2014). The interspecific
3 comparison of gene expression was based on 20,284 orthologous genes,
4 generated previously (Gan *et al.*, 2016), with a reciprocal gene sequence
5 similarity searching. The comparison of the lists of differentially expressed
6 genes (DEGs) in *C. hirsuta* and *A. thaliana* (Supplemental Data Sets 1-4)
7 resulted in six categories of genes: four groups of DEGs (up- or down-
8 regulated) in one species but not in the other, and two group of DEGs (up- or
9 down-regulated) in both species.
10

1
2
3
4
5
6
7
8
9
10
11
12
13
14
15
16
17
18
19
20
21
22
23
24
25
26
27
28
29
30
31
32
33
34

SUPPLEMENTAL FIGURE LEGENDS

Supplemental Figure 1 (Supports Figure 1). Photosynthetic-related responses of *A. thaliana* and *C. hirsuta* seedlings to changing light conditions. **(A)** Maximum photochemical efficiency of PSII in the dark-adapted state (F_v/F_m) of seedlings germinated and grown for 7 days under W (20-24 PAR, white) and then either transferred to high light (HL, 200 PAR, yellow) for 7 more days followed by low light (LL, 4 PAR, grey) for another week (left plot) or first to LL and then to HL (right plot). Values represent mean and standard error of $n=7$ seedlings per treatment. **(B)** Chlorophyll levels in *A. thaliana* and *C. hirsuta* seedlings transferred from W to HL for 7 days as described in **A**. Mean and standard deviation of $n=3$ pools of seedlings are represented relative to the levels in W-grown seedlings. **(C)** Rapid light curves of relative photosynthetic electron transport rate (rETR) versus incident photon irradiance (PAR) in *A. thaliana* (left) and *C. hirsuta* (right) seedlings germinated and grown for 7 days under W and then exposed for one day to either W or LL. Values shown are mean and standard error of $n = 5$ samples.

Supplemental Figure 2 (Supports Figure 1). Light spectra of the treatments used in this study. Spectral photon distribution of control white light (R:FR = 5.83, upper), low R:FR (0.055, middle) and very low R:FR (R:FR = 0.020, lower) treatments. Units of irradiance are given per nm. Bars indicate wavelengths used for estimating the R:FR.

Supplemental Figure 3 (Supports Figure 1). Longitudinal length of *A. thaliana* and *C. hirsuta* leaves respond differently to simulated shade. **(A)** Aspect of representative leaves of *A. thaliana* (left) and *C. hirsuta* (right). A red-dotted line illustrates the limits of the organs measured in *A. thaliana* (petiole) and *C. hirsuta* (petiole and rachis). Heteroblastic leaf series of *A. thaliana* **(B)** and *C. hirsuta* **(C)** wild-type genotypes of plants grown under W or W+FR. The two cotyledons and rosette leaves 1 to 9 (*A. thaliana*) or 1 to 8 (*C. hirsuta*) are shown from left to right. Leaves used to measure petiole and rachis length are indicated with numbers. Scale bar is 1 cm.

1
2
3
4
5
6
7
8
9
10
11
12
13
14
15
16
17
18
19
20
21
22
23
24
25
26
27
28
29
30
31
32
33
34

Supplemental Figure 4 (Supports Figure 2). *A. thaliana* and *C. hirsuta* seedlings change gene expression differently in response to simulated shade. **(A)** Venn diagram representing the overlap of simulated shade-regulated genes (up- and down-regulated genes) between *At*^{WT} and *Ch*^{WT} seedlings grown as indicated in Figure 2A. **(B)** Venn diagrams representing the overlap in significantly overrepresented gene ontology (GO) biological process (left) and molecular function (right) terms among genes up-regulated by the W+FR treatment only in *At*^{WT} or *Ch*^{WT}, or in both species. **(C)** Shade-induced changes in *A. thaliana* and *C. hirsuta* gene expression profiles differ from those of two *Geranium* species displaying divergent responses to vegetation proximity. Venn diagrams representing the overlap of up- (left) and down-regulated (right) genes in response to simulated shade between *At*^{WT} and *Ch*^{WT} seedlings, and *G. pyrenaicum* (*Gpyr*) and *G. robertianum* (*Grob*) petioles (Gommers *et al.*, 2017).

Supplemental Figure 5 (Supports Figure 2). The expression of a set of shade-induced but auxin-dependent genes, identified in *A. thaliana*, is also shade-induced in *C. hirsuta*. Expression values were obtained from (1) RNA-seq data on *At*^{WT} (*Col-0*), *pif7-1* and *sav3-2* (Li *et al.*, 2012), (2) Affymetrix array data on *At*^{WT} and *sav3-2* (Bou-Torrent *et al.*, 2014; Tao *et al.*, 2008), and RNA-seq data on *At*^{WT} and *Ch*^{WT} (Supplemental Data Sets 1-4). **(A)** Venn diagram analyses were used to identify a set of 13 genes significantly induced in response to 1h of shade in *At*^{WT} but not in *sav3-2* and *pif7-1* mutant seedlings. **(B)** Fold change induction of the expression of the indicated set of 13 genes after 1 h of low R:FR in *At*^{WT} (*Col-0*), *pif7-1* and *sav3-2* (Li *et al.*, 2012) (upper graph), *At*^{WT} and *sav3-2* (Bou-Torrent *et al.*, 2014; Tao *et al.*, 2008) (middle graph), and *At*^{WT} and *Ch*^{WT} (lower graph; in this experiment, expression of *IAA6*, *SAUR46* and *At3g28420* was not found as shade induced). Asterisks indicate those values shown to be significantly induced by shade in the corresponding statistics analyses.

Supplemental Figure 6 (Supports Figure 3). Reduction of phyA activity in *C. hirsuta* seedlings results in a *sis* phenotype. **(A)** Alignment of PHYA amino acid sequences around the G913 (red arrow) identified as mutated in the *PHYA*

1 gene of *sis1-2* plants from a broad range of angiosperms plant species:
2 *Arabidopsis lyrata* (*A. lyrata*, 1122 residues), *Arabidopsis thaliana* (*A. thaliana*,
3 1122 residues), *Brassica rapa* (*B. rapa*, 1210 residues), *Carica papaya* (*C.*
4 *papaya*, 986 residues), *Capsella rubella* (*C. rubella*, 1122 residues), *Cardamine*
5 *hirsuta* (*C. hirsuta*, 1122 residues), *Citrus sinensis* (*C. sinensis*, 1117 residues),
6 *Manihot esculenta* (*M. esculenta*, 1123 residues), *Oryza sativa* (*O. sativa*, 1128
7 residues), *Populus trichocarpa* (*P. trichocarpa*, 1126 residues), *Phaseolus*
8 *vulgaris* (*Ph. vulgaris*, 1123 residues), *Solanum lycopersicum* (*S. lycopersicum*,
9 1123 residues), *Solanum tuberosum* (*S. tuberosum*, 1123 residues), *Sorghum*
10 *bicolor* (*S. bicolor*, 1131 residues), *Thellungiella halophila* (*T. halophila*, 1122
11 residues) and *Zea mays* (*Z. mays*, 1131 residues). **(B)** *ChPHYA* gene
12 expression analysis in 6-day-old etiolated seedlings of wild-type (Ch^{WT}) and
13 three independent RNAi:*ChPHYA* lines. Transcript abundance, normalized to
14 *ChEF1 α* is shown. Values are means and s.e.m. of three independent RT-
15 qPCR biological replicates relative to Ch^{WT} values. Asterisks indicate significant
16 differences (** $p < 0.01$) relative to Ch^{WT} levels. **(C)** Immunoblot detection of
17 PHYA (upper band) and tubulin (lower band) with mouse monoclonal anti-PHYA
18 and anti-TUB antibodies in extracts of 6-day-old etiolated seedlings of Ch^{WT} ,
19 and three independent RNAi:*ChPHYA* lines. **(D)** Hypocotyl length of d7
20 seedlings of Ch^{WT} and three independent RNAi:*ChPHYA* lines grown as
21 indicated in Figure 1A. Asterisks indicate significant differences (** $p < 0.01$)
22 relative to Ch^{WT} growing under the same light conditions.

23

24 **Supplemental Figure 7** (Supports Figure 5). Partial alignment of
25 *ChPHYA/AtPHYA*, *ChEF1 α /AtEF1 α* , *ChSPC25/AtSPC25* and *ChYLS8/AtYLS8*
26 sequences. The location of the common primers used to quantify and compare
27 expression levels by RT-qPCR between species is shown.

28

29 **Supplemental Figure 8** (Supports Figure 6). Strategies to compare biological
30 activity between *AtphyA* and *ChphyA* in transgenic lines. **(A)** Cartoons
31 describing the growth conditions employed to analyze the expression of
32 *AtPHYA* and *ChPHYA* and/or *phyA* protein levels in the different lines analyzed.
33 Etiolated seedlings were grown for 4 days in the dark before harvesting (white
34 asterisk, upper panel) for RNA and protein extraction. Seedlings were grown for

1 2 days under W then for 5 additional days under W+FR before harvesting (white
2 asterisk, lower panels) for RNA extraction. **(B)** Correlation between levels of
3 *PHYA* expression in seedlings grown under simulated shade (*PHYA*_{W+FR}) and
4 in darkness (*PHYA*_D). **(C-E)** Correlation between Hyp_{W+FR}-Hyp_W (estimated
5 phyA activity in simulated shade) and relative levels of *PHYA* expression in **(C)**
6 etiolated seedlings (*PHYA*_D, left panel) or seedlings grown under simulated
7 shade (*PHYA*_{W+FR}, right panel), **(D)** relative phyA protein levels in etiolated
8 seedlings (*PHYA*:TUB), and Hyp_D-Hyp_{FR} (estimated phyA activity during
9 seedling de-etiolation under FR) for the different lines analyzed. In **B** to **E**, the
10 estimated regression equation (top of graph) and the estimated R² values are
11 shown for each plot, and grey arrows indicate the lines shown in Figure 6. **(F)**
12 Summary of the correlations observed between the estimated AtphyA and
13 ChphyA biological activities and transgenic *PHYA* expression and phyA protein
14 levels in the various *phyA>AtPHYA* and *phyA>ChPHYA* complementation lines.
15 Only positive correlations, indicated with discontinuous green lines with arrows
16 in both ends, are shown.

17

18 **Supplemental Figure 9** (Supports Figure 7). The expression of a set of shade-
19 induced phyA-repressed genes, identified in *A. thaliana*, is attenuated in *C.*
20 *hirsuta*. **(A)** Fold change induction after 1 h of low R:FR of the expression of the
21 top genes induced in *phyA-211* (but not in At^{WT}) (Yang *et al.*, 2018) (upper
22 graph), and At^{WT} and Ch^{WT} (lower graph). **(B)** Fold change induction after 1 h of
23 low R:FR of the expression of the top genes (and *GH3.3*) more induced in
24 *phyA-211* than At^{WT} (Yang *et al.*, 2018) (upper graph), and At^{WT} and Ch^{WT}
25 (lower graph). In **A** and **B**, only those genes found as shade induced in At^{WT} or
26 Ch^{WT} are included. Asterisks indicate those values shown to be significantly
27 induced by shade in At^{WT} or Ch^{WT}.

28

29 **Supplemental Figure 10** (Supports Figures 6 and 7). Alignment of *C. hirsuta*
30 and *A. thaliana* phyA amino acid sequences. The three different types of point
31 differences found are highlighted in green, pink or blue colors. In red are
32 pointed the two residues in the ChphyA sequence mutated in *sis1-1* and *sis1-2*
33 lines.

34

1 **SUPPLEMENTAL REFERENCES**

2 **Anders, S. and Huber, W.** (2010) Differential expression analysis for sequence
3 count data. *Genome Biol*, **11**, R106.

4 **Bou-Torrent, J., Galstyan, A., Gallemi, M., Cifuentes-Esquivel, N., Molina-**
5 **Contreras, M.J., Salla-Martret, M., Jikumaru, Y., Yamaguchi, S., Kamiya,**
6 **Y. and Martinez-Garcia, J.F.** (2014) Plant proximity perception dynamically
7 modulates hormone levels and sensitivity in Arabidopsis. *J Exp Bot*, **65**,
8 2937-2947.

9 **Galbiati, F., Sinha Roy, D., Simonini, S., Cucinotta, M., Ceccato, L., Cuesta,**
10 **C., Simaskova, M., Benkova, E., Kamiuchi, Y., Aida, M., Weijers, D.,**
11 **Simon, R., Masiero, S. and Colombo, L.** (2013) An integrative model of the
12 control of ovule primordia formation. *Plant J*, **76**, 446-455.

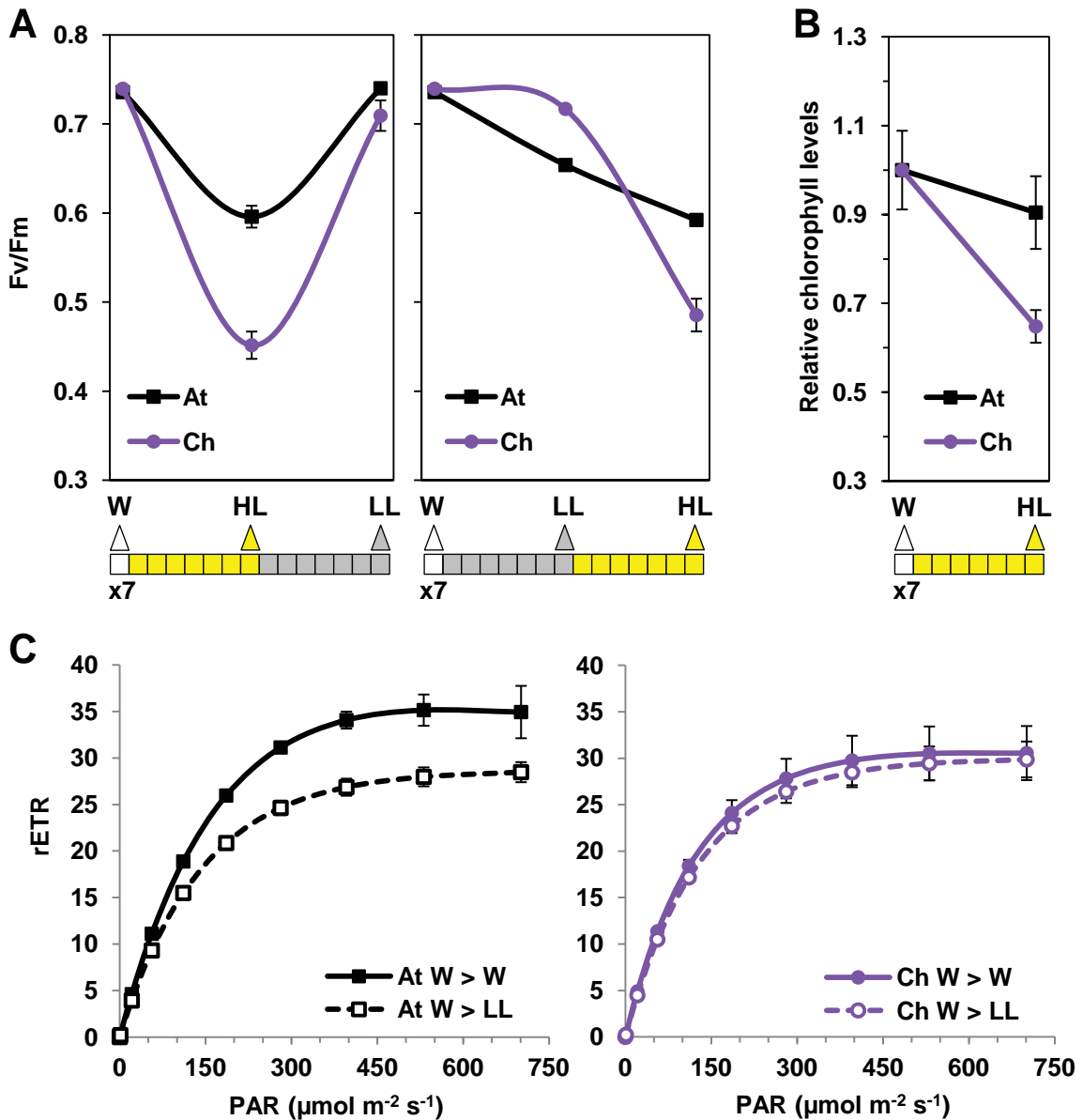
13 **Gallemi, M., Galstyan, A., Paulisic, S., Then, C., Ferrandez-Ayela, A.,**
14 **Lorenzo-Orts, L., Roig-Villanova, I., Wang, X., Micol, J.L., Ponce, M.R.,**
15 **Devlin, P.F. and Martinez-Garcia, J.F.** (2016) DRACULA2 is a dynamic
16 nucleoporin with a role in regulating the shade avoidance syndrome in
17 Arabidopsis. *Development*, **143**, 1623-1631.

18 **Gallemi, M., Molina-Contreras, M.J., Paulisic, S., Salla-Martret, M., Sorin,**
19 **C., Godoy, M., Franco-Zorrilla, J.M., Solano, R. and Martinez-Garcia, J.F.**
20 (2017) A non-DNA-binding activity for the ATHB4 transcription factor in the
21 control of vegetation proximity. *New Phytol*.

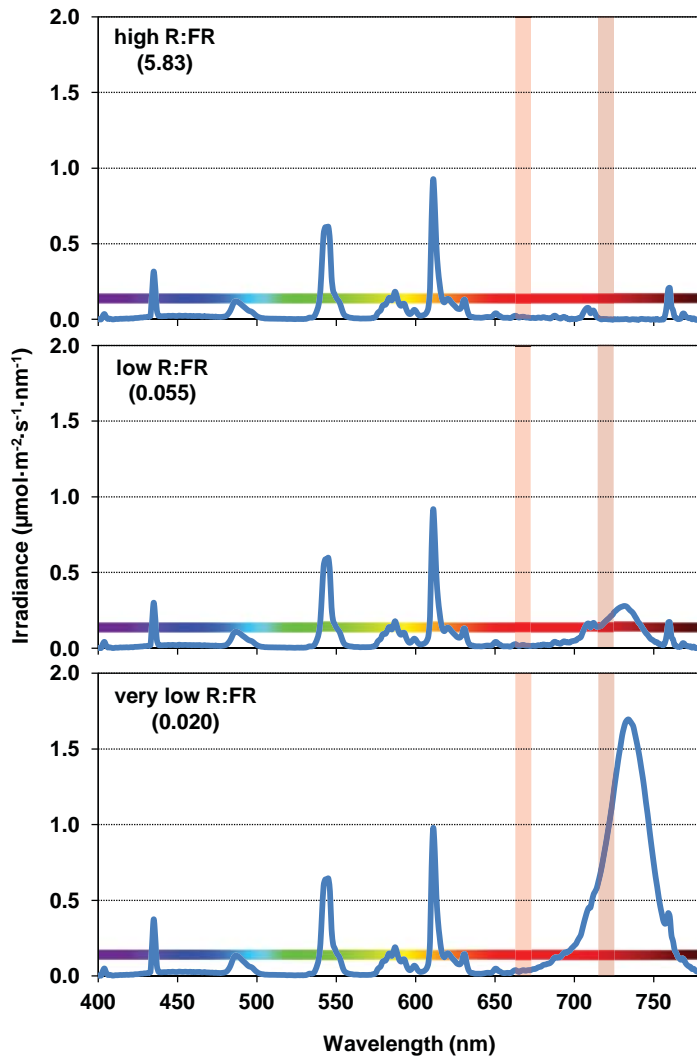
22 **Gan, X., Hay, A., Kwantes, M., Haberer, G., Hallab, A., Ioio, R.D., Hofhuis,**
23 **H., Pieper, B., Cartolano, M., Neumann, U., Nikolov, L.A., Song, B.,**
24 **Hajheidari, M., Briskine, R., Kougioumoutzi, E., Vlad, D., Broholm, S.,**
25 **Hein, J., Meksem, K., Lightfoot, D., Shimizu, K.K., Shimizu-Inatsugi, R.,**
26 **Imprialou, M., Kudrna, D., Wing, R., Sato, S., Huijser, P., Filatov, D.,**
27 **Mayer, K.F., Mott, R. and Tsiantis, M.** (2016) The Cardamine hirsuta
28 genome offers insight into the evolution of morphological diversity. *Nat*
29 *Plants*, **2**, 16167.

30 **Gommers, C.M., Keuskamp, D.H., Buti, S., van Veen, H., Koevoets, I.T.,**
31 **Reinen, E., Voesenek, L.A. and Pierik, R.** (2017) Molecular Profiles of
32 Contrasting Shade Response Strategies in Wild Plants: Differential Control of
33 Immunity and Shoot Elongation. *Plant Cell*, **29**, 331-344.

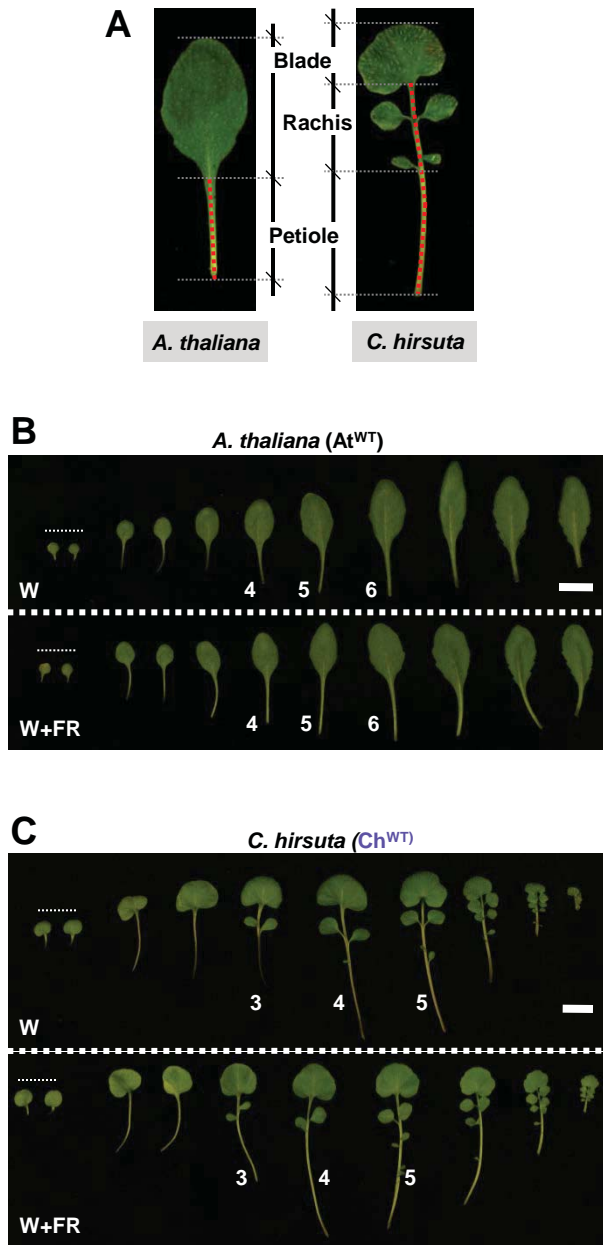
- 1 **Kim, D., Perteza, G., Trapnell, C., Pimentel, H., Kelley, R. and Salzberg, S.L.**
2 (2013) TopHat2: accurate alignment of transcriptomes in the presence of
3 insertions, deletions and gene fusions. *Genome Biol*, **14**, R36.
- 4 **Li, L., Ljung, K., Breton, G., Schmitz, R.J., Pruneda-Paz, J., Cowing-Zitron,**
5 **C., Cole, B.J., Ivans, L.J., Pedmale, U.V., Jung, H.S., Ecker, J.R., Kay,**
6 **S.A. and Chory, J.** (2012) Linking photoreceptor excitation to changes in
7 plant architecture. *Genes Dev*, **26**, 785-790.
- 8 **Mott, R., Yuan, W., Kaisaki, P., Gan, X., Cleak, J., Edwards, A., Baud, A.**
9 **and Flint, J.** (2014) The architecture of parent-of-origin effects in mice. *Cell*,
10 **156**, 332-342.
- 11 **Roig-Villanova, I., Bou, J., Sorin, C., Devlin, P.F. and Martinez-Garcia, J.F.**
12 (2006) Identification of primary target genes of phytochrome signaling. Early
13 transcriptional control during shade avoidance responses in Arabidopsis.
14 *Plant Physiology*, **141**, 85-96.
- 15 **Somers, D.E., Sharrock, R.A., Tepperman, J.M. and Quail, P.H.** (1991) The
16 *hy3* Long Hypocotyl Mutant of Arabidopsis Is Deficient in Phytochrome B.
17 *Plant Cell*, **3**, 1263-1274.
- 18 **Tao, Y., Ferrer, J.L., Ljung, K., Pojer, F., Hong, F., Long, J.A., Li, L.,**
19 **Moreno, J.E., Bowman, M.E., Ivans, L.J., Cheng, Y., Lim, J., Zhao, Y.,**
20 **Ballare, C.L., Sandberg, G., Noel, J.P. and Chory, J.** (2008) Rapid
21 synthesis of auxin via a new tryptophan-dependent pathway is required for
22 shade avoidance in plants. *Cell*, **133**, 164-176.
- 23 **Toledo-Ortiz, G., Kiryu, Y., Kobayashi, J., Oka, Y., Kim, Y., Nam, H.G.,**
24 **Mochizuki, N. and Nagatani, A.** (2010) Subcellular sites of the signal
25 transduction and degradation of phytochrome A. *Plant Cell Physiol*, **51**, 1648-
26 1660.
- 27 **Yang, C., Xie, F., Jiang, Y., Li, Z., Huang, X. and Li, L.** (2018) Phytochrome A
28 Negatively Regulates the Shade Avoidance Response by Increasing
29 Auxin/Indole Acetic Acid Protein Stability. *Dev Cell*, **44**, 29-41 e24.
- 30
31
32

**Supplemental Figure 1.** (Supports Figure 1)

Photosynthetic-related responses of *A. thaliana* and *C. hirsuta* seedlings to changing light conditions. **(A)** Maximum photochemical efficiency of PSII in the dark-adapted state (F_v/F_m) of seedlings germinated and grown for 7 days under W (20-24 PAR, white) and then either transferred to high light (HL, 200 PAR, yellow) for 7 more days followed by low light (LL, 4 PAR, grey) for another week (left plot) or first to LL and then to HL (right plot). Values represent mean and standard error of $n=7$ seedlings per treatment. **(B)** Chlorophyll levels in *A. thaliana* and *C. hirsuta* seedlings transferred from W to HL for 7 days as described in **A**. Mean and standard deviation of $n=3$ pools of seedlings are represented relative to the levels in W-grown seedlings. **(C)** Rapid light curves of relative photosynthetic electron transport rate (rETR) versus incident photon irradiance (PAR) in *A. thaliana* (left) and *C. hirsuta* (right) seedlings germinated and grown for 7 days under W and then exposed for one day to either W or LL. Values shown are mean and standard error of $n = 5$ samples.

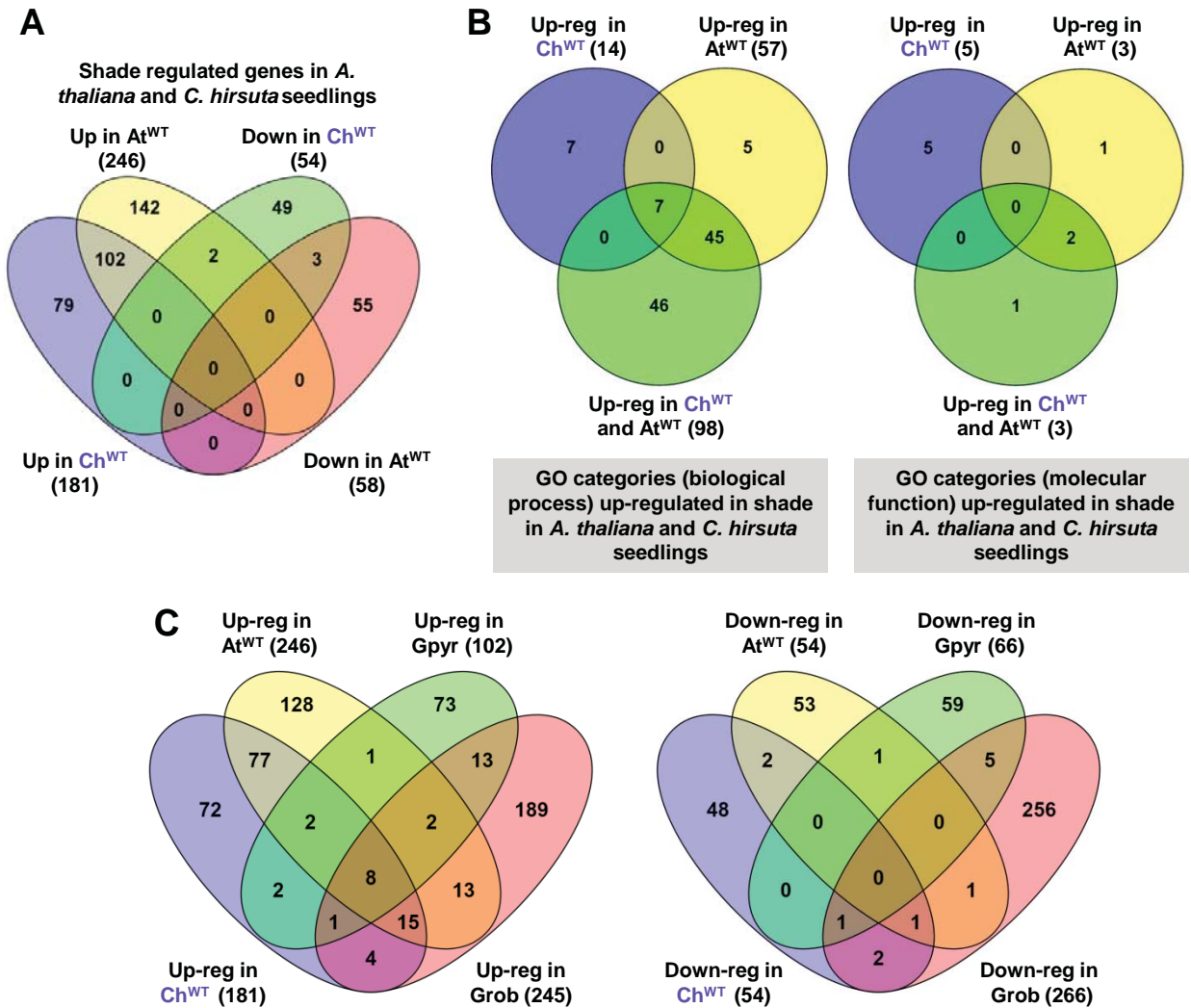


Supplemental Figure 2. Light spectra of the treatments used in this study. Spectral photon distribution of control white light (R:FR = 5.83, upper), low R:FR (0.055, middle) and very low R:FR (R:FR = 0.020, lower) treatments. Units of irradiance are given per nm. Bars indicate wavelengths used for estimating the R:FR.



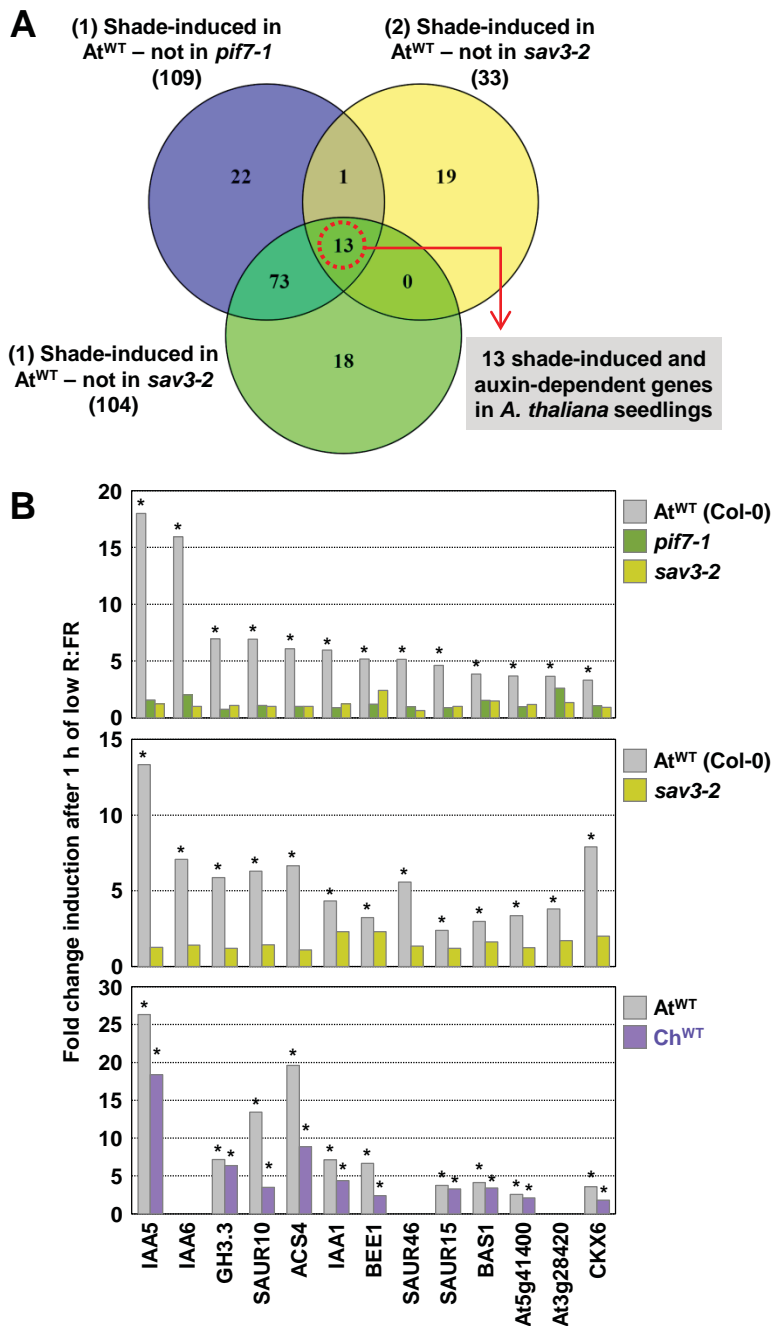
Supplemental Figure 3. (Supports Figure 1)

Longitudinal length of *A. thaliana* and *C. hirsuta* leaves respond differently to simulated shade. **(A)** Aspect of representative leaves of *A. thaliana* (left) and *C. hirsuta* (right). A red-dotted line illustrates the limits of the organs measured in *A. thaliana* (petiole) and *C. hirsuta* (petiole and rachis). Heteroblastic leaf series of *A. thaliana* **(B)** and *C. hirsuta* **(C)** wild-type genotypes of plants grown under W or W+FR. The two cotyledons and rosette leaves 1 to 9 (*A. thaliana*) or 1 to 8 (*C. hirsuta*) are shown from left to right. Leaves used to measure petiole and rachis length are indicated with numbers. Scale bar is 1 cm.



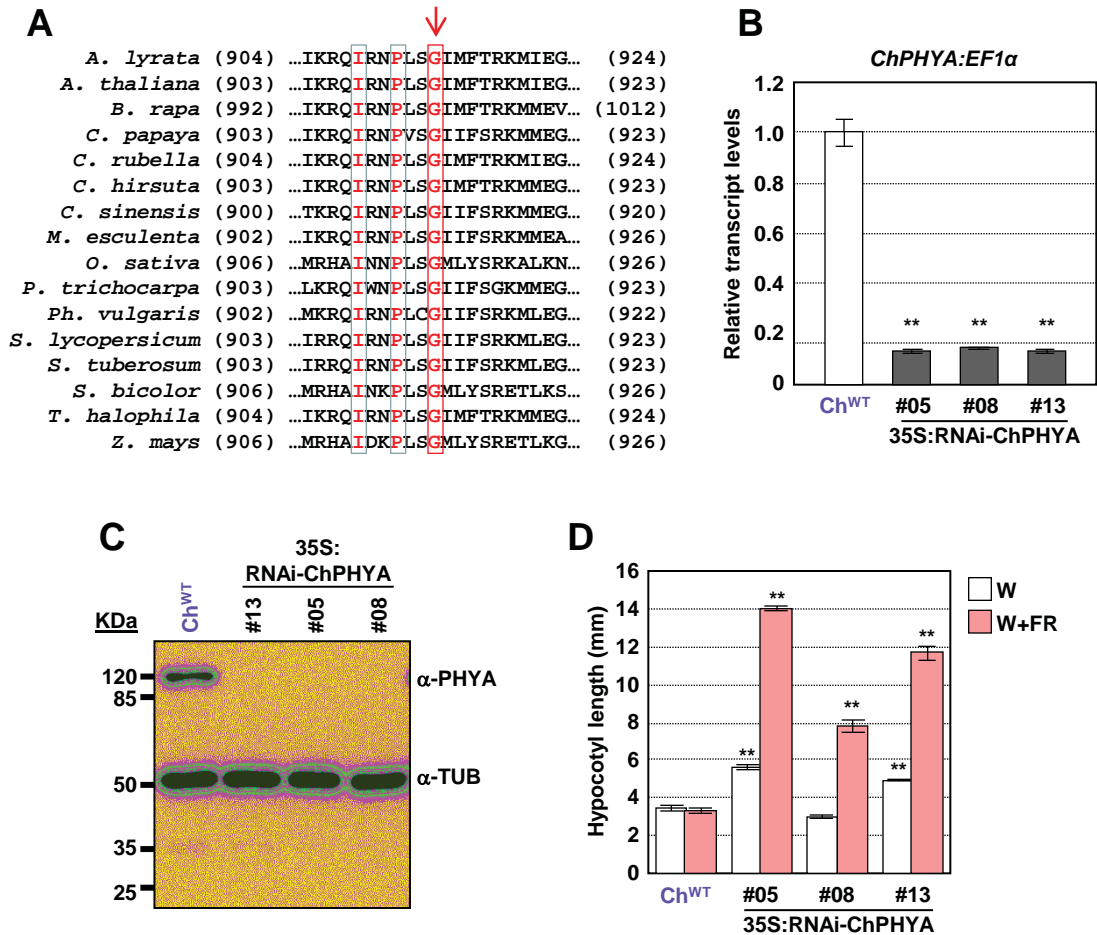
Supplemental Figure 4. (Supports Figure 2)

A. thaliana and *C. hirsuta* seedlings change gene expression differently in response to simulated shade. **(A)** Venn diagram representing the overlap of simulated shade-regulated genes (up- and down-regulated genes) between *At*^{WT} and *Ch*^{WT} seedlings grown as indicated in Figure 2A. **(B)** Venn diagrams representing the overlap in significantly overrepresented gene ontology (GO) biological process (left) and molecular function (right) terms among genes up-regulated by the W+FR treatment only in *At*^{WT} or *Ch*^{WT}, or in both species. **(C)** Shade-induced changes in *A. thaliana* and *C. hirsuta* gene expression profiles differ from those of two *Geranium* species displaying divergent responses to vegetation proximity. Venn diagrams representing the overlap of up- (left) and down-regulated (right) genes in response to simulated shade between *At*^{WT} and *Ch*^{WT} seedlings, and *G. pyrenaicum* (*Gpyr*) and *G. robertianum* (*Grob*) petioles (Gommers et al., 2017).



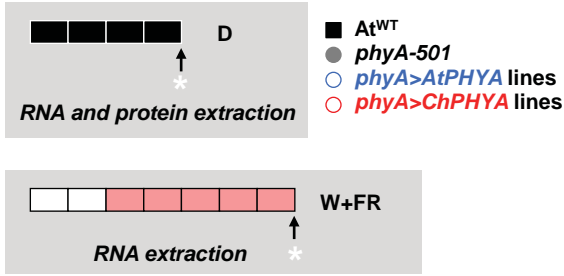
Supplemental Figure 5. (Supports Figure 2)

The expression of a set of shade-induced but auxin-dependent genes, identified in *A. thaliana*, is also shade-induced in *C. hirsuta*. Expression values were obtained from (1) RNA-seq data on *At*^{WT} (Col-0), *pif7-1* and *sav3-2* (Li et al., 2012), (2) Affymetrix array data on *At*^{WT} and *sav3-2* (Bou-Torrent et al., 2014; Tao et al., 2008), and RNA-seq data on *At*^{WT} and *Ch*^{WT} (Supplemental Data Sets 1-4). **(A)** Venn diagram analyses were used to identify a set of 13 genes significantly induced in response to 1h of shade in *At*^{WT} but not in *sav3-2* and *pif7-1* mutant seedlings. **(B)** Fold change induction of the expression of the indicated set of 13 genes after 1 h of low R:FR in *At*^{WT} (Col-0), *pif7-1* and *sav3-2* (Li et al., 2012) (upper graph), *At*^{WT} and *sav3-2* (Bou-Torrent et al., 2014; Tao et al., 2008) (middle graph), and *At*^{WT} and *Ch*^{WT} (lower graph; in this experiment, expression of *IAA6*, *SAUR46* and *At3g28420* was not found as shade induced). Asterisks indicate those values shown to be significantly induced by shade in the corresponding statistics analyses.

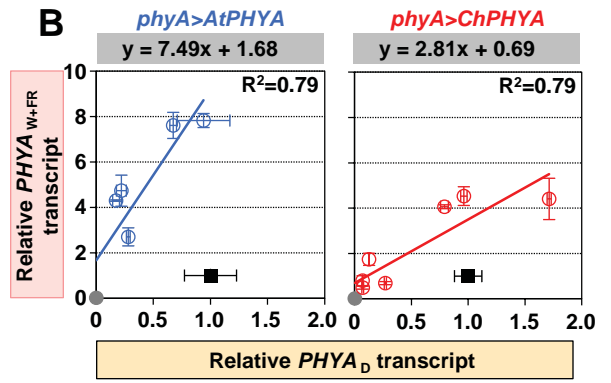
**Supplemental Figure 6.** (Supports Figure 3)

Reduction of *phyA* activity in *C. hirsuta* seedlings results in a *sis* phenotype. **(A)** Alignment of PHYA amino acid sequences around the G913 (red arrow) identified as mutated in the *PHYA* gene of *sis1-2* plants from a broad range of angiosperms plant species: *Arabidopsis lyrata* (*A. lyrata*, 1122 residues), *Arabidopsis thaliana* (*A. thaliana*, 1122 residues), *Brassica rapa* (*B. rapa*, 1210 residues), *Carica papaya* (*C. papaya*, 986 residues), *Capsella rubella* (*C. rubella*, 1122 residues), *Cardamine hirsuta* (*C. hirsuta*, 1122 residues), *Citrus sinensis* (*C. sinensis*, 1117 residues), *Manihot esculenta* (*M. esculenta*, 1123 residues), *Oryza sativa* (*O. sativa*, 1128 residues), *Populus trichocarpa* (*P. trichocarpa*, 1126 residues), *Phaseolus vulgaris* (*Ph. vulgaris*, 1123 residues), *Solanum lycopersicum* (*S. lycopersicum*, 1123 residues), *Solanum tuberosum* (*S. tuberosum*, 1123 residues), *Sorghum bicolor* (*S. bicolor*, 1131 residues), *Thellungiella halophila* (*T. halophila*, 1122 residues) and *Zea mays* (*Z. mays*, 1131 residues). **(B)** *ChPHYA* gene expression analysis in 6-day-old etiolated seedlings of wild-type (Ch^{WT}) and three independent RNAi:ChPHYA lines. Transcript abundance, normalized to *ChEF1α* is shown. Values are means and s.e.m. of three independent RT-qPCR biological replicates relative to Ch^{WT} values. Asterisks indicate significant differences (***p*<0.01) relative to Ch^{WT} levels. **(C)** Immunoblot detection of PHYA (upper band) and tubulin (lower band) with mouse monoclonal anti-PHYA and anti-TUB antibodies in extracts of 6-day-old etiolated seedlings of Ch^{WT}, and three independent RNAi:ChPHYA lines. **(D)** Hypocotyl length of d7 seedlings of Ch^{WT} and three independent RNAi:ChPHYA lines grown as indicated in Figure 1A. Asterisks indicate significant differences (***p*<0.01) relative to Ch^{WT} growing under the same light conditions.

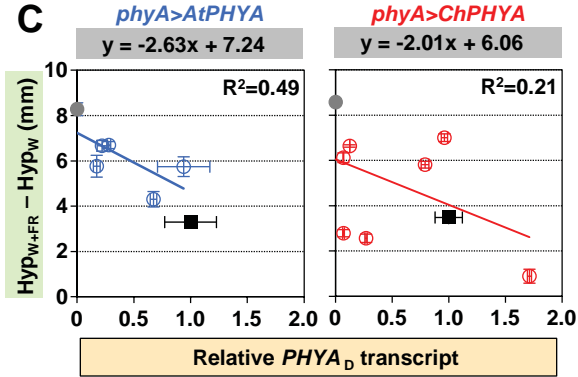
A



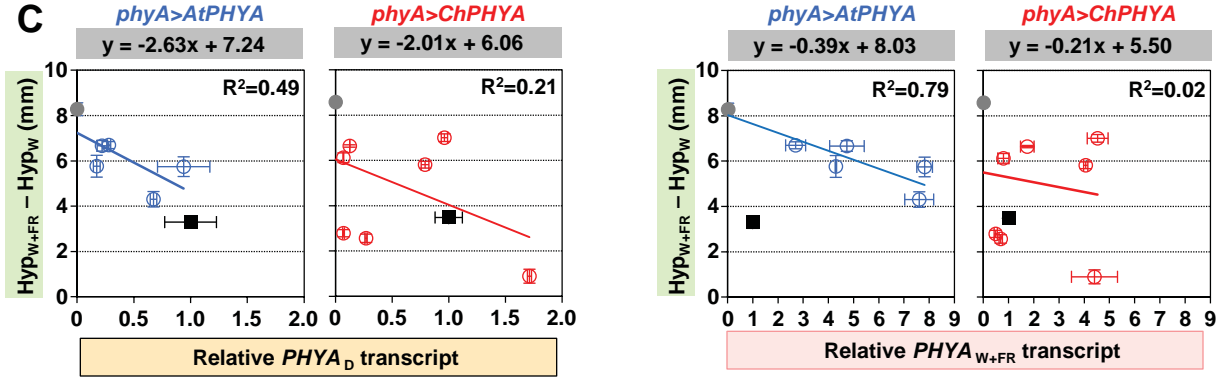
B



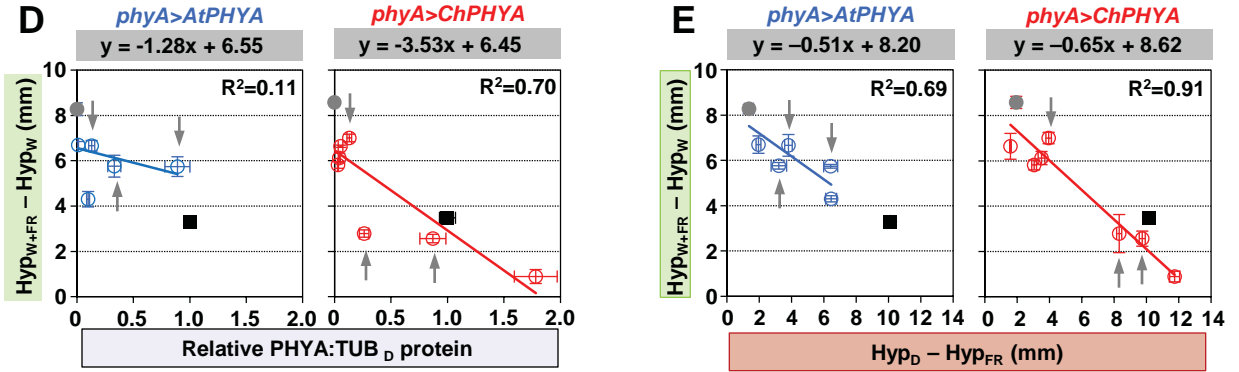
C



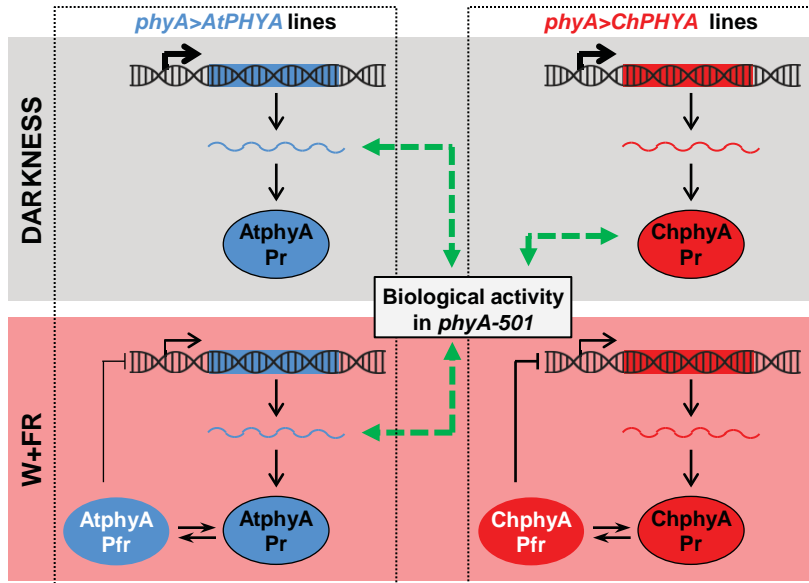
D



E

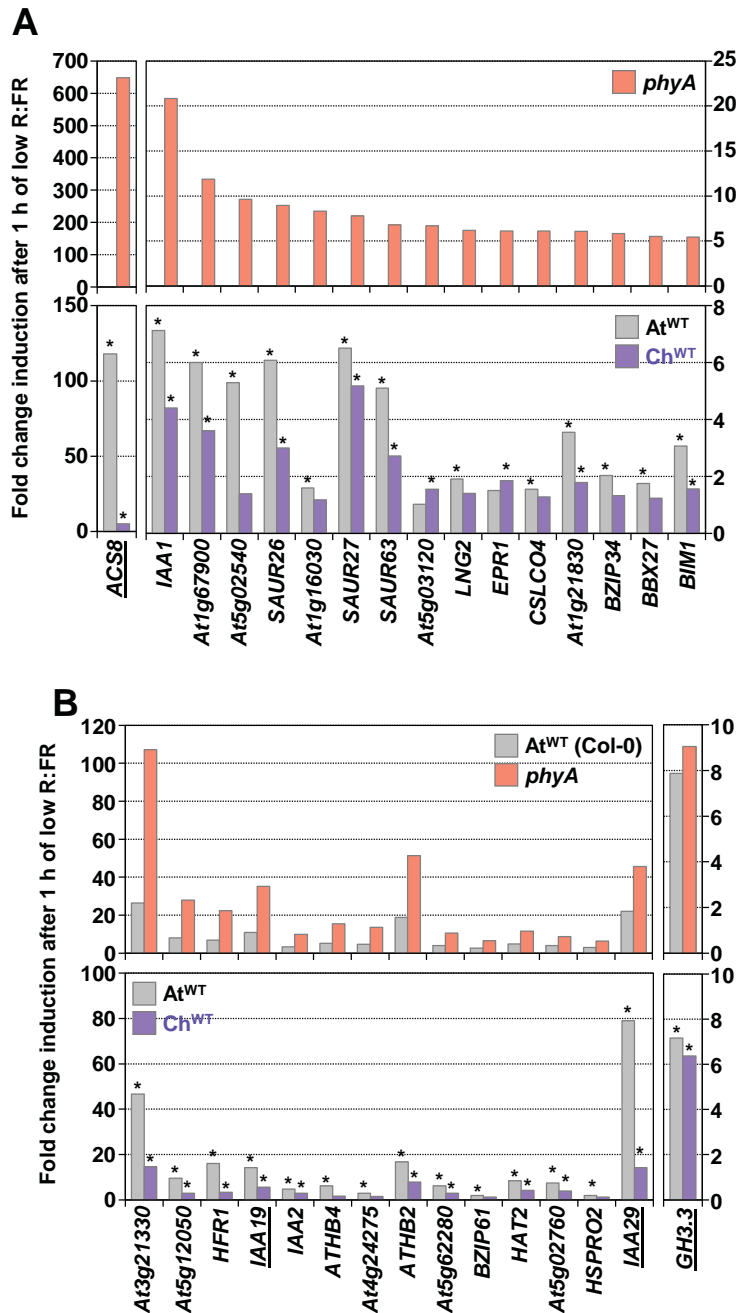


F



Supplemental Figure 8. (Supports Figure 6)

Strategies to compare biological activity between AtphyA and ChphyA in transgenic lines. **(A)** Cartoons describing the growth conditions employed to analyze the expression of *AtPHYA* and *ChPHYA* and/or phyA protein levels in the different lines analyzed. Etiolated seedlings were grown for 4 days in the dark before harvesting (white asterisk, upper panel) for RNA and protein extraction. Seedlings were grown for 2 days under W then for 5 additional days under W+FR before harvesting (white asterisk, lower panels) for RNA extraction. **(B)** Correlation between levels of *PHYA* expression in seedlings grown under simulated shade ($PHYA_{W+FR}$) and in darkness ($PHYA_D$). **(C-E)** Correlation between $Hyp_{W+FR}-Hyp_W$ (estimated phyA activity in simulated shade) and relative levels of *PHYA* expression in **(C)** etiolated seedlings ($PHYA_D$, left panel) or seedlings grown under simulated shade ($PHYA_{W+FR}$, right panel), **(D)** relative phyA protein levels in etiolated seedlings (PHYA:TUB), and Hyp_D-Hyp_{FR} (estimated phyA activity during seedling de-etiolation under FR) for the different lines analyzed. In **B** to **E**, the estimated regression equation (top of graph) and the estimated R^2 values are shown for each plot, and grey arrows indicate the lines shown in Figure 6. **(F)** Summary of the correlations observed between the estimated AtphyA and ChphyA biological activities and transgenic *PHYA* expression and phyA protein levels in the various *phyA>AtPHYA* and *phyA>ChPHYA* complementation lines. Only positive correlations, indicated with discontinuous green lines with arrows in both ends, are shown.



Supplemental Figure 9. (Supports Figure 7)

The expression of a set of shade-induced *phyA*-repressed genes, identified in *A. thaliana*, is attenuated in *C. hirsuta*. **(A)** Fold change induction after 1 h of low R:FR of the expression of the top genes induced in *phyA-211* (but not in *At*^{WT}) (Yang et al., 2018) (upper graph), and *At*^{WT} and *Ch*^{WT} (lower graph). **(B)** Fold change induction after 1 h of low R:FR of the expression of the top genes (and *GH3.3*) more induced in *phyA-211* than *At*^{WT} (Yang et al., 2018) (upper graph), and *At*^{WT} and *Ch*^{WT} (lower graph). In **A** and **B**, only those genes found as shade induced in *At*^{WT} or *Ch*^{WT} are included. Asterisks indicate those values shown to be significantly induced by shade in *At*^{WT} or *Ch*^{WT}.

```

ChPHYA  MSGSRPSQSSEGSRRSRHSARIAIAQTTVDAKLHADFEESGSSFDYSTSVRVTGPVVENQP 60
AtPHYA  MSGSRPQSSEGSRRSRHSARIAIAQTTVDAKLHADFEESGSSFDYSTSVRVTGPVVENQP 60
*****.*****

ChPHYA  PRSDKVTTTYLHHIQGKLIQPFGLLALDEKTFKVIAYSENAPPELLTMASHAVPSVGEH 120
AtPHYA  PRSDKVTTTYLHHIQGKLIQPFGLLALDEKTFKVIAYSENASELLTMASHAVPSVGEH 120
*****.*****

ChPHYA  PVLGIGTDIRSLFTAPSASALQKALGFGDVSLNLPILVHCKTSAPFFYAIVHRVTGSII 180
AtPHYA  PVLGIGTDIRSLFTAPSASALQKALGFGDVSLNLPILVHCRRTSAPFFYAIHRVTGSII 180
*****.*****

ChPHYA  DFEPVKPYEVPMTAAGALQSYKLAAKAITRLQSLPSGSMERLCDTMVQEVFELTGYDRVM 240
AtPHYA  DFEPVKPYEVPMTAAGALQSYKLAAKAITRLQSLPSGSMERLCDTMVQEVFELTGYDRVM 240
*****.*****

ChPHYA  AYKFHEDDHGEVVEVTKPGLEPYLGLHYPATDIPQAARFLFMKNKVRMIVDCNAKHARV 300
AtPHYA  AYKFHEDDHGEVVEVTKPGLEPYLGLHYPATDIPQAARFLFMKNKVRMIVDCNAKHARV 300
*****.*****

ChPHYA  LQDEKLSFDLTLGCGSTLRAPHSCHLQYMANMDSIASLVMVAVVNEEDGEGDAPDSTTPQ 360
AtPHYA  LQDEKLSFDLTLGCGSTLRAPHSCHLQYMANMDSIASLVMVAVVNEEDGEGDAPDATTTPQ 360
*****.*****

ChPHYA  KRKRLWGLVVCNTTFRFVFPFLRYACEFLAQVFAIHVNKEVELENQIVEKNILRTQTLL 420
AtPHYA  KRKRLWGLVVCNTTFRFVFPFLRYACEFLAQVFAIHVNKEVELDNQIVEKNILRTQTLL 420
*****.*****

ChPHYA  CDMLMRDAPLGIIVSQSPNIMDLVKCDGAALLYKDKIWKLGTTSPDFHLQEIASWLEYHT 480
AtPHYA  CDMLMRDAPLGIIVSQSPNIMDLVKCDGAALLYKDKIWKLGTTSPDFHLQEIASWLEYHM 480
*****.*****

ChPHYA  DSTGLSTDSLHDAGFPKALGLGDSVCGMAAVRISSKDMIFWFRSHTAGEVRRWGAKHDPD 540
AtPHYA  DSTGLSTDSLHDAGFPKALGLGDSVCGMAAVRISSKDMIFWFRSHTAGEVRRWGAKHDPD 540
*****.*****

ChPHYA  DRDDARRMHPRSSFKAFLEVVKTRSLPWKDYEMDAIHSLQLLRNAFKDSESTDVNTKTI 600
AtPHYA  DRDDARRMHPRSSFKAFLEVVKTRSLPWKDYEMDAIHSLQLLRNAFKDSESTDVNTKVI 600
*****.*****

ChPHYA  HSKLNLKIDIGIQELEAVTSEMVRLETATVPIILAVSDGLVNGWNTKIAELTGLVDEA 660
AtPHYA  VSKLNLKIDIGIQELEAVTSEMVRLETATVPIILAVSDGLVNGWNTKIAELTGLVDEA 660
*****.*****

ChPHYA  IGKHLTLVEDSSVEIVKRMLENALEGTEEQNVQFEIKTHLSRADAGPISLVVNACASRD 720
AtPHYA  IGKHLTLVEDSSVEIVKRMLENALEGTEEQNVQFEIKTHLSRADAGPISLVVNACASRD 720
*****.*****

ChPHYA  LHENVVGVCFVAHDLTGQKTVMDFTRIEGDYKAIIQNPPLIPPIFGTDFEGWCTEWNP 780
AtPHYA  LHENVVGVCFVAHDLTGQKTVMDFTRIEGDYKAIIQNPPLIPPIFGTDFEGWCTEWNP 780
*****.*****

ChPHYA  AMSKLTGLKREEVMDKMLLGEVFGTQKSCCRLKNQEAFFVNLGIVLNSAVTSQSEKVSFA 840
AtPHYA  AMSKLTGLKREEVIDKMLLGEVFGTQKSCCRLKNQEAFFVNLGIVLNNAVTSQDEKVSFA 840
*****.*****

ChPHYA  FFTRGGKYTECLLCVSKKLDREGVVTGVFCFLQLASHLQALHVQRLAERTAVKRLKAL 900
AtPHYA  FFTRGGKYTECLLCVSKKLDREGVVTGVFCFLQLASHLQALHVQRLAERTAVKRLKAL 900
*****.*****

ChPHYA  AYIKRQIRNPLSGIMFTRKMEGTELGPEQRRILQTSALCQKQLSKVLDDSDLESIEGC 960
AtPHYA  AYIKRQIRNPLSGIMFTRKMEGTELGPEQRRILQTSALCQKQLSKVLDDSDLESIEGC 960
*****.*****

ChPHYA  LDLEMKEFSLNEVLTASTSQVMMKSNKSVRI TNETGEEVMSDTLYGDSIRLQQLADFM 1020
AtPHYA  LDLEMKEFSLNEVLTASTSQVMMKSNKSVRI TNETGEEVMSDTLYGDSIRLQQLADFM 1020
*****.*****

ChPHYA  LMSVNFPTSGGQLTVASLRKDQLGRSVHLAILEIRLTHTGAGMPEFLLNQMGFTEEDVS 1080
AtPHYA  LMAVNFPTSGGQLTVASLRKDQLGRSVHLAILEIRLTHTGAGMPEFLLNQMGFTEEDVS 1080
*****.*****

ChPHYA  EEGLSLMVSRLVKLMNGDVQYLRQAGKSSFIITAEALAAANK 1122
AtPHYA  EEGLSLMVSRLVKLMNGDVQYLRQAGKSSFIITAEALAAANK 1122
*****.*****

```

Supplemental Figure 10. (Supports Figure 6)

Alignment of *C. hirsuta* and *A. thaliana* phyA amino acid sequences. The three different types of point differences found are highlighted in green, pink or blue colors. In red are pointed the two residues in the ChphyA sequence mutated in *sis1-1* and *sis1-2* lines.

Supplemental Table 1 (Supports Figure 5). RPKM of eight genes commonly used for normalizing in RT-qPCR analyses. Data were extracted from our RNA-seq experiments in *A. thaliana* and *C. hirsuta* seedlings, described in Figure 2A. Transcript levels (read counts) were normalized as RPKM (Reads Per Kilobase of transcript, per Million mapped reads). The expression of most of the orthologous pairs of genes (e.g., a_1 vs. c_1) was within the same range. Shade treatment was not affecting the expression of these normalizing genes in any of the two species. As a positive control, *PIL1* expression was incorporated (row in grey).

		RPKM					
		At ^{WT} - 0 h			At ^{WT} - 1 h W+FR		
		rep1	rep2	rep3	rep1	rep2	rep3
<i>EF1α</i>	At5g60390 (a_1)	1439.643	1642.496	2047.051	1797.248	1625.529	1862.771
<i>SPC25</i>	At2g39960 (a_2)	62.396	66.872	76.918	83.291	77.484	78.664
<i>YLS8</i>	At5g08290 (a_3)	115.577	109.004	142.605	132.587	109.305	130.746
<i>PP2A</i>	At1g13320 (a_4)	23.699	26.735	23.152	25.637	23.123	23.009
<i>SAND</i>	At2g28390 (a_5)	17.314	20.024	18.496	21.273	21.726	25.085
<i>UBC</i>	At5g25760 (a_6)	52.030	51.076	45.266	64.194	55.429	55.481
<i>APX3</i>	At4g35000 (a_7)	85.285	85.520	113.034	92.083	85.010	88.498
<i>ACT2</i>	At3g18780 (a_8)	386.295	378.730	431.258	407.656	386.058	436.198
<i>PIL1</i>	At2g46970	1.202	1.007	0.710	45.187	55.811	51.400
		Ch ^{WT} - 0 h					
		Ch ^{WT} - 0 h			Ch ^{WT} - 1 h W+FR		
		rep1	rep2	rep3	rep1	rep2	rep3
<i>EF1α</i>	CARHR274060 + CARHR274080 (c_1)	1599.331	1589.089	1741.301	1839.943	1584.613	1656.329
<i>SPC25</i>	CARHR134880 + CARHR134890 (c_2)	38.307	27.580	35.691	40.726	38.702	40.127
<i>YLS8</i>	CARHR204840 (c_3)	127.433	95.962	122.678	135.796	127.408	121.078
<i>PP2A</i>	CARHR013700 (c_4)	35.479	32.030	39.510	35.357	35.165	32.101
<i>SAND</i>	CARHR121340 (c_5)	16.898	15.447	17.226	18.281	14.384	14.221
<i>UBC</i>	CARHR187650 (c_6)	48.770	45.744	57.398	55.274	69.315	64.938
<i>APX3</i>	CARHR243280 (c_7)	205.188	178.722	183.599	179.091	188.908	170.422
<i>ACT2</i>	CARHR094190 (c_8)	1017.891	965.459	1073.328	983.693	1018.058	813.392
<i>PIL1</i>	CARHR142340	0.409	0.128	0.130	14.255	20.875	14.204

11
12
13

1 **Supplemental Table 2.** Primers used in this work. Primers for transcript level
 2 analyses by RT-qPCR of *A. thaliana* *ATHB2*, *PIL1* and *UBQ10* have been
 3 described elsewhere (Gallemi *et al.*, 2016; Gallemi *et al.*, 2017).

4

Primers used for cloning	
Gene name (AGI)	Name, oligonucleotide sequences (5'→3')
<i>ChPHYA</i>	CTO31, ATG-TCC-GGG-TCT-AGG-CCG-AG
	CTO32, GAA-CCG-AAG-GGC-TGA-ATC-AGC-T
	MBO9, CAT-CCA-TAT-TTA-CAG-CTC-CAG
Primers used for qPCR analyses	
Gene name (AGI)	Name, oligonucleotide sequences (5'→3')
<i>AtATHB2</i>	MGO26, GGA-GGT-AGA-CTG-CGA-GTT-CTT-ACG
<i>(At4g16780)</i>	MGO27, TGC-ATG-TAG-AAC-TGA-GGA-GAG-AGC
<i>ChATHB2</i>	CTO39, AGC-CCA-CCC-ACT-ACT-TTG-ACC
	CTO40, CGT-GGC-AGC-TTG-ATT-TGG-T
<i>AtPIL1</i>	BO87, GGA-AGC-AAA-ACC-CTT-AGC-ATC-AT
<i>(At2g46970)</i>	BO88, TCC-ATA-TAA-TCT-TCA-TCT-TTT-AAT-TTT-GGT-TTA
<i>ChPIL1</i>	CTO17, GAA-GAC-CCC-AAA-ACA-ACG-GTT
	CTO18, CCC-TCA-TCG-TAC-TCG-GTC-TCA
<i>AtUBQ10</i>	BO40, AAA-TCT-CGT-CTC-TGT-TAT-GCT-TAA-GAA-G
<i>(At4g05320)</i>	BO41, TTT-TAC-ATG-AAA-CGA-AAC-ATT-GAA-CTT
<i>AtPHYA</i> and <i>ChPHYA</i>	MJO75, TCG-GAT-AAC-AAA-TGA-GAC
	MJO76, CGG-ATG-GTG-TAA-AGT-TTA
<i>AtEF1α</i>	BO95, TGG-TGT-CAA-GCA-GAT-GAT-TTG-C
<i>(At5g60390)</i>	BO96, ATG-AAG-ACA-CCT-CCT-TGA-TGA-TTT-C
<i>ChEF1α</i>	CTO9, GGC-CGA-TTG-TGC-TGT-CCT-TA
	CTO10, TCA-CGG-GTC-TGA-CCA-TCC-TTA
<i>AtEF1α</i> and <i>ChEF1α</i>	SPO102, ATG-ATT-ACT-GGT-ACC-TCC-CAG-GC
	SPO103, CTC-ACG-GGT-CTG-ACC-ATC-CT

<i>ACS8</i> (<i>At4g37770</i>)	JRO46, GCA-GCC-AAT-TTC-CAA-AGA-GA
	JRO47, CGA-CAT-GAA-ATC-CGC-CAT-AG
<i>GH3.3</i> (<i>At2g23170</i>)	JRO38, TTC-TCC-CTC-ATC-ATG-AAG-TCC
	JRO39, AAC-GGT-TAA-GCC-CAG-CAT-AG
<i>IAA19</i> (<i>At3g15540</i>)	NCO89, TGC-TCT-TGA-TAA-GCT-CTT-CGG-TT
	NCO90, TCT-TTC-AAG-GCC-ACA-CCG-AT
<i>IAA29</i> (<i>At3g15540</i>)	MGO38, CTT-CCA-AGG-GAA-AGA-GGG-TGA
	MGO39, TTC-CGC-AAA-GAT-CTT-CCA-TGT-AAC
<i>SPC25</i> (<i>At2g39960</i>) and <i>ChSPC25</i>	SPO113, ATC-AAT-CTC-AGC-TGG-GAA-GTC
	SPO114, TCT-TTC-CAG-AAT-AAA-CCC-TC
<i>YLS8</i> (<i>At5g08290</i>) and <i>ChYLS8</i>	SPO115, AGA-TCA-ACT-GGG-CTC-TCA-AGG
	SPO116, TTG-GAG-CAA-TCA-CCA-ACC-CAC

1

2

Annex III

Light signals generated by vegetation shade facilitate acclimation to low light in shade-avoider plants.

Morelli, L., Paulišić, S., Qin, W., Iglesias-Sanchez, A., Roig-Villanova, I., Florez-Sarasa, I., Rodriguez-Concepcion, M., and Martinez-Garcia, J.F.

The PhD candidate contributed with his work to the following datasets:

Figure 1

Figure 2

Figure 4

Figure 5

Figure 6

Figure 7

Figure 8

Figure S1

Figure S2

Figure S3

Figure S4



Synthetic conversion of leaf chloroplasts into carotenoid-rich plastids reveals mechanistic basis of natural chromoplast development

Briardo Llorente^{a,b,c,1}, Salvador Torres-Montilla^a, Luca Morelli^a, Igor Florez-Sarasa^a, José Tomás Matus^{a,d}, Miguel Ezquerro^a, Lucio D'Andrea^{a,e}, Fakhreddine Houhou^f, Eszter Majer^f, Belén Picó^g, Jaime Cebolla^g, Adrian Troncoso^h, Alisdair R. Fernie^e, José-Antonio Daròs^f, and Manuel Rodríguez-Concepción^{a,f,1}

^aCentre for Research in Agricultural Genomics (CRAG) CSIC-IRTA-UAB-UB, Campus UAB Bellaterra, 08193 Barcelona, Spain; ^bARC Center of Excellence in Synthetic Biology, Department of Molecular Sciences, Macquarie University, Sydney NSW 2109, Australia; ^cCSIRO Synthetic Biology Future Science Platform, Sydney NSW 2109, Australia; ^dInstitute for Integrative Systems Biology (I2SysBio), Universitat de València-CSIC, 46908 Paterna, Valencia, Spain; ^eMax-Planck-Institut für Molekulare Pflanzenphysiologie, 14476 Potsdam-Golm, Germany; ^fInstituto de Biología Molecular y Celular de Plantas, CSIC-Universitat Politècnica de València, 46022 Valencia, Spain; ^gInstituto de Conservación y Mejora de la Agrodiversidad, Universitat Politècnica de València, 46022 Valencia, Spain; and ^hSorbonne Universités, Université de Technologie de Compiègne, Génie Enzymatique et Cellulaire, UMR-CNRS 7025, CS 60319, 60203 Compiègne Cedex, France

Edited by Krishna K. Niyogi, University of California, Berkeley, CA, and approved July 29, 2020 (received for review March 9, 2020)

Plastids, the defining organelles of plant cells, undergo physiological and morphological changes to fulfill distinct biological functions. In particular, the differentiation of chloroplasts into chromoplasts results in an enhanced storage capacity for carotenoids with industrial and nutritional value such as beta-carotene (provitamin A). Here, we show that synthetically inducing a burst in the production of phytoene, the first committed intermediate of the carotenoid pathway, elicits an artificial chloroplast-to-chromoplast differentiation in leaves. Phytoene overproduction initially interferes with photosynthesis, acting as a metabolic threshold switch mechanism that weakens chloroplast identity. In a second stage, phytoene conversion into downstream carotenoids is required for the differentiation of chromoplasts, a process that involves a concurrent reprogramming of nuclear gene expression and plastid morphology for improved carotenoid storage. We hence demonstrate that loss of photosynthetic competence and enhanced production of carotenoids are not just consequences but requirements for chloroplasts to differentiate into chromoplasts.

carotenoid | chromoplast | differentiation | phytoene | synthetic

Plastids comprise a group of morphologically and functionally diverse plant organelles capable of differentiating from one plastid type to another in response to developmental and environmental stimuli (1, 2). Such plastidial conversions are essential to sustain many fundamental biological processes and largely contribute to cell specialization in the different plant tissues. Among the different plastid types, chromoplasts are of great importance in nature and agriculture because of their capacity to accumulate high levels of carotenoids, plant pigments of isoprenoid nature that provide color in the yellow to red range (3–5). Carotenoids such as beta-carotene (provitamin A) are health-promoting nutrients that animals cannot synthesize but take up in their diets. They are also added-value compounds widely used in cosmetics, pharma, food, and feed industries as natural pigments and phytonutrients (4, 6).

Chromoplasts differentiate from preexisting plastids such as proplastids (i.e., undifferentiated plastids), leucoplasts (i.e., uncolored plastids in nonphotosynthetic tissues), and chloroplasts (i.e., photosynthetic plastids). Chloroplasts transform into chromoplasts during the development of many flowers and fruits, but only a few plant species differentiate chromoplasts in leaves (1, 5). The yellow to red colors that some leaves acquire as they senesce (e.g., in the autumn or when they are exposed to continuous darkness) are due to chloroplast carotenoids becoming visible when the chlorophylls degrade. This senescence process, however, does not involve the transformation of chloroplasts into

chromoplasts but into a completely different type of plastids named gerontoplasts (1, 2).

The most prominent changes during chloroplast-to-chromoplast differentiation are the reorganization of the internal plastid structures, together with a concurrent loss of photosynthetic competence and overaccumulation of carotenoid pigments (1–3, 5, 7, 8). The remodeling of the internal plastid structures generates an increased metabolic sink capacity but it also promotes carotenoid biosynthesis. The control of chromoplast differentiation appears as a very promising strategy for improving the nutritional and health benefits of crops (5–9). The overall process is known to involve changes in gene expression (e.g., via retrograde signaling from plastids to the nucleus), hormonal regulation, protein quality control, and plastid protein import (1, 3, 5). However, very few inducers of chromoplast development have been identified to date. Orange (OR) chaperones are among the best characterized,

Significance

Carotenoids are natural pigments whose properties as provitamin A and health-promoting phytonutrients make them ideal targets for biofortification. Here, we show that plastids specialized in carotenoid overaccumulation named chromoplasts can be synthetically produced in plant tissues that do not naturally develop them. We further demonstrate that differentiation of chromoplasts from leaf chloroplasts not just causes but requires both a reduction in photosynthetic activity and a stimulation of carotenoid biosynthesis in a process hardwired to a major reprogramming of global gene expression and cell metabolism. The synthetic system that we report here should allow to boost the nutritional quality of green vegetables and forage crops once their photosynthetic activity is dispensable (e.g., just before harvesting).

Author contributions: B.L., S.T.-M., L.M., I.F.-S., E.M., J.-A.D., and M.R.-C. designed research; B.L., S.T.-M., L.M., I.F.-S., J.T.M., M.E., L.D., F.H., E.M., B.P., J.C., and A.T. performed research; B.L., S.T.-M., L.M., I.F.-S., J.T.M., M.E., B.P., J.C., A.T., A.R.F., J.-A.D., and M.R.-C. contributed new reagents/analytic tools; B.L., S.T.-M., L.M., I.F.-S., J.T.M., M.E., L.D., F.H., E.M., B.P., J.C., A.T., A.R.F., J.-A.D., and M.R.-C. analyzed data; and B.L. and M.R.-C. wrote the paper.

The authors declare no competing interest.

This article is a PNAS Direct Submission.






Published under the PNAS license.

¹To whom correspondence may be addressed. Email: briardo.llorente@mq.edu.au or manuelrc@ibmcp.upv.es.

This article contains supporting information online at <https://www.pnas.org/lookup/suppl/doi:10.1073/pnas.2004405117/-DCSupplemental>.

First published August 19, 2020.

Light signals generated by vegetation shade facilitate acclimation to low light in shade-avoider plants

Luca Morelli ^{1,2}, Sandi Paulišić,² Wenting Qin,^{1,2} Ariadna Iglesias-Sanchez ², Irma Roig-Villanova ^{2,†}, Igor Florez-Sarasa ², Manuel Rodriguez-Concepcion^{1,2,‡} and Jaime F. Martinez-Garcia ^{1,2,3,*,‡}

1 Institute for Plant Molecular and Cell Biology (IBMCP), CSIC-UPV, València 46022, Spain

2 Centre for Research in Agricultural Genomics (CRAG) CSIC-IRTA-UAB-UB, Campus UAB Bellaterra, Barcelona 08193, Spain

3 Institució Catalana de Recerca i Estudis Avançats (ICREA), Passeig Lluís Companys 23, Barcelona 08010, Spain

*Author for communication: jaume.martinez@ibmcp.upv.es

†Present address: Barcelona School of Agricultural Engineering (ESAB), Universitat Politècnica de Catalunya (UPC), Castelldefels, Barcelona 08860, Spain.

‡Senior authors.

M.R.-C. and J.F.M.-G. conceived the original research plan, directed, and coordinated the study. L.M., I.F.-S., A.I.-S., and M.R.-C. measured and analyzed photosynthetic parameters, respiration, and pigment levels; S.P., I.R.-V., and W.Q. performed all the other experiments. All authors analyzed their data and discussed the results. M.R.-C. and J.F.M.-G. wrote the paper with revisions and contributions or/and comments of all other authors.

The author responsible for distribution of materials integral to the findings presented in this article in accordance with the policy described in the Instructions for Authors (<https://academic.oup.com/plphys/pages/general-instructions>) is: Jaime F. Martinez-Garcia (jaume.martinez@ibmcp.upv.es)

Abstract

When growing in search for light, plants can experience continuous or occasional shading by other plants. Plant proximity causes a decrease in the ratio of R to far-red light (low R:FR) due to the preferential absorbance of R light and reflection of FR light by photosynthetic tissues of neighboring plants. This signal is often perceived before actual shading causes a reduction in photosynthetically active radiation (low PAR). Here, we investigated how several Brassicaceae species from different habitats respond to low R:FR and low PAR in terms of elongation, photosynthesis, and photoacclimation. Shade-tolerant plants such as hairy bittercress (*Cardamine hirsuta*) displayed a good adaptation to low PAR but a poor or null response to low R:FR exposure. In contrast, shade-avoider species, such as Arabidopsis (*Arabidopsis thaliana*), showed a weak photosynthetic performance under low PAR but they strongly elongated when exposed to low R:FR. These responses could be genetically uncoupled. Most interestingly, exposure to low R:FR of shade-avoider (but not shade-tolerant) plants improved their photoacclimation to low PAR by triggering changes in photosynthesis-related gene expression, pigment accumulation, and chloroplast ultrastructure. These results indicate that low R:FR signaling unleashes molecular, metabolic, and developmental responses that allow shade-avoider plants (including most crops) to adjust their photosynthetic capacity in anticipation of eventual shading by nearby plants.

Introduction

Light is essential for plants as a source of energy and environmental information. Shading by nearby individuals can reduce light quantity (i.e. photon supply) and hence compromise photosynthetic activity and growth, a problematic situation in intensive cropping systems. To deal with the

outcomes of mutual shading, plants have developed response mechanisms based on the perception of light quality, i.e. spectral information (Casal, 2013; Martinez-Garcia et al., 2010). The preferential absorbance of red (R) light and reflection of far-red (FR) light by photosynthetic tissues results in a decreased ratio of R to FR (R:FR) when light is reflected

from or filtered through green stems and leaves. The low R:FR is a very reliable light signal that announces the close presence of nearby plants that may compete for resources.

Plants growing in ecosystems where access to light is restricted (e.g. in forest understories) show a shade-tolerant habit by adapting their light capture and utilization systems to low light intensity conditions. In contrast, plants growing in open habitats are shade-avoiders (also referred to as shade-intolerant or sun-loving). In shade-avoider plant species, such as *Arabidopsis* (*Arabidopsis thaliana*) and most sun-loving crops, perception of the low R:FR signal by the phytochrome photoreceptors activates a signaling pathway that eventually triggers a set of responses known as the shade-avoidance syndrome (SAS). The most prominent phenotype following exposure to low R:FR is elongation (e.g. of seedling hypocotyl, leaf petiole, and stem internode tissues), intended to overgrow neighboring competitors and outcompete them in the access to light. If the neighboring individuals overgrow and eventually shade the plant, the consequent reduction in light quantity (i.e. in the amount of radiation available for photosynthesis) results in additional and stronger SAS responses such as reduced leaf size, attenuated defense mechanisms, and early flowering (Roig-Villanova and Martinez-Garcia, 2016).

The most extensively studied SAS response by far is hypocotyl elongation in *A. thaliana* (At). In this species, low R:FR inactivates phytochrome B (phyB), releasing PHYTOCHROME INTERACTING FACTORS (PIFs) that can then regulate gene expression and promote elongation growth. This response is also repressed by negative SAS regulators such as ELONGATED HYPOCOTYL 5 (HY5), amongst many others (Cifuentes-Esquivel et al., 2013; Ciolfi et al., 2013). Biological activity of these transcription factors can be modulated by additional components of the SAS regulatory network such as LONG HYPOCOTYL IN FAR-RED 1 (HFR1, which binds PIFs to prevent their binding to target genes) and phytochrome A (phyA, which gets stabilized in shade and then promotes HY5 accumulation; Ciolfi et al., 2013; Martinez-Garcia et al., 2014; Yang et al., 2018). Both HFR1 and phyA hence act as additional SAS repressors that were recently found to be instrumental for the adaptation to shade. Indeed, the shade-tolerant hairy bittercress (*Cardamine hirsuta*), a close relative of At, does not elongate when exposed to low R:FR unless the function of phyA or HFR1 is genetically lost in mutant plants (Hay et al., 2014; Molina-Contreras et al., 2019; Paulisic et al., 2021).

Differences between shade-avoider and shade-tolerant species are not restricted to changes in elongation after exposure to low R:FR. Photoacclimation (i.e. the ability of plants to adjust photosynthesis to changes in the incident light with specific phenotypic changes) also diverges. Variation of photoacclimation responses among species on day-to-week time scale has been associated to two main strategies (Murchie and Horton, 1997; Ptushenko and Ptushenko, 2019). The first one consists of an alteration of photosynthetic pigment content, which positively corresponds with

photosynthetic capacity. The second one involves changes in the photosynthetic machinery, which appears to be more important in plant species from environments where temporal and spatial variations in light irradiance are common, e.g. margins of woodlands. Combinations of these two main strategies give rise to the observed diversity in photoacclimation. In the case of At and *C. hirsuta* (Ch), a differential response to low R:FR in terms of photosynthetic pigment accumulation has been observed. Chlorophyll and carotenoid levels drop about 20% in At plants grown under low R:FR conditions, whereas the decrease is attenuated in Ch plants (Molina-Contreras et al., 2019). Whether photosynthetic capacity and/or chloroplast ultrastructure is differentially impacted by low R:FR in these species remains unknown. In terms of light quantity, the shade-avoider At showed a lower capacity to acclimate to reduced photosynthetically active radiation (low PAR) but a higher capacity to acclimate to intense light (high PAR) compared to the shade-tolerant Ch (Molina-Contreras et al., 2019). A similar physiological behavior has been described for shade-avoider and shade-tolerant species of the genus *Tradescantia* (Benkov et al., 2019), a model to study the ecology of photosynthesis and the mechanisms of photoacclimation in plants (Ptushenko and Ptushenko, 2019). The possible connections between low R:FR signaling and photoacclimation responses in plants remain, however, virtually unknown. Here, we explored natural and engineered genetic diversity to investigate this connection using different Brassicaceae species.

Results

Different Brassicaceae species present divergent photoacclimation responses

We previously showed that, compared to sun-loving At Col-0, shade-tolerant Ch Ox exhibits a better ability to maintain photosynthesis after transfer to low PAR but a stronger chlorophyll loss when light intensity increases (Molina-Contreras et al., 2019). To better characterize the photoacclimation responses of these two Brassicaceae species, both At and Ch were germinated and grown for 7 d under control conditions of a photosynthetic photon flux density (PPFD) in the PAR region of 20–24 $\mu\text{mol m}^{-2} \text{s}^{-1}$ (W_{20}). Then they were transferred to either lower PAR (W_4 , PPFD of 4 $\mu\text{mol m}^{-2} \text{s}^{-1}$) or higher PAR (W_{200} , PPFD of 200 $\mu\text{mol m}^{-2} \text{s}^{-1}$) for up to seven more days (Figure 1). Light curve analysis at day 3 after the transfer already showed clearly opposite responses of At and Ch, i.e. a better photosynthetic activity of Ch compared to At when transferred to W_4 and a better activity of At compared to Ch when transferred to W_{200} (Figure 1A). Derived parameters such as maximum electron transport rate (ETR_m) and photosynthetic rate in light-limited region of the light curve (alpha) also illustrated that At performed better than Ch after transfer to higher light (W_{200}) but worst after transfer to lower light (W_4 ; Figure 1B). Other photosynthetic parameters such as maximum quantum efficiency of PSII (Fv/Fm) and light use

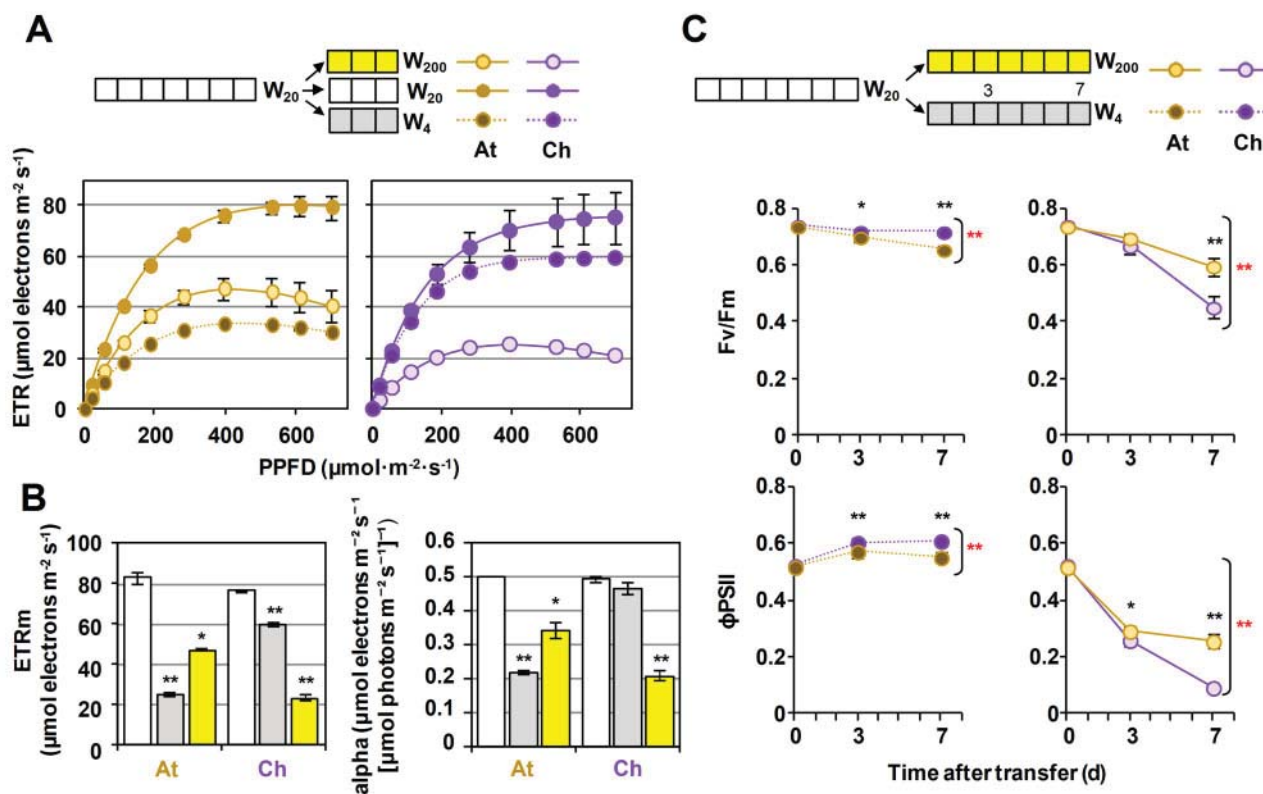


Figure 1 *Arabidopsis thaliana* and *Cardamine hirsuta* show antagonistic photoacclimation responses to higher and lower PAR. A, Light curves of At and Ch seedlings germinated and grown under white light of $20\text{-}\mu\text{mol}\cdot\text{m}^{-2}\cdot\text{s}^{-1}$ PPFD (W_{20}) for 7 d and then either kept under W_{20} or transferred to either 200 (W_{200}) or 4 (W_4) $\mu\text{mol}\cdot\text{m}^{-2}\cdot\text{s}^{-1}$ PPFD for 3 more days. Values represent the mean and standard error of $n = 3$ plants for treatment. B, ETRm and photosynthetic rate in the light-limited region of the light curve (alpha) calculated from the curves shown in (A). Asterisks mark statistically significant changes (t test $*P < 0.05$, $**P < 0.01$) in W_4 or W_{200} relative to W_{20} . C, Maximum photochemical efficiency of PSII in the dark-adapted state (Fv/Fm) and effective quantum yield calculated at growth light (ΦPSII) of seedlings germinated and grown for 7 d under W_{20} and then transferred to either W_{200} or W_4 for seven more days. Data were taken at 0, 3, and 7 d after the transfer. Values are mean and standard error of $n = 7$ seedlings per treatment. Black asterisks mark statistically significant differences between At and Ch at each time point (t test $*P < 0.05$, $**P < 0.01$). Red asterisks indicate statistically significant differences between genotypes over time (two-way ANOVA, $**P < 0.01$).

efficiency of PSII (ΦPSII) also showed differences between At and Ch at day 3 after transfer, but these differences became clearer at longer times of exposure to either W_{200} or W_4 (Figure 1C). Specifically, Fv/Fm values were lower in Ch than in At after transfer to higher light, while the opposite was observed when transferred to lower light. A similar trend was observed in the case of ΦPSII (Figure 1C). These results together indicate that Ch tolerates better the transfer to lower PAR (consistent with Ch being more tolerant to shade), while an increase in light irradiance compromises photosynthetic efficiency in Ch more than in shade-avoider At. Based on these results, we used light curve analysis at day 3 or earlier to estimate photoacclimation to lower PAR and Fv/Fm measurements at day 7 to estimate photoacclimation to higher PAR.

Besides At and Ch, the Brassicaceae family (mustards) includes many food crops (e.g. cauliflower, broccoli, radish, cabbage, kale, and similar green leafy vegetables) and a diversity of wild species from forested and open habitats. As a first step to explore the possible connection between low PAR and low R:FR responses, we analyzed photoacclimation

and hypocotyl elongation in six different Brassicaceae species or accessions, including At and Ch as controls. The selected wild mustards were alpine rock cress (*Arabis alpina*, Aa), two accessions of shepherd's purse (*Capsella bursa-pastoris*, Freiburg-1 (Cb-F) and Strasbourg-1 (Cb-S), pink shepherd's-purse (*Capsella rubella*, Cr), watercress (*Nasturtium officinale*, No), and London rocket (*Sisymbrium irio*, Si). Initially, we aimed to classify them as shade-avoider or shade-tolerant based on photoacclimation responses. After germination and growth for 7 d under W , seedlings were either kept under control W_{20} or transferred to lower light (W_4). Light curve analyses at day 1 after the transfer already showed differential responses that served to classify the accessions in two groups (Figure 2). Similar to the shade-avoider At, seedlings of Cb-F, Cb-S, and Cr showed a lowering of the curve under W_4 conditions, whereas those of Aa, No, and Si behaved as the shade-tolerant Ch and showed virtually identical light curves under W_{20} and W_4 (Figure 2A). ETRm and alpha values also illustrated that the W_4 treatment led to decreased photosynthetic performance in At, Cb-F, Cb-S, and Cr but not in Ch, Aa, No, and Si (Figure 2B;

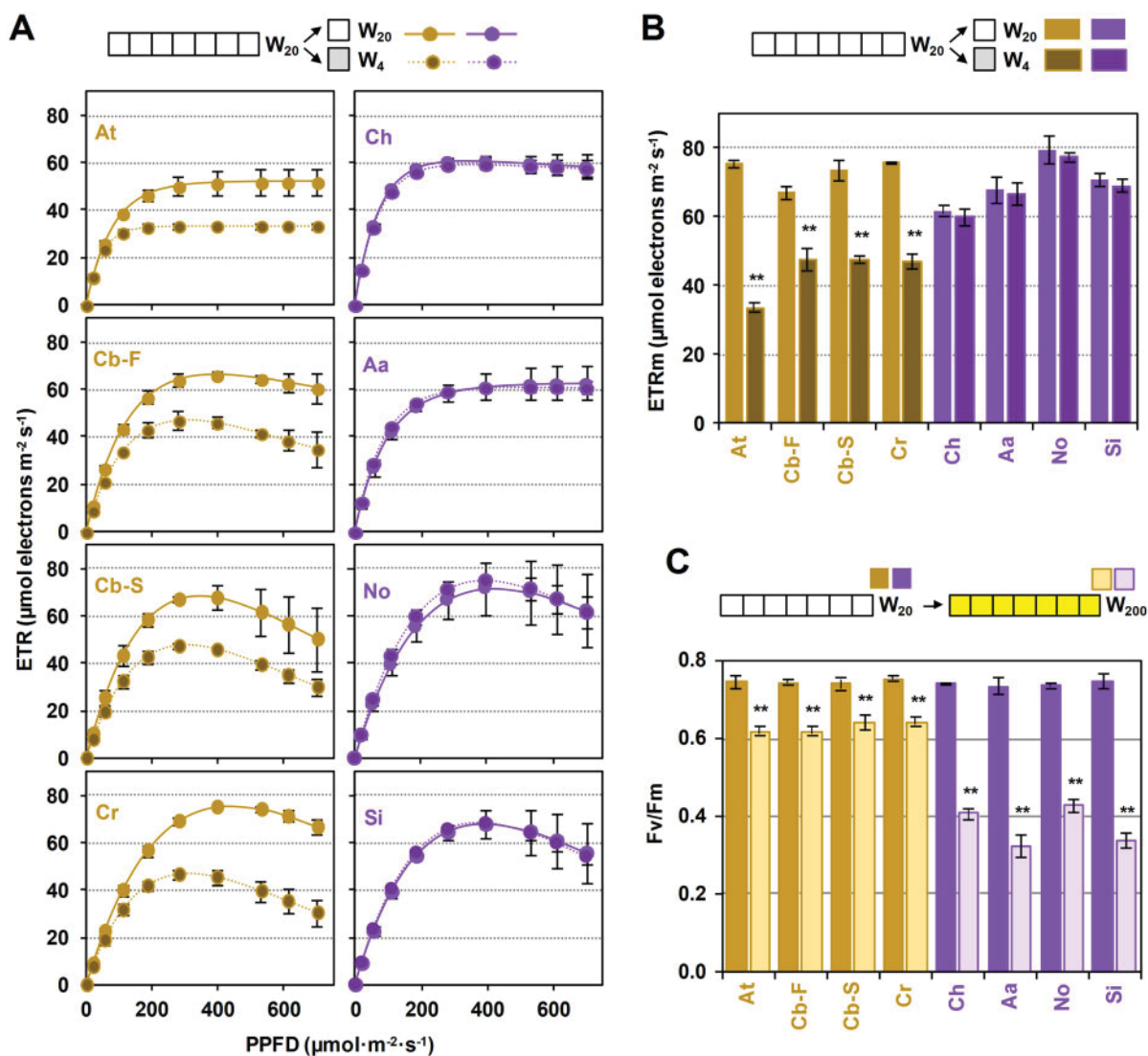


Figure 2 Brassicaceae plants can be grouped with either *A. thaliana* or *C. hirsuta* based on their photoacclimation responses. A, Light curves of *Arabidopsis thaliana* (At), *Capsella bursa-pastoris* (Cb-F and Cb-S), *Capsella rubella* (Cr), *Cardamine hirsuta* (Ch), *Arabis alpina* (Aa), *Nasturtium officinale* (No), and *Sisymbrium irio* (Si) seedlings germinated and grown under white light (W₂₀) for 7 d and then either kept under W₂₀ or transferred to lower PAR (W₄) for one more day. Values represent the mean and standard error of $n = 3$ plants for treatment. B, ETRm values calculated from the curves shown in (A). C, Fv/Fm values of seedlings grown for 7 d under W₂₀ and then transferred to higher PAR (W₂₀₀) for seven more days. Mean and standard error of $n = 9$ seedlings per treatment are represented. Asterisks in (B) and (C) mark statistically significant changes (t test, **P < 0.01) relative to W₂₀.

Supplemental Figure S1). We next analyzed photoacclimation to increased irradiation quantifying Fv/Fm before or after transferring 7-d-old W₂₀-grown seedlings to W₂₀₀ for seven additional days. Again, At grouped together with the two accessions of Cb and with Cr as they acclimated much better to high PAR compared to the group formed by Ch, Aa, No, and Si (Figure 2C). Together, these photoacclimation results led to classify the former group as shade-avoiders, and the latter as shade-tolerant species.

Photoacclimation responses can be uncoupled from shade-driven hypocotyl elongation

Next, we investigated whether the classification of the selected mustard species as shade-avoider or shade-tolerant

based on their photoacclimation features corresponded with their elongation response to low R:FR. After germination and growth for 3 d under W₂₀ (R:FR = 1.5–3.3), seedlings were either kept under W₂₀ or transferred to FR-supplemented W₂₀ (W₂₀+FR, R:FR = 0.02) for four additional days, and then hypocotyl length was measured (Figure 3). Similar to At, the Cb-F accession showed a strong hypocotyl elongation response, whereas Cb-S, Cr, and No elongated moderately in response to low R:FR. In contrast, Ch, Aa, and Si did not elongate in response to low R:FR (Figure 3A). These results confirm that the elongation response to low R:FR cannot be fully predicted based on the photoacclimation phenotype of a particular accession. Nonetheless, accessions classified as shade-avoider based on their photoacclimation

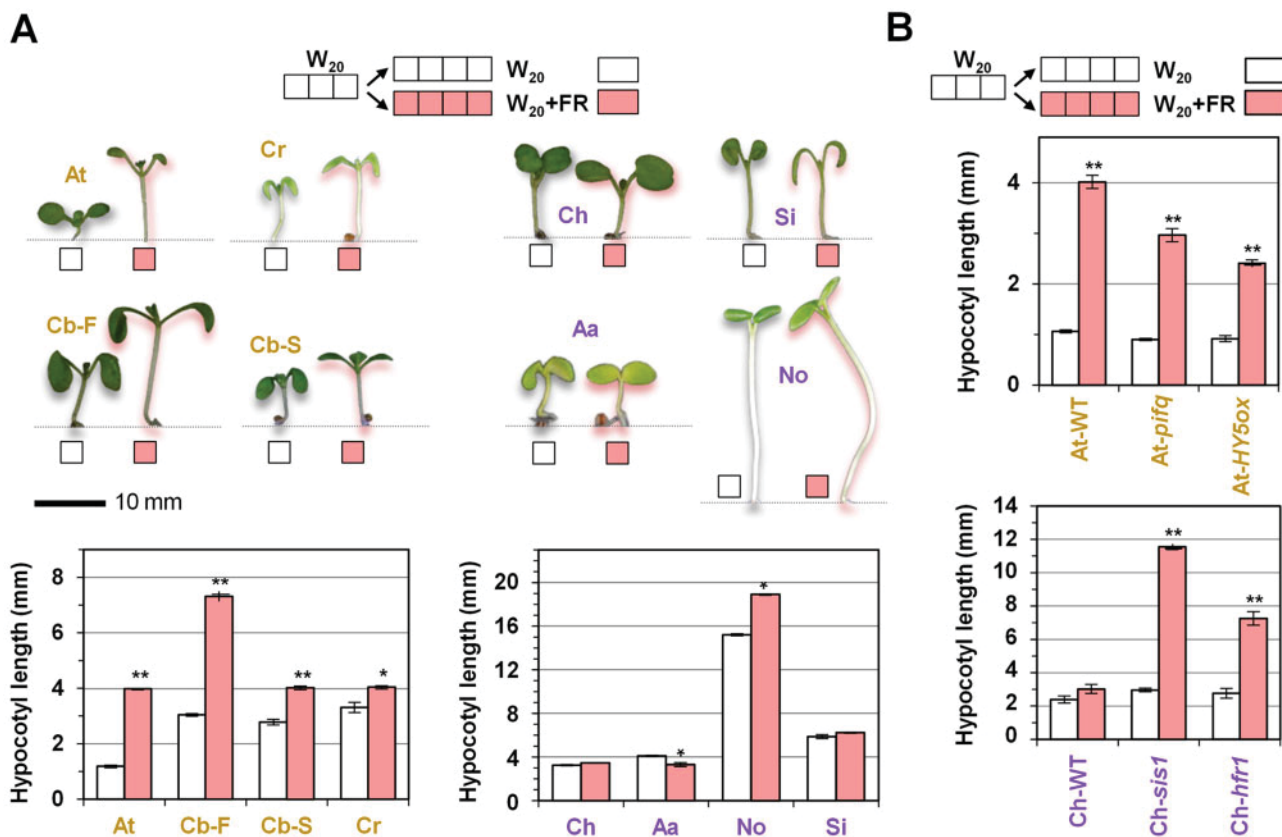


Figure 3 The hypocotyl elongation response to low R:FR is plastic in Brassicaceae plants. A, The indicated genotypes were germinated and grown under W_{20} for 3 d and then either kept under W_{20} or transferred to low R:FR ($W_{20}+FR$) for four more days. Then, pictures were taken and hypocotyl length was measured. B, Hypocotyl length of the indicated mutants grown as indicated in (A). In both (A) and (B), mean and standard error of measurements from at least 20 seedlings in $n = 3$ independent experiments per treatment are represented. Asterisks mark statistically significant changes in $W_{20}+FR$ relative to W_{20} (t test, * $P < 0.05$, ** $P < 0.01$).

behavior (i.e. poor photoacclimation to decreased PAR but good photoacclimation to increased PAR) exhibit a range of elongation responses to low R:FR (i.e. from moderate to strong elongation), whereas plant species with a shade-tolerant photoacclimation responses display either no elongation or a mild shade-avoider phenotype in terms of hypocotyl elongation when exposed to low R:FR (e.g. No).

The shade-avoider or shade-tolerant elongation phenotype in response to low R:FR can be reversed by manipulating the levels of specific SAS regulators. Previous results have shown that At lines overexpressing *HYS* (*At-HY5ox*) display an attenuated hypocotyl response to low R:FR (Ortiz-Alcaide et al., 2019), whereas a similar but weaker response was observed in a quadruple mutant defective in all members of the photolabile PIF quartet (PIFQ), PIF1, PIF3, PIF4 and PIF5 (*At-pifq*; Figure 3B). Despite the different degrees of elongation response to low R:FR, these two lines showed photoacclimation responses to lower PAR very similar to those of wild-type (*At-WT*) controls (Figure 4). Both light curves (Figure 4A) and ETRm values (Figure 4B) were almost identical in *At-WT* plants and mutants hypersensitive to low R:FR. In the case of Ch, lines deficient in phyA (*Ch-sis1*) or HFR1 (*Ch-hfr1*) gain the ability to elongate when exposed to low R:FR (Molina-Contreras et al., 2019; Paulisic et al., 2021; Figure 3B). In contrast to the shade-hyposensitive At mutants,

the hypersensitive Ch mutant lines appeared to gain a partial shade-avoider phenotype in terms of photoacclimation to low PAR, as lower values of light curves (Figure 4A) and ETRm (Figure 4B) were observed under W_4 compared to W_{20} . However, photoacclimation to increased PAR (W_{200}) estimated from Fv/Fm values and also from chlorophyll levels (Molina-Contreras et al., 2019) was similar for *Ch-WT*, *Ch-sis1*, and *Ch-hfr1* plants (Figure 4C). We therefore concluded that manipulation of the plant ability to elongate in response to proximity shade hardly impacts their photoacclimation capacity, at least when plants are growing in the absence of the low R:FR signal.

Activation of low R:FR signaling causes a decrease in pigment levels and photosynthetic activity

Low R:FR signals not only influence hypocotyl elongation but they are also known to reduce the contents of photosynthetic pigments (chlorophylls and carotenoids) in many plant species (Roig-Villanova et al., 2007; Cagnola et al., 2012; Patel et al., 2013; Bou-Torrent et al., 2015; Molina-Contreras et al., 2019). The reduction is observed in both elongating (*At-WT*) and nonelongating (*Ch-WT*) seedlings, but it is stronger in the former (Figure 5). *Cardamine hirsuta* mutants that gained the ability to elongate in response to shade, such as *Ch-sis1* and *Ch-hfr1*, also displayed stronger

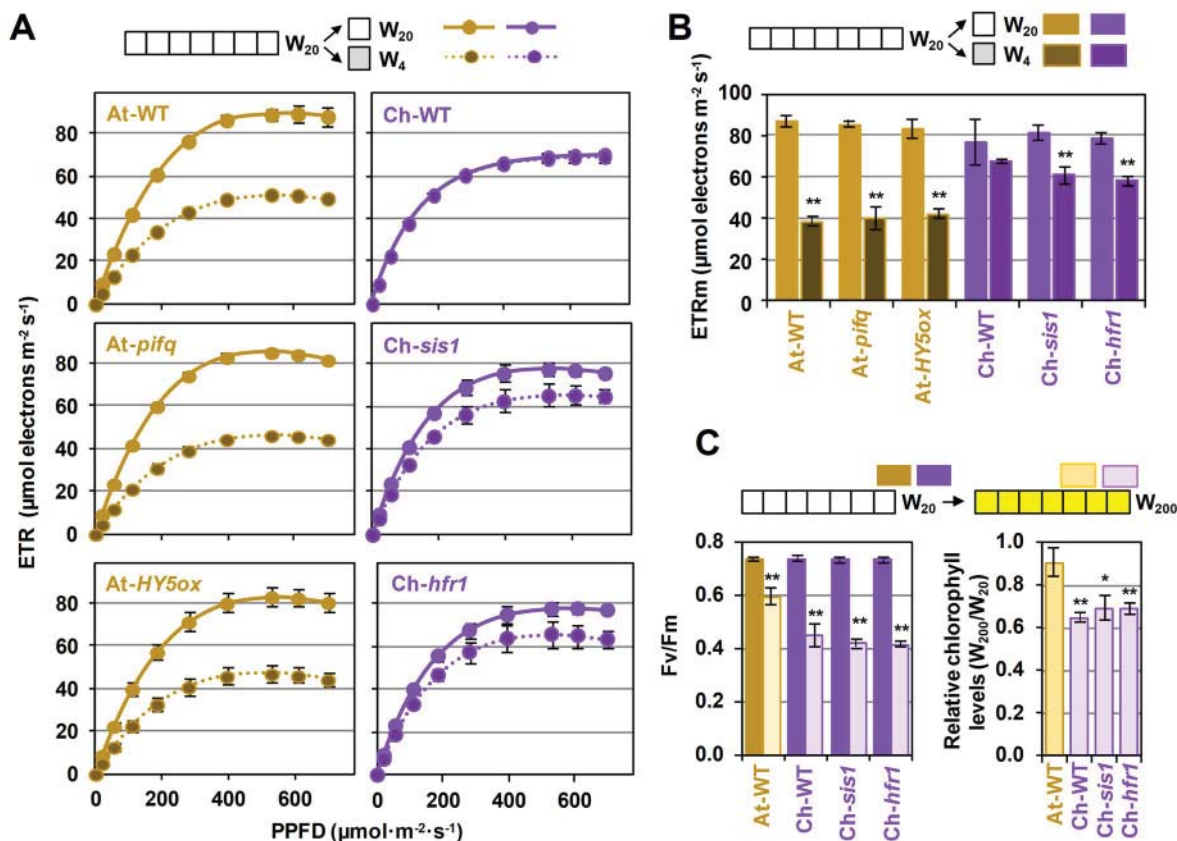


Figure 4 Mutations that alter sensitivity to low R:FR do not impact photoacclimation responses. A, Light curves of At and Ch wild-type and mutant seedlings germinated and grown under W₂₀ for 7 d and then either kept under W₂₀ or transferred to lower PAR (W₄) for one more day. Values represent the mean and standard error of $n = 3$ plants for treatment. B, ETRm values calculated from the curves shown in (A). C, Fv/Fm values and HPLC-determined relative chlorophyll levels of seedlings grown for 7 d under W₂₀ and then transferred to higher PAR (W₂₀₀) for seven more days. Mean and standard error of $n = 9$ seedlings (Fv/Fm) or $n = 3$ independent pools (HPLC) per treatment are represented. Asterisks in (B) and (C) mark statistically significant changes (t test, * $P < 0.05$, ** $P < 0.01$) relative to W₂₀.

reductions in photosynthetic pigment contents relative to Ch-WT after low R:FR exposure (Figure 5A; Molina-Contreras et al., 2019). Conversely, At mutants with a reduced ability to elongate in response to shade, such as At-*pifq* and At-*HY5ox* (Figure 3B), showed attenuated reduction of pigment contents relative to At-WT when exposed to low R:FR (Figure 5A).

To test whether decreases in photosynthetic pigment levels driven by simulated shade exposure might affect photosynthetic activity, we next measured Fv/Fm and Φ PSII in seedlings grown either under W₂₀ or under W₂₀+FR (Figure 5B; Supplemental Figure S2A). Indeed, low R:FR was found to result in decreased photosynthetic activity in the lines with strong pigment loss responses independently on the species (At-WT, Ch-*sis1*, and Ch-*hfr1*). ETRm and alpha parameters also tended to be lower in W+FR-exposed At-WT, Ch-*sis1*, and Ch-*hfr1* seedlings compared to W controls (Figure 5C; Supplemental Figure S2B). The effect of low R:FR on photosynthesis was much less dramatic in the rest of the lines (At-*pifq*, At-*HY5ox*, and Ch-WT), which consistently displayed a reduced impact of W₂₀+FR exposure on their photosynthetic pigment levels (Figure 5).

Proximity shade signals have also been found to impact photosynthesis at the level of gene expression. Analyses of low R:FR-triggered transcriptomic changes showed reduced levels of transcripts encoding photosynthesis-related proteins (e.g. enzymes involved in chlorophyll and carotenoid biosynthesis, components of the photosynthetic apparatus, and/or members of the carbon fixation process) in several species, including alfalfa (Lorenzo et al., 2019), maize (Shi et al., 2019), tomato (Cagnola et al., 2012), and At (Leivar et al., 2012). Interestingly, the changes in the expression of photosynthesis-related genes triggered by low R:FR are attenuated in the At-*pifq* mutant compared to At-WT seedlings (Figure 6). This is particularly evident in the case of low R:FR-repressed photosynthetic genes (Figure 6), suggesting that the PIF-mediated regulation of gene expression in response to low R:FR is instrumental for the observed changes in photosynthesis (Figure 5).

Exposure of shade-avoider plants to low R:FR improves their photoacclimation to low PAR

The observation that exposure of low R:FR caused a decreased in photosynthetic activity of At-WT seedlings and

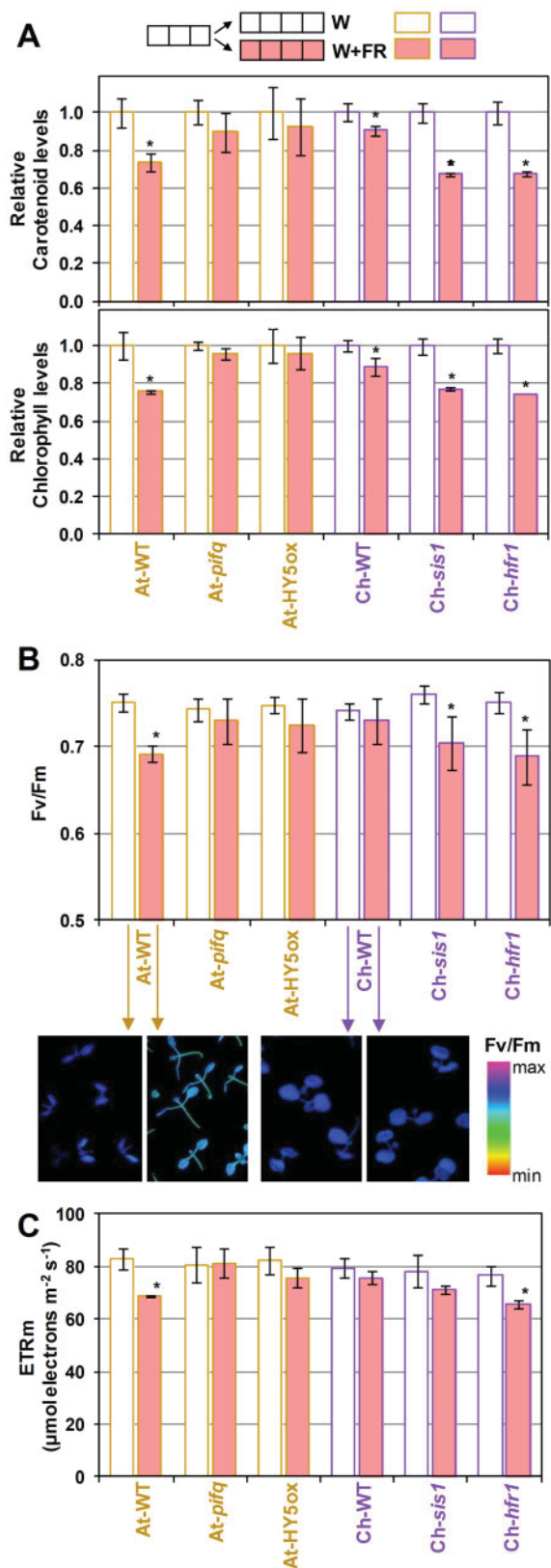


Figure 5 Activation of low R:FR signaling reduces photosynthetic pigment levels and activity. A, The indicated genotypes were germinated and grown under W_{20} for 3 d and then either kept under W_{20} or transferred to low R:FR ($W_{20}+\text{FR}$) for four more days. Then, the levels of photosynthetic pigments (carotenoids and chlorophylls) were

shade-hypersensitive Ch mutants prompted us to analyze whether this light signal may also cause changes in chloroplast ultrastructure. Cotyledons from At-WT seedlings germinated and grown for 2 d under W_{20} and then either kept in W_{20} or transferred to $W_{20}+\text{FR}$ for five additional days were collected and used for transmission electron microscopy (TEM). Chloroplasts from low R:FR-exposed samples were found to exhibit larger grana stacks and contain less and smaller plastoglobules compared to W -grown controls (Figure 7). Interestingly, similar changes are associated to low PAR photoacclimation (Rozak et al., 2002; Lichtenthaler, 2007; Wood et al., 2018). We therefore reasoned that exposure to low R:FR in the absence of any light intensity change might trigger responses to anticipate a foreseeable shading involving a decrease in PAR. To test this hypothesis, we analyzed light curves of WT and mutant seedlings grown in either W_{20} or $W_{20}+\text{FR}$ and then transferred to lower PAR (W_4) for 3 d (Figure 8). Pre-exposure of At-WT seedlings to low R:FR ($W_{20}+\text{FR}$) resulted in a strongly attenuated reduction in ETRm after their transfer to lower PAR (Figure 8A). In contrast, At mutants with reduced SAS elongation responses also lost the response to low R:FR in terms of improved photoacclimation to lower PAR (W_4 ; Figure 8A). Pretreatment with $W_{20}+\text{FR}$ had virtually no effect on the photoacclimation of Ch-WT seedlings to lower PAR (W_4) but caused a slight but significant improvement of ETRm in shade-hypersensitive Ch mutants at day 1 after transfer to W_4 (Figure 8A). When analyzing photoacclimation to higher PAR, pre-exposure of At-WT or Ch-WT seedlings to $W_{20}+\text{FR}$ resulted in no improvement compared to W_{20} -grown controls (Figure 8B). If anything, Ch-WT seedlings grown under $W_{20}+\text{FR}$ photoacclimated worse than W_{20} -grown seedlings when exposed to higher light intensity (Figure 8B).

The battery of mustards that grouped together with At in terms of photoacclimation responses (Cb-F, Cb-S, and Cr; Figure 2; Supplemental Figure S1) also showed improved photoacclimation to reduced PAR when pre-exposed to low R:FR, whereas the simulated shade signal did not have an effect on those clustered with Ch (Aa, No, and Si; Figure 8A). This low R:FR-dependent phenotype was independent of the growing light intensity and photoperiod, as it was also observed in At-WT seedlings growing under W_{200} or $W_{200}+\text{FR}$ for 8 h or 16 h a day (i.e. under long day or short day conditions, respectively) and then transferred to W_{15} (Supplemental Figure S3). Because both the response of shade-avoider plants to low R:FR and the acclimation to low light involve a reduced respiration rate to cope with the limited generation of photoassimilates and hence contribute to

quantified spectrophotometrically. B, Fv/Fm values of seedlings germinated and grown as indicated in (A). Lower pictures show false-color images in wild-type seedlings. (C) ETRm values of seedlings germinated and grown as indicated in (A). Mean and standard error of $n = 3$ independent pools of seedlings (A) or $n = 9$ seedlings (B and C) per treatment are represented. Asterisks mark statistically significant changes in $W_{20}+\text{FR}$ relative to W_{20} (t test, $*P < 0.05$).

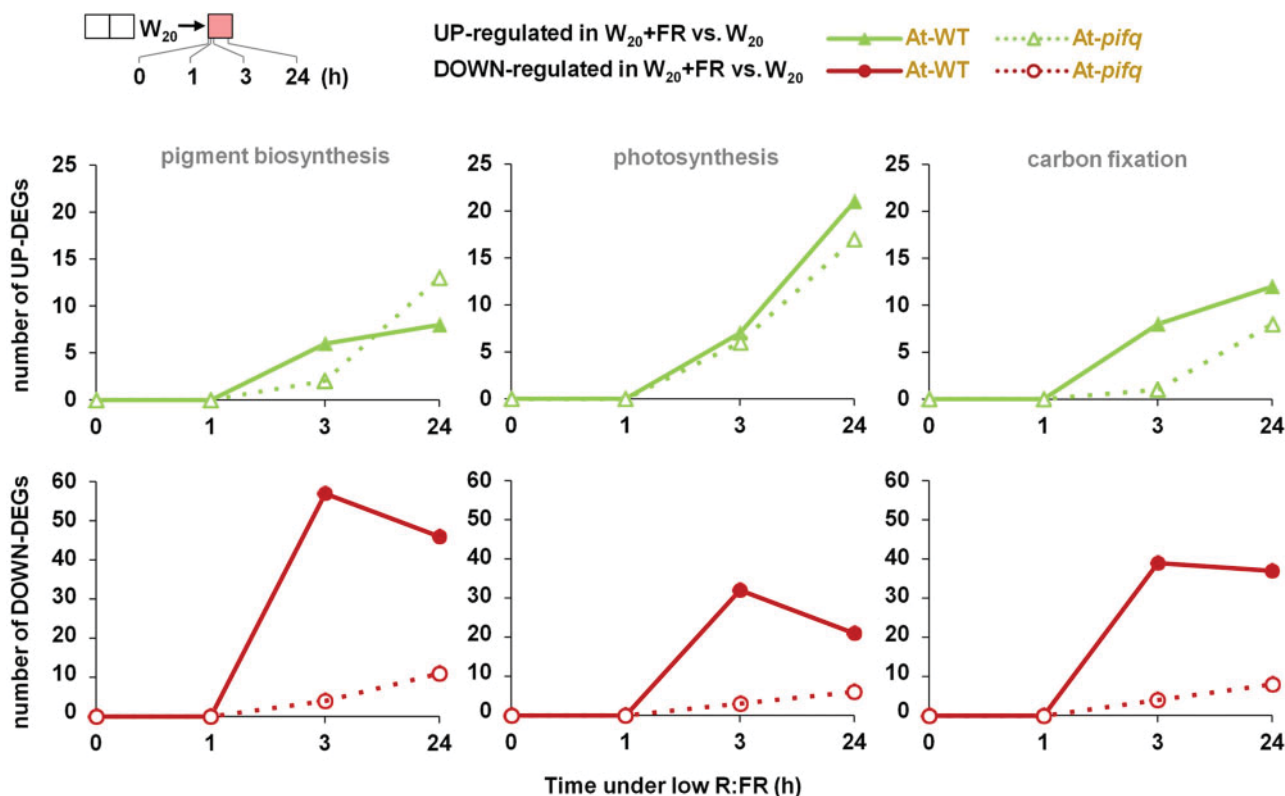


Figure 6 Exposure to low R:FR triggers changes in photosynthetic gene expression that are attenuated in the hyposensitive *At-pifq* mutant. Data were extracted from a publicly available experiment (Leivar et al., 2012). *At-WT* and *At-pifq* lines were germinated and grown under $19 \mu\text{mol}\cdot\text{m}^{-2}\cdot\text{s}^{-1}$ PAR white light (W_{20} , R:FR of 6.48) for 2 d and exposed to low R:FR ($W_{20}+FR$, R:FR of 0.006) for 0, 1, 3, or 24 h. Plots represent the number of DEGs either up- or downregulated in $W_{20}+FR$ versus W_{20} that are involved in photosynthetic pigment biosynthesis (Kyoto Encyclopedia of Genes and Genomes pathways ath00906 and ath00860), photosynthesis (ath00195 and ath00196), and carbon fixation (ath00710).

carbon balance (Cagnola et al., 2012; Casal, 2013), we next measured changes in respiration in whole wild-type *At* and *Ch* seedlings exposed or not to low R:FR and then transferred to reduced PAR (Supplemental Figure S4). In W_{20} controls, respiration (estimated as total oxygen consumption in darkness) was reduced in *At* seedlings when they were moved to W_4 . When exposed to $W_{20}+FR$, however, respiration was already lower and did not significantly change after transferring to lower PAR. In contrast, *Ch* seedlings showed similar respiration values in all conditions (Supplemental Figure S4). Based on these data we conclude that detection and transduction of low R:FR signals not only allows shade-avoider plants to overgrow their neighbors but also to pre-adapt their photosynthetic and respiratory machinery to foreseeable conditions of actual shading involving reduced PAR. In contrast, shade-tolerant plants have a better adapted capacity to grow under reduce PAR and do not seem to use the low R:FR signal.

Discussion

Plants have been traditionally classified as shade avoider and tolerant based mostly on their natural habitat, although virtually all plants are exposed to at least some degree of shade during their lifetime. As an ecological concept, shade

tolerance refers to the capacity of a given plant to tolerate low light levels, but it is also associated with a wide range of traits, including phenotypic plasticity to optimize light capture (Valladares and Niinemets, 2008). Analyzing a range of caulescent herbs, it was suggested that the elongation response upon exposure to low R:FR was dependent on the shade habit, the shade-avoiders elongating the most and the shade-tolerant showing a mild or no elongation response (Smith, 1982). Indeed, elongation might not be the best solution for plants that spend all their lives under a canopy or permanently shaded by other plants. Another important parameter to ascertain the degree of shade tolerance of a plant is photoacclimation capacity, which is essential for plant fitness in environments with changing light input conditions (e.g. those where the growth of nearby plants may suddenly compromise access to light). By taking into account both parameters (the hypocotyl elongation response and the capacity to acclimate to low or high PAR), here we analyzed the shade tolerance of several Brassicaceae species, including the closely related mustard model systems *At* and *Ch*. As a rule of thumb, we observed that *Ch* and other species showing a good photoacclimation response to lower PAR (and badly performing after transfer to higher PAR) showed a poor or null elongation response to low R:FR (Figures 2 and

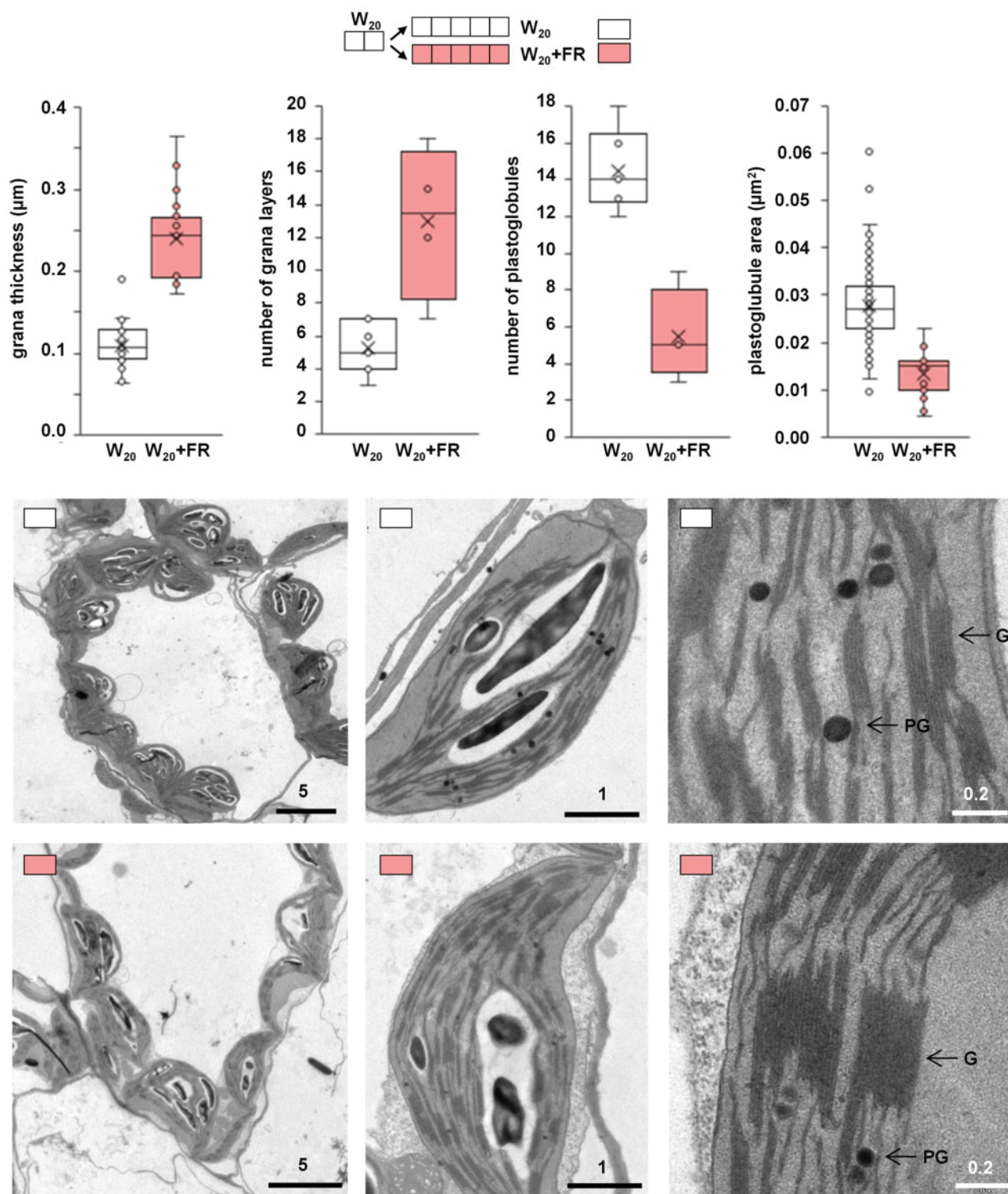


Figure 7 Low R:FR triggers ultrastructural changes in *At* chloroplasts. *At*-WT seeds were germinated and grown under W_{20} for 2 d and then either kept under W_{20} or transferred to low R:FR ($W_{20}+FR$) for 5 more days. Cotyledons were then used for TEM analysis of chloroplast ultrastructure. Representative pictures at different scales (numbers indicate micrometer) are shown. Boxplots show quantification of the indicated parameters from the images. Boxes show the values between the upper and the lower quartile, the cross represents the mean and the horizontal line the median. Whiskers (the upper and lower extremes) and circles represent single data and the ones located outside of the whiskers limit are the outliers (data with the same numerical value are visualized as a single point). For quantifying grana thickness, all the distinguishable structures were used (W_{20} $n = 30$, $W_{20}+FR$ $n = 20$). For quantifying grana layers, four major grana complexes from higher magnifications were measured. For quantifying the number of plastoglobules, at least six individual chloroplasts for each treatment were used. Plastoglobule area was measured for all the plastoglobules (W_{20} $n = 87$, $W_{20}+FR$ $n = 22$). PG, plastoglobules; G, grana.

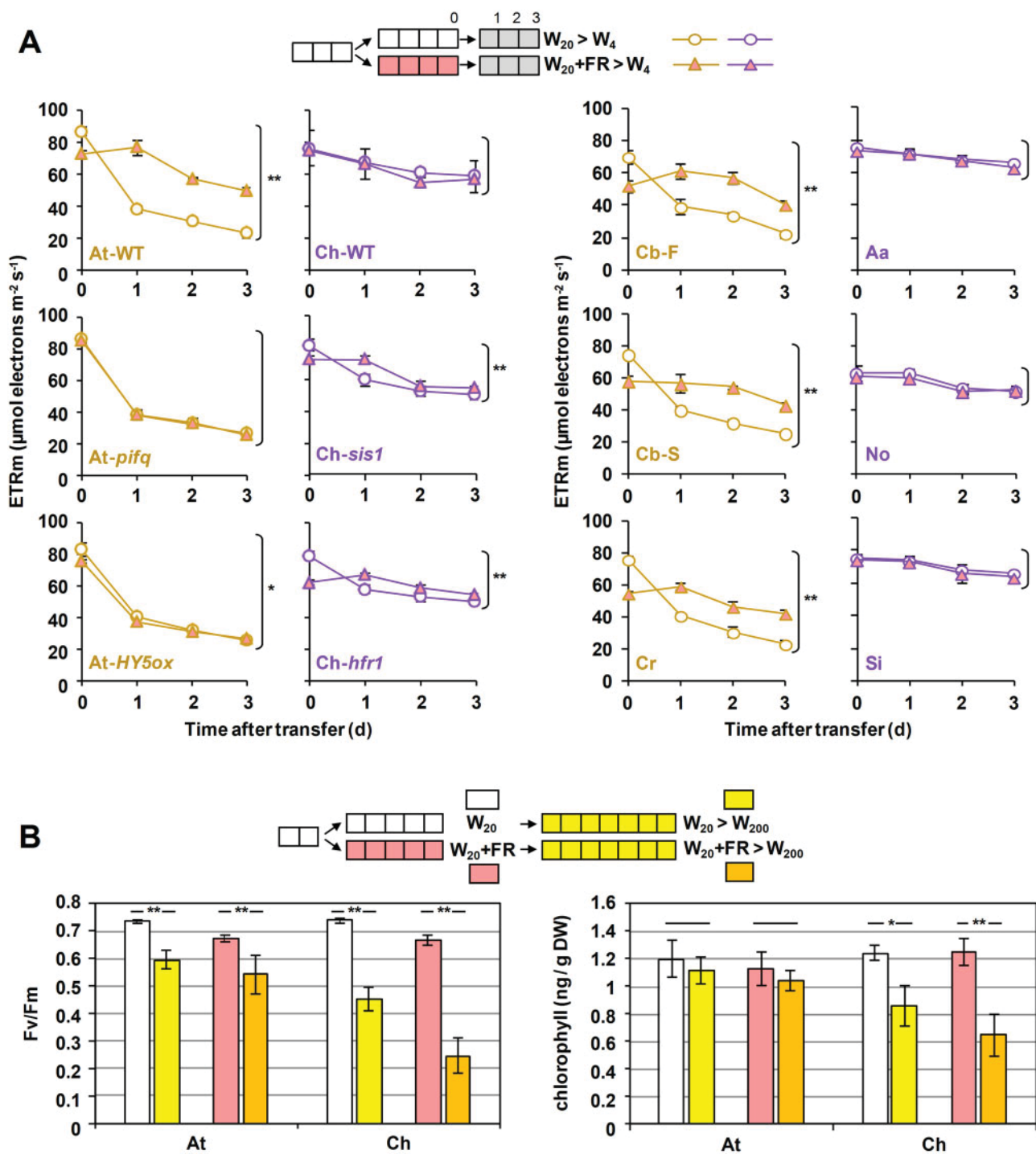


Figure 8 Pre-exposure to low R:FR improves the photoacclimation to low PAR in shade-avoider plants. A, The indicated genotypes were germinated and grown under W_{20} for 3 d, transferred to either W_{20} or $W_{20}+FR$ for 4 d, and then exposed to W_4 . Mean and standard error of ETRm values at 0, 1, 2, and 3 d after transfer to W_4 are shown ($n = 3$ seedlings per treatment). Asterisks indicate statistically significant differences between treatments (W_{20} or $W_{20}+FR$) over time (two-way ANOVA, $*P < 0.05$, $**P < 0.01$). B, Wild-type At and Ch lines were germinated and grown under W_{20} for 2 d, transferred to either W_{20} or $W_{20}+FR$ for 5 d, and then exposed to W_{200} for 7 more days. Fv/Fm values and HPLC-quantified chlorophyll levels were determined. Mean and standard error of $n = 7$ seedlings (Fv/Fm) or $n = 3$ independent pools (HPLC) per treatment are represented. Asterisks mark statistically significant differences between values before and after exposure to W_{200} (t test, $*P < 0.05$; $**P < 0.01$).

3). Mustards such as At that photoacclimated poorly to lower PAR but better to higher PAR tended to more conspicuously elongate their hypocotyls in response to low

R:FR, but there were exceptions of poorly elongating species such as No (Figures 2 and 3). Furthermore, mutation of genes encoding SAS regulators can dramatically change the

elongation response to low R:FR without improving the photoacclimation phenotype (Figure 4). Together, these results confirm that the capacity for photosynthetic acclimation to changing irradiance is a species-specific trend (Bailey et al., 2001) and a reliable indicator of shade tolerance. The shade-induced hypocotyl elongation response should only be used as a complementary phenotype to classify a plant as shade-tolerant (badly adapted to higher PAR exposure, well adapted to live under lower PAR and poorly responsive to low R:FR) or shade-avoider (well adapted to higher PAR, poor performers under lower PAR that elongate when exposed to low R:FR).

Our results also unveiled that an activation of low R:FR signaling in shade-avoider species such as *AtAt*-WT and shade-tolerant *Ch* plants with mutations causing low R:FR hypersensitivity (*Ch-sis1* and *Ch-hfr1*) regulated photosynthesis at multiple levels. We confirmed that exposure to W+FR caused a substantial decrease in the levels of photosynthetic pigments (chlorophylls and carotenoids) in these lines (Roig-Villanova et al., 2007; Bou-Torrent et al., 2015; Molina-Contreras et al., 2019; Paulisic et al., 2021) and proved that the changes had a direct impact on decreasing photosynthetic activity (Figure 5). Low R:FR treatments are known to trigger changes in gene expression within minutes (Kohnen et al., 2016). These changes, which are often instrumental for altering rapid growth responses, such as hypocotyl or petiole elongation, are usually mediated by PIFs (Hornitschek et al., 2009; Galstyan et al., 2011; Cifuentes-Esquivel et al., 2013; de Wit et al., 2015; Gallemi et al., 2017). PIFs were also found to regulate longer-term changes in gene expression such as those affecting photosynthetic genes (Figure 6). Because loss of PIFQ function in the *At-pifq* mutant resulted in a much attenuated response to W+FR compared to *At*-WT in terms of photosynthetic gene expression (Figure 6) but it also prevented photosynthetic pigment and activity loss (Figure 5), we propose that stabilization of PIFQ proteins following low R:FR exposure triggers a reprogramming of photosynthesis-related gene expression that eventually results in lower pigment levels and reduced photosynthetic activity. Based on the results obtained with other mutants (Figure 5), we speculate that this signaling network is further influenced by factors such as HFR1 and HY5, which prevent PIF binding to target genes by heterodimerization (Hornitschek et al., 2009) or competition for promoter binding sites (Toledo-Ortiz et al., 2014), respectively.

Concomitant with the described molecular and physiological changes, we discovered that low R:FR treatment of *At*-WT seedlings triggered ultrastructural changes in the chloroplast endomembrane systems resembling those occurring after transfer to low PAR (Figure 7). Grana with more thylakoid layers and increased thickness were observed in the chloroplasts of *At* seedlings exposed to simulated shade. In contrast, chloroplasts from tobacco (*Nicotiana tabacum*) leaves that received end-of-day-FR treatments (considered to induce similar shade responses as low R:FR) showed fewer

thylakoid layers per granum but more small grana spread throughout the chloroplast compared to end-of-day R controls (Kasperbauer and Hamilton, 1984). While these differences in chloroplast ultrastructure might derive from distinct treatments being applied to diverse species, both solutions likely contribute to optimize photosynthesis in the shade, when relatively less photons would strike a leaf. Indeed, leaves that develop under low PAR have chloroplasts with less plastoglobules (which are derived from thylakoid membranes) and more thylakoids per granum (Rozak et al., 2002; Lichtenthaler, 2007; Wood et al., 2018). Based on these results, we suggest that the chloroplast ultrastructural changes observed in *At*-WT plants grown under low R:FR are most likely aimed to acclimate their photosynthetic machinery to perform better under low PAR by, for instance, allowing a more efficient energy transfer. In agreement, pre-treatment with low R:FR improved photoacclimation to low PAR of *At*-WT seedlings but had no effect in *At* mutants defective in low R:FR signaling (Figure 8). Further experiments showed that the observed positive effect of low R:FR exposure for acclimation to low PAR can be observed in *At*-WT plants growing under different light conditions (Supplemental Figure S3) and in other shade-avoider Brassicaceae (*Cb-F*, *Cb-S*, and *Cr*), but not in shade-tolerant species such as *Ch*, *Aa*, *No*, and *Si* (Figure 8A).

At low irradiances, a proper balance between carbon allocation to growth and to respiration is important to meet the challenges associated with a shade environment. Wild-type *At* (shade-avoider) but not *Ch* (shade-tolerant) seedlings showed a drop in dark respiration when irradiation was reduced (Supplemental Figure S4), likely to reduce carbon loss for a better carbon balance. This adaptive mechanism might contribute to explain why shade-avoider and shade-tolerant species appear to show little or no differences in carbon balance under low light conditions (Sterck et al., 2013; Pons and Poorter, 2014). Similar to that observed for photosynthetic activity (Figure 8), the respiration drop observed in *At*-WT seedlings was attenuated by pre-exposure to low R:FR (Supplemental Figure S4). Interestingly, there is evidence for the specific activation/deactivation of respiratory pathways by the phytochrome system at different levels (Ribas-Carbo et al., 2008; Igamberdiev et al., 2014). Regardless of the signaling pathway connecting low R:FR perception to reduced photosynthesis and respiration, this is likely part of an anticipation mechanism for shade-avoider plants to prepare for the foreseeable reduction in PAR associated with shading. Indeed, low R:FR signals are perceived before actual shading takes place and light becomes limiting, and hence they are considered to act as a warning signal that shading might occur (Martinez-Garcia et al., 2010; Casal, 2013). When shade-avoider plants such as *At* and most crops (including tomato, cereals, or legumes) grow among taller plants or in a forest understory, they will use the low R:FR signals coming from a closing canopy to elongate (to overgrow its neighbors) but also to readapt its photosynthetic and respiratory machinery to low PAR before

actual shading takes place. In contrast, shade-tolerant plants are adapted to grow under dim light and hence photoacclimation to low PAR is hardly improved even when hypersensitive mutants that show shade-avoider responses in terms of elongation (Figure 3) and photosynthesis (Figure 6) are pre-exposed to low R:FR (Figure 8).

While the observed decrease in respiration and photosynthetic pigment and activity levels in shade-avoider plants appears to be part of the anticipation mechanism to an eventual reduction in PAR, a too committed response might be detrimental if light conditions change (e.g. if shading does not occur or shade plants become exposed again to direct sunlight). We have previously shown that a compensation mechanism exist that represses the response to low R:FR when the photosynthetic capacity of chloroplasts is compromised (Ortiz-Alcaide et al., 2019). The retrograde (i.e. chloroplast-to-nucleus) pathway that adapts low R:FR perception and signaling to the photosynthetic status of the plant involves the antagonistic factors PIFs and HY5, which also participate in retrograde signaling when underground seedlings are illuminated and start their photomorphogenic (i.e. photosynthetic) development (Ruckle et al., 2007; Martin et al., 2016; Xu et al., 2016; Ortiz-Alcaide et al., 2019). The balance of positive and negative regulators together with the chloroplast-mediated control of SAS likely contribute to prevent an excessive response to shade, hence preventing photooxidative damage (resulting from light intensity exceeding the photosynthetic capacity of the plant) and facilitating the return to high R:FR conditions if the low R:FR signal disappears (e.g. if a commitment to the shade-avoidance lifestyle is unnecessary). Together, our work demonstrates that regulation of photosynthetic (chloroplast) performance is both an output and an input of the response of plants to shade. Our results therefore contribute to a better understanding of how plants respond to shade, a knowledge that will contribute to optimally grow crop plants closer together or/and under canopies (e.g. in intercropping settings).

Materials and methods

Plant material and growth conditions

Alpine rock cress (*Arabis alpina*, *pep1-1* mutant; Wang et al., 2009), *Arabidopsis* (*Arabidopsis thaliana*, Col-0 accession), hairy bittercress (*Cardamine hirsuta*, Oxford, Ox accession; Molina-Contreras et al., 2019), shepherd's purse (*Capsella bursa-pastoris*, accessions Strasbourg-1, Str-1 and Freiburg-1, Fre-1), pink shepherd's-purse (*Capsella rubella*), and London rocket (*Sisymbrium irio*) plants were grown in the greenhouse under long-day photoperiods (16-h light and 8-h dark) to produce seeds, as described (Gallemí et al., 2017). Seeds of *C. bursa-pastoris* were collected by Ruben Alcazar (University of Barcelona, Spain) from wild populations in Strasbourg (France, coordinates: 48.612436, 7.767881; Str-1) and Freiburg (Germany, coordinates: 47.994945, 7.861979; Fre-1). Seeds of *C. rubella*, collected from wild populations in Crete (Greece, coordinates 35.29, 24.42; accession 879) were

previously described (Koenig et al., 2019). Seeds of *S. irio* were collected from wild populations in Bellaterra (Barcelona, Spain, coordinates: 41.497731, 2.109558). Seeds of watercress (*Nasturtium officinale*) were provided by a seed company (www.semillasfito.es). *Arabidopsis thaliana* and Ch mutant and transgenic lines were previously available in our laboratories (Molina-Contreras et al., 2019; Ortiz-Alcaide et al., 2019; Paulisic et al., 2021).

For the light acclimation experiments seedlings were germinated and grown in Petri dishes containing solid medium without sucrose (0.5× MS): 2.2 g·L⁻¹ MS basal salt mixture (Duchefa), 1% (w/v) agar, 0.25 g·L⁻¹ 2-(*N*-morpholino)ethanesulfonic acid (MES; Sigma Aldrich), pH 5.7). Normal light conditions refer to white light (W) produced by cool-white vertical fluorescent tubes of a photosynthetic photon flux density in the PAR region (PPFD) of 20–24 μmol m⁻² s⁻¹ (W₂₀) with a R:FR of 1.5–3.3. Low light and high light conditions corresponded to W of PPFD of 4 (W₄) and 200 (W₂₀₀) μmol m⁻² s⁻¹, respectively, produced by horizontal fluorescent tubes. Low R:FR treatment was produced by supplementing W₂₀ with FR (W₂₀+FR). FR was emitted from a GreenPower LED module HF FR (Philips), providing a R:FR of 0.02 (Martinez-Garcia et al., 2014). For the light acclimation experiments shown in Supplemental Figure S3, seedlings were germinated and grown in Petri dishes, as previously described, but exposed to long-day (16-h light/8-h darkness) or short-day (8-h light/16-h darkness) photoperiods. The light part of the photoperiod was produced by cool-white horizontal fluorescent tubes of 200–210 μmol m⁻² s⁻¹ of PPFD (W₂₀₀) with R:FR of 2–3.5). In that case, low light conditions corresponded to values of 15 μmol m⁻² s⁻¹ PPFD (W₁₅). In this set-up, low R:FR treatment was produced by supplementing W₂₀₀ with the same FR lamps described above (W₂₀₀+FR), obtaining a R:FR of 0.2–0.25. Light fluence rates were measured with a Spectrosense2 meter (Skye Instruments Ltd), which provides PPFD (400–700 nm), and photon flux density in 10 nm windows of R (664–674 nm) and FR (725–735 nm) regions to calculate the R:FR (Martinez-Garcia et al., 2014). Full spectra photon distribution of W and W+FR treatments have been described elsewhere (Molina-Contreras et al., 2019).

Measurement of hypocotyl length

For hypocotyl measurement, about 30 seeds of each genotype were germinated and grown on plates containing 0.5× MS solid media. For quantification of hypocotyl length, at least 20 seedlings were analyzed with the Fiji-ImageJ software (Schindelin et al., 2012), as described (Roig-Villanova et al., 2019). All experiments were repeated at least three times with consistent results. Hypocotyl measurements from all the different experiments were averaged.

Photosynthetic measurements and pigment quantification

Whole seedlings were harvested, ground in liquid nitrogen, and the resulting powder was used for quantification of chlorophylls and carotenoids either spectrophotometrically

or by high performance liquid chromatography (HPLC) as described (Bou-Torrent et al., 2015). Chlorophyll fluorescence measurements were carried out on seedlings using a MAXI-PAM fluorometer (Heinz Walz GmbH) as described (Molina-Contreras et al., 2019). Briefly, for every measurement the whole cotyledons of seven seedlings were considered. Effective quantum yield of photosystem II (PSII) under growth light, Φ_{PSII} , was measured as $\Delta F/F_m'$, where ΔF corresponds to $F_m' - F$ (the maximum minus the minimum fluorescence of light-exposed plants). Maximum quantum yield of PSII, F_v/F_m , was calculated as $(F_m - F_o)/F_m$, where F_m and F_o are, respectively, the maximum and the minimum fluorescence of dark-adapted samples. For dark acclimation, plates were incubated for at least 30 min in darkness to allow the full relaxation of photosystems. Light curves were constructed with 10 incremental steps of actinic irradiance (E ; 0, 20, 55, 110, 185, 280, 395, 530, 610, 700 $\mu\text{mol photons}\cdot\text{m}^{-2}\cdot\text{s}^{-1}$ of PPF). For each step, Φ_{PSII} was monitored every minute and electron transport rate (ETR) was calculated as $E \times \Phi_{PSII} \times 0.84 \times 0.5$ (where 0.84 is the light absorbance by an average green leaf and 0.5 is the fraction of absorbed quanta available for PSII). The light response and associated parameters ETR_m (maximum electron transport rate) and alpha (photosynthetic rate in light-limited region of the light curve) were characterized by fitting iteratively the model of the rETR versus E curves using MS Excel Solver (Platt et al., 1980). The fit was very good in all the cases ($r > 0.98$).

Respiration measurements

Seedlings were germinated and grown on $0.5 \times$ MS plates, as described (Supplemental Figure S4). Before the measurements, seedlings were placed in the dark for about 30 min to avoid light-enhanced dark respiration. Five to 10 seedlings were then collected, immediately weighed, and placed into the respiration cuvette containing the respiration buffer (30-mM MES, pH 6.2, 0.2-mM CaCl_2). Oxygen uptake rates were measured in darkness using a liquid-phase Clark-type oxygen electrode (Rank Brothers Ltd.) as previously described (Florez-Sarasa et al., 2009) at a constant temperature of 23°C.

Microarray data analyses

Microarray data corresponding to Col-0 At-WT and At-*pifq* seedlings exposed to low-R:FR for 0, 1, 3, and 24 h (Leivar et al., 2012) were analyzed to select for differentially expressed genes (DEGs) specifically related to photosynthesis. The reported list of DEGs was further filtered using cut-offs of FDR < 0.05 and log₂-transformed fold change higher than 0.585 for upregulated genes and lower than -0.599 for downregulated genes. Then, photosynthesis-related genes were identified by using the Kyoto Encyclopedia of Genes and Genomes Mapper tool (Kanehisa and Sato, 2020).

Transmission electron microscopy

TEM was carried out as described (Flores-Perez et al., 2008). Chloroplast features in the pictures were quantified by using the FIJI-ImageJ software (Schindelin et al., 2012).

Accession numbers

Sequence data from this article can be found in the EMBL/Genbank and *C. hirsuta* genetic and genomic resource (<http://chi.mpipz.mpg.de>) data libraries under the following accession numbers: AT1G02340 (*AtHFR1*), AT5G11260 (*AtHY5*), AT2G20180 (*AtPIF1*), AT1G09530 (*AtPIF3*), AT2G43010 (*AtPIF4*), AT3G59060 (*AtPIF5*), CARHR001660 (*ChHFR1*), and CARHR009540 (*SIS1/ChPHYA*).

Supplemental data

The following materials are available in the online version of this article.

Supplemental Figure S1. Alpha values calculated from the light curves shown in Figure 2A.

Supplemental Figure S2. Activation of low R:FR signaling reduces photosynthetic activity.

Supplemental Figure S3. Pre-exposure to low R:FR improves photoacclimation to lower PAR in *A. thaliana* plants grown under photoperiods.

Supplemental Figure S4. Exposure to low R:FR differentially impacts respiration rate of shade-avoider and shade-tolerant plants.

Acknowledgments

We thank M^a Rosa Rodríguez (CRAG) for technical support, and George Coupland (MPI for Plant Breeding Research, Cologne, Germany), Rubén Alcazar (Universitat de Barcelona, Spain) and Ignacio Rubio (CRAG) for providing mustard seeds.

Funding

L.M. received a predoctoral fellowships from *La Caixa Foundation* (INPhINIT fellowship LCF/BQ/IN18/11660004). W.Q. is a recipient of a predoctoral Chinese Scholarship Council (CSC) fellowship. A.I.-S. is supported by a predoctoral fellowship from MICINN (PRE2018-083610). I.F.-S. has received funding from the European Union's Horizon 2020 research and innovation programme under the Marie Skłodowska-Curie grant agreement no. 753301. Our research is supported by grants from MICINN-FEDER (BIO2017-85316-R, and BIO2017-84041-P) and AGAUR (2017-SGR1211, 2017-SGR710 and Xarba) to J.F.M.-G. and M.R.-C. We also acknowledge the support of the MINECO for the "Centro de Excelencia Severo Ochoa 2016-2019" award SEV-2015-0533 and by the CERCA Programme/Generalitat de Catalunya.

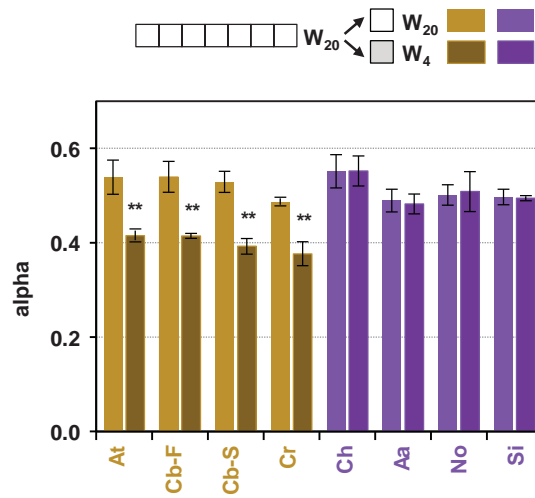
Conflict of interest statement. The authors declare no competing interests.

References

- Bailey S, Walters RG, Jansson S, Horton P (2001) Acclimation of *Arabidopsis thaliana* to the light environment: the existence of separate low light and high light responses. *Planta* **213**: 794–801
- Benkov MA, Yatsenko AM, Tikhonov AN (2019) Light acclimation of shade-tolerant and sun-resistant *Tradescantia* species: photochemical activity of PSII and its sensitivity to heat treatment. *Photosynth Res* **139**: 203–214
- Bou-Torrent J, Toledo-Ortiz G, Ortiz-Alcaide M, Cifuentes-Esquivel N, Halliday KJ, Martinez-Garcia JF, Rodriguez-Concepcion M (2015) Regulation of carotenoid biosynthesis by shade relies on specific subsets of antagonistic transcription factors and cofactors. *Plant Physiol* **169**: 1584–1594
- Cagnola JI, Ploschuk E, Benech-Arnold T, Finlayson SA, Casal JJ (2012) Stem transcriptome reveals mechanisms to reduce the energetic cost of shade-avoidance responses in tomato. *Plant Physiol* **160**: 1110–1119
- Casal JJ (2013) Photoreceptor signaling networks in plant responses to shade. *Annu Rev Plant Biol* **64**: 403–427
- Cifuentes-Esquivel N, Bou-Torrent J, Galstyan A, Gallemi M, Sessa G, Salla Martret M, Roig-Villanova I, Ruberti I, Martinez-Garcia JF (2013) The bHLH proteins BEE and BIM positively modulate the shade avoidance syndrome in *Arabidopsis* seedlings. *Plant J* **75**: 989–1002
- Ciolfi A, Sessa G, Sassi M, Possenti M, Salvucci S, Carabelli M, Morelli G, Ruberti I (2013) Dynamics of the shade-avoidance response in *Arabidopsis*. *Plant Physiol* **163**: 331–353
- de Wit M, Ljung K, Fankhauser C (2015) Contrasting growth responses in lamina and petiole during neighbor detection depend on differential auxin responsiveness rather than different auxin levels. *New Phytol* **208**: 198–209
- Flores-Perez U, Sauret-Gueto S, Gas E, Jarvis P, Rodriguez-Concepcion M (2008) A mutant impaired in the production of plastome-encoded proteins uncovers a mechanism for the homeostasis of isoprenoid biosynthetic enzymes in *Arabidopsis* plastids. *Plant Cell* **20**: 1303–1315
- Florez-Sarasa I, Ostaszewska M, Galle A, Flexas J, Rychter AM, Ribas-Carbo M (2009) Changes of alternative oxidase activity, capacity and protein content in leaves of *Cucumis sativus* wild-type and MSC16 mutant grown under different light intensities. *Physiol Plant* **137**: 419–426
- Galstyan A, Cifuentes-Esquivel N, Bou-Torrent J, Martinez-Garcia JF (2011) The shade avoidance syndrome in *Arabidopsis*: a fundamental role for atypical basic helix-loop-helix proteins as transcriptional cofactors. *Plant J* **66**: 258–267
- Gallemi M, Molina-Contreras MJ, Paulisic S, Salla-Martret M, Sorin C, Godoy M, Franco-Zorrilla JM, Solano R, Martinez-Garcia JF (2017) A non-DNA-binding activity for the ATHB4 transcription factor in the control of vegetation proximity. *New Phytol* **216**: 798–813
- Hay AS, Pieper B, Cooke E, Mandakova T, Cartolano M, Tattersall AD, Ioio RD, McGowan SJ, Barkoulas M, Galinha C, et al. (2014) *Cardamine hirsuta*: a versatile genetic system for comparative studies. *Plant J* **78**: 1–15
- Hornitschek P, Lorrain S, Zoete V, Michielin O, Fankhauser C (2009) Inhibition of the shade avoidance response by formation of non-DNA binding bHLH heterodimers. *EMBO J* **28**: 3893–3902
- Igamberdiev AU, Eprintsev AT, Fedorin DN, Popov VN (2014) Phytochrome-mediated regulation of plant respiration and photorespiration. *Plant Cell Environ* **37**: 290–299
- Kanehisa M, Sato Y (2020) KEGG Mapper for inferring cellular functions from protein sequences. *Protein Sci* **29**: 28–35
- Kasperbauer MJ, Hamilton JL (1984) Chloroplast structure and starch grain accumulation in leaves that received different red and far-red levels during development. *Plant Physiol* **74**: 967–970
- Koenig D, Hagmann J, Li R, Bemm F, Slotte T, Neuffer B, Wright SI, Weigel D (2019) Long-term balancing selection drives evolution of immunity genes in *Capsella*. *eLife* **8**
- Kohnen MV, Schmid-Siegert E, Trevisan M, Petrolati LA, Senechal F, Muller-Moule P, Maloof J, Xenarios I, Fankhauser C (2016) Neighbor detection induces organ-specific transcriptomes, revealing patterns underlying hypocotyl-specific growth. *Plant Cell* **28**: 2889–2904
- Leivar P, Tepperman JM, Cohn MM, Monte E, Al-Sady B, Erickson E, Quail PH (2012) Dynamic antagonism between phytochromes and PIF family basic helix-loop-helix factors induces selective reciprocal responses to light and shade in a rapidly responsive transcriptional network in *Arabidopsis*. *Plant Cell* **24**: 1398–1419
- Lichtenthaler HK (2007) Biosynthesis, accumulation and emission of carotenoids, alpha-tocopherol, plastoquinone, and isoprene in leaves under high photosynthetic irradiance. *Photosynth Res* **92**: 163–179
- Lorenzo CD, Alonso Iserte J, Sanchez Lamas M, Antonietti MS, Garcia Gagliardi P, Hernando CE, Dezar CAA, Vazquez M, Casal JJ, Yanovsky MJ, et al. (2019) Shade delays flowering in *Medicago sativa*. *Plant J* **99**: 7–22
- Martin G, Leivar P, Ludevid D, Tepperman JM, Quail PH, Monte E (2016) Phytochrome and retrograde signalling pathways converge to antagonistically regulate a light-induced transcriptional network. *Nat Commun* **7**: 11431
- Martinez-Garcia JF, Galstyan A, Salla-Martret M, Cifuentes-Esquivel N, Gallemi M, Bou-Torrent J (2010) Regulatory components of shade avoidance syndrome. *Adv Bot Res* **53**: 65–116
- Martinez-Garcia JF, Gallemi M, Molina-Contreras MJ, Llorente B, Bevilaqua MR, Quail PH (2014) The shade avoidance syndrome in *Arabidopsis*: the antagonistic role of phytochrome a and B differentiates vegetation proximity and canopy shade. *PLoS One* **9**: e109275
- Molina-Contreras MJ, Paulisic S, Then C, Moreno-Romero J, Pastor-Andreu P, Morelli L, Roig-Villanova I, Jenkins H, Hallab A, Gan X, et al. (2019) Photoreceptor activity contributes to contrasting responses to shade in *Cardamine* and *Arabidopsis* seedlings. *Plant Cell* **31**: 2649–2663
- Murchie EH, Horton P (1997) Acclimation of photosynthesis to irradiance and spectral quality in British plant species: chlorophyll content, photosynthetic capacity and habitat preference *Plant Cell Environ* **20**: 438–448
- Ortiz-Alcaide M, Llamas E, Gomez-Cadenas A, Nagatani A, Martinez-Garcia JF, Rodriguez-Concepcion M (2019) Chloroplasts modulate elongation responses to canopy shade by retrograde pathways involving HY5 and ABA. *Plant Cell*
- Patel D, Basu M, Hayes S, Majlath I, Hetherington FM, Tschaplinski TJ, Franklin KA (2013) Temperature-dependent shade avoidance involves the receptor-like kinase ERECTA. *Plant J* **73**: 980–992
- Paulisic S, Qin W, Arora Veraszto H, Then C, Alary B, Nogue F, Tsiantis M, Hothorn M, Martinez-Garcia JF (2021) Adjustment of the PIF7-HFR1 transcriptional module activity controls plant shade adaptation. *EMBO J* **40**: e104273
- Platt T, Gallegos CL, Harrison WG (1980) Photoinhibition of photosynthesis in natural assemblages of marine phytoplankton. *J Mar Res* **38**: 687–701
- Pons TL, Poorter H (2014) The effect of irradiance on the carbon balance and tissue characteristics of five herbaceous species differing in shade-tolerance. *Front Plant Sci* **5**: 12
- Ptushenko OS, Ptushenko VV (2019) *Tradescantia*-based models: a powerful looking glass for investigation of photoacclimation and photoadaptation in plants. *Physiol Plant* **166**: 120–133
- Ribas-Carbo M, Giles L, Flexas J, Briggs W, Berry JA (2008) Phytochrome-driven changes in respiratory electron transport partitioning in soybean (*Glycine max. L.*) cotyledons. *Plant Biol (Stuttg)* **10**: 281–287
- Roig-Villanova I, Bou-Torrent J, Galstyan A, Carretero-Paulet L, Portoles S, Rodriguez-Concepcion M, Martinez-Garcia JF (2007) Interaction of shade avoidance and auxin responses: a role for two novel atypical bHLH proteins. *EMBO J* **26**: 4756–4767

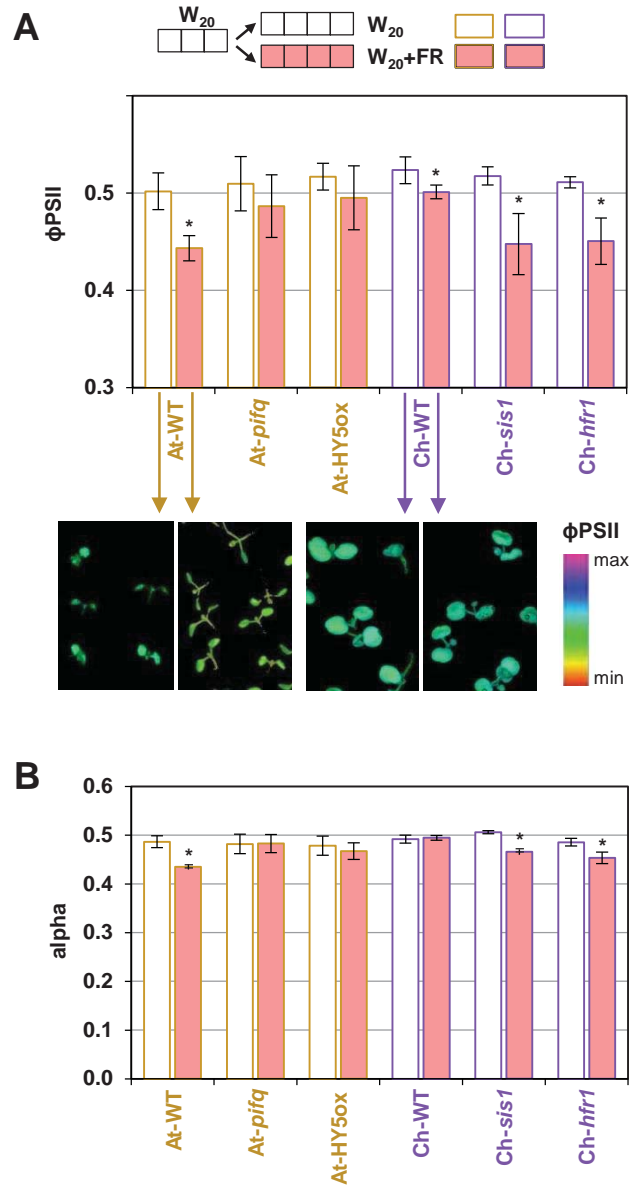
- Roig-Villanova I, Martinez-Garcia JF** (2016) Plant responses to vegetation proximity: a whole life avoiding shade. *Front Plant Sci* **7**: 236
- Roig-Villanova I, Paulisic S, Martinez-Garcia JF** (2019) Shade avoidance and neighbor detection. *Methods Mol Biol* **2026**: 157–168
- Rozak PR, Seiser RM, Wacholtz WF, Wise RR** (2002) Rapid, reversible alterations in spinach thylakoid appression upon changes in light intensity. *Plant Cell Environ* **25**: 421–429
- Ruckle ME, DeMarco SM, Larkin RM** (2007) Plastid signals remodel light signaling networks and are essential for efficient chloroplast biogenesis in *Arabidopsis*. *Plant Cell* **19**: 3944–3960
- Schindelin J, Arganda-Carreras I, Frise E, Kaynig V, Longair M, Pietzsch T, Preibisch S, Rueden C, Saalfeld S, Schmid B, et al.** (2012) Fiji: an open-source platform for biological-image analysis. *Nat Methods* **9**: 676–682
- Shi Q, Kong F, Zhang H, Jiang Y, Heng S, Liang R, Ma L, Liu J, Lu X, Li P, et al.** (2019) Molecular mechanisms governing shade responses in maize. *Biochem Biophys Res Commun* **516**: 112–119
- Smith H** (1982) Light quality, photoperception, and plant strategy. *Ann Rev Plant Physiol* **33**: 481–518
- Sterck FJ, Duurssma RA, Pearcy RW, Valladares F, Cieslak M, Weemstra M** (2013) Plasticity influencing the light compensation point offsets the specialization for light niches across shrub species in a tropical forest understorey. *J Ecol* **101**: 971–980
- Toledo-Ortiz G, Johansson H, Lee KP, Bou-Torrent J, Stewart K, Steel G, Rodriguez-Concepcion M, Halliday KJ** (2014) The HY5-PIF regulatory module coordinates light and temperature control of photosynthetic gene transcription. *PLoS Genet* **10**: e1004416
- Valladares F, Niinemets U** (2008) Shade tolerance, a key plant feature of complex nature and consequences. *Ann Rev Ecol Evol Syst* **39**: 237–257
- Wang R, Farrona S, Vincent C, Joecker A, Schoof H, Turck F, Alonso-Blanco C, Coupland G, Albani MC** (2009) PEP1 regulates perennial flowering in *Arabidopsis*. *Nature* **459**: 423–427
- Wood WHJ, MacGregor-Chatwin C, Barnett SFH, Mayneord GE, Huang X, Hobbs JK, Hunter CN, Johnson MP** (2018) Dynamic thylakoid stacking regulates the balance between linear and cyclic photosynthetic electron transfer. *Nat Plants* **4**: 116–127
- Xu X, Chi W, Sun X, Feng P, Guo H, Li J, Lin R, Lu C, Wang H, Leister D, et al.** (2016) Convergence of light and chloroplast signals for de-etiolation through ABI4-HY5 and COP1. *Nat Plants* **2**: 16066
- Yang C, Xie F, Jiang Y, Li Z, Huang X, Li L** (2018) Phytochrome a negatively regulates the shade avoidance response by increasing auxin/indole acetic acid protein stability. *Dev Cell* **44**: 29–41 e24

Supplemental Figure S1



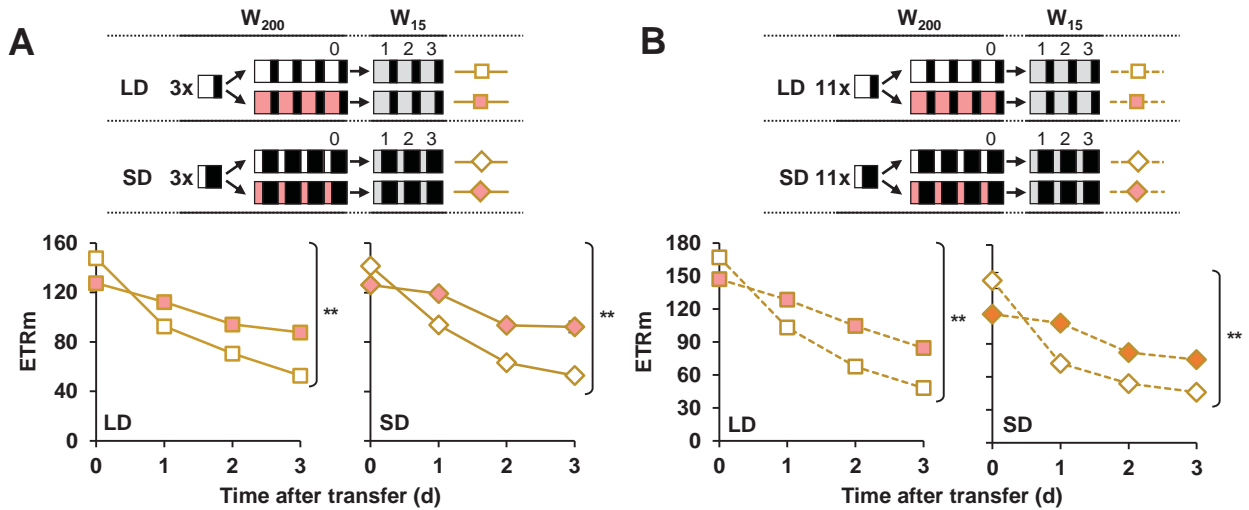
Supplemental Figure S1. Alpha values calculated from the light curves shown in Fig. 2A corresponding to *Arabidopsis thaliana* (At), *Capsella bursa-pastoris* (Cb-F and Cb-S), *Capsella rubella* (Cr), *Cardamine hirsuta* (Ch), *Arabis alpina* (Aa), *Nasturtium officinale* (No), and *Sisymbrium irio* (Si) seedlings germinated and grown under W₂₀ for 7 days and then either kept under W₂₀ or transferred to lower PAR (W₄) for 1 more day. Values represent the mean and standard error of n=3 plants for treatment. Asterisks mark statistically significant changes (*t* test ** *P*<0.01) relative to W₂₀.

Supplemental Figure S2



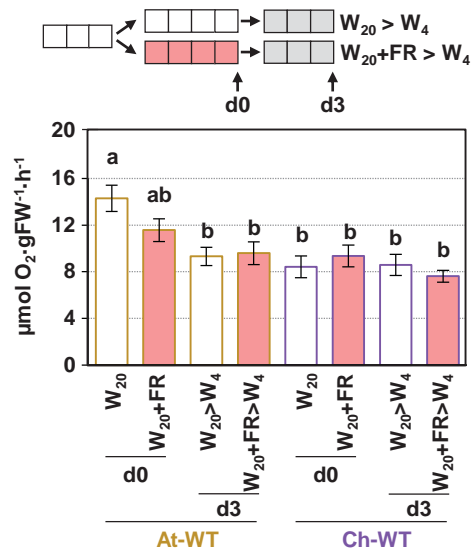
Supplemental Figure S2. Activation of low R:FR signaling reduces photosynthetic activity. (A) ϕPSII values of seedlings germinated and grown as indicated in Fig. 5A and summarized at the top of the section. Lower pictures show false-color images of this parameter in wild-type seedlings. **(B)** Alpha values of seedlings germinated and grown as indicated in **A**. Mean and standard error of $n=9$ seedlings per treatment are represented. Asterisks mark statistically significant changes in W₂₀+FR relative to W₂₀ (t test, $*P<0.05$).

Supplemental Figure S3



Supplemental Figure S3. Pre-exposure to low R:FR improves photoacclimation to lower PAR in *Arabidopsis thaliana* plants grown under photoperiods. *A.* *thaliana* plants were germinated and grown under $200 \mu\text{mol}\cdot\text{m}^{-2}\cdot\text{s}^{-1}$ PAR (W_{200}) for **(A)** 3 or **(B)** 11 days, transferred to either W_{200} or $W_{200}+\text{FR}$ for 4 days, and then exposed to $15 \mu\text{mol}\cdot\text{m}^{-2}\cdot\text{s}^{-1}$ PAR (W_{15}) for 3 more days. Mean and standard error of ETRm values at 0, 1, 2 and 3 days after transfer to W_{15} are shown ($n=3$ seedlings per treatment). Asterisks indicate statistically significant differences between treatments (W_{200} or $W_{200}+\text{FR}$) over time (two-way ANOVA, ** $P<0.01$).

Supplemental Figure S4



Supplemental Figure S4. Exposure to low R:FR differentially impacts respiration rate of shade-avoider and shade-tolerant plants. *A. thaliana* (At-WT) and *C. hirsuta* (Ch-WT) seedlings were germinated and grown under W_{20} for 3 days, transferred to either W_{20} or $W_{20} + FR$ for 4 days, and then exposed to lower PAR (W_4) for 3 more days. Mean and standard error of respiration rate values (expressed as $\mu\text{mol O}_2 \cdot \text{gFW}^{-1} \cdot \text{h}^{-1}$) at 0 and 3 days after transfer to W_4 are shown ($n=8$ seedlings per treatment). Different lowercase letters denote significant differences among means according to one-way ANOVA followed by a Tuckey post-hoc test ($P=0.05$).

Annex IV

An engineered extraplastidial pathway for carotenoid biofortification of leaves.

Andersen, T.B., Llorente, B., **Morelli, L.**, Torres-Montilla, S., Bordanaba-Florit, G., Espinosa, F.A., Rodriguez-Goberna, M.R., Campos, N., Olmedilla-Alonso, B., Llansola-Portoles, M.J., Pascal, A.A., and Rodriguez-Concepcion, M.

The PhD candidate contributed with his work to the following datasets:

Figure 5

Figure 8



Synthetic conversion of leaf chloroplasts into carotenoid-rich plastids reveals mechanistic basis of natural chromoplast development

Briardo Llorente^{a,b,c,1}, Salvador Torres-Montilla^a, Luca Morelli^a, Igor Florez-Sarasa^a, José Tomás Matus^{a,d}, Miguel Ezquerro^a, Lucio D'Andrea^{a,e}, Fakhreddine Houhou^f, Eszter Majer^f, Belén Picó^g, Jaime Cebolla^g, Adrian Troncoso^h, Alisdair R. Fernie^e, José-Antonio Daròs^f, and Manuel Rodríguez-Concepción^{a,f,1}

^aCentre for Research in Agricultural Genomics (CRAG) CSIC-IRTA-UAB-UB, Campus UAB Bellaterra, 08193 Barcelona, Spain; ^bARC Center of Excellence in Synthetic Biology, Department of Molecular Sciences, Macquarie University, Sydney NSW 2109, Australia; ^cCSIRO Synthetic Biology Future Science Platform, Sydney NSW 2109, Australia; ^dInstitute for Integrative Systems Biology (I2SysBio), Universitat de València-CSIC, 46908 Paterna, Valencia, Spain; ^eMax-Planck-Institut für Molekulare Pflanzenphysiologie, 14476 Potsdam-Golm, Germany; ^fInstituto de Biología Molecular y Celular de Plantas, CSIC-Universitat Politècnica de València, 46022 Valencia, Spain; ^gInstituto de Conservación y Mejora de la Agrodiversidad, Universitat Politècnica de València, 46022 Valencia, Spain; and ^hSorbonne Universités, Université de Technologie de Compiègne, Génie Enzymatique et Cellulaire, UMR-CNRS 7025, CS 60319, 60203 Compiègne Cedex, France

Edited by Krishna K. Niyogi, University of California, Berkeley, CA, and approved July 29, 2020 (received for review March 9, 2020)

Plastids, the defining organelles of plant cells, undergo physiological and morphological changes to fulfill distinct biological functions. In particular, the differentiation of chloroplasts into chromoplasts results in an enhanced storage capacity for carotenoids with industrial and nutritional value such as beta-carotene (provitamin A). Here, we show that synthetically inducing a burst in the production of phytoene, the first committed intermediate of the carotenoid pathway, elicits an artificial chloroplast-to-chromoplast differentiation in leaves. Phytoene overproduction initially interferes with photosynthesis, acting as a metabolic threshold switch mechanism that weakens chloroplast identity. In a second stage, phytoene conversion into downstream carotenoids is required for the differentiation of chromoplasts, a process that involves a concurrent reprogramming of nuclear gene expression and plastid morphology for improved carotenoid storage. We hence demonstrate that loss of photosynthetic competence and enhanced production of carotenoids are not just consequences but requirements for chloroplasts to differentiate into chromoplasts.

carotenoid | chromoplast | differentiation | phytoene | synthetic

Plastids comprise a group of morphologically and functionally diverse plant organelles capable of differentiating from one plastid type to another in response to developmental and environmental stimuli (1, 2). Such plastidial conversions are essential to sustain many fundamental biological processes and largely contribute to cell specialization in the different plant tissues. Among the different plastid types, chromoplasts are of great importance in nature and agriculture because of their capacity to accumulate high levels of carotenoids, plant pigments of isoprenoid nature that provide color in the yellow to red range (3–5). Carotenoids such as beta-carotene (provitamin A) are health-promoting nutrients that animals cannot synthesize but take up in their diets. They are also added-value compounds widely used in cosmetics, pharma, food, and feed industries as natural pigments and phytonutrients (4, 6).

Chromoplasts differentiate from preexisting plastids such as proplastids (i.e., undifferentiated plastids), leucoplasts (i.e., uncolored plastids in nonphotosynthetic tissues), and chloroplasts (i.e., photosynthetic plastids). Chloroplasts transform into chromoplasts during the development of many flowers and fruits, but only a few plant species differentiate chromoplasts in leaves (1, 5). The yellow to red colors that some leaves acquire as they senesce (e.g., in the autumn or when they are exposed to continuous darkness) are due to chloroplast carotenoids becoming visible when the chlorophylls degrade. This senescence process, however, does not involve the transformation of chloroplasts into

chromoplasts but into a completely different type of plastids named gerontoplasts (1, 2).

The most prominent changes during chloroplast-to-chromoplast differentiation are the reorganization of the internal plastid structures, together with a concurrent loss of photosynthetic competence and overaccumulation of carotenoid pigments (1–3, 5, 7, 8). The remodeling of the internal plastid structures generates an increased metabolic sink capacity but it also promotes carotenoid biosynthesis. The control of chromoplast differentiation appears as a very promising strategy for improving the nutritional and health benefits of crops (5–9). The overall process is known to involve changes in gene expression (e.g., via retrograde signaling from plastids to the nucleus), hormonal regulation, protein quality control, and plastid protein import (1, 3, 5). However, very few inducers of chromoplast development have been identified to date. Orange (OR) chaperones are among the best characterized,

Significance

Carotenoids are natural pigments whose properties as provitamin A and health-promoting phytonutrients make them ideal targets for biofortification. Here, we show that plastids specialized in carotenoid overaccumulation named chromoplasts can be synthetically produced in plant tissues that do not naturally develop them. We further demonstrate that differentiation of chromoplasts from leaf chloroplasts not just causes but requires both a reduction in photosynthetic activity and a stimulation of carotenoid biosynthesis in a process hardwired to a major reprogramming of global gene expression and cell metabolism. The synthetic system that we report here should allow to boost the nutritional quality of green vegetables and forage crops once their photosynthetic activity is dispensable (e.g., just before harvesting).

Author contributions: B.L., S.T.-M., L.M., I.F.-S., E.M., J.-A.D., and M.R.-C. designed research; B.L., S.T.-M., L.M., I.F.-S., J.T.M., M.E., L.D., F.H., E.M., B.P., J.C., and A.T. performed research; B.L., S.T.-M., L.M., I.F.-S., J.T.M., M.E., B.P., J.C., A.T., A.R.F., J.-A.D., and M.R.-C. contributed new reagents/analytic tools; B.L., S.T.-M., L.M., I.F.-S., J.T.M., M.E., L.D., F.H., E.M., B.P., J.C., A.T., A.R.F., J.-A.D., and M.R.-C. analyzed data; and B.L. and M.R.-C. wrote the paper.

The authors declare no competing interest.

This article is a PNAS Direct Submission.

Published under the PNAS license.

¹To whom correspondence may be addressed. Email: briardo.llorente@mq.edu.au or manuelrc@ibmcp.upv.es.

This article contains supporting information online at <https://www.pnas.org/lookup/suppl/doi:10.1073/pnas.2004405117/-DCSupplemental>.

First published August 19, 2020.

An engineered extraplastidial pathway for carotenoid biofortification of leaves

Trine B. Andersen^{1,†} , Briardo Llorente^{1,2,3} , Luca Morelli¹ , Salvador Torres-Montilla¹ , Guillermo Bordanaba-Florit¹, Fausto A. Espinosa¹, Maria Rosa Rodriguez-Goberna¹, Narciso Campos^{1,4} , Begoña Olmedilla-Alonso⁵ , Manuel J. Llansola-Portoles⁶ , Andrew A. Pascal⁶  and Manuel Rodriguez-Concepcion^{1,7,*} 

¹Centre for Research in Agricultural Genomics (CRAG), CSIC-IRTA-UAB-UB, Barcelona, Spain

²Department of Molecular Sciences, ARC Center of Excellence in Synthetic Biology, Macquarie University, Sydney, NSW, Australia

³CSIRO Synthetic Biology Future Science Platform, Sydney, NSW, Australia

⁴Departament de Bioquímica i Biologia Molecular, Universitat de Barcelona, Barcelona, Spain, 08028

⁵Instituto de Ciencia y Tecnología de Alimentos y Nutrición (ICTAN-CSIC), Madrid, Spain

⁶CEA, CNRS, Institute for Integrative Biology of the Cell (I2BC), Université Paris-Saclay, Gif-sur-Yvette, France

⁷Instituto de Biología Molecular y Celular de Plantas (IBMCP), CSIC-Universitat Politècnica de València, Valencia, Spain

Received 2 April 2020;

accepted 9 December 2020.

*Correspondence (Tel (+34) 963 877 725;

fax (+34) 963 877 859; email

manuelrc@ibmcp.upv.es)

†Present address: Great Lakes Bioenergy

Research Center, Michigan State University,

East Lansing, MI, 48824, USA

Summary

Carotenoids are lipophilic plastidial isoprenoids highly valued as nutrients and natural pigments. A correct balance of chlorophylls and carotenoids is required for photosynthesis and therefore highly regulated, making carotenoid enrichment of green tissues challenging. Here we show that leaf carotenoid levels can be boosted through engineering their biosynthesis outside the chloroplast. Transient expression experiments in *Nicotiana benthamiana* leaves indicated that high extraplastidial production of carotenoids requires an enhanced supply of their isoprenoid precursors in the cytosol, which was achieved using a deregulated form of the main rate-determining enzyme of the mevalonic acid (MVA) pathway. Constructs encoding bacterial enzymes were used to convert these MVA-derived precursors into carotenoid biosynthetic intermediates that do not normally accumulate in leaves, such as phytoene and lycopene. Cytosolic versions of these enzymes produced extraplastidial carotenoids at levels similar to those of total endogenous (i.e. chloroplast) carotenoids. Strategies to enhance the development of endomembrane structures and lipid bodies as potential extraplastidial carotenoid storage systems were not successful to further increase carotenoid contents. Phytoene was found to be more bioaccessible when accumulated outside plastids, whereas lycopene formed cytosolic crystalloids very similar to those found in the chromoplasts of ripe tomatoes. This extraplastidial production of phytoene and lycopene led to an increased antioxidant capacity of leaves. Finally, we demonstrate that our system can be adapted for the biofortification of leafy vegetables such as lettuce.

Keywords: carotenoids, phytoene, lycopene, biosynthesis, *Nicotiana benthamiana*, lettuce, bioaccessibility, antioxidant, biofortification.

Introduction

Carotenoids are lipophilic isoprenoids distributed throughout all kingdoms of life. Plants and some bacteria, archaea and fungi can biosynthesize these compounds *de novo*, whereas the vast majority of animals acquire them through their diet (Rodriguez-Concepcion *et al.*, 2018; Zheng *et al.*, 2020). Carotenoids are an essential part of the human diet, acting as precursors of retinoids (including vitamin A) and health-promoting molecules. They are also economically relevant as natural pigments that provide colours in the yellow to red range to many fruits, vegetables, seafood, fish, poultry and dairy products. One example is lycopene, which gives rise to the red colour in ripe tomatoes. Carotenoids with a shorter conjugation length such as phytoene (the first committed intermediate of the

biosynthetic pathway) are colourless (Rodriguez-Concepcion *et al.*, 2018).

In plants, carotenoids are synthesized in plastids from the universal C5 isoprenoid precursors isopentenyl diphosphate (IPP) and dimethylallyl diphosphate (DMAPP) produced by the methylerythritol 4-phosphate (MEP) pathway (Figure 1). Other plastidial isoprenoids, such as monoterpenoids and the prenyl moieties of chlorophylls and tocopherols, are produced using the same pool of substrates. In the cytosol, a second pool of IPP and DMAPP is synthesized by the mevalonic acid (MVA) pathway for the production of sesquiterpenoids and triterpenoids (including sterols). Plastid-localized isoforms of geranylgeranyl diphosphate (GGPP) synthases catalyse the condensation of three IPP and one DMAPP into one C20 GGPP. Two GGPP molecules are then converted into one C40 phytoene by phytoene synthase.

Desaturation and isomerization of phytoene produce lycopene, a linear carotenoid whose ends may then be cyclized into β and/or ϵ rings. The formation of two β rings results in the production of β -carotene, from which β - β xanthophylls such as violaxanthin and neoxanthin are formed through oxidation. The formation of one β and one ϵ ring leads to the production of lutein, the most abundant xanthophyll in photosynthetic tissues (Figure 1a). In chloroplasts, carotenoids are involved in light harvesting and photoprotection against excess light, and their levels are finely balanced with those of chlorophylls for the efficient assembly and functionality of photosynthetic complexes (Domonkos *et al.*, 2013; Esteban *et al.*, 2015; Hashimoto *et al.*, 2016). Carotenoids can also be produced and stored at high levels in chromoplasts, which are specialized plastids found in some non-photosynthetic tissues of flowers, fruits and other carotenoid-accumulating tissues (Sadali *et al.*, 2019; Sun *et al.*, 2018).

Several biotechnological strategies have been tested to enrich plant-derived feed and food products with carotenoids to improve their nutritional and economic value (Alos *et al.*, 2016; Zheng *et al.*, 2020). While highly successful results have been obtained in non-photosynthetic tissues, including Golden Rice, manipulation of carotenoid levels in photosynthetic tissues has been much more challenging. We have investigated methods to produce carotenoids in green tissues without interfering with photosynthetic function by moving their biosynthesis away from the chloroplast. The cytosol was a logical choice since the metabolic precursors of carotenoids (IPP and DMAPP) are already present due to the activity of the MVA pathway (Figure 1a). A previous attempt using virus-mediated expression of bacterial enzymes encoding GGPP synthase (*crtE*), phytoene synthase (*crtB*) and a desaturase/isomerase transforming phytoene into lycopene

(*crtI*) resulted in the production of lycopene in the cytosol of tobacco (*Nicotiana tabacum*) cells (Majer *et al.*, 2017). Virus-infected tissues accumulated lycopene to levels up to 10% of the total leaf carotenoid content, but only for 1–2 days, as carotenoid-producing leaves soon became necrotized. Such deleterious phenotype may be caused by side-effects of the viral infection, by the diversion of metabolic substrates away from cytosolic isoprenoid pathways, and/or by negative interference of the lipophilic lycopene with cell membrane function. Here we tested new strategies to circumvent these problems using phytoene and lycopene as the target products. The choice of these carotenoid intermediates (Figure 1a) was based on three main reasons. First, they are virtually absent in non-engineered leaves as they are readily converted into downstream chloroplast carotenoids (Domonkos *et al.*, 2013; Esteban *et al.*, 2015; Hashimoto *et al.*, 2016; Rodriguez-Concepcion *et al.*, 2018). Second, their supply is essential for the eventual production of any downstream carotenoid of interest. And third, they are health-promoting phytonutrients that are only found in a few food sources (Melendez-Martinez *et al.*, 2015; Melendez-Martinez *et al.*, 2018; Müller *et al.*, 2011; Rodriguez-Concepcion *et al.*, 2018).

Results

Agroinfiltrated leaves can produce extrastidial phytoene and lycopene at levels similar to those of endogenous chloroplast carotenoids

To produce phytoene and lycopene in the cytosol without the deleterious effects previously observed using viral vectors (Majer *et al.*, 2017), we tested a combination of strategies using

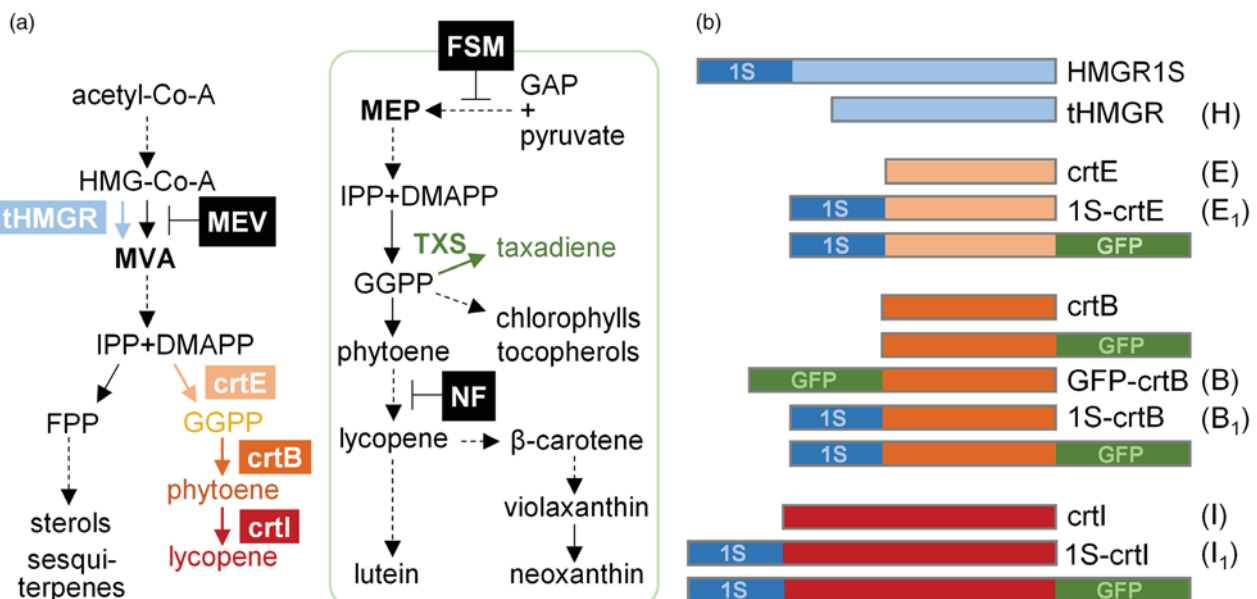


Figure 1 Schematic representation of the pathways and enzymes related to this work. (a) Carotenoid biosynthesis and related isoprenoid pathways in plants. Inhibitors of the MVA pathway (mevinolin, MEV), the MEP pathway (fosmidomycin, FSM) and the carotenoid pathway (norflurazon, NF) are boxed in black. HMG-CoA, hydroxymethylglutaryl coenzyme-A; MVA, mevalonic acid; IPP, isopentenyl diphosphate; DMAPP, dimethylallyl diphosphate; FPP, farnesyl diphosphate; GGPP, geranylgeranyl diphosphate; GAP, glyceraldehyde 3-phosphate; MEP, methylerythritol 4-phosphate. Enzymes produced in our system are shown in colour: tHMGR, truncated HMGR-CoA reductase; crtE, bacterial GGPP synthase; crtB, bacterial phytoene synthase; crtI, bacterial desaturase/isomerase; TXS, taxadiene synthase. The green box encloses reactions taking place in plastids. (b) Proteins used in this work. HMGR1S, crtE, crtB and crtI are unmodified enzymes. The rest are either truncated or fusion proteins. Boxes represent different enzymes and tags drawn to scale.

agroinfiltration of *Nicotiana benthamiana* as a less aggressive transient expression system (Schwach *et al.*, 2005). Plasmid vectors expressing the constructs under the control of the constitutive cauliflower mosaic virus 35S promoter together with a plasmid carrying the viral RNA silencing suppressor HCPro were used for transformation of *Agrobacterium tumefaciens* strain GV3101. *N. benthamiana* leaves were infiltrated with *A. tumefaciens* cultures carrying the selected constructs in identical proportions. To convert MVA-derived IPP and DMAPP into carotenoids, the bacterial *Pantoea ananatis* genes encoding crtE (to produce GGPP), crtB (to transform GGPP into phytoene) and crtI (to synthesize lycopene from phytoene) were used (Figure 1a). Unmodified versions of these three bacterial enzymes are active and synthesize lycopene in the cytosol of tobacco leaf cells (Majer *et al.*, 2017). In the case of crtB, however, part of the protein is targeted to chloroplasts (Figure 2) (Llorente *et al.*, 2020). To prevent this, we tested a version of the crtB enzyme with GFP fused to its N-terminus referred to as GFP-crtB (Figure 1b), which is retained in the cytosol of agroinfiltrated *N. benthamiana* leaf cells (Figure 2) (Llorente *et al.*, 2020). When we compared the production of phytoene by crtB and GFP-crtB enzymes at 5 days post-infiltration (dpi) (Figure 3), the amounts were 10-fold higher in the case of the unmodified crtB enzyme. This could be due to the N-terminal GFP tag interfering with crtB activity. Alternatively, the localization of at least some crtB protein in chloroplasts (Figure 2) might involve access to a higher supply of GGPP for phytoene production. Consistent with the latter hypothesis, inhibition of the MEP pathway with fosmidomycin (Figure 1a) strongly decreased the production of phytoene by crtB but not by GFP-crtB (Figure 3a). A similar result was observed when plastidial GGPP levels were decreased by co-expressing a *Taxus baccata* gene encoding taxadiene synthase (Figure 3b), a chloroplast-targeted enzyme that directly converts MEP-derived GGPP into the non-native diterpene taxadiene (Besumbes *et al.*, 2004) (Figure 1a). These results support the conclusion that unmodified crtB produces most of the detected phytoene from plastidial GGPP. In agreement, specific blockage of cytosolic IPP and DMAPP supply with the MVA pathway inhibitor mevinolin (Figure 1a) decreased the production of phytoene by GFP-crtB but not by crtB (Figure 3a). Conversely, increasing cytosolic GGPP levels by co-agroinfiltration of the crtE enzyme resulted in a marginal increment in the production of phytoene by crtB while it doubled the levels of phytoene synthesized by GFP-crtB (Figure 3b). These results indicate that GFP-crtB is enzymatically active and uses MVA-derived GGPP precursors to produce phytoene.

To minimize competition with endogenous cytosolic isoprenoid pathways (Figure 1a), we next increased MVA pathway flux using a truncated version of hydroxymethylglutaryl CoA reductase (HMGR), the main rate-limiting enzyme of the MVA

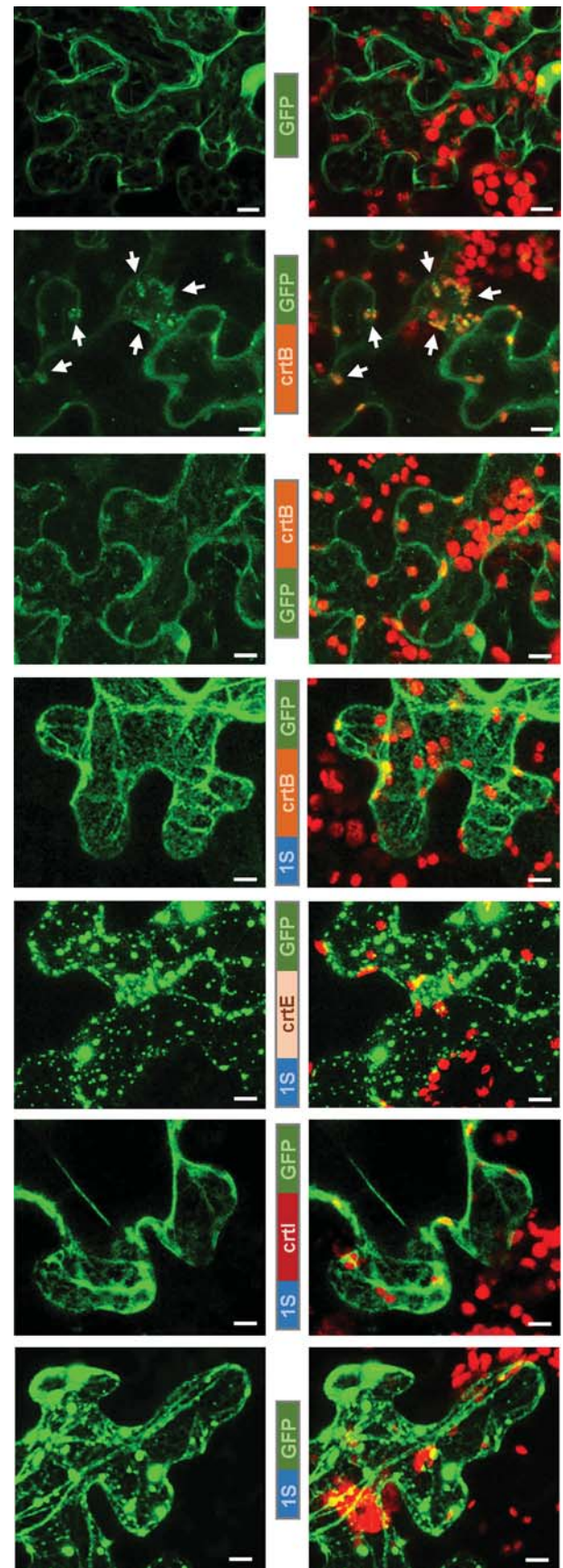


Figure 2 Subcellular localization of GFP-tagged proteins. *N. benthamiana* leaves were agroinfiltrated with constructs to express the indicated proteins and investigate their subcellular distribution based on GFP fluorescence by confocal microscopy at 3 dpi. Pictures show Z-stacks of selected regions of leaf cells displaying GFP fluorescence either alone (in green; left panels) or in combination with chlorophyll autofluorescence (in red; right panels). Arrows mark chloroplasts showing GFP fluorescence. Scale bars are 10 μm .

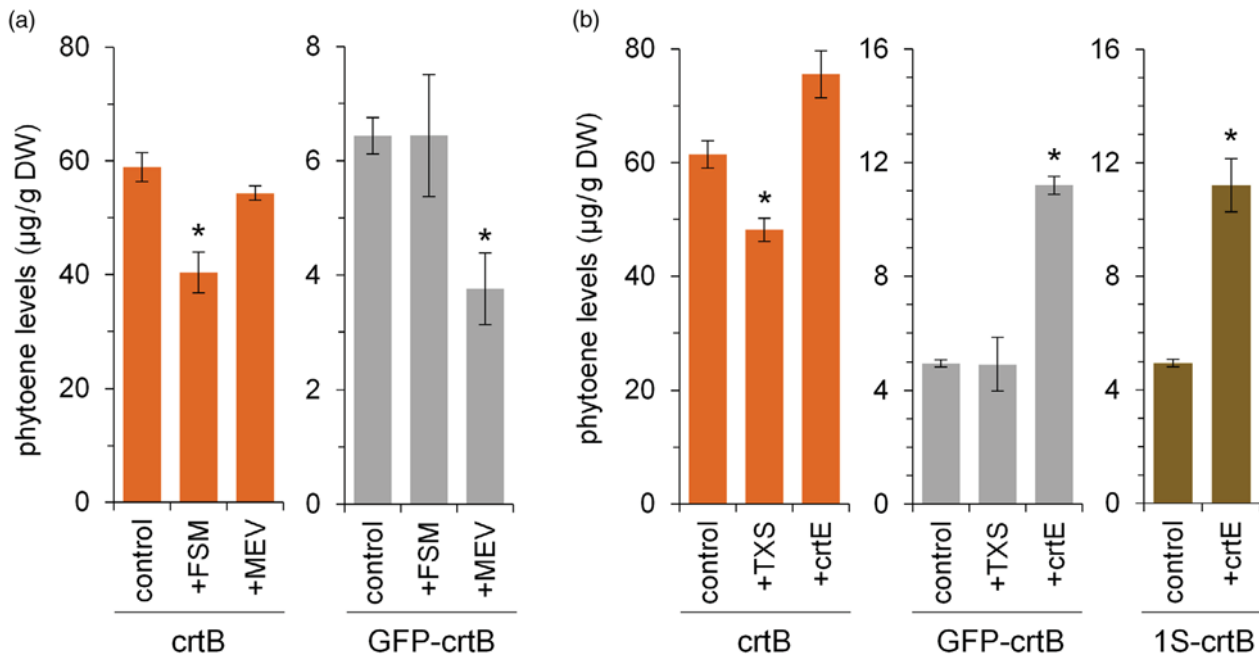


Figure 3 Supply of isoprenoid precursors is limiting for phytoene biosynthesis in the cytosol. *N. benthamiana* leaves were agroinfiltrated with the indicated constructs and samples were collected at 5 dpi for HPLC analysis. (a) Phytoene accumulation in leaf areas expressing either *crtB* or GFP-*crtB*, after treatment with the indicated inhibitors of the MEP or MVA pathways (FSM and MEV, respectively) or a mock solution (control). (b) Phytoene accumulation in leaf areas expressing *crtB*, GFP-*crtB* or 1S-*crtB* either alone (control) or together with yew *TXS* or bacterial *crtE*. Plots show the mean and standard error of $n = 4$ independent samples. Asterisks mark statistically significant changes relative to control samples (t -test, $P < 0.05$).

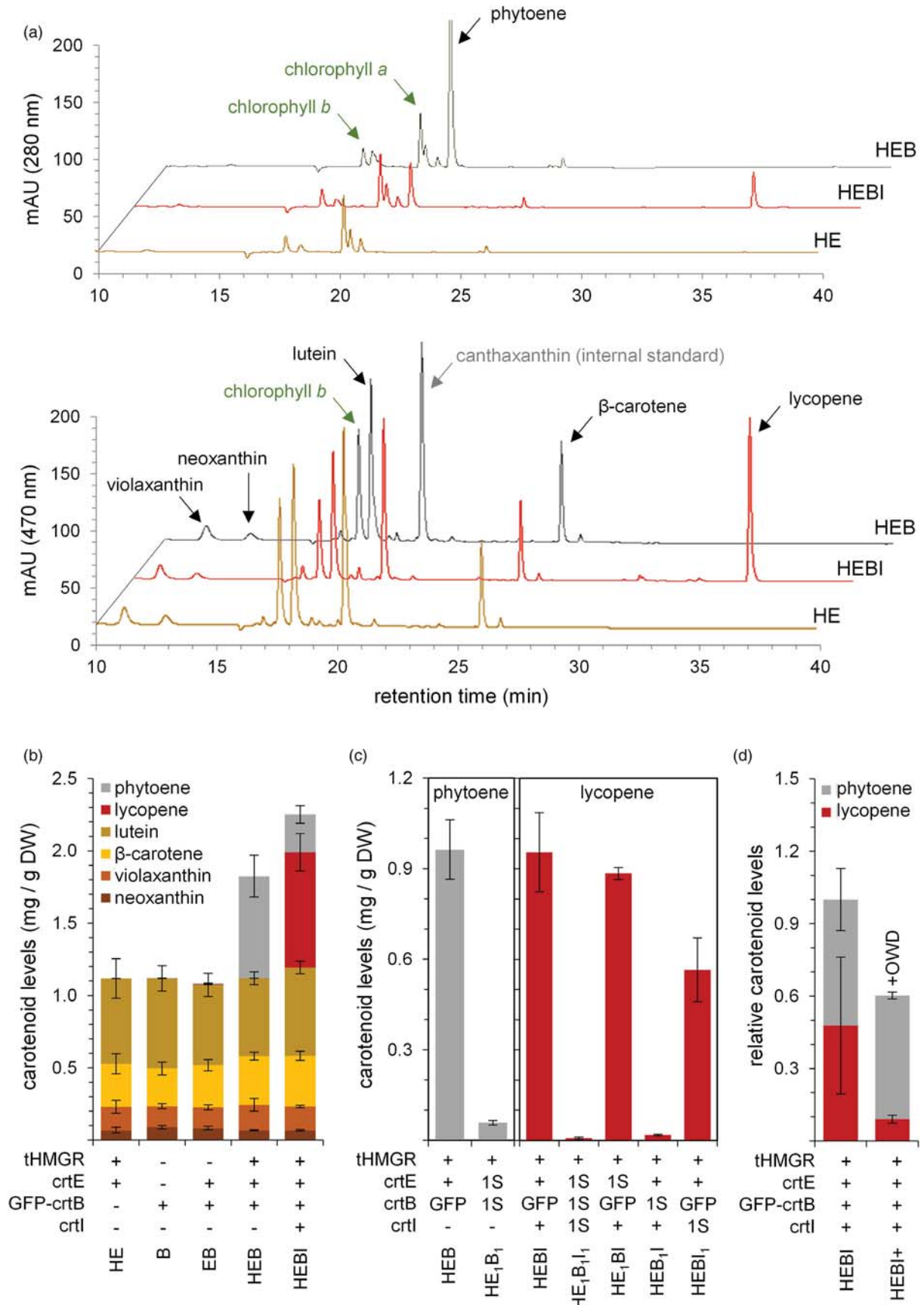
pathway (Rodríguez-Concepción and Boronat, 2015). In particular, we used the *Arabidopsis thaliana* HMGR1 enzyme (At1g76490) lacking the N-terminal regulatory domain (Figure 1b). This truncated version, referred to as tHMGR (Cankar *et al.*, 2015; van Herpen *et al.*, 2010), is not feedback-regulated and localizes to the cytosol as it lacks the N-terminal transmembrane domain that anchors the enzyme to the endoplasmic reticulum (ER). Constructs encoding tHMGR were co-infiltrated with the corresponding bacterial enzymes into *N. benthamiana* leaves and their carotenoid profile was analysed at 5 dpi (Figure 4). Co-agroinfiltration of constructs for tHMGR, *crtE* and GFP-*crtB* (HEB combination) led to an astounding accumulation of phytoene (Figure 4a). While addition of the *crtE* enzyme doubled the production of phytoene compared to GFP-*crtB* alone (EB relative to B, respectively; Figure 3b), a dramatic 200-fold increase in phytoene levels was detected in HEB samples additionally producing tHMGR (Figure 4b). Strikingly, this newly produced cytosolic phytoene increased total carotenoid levels by more than 60%. Further addition of *crtI* (HEBI combination) resulted in the production of very high levels of lycopene but also phytoene, probably reflecting incomplete enzymatic

conversion by *crtI* (Figure 4b). The level of cytosolic carotenoids accumulated in HEBI leaves was similar to the total amount of endogenous chloroplast carotenoids (Figure 4b). In particular, lycopene levels were in the same range of those found in chromoplasts from natural sources specialized for the accumulation of high lycopene levels such as tomato ripe fruit (D'Andrea *et al.*, 2018; Diretto *et al.*, 2020; Flores *et al.*, 2016; Massaretto *et al.*, 2018; Nogueira *et al.*, 2013; Pankratov *et al.*, 2016; Suzuki *et al.*, 2015).

Enhancing the development of endomembrane structures does not improve carotenoid contents

Next, we evaluated the potential of anchoring the bacterial enzymes to cell endomembranes while stimulating the proliferation of such lipid-storage structures to accommodate even higher carotenoid levels without interfering with other cell functions. To do this, we used the N-terminal 178 aa sequence of the *Arabidopsis* HMGR1S isoform. This sequence (named 1S) lacks any catalytic activity, but it includes transmembrane domains for ER membrane anchoring and is sufficient to stimulate a massive proliferation of ER-derived membranes and vesicular

Figure 4 Extrastidial carotenoids are produced at levels similar to those naturally found in chloroplasts. *N. benthamiana* leaf areas agroinfiltrated with different combinations of constructs were collected at 5 dpi for HPLC analysis. (a) HPLC chromatograms of HE, HEB and HEBI samples at 280 nm (to detect phytoene) and 470 nm (to detect coloured carotenoids). The non-plant carotenoid canthaxanthin is used as an internal standard. (b) Levels of carotenoids in leaf areas agroinfiltrated with the indicated combinations. (c) Levels of phytoene and lycopene in leaf areas expressing untagged enzymes (+) or versions with N-terminal GFP or 1S sequences. (d) Levels of phytoene and lycopene in HEBI leaf areas either co-infiltrated or not with a set of three more proteins promoting lipid body formation (indicated as + OWD). Levels are expressed relative to those without OWD. In all cases, plots represent the mean and standard error of $n \geq 3$ independent samples.



structures (Ferrero *et al.*, 2015). Indeed, N-terminal fusion of the 1S sequence to GFP resulted in the localization of the resulting 1S-GFP protein in highly fluorescent bodies corresponding to these proliferating structures (Figure 2). A very similar distribution was observed for 1S-crtE-GFP. In the case of the 1S-crtB-GFP and 1S-crtI-GFP fusions, however, the fluorescent bodies were not observed and the proteins localized only in ER membranes (Figure 2).

The combination tHMGR, 1S-crtE and 1S-crtB (HE₁B₁) produced 0.06 mg of phytoene per g of DW (or 60 µg/g DW), which is about 15-fold lower than that produced by the HEB samples (Figure 4c) but fivefold higher than that produced by crtE and 1S-crtB (Figure 3b). These results suggest that the addition of the 1S domain to crtB or crtE does not block their enzymatic activity, but rather inhibits correct use of the extra MVA-derived precursors that result from tHMGR activity. Consistent with this interpretation, when tHMGR and 1S-fused crtE, crtB and crtI enzymes were used (HE₁B₁ combination), the production of lycopene showed a dramatic drop (Figure 4c). By using only one of the three bacterial enzymes fused to 1S, however, different effects were observed. The use of 1S-crtE did not have a significant impact compared to crtE, but a reduction occurred when crtI was substituted with 1S-crtI, and a major inhibition resulted from using 1S-crtB in place of GFP-crtB (Figure 4c).

As an alternative strategy to improve carotenoid storage in extrastidial compartments, we next stimulated the proliferation of oleosin-coated lipid bodies. The strategy, based on the agroinfiltration of sequences encoding oleosins, diacylglycerol acyltransferase, and the transcription factor WRINKL1, has recently been reported as contributing successfully to the storage of lipophilic MVA-derived sesquiterpenes (Figure 1a) in *N. benthamiana* leaves (Delatte *et al.*, 2018). Addition of the plasmids encoding these proteins to the HEBI mix, however, was detrimental to lycopene accumulation and neutral for phytoene (Figure 4d).

Extrastidial phytoene and lycopene accumulation eventually reduce chlorophyll contents and photosynthetic activity

The massive levels of lycopene that accumulated in *N. benthamiana* leaves agroinfiltrated with HEBI constructs resulted in a characteristic red colour in the sectors that produced the pigment (Figure 5). By contrast, HEB areas producing only phytoene were visually indistinguishable from agroinfiltrated control HE areas, as expected due to the colourless nature of phytoene (Figure 5a). At the cell level, tubular structures of distinctive red colour were observed inside HEBI cells (Figure 5b), suggesting that they might correspond to lycopene crystals. The red colour of lycopene-accumulating areas was stable for about a week and then it gradually faded. Leaf pigmentation actually paralleled the accumulation profile of lycopene, which steadily increased to 5 dpi, and then remained high for at least two more days (Figure 5c). Interestingly, the levels of endogenous (i.e. chloroplastidial) carotenoids in HEBI leaves remained unchanged, whereas chlorophyll levels started to decrease at 5 dpi and by 7 dpi they had dropped about 20% (Figure 5c). Phytoene production in *N. benthamiana* leaves agroinfiltrated with HEB constructs appeared to be still active at 7 dpi (Figure 5c). Similar to lycopene-producing HEBI leaf tissues, HEB areas accumulating cytosolic phytoene showed a decrease in chlorophyll levels and no changes in chloroplast-associated carotenoids. In this case, however, the reduction in chlorophyll contents occurred later (at 7 dpi) and to a

lower degree (10%) compared to lycopene-producing HEBI leaf tissues (Figure 5c). No changes in carotenoid or chlorophyll levels were observed in control HE leaves (Figure 5c), suggesting that the decrease in chlorophyll levels observed in leaves producing phytoene and lycopene is not due to the agroinfiltration procedure but to the accumulation of those carotenoids outside chloroplasts. Analysis of chloroplast ultrastructure by transmission electron microscopy (TEM) of leaf cells at 7 dpi showed a higher abundance of plastoglobules in HEB chloroplasts compared to HE controls (Figure 5d). The development of plastoglobules was more evident in HEBI chloroplasts, which also showed a decreased abundance of thylakoid membranes and grana (Figure 5d).

To check whether the changes in leaf chlorophyll levels and chloroplast ultrastructure caused by extrastidial accumulation of phytoene and lycopene had any impact on photosynthesis, we next quantified effective quantum yield of photosystem II (ϕPSII) at different time points after agroinfiltration with HE, HEB or HEBI combinations (Figure 5e). Phytoene-producing HEB leaves only showed a statistically significant decrease in the ϕPSII value at 7 dpi, whereas HEBI tissues producing lycopene showed a stronger reduction even at earlier time points (Figure 5e). While our results demonstrate that leaf cells remain photosynthetically active despite accumulating phytoene and lycopene at levels similar to those of photosynthesis-related chloroplast carotenoids (i.e. lutein, β-carotene, violaxanthin and neoxanthin), they also show that chloroplast features are altered by the accumulation of phytoene and, particularly, lycopene in extrastidial locations.

Phytoene shows improved bioaccessibility when accumulated outside plastids

Phytoene is a health-promoting carotenoid naturally found in some non-green fruits and vegetables such as tomatoes but normally absent from leaves (Melendez-Martinez *et al.*, 2015; Melendez-Martinez *et al.*, 2018). The accumulation of phytoene in HEB leaves reached levels of ca. 1 mg/g DW, similar or even higher than those found in ripe tomatoes (D'Andrea *et al.*, 2018; Dretto *et al.*, 2020; Flores *et al.*, 2016; Massaretto *et al.*, 2018; Nogueira *et al.*, 2013; Pankratov *et al.*, 2016; Suzuki *et al.*, 2015). However, it was unknown whether the subcellular localization of phytoene might impact its bioaccessibility (i.e. the quantity released from the plant matrix in the gastrointestinal tract that becomes available for absorption and eventual biological activity). To address this question, we compared bioaccessibility of extrastidial phytoene from agroinfiltrated HEB leaves and plastidial phytoene from non-infiltrated leaves treated with norflurazon (NF), an inhibitor of phytoene desaturation (Figure 1a). *N. benthamiana* leaves were infiltrated either with *A. tumefaciens* cultures carrying the HEB constructs or with NF and collected 5 days later. Non-infiltrated leaves were also collected as a control, and tissue from all samples was freeze-dried and ground to a fine powder that was used for both HPLC and *in vitro* digestion assays (Figure 6). HPLC analysis of the samples showed that the NF treatment resulted in the accumulation of some phytoene and only caused a slight reduction in the levels of downstream carotenoids compared to control leaves (Figure 6a). The levels of phytoene in HEB leaf samples were much higher than those in NF-treated samples, whereas the amount of chloroplast carotenoids remained unchanged compared to control leaves (Figure 6a). To facilitate bioaccessibility comparisons, we mixed 1 volume of lyophilized HEB tissue with 5 volumes of

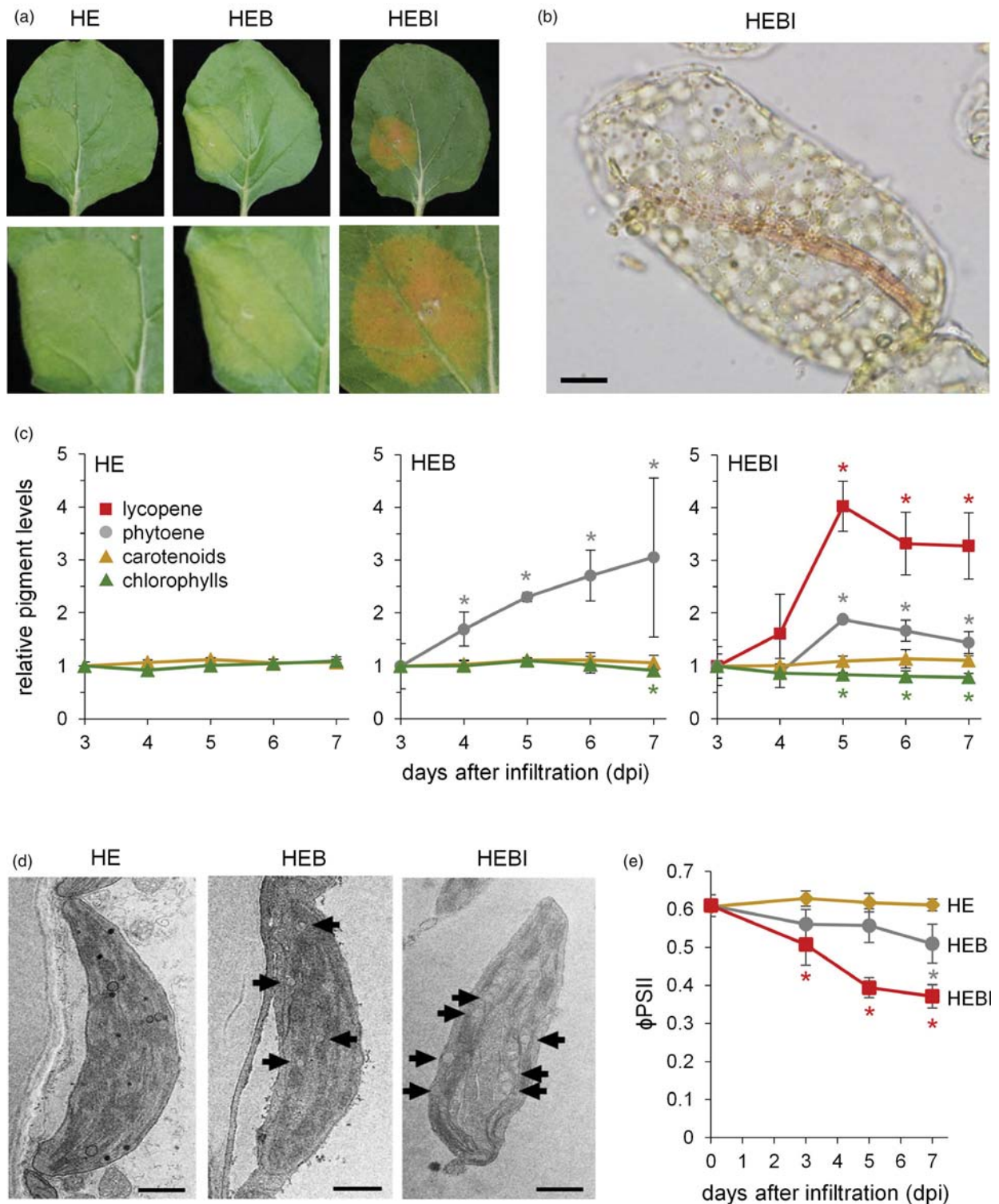


Figure 5 Accumulation of extraplasmidial phytoene and lycopene indirectly impacts photosynthesis. (a) Representative pictures of *N. benthamiana* leaves agroinfiltrated in their lower left-hand side with constructs to express HE, HEB and HEBI combinations. The lower panels show a magnification of the agroinfiltrated areas. (b) Picture of a leaf cell from a HEBI-infiltrated area. Note the distinctive red tubular structure within the cell, likely to be a large lycopene crystal. Scale bar is 10 μm . (c) Photosynthetic pigment levels in HE, HEB and HEBI leaf areas at the indicated times after agroinfiltration. Carotenoid contents refer to endogenous (i.e. chloroplastic) species, excluding phytoene and lycopene. Values are the mean and standard error of $n \geq 3$ independent samples relative to levels at 3 dpi. Asterisks mark statistically significant changes (*t*-test, $P < 0.05$) relative to 3 dpi. (d) TEM images of representative chloroplasts from leaf areas like those shown in (a) at 7 dpi. Arrows mark plastoglobules in HEB and HEBI chloroplasts. Scale bars are 1 μm . (e) Effective quantum yield of PSII (ϕPSII) in leaf sections agroinfiltrated with the indicated combinations. Plots represent the mean and standard error of $n \geq 3$ independent samples. Asterisks mark statistically significant changes (*t*-test, $P < 0.05$) relative to 0 dpi.

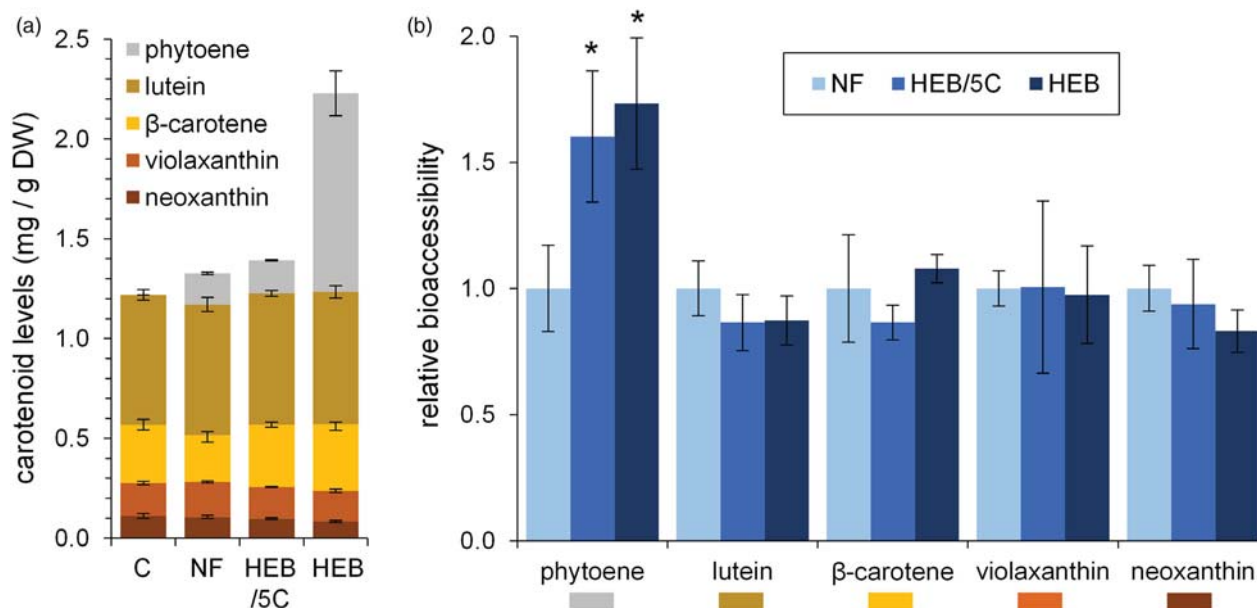


Figure 6 Bioaccessibility of phytoene changes depending on its subcellular accumulation site. *N. benthamiana* leaves were agroinfiltrated with HEB constructs to produce extraplasmidial phytoene or treated with norflurazon (NF) to accumulate phytoene inside chloroplasts and collected 5 days later. Non-infiltrated, untreated leaves were collected at the same time as a control (sample C). Freeze-dried tissue from these leaf samples was ground and used for both for HPLC and bioaccessibility analysis. A sample combining one part of HEB and five parts of C ground tissue (named HEB/5C) was also used for experiments. (a) HPLC analysis of carotenoids in the indicated samples. (b) Bioaccessibility of the carotenoids shown in (a). Values correspond to the mean and standard error of $n = 3$ independent samples per treatment represented relative to those of NF-treated leaves. Asterisks mark statistically significant changes relative to NF-treated samples (t -test, $P < 0.05$).

control tissue to create a new sample (named HEB/5C) with levels of extraplasmidial phytoene similar to the plastidial phytoene contents of NF samples (Figure 6a). Then, a standardized *in vitro* method that simulates digestion was used to estimate the bioaccessibility of phytoene in leaves when accumulated either inside or outside plastids (NF-treated leaves or HEB and HEB/5C samples, respectively). Using this *in vitro* method, which reproduces physiological conditions *in vivo* by using specific digestive enzymes under conditions mimicking oral, gastric and small intestinal digestion phases, bioaccessibility of phytoene was found to be 60–70% higher in HEB and HEB/5C samples compared to NF-treated leaves (Figure 6b). By contrast, bioaccessibility of the endogenous (chloroplast) carotenoids was similar in all the samples (Figure 6b). The results support the conclusion that extraplasmidial accumulation improves phytoene bioaccessibility.

Cytosolic lycopene crystals in leaves are similar to those present in tomato fruit chromoplasts and contribute to increase antioxidant capacity

Like phytoene, lycopene is associated with health benefits but its bioaccessibility is much lower in part because lycopene-rich products such as a ripe tomato fruits accumulate this carotenoid as intraplasmidial crystals (Cooperstone *et al.*, 2015; Mapelli-Brahm *et al.*, 2018). To test whether the tubular structures that were visible in HEBI cells (Figure 5b) correspond to lycopene crystalloids, we initially recorded the absorption spectra of *N. benthamiana* HE, HEB and HEBI leaves and then calculated the difference spectra for HEB-minus-HE and HEBI-minus-HE (Figure 7a). The HEBI-HE difference spectrum exhibited two peaks in the carotenoid region at 528 and 568 nm, that were absent in

the HEB-HE spectrum. This indicates the presence of a new carotenoid species absorbing in this region in HEBI. The peaks are coincident with the 0-1 and 0-0 vibronic transitions, respectively, reported for lycopene crystalloids in tomatoes (Ishigaki *et al.*, 2017; Llansola-Portoles *et al.*, 2018). To analyse the features of the HEBI lycopene crystals further, we turned to resonance Raman spectroscopy, a technique that provides rich information about the vibrational properties of carotenoids. The vibrational modes in the ν_7 region, around 1520 cm^{-1} , arise from stretching vibrations of the double bonds of the linear carotenoid skeleton (Koyama and Fujii, 1999; Robert, 1999). Resonance Raman spectra at 77 K upon 514.5 and 577 nm excitation were recorded for HEBI and control HE leaves, and compared with that of ripe tomatoes (Figure 7b). At 514.5 nm, both HE and HEBI leaves exhibit a wide ν_7 mode but with somewhat shifted maxima – 1525.8 cm^{-1} in HE and 1523.8 cm^{-1} in HEBI. An even lower frequency is observed in the case of ripe tomato fruit (peak at 1521.5 cm^{-1} ; Figure 7b), as previously described (Llansola-Portoles *et al.*, 2018). HE samples excited at 577 nm exhibited a wide vibrational mode, peaking at the same frequency as at 514.5 nm (1525.8 cm^{-1}). In contrast, the ν_7 mode for HEBI at 577 nm is significantly narrower and down-shifted to 1513.1 cm^{-1} , overlapping with the spectrum of tomatoes at this wavelength (Figure 7b). Note that the signals recorded in leaves for 577 nm excitation are very noisy, as they overlap with the blue tail of the large chlorophyll fluorescence signal. Taken together, these data indicate that HEBI leaves exhibit contributions both from chloroplast carotenoids and from a new red-absorbing species. This red-shifted carotenoid dominates the spectrum at 577 nm, as it is in pre-resonance with its 0-0 absorption transition at 568 nm (see above) giving a narrow ν_7 contribution at 1513.1 cm^{-1} , as

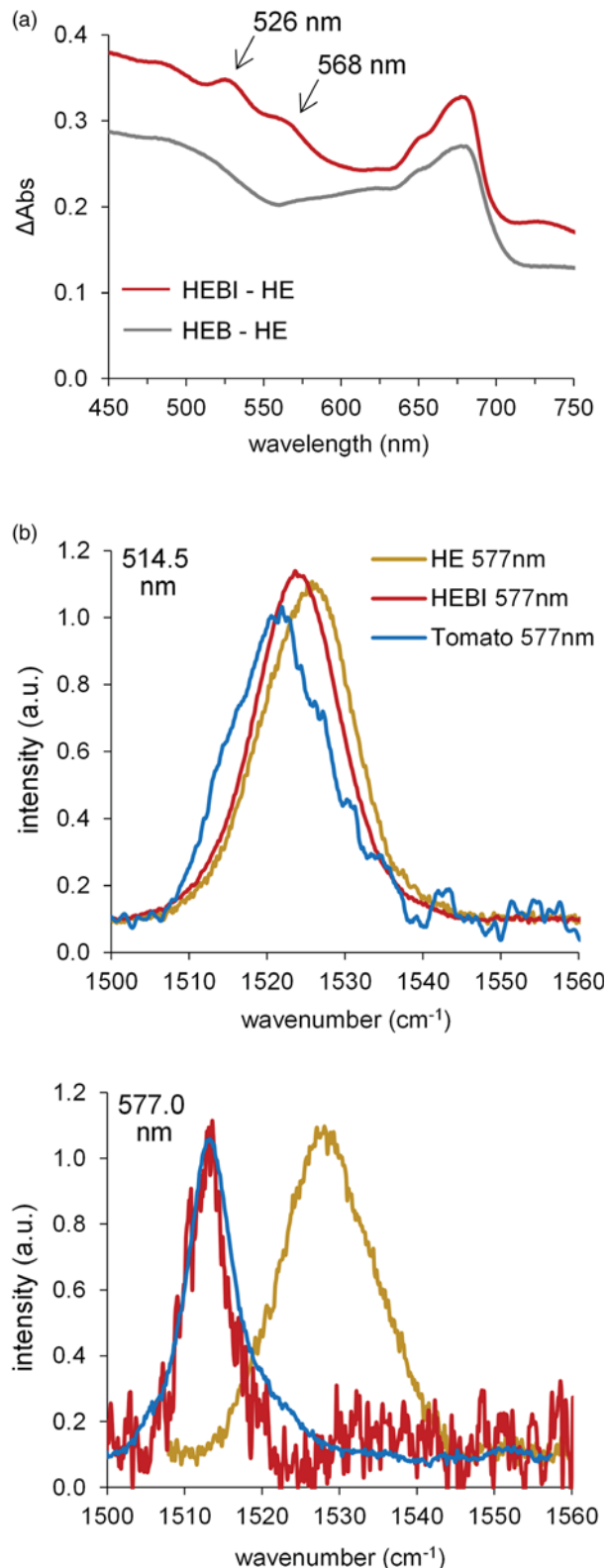


Figure 7 Lycopene crystalloids in HEBI leaves are similar to those in tomato fruit chromoplasts. (a) Absorption difference spectra of *N. benthamiana* leaves (HEB and HEBI-minus-HE) obtained at room temperature in reflectance mode. (b) 77 K resonance Raman spectra in the ν_7 region for *N. benthamiana* HE and HEBI leaves and red (ripe) tomato fruit at 514.5 and 577 nm excitation.

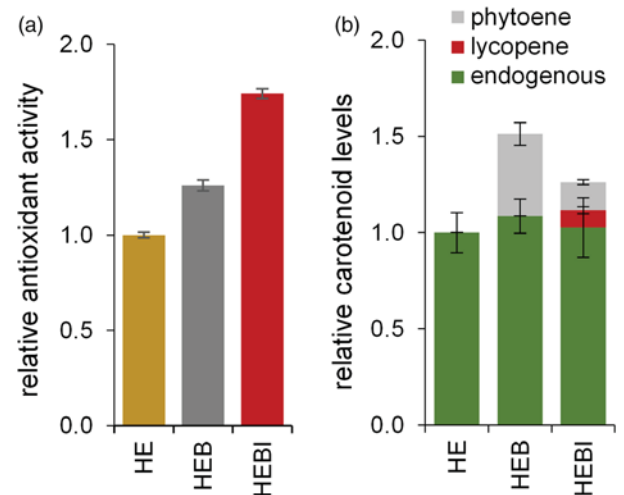


Figure 8 Cytosolic production of phytoene and lycopene contribute to biofortification. (a) Antioxidant capacity of *N. benthamiana* HE, HEB and HEBI leaves. Values correspond to the mean and standard error of $n = 3$ independent samples represented relative to those of control (HE) leaves. (b) Levels of carotenoids in lettuce leaves agroinfiltrated with the indicated combinations of constructs. Mean and standard error of $n \geq 4$ independent samples are represented relative to those in HE leaves.

observed in tomatoes. A mixture of both carotenoid populations (new red species and chloroplast carotenoids) is observed when exciting HEBI at 514.5 nm, as this wavelength is midway between the newly observed 0-1 band (528 nm) and the 0-0 transitions of photosynthetic carotenoids (~ 500 nm and below). In this case, ν_7 exhibits a frequency intermediate between 1513.1 cm^{-1} (red species) and 1525.8 cm^{-1} (chloroplast carotenoids; see HEB at this wavelength). The marked similarity between the extraplastidial lycopene crystals formed in HEBI leaves and the lycopene crystalloids naturally present in ripe tomatoes, in terms of their vibrational and electronic properties, indicates a very similar organization and aggregation state in both cases.

Lycopene is a major contributor to the antioxidant properties of carotenoid-containing foods (Müller *et al.*, 2011). In agreement, the accumulation of lycopene in HEBI leaves resulted in an astounding 80% increase in antioxidant activity of the leaf tissue as determined using the Trolox equivalent antioxidant capacity (TEAC) test (Figure 8a). Also consistent with the much lower antioxidant capacity of phytoene (Müller *et al.*, 2011), the TEAC value of phytoene-producing HEB leaves was only 30% higher than that of HE controls (Figure 8a).

Cytosolic carotenoid production in edible lettuce leaves

Our strategy of engineering a synthetic cytosolic pathway to boost carotenoid levels in green (i.e. chloroplast-containing) tissues could be readily applied to the biofortification of edible leafy vegetables. As a proof of concept, we tested whether agroinfiltration could also work to transiently express the required genes in romaine lettuce (*Lactuca sativa*), a widely consumed and inexpensive salad vegetable with a relatively low nutritional value (Mou, 2009). Lettuce leaves were found to be more difficult to agroinfiltrate than those of *N. benthamiana*, but vacuum agroinfiltration was successful in transiently expressing HEB and HEBI combinations leading to extraplastidial phytoene and/or lycopene overproduction in some leaf areas (Figure 8b). The levels of total

carotenoids (i.e. extraplasmidial and chloroplastic) were clearly enhanced in agroinfiltrated areas, although the accumulation of phytoene and/or lycopene was lower than that achieved in *N. benthamiana*.

Discussion

In this paper, we show that carotenoids can be produced and accumulated in very high amounts for over a week in the cytosol of leaf cells. We demonstrate major improvements compared to our first attempts in *N. tabacum* using viral vectors carrying untagged crtE, crtB and crtI enzymes (Majer *et al.*, 2017). First, agroinfiltration of *N. benthamiana* leaves was found to be a much faster and reliable method to test enzyme combinations with minimal interference from chlorosis and necrosis. Second, using the GFP-crtB protein ensured cytosolic localization of the phytoene-producing crtB enzyme (Llorente *et al.*, 2020). Third, adding a deregulated version of the HMGR enzyme (tHMGR) boosted cytosolic GGPP supply to reach much higher phytoene and lycopene levels than those achieved in our previous work. Fourth, extraplasmidial carotenoid levels remained high for much longer than when using viral vectors. And fifth, we showed that the accumulation of these extraplasmidial carotenoids provides nutritional benefits that can be transferred to leafy vegetables such as lettuce, hence demonstrating the feasibility of using this strategy for food biofortification.

Rapid testing of different gene combinations by agroinfiltration led to establish that a major limiting step for carotenoid biosynthesis outside plastids was the supply of their metabolic precursors (Figure 3). To enhance the production of these precursors, we used a truncated form of HMGR, considered to be the main rate-determining enzyme of the MVA pathway (Rodríguez-Concepción and Boronat, 2015). This truncated form (tHMGR) retains the cytosolic domain bearing its catalytic activity but lacks the N-terminal 1S region required to anchor the enzyme to the ER (Figure 1). As the N-terminal region is also key for the regulation of HMGR enzyme levels and activity, the tHMGR protein is a deregulated and more stable version of the enzyme (Doblas *et al.*, 2013; Leivar *et al.*, 2011; Pollier *et al.*, 2013; Rodríguez-Concepción and Boronat, 2015). The use of tHMGR enzymes has already been shown to increase the production of MVA-derived isoprenoids such as sesquiterpenes and sterols (Figure 1) (Andersen *et al.*, 2017; Cankar *et al.*, 2015; Chappell *et al.*, 1995; Harker *et al.*, 2003; van Herpen *et al.*, 2010; Lee *et al.*, 2019; Wu *et al.*, 2006; Yin and Wong, 2019). The highest increases have been typically obtained in transient expression assays with *N. benthamiana* leaves similar to those used in our work. In particular, addition of *Arabidopsis* tHMGR to agroinfiltrated gene combinations caused a 37-fold increase in endogenous sesquiterpenes levels (Cankar *et al.*, 2015) and boosted the production of exogenous sesquiterpenes (i.e. those not naturally found in *N. benthamiana*) up to 300-fold (van Herpen *et al.*, 2010). The ca. 100-fold increase in phytoene levels observed after incorporating tHMGR with the combination of GFP-crtB and crtE (i.e. HEB vs. EB; Figures 3b and 4b) falls within the same range.

Unlike sesquiterpenoids, carotenoids such as phytoene and lycopene are not naturally produced in the cytosol of plant cells. We therefore reasoned that the levels of carotenoids accumulated outside plastids could be further increased by improving the capacity of leaf cells to sequester and store these lipophilic isoprenoids through the development of ER-derived membrane systems and lipid bodies. Fusion of the 1S domain of the

Arabidopsis HMGR1S isoform to crtE successfully targeted the resulting enzyme to the ER, and also stimulated a massive development of ER-derived membranes and vesicular structures similar to those observed with the 1S-GFP protein (Figure 2) (Ferrero *et al.*, 2015). In the case of crtB and crtI, however, the proteins 1S-crtB-GFP and 1S-crtI-GFP were targeted to the ER membranes but did not stimulate the proliferation of fluorescent bodies (Figure 2), perhaps because they were produced at lower levels than the 1S-crtE-GFP fusion. Consistently, the number of cells showing detectable GFP fluorescence was much lower in leaf areas agroinfiltrated with 1S-crtB-GFP or 1S-crtI-GFP compared to those agroinfiltrated with 1S-crtE-GFP or 1S-GFP. In addition, the fusion to 1S did not have a substantial impact on crtE activity (i.e. in the production of GGPP) but it dramatically prevented the conversion of GGPP into phytoene and had a negative impact on the synthesis of lycopene from phytoene (Figure 4c). It is possible that cytosolic (i.e. soluble) GFP-crtB and crtI enzymes could associate for efficient channelling of GGPP provided by either soluble or membrane-bound crtE to lycopene, which would then be released to form crystals. Indeed, it has been suggested that these bacterial enzymes might interact to form a multiprotein complex and/or create a microenvironment to function as a metabolon for efficient substrate channelling when produced inside plastids (Nogueira *et al.*, 2013; Ravanello *et al.*, 2003). ER-membrane association might prevent such direct interaction of the enzymes, negatively impacting lycopene production. The observation that ER-targeting of crtB results in a dramatic block of phytoene production in samples containing soluble tHMGR (Figure 4c) but not in those harbouring only the endogenous ER-anchored HMGR enzymes (Figure 3b) further supports the conclusion that high phytoene (and lycopene) titres require a completely soluble synthetic pathway for efficient metabolite channelling.

Another remarkable observation of our work was that proliferation of ER-derived membrane structures (e.g. in leaf areas expressing 1S-crtE) or lipid bodies did not provide an advantage for the accumulation of extraplasmidial carotenoids (Figure 4). This might not be so surprising in the case of lycopene, which was later found to form cytosolic crystals (Figure 7). It is likely, however, that lycopene produced in HEBI leaves is initially stored in association with cell membranes before reaching a concentration high enough to crystallize. In the case of phytoene, fruits that produce high amounts of this carotenoid store it in lipophilic vesicles inside chromoplasts that are sometimes released into the cytosol, probably to remove excess amounts accumulated in plastidial membranes (Lado *et al.*, 2015; Nogueira *et al.*, 2013). Whether the massive amounts of phytoene produced in HEB and HEBI cells are sequestered in cell membrane systems other than those derived from the ER (e.g. vacuoles or plasma membrane) remains unknown. However, the observation that the bioaccessibility of phytoene produced in HEB leaves is significantly higher than that accumulated in the plastids of NF-treated leaves (Figure 6b) suggests that phytoene might be less tightly associated to membranes when produced and stored at extraplasmidial locations.

Regardless of the storage mechanism, the accumulation of extraplasmidial carotenoids in our system achieved levels comparable to those of endogenous chloroplast carotenoids and, significantly, these levels remained high for over a week. This represents a dramatic increase in stability relative to our previous results using viral vectors, when lycopene levels dropped soon after the leaves exhibited a red colour (Majer *et al.*, 2017). It is

possible that crystallization of lycopene in HEBI leaves after reaching levels similar to those found in tomato fruit chromoplasts could contribute to its higher stability, as crystals are metabolically and osmotically inert and probably less prone to oxidative or enzymatic degradation. Nevertheless, the formation of cytosolic lycopene crystals in HEBI cells and the accumulation of similarly high levels of phytoene in HEB cells had a negative effect on cell fitness. Indeed, several signs of cell damage, including chlorosis and eventual necrosis, developed about a week after agroinfiltration in HEB and HEBI leaves. The reduction in chlorophyll levels, the increased number of chloroplast plastoglobules, the decreased abundance of thylakoids and grana, and the defects in photosynthetic activity detected in these leaves (Figure 5) strongly suggest that extraplastidial accumulation of lycopene and, to a lesser extent, phytoene triggered a leaf senescence process. Indeed, the earliest changes associated with leaf senescence occur in the chloroplast and cause chlorosis before necrotic symptoms are observed (Tamary et al., 2019). It seems likely that these deleterious, senescence-like effects observed in HEB and HEBI leaves might be related to cell damage caused by the disruption of normal cell compartments, functions and/or metabolism upon accumulation of extraplastidial isoprenoids. Alternatively, signals derived from the cleavage of cytosolic phytoene, lycopene or intermediate carotenoid species might be transduced to regulate chloroplast structure and function, including photosynthetic activity (Avendano-Vazquez et al., 2014; Cazzonelli et al., 2020).

Very little attention has been paid to carotenoid biofortification of green vegetables to date, in part because of the challenges associated with changing the balance between carotenoids and chlorophylls (Alos et al., 2016; Domonkos et al., 2013; Esteban et al., 2015; Hashimoto et al., 2016; Zheng et al., 2020). Nonetheless, recent reports have shown that *N. benthamiana* leaves overexpressing regulators of carotenoid gene expression and storage were able to double their carotenoid content in chloroplasts (Ampomah-Dwamena et al., 2019; D'Amelia et al., 2019; Llorente et al., 2020; Wang et al., 2018). Here we report a similar twofold increase in total carotenoid levels in *N. benthamiana* leaves (Figure 4b). Despite the defects on cell function described above, our system for cytosolic production of carotenoids offers multiple advantages over those modifying the plastidial carotenoid content. Firstly, the composition of chloroplast carotenoids remains unchanged in our system (Figure 5c) and therefore their photosynthetic and photoprotective functions are not directly impacted. Although a likely secondary cell damage-associated effect does cause photosynthesis to slow down (Figure 5e), it is not blocked and can therefore continue to support plant growth while the extraplastidial carotenoids are produced and stored. Secondly, our system separates the carotenoid intermediates from those plastidial enzymes that convert them into downstream products or degrade them into cleavage products, including apocarotenoid signals (Rodríguez-Concepcion et al., 2018). While non-enzymatic degradation could still occur, it does not appear to be a problem to achieve high titres of extraplastidial carotenoids in our system. Together with the unexpected capacity of leaf cells to accumulate carotenoids outside chloroplasts, this resulted in levels of phytoene and lycopene up to 1 mg/g DW, in the range of those found in chromoplasts from natural sources such as ripe tomato fruit (D'Andrea et al., 2018; Diretto et al., 2020; Flores et al., 2016; Massaretto et al., 2018; Nogueira et al., 2013; Pankratov et al., 2016; Suzuki et al., 2015). Thirdly, the system is very

flexible, and the incorporation of additional enzymes catalysing downstream steps is feasible so that a much broader variety of carotenoids could be produced (Nogueira et al., 2019). Finally, we demonstrate that this system can be adapted to the bioengineering of leafy vegetables such as lettuce, improving their antioxidant capacity, bioaccessibility and overall nutritional quality.

N. benthamiana is particularly well suited to produce high titres of valuable enzymes and metabolites for molecular pharming due to a fast growth rate and a natural ability to express heterologous gene sequences, among other traits (Lomonosoff and D'Aoust, 2016). While agroinfiltration assays can be scaled up for industrial production of carotenoids and other metabolites in *N. benthamiana*, adaptation to crops such as lettuce for human or animal consumption should require further efforts in the development and optimization of safe and reliable transient expression methods with no health risks. Stable expression of transgenes appears as a valid alternative from the technical point of view. However, the poor consumer acceptance of transgenesis has turned the attention to genome editing. New varieties of leafy food (e.g. lettuce, spinach, cabbage, kale, chard) and forage crops (e.g. alfalfa, grasses) could be generated by editing endogenous genes to overaccumulate carotenoids in extraplastidial locations. Flux-controlling enzymes involved in isoprenoid biosynthesis (including HMGR, GGPP synthase and phytoene synthase) are encoded by small gene families in most plants. In the case of GGPP synthase, cytosolic isoforms are naturally present (Ruiz-Sola et al., 2016). For the rest, CRISPR-Cas9 technology could be used to remove the N-terminal region from non-essential and/or tissue-specific isoforms of HMGR (to create truncated forms similar to the tHMGR version used here) and carotenoid biosynthetic enzymes such as phytoene synthase (to remove the plastid transit peptide and create a cytosolic version). Furthermore, our results open the door to the biofortification of leafy vegetables with other health-promoting isoprenoids such as tocopherols (vitamin E), phylloquinones (vitamin K1) and plastoquinone by engineering extraplastidial biosynthetic pathways using MVA-derived precursors.

Methods

Plant material, growth conditions and treatments

Nicotiana benthamiana RDR6i, tomato (*Solanum lycopersicum*) MicroTom and lettuce (*Lactuca sativa*) Romaine plants were grown in a greenhouse under standard long-day conditions as described (D'Andrea et al., 2018; Llorente et al., 2016; Majer et al., 2017). For *N. benthamiana* agroinfiltration, the second or third youngest leaves of 4-5-week-old plants were infiltrated with LB-grown cultures of *Agrobacterium tumefaciens* strain GV3101 cells transformed with the plasmids of interest as described (Sparkes et al., 2006). Cultures were typically used at an optical density at 600 nm of 1 and mixed in identical proportions for the various combinations. Gene silencing was prevented by co-agroinfiltration with the *A. tumefaciens* strain EHA101 carrying the helper component protease (HCPro) of the watermelon mosaic virus (WMV) in plasmid pGWB702-HCProWMV (the kind gift of Juan José López-Moya and Maria Luisa Domingo-Calap). For pharmacological treatments, stock solutions of mevinolin (MEV), fosmidomycin (FSM) and norflurazon (NF) prepared as described (Llamas et al., 2017; Perello et al., 2014) were diluted in water and 0.05 % Tween 20 right to final concentrations of 10 μ M MEV, 200 μ M FSM and 20 μ M NF. Working solutions were

then infiltrated with a syringe. Infiltration of MEV and FSM was carried out in leaf areas that had been agroinfiltrated with different constructs 24 h earlier. Agroinfiltration of lettuce was performed by vacuum as described (Yamamoto *et al.*, 2018).

Constructs

A truncated version of *Arabidopsis thaliana* HMGR1 (At1g76490) missing the N-terminal 164 aa, referred to as tHMGR (Cankar *et al.*, 2015), was cloned into a pEAQ-USER version of the pEAQ-HT vector kindly provided by George Lomonosoff (Luo *et al.*, 2016; Peyret and Lomonosoff, 2013). Full-length sequences encoding *Pantoea ananatis* crtE, crtB and crtI enzymes were amplified by PCR from plasmid pACCRT-E1B and cloned using the Gateway system into plasmid pDONR207 as described (Majer *et al.*, 2017). Plasmid pGWB506 was used to generate construct 35S:GFP-crtB and plasmid pGWB405 to generate constructs 35S:crtE, 35S:crtE-GFP, 35S:crtB, 35S:crtB-GFP, 35S:crtI and 35S:crtI-GFP (Majer *et al.*, 2017; Nakagawa *et al.*, 2007). Some of these constructs were later used to generate 15-tagged versions by fusing the sequence encoding the first 178 aa residues of the *A. thaliana* HMGR1S isoform to the N-terminal region of the crtE, crtB or crtI enzymes using overlap extension PCR. Plasmid pCA-TXS-His (Besumbes *et al.*, 2004) was used for the expression of a yew (*Taxus baccata*) sequence encoding TXS. Constructs to stimulate lipid body formation (Delatte *et al.*, 2018) were kindly provided by Maria Coca and Tarik Ruiz.

Microscopy

Subcellular localization of GFP-tagged proteins was observed by direct examination of agroinfiltrated leaf tissue at 3 dpi with a Leica TCS SP5 Confocal Laser Scanning Microscope. GFP fluorescence was detected using a BP515-525 filter after excitation at 488 nm, whereas chlorophyll autofluorescence was detected using a LP590 filter after excitation at 568 nm. For light microscopy, leaves were cut into small pieces and cells were separated as described (Lu *et al.*, 2017). Transmission electron microscopy (TEM) of agroinfiltrated leaf areas was performed as described (D'Andrea *et al.*, 2018).

HPLC analysis of pigments

Leaf areas of interest were harvested, snap-frozen in liquid nitrogen and lyophilized until they were completely dry. Approximately 4 mg of this freeze-dried tissue (corresponding to samples from different leaves pooled together) was mixed with 375 μ L of methanol and 25 μ L of a 10 % (w/v) solution of canthaxanthin (Sigma) in chloroform. Extraction and separation of chlorophylls and carotenoids were then performed as described (Emiliani *et al.*, 2018). Eluting compounds were monitored using a photodiode array detector. Peak areas of chlorophylls at 650 nm and carotenoids at 470 nm (lycopene, lutein, β -carotene, violaxanthin, neoxanthin, canthaxanthin) or 280 nm (phytoene) were determined using the Agilent ChemStation software. Quantification was performed by comparison with commercial standards (Sigma).

UV-Vis absorption and resonance Raman

Absorption spectra were measured using a CARY5000 UV/Vis/NIR spectrophotometer (Agilent). Because the analysed tissues were not transparent, we used an integration sphere in reflectance mode, transforming into absorbance using the Kubelka – Munk function (Nobbs, 1985). Resonance Raman spectra were recorded at room temperature and 77 K, the latter with an LN2-flow

cryostat (Air Liquide). Laser excitations at 488, 501.7 and 514.5 nm were obtained with an Ar + Sabre laser (Coherent), and at 577 nm with a Genesis CX STM laser (Coherent). Output laser powers of 10–100 mW were attenuated to <5 mW at the sample. Scattered light was focused into a Jobin-Yvon U1000 double-grating spectrometer (1800 grooves/mm gratings) equipped with a red-sensitive, back-illuminated, LN2-cooled CCD camera. Sample stability and integrity were assessed based on the similarity between the first and last Raman spectra.

Photosynthetic measurements

Photosynthetic efficiencies were assessed by measuring chlorophyll *a* fluorescence with a MAXI-PAM fluorimeter (Heinz Walz GmbH). Photosynthetic parameters were evaluated at 0, 3, 5 and 7 dpi in plants that were previously kept in darkness for at least 30 min to fully open and relax PSII reaction centres. Effective quantum yield of PSII (Φ PSII) was measured as $(F_m' - F_s)/F_m'$, where F_m' and F_s are the maximum and minimum fluorescence of light-exposed plants, respectively. The chosen light intensity was 21 PAR (AL = 2). Average values were calculated from three biological replicates with three different leaf areas for each replicate.

Antioxidant capacity

Carotenoid extracts prepared as described above were diluted in 400 μ L of diethyl ether and saponified by adding 100 μ L of 10% (w/v) KOH in methanol to avoid interference from chlorophylls. Samples were left shaking for 30 min at 4 °C and then diluted with 400 μ L of milliQ water before centrifugation for 5 min at 13 000 rpm and 4 °C. The upper phase was collected, dried in a SpeedVac and resuspended in 200 μ L of acetone. Total antioxidant capacity of the mixture was carried out as described (Re *et al.*, 1999).

Bioaccessibility assays

N. benthamiana leaves were either agroinfiltrated with constructs encoding tHMGR, crtE and GFP-crtB (HEB) to produce extrastidial phytoene or syringe-infiltrated with a 20 μ M NF solution in water and 0.05 % Tween 20 to accumulate plastidial phytoene by preventing its conversion into downstream carotenoids. Samples from several HEB and NF-treated leaves were collected 5 days after infiltration; non-infiltrated leaves were also collected as controls. Bioaccessibility assays were carried out as described (Estevez-Santiago *et al.*, 2016) using lyophilized tissue samples.

Statistical analyses

Student's *t*-tests were used for statistical analyses using Prism 5.0a (GraphPad) and Office Excel 2010 (Microsoft).

Acknowledgments

We greatly thank Juan José López-Moya, Maria Luisa Domingo-Calap, George Lomonosoff, Maria Coca and Tarik Ruiz for the gift of plasmids, and Christophe Humbert for his help measuring diffuse absorption spectra. This work was funded by the European Regional Development Fund (FEDER) and the Spanish Agencia Estatal de Investigación (grants BIO2017-84041-P and, BIO2017-90877-REDT), Generalitat de Catalunya (2017SGR-710), and European Union's Horizon 2020 (EU-H2020) COST Action CA15136 (EuroCaroten) to MRC. We also acknowledge the financial support of the Severo Ochoa Programme for Centres of Excellence in R&D 2016-2019 (SEV-2015-0533) and the

Generalitat de Catalunya CERCA Programme to CRAG. This work also benefited from the Biophysics Platform of I2BC, supported by iBISA and by the French Infrastructure for Integrated Structural Biology (FRISBI) ANR-10-INBS-05. TBA was funded by a Carlsberg Foundation fellowship. BL is supported by grants from the CSIRO Synthetic Biology Future Science Platform and Macquarie University. LM is supported by La Caixa Foundation PhD INPhINIT (ID 100010434) fellowship LCF/BQ/IN18/11660004, which received funding from the EU-H2020 (MSCA grant 713673). STM is supported by a PhD fellowship from the Spanish Ministry of Education, Culture and Sports (FPU16/04054).

Conflicts of interest

The authors declare no conflict of interest.

Author contributions

T.B.A., B.L., N.C. and M.R.C. designed the research. T.B.A., B.L., L.M., S.T.M., G.B.F., F.A.E., B.O.A., and M.J.L. performed experiments. N.C., B.O.A., M.J.L. and A.A.P. contributed analytic tools; T.B.A., B.L., L.M., S.T.M., G.B.F., F.A.E., B.O.A., A.A.P. and M.R.C. analysed data; T.B.A. and M.R.C. wrote the paper. All authors reviewed and discussed the manuscript.

References

- Alos, E., Rodrigo, M.J. and Zacarias, L. (2016) Manipulation of carotenoid content in plants to improve human health. *Sub-Cell. Biochem.* **79**, 311–343.
- Ampomah-Dwamena, C., Thrimawithana, A.H., Dejnopratt, S., Lewis, D., Easley, R.V. and Allan, A.C. (2019) A kiwifruit (*Actinidia deliciosa*) R2R3-MYB transcription factor modulates chlorophyll and carotenoid accumulation. *New Phytol.* **221**, 309–325.
- Andersen, T.B., Martinez-Swatson, K.A., Rasmussen, S.A., Boughton, B.A., Jorgensen, K., Andersen-Ranberg, J., Nyberg, N. et al. (2017) Localization and in-vivo characterization of *Thapsia garganica* CYP76AE2 indicates a role in Thapsigargin biosynthesis. *Plant Physiol.* **174**, 56–72.
- Avendano-Vazquez, A.O., Cordoba, E., Llamas, E., San Roman, C., Nisar, N., De la Torre, S., Ramos-Vega, M. et al. (2014) An uncharacterized apocarotenoid-derived signal generated in zeta-carotene desaturase mutants regulates leaf development and the expression of chloroplast and nuclear genes in Arabidopsis. *Plant Cell*, **26**, 2524–2537.
- Besumbes, O., Sauret-Gueto, S., Phillips, M.A., Imperial, S., Rodriguez-Concepcion, M. and Boronat, A. (2004) Metabolic engineering of isoprenoid biosynthesis in Arabidopsis for the production of taxadiene, the first committed precursor of Taxol. *Biotechnol. Bioeng.* **88**, 168–175.
- Cankar, K., Jongedijk, E., Klompmaker, M., Majdic, T., Mumm, R., Bouwmeester, H., Bosch, D. et al. (2015) (+)-Valencene production in *Nicotiana benthamiana* is increased by down-regulation of competing pathways. *Biotechnol. J.* **10**, 180–189.
- Cazzonelli, C.I., Hou, X., Alagöz, Y., Rivers, J., Dhimi, N., Lee, J., Marri, S. et al. (2020) A cis-carotene derived apocarotenoid regulates etioplast and chloroplast development. *eLife* **9**, e45310.
- Chappell, J., Wolf, F., Proulx, J., Cuellar, R. and Saunders, C. (1995) Is the reaction catalyzed by 3-hydroxy-3-methylglutaryl coenzyme A reductase a rate-limiting step for isoprenoid biosynthesis in plants? *Plant Physiol.* **109**, 1337–1343.
- Cooperstone, J.L., Ralston, R.A., Riedl, K.M., Haufe, T.C., Schweiggert, R.M., King, S.A., Timmers, C.D. et al. (2015) Enhanced bioavailability of lycopene when consumed as cis-isomers from tangerine compared to red tomato juice, a randomized, cross-over clinical trial. *Mol. Nutr. Food Res.* **59**, 658–669.
- D'Amelia, V., Raiola, A., Carputo, D., Filippone, E., Barone, A. and Rigano, M.M. (2019) A basic Helix-Loop-Helix (SIARANCIO), identified from a *Solanum pennellii* introgression line, affects carotenoid accumulation in tomato fruits. *Sci. Rep.* **9**, 3699.
- D'Andrea, L., Simon-Moya, M., Llorente, B., Llamas, E., Marro, M., Loza-Alvarez, P., Li, L. et al. (2018) Interference with Clp protease impairs carotenoid accumulation during tomato fruit ripening. *J. Exp. Bot.* **69**, 1557–1568.
- Delatte, T.L., Scaiola, G., Molenaar, J., de Sousa Farias, K., L. Alves Gomes Albertti, Busscher, J., Verstappen, F. et al. (2018) Engineering storage capacity for volatile sesquiterpenes in *Nicotiana benthamiana* leaves. *Plant Biotechnol. J.* **16**, 1997–2006.
- Diretto, G., Frusciantè, S., Fabbri, C., Schauer, N., Busta, L., Wang, Z., Matas, A.J. et al. (2020) Manipulation of β -carotene levels in tomato fruits results in increased ABA content and extended shelf life. *Plant Biotechnol. J.* **18**, 1185–1199.
- Doblas, V.G., Amorim-Silva, V., Pose, D., Rosado, A., Esteban, A., Arro, M., Azevedo, H. et al. (2013) The SUD1 gene encodes a putative E3 ubiquitin ligase and is a positive regulator of 3-hydroxy-3-methylglutaryl coenzyme A reductase activity in Arabidopsis. *Plant Cell*, **25**, 728–743.
- Domonkos, I., Kis, M., Gombos, Z. and Ughy, B. (2013) Carotenoids, versatile components of oxygenic photosynthesis. *Prog. Lipid Res.* **52**, 539–561.
- Emiliani, J., D'Andrea, L., Ferreyra Lorena Falcone, E., Maulion, E., Rodriguez, E., Rodriguez-Concepcion, M. and Casati, P. (2018) A role for beta, beta-xanthophylls in Arabidopsis UV-B photoprotection. *J. Exp. Bot.* **69**, 4921–4933.
- Esteban, R., Barrutia, O., Artetxe, U., Fernandez-Marin, B., Hernandez, A. and Garcia-Plazaola, J.I. (2015) Internal and external factors affecting photosynthetic pigment composition in plants: a meta-analytical approach. *New Phytol.* **206**, 268–280.
- Estevez-Santiago, R., Olmedilla-Alonso, B. and Fernandez-Jalao, I. (2016) Bioaccessibility of provitamin A carotenoids from fruits: application of a standardised static in vitro digestion method. *Food Funct.* **7**, 1354–1366.
- Ferrero, S., Grados-Torrez, R.E., Leivar, P., Antolin-Llovera, M., Lopez-Iglesias, C., Cortadellas, N., Ferrer, J.C. et al. (2015) Proliferation and morphogenesis of the endoplasmic reticulum driven by the membrane domain of 3-hydroxy-3-methylglutaryl coenzyme A reductase in plant cells. *Plant Physiol.* **168**, 899–914.
- Flores, P., Hernández, V., Hellín, P., Fenoll, J., Cava, J., Mestre, T. and Martínez, V. (2016) Metabolite profile of the tomato dwarf cultivar Micro-Tom and comparative response to saline and nutritional stresses with regard to a commercial cultivar. *J. Sci. Food Agric.* **96**, 1562–1570.
- Harker, M., Holmberg, N., Clayton, J.C., Gibbard, C.L., Wallace, A.D., Rawlins, S., Hellyer, S.A. et al. (2003) Enhancement of seed phytoester levels by expression of an N-terminal truncated *Hevea brasiliensis* (rubber tree) 3-hydroxy-3-methylglutaryl-CoA reductase. *Plant Biotechnol. J.* **1**, 113–121.
- Hashimoto, H., Uragami, C. and Cogdell, R.J. (2016) Carotenoids and Photosynthesis. *Sub-Cell. Biochem.* **79**, 111–139.
- van Herpen, T.W., Cankar, K., Nogueira, M., Bosch, D., Bouwmeester, H.J. and Beekwilder, J. (2010) *Nicotiana benthamiana* as a production platform for artemisinin precursors. *PLoS One* **5**, e14222.
- Ishigaki, M., Mekislarun, P., Kitahama, Y., Zhang, L., Hashimoto, H., Genkawa, T. and Ozaki, Y. (2017) Unveiling the aggregation of lycopene in vitro and in vivo: UV-Vis, resonance Raman, and Raman imaging studies. *J. Phys. Chem. B* **121**, 8046–8057.
- Koyama, Y. and Fujii, R. (1999) Cis-trans carotenoids in photosynthesis: configurations, excited-state properties and physiological functions. In *The photochemistry of carotenoids* (Frank, H.A., Young, A.J., Britton, G. and Cogdell, R.J., eds), pp. 161–188. Dordrecht, Netherlands: Springer Netherlands.
- Lado, J., Zacarias, L., Gurrea, A., Page, A., Stead, A. and Rodrigo, M.J. (2015) Exploring the diversity in Citrus fruit colouration to decipher the relationship between plastid ultrastructure and carotenoid composition. *Planta*, **242**, 645–661.
- Lee, A.R., Kwon, M., Kang, M.K., Kim, J., Kim, S.U. and Ro, D.K. (2019) Increased sesqui- and triterpene production by co-expression of HMG-CoA reductase and biotin carboxyl carrier protein in tobacco (*Nicotiana benthamiana*). *Metab. Eng.* **52**, 20–28.
- Leivar, P., Antolin-Llovera, M., Ferrero, S., Closa, M., Arro, M., Ferrer, A., Boronat, A. et al. (2011) Multilevel control of Arabidopsis 3-hydroxy-3-methylglutaryl coenzyme A reductase by protein phosphatase 2A. *Plant Cell*, **23**, 1494–1511.
- Llamas, E., Pulido, P. and Rodriguez-Concepcion, M. (2017) Interference with plastome gene expression and Clp protease activity in Arabidopsis triggers a

- chloroplast unfolded protein response to restore protein homeostasis. *PLoS Genet.* **13**, e1007022.
- Llansola-Portoles, M.J., Redeckas, K., Streckaite, S., Iliaoa, C., Pascal, A.A., Telfer, A., Vengris, M. et al. (2018) Lycopene crystalloids exhibit singlet exciton fission in tomatoes. *Phys. Chem. Chem. Phys.* **20**, 8640–8646.
- Llorente, B., D'Andrea, L., Ruiz-Sola, M.A., Botterweg, E., Pulido, P., Andilla, J., Loza-Alvarez, P. et al. (2016) Tomato fruit carotenoid biosynthesis is adjusted to actual ripening progression by a light-dependent mechanism. *Plant J.* **85**, 107–119.
- Llorente, B., Torres-Montilla, S., Morelli, L., Florez-Sarasa, I., Matus, J.T., Ezquerro, M., D'Andrea, L. et al. (2020) Synthetic conversion of leaf chloroplasts into carotenoid-rich plastids reveals mechanistic basis of natural chromoplast development. *Proc. Natl Acad Sci USA*, **117**, 21796–21803.
- Lomonosoff, G.P. and D'Aoust, M.A. (2016) Plant-produced biopharmaceuticals: a case of technical developments driving clinical deployment. *Science*, **353**, 1237–1240.
- Lu, Y., Stegemann, S., Agrawal, S., Karcher, D., Ruf, S. and Bock, R. (2017) Horizontal transfer of a synthetic metabolic pathway between plant species. *Curr. Biol.* **27**, 3034–3041.e3033.
- Luo, D., Callari, R., Hamberger, B., Wubshet, S.G., Nielsen, M.T., Andersen-Ranberg, J., Hallstrom, B.M. et al. (2016) Oxidation and cyclization of casbene in the biosynthesis of Euphorbia factors from mature seeds of *Euphorbia lathyris* L. *Proc. Natl Acad. Sci. USA*, **113**, E5082–5089.
- Majer, E., Llorente, B., Rodriguez-Concepcion, M. and Daros, J.A. (2017) Rewiring carotenoid biosynthesis in plants using a viral vector. *Sci. Rep.* **7**, 41645.
- Mapelli-Brahm, P., Desmarchelier, C., Margier, M., Reboul, E., Melendez-Martinez, A.J. and Borel, P. (2018) Phytoene and phytofluene isolated from a tomato extract are readily incorporated in mixed micelles and absorbed by caco-2 cells, as compared to lycopene, and SR-BI is involved in their cellular uptake. *Mol. Nutr. Food Res.* **62**, e1800703.
- Massaretto, I.L., Albaladejo, I., Purgatto, E., Flores, F.B., Plasencia, F., Egea-Ranández, J.M., Bolarin, M.C. et al. (2018) Recovering tomato landraces to simultaneously improve fruit yield and nutritional quality against salt stress. *Front Plant Sci.* **9**, 1778.
- Melendez-Martinez, A.J., Mapelli-Brahm, P., Benitez-Gonzalez, A. and Stinco, C.M. (2015) A comprehensive review on the colorless carotenoids phytoene and phytofluene. *Arch. Biochem. Biophys.* **572**, 188–200.
- Melendez-Martinez, A.J., Mapelli-Brahm, P. and Stinco, C.M. (2018) The colourless carotenoids phytoene and phytofluene: from dietary sources to their usefulness for the functional foods and nutraceuticals industries. *J. Food Compos. Anal.* **67**, 91–103.
- Mou, B. (2009) Nutrient content of lettuce and its improvement. *Curr. Nutr. Food Sci.* **5**, 242–248.
- Müller, L., Fröhlich, K. and Böhm, V. (2011) Comparative antioxidant activities of carotenoids measured by ferric reducing antioxidant power (FRAP), ABTS bleaching assay (α TEAC), DPPH assay and peroxy radical scavenging assay. *Food Chem.* **129**, 139–148.
- Nakagawa, T., Suzuki, T., Murata, S., Nakamura, S., Hino, T., Maeo, K., Tabata, R. et al. (2007) Improved Gateway binary vectors: high-performance vectors for creation of fusion constructs in transgenic analysis of plants. *Biosci. Biotechnol. Biochem.* **71**, 2095–2100.
- Nobbs, J.H. (1985) Kubelka-munk theory and the prediction of reflectance. *Prog. Color. Relat. Top.* **15**, 66–75.
- Nogueira, M., Enfissi, E.M.A., Welsch, R., Beyer, P., Zurbriggen, M.D. and Fraser, P.D. (2019) Construction of a fusion enzyme for astaxanthin formation and its characterisation in microbial and plant hosts: A new tool for engineering ketocarotenoids. *Metab. Eng.* **52**, 243–252.
- Nogueira, M., Mora, L., Enfissi, E.M., Bramley, P.M. and Fraser, P.D. (2013) Subchromoplast sequestration of carotenoids affects regulatory mechanisms in tomato lines expressing different carotenoid gene combinations. *Plant Cell*, **25**, 4560–4579.
- Pankratov, I., McQuinn, R., Schwartz, J., Bar, E., Fei, Z., Lewinsohn, E., Zamir, D. et al. (2016) Fruit carotenoid-deficient mutants in tomato reveal a function of the plastidial isopentenyl diphosphate isomerase (IDI1) in carotenoid biosynthesis. *Plant J.* **88**, 82–94.
- Perello, C., Rodriguez-Concepcion, M. and Pulido, P. (2014) Quantification of plant resistance to isoprenoid biosynthesis inhibitors. *Methods Mol. Biol.* **1153**, 273–283.
- Peyret, H. and Lomonosoff, G.P. (2013) The pEAQ vector series: the easy and quick way to produce recombinant proteins in plants. *Plant Mol. Biol.* **83**, 51–58.
- Pollier, J., Moses, T., Gonzalez-Guzman, M., De Geyter, N., Lippens, S., Vanden Bossche, R., Marhavy, P. et al. (2013) The protein quality control system manages plant defence compound synthesis. *Nature*, **504**, 148–152.
- Ravanello, M.P., Ke, D., Alvarez, J., Huang, B. and Shewmaker, C.K. (2003) Coordinate expression of multiple bacterial carotenoid genes in canola leading to altered carotenoid production. *Metab. Eng.* **5**, 255–263.
- Re, R., Pellegrini, N., Prottogente, A., Pannala, A., Yang, M. and Rice-Evans, C. (1999) Antioxidant activity applying an improved ABTS radical cation decolorization assay. *Free Radic. Biol. Med.* **26**, 1231–1237.
- Robert, B. (1999) The electronic structure, stereochemistry and resonance Raman spectroscopy of carotenoids. In *The Photochemistry of Carotenoids* (Frank, H.A., Young, A.J., Britton, G. and Cogdell, R.J., eds), pp. 189–201. Dordrecht, Netherlands: Springer Netherlands.
- Rodriguez-Concepcion, M., Avalos, J., Bonet, M.L., Boronat, A., Gomez-Gomez, L., Hornero-Mendez, D., Limon, M.C. et al. (2018) A global perspective on carotenoids: Metabolism, biotechnology, and benefits for nutrition and health. *Prog. Lipid Res.* **70**, 62–93.
- Rodriguez-Concepcion, M. and Boronat, A. (2015) Breaking new ground in the regulation of the early steps of plant isoprenoid biosynthesis. *Curr. Opin. Plant Biol.* **25**, 17–22.
- Ruiz-Sola, M.A., Barja, M.V., Manzano, D., Llorente, B., Schipper, B., Beekwilder, J. and Rodriguez-Concepcion, M. (2016) A single arabidopsis gene encodes two differentially targeted geranylgeranyl diphosphate synthase isoforms. *Plant Physiol.* **172**, 1393–1402.
- Sadali, N.M., Sowden, R.G., Ling, Q. and Jarvis, R.P. (2019) Differentiation of chromoplasts and other plastids in plants. *Plant Cell Rep.* **38**, 803–818.
- Schwach, F., Vaistij, F.E., Jones, L. and Baulcombe, D.C. (2005) An RNA-dependent RNA polymerase prevents meristem invasion by potato virus X and is required for the activity but not the production of a systemic silencing signal. *Plant Physiol.* **138**, 1842–1852.
- Sparkes, I.A., Runions, J., Kearns, A. and Hawes, C. (2006) Rapid, transient expression of fluorescent fusion proteins in tobacco plants and generation of stably transformed plants. *Nat. Protoc.* **1**, 2019–2025.
- Sun, T., Yuan, H., Cao, H., Yazdani, M., Tadmor, Y. and Li, L. (2018) Carotenoid metabolism in plants: the role of plastids. *Mol. Plant*, **11**, 58–74.
- Suzuki, M., Takahashi, S., Kondo, T., Dohra, H., Ito, Y., Kiriiwa, Y., Hayashi, M., et al. (2015) Plastid Proteomic Analysis in Tomato Fruit Development. *PLoS One* **10**, e0137266. <https://doi.org/10.1371/journal.pone.0137266>.
- Tamary, E., Nevo, R., Naveh, L., Levin-Zaidman, S., Kiss, V., Savidor, A., Levin, Y. et al. (2019) Chlorophyll catabolism precedes changes in chloroplast structure and proteome during leaf senescence. *Plant Direct*, **3**, e00127.
- Wang, Z., Xu, W., Kang, J., Li, M., Huang, J., Ke, Q., Kim, H.S. et al. (2018) Overexpression of alfalfa Orange gene in tobacco enhances carotenoid accumulation and tolerance to multiple abiotic stresses. *Plant Physiol. Biochem.* **130**, 613–622.
- Wu, S., Schalk, M., Clark, A., Miles, R.B., Coates, R. and Chappell, J. (2006) Redirection of cytosolic or plastidial isoprenoid precursors elevates terpene production in plants. *Nat. Biotechnol.* **24**, 1441–1447.
- Yamamoto, T., Hoshikawa, K., Ezura, K., Okazawa, R., Fujita, S., Takaoka, M., Mason, H.S. et al. (2018) Improvement of the transient expression system for production of recombinant proteins in plants. *Sci. Rep.* **8**, 4755.
- Yin, J.L. and Wong, W.S. (2019) Production of santalenes and bergamotene in *Nicotiana tabacum* plants. *PLoS One*, **14**, e0203249.
- Zheng, X., Giuliano, G. and Al-Babili, S. (2020) Carotenoid biofortification in crop plants: citius, altius, fortius. *Biochim. Biophys. Acta Mol. Cell Biol. Lipids*, **1865**, 158664.